Transactions

of the

ASME

JULY, 1948

VOL. 70, NO. 5

Transactions

of The American Society of Mechanical Engineers

Published on the tenth of every month, except March, June, September, and December

---

Published monthly by The American Society of Mechanical Engineers. Publication office at 20th and Northampton Streets, Easton, Pa. The editorial department is located at the headquarters of the Society, 29 West Thirty-Ninth Street, New York 18, N. Y. Cable address, "Dynamic," New York. Price $1.50 a copy, $12.00 a year; to members and affiliates, $1.00 a copy, $6.00 a year. Changes of address must be received at Society headquarters three weeks before they are to be effective on the mailing list. Please send old as well as new address. . . . By-Law: The Society shall not be responsible for statements or opinions advanced in papers or . . . printed in its publications (B13, Par. 4). . . . Entered as second-class matter March 2, 1928, at the Post Office at Easton, Pa., under the Act of August 24, 1912. . . .

Laboratory Investigations of the Mechanism of Cavitation

By R. T. KNAPP[1] and A. HOLLANDER,[2] PASADENA, CALIF.

The paper describes some experimental investigations of the formation and collapse of cavitation bubbles. The experiments were carried on in the high-speed water tunnel of the Hydrodynamics Laboratory of the California Institute of Technology under the sponsorship of the Research and Development Division of the Bureau of Ordnance of the U. S. Navy and the Fluid Mechanics Section of the Office of Naval Research. A detailed study of the formation and collapse of the individual bubbles has been carried on by the use of high-speed motion pictures taken at rates up to 20,000 per sec. From these records calculations have been made of rate of formation and collapse of the bubbles. Deductions have been drawn from these results concerning the physical mechanism of the cavitation phenomenon.

Inherent Difficulties of Observation of Cavitation Process

THERE is little doubt but that most workers in the field of cavitation would agree that there is considerably more conjecture than knowledge on the physical events that take place during cavitation. Much of this lack of knowledge is due to the fact that it is inherently difficult to observe and record the details of the phenomenon. The individual bubbles or voids form and collapse with great rapidity. Furthermore, cavitation is generally caused by fast-moving bodies in liquid, either with a free surface (propeller, torpedo), or in closed conduits (pump or turbine impeller), so that even the study of simpler cases with a stationary object and fast-moving liquid to attain the same relative speed is difficult. The result is that most of the experimental observations in the past have been restricted either to the study of the effect of cavitation, i.e., cavitation damage, or to the recording of the over-all or instantaneous pictures of some stage of the cavitation process. As a consequence of the lack of such detailed information, no quantitative description has been developed of the actual physical processes which take place during cavitation. Thus although many attempts have been made to develop analytical interpretations they have been based upon widely different physical assumptions, many of which have little background of experimental fact. The objective of the present study has been to attempt to furnish a more quantitative physical knowledge concerning the mechanism of cavitation and to formulate some elementary analytical descriptions of the phenomenon on the basis of these physical observations. This paper, in turn, is only a preliminary report for the purpose of presenting some of the first experimental observations, together with tentative analyses of their significance and implications.

Experimental Methods and Equipment

The experimental approach to the problem may be divided naturally as follows:

1 The production of the desired degree of cavitation under measurable and reproducible conditions which are suitable for observation.

2 The photographic recording of the details of the cavitation process.

The equipment and technique required for each part will be described separately.

Production of Cavitation in High-Speeed Water Tunnel. The high-speed water tunnel was chosen as the major piece of equipment for use with this project because the pressure, velocity, and temperature of the liquid in the working section could be controlled accurately at any desired set of values within the range necessary to produce or eliminate cavitation on a wide variety of experimental shapes. A detailed description of the construction and operation of this tunnel has been given in another paper.[3]

In the series of experiments now under consideration, measurements have been made at velocities of from 30 to 70 fps, with absolute pressures at the wall of the working section ranging from about $1^1/_2$ to 50 psi above vapor pressure. Temperature range has been held to within a few degrees of room temperature. Nearly all the observations have been made on flow around bodies of revolution which have been mounted with their axes either parallel or within a few degrees of parallel with the direction of flow. Wide ranges of forebody or nose shapes and afterbody shapes have been studied. Pressure-distribution measurements have been made on some selected shapes of these series. All of the bodies studied have had a uniform maximum diameter of 2 in. The observations under consideration at this time have all been made on cavitation occurring on or adjacent to a series of ogive noses. The ogive nose is a very simple shape, as may be seen from Fig. 1. It can be defined as being generated by revolving a circular arc about the axis of revolution of the cylinder. One end of the arc is tangent to an element of the cylinder; the

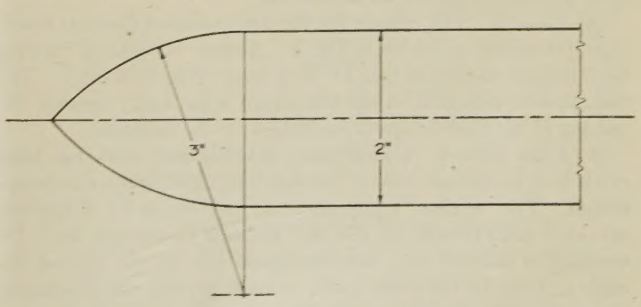

Fig. 1 1.5-Caliber Ogive Nose

[1] Director, Hydrodynamics Laboratory, California Institute of Technology. Mem. ASME.

[2] Research Engineer, Hydrodynamics Laboratory, California Institute of Technology. Mem. ASME.

Contributed by the Hydraulic Division and presented at the Annual Meeting, Atlantic City, N. J., December 1–5, 1947, of The American Society of Mechanical Engineers.

 Paper No. 47—A-150.

[3] "The Hydrodynamics Laboratory at the California Institute of Technology," by R. T. Knapp, Joseph Levy, F. Barton Brown, and J. Pat O'Neill, Trans. ASME, this issue, pp. 437–457.

other end intersects the axis. It is convenient to express the radius of this arc in terms of the diameter of the cylinder, i.e., the generatrix of a $1^1/_2$ d ogive is an arc whose radius is $1^1/_2$ times the diameter of the cylinder.

High-Speed Motion-Picture Photography. The tool selected to record the physical details of the cavitation phenomenon is high-speed motion-picture photography. Motion pictures taken at one speed and projected at another can be thought of as performing the function of a time telescope or microscope. With this conception, the ratio of magnification will be measured by the ratio of the picture-taking speed to the projecting speed of the picture. For example, if pictures are taken of a given phenomenon at relatively long intervals and then projected at the normal speed necessary for viewing movies, the time scale of the phenomenon is changed in a manner similar to the way the distance scale of an object is changed when observed through a telescope. The telescope brings the distant object close enough to the observer, so that details of its structure can be observed; the speeded-up projection of the pictures brings the time details of the phenomenon close enough together, so that they can be observed. Conversely, motion pictures taken at a high rate of speed and projected at a much lower rate of speed serve as a time microscope, since the process resolves the details in time in the same manner as the microscope resolves the details in space.

In the present study, pictures of cavitation have been taken at varying rates from 64 per sec to 20,000 per sec. When these are projected at the normal viewing speed of 16 per sec, time magnifications covering ratios of 4:1 to 1250:1 are secured. Equipment such as this is needed to change the time scale for exactly the same reason that telescopes and microscopes are needed to change the length scale. The human senses and brain have a limited range in which they can get an undistorted concept of what is occurring. Therefore it is necessary to transform the actual times and distances involved in a given phenomenon until they fall within these limited ranges.

Description of Photographic Equipment. Photographic equipment used in this study is of the multiflash type. The pioneer development in this field was carried on by Prof. Harold E. Edgerton and his associates at the Massachusetts Institute of Technology. It consists of a simple camera in which the recording film moves constantly past the focal plane at a high speed. The camera has no shutter. Illumination required to take the picture is provided by one or more synchronized flash lamps, which also act as the camera shutter. This requires that the flash duration be so short that neither the image of the object on the film nor the film itself move an appreciable distance while the light is on. As the number of the pictures taken per second increases, the film motion becomes the controlling factor in most cases. Up to the present time satisfactory pictures have been taken at rates up to 30,000 exposures per sec. The lamp equipment has been operated up to 50,000 flashes per sec, but as yet the obtainable film speeds have not been high enough to give a satisfactory frame height for use at this rate.

(*a*) *Camera.* The camera itself is the standard General Radio type instrument as shown in Fig. 2. A series of lenses of varying focal lengths have been fitted to it to increase its flexibility. The commutator provided on the film drum is not used; instead, the pulsing of the flash lamps is controlled by an oscillator.

(*b*) *Flash Lamps.* Considerable development work has been carried on to increase the rate at which the flash lamps can be operated. The original equipment, as developed by Edgerton, operated satisfactorily at the rate of 3000 flashes per sec. Investigation showed that this limitation was in the control circuits and not in the lamp itself. Consequently, the laboratory has undertaken the development of a system which utilizes several control circuits synchronized through a common multiphase

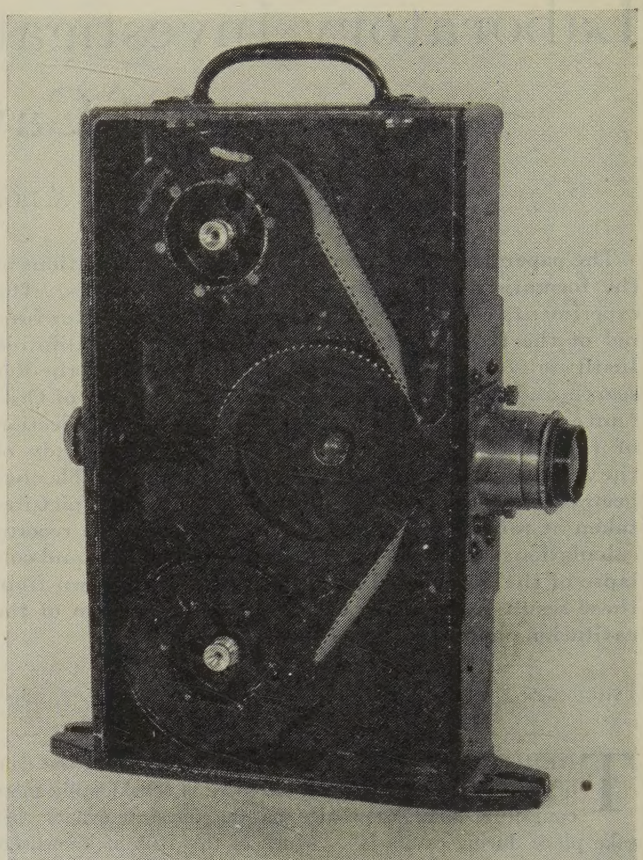

FIG. 2 HIGH-SPEED MOTION-PICTURE CAMERA

oscillator circuit, but discharging in rotation through a single lamp.

By the use of this system the flash rate becomes equal to the maximum rate at which a single control circuit can be operated, multiplied by the number of circuits involved. At the present time six circuits have been used simultaneously in 6-phase array with proper electronic switching devices to permit all of the circuits to discharge through a common lamp.

In the design and development of a combination camera and flash-lamp system of this type, it is necessary to bear in mind the extreme importance of the relationship between the camera and the lights because the lights function as the camera shutter. In fact, the characteristics of the flash lamps exert a controlling influence upon the work that can be done with the combination. The most important characteristic of the flash lamp is the effective duration of the flash. The minimum available flash duration limits the maximum usable film speed.

In this system of photography, the film moves continuously. Therefore the flash duration must be short enough to stop the motion of the film; otherwise, the record will be blurred. For critically sharp results, the maximum usable film speed can be calculated from the criterion that the allowable film motion during one flash should not be greater than the diameter of the circle of confusion of the lens system. For extremely high-speed work it may be necessary to lower this requirement somewhat. The permissible deviation will depend upon the accuracy of measurements required from the record. At first sight this criterion may seem incomplete, since no consideration is given to the speed of the object being photographed.

A simple example will show that, at least for the present use, this is not the case. Blurring is caused by a relative movement

between the image and the film during exposure. While making cavitation photographs in the laboratory, the flow is at right angles to the motion of the film. The motion with respect to the film will be the vector sum of the motion of the image of the bubble with respect to the camera frame and the motion of the film with respect to the camera frame. The maximum flow velocity in the tunnel that has been photographed is about 75 fps. The smallest reduction ratio used in the photograph is about 6:1, i.e., the image on the film, and hence the image velocity on the film is not over $^1/_6$ of the bubble velocity in the tunnel. Thus the maximum velocity of the image with respect to the camera frame is $12^1/_2$ fps.

Most of the pictures were taken at a rate of 20,000 frames per sec. In order to keep the film speed to a minimum, very small frame heights were employed. Thus, on the average, each individual picture was about 1 in. wide × $^1/_{16}$ in. high. This frame height of $^1/_{16}$ in. requires a film speed of over 100 fps when the taking rate is 20,000 per sec and, even at this speed, all spacing between frames has to be eliminated. The vector sum of 100 and $12^1/_2$ is less than 101, i.e., the speed of the object had something less than 1 per cent effect upon the relative speed between the image and the film. When the camera is further from the tunnel, or if a shorter-focal-length lens is used, the effect is even smaller. It is safe to conclude, therefore, that in the design of photographic equipment of this kind the speed of the object can be ignored safely.

Another very important characteristic of the flash lamp when used in this system of photography is the intensity of the light. This intensity must be very high to produce an image of reasonable density in the very short exposure time available. The importance of illumination intensity can be seen clearly if the operation of this type of equipment is compared to that of a hypothetical motion-picture camera of the standard type, using a normal shutter but operating at 20,000 exposures per sec. The normal type of shutter has an opening of about 180 deg, which means that the effective exposure time is one half of the elapsed time between successive pictures. In this case the exposure would be $^1/_{40,000}$ sec. If this is compared to the exposure time of $^1/_{30}$ to $^1/_{50}$ sec for a normal camera operating at a conventional speed, it will be seen that an extremely intense illumination would be required if an adequate exposure were to be secured. However, $^1/_{40,000}$ sec is 25 microseconds. This is 25 times as long as the flash duration, which is 1 microsecond. Hence the flash intensity must be at least 25 times as great ast hat required for this hypothetical conventional-type camera. The energy input to the lamp is at a rate corresponding to a continuous flow of 20 kw; however, as the lamp is burning only $^1/_{50}$ of the total time, the energy input during the exposure is at the rate of 1000 kw.

An example of the difference in the information obtainable with different taking rates is seen in Figs. 3(*a* to *d*). The film strips are all taken under the same conditions in the tunnel for the same degree of cavitation on the same model. In comparing strips 3(*a*) and 3(*d*), it should be remembered that there are 1250 individual exposures on the *d* strip between each one on the *a* strip. The *a* strip was taken at the normal motion-picture rate.

Experimental Observations

An examination of some of the records shows that if all stages of cavitation are considered the phenomenon is very complex. For example, Fig. 4 presents a series of pictures showing increasing degrees of cavitation from the incipient point to the formation of a cavity large enough to contain the entire body. In this case, the shape is a hemispherical nose with a straight cylindrical afterbody. This entire series was obtained while the tunnel was operating at constant velocity with gradually decreasing pressure in the working section. It will be observed in each picture that many complex bubble groups are formed and if the life history of such a group is examined it will be seen that the individual bubbles interact and often combine in either the formation or the collapse stage. At the present time no attempt will be made to investigate these complicated interactions. Instead, consideration will be restricted to the simplest appearances that can be found on the records. For that reason a shape was chosen which, at least for low degrees of cavitation, tends to produce individual bubbles spaced far enough apart so that occasional ones can be found which throughout their entire life history of formation, collapse, and rebound are not seriously affected by interference from other bubbles.

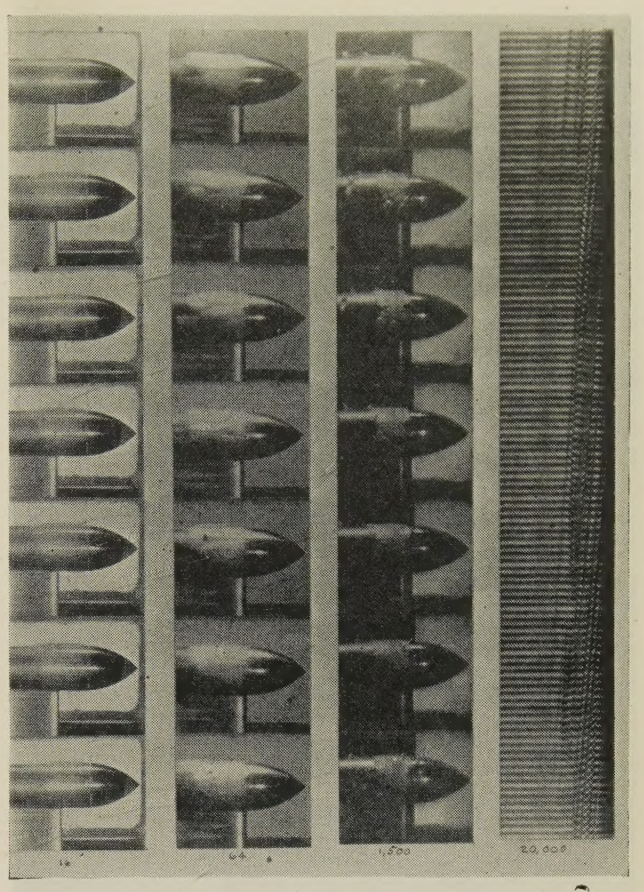

(*a*) (*b*) (*c*) (*d*)
(*a*) 16 per sec (*b*) 64 per sec (*c*) 1500 per sec (*d*) 20,000 per sec

Fig. 3 Comparison of Picture-Taking Rates

An example of the effect of surface curvature of the body on the appearance of the cavitation is shown in Figs. 5(*a*, *b*, and *c*). These pictures were taken for approximately the same degree of cavitation. However, the body noses are different. Fig. 5(*a*) is a hemispherical nose, Fig. 5(*b*) an 0.875-caliber ogive, and Fig. 5(*c*) a 1.5-caliber ogive. The appearance of the cavitation in Fig. 5(*a*) is typical of that found on the blunter nose forms; whereas that in Fig. 5(*c*) is characteristic of the finer shapes. Fig. 5(*b*) is a transition shape, showing some of the characteristics of both. The experimental material used in the rest of this presentation has all been obtained from records taken with a 1.5-caliber ogive nose mounted on a long cylindrical afterbody.

Fig. 6 shows a record of the complete life history of a cavitation bubble. Strip (*b*) is a direct continuation of strip (*a*). These photographs were obtained at a tunnel velocity of 40 fps and a picture-taking rate of 20,000 frames per sec. It will be

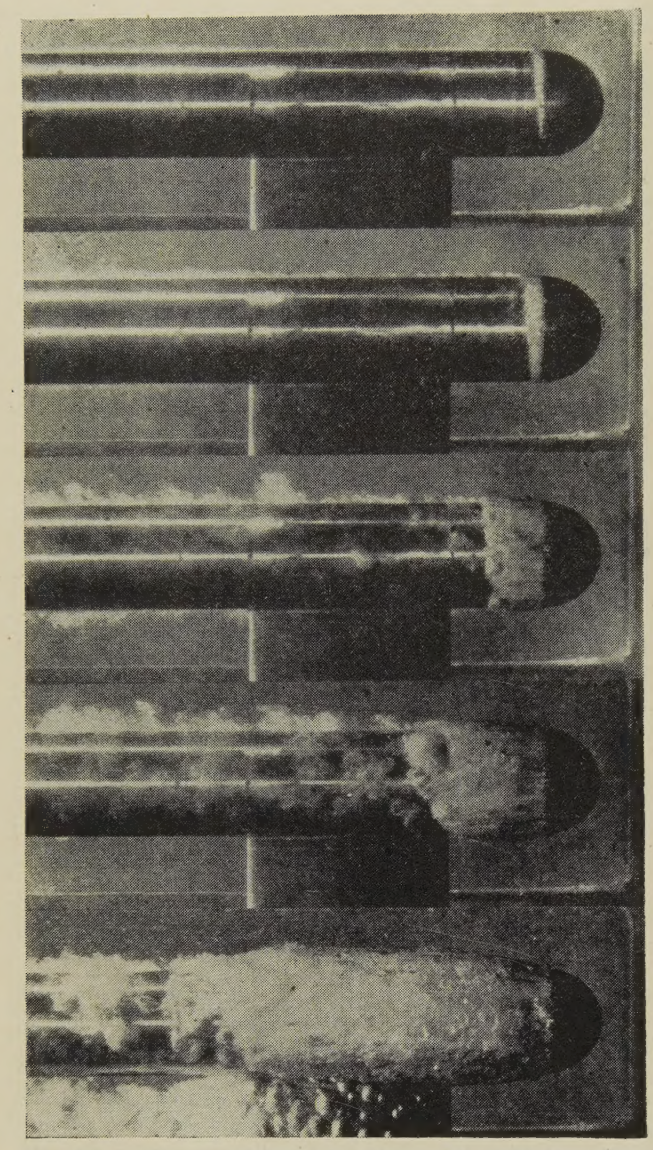

FIG. 4 CAVITATION DEVELOPMENT ON BODY WITH HEMISPHERICAL NOSE

[Views from top down: (*a*) $K = 0.62$; (*b*) $K = 0.55$; (*c*) $K = 0.45$; (*d*) $K = 0.40$; (*e*) $K = 0.31$, respectively.]

seen that the life cycle of a bubble can be divided into a series of natural stages, as follows:

1 Formation and growth, from first appearance to maximum diameter.

2 First collapse, from maximum diameter to first disappearance.

3 First rebound, from first disappearance to second maximum.

4 Second collapse, from second maximum to second disappearance.

5 Second rebound.

6 Third collapse.

7 Final rebound, collapse, and disappearance.

A large share of the existing literature on cavitation has considered only the second stage. The growth, rebound, and recollapse phases have been ignored, in general, either because their existence was unknown or because they were considered an unwarranted complication. This can be understood on the basis discussed previously, i.e., most of the investigators have been concerned either with the investigation of methods for preventing the occurrence of cavitation, or with the determination of cavitation damage and the relative resistance of different materials to such damage.

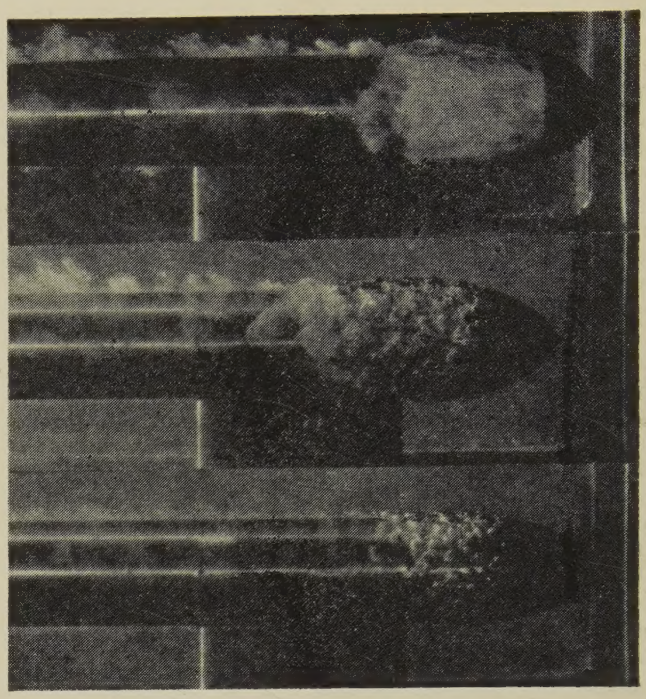

FIG. 5 EFFECT OF SURFACE CURVATURE ON APPEARANCE OF CAVITATION

[Views from top down: (*a*), (*b*), (*c*)]

One of the assumptions commonly made is that the pressure in the bubble is approximately equal to the vapor pressure of the liquid at the mean temperature of the flow. There is much indirect evidence to support the belief that this is the right order of magnitude for the pressure. For example, Fig. 4 shows a series of pictures of the development of cavitation on the hemispherical nose. It will be noted that in the initial stages, Figs. 4 (*a* to *c*), the cavitation area is not symmetrical around the nose, but in each case it is wider at the top than at the bottom of the model. The only significant difference in the flow conditions from top to bottom is a change in the hydrostatic pressure which has an over-all magnitude of 2 in. of water. Thus the degree of cavitation is sensitive to a fraction of this very slight change of pressure. This furnishes a strong inference that the pressure within the bubble must likewise be small, that is, of the same order as the vapor pressure at the existing temperature, or it would not be affected by this small change in pressure. Similar evidence is given by the difference betwen the successive pictures. The change of the measured tunnel pressure between the pictures is very small in contrast to the great change in the cavitation areas. More direct evidence is given by the agreement between pressure-distribution measurements made under noncavitating conditions on a specific shape, with the pressure at which cavitation first appears on that shape.

In the analysis of cavitation phenomena, the cavitation parameter has been found very useful. This is defined as follows

$$K = \frac{p_L - p_B}{\rho \frac{V^2}{2}} = \frac{h_L - h_B}{\frac{V^2}{2g}}$$

in which

K = cavitation parameter
p_L = absolute pressure in the undisturbed liquid, psf
h_L = same in feet of liquid, $h_L = \frac{p_L}{\gamma}$
p_B = vapor pressure corresponding to water temperature, psf
h_B = same as p_B in feet of liquid, $h_B = \frac{p_B}{\gamma}$
V = relative velocity between body and liquid, fps
ρ = mass density of liquid, slugs per cu ft = γ/g
γ = specific weight of liquid, lb per cu ft
g = acceleration of gravity, fps per sec

It will be seen that the numerator of both expressions is simply the net pressure or head acting to collapse the cavity or bubble. The denominator is the velocity pressure or head. Since the entire variation in pressure around the moving body is a result of the velocity, the velocity head may be considered a measure of the pressure available to open up a cavitation void. From this point of view, the cavitation parameter is simply the ratio of the pressure available for keeping the stream in contact with the body to the pressure available for opening the stream and permitting bubble formation. If the K for incipient cavitation is considered, (designated K_i), it can be interpreted to mean the maximum reduction in pressure on the surface of the body measured in terms of the velocity head. Thus if a body starts to cavitate at the cavitation parameter of 1, it means that the lowest pressure at any point on the surface is one velocity head below that of the undisturbed fluid.

It was found that for greater degrees of cavitation, measured by the extension of the bubble-covered section to $^1/_4$, $^1/_2$, $^3/_4$, or full length of the body, the parameter K is equally significant, i.e., it signifies similar extensions for the same K values independently of the velocity.

Analysis of Observations

The high-speed water tunnel is a piece of equipment which can be operated under accurately known and controlled conditions. The associated instruments and apparatus, including the photographic equipment used in making the records of the formation and collapse of the cavitation bubble are quantitative instruments. Therefore it is possible to evaluate the records of the cavitation bubbles with reasonable accuracy. Time measurements are based upon the interval between the individual exposures on the high-speed motion pictures. This interval is determined by the flash rate of the lamps. This rate is controlled by an oscillator whose frequency is known with great accuracy. Thus the flashes are spaced at very uniform known intervals. The time measurement is completely unaffected by the film speed in this system of measurements. Motion is determined by measuring the position of the bubble on the individual pictures on the film. The light path from the camera to the bubble traverses air, lucite, and water, which produces some optical distortion. This distortion is comparatively small because the outside surfaces of the lucite windows are planes. Therefore the cylindrical lens effect of the water-filled circular working section is largely eliminated. The amount of distortion which does exist is eliminated by applying correction factors that have been determined by photographing horizontal and vertical test scales mounted in the tunnel area in the position normally occupied by the model. Thus the actual dimensions of the bubbles and the amount of their movement can be determined with a good degree of approximation.

Fig. 6 is a suitable record for this purpose. It shows the life cycle of an isolated bubble which happens to be far enough removed from other similar bubbles to make it reasonable to

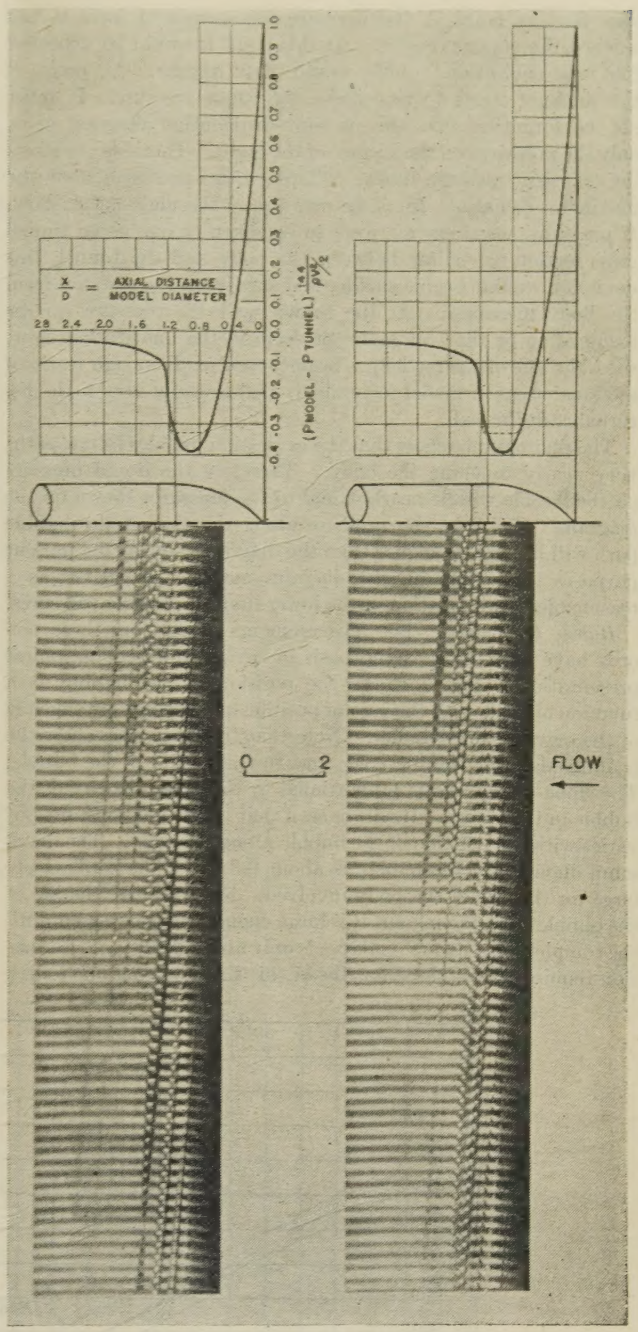

(a) (b)

Fig. 6 Life History of a Cavitation Bubble

assume that it is relatively unaffected by other elements of the cavitation. The diagram at the top of the figure shows the pressure distribution on the surface of the body. This distribution was measured on the model in the tunnel. The full line is for noncavitating conditions, and the dotted line is for the degree of cavitation shown in the photographs. For these measurements the tunnel was operated at a cavitation parameter of $K = 0.33$. The tunnel velocity was 40 fps. This corresponds to a dynamic head of about 24.8 ft or 10.7 psi. The vapor pressure of the water at the temperature of the measurements was approximately 0.4 psi. The absolute pressure in the undisturbed flow, corresponding to these conditions, is about 4 psi. (See also Fig. 8)

If we examine the pressure-distribution diagram it will be

seen that at point A the pressure has decreased until it has reached the vapor pressure. At this point it would be expected that the cavitation bubble would first appear. At point B the pressure starts to rise above the vapor pressure. It must not be forgotten that the pressure-distribution diagram gives only the pressures on the surface of the body. Therefore, neglecting transient pressure during collapse, these pressures show the maximum deviations from the pressure in the undisturbed flow. If pressure measurements were to be taken at one given tunnel cross section for points between the body and the tunnel, this deviation would become smaller and smaller as the distance from the body increased. At the tunnel wall the pressure can be assumed to be the true static pressure in the undisturbed flow, since the size of the model has been chosen small enough (ratio of sectional areas of model to tunnel is $^1/_{80}$) to cause very little disturbance at the wall.

The photographs show that the cavitation bubbles follow paths very nearly touching the body. Therefore the liquid pressure on the bubble will be nearly equal to the pressures shown on the diagram. Probably the pressure along the line of the bubble path will be slightly higher than the diagram, but for the present purposes the values on the diagram may be considered as a reasonable approximation of the lower limit of possible pressures.

Bubble Formation. The measurements made from these records have been used as the basis of several different graphical presentations. Fig. 7 shows the position of the bubble as a function of time, with the zero of position at the point of tangency of the ogive to the cylinder. Note that the three lines show the leading edge, the trailing edge, and the mid-point of the bubble. The slope of the line is proportional to the axial velocity of the bubble in the tunnel. It will be seen that this is not constant but varies with the position of the bubble along the body. The maximum diameter of the bubble is about 0.3 in. This is relatively large for the size of the body involved. Nevertheless, the life of the bubble from the instant it is large enough to be detected until the completion of its first collapse is only about 0.003 sec. Formation requires about three fourths of this time, leaving one fourth for the collapse. An interesting point to observe in passing is that during the final stages of the first collapse the leading edge of the bubble is moving radially inward so rapidly that it is actually moving upstream in the tunnel. Fig. 8 gives the measured radius and volume of the bubble, plotted on the pressure-distribution diagram from Fig. 6. Fig. 9 shows the bubble radius and volume as functions of time. For this diagram the bubbles have been assumed to be spheres having a radius equal to the average of the horizontal and vertical dimensions measured in the photographs.

In the analysis of these diagrams it is necessary to consider some of the physical factors which must influence the growth and collapse of the bubble.

Any fluid particle may be considered as a free body moving in accordance with the forces acting upon it. In such an analysis the inertia of the particle plays a very important role. If particles of liquid on the bubble surface are studied, it may be assumed as a first approximation that they move symmetrically, i.e., that the bubble remains spherical. Thus spheres are equal pressure surfaces, hence only radial forces and velocities are involved.

A consideration of the shape of the body and the pressure-distribution diagram on its surface leads to the explanation of why the cavitation bubble forms. Imagine a particle of liquid in the flow impinging on the nose of the body and following along the surface. First it is forced radially outward and the pressure-distribution diagram shows the amount of force required to make it conform to this portion of the body shape. Outward acceleration continues for a short distance but decreases rapidly in magnitude as shown by the rapid fall in the pressure on the surface. At the point where the pressure on the body has fallen until it is equal to the static pressure in the undisturbed flow, outward acceleration ceases, i.e., the particle is moving out fast enough to keep out of the way of the body. Downstream from this point it is necessary to apply a force acting toward the body to keep the particle in contact with it, because now the surface is curving away from the path of the particle. Since the pressure in the

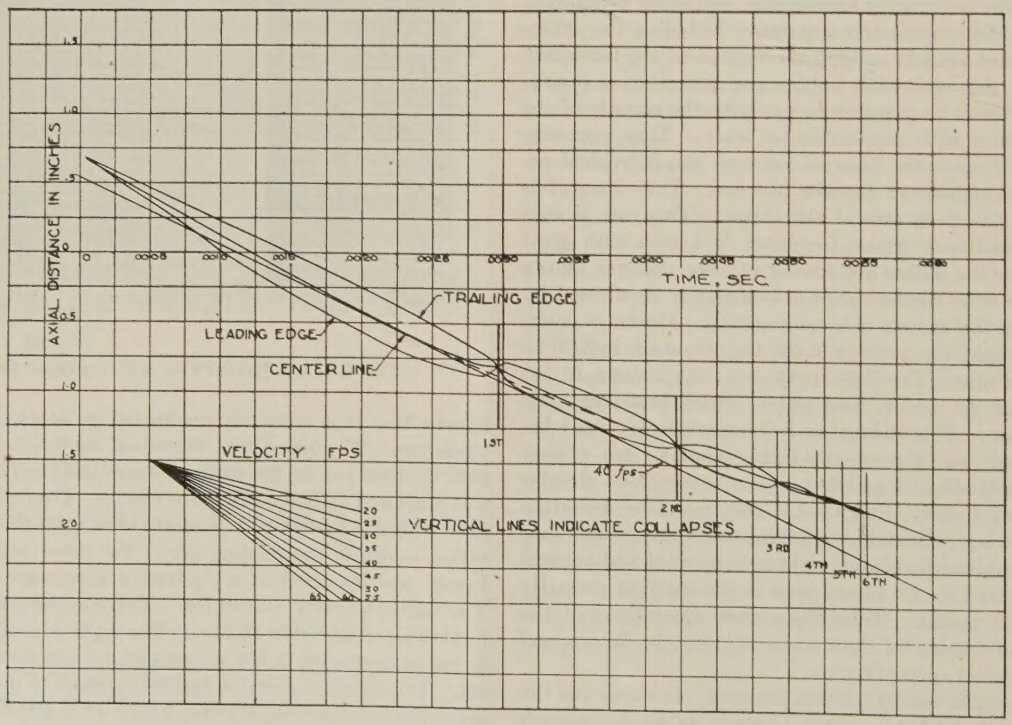

FIG. 7 BUBBLE MOVEMENT DURING FORMATION AND COLLAPSE

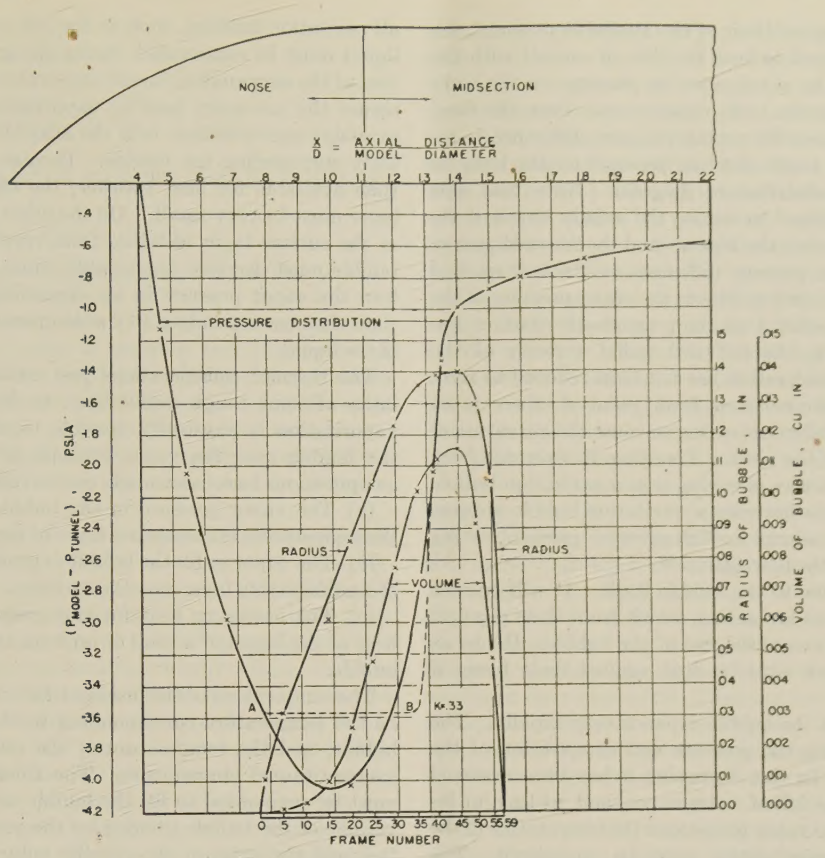

FIG. 8 RELATION OF BUBBLE GROWTH AND COLLAPSE TO PRESSURE FIELD

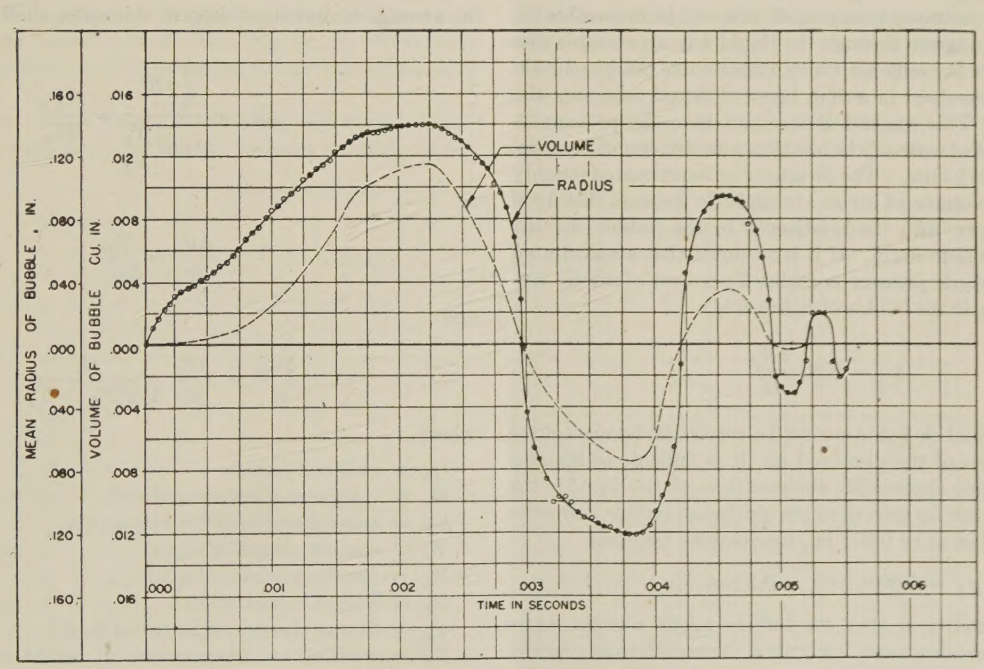

FIG. 9 TIME HISTORY OF LIFE OF BUBBLE

undisturbed flow is the upper limit of the available pressure, the pressure differences required to keep the flow in contact with the body must be produced by a reduction in pressure on the body surface. As the body curves more rapidly away from the flow, a greater and greater inwardly acting pressure difference is required, i.e., a lower and lower absolute pressure on the body as shown on the pressure-distribution diagram. Note that this pressure difference is utilized to reduce the axially outward velocity that was set up during the flow around the forward part of the nose. The maximum pressure difference available is reached when the pressure on the surface falls to the vapor pressure of the liquid. This occurs at point A on the pressure-distribution diagram, Fig. 8. However, the outward radial velocity of the liquid particle under consideration has not been reduced to zero; hence when it moves downstream from point A, there is no longer enough pressure difference acting to cause the curvature of its path to match that of the body. Therefore it separates from the body, which is just a way of saying that a cavitation bubble is formed. Putting it another way, a cavitation bubble appears when there is no longer a large enough pressure gradient acting toward the body to hold the flow against it.

Attention is shifted now to the bubble itself. It will be seen that surface tension forces are acting, which from their physical nature always tend to decrease the size of the bubble. Hence as the bubble expands, work must be done against these forces if growth is to take place.

The record shows that the bubble expands very rapidly. The question arises concerning the pressure and composition of the gas inside the bubble. In this discussion it has been assumed tacitly that the bubble is full of water vapor, and, at least at inception, the pressure is the vapor pressure at the temperature of the liquid. Several other possibilities must be considered. The bubble might contain air, which was previously dissolved in the water, since the present experiments were made with water saturated with air at atmospheric pressure. As the total time from formation to collapse is very small, it would be impossible for air molecules to migrate through the liquid any appreciable distance. Therefore the only air which might come out of solution would be that dissolved in a thin layer of liquid adjoining the bubble surface. This amount is so small that the pressure in the bubble would of necessity be less than a millimeter of mercury during the most of its life. The pressure can be estimated roughly by dividing the volume of air at atmospheric pressure dissolved in the liquid layer ΔR_A thick adjacent to the bubble, by the volume of the bubble itself. If it is assumed that air-saturated water at atmospheric pressure contains 2 per cent of air by volume, the pressure in the bubble of radius R is

$$p_A = 0.06 \frac{\Delta R_A}{R}$$

Since the individual air bubbles must be very small because of the low concentration of the dissolved air, it is difficult to imagine their migrating any appreciable distance through the liquid in the 0.0022 sec available for growth to the maximum bubble diameter. If ΔR is estimated to be 0.001 in., the pressure becomes

$$p_A = 0.0004 \text{ atm} = 0.3 \text{ mm Hg}$$

Another possibility is that the bubble might contain water vapor but at a pressure much lower than the equilibrium pressure corresponding to the average temperature of the flow (0.39 psi at 72 F). However, physical measurements obtained from pressure-distribution models show that when the cavitation voids touch the body and are large enough to cover some of the piezometer openings, the pressure in these voids is approximately equal to the vapor pressure of the liquid. If this is actually the case in all cavitation bubbles, such as the one under consideration, then liquid must be evaporated during the growth period. If a portion of the surrounding liquid evaporates into the bubble, it must secure the necessary heat of vaporization to do so. The only available source of heat is in the heat of the liquid layer immediately surrounding the bubble. Because of the extremely short time available for heat transfer, the effective thickness of this layer must be very small. On the other hand, if the temperature of the surface layer of liquid falls very far, the pressure in the bubble must decrease appreciably, since it is difficult to imagine how the vapor pressure in an expanding bubble can be greater than that corresponding to the temperature of the surface layer of the liquid.

The thermal considerations just outlined suggest the desirability of some rough calculations to determine whether enough vaporization is physically possible to maintain the pressure in the bubble near the vapor pressure of the liquid. Therefore computations have been made on the following assumptions:

(*a*) The vapor pressure in the bubble is in equilibrium with the temperature of the surface layer of liquid.

(*b*) The vapor to fill the bubble is produced by the evaporation of a uniform thin layer over the surface.

(*c*) The necessary heat for this evaporation comes from the heat of the liquid of a shell of uniform thickness surrounding the bubble.

The temperature of the inside surface of this shell is assumed to be the temperature corresponding to the vapor pressure in the bubble, and the temperature of the outside of the shell is the average tunnel temperature. The thickness of the shell which must be evaporated to fill the bubble with vapor is equal to the volume of the bubble divided by the product of the bubble surface and the ratio of the specific volumes of the vapor to the liquid. The ratio of the thickness of the outer shell which furnishes the heat to evaporate this liquid to the thickness of the evaporated layer is equal to the heat of vaporization divided by the average temperature drop of this outer shell. Thus

$$\Delta R_v = \frac{\frac{4}{3}\pi R^3}{4\pi R^2 \frac{V_v}{V_L}} = \frac{R V_L}{3 V_v}$$

or

$$\frac{\Delta R_v}{R} = \frac{V_L}{3 V_v}$$

and

$$\frac{\Delta R_H}{R} = \frac{\Delta R_v}{R} \frac{H_v}{1/2(T_L - T_B)}$$

where

R = radius of bubble
R_v = thickness of evaporated shell
R_H = thickness of shell furnishing heat
V_v = specific volume of vapor
V_L = specific volume of liquid
H_v = heat of vaporization
T_L = temperature of undisturbed liquid
T_B = equilibrium temperature of liquid corresponding to pressure in bubble

For the bubble shown in Fig. 6, T_L was 72 F. If the vapor in the bubble is assumed to be 10 F below this, i.e., 62 F, $\frac{V_v}{V_L} = 70{,}000$, $H_v = 1050$. Therefore

$$\frac{\Delta R_\sigma}{R} = \frac{1}{210{,}000}$$

$$\frac{\Delta R_H}{R} = \frac{1}{210{,}000} \times \frac{1050}{5} = \frac{1}{1000}$$

When the bubble has grown to maximum size, $R_0 = 0.15$ in., hence

$$\Delta R_\sigma = 7 \times 10^{-7} \text{ in.}$$

$$\Delta R_H = 1.5 \times 10^{-4} \text{ in.}$$

These thicknesses are so small that the evaporative process appears very plausible even in face of the short time of growth and much more plausible than the evolution and migration of minute air bubbles through a layer of liquid 7 times as thick as the heating shell. Furthermore the vapor pressure corresponding to 62 F is 0.019 atmosphere, which is 47 times greater than the 0.004 atmosphere calculated for the air migration from the 0.001-in-thick shell.

A further inspection of the pressure-distribution diagram yields some additional facts. As previously stated, point *A* should be the point at which the bubble first appears. Point *B* should be the point of the maximum rate of bubble growth. Up to this point the outward radial velocity of the bubble surface should have increased. Here the acceleration should reverse, i.e., the rate of growth should slow down. Note, however, that the growth should continue until the radial kinetic energy is expended in working against the pressure difference. Thus, the point of maximum bubble diameter should be downstream from point *B*. At the point of the maximum bubble diameter, the liquid no longer has any kinetic energy with respect to the center of the bubble. However, the kinetic energy has been expended in a conservative manner, i.e., it has done work against the pressure difference and against the surface tension. The point of maximum diameter is not an equilibrium condition, the bubble starts to collapse immediately. If in Fig. 8 the bubble size is compared with the pressure-distribution diagram, it will be seen that at least qualitatively the foregoing deductions agree with the observations.

Bubble Collapse. All of the factors investigated during bubble growth must be considered during the collapse period. In examining this collapse, it might be well to state explicitly an assumption that is implicit in the previous discussion. The fluid system is thought of not as a purely mechanical one, but as a thermodynamic one as well. Two sources of energy have been considered during the bubble growth, the mechanical energy present, as a result of the motion of the fluid, and the thermal energy made available by a change in temperature of the liquid. It was assumed that none of the mechanical energy was transferred from the liquid to the gas. During the collapse period it may not be possible to avoid considering energy interchange between the liquid and the gas and vapor in the bubble. The collapse period begins at the maximum diameter of the bubble. At this point the vapor may be assumed to be in thermal equilibrium with the inner surface of the liquid which is at a lower temperature than that of the surrounding liquid. The progress of the collapse furnishes the mechanism for compressing the vapor in the bubble, thus raising its temperature above the surface of the liquid and reversing the temperature gradient, which provides a means for carrying away the heat of condensation.

It will be seen from Fig. 9 that the rate of collapse is considerably higher than the growth; consequently the rate of condensation must be similarly increased. Furthermore, as the bubble gets smaller, the thickness of the shell of surrounding liquid, whose temperature has been raised by the heat of condensation, increases appreciably. Both factors require corresponding increases in the temperature difference between the vapor and the average temperature of the liquid. This is easily available when the bubble has grown small because the necessary energy for compressing and raising the temperature of the vapor can be taken from the kinetic energy of the surrounding liquid.

Fig. 10 is a plot of the radial velocity of the bubble surface during the collapse period. It is seen that this velocity increases very rapidly as the bubble becomes small. The accuracy of the calculation is limited by the experimental measurements. The points show the consecutive frames of the photographic record. In the final collapse and initial rebound phases, the readings are too far apart even though they are separated by only $^1/_{4000}$ sec. For this reason, an attempt is being made to increase the photographic rates to at least 50,000 per sec.

In analyzing the mechanism of collapse and rebound, it is necessary to explain what happens to the kinetic energy of the liquid.

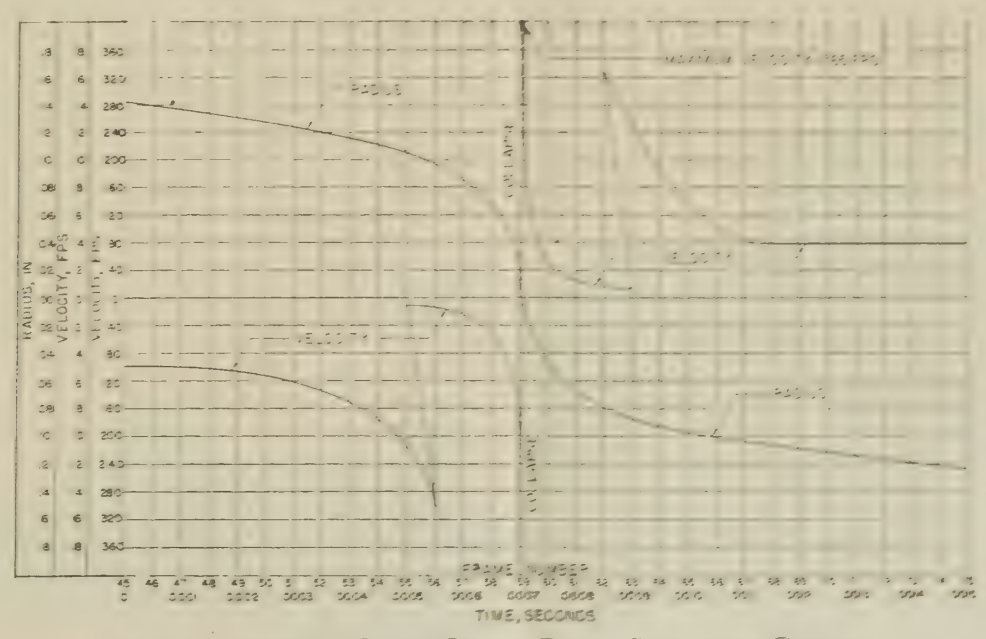

FIG. 10 VELOCITY OF BUBBLE SURFACE DURING COLLAPSE AND REBOUND

Since there is no apparent way of dissipating this energy, it must be assumed to be stored in some other form when the bubble is completely collapsed. The very fact that rebound occurs and the cavity reopens to nearly the same size as the original maximum radius is strong evidence that the kinetic energy was stored and given back essentially undiminished. Several possible methods of storing the energy suggest themselves. The most probable energy storage is in the compression of the liquid itself. Other possible ways are in the energy of compression of the noncondensable gas or the vapor in the bubble. However, as will be shown later, storage of a major part of the energy in the gas or vapor leads to impossible values of pressure and volume. The storage of the energy in the liquid is accomplished by the common "water-hammer" phenomenon. This method of energy storage permits the development of extremely high localized pressures. If particles of the liquid from opposite sides of the bubble are assumed to hit each other and come to rest, the resultant pressure may be estimated by the normal water-hammer calculations provided that the velocity of the liquid (V), at the time of impact is known. The resulting pressure is given by the simple water-hammer equation

$$P = \frac{\rho c V}{144}$$

where

P = pressure, psi
c = velocity of sound in liquid, fps

If values for c and ρ for cold water are substituted in the equation, this becomes

$$P = 65\,V$$

It must be remembered that this water-hammer equation is derived on the basic concept that the kinetic energy of a given element of moving liquid is stored within that same element in elastic compression when the element is brought to rest. This concept explains the "rebound" or re-formation of the bubble after collapse. Since there is no way to hold the liquid in a compressed condition after the inward radial velocity has been reduced to zero, the stored elastic energy goes into producing outward radial velocity. Since there has been nothing to cause appreciable energy loss, the bubble should grow to its original size at the same rate it collapsed, provided that the surrounding pressure remained constant. This cycle of growth and collapse should continue indefinitely. Actually, losses through fluid friction or possibly heat conduction, damp this oscillation. The photographic records show clearly that many bubbles go through 4 or 5 cycles before final decay. The pressure diagram shows that, except for the original formation period, the rest of the life of the bubble occurs in a relatively constant pressure field.

It is interesting to compare this measured history of an actual bubble with the analysis presented by Rayleigh in his classical paper[4] of 1917. He considered the collapse of an empty spherical bubble in an incompressible fluid having a constant pressure at infinity. He equated the kinetic energy of the resulting motion of the fluid to the work done at infinity by the constant pressure acting through a change of volume equal to the change of bubble volume. He obtained expressions for the velocity of the bubble surface as a function of the radius, for the time of collapse, for the acceleration of a point on the surface, and for the pressure distribution in the surrounding fluid. He also calculated the behavior of the bubble if it were filled with a gas at an arbitrary pressure at the beginning of collapse, on the assumption of isothermal compression. This included an expression for the ratio of initial to final volume of the bubble if all of the kinetic energy of the incompressible fluid was stored in compressing the gas. Finally, he calculated the pressure produced if an empty bubble collapsed on an absolutely rigid sphere of arbitrary radius. Here he abandoned the assumption of an incompressible fluid, but only after contact with the rigid sphere. He found the resulting pressure to be given by the water-hammer equation.

Fig. 11 shows a comparison of the Rayleigh prediction for the empty bubble with the measured radius versus time for the collapse of the bubble in Fig. 6. It is felt that the agreement is quite remarkable. In the calculation, the pressure acting is assumed to be the pressure at the tunnel wall minus the vapor pressure of the water. Rayleigh's derivation permits of such a constant bubble pressure. The curve in Fig. 12 is Rayleigh's calculated velocity of the surface as a function of the time measured from the beginning of collapse. The points shown are the slope of the measured curve in Fig. 11. The deviations of the measured from the predicted curves are in the right direction to agree with physical conditions. Rayleigh assumed no energy storage up to the instant of complete collapse, because up to that instant he assumed an incompressible fluid. Actually, there is some energy storage, especially in the last stages, in the liquid and also in the gas or vapor in the bubble. All of this energy storage reduces the work available for increasing the velocity; hence the collapse time must be longer.

In a previous section of this paper it was estimated that the amount of air available would fill the bubble to a pressure of 0.0004 atm at maximum diameter. If all of the kinetic energy of the liquid were to be stored in this air by isothermal compression, Rayleigh's calculations indicate a required compression ratio of 4×10^{26}, or a radius ratio of 7.3×10^{8}. The initial radius of the actual bubble was 0.140 in. This means the compressed air bubble would be 2×10^{-10} in. diam and would have a pressure of 1.6×10^{23} atm. Obviously, this is impossible since the energy could all be stored in the liquid at a much lower pressure. It seems most probable that the energy is stored in compression in all three fluids, i.e., liquid, vapor, and gas, and that the compression processes of the vapor and the gas lie between the adiabatic and the isothermal.

Cavitation Damage.[5] At the beginning of this discussion it was stated that the objective of this investigation is the study of the mechanism of cavitation and not of cavitation damage. However, there are a few tentative conclusions which can be formulated concerning certain phases of cavitation damage on the basis of the results obtained to date. It has been seen that the maximum collapse velocity of the cavitation bubble is controlled by (1) the maximum bubble size, and (2) the pressure difference existing between the surrounding fluid and the bubble. Factors which affect the maximum bubble size are the length of the zone in which bubble growth occurs, the average velocity of flow, and the velocity component normal to the guiding surface. The length of the zone is determined by the size and the shape of the guiding surface that is responsible for the cavitation. This alone would indicate that there should be a scale effect in cavitation damage. Consider, for example, two shapes geometrically similar but differing in size. If the velocity of flow past these two shapes is the same, the pressure and also the cavi-

[4] "On the Pressure Developed in a Liquid During the Collapse of a Spherical Cavity," by Lord Rayleigh, *Philosophical Magazine*, vol. 34, 1917, pp. 94–98 (see Appendix).

[5] No bibliography of cavitation literature is included in this paper because many exhaustive lists have already been published. One of the most recent of these will be found in the paper by A. J. Stepanoff, "Cavitation in Centrifugal Pumps," Trans. ASME, vol. 67, 1945, p. 539. Another which refers particularly to cavitation damage, but includes much work on cavitation, is contained in the book on "Werkstoffzerstörung durch Kavitation" by Nowotny, published by V.D.I. Verlag, 1942, and reprinted by J. W. Edwards, Ann Arbor, Mich., 1946.

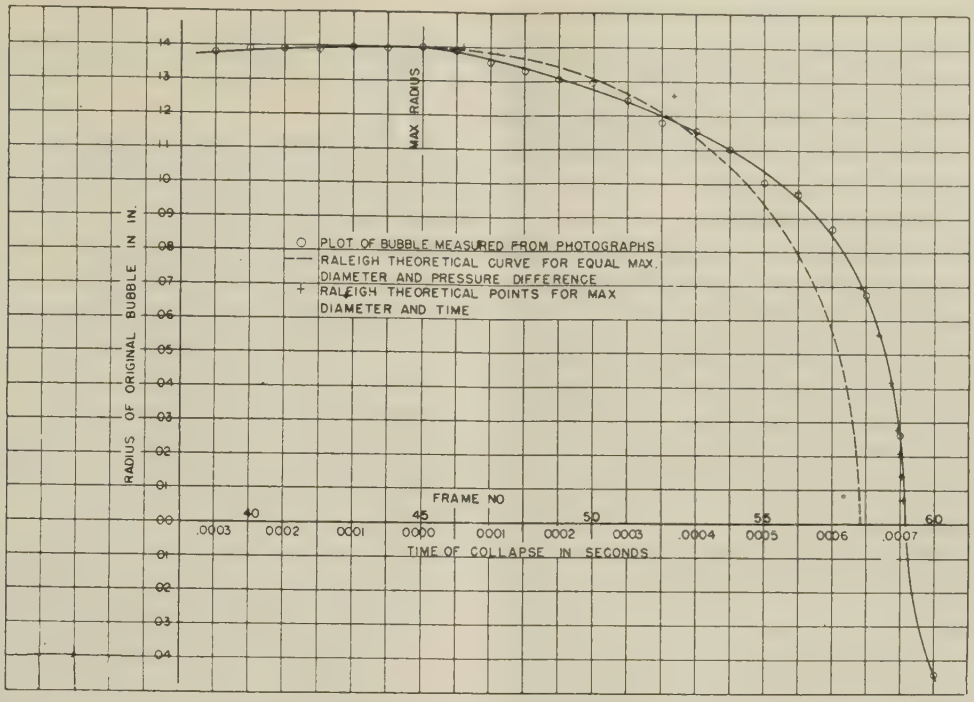

FIG. 11 COMPARISON OF MEASURED BUBBLE SIZE WITH RAYLEIGH PREDICTION

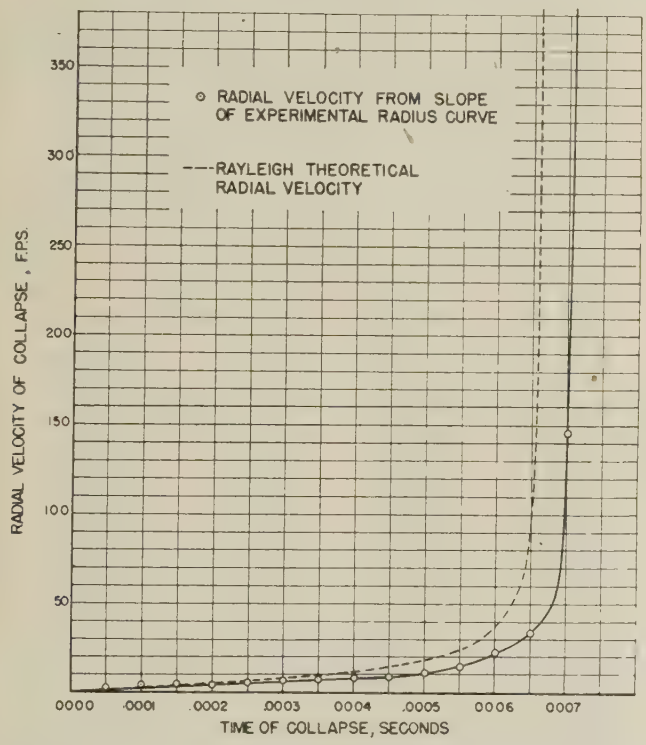

FIG. 12 COMPARISON OF MEASURED SURFACE VELOCITY DURING COLLAPSE WITH RAYLEIGH PREDICTION

tation parameter, K, at corresponding points will be identical. If one shape is twice as large as the other, the length of the formation zone will be twice as long, which means that since the velocities are the same, the bubble should grow under the same pressure difference for twice as long a time; hence it should be larger. The two bubbles will collapse under identical pressure conditions; hence the final collapsing velocity will be higher for the larger bubble. Thus cavitation damage may be expected to increase in severity with increase in size. A similar line of reasoning leads to the conclusion that if the flow velocity is increased over a given surface while the flow pressure is adjusted to keep the cavitation parameter K constant, the collapsing velocity, and hence the cavitation damage, will increase. Both of these conclusions are contrary to the concept that the cavitation parameter alone determines the severity of cavitation damage.

These two cases deal with similar geometric shapes. As a third case, consider two different shapes which, however, have the same incipient cavitation parameter. If these are operated at the same velocity but at a lower cavitation parameter identical for both shapes, the cavitation damage may be quite different. If the velocity component of the flow normal to and away from the surface of one shape is lower than that of the other, the maximum bubble size for the shape having the lower normal velocity component should be smaller and the damage less.

CONCLUSION

In conclusion, the authors wish to emphasize that the foregoing interpretation of the experimental measurements of the life history of a cavitation bubble is only a tentative presentation of the simplest possible case, i.e., a bubble which forms and collapses without interference from other bubbles. An examination of the photographic record shows that this is a relatively rare occurrence; more often clusters of bubbles form and collapse very close together. In many of the records it is obvious that the collapse of one bubble has a major effect on the collapse of its neighbor. Furthermore, as the severity of the cavitation is increased, the bubble concentration builds up very rapidly, so that rarely if ever can a single bubble be seen to form and collapse without interference. An inspection of the records indicates that the presence of many bubbles offers complicating factors. Thus the most this discussion can represent is the first short step in the correlation of this new supply of experimental facts with the analysis of

the physical mechanism of the cavitation phenomenon. It is regretted that time has not permitted the presentation of a more complete comparison of the laboratory results with the various analytical descriptions of the cavitation process which are to be found in the literature. Such comparison will be included in the next step in the development of the cavitation program of the laboratory.

Acknowledgment

This program is being carried on in the Hydrodynamics Laboratory of the California Institute of Technology as a part of a research project which is being sponsored jointly by the Research and Development Division of the Bureau of Ordnance and the Fluid Mechanics Section of the Office of Naval Research, both of the U. S. Navy. Practically every member of the laboratory staff has contributed substantially to the experiments which furnish the basis of this paper. In addition, special appreciation is due to Haskell Shapiro and his staff who are responsible for the development and operation of the high-speed flash lamps, and to Hugh S. Bell and Donald Peterson for the photography and particularly for the development and perfection of methods of making projectionable motion-picture-film strips from the original high-speed pictures.

Appendix

In 1917 Lord Rayleigh presented his classical paper[4] on the pressure development in a liquid during the collapse of a spherical cavity. Since this paper is not regularly accessible to the engineer, a brief summary of it will be presented here.

Rayleigh quotes Besant's formulation of the problem: "An infinite mass of homogeneous incompressible fluid acted upon by no forces is at rest, and a spherical portion of the fluid is suddenly annihilated; it is required to find the instantaneous alteration of pressure at any point of the mass, and the time in which the cavity will be filled up, the pressure at an infinite distance being supposed to remain constant." Rayleigh first sets up an expression for the velocity u, at any distance r, which is greater than R, the radius of the cavity wall, that has a velocity U, at time t. It is

$$u/U = R^2/r^2 \quad \ldots\ldots [1]$$

Next, the expression for the kinetic energy of the entire body of fluid at time t, is developed by integrating the kinetic energy of a concentric fluid shell of thickness dr, and density ρ. The result is

$$\frac{\rho}{2}\int_R^\infty u^2\, 4\pi r^2 dr = 2\pi\rho U^2 R^3 \quad \ldots\ldots [2]$$

The work done on the entire body of fluid as the cavity is collapsing from the initial radius, R_0 to R is a product of the pressure, P at infinity and the change in volume of the cavity, i.e.

$$\frac{4\pi P}{3}(R_0^3 - R^3) \quad \ldots\ldots [3]$$

Since the fluid is incompressible, all of the work done must appear as kinetic energy. Therefore Equation [2] can be equated to Equation [3], which gives

$$U^2 = \frac{2P}{3\rho}\left(\frac{R_0^3}{R^3} - 1\right) \quad \ldots\ldots [4]$$

An expression for the time t, required for the cavity to collapse from R_0 to R can be obtained from Equation [4] by substituting for the velocity U, of the boundary, its equivalent dR/dt, and performing the necessary integration. This gives

$$t = \sqrt{\frac{3\rho}{2P}}\int_R^{R_0} \frac{R^{3/2}dR}{(R_0^3 - R^3)^{1/2}} = R_0\sqrt{\frac{3\rho}{2P}}\int_\beta^1 \frac{\beta^{3/2}d\beta}{(1-\beta^3)^{1/2}} \quad \ldots\ldots [5]$$

The new symbol β, is R/R_0. The time τ, of complete collapse is obtained if Equation [5] is evaluated for $\beta = 0$. For this special case the integration may be performed by means of Γ functions with the result that τ becomes

$$\tau = R_0\sqrt{\frac{\rho}{6P}}\,\frac{\Gamma\left(\frac{5}{6}\right)\Gamma\left(\frac{1}{2}\right)}{\Gamma\left(\frac{4}{3}\right)} = 0.91468\, R_0\sqrt{\frac{\rho}{P}} \quad \ldots\ldots [6]$$

Rayleigh does not integrate Equation [5] for any other value of β. In the detailed study of the time history of the collapse of a cavitation bubble, it is convenient to have a solution of all values between 0 and 1. Fig. 13 and Table 1 give the value of this integral over this range.

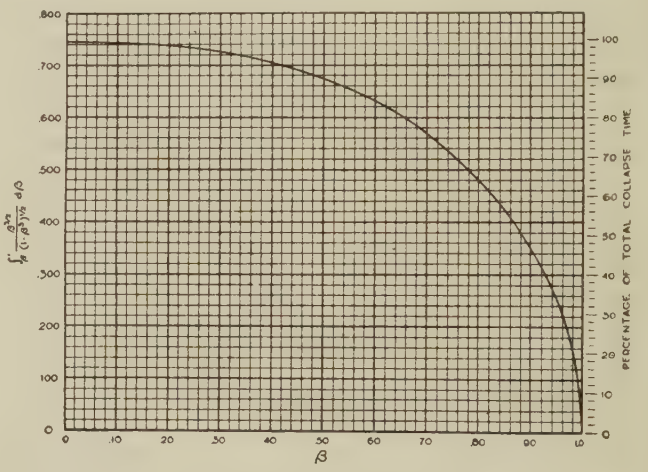

Fig. 13 Integral for Determining Time of Partial Collapse as Function of Radius Ratio

TABLE 1 VALUES OF THE INTEGRAL OF EQUATION [5]

β	$\int_\beta^1 \frac{\beta^{3/2}d\beta}{(1-\beta^3)^{1/2}}$	β	$\int_\beta^1 \frac{\beta^{3/2}d\beta}{(1-\beta^3)^{1/2}}$
0.000	0.74684	0.600	0.62915
0.040	0.74671	0.640	0.60676
0.080	0.74611	0.680	0.58133
0.120	0.74484	0.720	0.55240
0.160	0.74274	0.760	0.51935
0.200	0.73967	0.800	0.48128
0.240	0.73552	0.840	0.43684
0.280	0.73016	0.860	0.41159
0.320	0.72349	0.880	0.38380
0.360	0.71539	0.900	0.35285
0.400	0.70575	0.920	0.31782
0.440	0.69443	0.940	0.27716
0.480	0.68129	0.960	0.22785
0.520	0.66616	0.980	0.16220
0.560	0.64886	1.000	0.00000

Equation [4] shows that as R decreases to 0, the velocity U increases to infinity. In order to avoid this, Rayleigh calculates what would happen if, instead of having zero or constant pressure within the cavity, the cavity is filled with a gas which is compressed isothermally. In such a case, the external work done on the system as given by Equation [3] is equated to the sum of the kinetic energy of the liquid given by Equation [2], and the work of compression of the gas, which is $4QR_0^3 \log_e(R_0/R)$, where Q is the initial pressure of the gas. Thus Equation [4] is replaced by

$$U^2 = \frac{2P}{3\rho}\left(\frac{R_0^3}{R^3} - 1\right) - \frac{2Q}{\rho}\,\frac{R_0^3}{R^3}\log_e\frac{R_0}{R} \quad \ldots\ldots [7]$$

For any real (i.e., positive) value of Q, the cavity will not collapse completely, but U will come to 0 for a finite value of R. If Q is greater than P, the first movement of the boundary is outward. The limiting size of the cavity can be obtained by setting $U = 0$ in Equation [7], which gives

$$P\left(\frac{z-1}{z}\right) - Q \log_e z = 0 \quad \ldots\ldots [8]$$

in which z denotes the ratios of the volumes R_0^3/R^3. Equation [8] indicates that the radius oscillates between the initial value R_0 and another which is determined by the ratio P/Q from this equation. Although Rayleigh presents this example only for isothermal compression, it is obvious that any other thermodynamic process may be assumed for the case in the cavity and equations analogous to Equation [7] may be formulated.

As another interesting aspect of the bubble collapse, Rayleigh calculates the pressure field in the liquid surrounding the bubble, reverting to the empty cavity of zero pressure. He sets up the radial acceleration as the total differential of the liquid velocity u, at radius r, with respect to time, equates this to the radial pressure gradient divided by the density, and integrates to get the pressure at any point in the liquid. Hence

$$a_r = -\frac{du}{dt} = \frac{\delta u}{\delta t} - u\frac{\delta u}{\delta r} = \frac{1}{\rho}\frac{\delta p}{\delta r} \quad \ldots\ldots [9]$$

Expression for $\frac{\delta u}{\delta t}$ and $u\frac{\delta u}{\delta r}$ as functions of R and r are obtained from Equations [1] and [4], the partial differentials of Equation [1], with respect to r and t, and the partial differential of Equation [4], with respect to t. Substituting these expressions in Equation [9] yields

$$\frac{1}{P}\frac{\delta p}{\delta r} = \frac{R}{3r^2}\left[\frac{(4z-4)R^3}{r^3} - (z-4)\right] \quad \ldots\ldots [10]$$

By integration this becomes

$$\frac{1}{P}\int_P^p \delta p = \frac{R}{3}\left[(4z-4)R^3\int_\infty^r \frac{\delta r}{r^5} - (z-4)\int_\infty^r \frac{\delta r}{r^2}\right] \quad [11]$$

which gives

$$\frac{p}{P} - 1 = \frac{R}{3r}(z-4) - \frac{R^4}{3r^4}(z-1) \quad \ldots\ldots [12]$$

The pressure distribution in the liquid at the instant of release is obtained by substituting $R = R_0$ in Equation [12], which gives

$$p = P\left(1 - \frac{R_0}{r}\right) \quad \ldots\ldots [13]$$

The point of maximum pressure may be found by setting dp/dr equal to zero in Equation [10]. This gives a maximum value for p when

$$\frac{r_m^3}{R^3} = \frac{4z-4}{z-4} \quad \ldots\ldots [14]$$

If this value for r_m is substituted back into Equation [12], the maximum value of p is obtained

$$\frac{p_m}{P} = 1 + \frac{(z-4)R}{4r_m} = 1 + \frac{(z-4)^{4/3}}{4^{4/3}(z-1)^{1/3}} \quad \ldots\ldots [15]$$

If this equation is inspected it will be seen that so long as z is less than 4, the second term of the equation is negative; hence p_{max} and therefore all other pressures in the liquid are less than P at infinity; but when z exceeds 4, then p_{max} becomes greater than P. The radial location of p_{max} is given by Equation [14]. As the cavity approaches complete collapse, z becomes great and Equations [14] and [15] may be approximated by

$$r_m = 4^{1/3}R = 1.587\,R \quad \ldots\ldots [16]$$

and

$$\frac{p_m}{P} = \frac{z}{4^{4/3}} = \frac{R_0^3}{4^{4/3}R^3} \quad \ldots\ldots [17]$$

Equation [16] shows that as the cavity becomes very small, the pressure in the liquid near the boundary becomes very great in spite of the fact that the pressure at the boundary is always zero. Although Rayleigh does not mention it, this would suggest the possibility that some energy can be stored in compressing the liquid which would add an additional term to Equation [7]. Of course this would mean that the assumption of incompressibility would have to be abandoned for the entire calculation. This, however, would not change the physical concepts involved. Rayleigh himself abandons the assumption of the incompressible fluid to consider what happens if the cavity collapses on an absolutely rigid sphere of radius R, as proposed by his correspondence to Mr. Cook. However, he abandons the supposition of incompressibility only at the instant that the cavity wall comes in contact with the rigid sphere. From that instant on he makes the assumption common to all water-hammer calculations that the kinetic energy of each particle of fluid is changed to elastic energy of deformation of the same particle as determined by the volume modulus of elasticity of the fluid. On this basis he obtained

$$\frac{(P')^2}{2E} = \frac{1}{2}\rho U^2 = \frac{P}{3}\left(\frac{R_0^3}{R^3} - 1\right) = \frac{P}{3}(z-1) \quad \ldots\ldots [18]$$

where P' is the instantaneous pressure on the surface of the rigid sphere and E is the volume modulus of elasticity. Both must be expressed in the same units.

Discussion

J. M. Robertson[6] and Donald Ross.[7] This paper is an important contribution to the meager fund of knowledge of the mechanism of cavitation. The authors' development of techniques of superhigh-speed photography has made available an extremely useful tool for the study of the life of a cavitation bubble. Fig. 3 of the paper illustrates the manner in which knowledge of cavitation phenomena has increased with camera speed. The analysis of the growth and collapse of a single bubble, as presented in this paper, is in itself a major contribution to the subject. As more bubbles are analyzed and higher camera speeds are attained, more and more of the mysteries of cavitation will be dispelled.

By showing that the partial pressure of the air in the cavity is much smaller than the actual bubble pressure, the authors demonstrate that the gas in the bubble is primarily water vapor. This fact, which heretofore had only been surmised, should not be interpreted as indicating that air plays an insignificant role in the cavitation process. The cavitation studied by the authors was in water saturated with air at atmospheric pressure. In the case of the particular body studied, there was an appreciable distance preceding the cavitation region in which the pressure was below atmospheric and in which undissolved air bubbles

[6] Associate Professor of Civil Engineering; Ordnance Research Laboratory, Pennsylvania State College, State College, Pa. Jun. ASME.

[7] Assistant Professor, Ordnance Research Laboratory, Pennsylvania State College. State College, Pa.

could expand and dissolved air could come out of solution. Thus at the start of the cavitation region a number of air bubbles should have been available to act as nuclei for the formation of vapor cavities. The manner in which the bubble grows at the start of the cavitation region, as depicted in Figs. 8 and 9, would indicate that at the start of this region it may have had a radius of several thousandths of an inch.

The air content of the bubble plays an important role during the collapse period; since the air cannot be redissolved as rapidly as the water vapor, the bubble must collapse on an air nucleus. The minimum radius at the first collapse is thus primarily a function of the air content of the bubble. Osborne[8] has shown that "the abruptness and violence of the shock, the total acoustic energy produced and its frequency distribution are all highly dependent on the size of the residual air bubble around which the cavity collapses." The effectiveness of air in cushioning the cavitation shock is well known. It would be informative to know how the authors' results would be changed, if deaerated instead of saturated water were employed. The lack of air would not prevent cavitation, but its inception would be retarded. Briggs, Johnson, and Mason[9] have found that "when liquids are degassed, their natural cohesive pressure becomes effective and they will withstand a negative acoustic pressure." When air nuclei are absent, cavitation rupture is a molecular process, and the time the fluid element is in the negative pressure region is a very important factor. In tests made with model propellers at the David Taylor Model Basin,[10] and corroborated by one of the writers at the M.I.T. Propeller Tunnel, the critical pressure for the inception of cavitation was found to decrease with a reduction of air content. In an experiment in which the time in the negative pressure region was quite short, Numachi[11] found the critical pressure to be greatly affected by gas content. The critical pressure was found to be approximately vapor pressure with air-saturated water, while it was minus an atmosphere (absolute) with partially deaerated distilled water. The differences in the characteristics of the cavitation of the bodies, shown in Fig. 5 of the paper, can possibly be explained in terms of the time available for the formation of air nuclei before the fluid elements reach the cavitation region. This effect could be studied by cavitation measurements on several body shapes at different scales and with different air contents of the water.

Wilhelm Spannhake.[12] This admirable paper adds much to our present knowledge of cavitation even though the authors selected for investigation, as they state, only the simplest manifestations of the very complex phenomena they observed throughout a wide range of geometrical conditions and stages of cavitation. Specifically, they selected for study a situation which showed individual bubbles successively produced and spaced far enough apart so that from time to time some could be found which throughout their life history were not seriously affected by interference from other bubbles.

The possibility of maintaining a more or less stable stage of cavitation depends apparently upon the shape of the boundary surfaces against which cavitation occurs, or rather on the pressure distribution of the original flow pattern. This possibility will be seen from Fig. 5(*a*, *b*, and *c*) of the paper.

It is extremely interesting to notice that the same stage as in Fig. 5(*c*), showing distinctly separated bubbles, has been obtained recently at the David Taylor Model Basin in a small Venturi tube with circular cross section and a very slight longitudinal curvature in the throat, together with a small angle of divergence in the expanding passage. To a certain degree this case corresponds hydrodynamically to Fig. 5(*c*).

On the other hand, the authors mention that in other cases many complex groups of bubbles are formed in which the individual bubbles interact in either the formation or the collapse stages, as seems to be shown in Fig. 5(*a*), where the curvature of the nose of the body is sharper and consequently there are greater pressure differences along the surface.

Here there should be recalled the results obtained in 1933 and 1934 at the cavitation test stand of the Massachusetts Institute of Technology.[13]

These tests were made with a Venturi tube of rectangular cross section, and with both the longitudinal curvature in the throat and the angle of divergence in the expanding passage greater than in the circular tube mentioned as used at the Model Basin. Thus from the geometrical point of view and to a certain extent from the hydrodynamical point of view, this arrangement corresponds to the case of Fig. 5(*a*). During the tests at M.I.T., pictures were taken with a frequency of 3000 exposures per sec. No individual bubbles could be seen, but large cavitation volumes appeared separated from one another by compact volumes of water having rather definite outlines. The cavitation volumes and the intervening volumes of water were formed with a definite periodicity, and the cavitation volume collapsed as a whole when compressed between the alternate masses of water. Water completely filled the expanding passage after the collapse of the cavitation volume and was continuous with the water in the region of restored higher pressure. The writer believes that if the pictures had been taken with sufficiently higher frequency it is possible that individual bubbles and groups of bubbles would have been seen also in this case, and that the bubble groups would in turn be interacting and forming the large cavitation volumes.

The frequency of formation f, and collapse of the cavitation volumes turned out to be in direct proportion to the velocity v, in the Venturi throat and inversely in proportion to the distance l, over which the complete cavitation phenomenon extended. The dimensionless expression

$$\frac{f \cdot l}{v} = C$$

was the same for geometrically similar arrangements and for hydrodynamically similar stages of cavitation.

Considering the different cases described, the writer believes that cavitation is always periodical, and that the periodicity is always determined merely by the hydrodynamical boundary conditions of the original flow pattern. The formation of bubbles changes the boundary conditions and makes the flow unsteady. It likewise changes the pattern in such a way that there is a rise in pressure at the point where cavitation has started, and in this way the formation and further development of the cavity is stopped until the orig nal conditions are restored and the cycle begins again.

It is the writer's understanding that Dr. Knapp and his asso-

[8] "The Shock Produced by a Collapsing Cavity in Water," by M. F. M. Osborne, Trans. ASME, vol. 69, 1947, pp. 253–266.

[9] "Properties of Liquids at High Sound Pressures," by H. Briggs, J. B. Johnson, and W. P. Mason, *Journal of the Acoustical Society of America*, vol. 19, 1947, pp. 664–677.

[10] "Design, Operation, and Maintenance of a Meter for Recording the Air Content of Water in the David Taylor Model Basin Water Tunnels," by A. Borden, David Taylor Model Basin Report 549, December, 1946.

[11] "Translation and Commentary on F. Numachi's Articles on 'The Effect of Air Content on the Appearance of Cavitation in Distilled Salt, and Sea Water,'" Ordnance Research Laboratory Report, Serial No. NOrd 7958–27, August 1, 1946.

[12] Technische Hochschule Karlsruhe, Baden, American Zone. Contractee U. S. Navy.

[13] "Progress Report on M.I.T. Cavitation Research," by J. C. Hunsaker, Transactions of the 4th International Congress of Applied Mechanics, Cambridge, England, June, 1934.

ciates have under way a systematic investigation of the different stages of cavitation to clear up details of this most interesting hydrodynamic problem.

As to the rebound of the bubbles which has been observed for the first time in these California tests, the writer is not sure that this would have occurred had the air content in the water been distinctly smaller. This phenomenon reminds one in a way of the periodical expansion and compression of large gas bubbles formed by underwater explosions.

With respect to the damage done by cavitation, the writer believes that this problem cannot be regarded without considering the fact that even the smoothest surface of any material is not without slight crevices. These flaws present the weak points under the impact of water following the collapse of the bubbles. There is not only the force of the blow striking into the crevices but in addition the concentration of stresses at the sharp corners, and so on. On the other hand, it will be of the greatest importance to find out whether the individual bubbles or the large cavitation volumes do the more severe damage to the boundary walls.

It seems fitting at this time to recall the memory and do honor to the name of the late Dr. Foettinger who was one of the first to envisage the nature of cavitation damage.

Dr. Knapp and his staff are to be congratulated for the outstanding work reported in this paper. All concerned with cavitation will look forward to further results with the greatest interest.

A. J. Stepanoff.[14] Although considerable progress has been made in the last two decades in understanding cavitation in hydraulic machinery, the price to avoid or alleviate cavitation is still high. Part of this cost is due to the factor of ignorance. Any further progress in cavitation study without a knowledge of the mechanism of cavitation is well-nigh impossible.

Although the authors' study was confined to the life history of a bubble, its results are important from the practical point of view. It gives size and time scale of proceedings, which permits estimation of the thermodynamic process during the birth and collapse of the bubble. This in turn may lead to an estimation of how any liquid other than water will behave under cavitation conditions. The bubble reappearance as a result of an elastic water impact, never suspected before, may serve as an explanation of the appearance of cavitation pitting in places not expected.

Lack of exact cavitation knowledge has resulted in a variety of opinions as to the importance of several factors on conditions leading to cavitation in pumps and turbines. Thus some pump engineers evaluate their cavitation data in terms of absolute velocity through the impeller eye, others use relative velocity, and some use the peripheral velocity. Still another group uses the square root of the product of the radial and peripheral velocities. Similarly, the effect of the impeller entrance angle on cavitation is frequently misunderstood.

In describing the process of appearance and collapse of the bubble, the authors emphasize the hydrodynamic conditions leading to the formation of a cavity. The writer can imagine formation and disappearance of vapor bubbles by thermodynamic means only without pressure or velocity gradients in the surrounding liquid. If the ambient temperature is brought locally to the corresponding boiling pressure, vapor bubbles will appear. This is a regular boiling process in which no external mechanical forces are required to form a bubble, heat doing the work of volume expansion. During the collapsing period, temperature-pressure equilibrium is destroyed, vapor is condensed, and the liquid rushes into an empty space. The same is true also during the rebounding process although the elastic forces of the liquid play a more conspicuous role. Perhaps the difference is just a matter of point of view. The writer prefers to think in terms of thermodynamics of the process first because he believes that heat exchange limits the extent of cavitation. When dealing with liquids other than water, the main difference will appear in thermodynamic properties of the liquid and not in hydrodynamic forces.

The effect of degree of streamlining of the body nose on cavitation, as it appears in Fig. 5 of the paper, is interesting. This is contrary to a general belief that a blunt leading edge of impeller vanes is just as good as the hatchet-shaped one. Such a misconception originated from airfoil tests on air.

Under conditions of the authors' tests, it is reasonable to assume that all the kinetic energy of the bubble collapse is stored in the surrounding liquid and reappears as kinetic energy again during rebirth of the bubble. In hydraulic machinery, the minimum pressure appears at the boundary of the body, and, during collapse, a major portion of the energy may be absorbed by the body, resulting in noise and vibration. Large masses, sometimes including the supporting structure, may take part in dissipation of this energy. Thus rebounding of the bubbles may appear greatly subdued. In connection with hydraulic machinery, opinions have been expressed that, if cavitation bubbles appear and collapse in a body of water and do not contact the metal, there is no damage to the parts of the machine.[15]

The writer believes that the possibility of air in the vapor cavity is not to be excluded. This can happen not by air bubbles breaking through into the vapor space, for this they will have no energy, but by the liquid vaporizing into the air-bubble space when this reaches the low-pressure zone. Air liberation from water is quite common in hydraulic machinery when pressure drops below that of the atmosphere.

The difference in bubble grouping in the authors' tests due to a difference in elevation of 2 in. suggests that this difference alone (in the case of hydraulic machinery) may put a rotor out of balance and cause vibration. It is very unlikely that the force of buoyancy of the bubbles could have been responsible to any appreciable degree for the bubbles shifting upward due to lack of time.

In their conclusions regarding the effect of scale on cavitation in hydraulic machines of different sizes, the authors disregard the effect of Reynolds number. In larger machines, all turns will have larger radii of curvature and can be negotiated by the liquid with less velocity distortion than in a small machine. With the same linear velocities of flow, centrifugal forces, causing velocity shifting, are inversely proportional to the radius of curvature. Opinions have been expressed by several authorities on water turbines that, under the same head and submergence, the effects of cavitation are less harmful in the prototype than in the model.[16]

There is a great deal of confusion and misconception about the flow pattern in a turn or elbow. A study of cavitation under such conditions with the aid of high-speed photography would make an excellent topic for investigation. Most of the channels in hydraulic machinery where cavitation occurs are curved. There are no clear ideas as to what actually takes place under such conditions. What portion of the total flow is actually vaporized is of interest. Also, whether compound liquids, like petroleum oils, would behave similarly to water under cavitation conditions.

Research of this nature is beyond the testing facilities of the industry, and the authors and sponsors of this project deserve

[14] Development Engineer, Ingersoll-Rand Company, Phillipsburg, N. J. Mem. ASME.

[15] "Centrifugal and Axial Flow Pumps," by A. J. Stepanoff, John Wiley and Sons, New York, N. Y., 1948, p. 248.

[16] Ibid., p. 265.

credit for their undertaking and manner in which it was conducted. It is hoped that the authors will take full advantage of their equipment and recent progress in high-speed photography (5,000,000 pictures per sec) as recently reported.[17]

Authors' Closure

Before considering the specific points raised by the individual discussers, the authors wish to point out that as more and more information becomes available on the characteristics of cavitation, it is becoming more and more apparent that it is no longer possible to talk about cavitation as a single phenomenon; instead there are certainly a number of different types of cavitation which vary quite significantly in their characteristics. The existence of these various types of cavitation probably accounts for many of the discrepancies which occur in our empirical knowledge of the phenomenon, which in turn have inspired widely different interpretations of the basic mechanism. As was pointed out in the introduction, the paper presented only the first experimental observations of a single bubble, which was selected as the simplest possible case of one particular type of cavitation. In this type, the cavity forms and collapses while moving downstream with the local velocity of the rapidly moving fluid. It is probable that many of the points brought out by the discussion apply with much more force to other types of cavitation, but since the authors have experimental knowledge concerning this case and not the others, their comments will be limited to the type presented.

Messrs. Robertson and Ross bring out clearly in their interesting discussion the empirical fact that air is known to have a definite effect on the collapse of certain types of cavitation. They then suggest that it is very probable that the cavitation bubbles discussed by the authors had for a nucleus an air bubble of appreciable size and that this air did effectively cushion the collapse of the bubble. They suggest specifically that at the beginning of cavitation when vaporization first starts the air-bubble nuclei have a radius of several thousandths of an inch. The authors feel that air bubbles of this size could not be present without having been observed because the lighting used is very intense and a bubble of this diameter would be highly reflecting, as is evidenced by the small cavitation bubbles further downstream which are so easily seen both visually and on the photographs. However, it is interesting to investigate the order of magnitude of the effect which might have been produced if such an air nucleus had served as a starting point for the bubble whose life history was presented. Assume that the bubble radius was .005 of an inch, which is the upper imaginable size that could have escaped detection in the tunnel. Assume also that the pressure within the bubble was in equilibrium with the local pressure in the flowing stream. Thus at the beginning of the cavitation zone the air will have a pressure of about $^1/_3$ psia. Assume for convenience that this is one psi. This air will remain in the bubble during expansion and collapse; thus when the bubble has collapsed to the radius of .005 in., the air will be again in the same state, assuming that during expansion and collapse to this point the process has been reversible. Up to this point all work terms on the air are negligible. The work required to compress this bubble further may be calculated easily. Rayleigh assumed an isothermal process. The authors have indicated a possible pressure due to water hammer of approximately 50,000 psi, assuming an empty bubble. The isothermal work of compressing the air to the same pressure is given by the equation

$$W = p_1 V_1 \log_e \frac{V_1}{V_2}$$

in which $p_1 = 1$ psi

$$V_1 \cong \frac{d^3}{2} \text{ and } \frac{V_1}{V_2} = \frac{p_1}{p_2} = 50{,}000$$

The solution gives

$$W = 5 \times 10^{-6} \text{ inch-pounds}$$

Now the kinetic energy of the water which must be stored at collapse in compressing the air and the water is given by the simple product of the volume of the bubble at its maximum diameter multiplied by the pressure of the liquid in the collapse zone. By measurement the pressure is about 10 psia, the diameter is .30 in. Thus the kinetic energy to be stored is .135 in-lb. Therefore, it must be concluded that the effect of this amount of air on the collapse pressure is negligible since the best it could do would be to reduce the water-hammer pressure by less than .004 per cent. If the compression were assumed to be adiabatic rather than isothermal, the energy stored could be increased by a factor of, say, about 400, but this would still be negligible and on the other hand would produce tremendously high temperatures which would be brilliantly luminous, an effect completely contrary to the observations. It might also be noted that the amount of air in this bubble nucleus is quite small as compared to the amount that the authors calculated might be possible within the bubble due to coming out of solution in the shell immediately adjacent to the bubble. Thus assuming again isothermal expansion from the nucleus to the maximum diameter of the bubble, the partial pressure of the air at maximum diameter would be 2.5×10^{-6} atmospheres as compared to the 4×10^{-4} calculated in the original paper. Even the latter amount has of course a negligible effect upon the collapse pressure. Messrs. Robertson and Ross state that "it would be informative to know how the authors' results would be changed if deaerated instead of saturated water were employed." The authors are in hearty agreement with this desire and wish to call attention to the fact that as will be found in the description of the new installation of the water tunnel in the companion paper[3] provision has been made for the control of air content so that just this sort of study can and will be made. However, it is the present impression of the authors that one of the most important factors is the number of air nuclei present rather than the amount of air truly dissolved in the water. By air nuclei are meant minute undissolved bubbles which are probably associated with particles of solid matter found in the water. The number of nuclei may or may not be directly proportional to the amount of total air per unit volume of water. It would appear, at least in the type of cavitation under discussion, that the presence of an air nucleus is necessary to permit the cavitation bubble to start to form, but that after formation has commenced, the role of the air is insignificant.

The authors are indebted to Dr. Spannhake for a very interesting review of some of the significant features of his classical cavitation experiments. They deplore with him that the profession can no longer have the benefit of the discussion of Dr. Foettinger, the "old master" in the field. It is indeed interesting that a definite frequency was observed by Dr. Spannhake in fully-developed cavitation in special Venturi throats. However, it would seem to the authors that this is due at least partially to the interaction between the cavitation and the flow itself, since the development of the cavitation voids effectively changes the cross section of the conduit. On the other hand, as Prof. Hunsaker pointed out in his report[18] on this same research, "The

[17] "High-Speed Camera," *Mechanical Engineering*, vol. 69, December, 1947, pp. 1045–1046.

[18] "Progress Report on Cavitation Research at M.I.T." J. C. Hunsaker. Trans. ASME, vol. 57, October 1935, p. 423.

relation $\frac{fL}{V}$ can only be determined when cavitation is well developed and L is of substantial magnitude." On the other hand, as he states further in the same paper, "When cavitation is not well developed and L is but one or two throat diameters, the frequency observed is highly irregular....."

An examination of the records of the authors shows little evidence of a predominant frequency; in fact, the evidence is quite to the contrary. Not only does the period between the appearance of individual bubbles seem to be variable, but the life cycle of each bubble consists not of one formation and collapse but a series of them, each of which requires a different length of time. All of this indicates a wide band of frequencies. It should be pointed out that in the authors' experiments the cross section of the cavitation zone is small as compared with that of the tunnel. Thus, little or no interaction between the cavitation and the over-all flow is to be anticipated. Hence there seems to be little reason to expect correspondence between these experiments and those of M.I.T. Dr. Spannhake expresses some doubt as to whether or not the rebound of the bubbles observed by the authors is due to the air content of the water, and suggests the possibility that had the air content been distinctly smaller, the rebound might not have occurred. It is the belief of the authors that the rebound is a necessary concomitant of the energy storage at collapse and that it would continue to occur under all conditions in which it was possible to get the original cavitation bubble to form. To expand this statement further, it might be conceived that a liquid, containing no foreign nuclei or no undissolved or dissolved gas of any kind, might reach a state in which it would support a considerable tension. If this were the case, the formation of any cavitation bubbles could be inhibited at much higher velocity than under normal conditions. However, the forces causing the first void are of much smaller intensity than those available in the rebound of the highly compressed liquid following the collapse. Thus if the cavitation void can appear at all, there is good reason to believe that rebound will occur.

With reference to Dr. Spannhake's comments on cavitation damage, the authors wish again to emphasize that their remarks on cavitation damage were in no respect a discussion of the mechanism of the damage itself, but merely some tentative predictions as to the relative behavior of cavitation in producing damage as hydrodynamic conditions are varied. The basic idea underlying the authors' comments was to raise the question of the validity of the general concept of the similarity law with regard to cavitation damage, in which σ is usually considered as the only parameter of the hydrodynamic picture.

In reference to Dr. Stepanoff's discussion, the studies in the water tunnel demonstrated beyond any question that two of the most important variables in the production of cavitation are the shape of the body (guiding surface), and its alignment with respect to the flow. Without the knowledge and exact control of these variables it is impossible to classify cavitation in any significant and systematic form. Since this information is lacking in practically all cavitation tests of hydraulic machinery, the authors are forced to believe that the analyses of cavitation data based on any of various velocity parameters mentioned by Dr. Stepanoff as being in current use by the industry can only result at best in the determination of rules for the average design, which miss the optimum, usually by a large margin.

The authors agree that cavitation and boiling are closely related; however, they would hesitate to carry the relationship as far as Dr. Stepanoff suggests. As previously pointed out, unless the liquid can support very substantial tension, cavitation will occur with or without the benefit of heat transfer or vaporization. Fluid vaporizes into the cavity because the cavity is there; the vapor does not force the fluid away to form a cavity. The cavitation cavity is to the cavitation phenomenon as the hole is to the doughnut: It gives it its characteristic form, but not its substance.

The authors do not understand the comments regarding the effect of scale on cavitation in hydraulic machines of different sizes. If two similar passages of different size contain fluid flowing at the same absolute velocity, the pressure distribution and the flow lines will be identical if the units of length correspond to the scale of the two passages. This is one of the fundamental principles of similarity. The conditions initiating cavitation will be exactly the same for both channels.

Dr. Stepanoff calls attention to the lack of knowledge concerning the flow in curve channels even in such simple cases as stationary bends or elbows. This problem is treated in a most interesting manner in the first chapter of his new book, which includes a well-selected set of references. The authors agree that a study of this type of flow under cavitating conditions would be very valuable and are reasonably sure that the high-speed photographic technique could be adapted to this purpose.

In conclusion the authors wish to thank again the helpful discussers and to express their appreciation to many others in the field who came to them with oral and written comments and valuable suggestions.

The Hydrodynamics Laboratory of the California Institute of Technology

By R. T. KNAPP,[1] JOSEPH LEVY,[2] J. P. O'NEILL,[3] AND F. B. BROWN[4]

This paper presents a description of the Hydrodynamics Laboratory and its principal pieces of equipment that have been developed during the last five years. The field of investigations to be undertaken by the Laboratory is presented in general terms.

THE Hydrodynamics Laboratory is an outgrowth of the Hydraulic Machinery Laboratory of the California Institute of Technology.[5] In the fall of 1941 the Institute was requested to undertake the development and construction of a water tunnel for use in measuring the hydrodynamic forces on projectiles and other underwater bodies. This development was undertaken and the tunnel was put into operation early in the spring of 1942. Such rapid progress was made possible by the use of a large proportion of the apparatus and instruments already available in the existing Hydraulic Machinery Laboratory.

The tunnel has been in continuous operation ever since its completion. In the winter of 1943 it became evident that the equipment and the office and staff facilities were not sufficient for the problems at hand.

Therefore the design and construction of a new building and two additional pieces of major equipment were authorized. Construction of the building was commenced in July, 1944, and it was occupied in the spring of 1945. Design of the two major pieces of equipment, the controlled-atmosphere launching tank and the free-surface water tunnel was started simultaneously with that of the building.

During the war period the laboratory was operated under contract with the Office of Scientific Research and Development for Section 6.1 of the National Defense Research Committee. At the close of the emergency period, the sponsorship of the laboratory was taken over from the OSRD by the Research and Development Division of the Bureau of Ordnance of the U. S. Navy. This sponsorship has been continued and the Fluid Mechanics Branch of the Office of Naval Research has joined with it in the support of the more basic aspects of the current program. In addition to the program carried out under this sponsorship, the Laboratory and its equipment is also utilized for graduate instruction and research within the limitations of its capacity.

Field of Investigations. The primary objective of the Laboratory is to study the characteristics of bodies moving in a fluid. The major emphasis has been placed upon the motion of bodies in a liquid and in the motion from a gas to a liquid or vice versa. Some of the problems that have been and are being investigated within this field are as follows:

(*a*) The force systems acting on a moving submerged body, both in the steady and transient states. This includes the investigation of damping forces.

(*b*) The mechanism of cavitation from conditions of incipient cavitation to the fully developed state in which the cavitation bubble may envelop the entire body.

(*c*) The effect of shape on the production of cavitation and the development of cavitation-resistant shapes.

(*d*) The forces acting upon bodies passing through the interface between the gas and the liquid.

(*e*) Nonsymmetrical forces acting upon submerged bodies traveling close to the free surface.

Many of these studies have the possibility of wide nonmilitary application. For example, the results of the cavitation studies are applicable to ship hulls, propellers, hydraulic turbines, pumps, and flow in closed conduits.

This list in no sense exhausts the scope of the investigations which may be carried on in the laboratory. The equipment is rather unconventional in function and design and can be adapted to the study of many basic problems of interest to the engineering profession.

Building. At the close of the emergency period, plans were initiated to move the water tunnel out of the Hydraulic Machinery Laboratory and into the space provided for it in the new laboratory building. This move has now been completed, thus restoring the Hydraulic Machinery Laboratory to its original capacity for research in its field. The Hydraulic Machinery Laboratory is housed in the west end of the Guggenheim Aeronautics Laboratory. The Hydrodynamics Laboratory forms a south wing directly adjoining it. The new building consists of a sub-basement, basement, and first floor, with direct connection to the corresponding levels in the Hydraulic Machinery Laboratory. Fig. 1 shows the building with the Guggenheim Aeronautics Laboratory in the background. Fig. 2 is a plan of the basement level which shows the distribution of the experimental facilities. The three major pieces of equipment extend to the sub-basement level where, in addition, a well-equipped model and instrument shop is located. The ground floor is used for offices and design. The total available floor space is about 15,000 sq ft.

Laboratory Equipment and Field of Use. At present the Laboratory contains five pieces of research equipment. The three major ones are the high-speed water tunnel, the free-surface water tunnel, and the controlled-atmosphere launching tank. In addition, there is in operation a polarized-light flume and a ripple tank. The high-speed water tunnel is very much like a small wind tunnel except that water is used for the circulating fluid. It is equipped to study the hydrodynamic forces acting on bodies moving in a fluid, or on construction elements of moving bodies and hydraulic machines; for example, control surfaces, guide vanes, propeller blades, etc. The high velocity obtainable in the tunnel (upward to 100 fps), together with the fact that the pressure is controllable independent of the velocity, and that the amount of dissolved air can be controlled, make it particularly suitable for fundamental studies in cavitation.

[1] Director, Hydrodynamics Laboratory, California Institute of Technology, Pasadena, Calif. Mem. ASME.

[2] Principal Research Engineer, Hydrodynamics Laboratory, California Institute of Technology.

[3] Research Engineer, Hydrodynamics Laboratory, California Institute of Technology.

[4] Research Engineer, Hydrodynamics Laboratory, California Institute of Technology. Jun. ASME.

[5] "The Hydraulic Machinery Laboratory at the California Institute of Technology," by R. T. Knapp, Trans. ASME, vol. 58, 1936, pp. 663–676.

Contributed by the Hydraulic Division and presented at the Annual Meeting, Atlantic City, N. J., December 1–5, 1947, of THE AMERICAN SOCIETY OF MECHANICAL ENGINEERS.

 Paper No. 47—A-112.

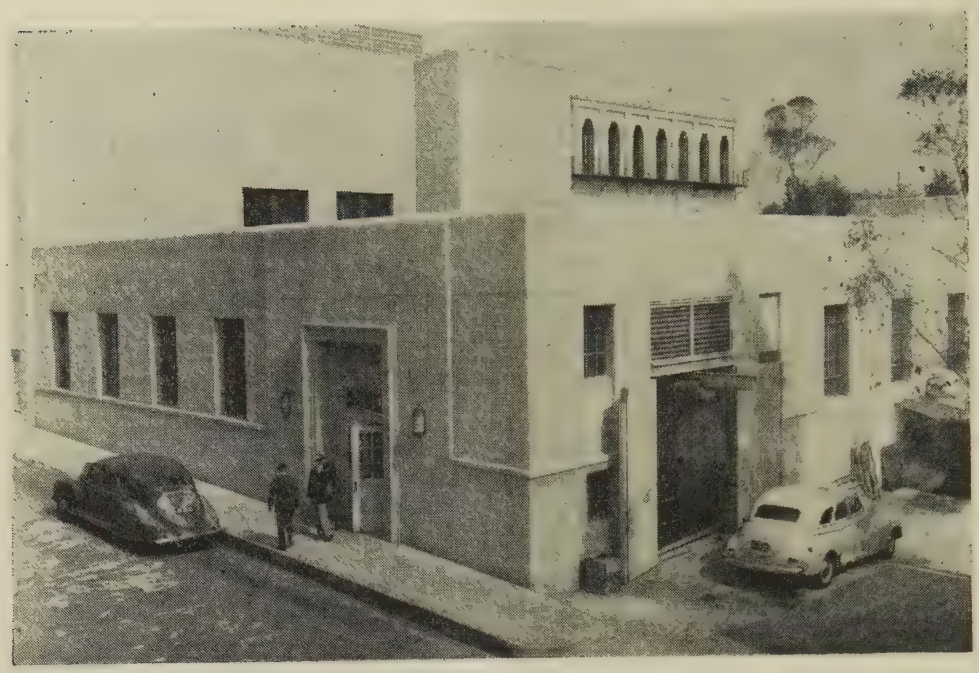

FIG. 1 HYDRODYNAMICS LABORATORY

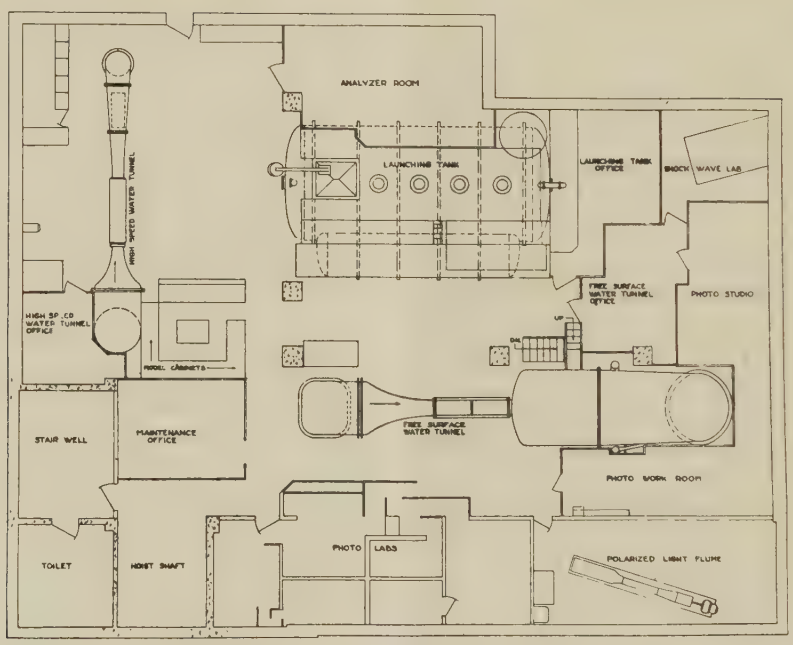

FIG. 2 BASEMENT PLAN OF HYDRODYNAMICS LABORATORY

The free-surface water tunnel is similar in many respects to the high-speed water tunnel. It operates at considerably lower velocity but has a much larger working section. Its distinguishing feature is indicated by its name, that is, the upper boundary of the stream in the working section is an air-water interface. The air pressure is controllable, thus making this apparatus particularly useful for model studies of bodies operating submerged, but very close to the surface. A rather elaborate air-separation system incorporated in the circuit makes it feasible to carry on studies involving the injection of large amounts of gas into the working section.

The controlled-atmosphere launching tank is a large, closed pressure vessel designed primarily for the study of the hydrodynamic problems involved in the transition period when a free-flying body, initially traveling through air, strikes the surface of a body of water and enters it. The design specifications were all based upon this objective, but the equipment, as built, may be employed in the investigation of other types of problems which require similar facilities. One of these auxiliary uses is the study of underwater explosions, including the effect of the interface on explosions occurring near the surface.

The polarized-light flume is a small low-velocity closed-circuit water channel having a rectangular glass-walled working section. It employs a dilute suspension of bentonite as a working fluid.

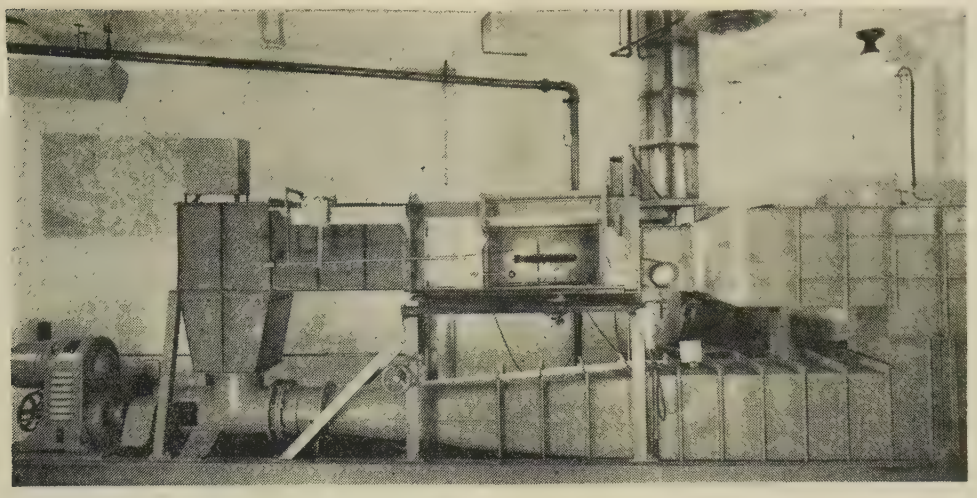

FIG. 3 POLARIZED-LIGHT FLUME

This material has the property of streaming double refraction. This makes it possible to study the flow pattern around any body placed in the working section, since, when the section is illuminated with polarized light, the shear pattern and, by inference, the flow pattern in the fluid becomes visible to the eye. Fig. 3 is a view of the flume, and Fig. 4 shows flow at low velocity around a typical body in the working section.

The ripple tank is a small shallow glass-bottom tank for the study of wave problems. This has proved useful not only in the investigation of surface-wave patterns on enclosed bodies of water, but also, through the good analogy between shallow-water surface waves and pressure waves in compressible fluids, for the investigation of shock waves and other supersonic phenomena in gases. Fig. 5 is a schematic sketch of the ripple tank, and Fig. 6 is a typical record of a Mach-type wave intersection.

The following sections will discuss in more detail the operating

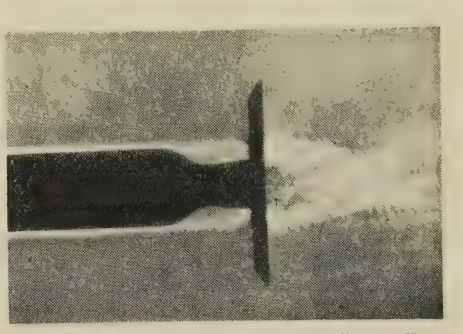

FIG. 4 FLOW PATTERN IN POLARIZED-LIGHT FLUME

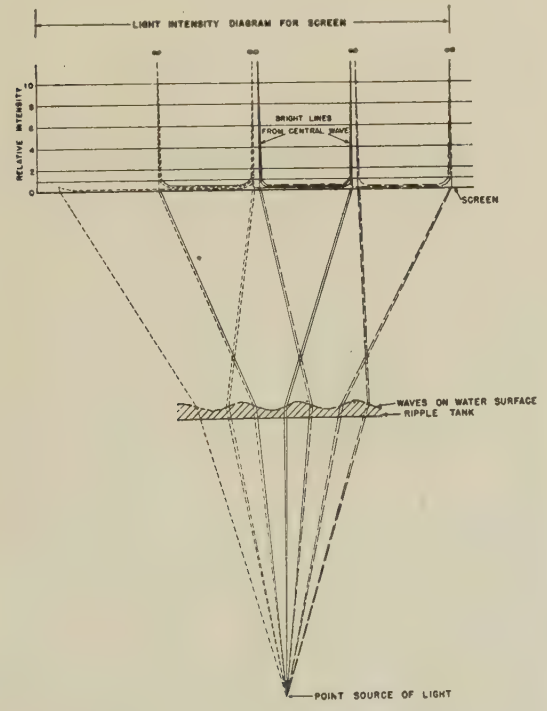

FIG. 5 SCHEMATIC ARRANGEMENT OF RIPPLE TANK

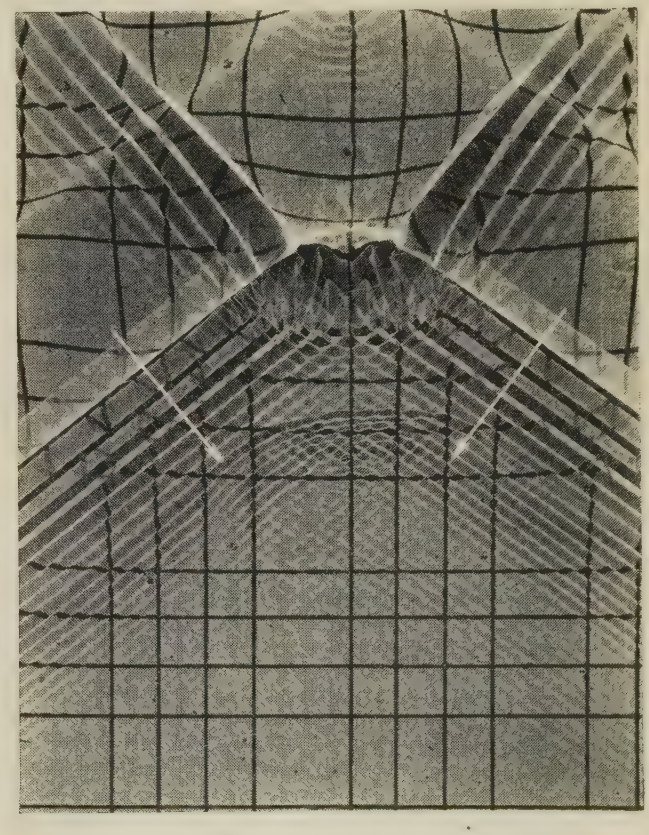

FIG. 6 MACH-TYPE WAVE INTERSECTION

characteristics and construction of the three major pieces of equipment.

High-Speed Water Tunnel

Specifications. The high-speed water tunnel was designed and constructed to permit the determination of the hydrodynamic forces on moving bodies. The design of the apparatus is based on the principle that the forces and flow pattern are determined by the relative flow and are the same whether the fluid is stationary and the object is moving, or vice versa. Therefore, as in wind tunnels, the flow pattern peculiar to the prototype moving through a stationary fluid is simulated by the flow pattern about a stationary model immersed in a moving fluid. The essential components of the tunnel are as follows:

(*a*) A working section in which the model may be mounted and observed.

(*b*) A circulating system, consisting basically of a pump and piping, by which the flow of water may be maintained through the working section.

(*c*) An absorption system, which resorbs any entrained air bubbles.

(*d*) An air-content control system which maintains at a constant value any desired amount of dissolved air in the flowing water.

(*e*) A control system by which the pressure, velocity, and temperature in the working section can be regulated and kept constant at any desired set of values.

(*f*) A balance by means of which the model may be put in different positions and the hydrodynamic forces acting upon it may be measured.

The tunnel design is determined by the size and operating characteristics of the working section. For this tunnel a 14-in-diam working section was chosen with a usable length of 6 ft. The design specifications also call for operation at any desired velocity up to 100 fps, and any pressure from 100 psi to vapor pressure.

A closed type of working section was selected because such a design reduces the energy loss, gives stable flow, results in a definite and calculable boundary correction to the measurements, and makes it possible to control pressure, velocity, and air content easily.

The tunnel has a carefully designed 340-ft path of travel for the water. Such a design avoids external disturbances, obtains a uniform flow in the working section, and permits a minimum power consumption. The effectiveness ratio, that is, the energy of the water in the working section compared with power input, is about $4^3/_4$ to 1.

The tunnel was designed to give as high a velocity in the working section as possible, considering the power available. High velocity is desirable in order to obtain a Reynolds number for the model which will approach that of the prototype. It also permits cavitation studies at speeds comparable to those associated with the prototype and in a velocity range where dissolved air is less likely to come out of solution.

The ability to control the amount of air in solution is of great help in the study of flow phenomena, particularly that of cavitation. In the high-speed water tunnel, a given air content can be kept constant because the water is not allowed to come in contact with the atmosphere. Air bubbles released as a result of cavitation can be a serious hindrance because the entrained air running through the complete tunnel circuit will change the cavitation conditions, the velocity, and will obscure the model in the working section in a very short time. For this reason, the tunnel has a "resorption" system which resorbs any air released before it has made a complete cycle.

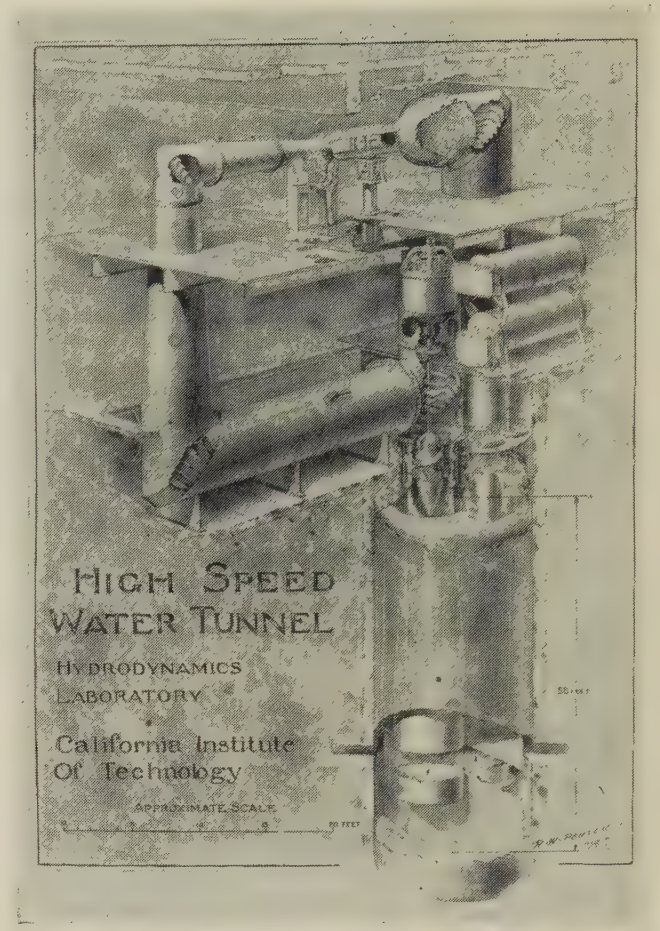

Fig. 7 High-Speed Water Tunnel

The closed system makes possible a simple pressure control. This pressure control which is independent of the velocity in the working section is necessary in the general study of cavitation, not only to simulate submergence of the prototype, but also to determine the cavitation parameter under all conditions.

Inasmuch as the energy from the 350-hp main circulating pump is dissipated in the tunnel as heat and thereby would cause an undesirable temperature rise, a refrigeration-and-temperature control system has been made a part of the tunnel system. Refrigeration was chosen instead of a cooling tower because of the necessity for controlling the air content.

The choice of the type of balance is one of the most difficult problems in connection with the tunnel. The forces on the body under study must be measured, but any connection to the body to provide means of measuring these forces changes the forces themselves and thus a correction must be made. An analysis of the measurements desired shows that the balance system can be relatively simple, since the bodies to be studied have axial symmetry. A three-component single-spindle-type balance therefore is capable of furnishing all the necessary information since the possible forces acting on the body can be reduced to a drag force in the direction of the flow, a cross or lift force, and a moment about an axis normal to the direction of flow.

Description of Main Circuit:

(*a*) *Flow Circuit.* The flow circuit can be traced in Fig. 8 from the circulating pump which discharges vertically through the downcomer to the bottom of the resorber. Here the water reverses and flows upward, passes over the top of the partition

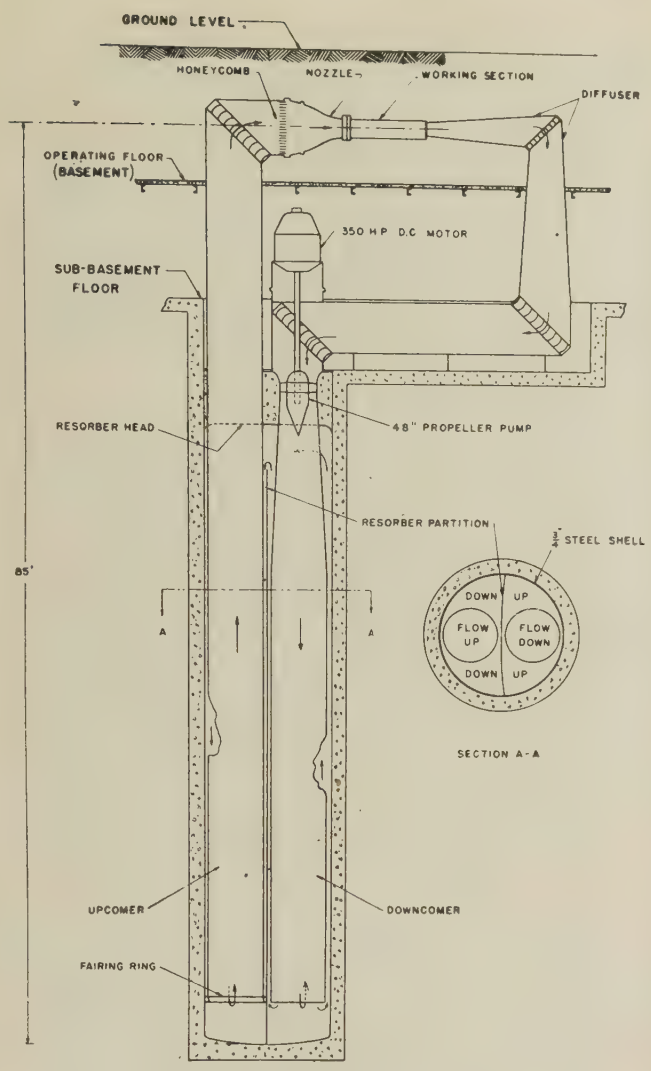

FIG. 8 MAIN TUNNEL CIRCUIT

and down to the bottom of the resorber again. The flow then rises through the upcomer to the vaned elbow where, at the working-section level, it is turned horizontally to the right. From there the water passes through a honeycomb, which, combined with the carefully designed elbow, insures a good entrance flow to the nozzle. The flow through the nozzle, with a reduction in area of about 18 to 1, results in a uniform velocity distribution in the working section with a very thin boundary layer. From the nozzle, the flow passes through the 14-in-diam working section and enters the horizontal diffuser which reduces its velocity to about $^3/_{10}$ of that in the working section. The flow then enters the diffuser elbow and passes downward through the third diffuser which completes the deceleration before it reaches the inlet of the circulating pump.

(*b*) *Circulating Pump and Drive.*. The source of power for the circulating pump is a direct-current separately excited stabilized shunt-wound vertical motor with a short-time rating of 500 hp. To save space the motor is mounted above the 48-in. propeller pump and connected directly to it by a long shaft. A pump of low speed and large size was selected and installed at a considerable depth below the working section in order to avoid pump cavitation.

(*c*) *Resorber.* The resorber, so-called because its function is to resorb entrained air bubbles into solution, is essentially a steel tank 11 ft 6 in. diam × 58 ft long, buried vertically in a concrete pit, the bottom being 70 ft from the level of the sub-basement. The resorber is split into two chambers by a light partition which extends from the bottom to within 4 ft of the top of the tank. A 5-ft-diam pipe extends into each chamber to within 4 ft of the bottom. These are called the downcomer and the upcomer.

The long time required for the water to pass through the resorber, due to its large capacity, plus the high pressure at the bottom, assures complete resorption of any entrained air in the circuit.

There are several additional advantages of this type of resorber construction. The vertical pit saves valuable space and permits a vertical pump drive with no side load on the pump bearings. The resorber, with a volume of approximately 45,000 gal, has a large heat-storage capacity which facilitates temperature control. Finally, the long straight approach of the upcomer gives uniform flow at the upcomer elbow.

Description of Auxiliary Circuits and Control Systems:

(*a*) *Temperature Control and Refrigeration System.* The refrigeration system used to maintain an even temperature level in the high-speed water tunnel is shown in Fig. 9. A small portion of the total volume of water circulated is pulled off the top of the resorber head by the chilled-water pump which forces it through the chiller coil of the refrigeration unit. The chilled water leaves the coil and returns to the main circuit at a point just upstream from the pump elbow. Complete mixture of the cold water is insured by passing through the main circulating pump and through the complete circuit of the resorber. Cooling water for the condenser coil is supplied from an induced-draft cooling tower located on the roof of an adjoining three-story building.

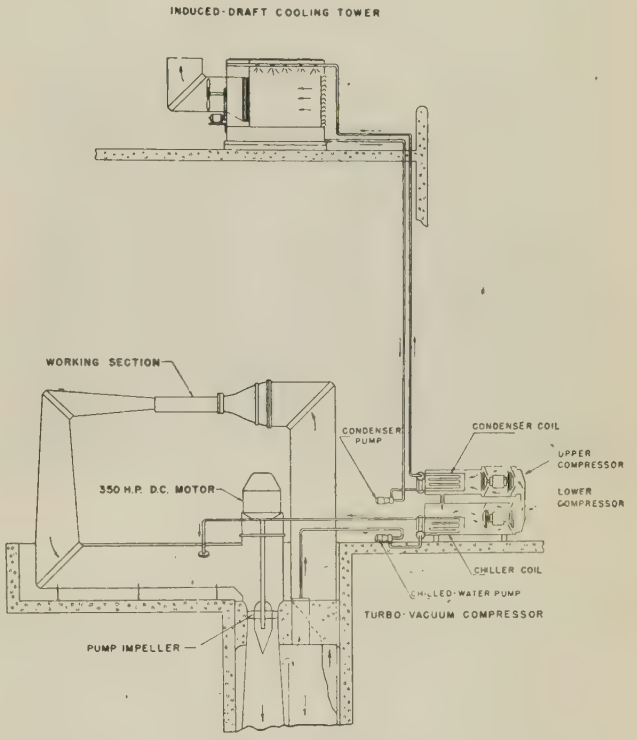

FIG. 9 COOLING SYSTEM

The turbovacuum compressor is a low-pressure self-contained refrigeration unit with the motors hermetically sealed inside.

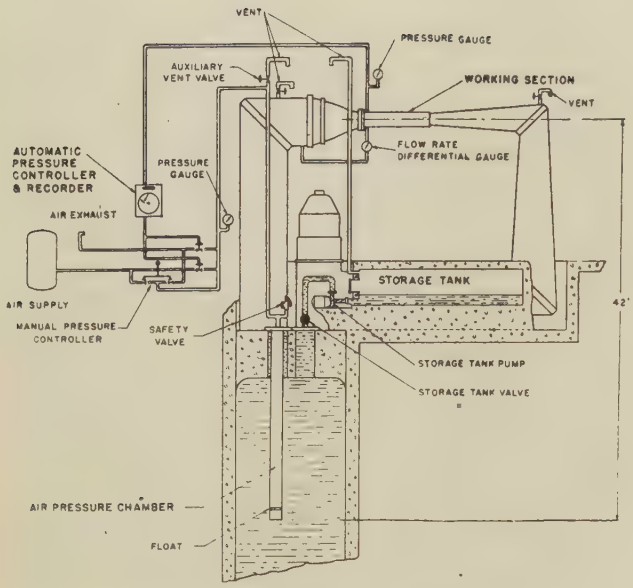

FIG. 10 PRESSURE-CONTROL SYSTEM

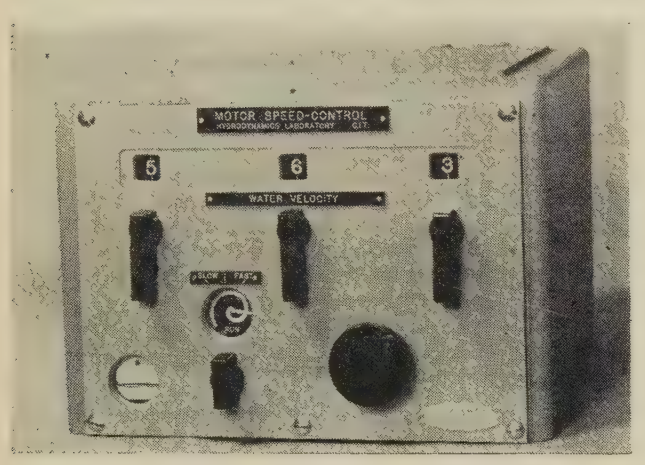

FIG. 11 SPEED-CONTROL UNIT

The compressors are of the centrifugal type, using a volatile refrigerant of the Freon family.

Temperature control is maintained by means of a Micromax temperature-recording device which operates relays so that the refrigeration unit cuts in and out at predetermined temperature levels.

(*b*) *Storage-Tank Pumping System.* In order to change models, the water level in the tunnel must be dropped to the bottom of the working section. This requires the transfer of 1100 gal of water between the tunnel and a suitable storage tank.

(*c*) *Pressure-Control System.* The pressure control system and also the storage tank and filling circuit are shown in Fig. 10. The pressure in the working section of the water tunnel is controlled by means of an air chamber with a water level approximately 40 ft below the center line of the working section. By this arrangement, it is possible to use a positive air supply at all times, even when the working section is operating under a vacuum. The relatively large volume of air is also desirable to compensate for changes of volume of the main tunnel circuit due to formation of vapor bubbles during cavitation tests. As Fig. 10 shows, even the minor absorption of air from the pressure chamber has been cut to a minimum by using a float to eliminate nearly all of the water-air interface. The air pressure may be controlled by means of the manual pressure controller valve or, if a more accurate control of the pressure in the working section is desired, by an automatic pressure-control system.

(*d*) *Speed Control.* It is essential that constant water velocity be maintained in the working section. This means that the circulating-pump and driving-motor speed must be controlled very accurately. Fig. 11 shows the unit used to control the velocity of the high-speed water tunnel. The system is the same as that used in the Hydraulic Machinery Laboratory,[5] except that the control box is very compact and has one gear cluster and three speed decades giving 1000 steps of control. This device is calibrated so as to permit settings of water velocity from 0 to 99.9 fps in steps of $^1/_{10}$ fps.

Description of Instruments:

(*a*) *Balance.* The balance, Fig. 12, is designed to measure three components of the hydrodynamic forces operating on the model, as previously outlined. The balance consists of a vertical spindle supported near the center with a universal pivot which permits rotation about any axis through this point but allows no translation. The model is attached rigidly to the top of the spindle. This assembly is prevented from rotating under the action of the hydrodynamic forces by applying restraining moments about three mutually perpendicular axes intersecting at the pivot. These moments are applied by hydraulic pressure through the three sets of pistons, cylinders, and yoke wires. The three restraining moments measure the components of the hydrodynamic forces acting on the model. The upper section of the spindle can be rotated so that the yaw of the model can be

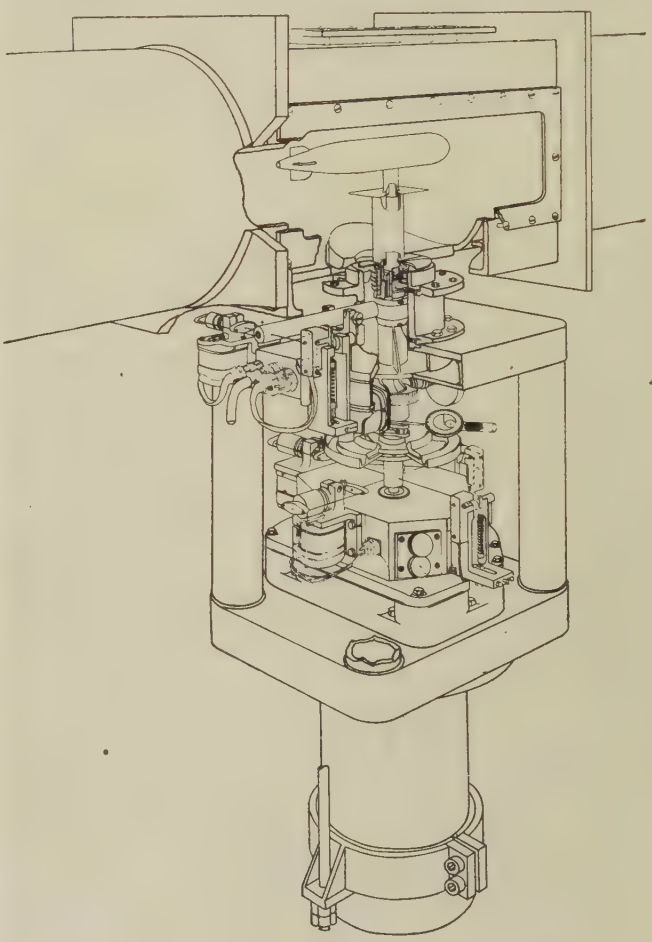

FIG. 12 BALANCE

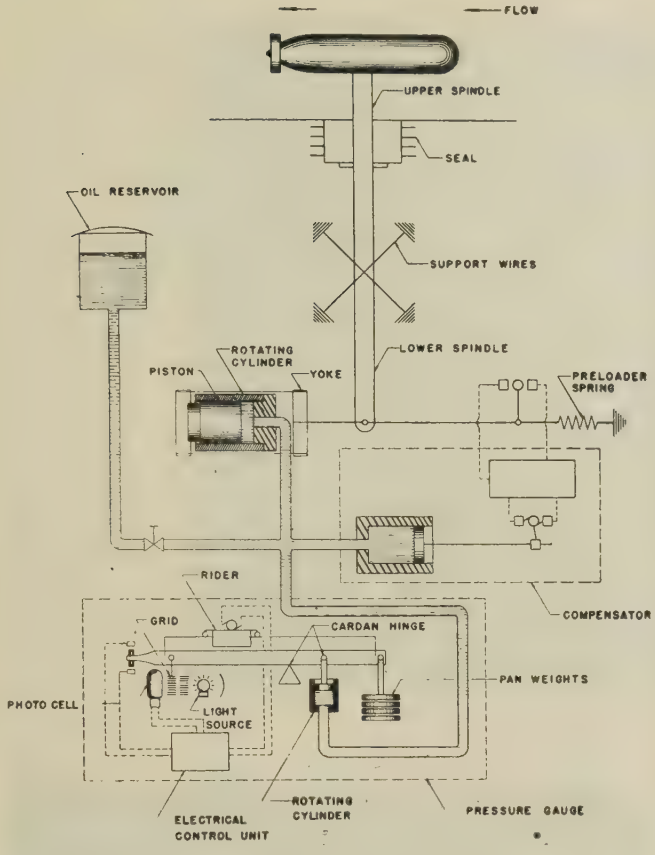

FIG. 13 FORCE-MEASURING SYSTEM

changed with respect to the flow without disturbing the remainder of the balance and measuring system.

Fig. 13 is a schematic diagram of the balance system, force-transmitting system, and pressure gage used to measure the drag force. Similar systems are used to measure cross-force and moment. The hydrodynamic force on the model and upper spindle is transmitted to the restraining wire at the bottom of the lower spindle. The wire and yoke transmit the force to the hydraulic piston. In order to measure positive and negative forces with one piston, a spring preloader is used. To eliminate static friction, the hydraulic cylinders are rotated at constant speed by individual motors.

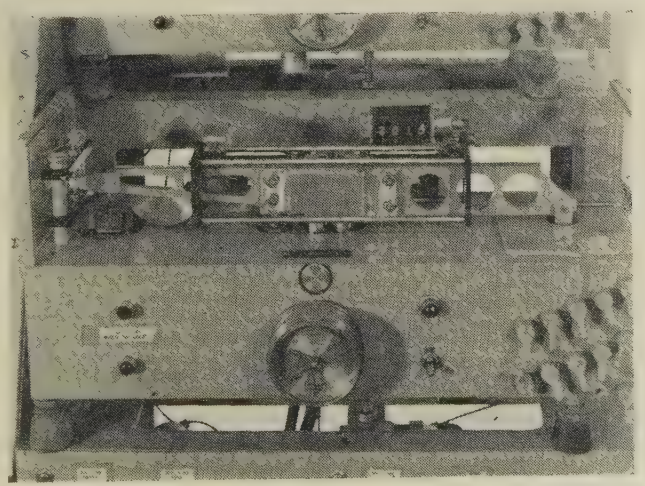

FIG. 14 PRESSURE GAGE

(*b*) *Pressure Gages.* The pressures in the cylinders on the balance are measured by weighing-type pressure gages, as shown schematically in Fig. 13. Fig. 14 shows one of these gages. It consists essentially of a beam supported on a Cardan hinge pivot. The pressure to be measured is applied through a piston attached to this beam, the piston being fitted in a cylinder which is rotated to avoid static friction, the same as in the case of the balance pistons and cylinders. The force exerted by the oil pressure on the piston is balanced by pan weights applied to the end of the beam and also by a rider weight running on the beam. Unbalance of this beam results in unbalance of the optical-electrical control system which, in turn, automatically moves the rider weight and changes pan weights until equilibrium is obtained. The positions of the rider and pan weights are indicated by counters which read directly in pounds per square inch to the nearest 0.01 psi. The maximum pressure reading is 750 psi.

(*c*) *Compensator.* The compensator shown in Fig. 15 is a small screw-operated piston which supplies oil to the system in a definite minute amount upon receiving an electrical signal from the balance contacts.

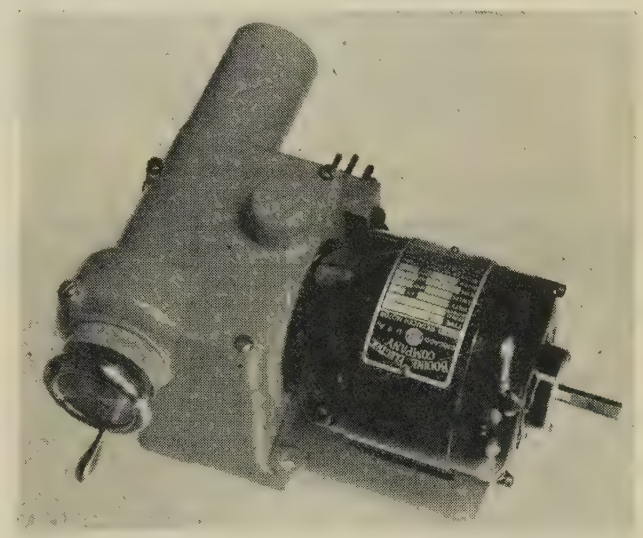

FIG. 15 COMPENSATOR

(*d*) *Differential Pressure Gage.* The differential pressure gage is employed primarily in the measurement of velocity of flow in the working section by means of the pressure difference across the nozzle, as shown diagrammatically in Fig. 10. It is similar in appearance and design to the pressure gages, the only difference being that the force applied to the beam is the result of the difference of two pressures applied to the opposite ends of the piston. The pressure lines from the nozzle are connected to the bottoms of two separating pots. The lower halves of these pots are filled with water and the upper halves with oil. Pressure leads from the oil domes go to the differential gage.

(*e*) *Control Panel.* Fig. 16 shows the instrument group with the cross-force, drag, moment, and the differential pressure gages. In the center is a panel with lights indicating the state of balance of the gages and other essential operating data. When all panel lights are out, a condition of gage balance and general instrument readiness is indicated. Thereupon a button is pushed which stops the gage rider motors so that simultaneous pressure readings may be recorded.

(*f*) *Models.* The models used are exact geometric replicas of the prototypes within the tolerances of the precision machine shops employed. A 2-in. body diameter has been chosen as

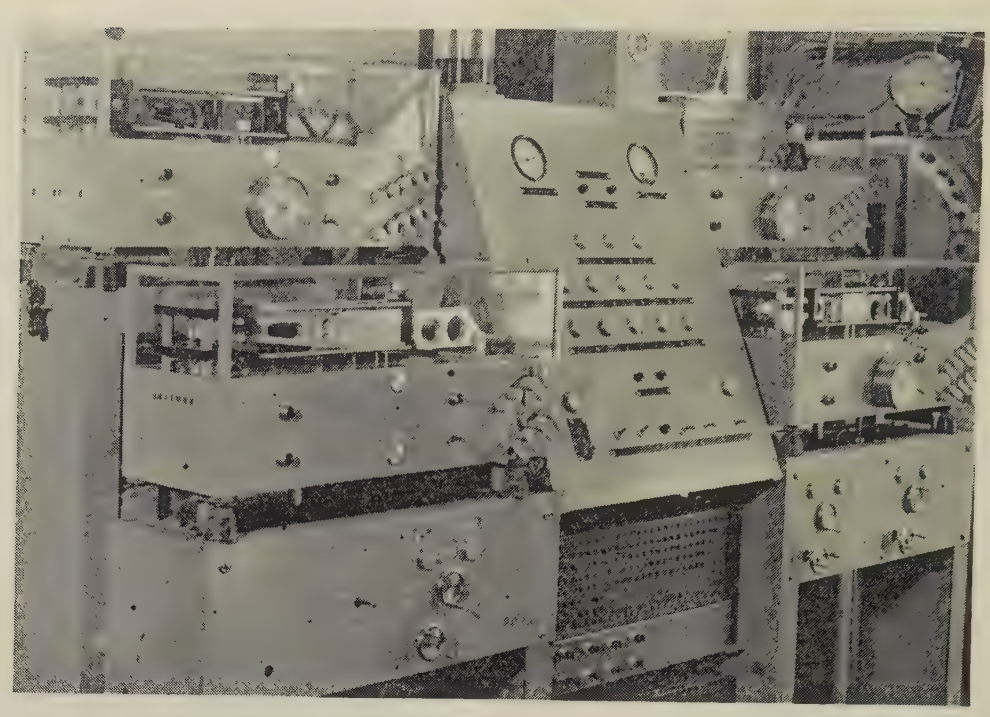

FIG. 16 INSTRUMENT GROUP

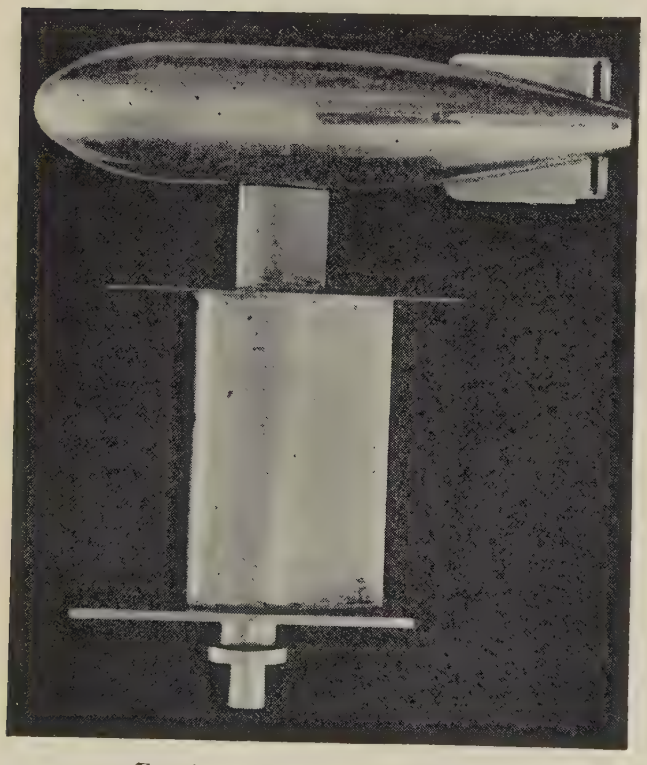

FIG. 17 TYPICAL MODEL AND SHIELD

standard. Fig. 17 shows a typical model and Fig. 18 its individual components, including the spindle and integral center section. A complete set of cylindrical body sections is available so that any desired length can be assembled from 0.100 in. to 12.000 in. in steps of 0.010 in. When a design of a new body is submitted for test, a quick survey of the model parts shows what elements are available and what new parts must be made.

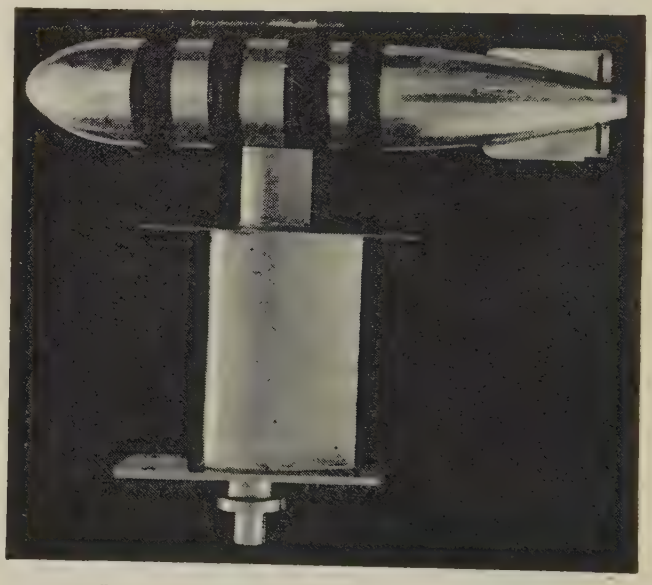

FIG. 18 EXPLODED VIEW OF TYPICAL MODEL

In general, the model parts are made of stainless steel to eliminate corrosion and to secure a reasonable hardness to reduce damage from handling.

THE FREE-SURFACE WATER TUNNEL

General Characteristics. The latest major piece of equipment of the laboratory is the free-surface water tunnel. It offers a working section in which bodies may be supported in a stream of flowing water so that their hydrodynamic characteristics can be determined. A unique feature is that the stream of water passing through the working section is confined by solid boundaries only at the bottom and sides; the top surface of the stream is not a solid boundary, but is here a free surface, i.e., an air-water interface. The hydrodynamic forces acting on a body when it is

near a surface are different from those acting during deep running. These forces and their variation with distance to the surface can be studied effectively in the free-surface water tunnel.

Large amounts of air or other gas may be injected into the working section during certain investigations. If it is not removed, it circulates with the water and returns to the working section. This is not permissible because it affects all the hydrodynamic forces and invalidates the measurements; therefore the free-surface tunnel has a high-capacity air-removal system to remove bubbles before they return to the working section.

The air pressure above the free surface in the working section can be controlled at any value from atmospheric pressure down to $^1/_{12}$ or $^1/_{15}$ atm. This permits control of cavitation on a model; therefore the effect of cavitation on the hydrodynamic forces on a body can be investigated. It is now possible to model properly and simultaneously the submergence, the surface-wave pattern, and the cavitation characteristics.

Velocities as high as 30 fps can be obtained in the working section. The channel is 20 in. wide and 30 in. deep; the normal depth of flow, however, is 21 in., in order to allow a 9-in. air space above the interface. Throughout its 8-ft length, the working section is bounded by transparent windows on the sides, bottom, and top to permit photographic and visual observation of cavitation, surface configuration, and air entrainment caused by the model under test.

Special Operating Characteristics. Because of the wave phenomena associated with the movement of objects near a free surface, this test channel is made wider than the 14-in. diam of the working section in the high-speed tunnel. The 20-in. width used here should allow the standardized models with a diameter of 2 in. to be used in both tunnels even when the submergence in the free-surface tunnel is so small that the surface-wave phenomena are significant.

Since the top of the free surface must be level before it is disturbed by a model, a rectangular cross section is used. Any other shape would complicate the design of the viewing windows and the accelerating nozzle which precedes the working section. The 21-in. depth of flow where it discharges into the working section will allow a variation in submergence of the model throughout a range from any degree of intersection with the surface to a submersion so great that the free surface does not affect the results.

Continuous operation at velocities as high as 25 or 30 fps can be obtained. For a channel with a depth of 21 in., the critical velocity, i.e., the velocity of a gravity wave, is about $7^1/_2$ fps. At 30 fps, the ratio of the velocity of flow to the wave velocity will be 4. This ratio, the Froude number for the open channel, is a characteristic parameter describing the behavior of a surface wave in the working section. It is analogous to the Mach number, the flow parameter used with supersonic gas flow.

Another type of surface-wave phenomenon studied by William Froude in 1872, was caused by geometrically similar forms moving parallel to the surface. He found that surface waves of identical geometrical configuration would be produced if the speed-length ratio, $V/\sqrt{l}$ were the same. In adjusting this ratio for geometrical modeling of the surface-wave pattern, values as high as 30 can be obtained for models that are 1 ft long by bringing the tunnel velocity up to 30 fps. By making speed adjustments to produce identical values of $V/\sqrt{l}$ and by providing geometrical modeling of the submergence, the flow pattern around the model should be geometrically similar to the pattern around the prototype. With the 30-fps velocity around a model that is 1 ft long, the Reynolds number will be 3,000,000. This parameter will be high enough in the majority of tests so that exact modeling for skin friction will be considerably less significant than proper modeling of the surface wave.

In order to regulate the cavitation parameter, it is necessary to control the pressure of the air above the water surface. This is done by connecting this space to a high-capacity vacuum pump and regulating the flow of air to the pump with control valves. The valves are positioned by an automatic vacuum regulator. At 30 fps and $^1/_{15}$ atm the cavitation parameter is about 0.11.

Arrangement and Construction of the Main Circuit. The free-surface water tunnel has a closed-circuit circulation system which is driven by a propeller pump, powered by a variable-speed direct-current motor. The circuit is arranged in a vertical plane with the working section in the upper horizontal run. The return circuit, containing the circulation pump, is located one floor below the upper level.

Fig. 19 shows a sketch of the entire tunnel. The observer is watching the operation of a model mounted on the balance in the working section. Downstream from the working section, the jet enters a series of vane diffusers which increase the cross section and decrease the velocity. The low-velocity flow enters an air separator which can be seen through the cutaway opening in the upper left-hand corner of the sketch. At the lower level, the discharge from the pump goes into a circular diffuser section which again decreases the velocity. At the maximum diameter, a transition section gradually changes the cross section from round to square. The acceleration of the flow to the working velocity begins in the vertical riser, continues in the accelerating elbow above this riser, and is completed in a two-dimensional nozzle which discharges a 20-in-wide × 21-in-deep jet of water into the working section.

Since the working section may be operated at very low pressures, the entire structure is designed to support an external pressure of 1 atm. This requires heavy strengthening ribs on all the exterior surfaces where the cross section is not circular.

Construction of Working Section. All faces of the working section shown in Fig. 20 contain lucite windows which are held in a comparatively light steel framework. Deflection of this framework allows the windows to take a share of the stresses involved in the low-pressure operation. The pressure on the top and bottom windows loads the side windows in a vertical direction and vice versa. Positive pressures must be limited to a few pounds per square inch because the windows do not assist in taking the load in such cases. In order to limit deflections, the 30-in-high side windows are $4^1/_2$ in. thick, and the 20-in-wide top and bottom windows are 3 in. thick. The length is divided into two sections in order to decrease the size of the lucite castings.

Deceleration Downstream From Working Section. The velocity must be reduced before the flow enters the air separator since time must be allowed for the bubbles to rise. The purpose of the diffuser is to take the water discharged by the working section and distribute it evenly over a cross-sectional area about 16 times as great, thereby reducing the velocity by this ratio.

An efficient diffuser should regain a large portion of the difference in the velocity heads at the entrance and discharge. A number of factors complicate the problem of getting efficient diffusion in the free-surface water tunnel. There is a transition from an open surface to a closed diffuser. The size of the laboratory precludes the use of the customary long diffuser with a gradual expansion. Air bubbles in the flowing stream tend to prevent the flow from following the expanding channels; furthermore, work must be done in compressing these bubbles through the pressure regain obtainable. The necessity for a free surface in the air separator makes it difficult to apply the pressure across the diffuser which is required to realize whatever head the diffuser is capable of regaining.

A short diffuser with reasonable efficiency was secured by taking the flow through a series of four 60-deg turns with vane dif-

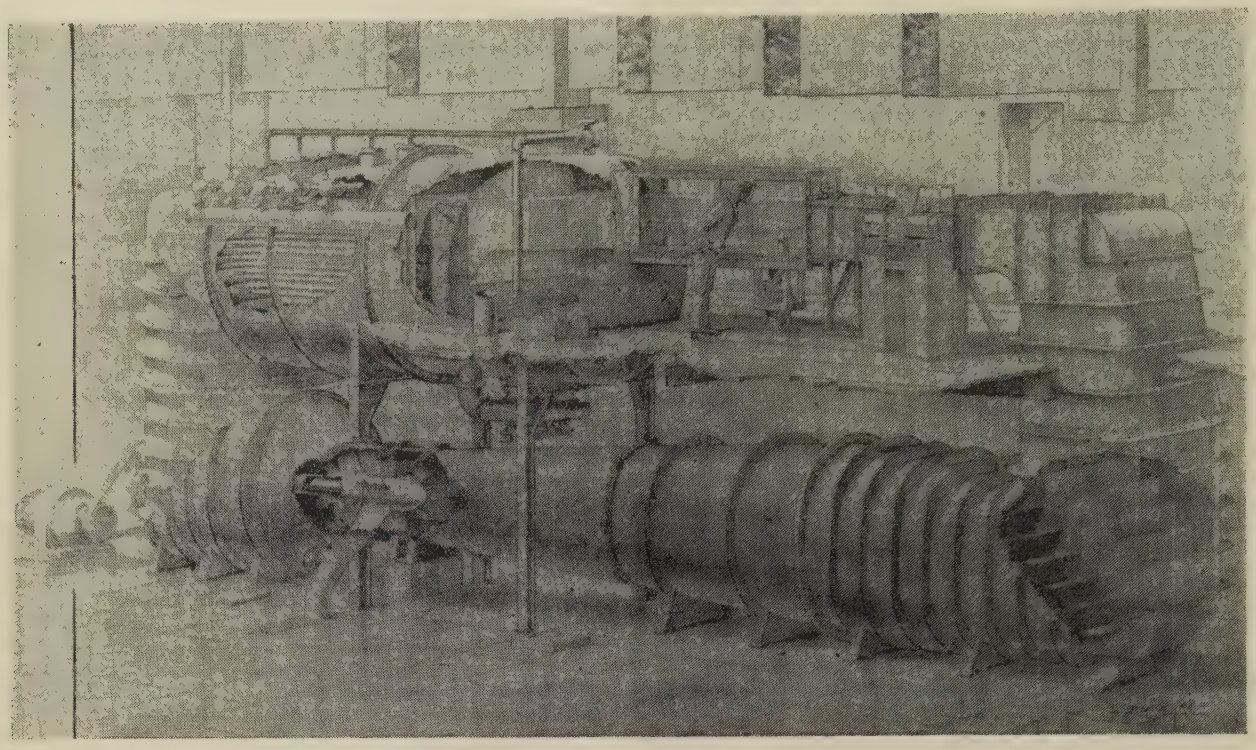

FIG. 19 FREE-SURFACE WATER TUNNEL

fusers which double the cross-sectional area at each turn. The vanes are curved on a 4-in. radius and the spacing transverse to the stream is small.

A regain of velocity head by the diffuser implies that the downstream pressure is higher than the upstream pressure. Since there are free surfaces on both sides of the diffuser, this pressure difference is maintained by adjusting the downstream level a few inches above the working-section level and by holding the air pressure above the air separator at a higher value than the air pressure in the working section. The total pressure across the diffuser, i.e., the head regained, is equal to the air-pressure difference plus the small surface-level difference between the air-separator chamber and the working section.

Pressure Controls. The working-section pressure can be controlled from atmospheric pressure down to about $^1/_{15}$ atm. Control valves are installed in the line connecting the working-section air chamber to the vacuum pump. They are actuated by a drift-compensated proportional controller, having a measuring element which is sensitive to the pressure in the working section. To simplify the control system, a manually controlled air bleed into the working section is provided. This makes it possible for a single automatic control system which operates valves in the vacuum line only to make pressure adjustments in both directions.

Air that is injected for powered models will enter the chamber above the air separator in varying amounts. Adjustments of the pressure in this chamber are made with control valves which are installed in the air-exit line. This line can be connected either to the working section or to the vacuum pump. Here again, manually controlled inbleed of compressed air is provided for changing operating conditions and for use, when necessary, in positioning the automatically controlled air-exit valves within their operating range. The controller operating these valves therefore is able to maintain the required back pressure on the diffuser.

The regulators for both the working-section pressure and the release of air from the air separator are shown on the control panel at the left in Fig. 20. The air piping and control valves can be seen in Fig. 21.

The Air Separator. The air introduced in the working section will at times appear in the form of small bubbles, many of which may be deeply submerged. The rate of rise of such bubbles is rather low. This means that either a long time or a short distance to a free surface is required for adequate separation. Although the velocity at which the flow leaves the battery of deceleration vanes will probably be under 2 fps, the depth will be very great—too great to permit the rise of a small bubble to the surface before the flow reaches the vane elbow and turns down toward the circulating pump. To reduce the effective depth, the air separator is divided into a series of shallow channels by means of a spaced stack of trays which have solid tops and perforated bottoms. The perforations permit free access of any bubble to the space within. This space contains dividers which permit the trapped air to flow across the stream to channels leading upward to the surface of the pool above the stack. Fig. 22 shows some of the trays after installation. They are $^1/_2$ in. thick and have a net separation of about 2 in. The minimum time required for the flow to pass through the tray section will be approximately 5 sec. Bubbles with an effective rate of rise of $^2/_5$ ips or greater will reach the perforations and be trapped. To assist the bubbles to separate there is a small flow from the main stream up through the perforations and out through the channels to the risers. This flow is induced by taking water from the pools above the trays (see one of the suction nozzles at the top of Fig. 22) and pumping it back into the main circuit between the diffuser vanes and the air-separator trays, i.e., just upstream from the air separator.

Many of the investigations may produce splash and spray above the free surface in the working section. Provisions are made to collect the water thus involved by skimming off the top layer and deflecting it to each side where it can drop into a stilling pool below the diffuser. From the stilling pool the skimmed

FIG. 20 WORKING SECTION AND AIR-CONTROL PANEL

FIG. 22 ENTRANCE TO AIR SEPARATOR WITH UPPER FOUR TRAYS INSTALLED

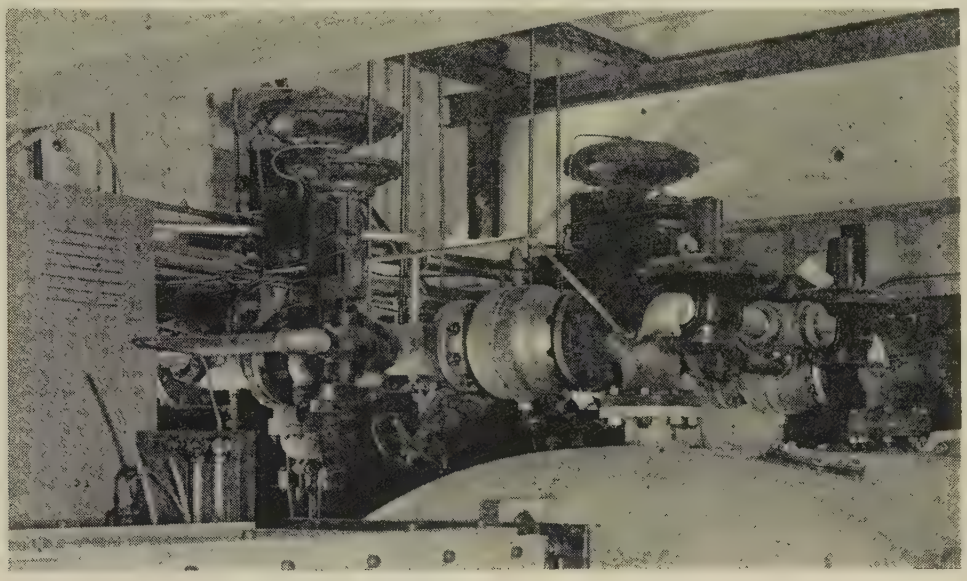

FIG. 21 AIR PIPING AND CONTROL VALVES

water is pumped back into the main circuit just upstream from the air separator. Entry at this point will give the air separator a chance to take out any remaining bubbles. The speed of the pump which takes the water out of the stilling pool is adjusted by a controller that is sensitive to the water level. By keeping this surface level fixed, the total water in the main circuit is practically constant, and this third free surface does not affect the operation of the main circuit.

Main-Circuit Pump and Driving Motor. A standard 42-in. propeller pump is used to circulate the water. The bearings are arranged for a horizontal drive and the shaft seal is designed for pressures acting in either direction, since the submergence is not sufficient to maintain a positive seal pressure during high-vacuum operation in the working section. Although this pump circulates approximately the same quantity of water as the one in the high-speed tunnel, the power requirements are greatly reduced because of the lower head required to produce the lower velocity in the working section. Therefore the pump of the free-surface tunnel is driven by a 75-hp direct-current motor which is powered with a 75-kw rectifier. The speed is controlled by a system which is identical with the one used in the high-speed tunnel.

Measurement of Hydrodynamic Forces. In order to determine the hydrodynamic characteristics of a body, it must be supported in the stream of flowing water by means of a balance capable of measuring the resultant forces. Since the forces resulting from tests in a free-surface channel have components that are different from those previously obtained, and since the position of the model relative to the interface should be adjustable, new balance systems are being developed for the free-surface water tunnel.

For most craft which operate at or near a free surface, variations in the pitch angle and degree of immersion greatly influence the resultant forces on the body. A great deal of valuable information can be obtained in the free-surface tunnel when models are supported with zero yaw. If the pitch angle is varied while maintaining zero yaw, a three-component balance, which measures drag, lift, and pitching moment, will define adequately the forces on models that are symmetrical about the drag-lift plane. Although in some investigations such a three-component

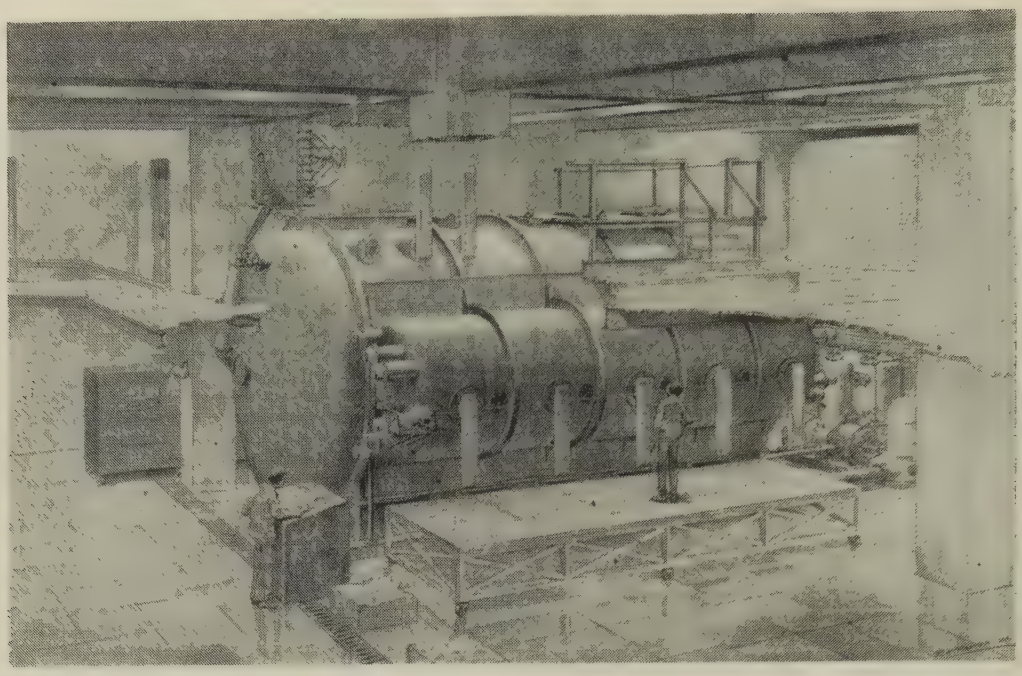

FIG. 23 GENERAL VIEW OF CONTROLLED-ATMOSPHERE LAUNCHING TANK

balance will secure all the information desired, its design and operation are considered only a part of the development of a five- or six-component weighing system. Six components will be necessary, in fact, before the balance can be considered complete, because even the rolling moment induced by yaw is significant for laterally steerable craft operating at or near a free surface.

CONTROLLED-ATMOSPHERE LAUNCHING TANK

General Description. The primary use of the controlled-atmosphere launching tank is in the study of the hydrodynamic problems involved as a free-flying body enters the water from the air. The equipment may be used for other studies, such as underwater explosions, which require similar facilities. In studying hydrodynamic phenomena occurring at an interface between a liquid and a gas, it is sometimes necessary to have control of the atmospheric pressure and density. For this reason the tank was built as a completely enclosed pressure vessel.

Fig. 23 is an artist's sketch showing an over-all view and Fig. 24 is a cutaway view of the launching end of the tank. The tank itself is a completely enclosed pressure vessel of welded-steel construction. In normal operation, the tank is filled with water to about three fourths of the total depth, leaving an air space above the water. A centrifugal launching device, mounted on the underside of a large hatch cover, launches the model under investigation at any desired trajectory angle from vertically downward to horizontal, with any pitch angle up to ±10 deg, and at any desired speed up to 250 fps. A battery of high-speed motion-picture cameras records the path of the model during both the air flight and the underwater travel. The cameras operate without shutters, and exposures are made by intermittent illumination of the interior of the tank with Edgerton-type flash lamps. The fields of view of adjacent cameras overlap by 60 per cent, so that at least two cameras photograph the model throughout its travel. The stereoscopic vision thus obtained makes it possible to recreate the path of the model step by step with the analyzing equipment which will be described later.

In Fig. 24 the launcher is seen in the launching position

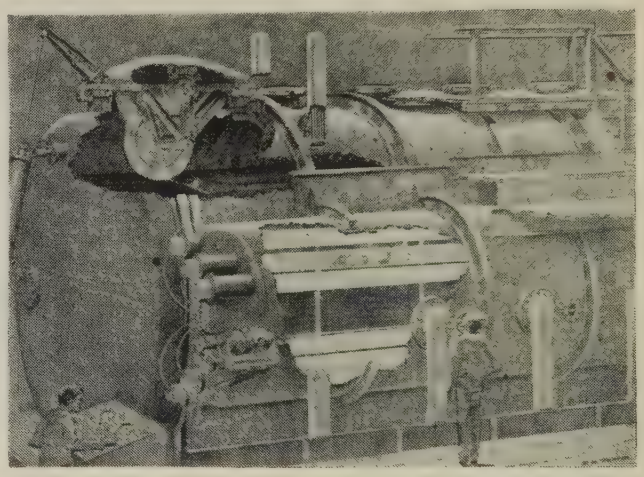

FIG. 24 CUTAWAY VIEW OF LAUNCHING END OF TANK

shortly after having released a model, and the model is seen entering the water. The air-trajectory cameras are approximately level with the launcher and slightly to the right. Four of the five underwater cameras are shown on the lower level. The flash lamps for illuminating the interior of the tank are installed in the six lucite tubes which pass through the tank, above and below the underwater cameras.

For convenience in description, the equipment will be subdivided into four components, namely, the tank, the launcher, the trajectory-recording system, and the data-analyzing system.

The Tank. The physical requirements for the study, as indicated in the previous section, call for control of the air pressure above the water in the tank. For this reason the tank was designed to withstand an external pressure of a full atmosphere and an internal pressure of 40 psi. The tank provides a clear launching plane 25 ft long with a water depth of 10 ft.

The tank structure, as may be seen in Fig. 25, consists of a large horizontal cylinder, 13 ft diam and 29 ft long, to one side of which is attached a section of a smaller cylinder 6 ft diam and

23 ft long. The purpose of the smaller cylinder is to provide the necessary distance from the cameras to the launching plane so that the launching plane can be covered with a reasonable number of cameras. The large openings in the shells of the two cylinders where they are joined together, require special provisions for carrying the hoop stress across the opening. This is done by means of the longitudinal T beams, 20 in. high, running the full length of the intersection, and 2-in. × 12-in. vertical columns spaced at 54-in. intervals which span the opening and transmit the load from one T beam to the other. These columns are spaced so that they will carry the load without ec-

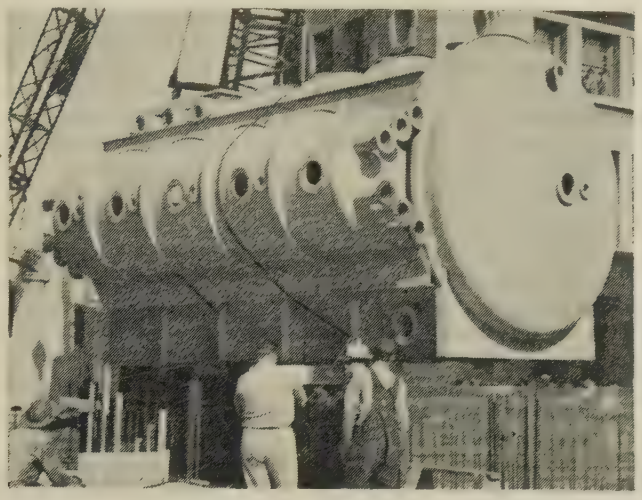

FIG. 25 CONTROLLED-ATMOSPHERE LAUNCHING TANK BEING LOWERED INTO BASEMENT FOR INSTALLATION

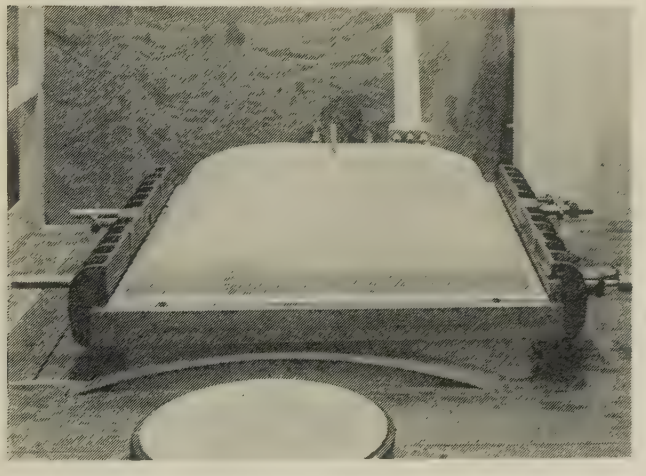

FIG. 26 HATCH COVER AND C-CLAMPS

centricity and at the same time stay out of the field of view of the recording cameras. The weight of the empty tank is approximately 40 tons, and when filled with water to a depth of 10 ft, the combined weight is about 150 tons.

The large rectangular hatch opening, which may be seen in Fig. 25, on top of the tank and near the far end, is off center to increase the distance between the launching plane and the cameras. The entire launching mechanism is mounted on the hinged cover which has an O-ring pressure seal. A hydraulic cylinder provides for rapid opening and closing of this hatch cover. Heavy C-clamp frames along the two longitudinal edges of the opening hold the cover rigidly in place during operation of the launcher. Fig. 26 shows the hatch cover, with the clamps and the opening lever. Four flanged openings along the top of the main cylinder are for access and recovery of models, ten on the side and ends are for attachment of recording cameras, five for visual observation windows, twelve for insertion of the lucite tubes which house the lamps, and two for control of the air pressure.

Since the tank is used for underwater photography, it is extremely important to maintain the water in it at a high degree of clarity. The lamps and the cameras are both on the same side of the tank. The light has to travel an average water path of 24 ft in going from the lamps to the model and back to the cameras. It is obvious that even a slight amount of color, fine suspension, or microscopic life in the water would absorb or scatter most of the light before it reached the cameras. Therefore the treatment of the interior of the tank was given a careful study. The requirements were to prevent corrosion of the steel tank, to avoid contamination of the water in any manner which might impair its optical properties, to provide a dark background, and to minimize the possibility of damage to models striking tank walls. Very few materials were found which could meet all these requirements. The one finally selected is a polyvinyl chloride plastic (Koroseal) which is cemented all over the interior of the tank, in

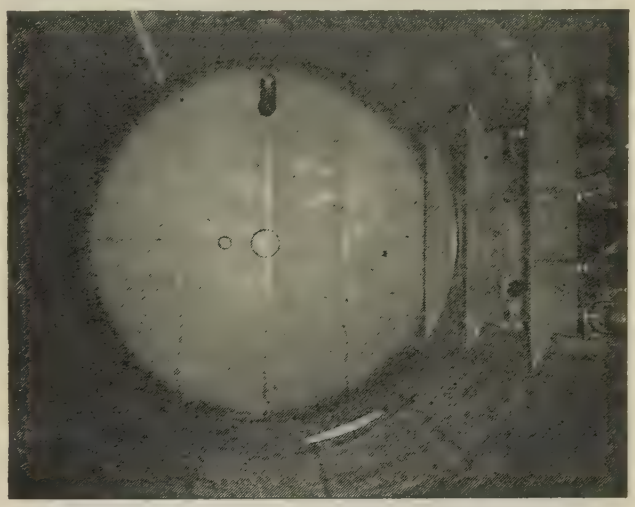

FIG. 27 INTERIOR OF TANK SHOWING TANK LINING, OVERHEAD ULTRAVIOLET LIGHT WITH COLUMNS, AND LUCITE TUBES AT RIGHT

sheets $^{3}/_{32}$ in. thick, with the seams between sheets heat-sealed with strips of similar material. Commercial sand and alum filters remove suspended materials from the water, and a string of germicidal ultraviolet lamps installed along the ceiling control bacterial growth. A vacuum pump is provided for controlling the atmospheric pressure. Fig. 27 shows the lined interior, the ultraviolet-light tubes along the ceiling and, incidentally, the reinforcing columns at the junction of the two cylinders and some of the lucite tubes in the smaller cylinder. Occasionally the local water supply contains traces of yellow coloring matter in solution which cannot be removed by filtration. This makes the water completely unusable in the tank since it filters out all the blue and violet light in which the flash lamps are rich. The difficulty has been overcome by distillation, which is done rather economically by means of vapor-compression stills.

The Launcher. The design specifications for the launcher call for a device which will produce accurately any desired speed up to 250 fps, be compact so it may be lowered easily into the tank for launching and brought out for loading and setting, and which will launch models with pitch angles (angle in vertical

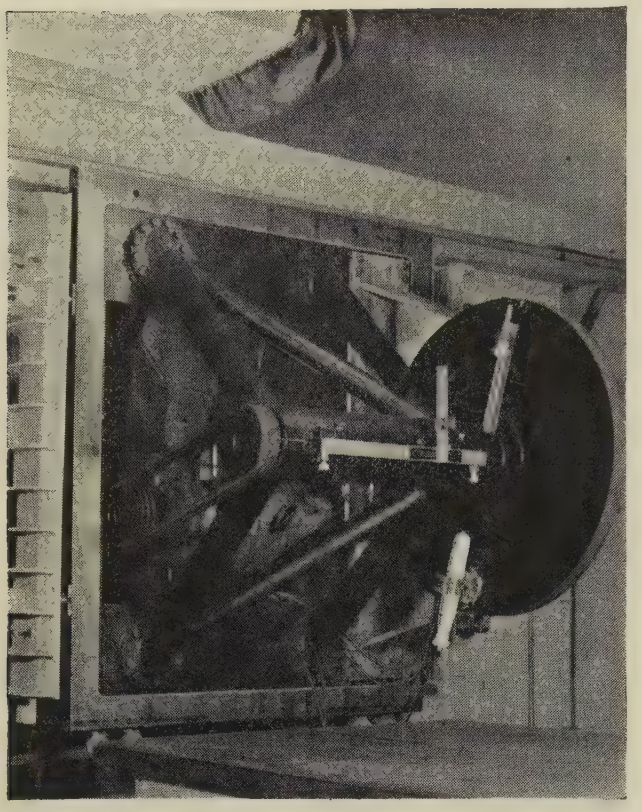

FIG. 28 LAUNCHER MOUNTED ON OPEN HATCH COVER

plane between axis of model and path of the center of gravity of the model) up to ±10 deg. It was also desired to provide for possible modification to include pitch angular velocity and yaw angles. After an extensive consideration of the possible launcher types, it was decided to use a centrifugal launcher.

The launcher consists basically of a rotating wheel which carries the model near its periphery, with a planetary-gear system to prevent the model from rotating about a transverse axis as it goes around with the wheel, and with a mechanism for releasing the model at any predetermined point along a 90-deg arc. Fig. 28 shows the launcher mounted on the open hatch cover with a model in place in the chuck. The wheel is a heavy steel plate having sufficient flywheel effect to insure uniform velocity. It is supported on a stainless-steel shaft which is mounted on four preloaded precision ball bearings, assembled in a quill to form an accurately aligned unit. The launcher is driven by a 10-hp d-c motor whose speed is controlled electronically by a device similar to the ones used with the water tunnels. The control is activated by a selsyn generator driven by chain from the launcher shaft. The model is counterbalanced by a movable weight on a screw in the plane of rotation of the model and displaced from it by 180 deg. No provision is made for shifting this counterbalance after the release of the model because the structure is massive enough not to suffer from this unbalance, and a slight unbalance is not critical once the model is free.

The chuck, with model in place, is seen in Fig. 29, and Fig. 30 shows the internal construction. It consists of a cylindrical seat, covering a 135-deg arc, into which the model is laid, and a gripping finger which holds the model in place. A locking lever, in turn holds the gripping finger against a spring which tends to open it. The locking lever extends slightly beyond the face of the wheel on the far side. To release the model, a tripper block is moved by a solenoid into the path of the protruding end of the locking lever. The open end of the model seat faces toward the periphery of the wheel. At the instant of release the model and the chuck have identically the same motion. From this instant the model moves along a tangential path, and the chuck, continuing its circular motion, gradually lifts away from it. After release, the heavy spring moves the gripping finger rapidly out of the way of the model to prevent interference. The model seat is made as rigid as possible to reduce to a minimum the energy stored in it which might affect the motion

FIG. 29 CHUCK WITH MODEL

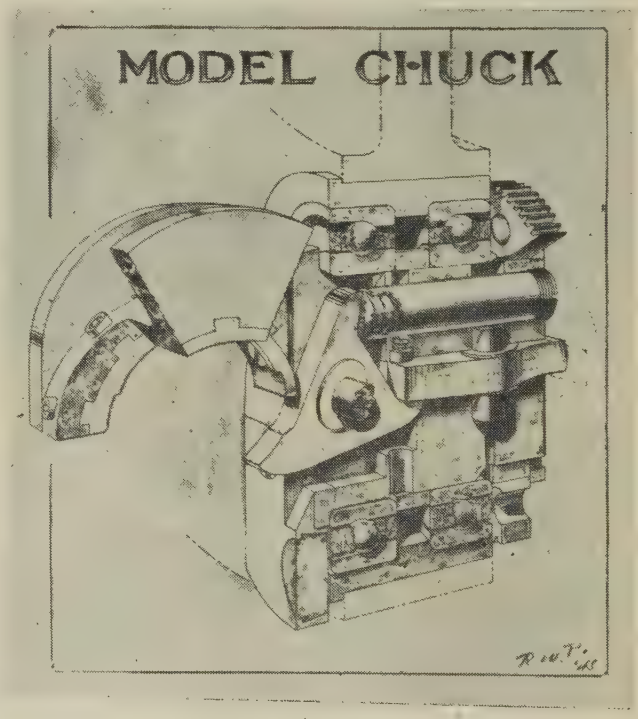

FIG. 30 INTERNAL CONSTRUCTION OF CHUCK

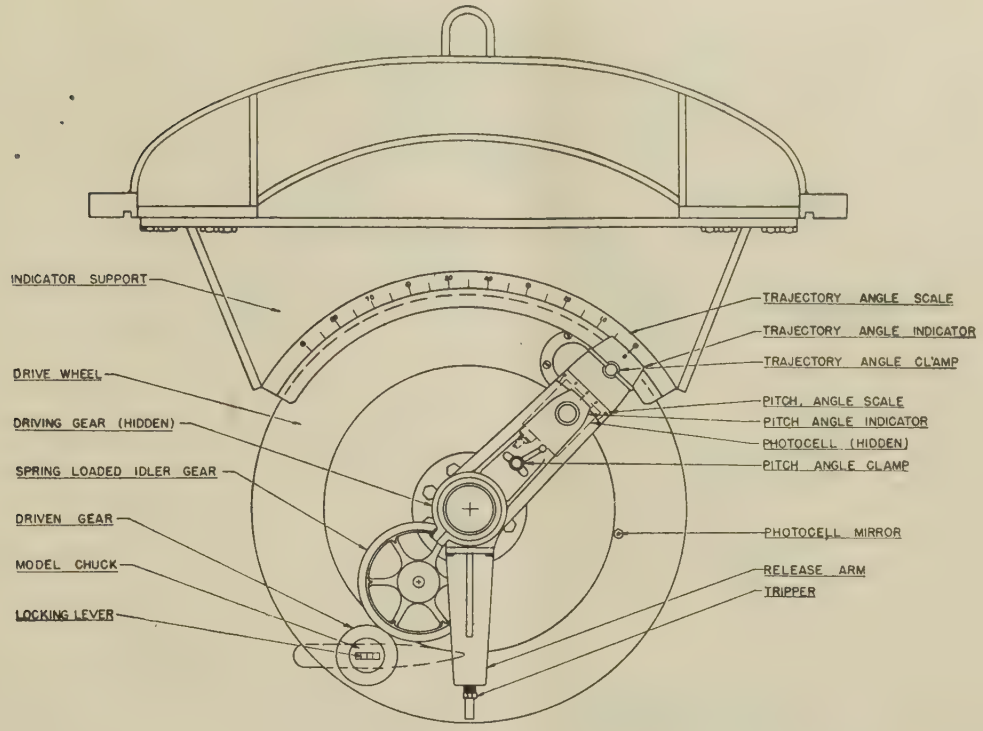

FIG. 31 MODEL LAUNCHER, CONTROL SIDE

of the model at the instant of release. The entire chuck mechanism is mounted in precision ball bearings.

Fig. 31 is a drawing of the launcher showing the opposite face of the wheel with planetary-gear system and launching controls. The planetary-gear system, which prevents the chuck from rotating around its own axis, is composed of specially cut fine-pitch precision gears. To insure smoothness of operation and to prevent backlash, the idler gear of this train is made in three layers. The central layer is integral with the spokes and hub. The two outer layers are ring gears and are loaded against the central layer by small tangential coil springs in the rim. The central layer and one outer layer mate with the hub gear, while the central and other layer engage the chuck gear. The hub and chuck gears are equal in diameter. There are two levers or arms, both bearing-mounted on the wheel shaft and prevented from rotating by clamps. The trajectory-angle arm clamps to the trajectory-angle scale, has a 90-deg adjustment, and is integral with the release arm which carries the solenoid-operated tripper. The pitch-angle arm is attached to the central gear of the planetary system, and is clamped to the trajectory-angle arm with an adjustment of ± 10 deg on the pitch-angle scale.

When the trajectory-angle arm is set at zero on its scale, the release arm hangs vertically down, and therefore would release the model on a horizontal trajectory. If, at the same time, the pitch-angle arm is set at zero on its scale, the axis of the model will be horizontal, i.e., parallel to the tangent at the point of release, and the model would fly with zero pitch angle. Now, if the trajectory-angle arm is moved a given number of degrees to any new position on its scale while leaving the pitch-angle arm clamped to it, then the release point is shifted the same number of degrees and the central gear is also rotated the same number of degrees in the same direction. The result is that the axis of the model is now parallel to the tangent at the new release point, and if released, the model would again travel with zero pitch. If, on the other hand, the trajectory-angle arm is left clamped while the pitch-angle arm is shifted, say, 5 deg, then the release point remains unchanged, whereas the model axis now makes an angle of 5 deg with the tangent at the release point. Thus the model would take off with a pitch angle of 5 deg.

On the trajectory-angle arm, on the side facing the wheel, there is a light source and a photocell. A small mirror mounted on the wheel reflects the light into the photocell every revolution when the chuck is about 20 deg before the launching point. This transmits a signal to the electronic interlocks which synchronize the operation of the tripper with that of the cameras and the lights.

Trajectory-Recording System. The cameras and flash lamps of this trajectory recording system have been described recently;[6] therefore only a brief description of this equipment will be given here.

In this installation the cameras are used as precision-measuring instruments, and many of the special features incorporated in their design were dictated by this requirement. To obtain all the necessary data from each launching, the camera system was designed to cover the entire underwater volume of the tank, as well as the above-water portion containing the trajectory from the launcher to the water surface. Since an entire test run occurs in 1 sec or less, it was decided that photographs should be taken at rates varying between 500 and 3000 per sec, per camera, depending upon the launching speed and the accelerations anticipated during a particular run.

The recording system consists of a battery of synchronized high-speed motion-picture cameras using standard 35-mm film. The main bank of five cameras records the underwater trajectory, while another bank of two or three cameras is used for recording the air trajectory. The optical coverage of the cameras is shown in Fig. 32. At the launching plane the adjacent camera fields have a 60 per cent overlap. In the vertical direction the field of view covers the entire water depth. This multiple cover-

[6] "Special Cameras and Flash Lamps for High-Speed Underwater Photography," R. T. Knapp, *Journal of the Society of Motion Picture Engineers*, vol. 49, no. 1, July, 1947, pp. 64–82.

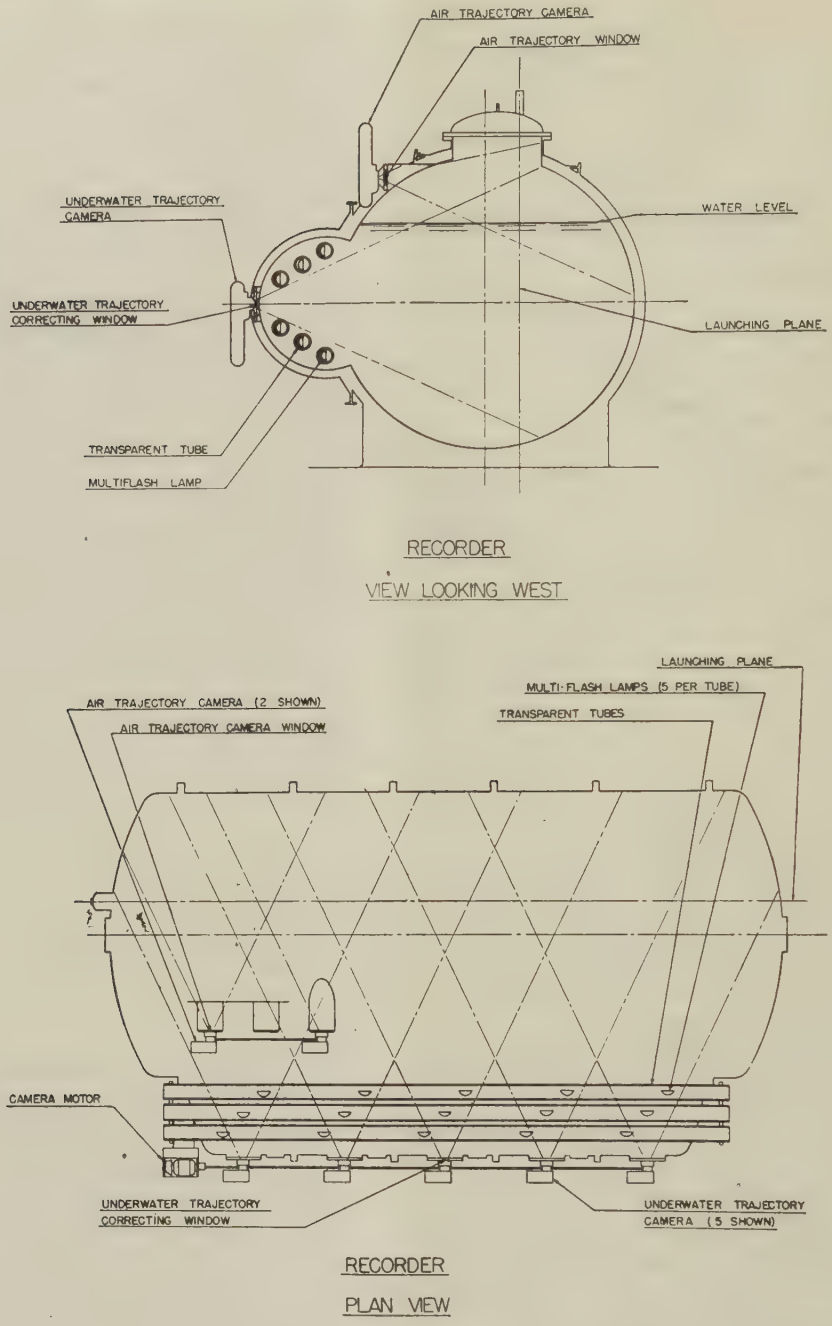

FIG. 32 ARRANGEMENT OF CAMERAS AND THEIR OVERLAPPING FIELDS OF VIEW

age makes it possible to use stereoscopic technique for the analysis of the recorded data to obtain five components of the motion, namely, longitudinal, lateral, and vertical movements, and rotation in the horizontal and vertical planes. Each camera is rigidly attached to a flanged opening in the tank shell and looks into the tank through a small window.

In the case of the underwater cameras, if a plane window were used, the result would have been reduction of the field of view due to refraction of the light in passing obliquely from the water to the air. This difficulty was overcome by using optically ground spherical windows, so positioned that the front nodal point of the camera lens is at the center of curvature of the window. Thus all primary rays pass through the interface at an angle of 90 deg and suffer no refraction; therefore there is no distortion or reduction of field. However, the curved water interface is, in effect, a negative lens which increases the effective focal length of the system and shifts the focal plane. Thus, for example, if the distance from the lens to the object is actually 12 ft, the lens must be set for a focal distance of about 14 in. when used with the spherical window. This shift in focal plane causes a field reduction of 4 per cent, compared to a field reduction of 29 per cent which would have resulted if a plane window were used.

The design requirement of a maximum rate of 3000 frames per sec made it necessary to use a continuous motion of the film because of the obvious difficulty involved in starting and stopping the film 3000 times per sec. Also, a rather high film speed was mandatory to provide a reasonable frame height. A speed of

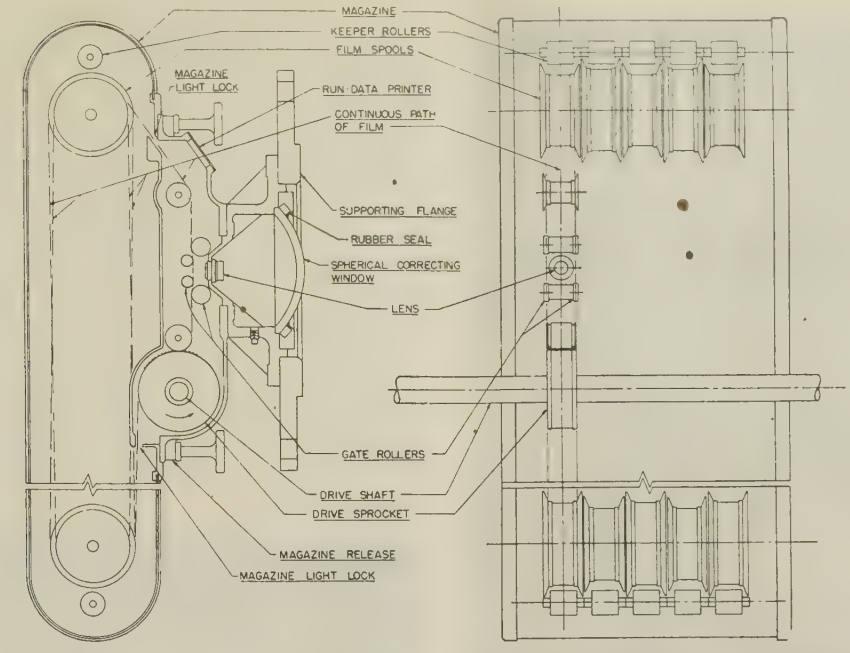

FIG. 33 UNDERWATER CAMERA WITH FILM MAGAZINE, SPHERICAL WINDOW, AND MOUNTING FLANGE

31.25 fps was selected, which at 500 frames per sec gives a standard 35-mm frame height of $^3/_4$ in., resulting directly in a projectionable motion-picture film. At the higher rates of 1000, 1500, and 3000 frames per sec, the frame heights are, respectively, $^3/_8$, $^1/_4$, and $^1/_8$ in. This high film speed makes it necessary to use extremely short exposures, of the order of two microsec, which are obtained by using flash lamps of the Edgerton type.

Fig. 33 is a drawing of one of the underwater cameras, with film magazine, spherical window, and mounting flange. The lens is a 1-in., f/2.3, Bausch and Lomb Baltar. To prevent friction, the film is guided through the focal plane by rollers instead of the usual pressure-plate arrangement. The film magazine may be detached from the camera and tilted to a horizontal position for loading. A thirty-two-ft length of film, sufficient for a single run, is stored in the magazine in a number of passes over the two sets of idler spools. The ends of the film, which extend through the light locks, are spliced together to form a slack loop about 2 ft long outside the magazine. Fig. 34 shows the arrangement of the film inside the magazine, and Fig. 35 shows a loaded magazine with the exposed loop containing the splice.

The loading operation is completed by tilting the magazine into the vertical position and threading the loop over the guide rollers and drive sprocket of the camera. With the film thus arranged in a continuous belt, it is possible to bring it up to speed gradually, expose it, and slow it down again without wasting any film or using long leaders.

All the cameras are driven through line shafting by a single synchronous motor.

Fig. 36 shows the underwater cameras and the driving motor. Fig. 37 is a close-up of the motor. To provide gradual acceleration and deceleration of the film, the motor housing is mounted in trunnion bearings so it may rotate, and the power to it is brought in through slip rings on its left-hand face. Two electrically operated brakes are provided, one to stop the shaft and one to stop the housing. To start the motor, the shaft brake is clamped, the housing brake is released, and the power is applied. The housing then begins to rotate, comes up to speed, and is

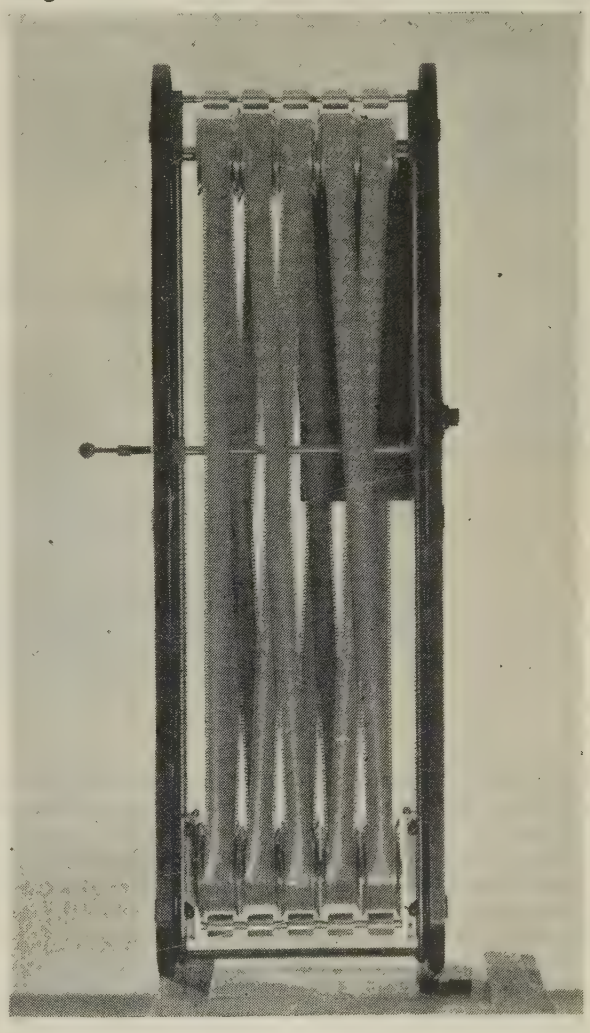

FIG. 34 BACK VIEW OF FILM MAGAZINE WITH COVER REMOEVD

FIG. 35 LOADED MAGAZINE WITH THREADING LOOP

camera during the actual recording period. Therefore provisions have been incorporated in the drive to synchronize the film travel with the instant of launching. A microswitch, actuated by a cam driven by a reduction gear from the camera shaft, makes contact once for every pass of the film belt. Before threading the film through the cameras, the camera shaft is rotated by hand until the microswitch closes, and then all the films are threaded into their respective cameras. When the camera drive is running, the microswitch signals each passage of the splices through the cameras, and controls the operation of the launcher release. Two other switches, actuated by the same cam, control the operation of the flash lamps. To insure that the splices remain abreast of each other throughout the run, it is necessary to make all the belts of exactly the same length, that is, have the same number of sprocket holes. This is accomplished by means of a film-loading device which counts the sprocket holes and thus measures out the required length.

As previously indicated, the cameras are operated with lenses continuously open and exposures are made by illuminating inter-

FIG. 37 CAMERA-DRIVE MOTOR WITH COVER REMOVED

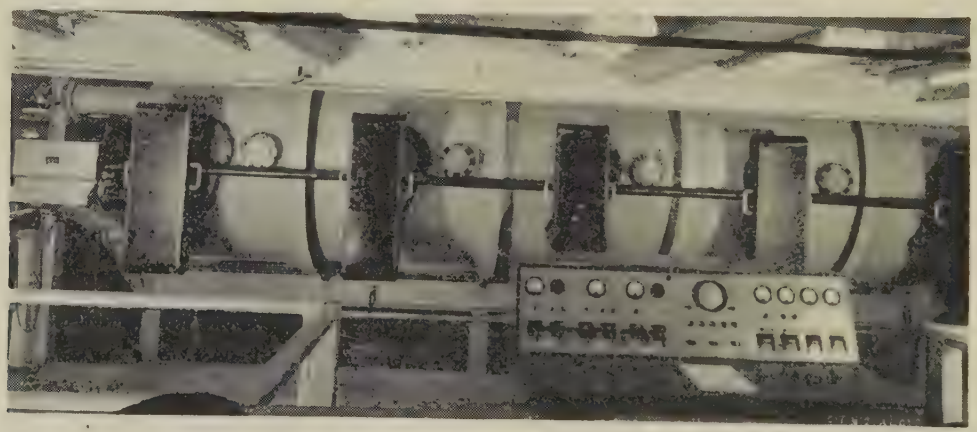

FIG. 36 UNDERWATER CAMERAS WITH DRIVE SHAFT AND MOTOR; CONTROL PANEL IN FOREGROUND

synchronized. The shaft brake is then released and the housing brake is gradually applied. As the housing slows down, the shaft takes up the difference between the synchronous speed and the housing speed, and, when the housing stops, the shaft is running at synchronous speed. By means of time-delay relays, this sequence of events proceeds automatically when the motor power is turned on. In slowing down the film after it had been exposed, this sequence is reversed.

It was noted before that in loading the film magazine, about 2 ft of film containing the splice is exposed to light. It would be undesirable to have this portion of the film pass through the

mittently the interior of the tank with flash lamps. A simple computation, involving the speed of the film and the projection ratio required for analysis, showed that the maximum effective flash duration usable would be about 2 microsec if sufficiently sharp images to give the required accuracy of measurement were to be obtained. This is approximately $^1/_{10,000}$ of the exposure time normally used in motion-picture photography. This means that extremely high light intensity is required, which could be obtained only by using a large battery of synchronized flash lamps. The assistance of Dr. Harold Edgerton of the Massachusetts Institute of Technology was enlisted because of

his wide experience in the development and use of flash lamps. The system consists of a battery of from 30 to 42 flash lamps, all operated simultaneously. Measurements indicate that the individual lamps are synchronized with each other within less than $^1/_4$ microsec.

Each lamp consists of a quartz tube about 8 in. long, filled with xenon, hydrogen, and a trace of radium bromide, with two metallic electrodes sealed into the ends of the tube. Two types of lamps are used. One consists of a straight tube with an aluminized lucite reflector designed by Dr. I. S. Bowen, Director of the Mount Wilson Observatory. The other type consists of a helical tube in a headlight-type sealed-beam reflector with smooth lens. Figs. 38 and 39 show the two types of lamps.

The power for the operation of each light is carried through an individual coaxial cable running from the light to the control panel. Each light is operated through an individual surge circuit which receives power from a large rectifier. The rectifier delivers direct current at 4000 volts, and the lights operate at twice this value through a voltage doubler incorporated in the circuit. The power consumption of each light is approximately 0.8 joules per flash. Thus at 3000 flashes per sec, the battery of 30 lamps requires a continuous input of approximately 80 kw. It must be remembered that at this speed the lights are lit only about $^1/_{200}$ of the time. This means that the power input during the period of illumination is at the rate of better than 16,000 kw. The heat generated in the tubes themselves limits the length of operation, since the tubes get quite hot and will collapse if they are operated too long. At flash rates of 1000 per sec, and above, the only significant heat dissipation is through radiation. Experiments have shown that 3600 flashes per run are the maximum that can be employed for successful high-speed operation.

A typical experiment is carried out as follows:

The camera magazines are loaded and attached to the cameras. The model is installed in the launcher, the desired trajectory and pitch angles are set, and the launcher is lowered into the tank by closing the hatch cover upon which it is mounted. The required air pressure, if below atmospheric, is adjusted by means of the vacuum pump. The launcher wheel is brought approximately to speed by manual control and is then put on automatic control which holds it exactly at the desired speed. The camera motor is turned on and the film comes up to speed automatically. The operator now starts a sequence necessary to launch the model by pressing and holding down the launching button. This operates the first of the three interlocks. The second interlock is actuated by the microswitch on the camera drive as the exposed film splices finish passing through the focal plane of the camera, and the third and final interlock, which trips the model and launches it, is actuated on the next revolution of the launching wheel after the film interlock operates. The flash lamps begin to function simultaneously with the release of the model and continue to flash until the entire length of film is exposed, at which time the lamps are automatically cut off. The equipment is then automatically shut down in reverse order of the starting sequence.

The camera motor runs at a constant speed of 31.25 rps. When the launcher runs at any multiple of that speed, the passage of the film splice through the camera and the passage of the model past the launching point occur with a fixed phase relation between them and may never coincide, in which case it would be impossible to launch the model. Provision is made therefore for changing the phase relation. This is done by rotating slowly the camera motor housing by means of a small

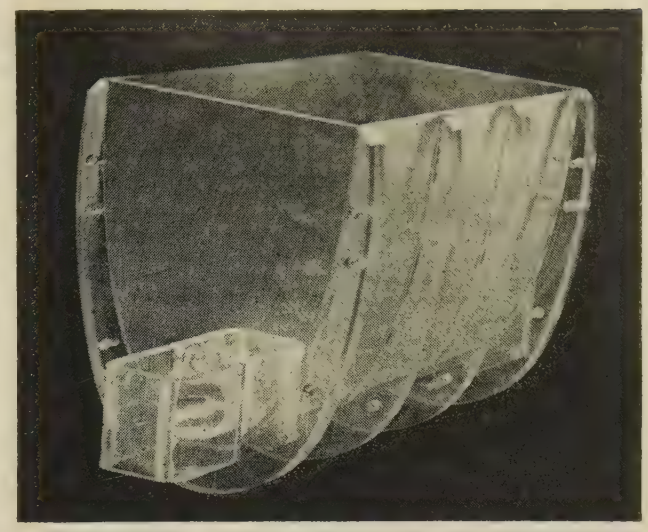

Fig. 38 Flash Lamp and Lucite Reflector

Fig. 39 Headlight-Type Lamp

electric motor geared to the housing brake. This may be seen in the lower left side of Fig. 37.

Data-Analyzing System. The basic principle of the analyzer is that it is essentially a duplicate of the recording system. Projectors take the place of the cameras and a movable screen replaces the model. All of the films from one run in the launching tank are placed in the corresponding projectors with the film strips synchronized so that the corresponding frames taken at the same time will be projected at the same time. The film drive of the projectors is a continuous shaft so that once the film strips are synchronized, they remain so during the projection of the entire run. Fig. 40 shows a line diagram of the analyzer system. It represents a point on the trajectory in which the projectile was in the field of view of cameras Nos. 2 and 3, so that projectors Nos. 2 and 3 are projecting the two images into the analyzer space. It is obvious that there is only one position in this space in which the two images will coincide. The exploring screen of the analyzer is then maneuvered until the two images both fall on it. Additional maneuvering causes the two images to fuse into one. This requires movements of the screen in three

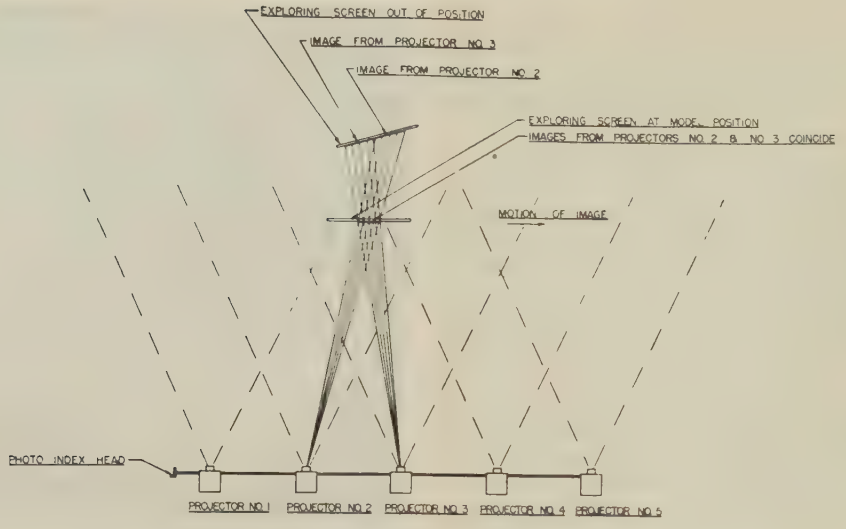

FIG. 40 SCHEMATIC DRAWING OF ANALYZER SYSTEM

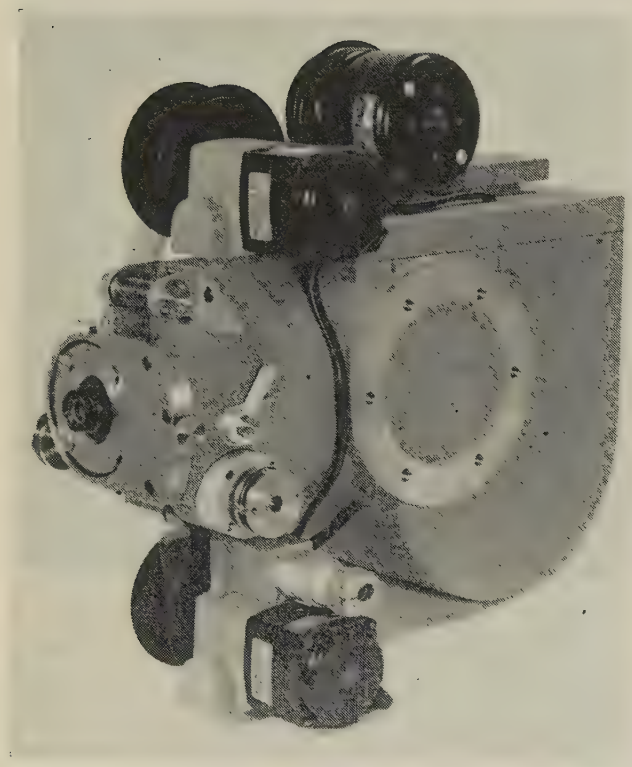

FIG. 41 ANALYZER PROJECTOR

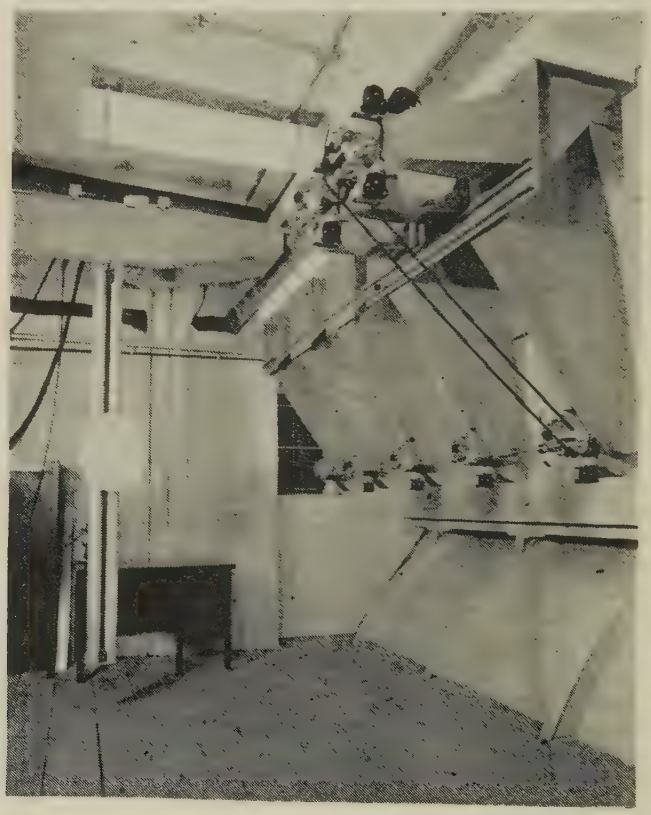

FIG. 42 DATA-ANALYZING EQUIPMENT

linear directions and also two angular motions. These movements are transferred to a battery of counters. When the screen is finally in the exact position required for the precise fusing of the images, the counters indicate the position of the projectile in space corresponding to that pair of photographs. The analyzer is built to a scale of one half that of the tank and recording equipment.

The projectors for this analyzer are precision instruments. As a first step in their construction, lenses were procured in matched pairs. One lens of the matched pair is used in the camera and the other lens in the corresponding projector. The gate mechanism is designed to hold the film exactly in the focal plane. The light source is kept at as low an intensity as is consistent with the accuracy of the readings that are required, in order to eliminate as much heat as possible which might affect both the dimensions of the film and those of the optical system. The temperature is controlled further by the employment of water cells and individual air cooling. Fig. 41 shows one of the projectors. To check the location of each frame, use is made of a series of reference marks on the rear wall of the launching tank. These marks are reproduced on a background screen at the rear of the analyzer, and before making a measurement a check is made to see that the images of the marks from the films in the

projector fall on the corresponding marks on this screen.

The exploring screen is a small disk with a half-model attached to it so the final projection is on a curved surface similar to the one photographed. The screen is carried on a mechanical transport which provides three linear and two angular motions. A carriage which spans the width of the room rides on longitudinal overhead rails. On this carriage is a pair of transverse rails on which travels a smaller carriage. Both carriages have rack-and-pinion drives. A pair of vertical guide tubes with a screw drive are suspended from the transverse carriage. These are arranged so they can be rotated in azimuth to provide one of the two angular motions. The other angular motion is obtained by rotation of the circular screen in its own plane. Selsyn repeaters and mechanical counters are used as position indicators to transmit the information to the operator's desk. Fig. 42 shows the data-analyzing equipment. It is planned to add another set of selsyn repeaters to operate recording pens at a plotting table where the three co-ordinates and two angles will be plotted against time.

Conclusions

In addition to the major pieces of equipment just described, the laboratory has available considerable auxiliary equipment which measurably widens the scope of work that can be undertaken. Three service facilities are also deserving of mention since they are of great utility to all of the laboratory research programs. These are the electronics laboratory, a photographic laboratory capable of processing both still and 16- and 35-mm film, and a precision instrument and model shop.

It is quite clear from the foregoing description that the fundamental interest of the laboratory is in basic research over a rather wide section of the field of hydrodynamics. At the same time the equipment is well adapted to yield accurate information on the characteristics of specific devices or machines. Much of the major equipment has been put into operation quite recently. Therefore it is hoped that this description of the laboratory will prove to be only the introduction to a series of studies in the field of hydrodynamics that will be referred by the laboratory to the engineering profession.

Hydraulic Problems in Connection With the Design of the Granby Pumping Plant

By E. B. MOSES,[1] DENVER, COLO.

Many unusual problems arose in the design of the Granby pumping plant which delivers water across the Continental Divide in Colorado. Owing to the 94-ft variation in suction head, the pumps are located far below ground level. A design for a subterranean plant with a cross section based upon the hydrostatic arch is analyzed. Because of limitation to voltage fluctuation when starting up, imposed by a comparatively small power supply, several methods of bringing the unit up to synchronous speed were studied. The final design comprises a discharge valve which is closed when starting, equipment for depressing the water below the runner when starting at reduced voltage or when using the unit as a synchronous condenser, a surge tank and a siphon at the upstream end of the discharge conduit. An air vent at top of the siphon is provided to stop reverse flow, and an automatic vacuum pump removes accumulation of air in the siphon.

Introduction

IT IS the purpose of this paper to discuss several new and unusual problems which were investigated during the design of the Granby pumping plant now being built for the Colorado-Big Thompson project by the United States Department of Interior, Bureau of Reclamation.

This plant is located near Granby Reservoir, 8 miles north of Granby, Colo., on the western slope of the Rocky Mountains. Water from the upper Colorado River and its tributaries will be stored in the reservoir during periods of high run-off. From the reservoir the plant will pump water up to Shadow Mountain and Grand Lakes which are joined by a short channel, and from Grand Lake it will run by gravity through the Alva B. Adams tunnel under the Continental Divide to the eastern slope of the Rocky Mountains where it will be used both for irrigation and power purposes. A plan and profile of the pumping plant are shown in Fig. 1.

There will be a 94-ft variation of water level in Granby Reservoir, from a maximum elevation of 8280 ft to a minimum elevation of 8186 ft. In the plant there are three vertical-shaft centrifugal single-stage pumps, each with a capacity of 200 cfs at the maximum pumping head of 186 ft. They are connected through flange couplings to 6000-hp 327-rpm 6600-v 3-phase 60-cycle synchronous motors. The suction line to each pump runs from a concrete intake structure located at a low point in the reservoir and consists of 87-in-ID concrete pipes each approximately 570 ft long.

Determination of Pump Setting

Because of the large fluctuation of inlet head, the long suction pipe, and the low barometric pressure at the 8180-ft altitude, it was necessary that the pump be installed well below the minimum reservoir level so as to insure freedom from cavitation throughout the wide range of head and discharge.

At the time of designing the plant, cavitation tests for this particular design of pump were not available. Sigma curves for the preliminary model of the Grand Coulee pump were studied and a minimum value of 0.112 for sigma was established. Then, since

$$\sigma = \frac{\text{Total inlet head above vapor pressure}}{\text{Net head across pump}}$$

or

$$\sigma = \frac{H_a - H_{vp} + h_s}{H}$$

then

$$\text{Total suction head, } h_s = \sigma H + H_{vp} - H_a$$

or using prototype values as follows:

		In feet
Maximum static head	=	185.00
Total suction plus velocity head (for 87-in. inlet and discharge lines)	=	4.00
Total head across pump, H	=	189.00
$\sigma H = 0.112 \times 189$	=	21.16
Vapor pressure, H_{vp} (at 70 deg F)	=	0.84
		22.00
Less barometric head, H_a (at elevation 8150)	=	—25.04
Net suction head	=	— 3.04
Velocity head at eye, $\frac{V_e^2}{2g}$ (at 200 cfs)	=	4.20
Total losses, trash rack to eye, H_{fs} (at 200 cfs)	=	1.40
Minimum static head above impeller crown required, h_s	=	2.56
Approximate height, crown above center line of pump	=	0.58
Minimum submergence required	=	3.14
Minimum reservoir elevation	=	8186.00
Center line of pump	=	8180.00
Actual submergence	=	6.00

From subsequent tests on the homologous model with a discharge corresponding to 200 cfs, a safe value for $\sigma = 0.10$ was obtained, while with a discharge of 270 cfs, corresponding to a head of 152 ft, $\sigma = 0.20$. These safe values of σ are based upon a permissible drop in efficiency of $^1/_2$ per cent. The corresponding values of σ in the plant were found to be 0.16 and 0.44, respectively, under these conditions, values sufficiently above the minimums to insure freedom from cavitation at the two extremes of normal operation.

Subterranean Plant Design Using Hydrostatic Arch

Due to topographic conditions and the setting of the pump below minimum reservoir level, the center of the pump is about 107 ft below the level of the surrounding ground.

Several designs for a subterranean station were investigated,

[1] Mechanical Engineer, Electrical Division, Hydraulic Equipment Section, Bureau of Reclamation, U. S. Department of the Interior. Mem. ASME.

Contributed by the Hydraulic Division and presented at the Annual Meeting, Atlantic City, N. J., December 1–5, 1947, of The American Society of Mechanical Engineers.

 Paper No. 47—A-93.

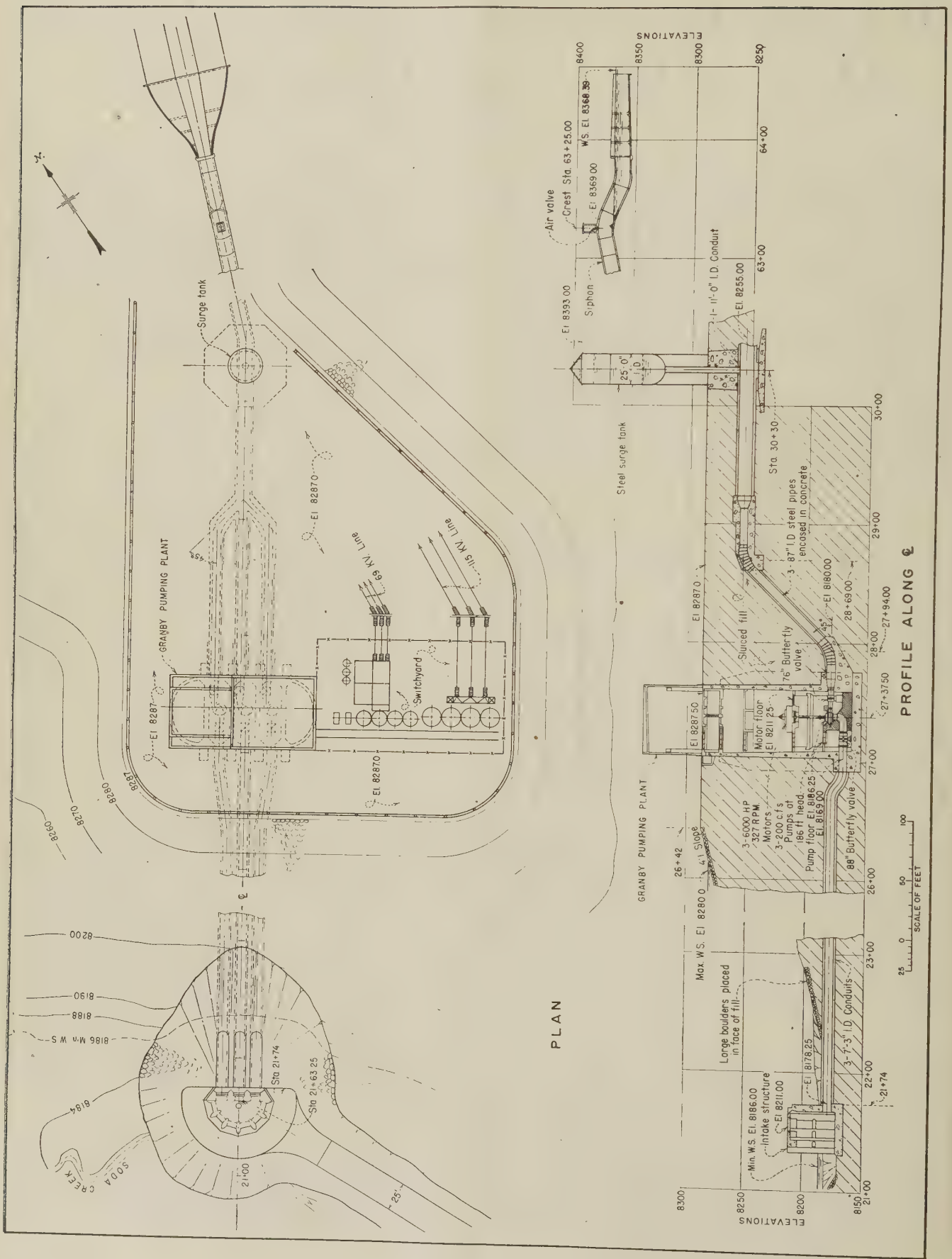
PLAN
PROFILE ALONG ℄
GRANBY PUMPING PLANT, PLAN AND PROFILE
Surge tank
GRANBY PUMPING PLANT
El 8287
El 82870
69 KV Line
115 KV Line
Switchyard
Steel surge tank
Air valve
Crest Sta. 63+25.00
W.S. El. 8368.39
El. 8369.00
Siphon
El 8393.00
11'-0" I.D. Conduit
El 8255.00
25'-0" I.D.
Sta 30+30
3-87" I.D. steel pipes encased in concrete
El 8180.00
Sluiced fill
76" Butterfly valve
El 8287.50
Motor floor El. 8211.25
3-6000 HP 327 R.P.M. Motors
3-200 c.f.s. Pumps at 186 ft. head
Pump floor El. 8186.25
El. 8169.00
88" Butterfly valve
Max W.S. El 8280.0
4:1 Slope
Large boulders placed in face of fill
Min W.S. El. 8186.00
Intake structure
El 8211.00
El. 8178.25
3-7'-3" I.D. Conduits
SCALE OF FEET
ELEVATIONS
SODA CREEK
Sta 21+74
Sta 21+63.25
8186 M.n. W.S.

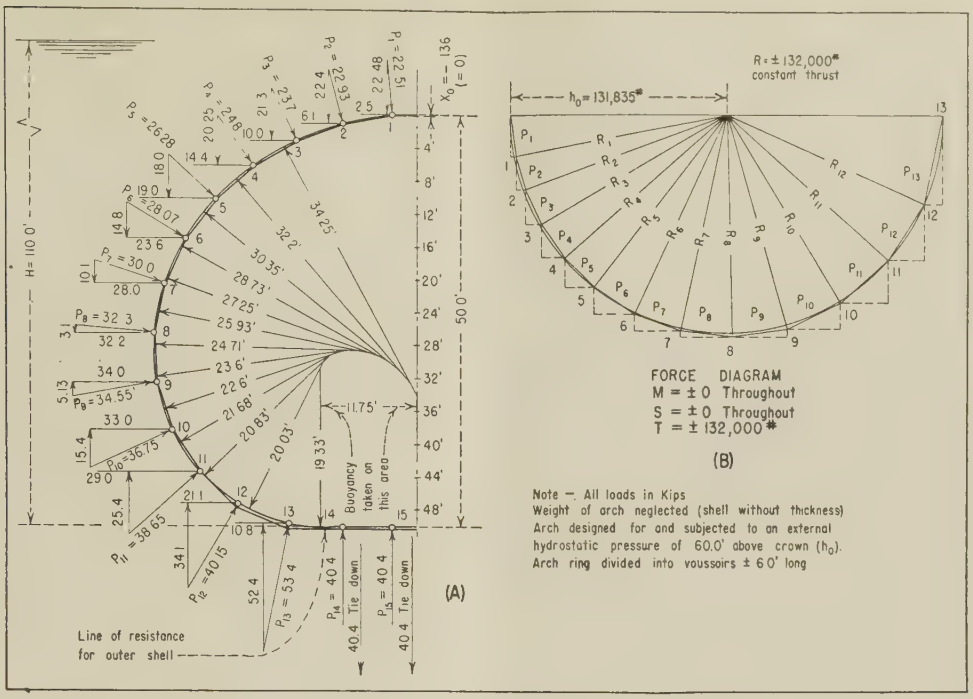

FIG. 2 ANALYSIS OF HYDROSTATIC ARCH; ARCH SHELL

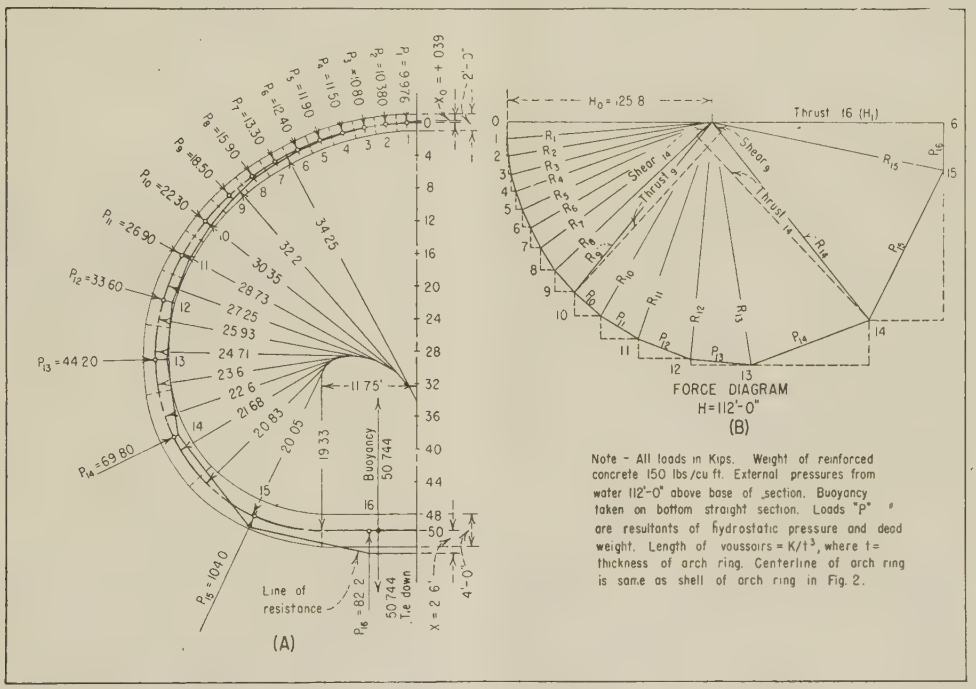

FIG. 3 ANALYSIS OF HYDROSTATIC ARCH; CONCRETE ARCH

the most interesting one being based on the principle of the hydrostatic spheroid and arch, the cross section of the station being that of a bubble or drop of water at rest on a flat surface, Fig. 2(*A*).

Figs. 2 and 3 are illustrative of the methods of designing a hydrostatic arch. In Figs. 2(*A*) and 15(*C*) the arch shape is determined from the formula

$$r_1 = \frac{H^2 - h_0^2}{4h_1}$$

where

H = hydrostatic head from surface of water level to base or invert of arch ring

h_0 = hydrostatic head from surface of water level to crown of arch ring

r_1 = radius of curvature of membrane at depth h_1 below surface of water level

In this example, the arch has been divided into zones of 4-ft

height and r_1, r_2, etc., calculated for the center of each zone. The dead weight of arch was neglected, the radial loads being those due to hydrostatic pressure only. The buoyancy or uplift is assumed to be taken by tie-down forces acting along the tangent at the base. The various stresses in the arch ring were analyzed by using the well-known method of analyzing concrete sewer sections by the elastic theory.[2] In this method, the moment and thrust at crown are computed, then the force diagram, Fig. 2(*B*), is plotted using the horizontal and vertical components of each applied load (P_1, etc.). The direction of these individual resultants (R_1, etc.) are then transferred back to the section layout, Fig. 2(*A*), starting at the crown; then the offset $x_0 = -0.136$ ft is found by the formula $x_0 = M_0/H_0$, using the previously obtained moment and horizontal thrust at the crown. The negative sign indicates that x_0 is to be laid off inside the center line of the arch ring. The directions of these resultants as they intersect their corresponding applied loads gives the "line of resistance." The closer this line of resistance is to the center line of the arch ring the less the bending moment. In this example the bending moment should be zero throughout but due to slight graphical errors and to using a finite number of radii in constructing the arch, the line of resistance departs slightly from the arch ring. It is to be noted that the shear is also zero and that the thrust (R_1, etc.) is constant throughout the arch ring.

Thus it is seen that for the example analyzed in Fig. 2, with an arch section 50 ft high, with a hydrostatic head of 110 ft above the base, that the ring, without dead weight, would merely have to resist a constant thrust of 132,000 lb per ft of width, the moment and shear being zero.

The example, analyzed in Fig. 3, uses for the center line of the arch ring the same shape as that developed in Fig. 2, but with a concrete arch ring tapering from 2 ft thick at the crown to 4 ft thick at the start of the tangent of the base section. The ring has been divided into voussoirs of lengths proportional to the moments of inertia of their cross sections about the center line of the arch ring, or dl/I is constant. The radial hydrostatic forces acting on the extrados are combined with the dead weight of the concrete, the resultant loads being assumed as acting at the center of the voussoirs. The hydrostatic head, as before, is taken as 110 ft above the center line of the arch ring at the base. The line of resistance departs somewhat from the center line of the ring, indicating small negative moments at midportion of the ring and large positive moments in the invert, the moment at the crown being very small. Again, the thrust is nearly constant throughout, and the shear values low, as shown by the semicircular form of the force diagram, Fig. 3(*B*).

Hydrostatic Arch Under Varying Head

The effect of a varying head on the moments at the crown, horizontal center line, and invert are shown by the corresponding influence lines in Fig. 4. For the designed head, the moments vary from +270,000 ft-lb to —285,000 ft-lb, while, with no external hydrostatic load, the moment reaches a maximum of +540,000 ft-lb at the invert, which is due to the dead weight only.

Fig. 5 shows the application of the hydrostatic arch to the design of a subterranean pumping station. The arch is built in a cave cut from the self-supporting rock and backfilled with loose material. Thus the arch ring has to withstand only the hydrostatic pressures due to percolation and the dead weight of the backfill and of the concrete ring. A gantry crane serves all the machinery; access to the plant is by an elevator shaft not shown. The plant is sufficiently long to accommodate the three units,

[2] "American Sewerage Practice," by L. Metcalf and H. P. Eddy, McGraw Hill Book Company, New York, N. Y., vol. 1, 1928, pp. 491–501.

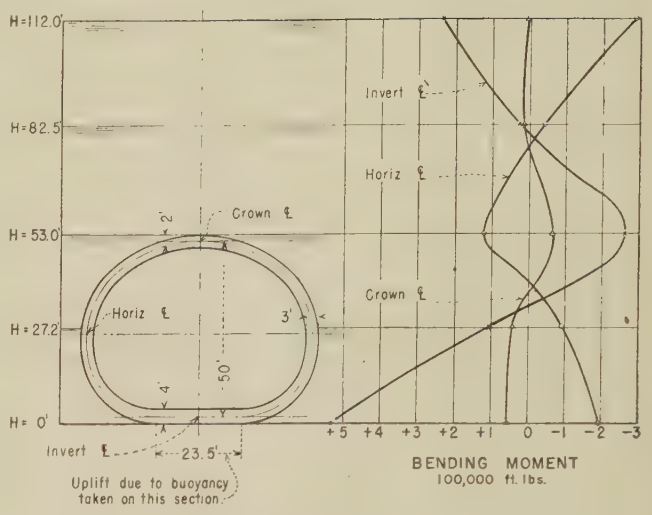

Influence diagram showing change in bending moments at crown, horizontal centerline and invert for varying depths of submergence.

Fig. 4 Analysis of Hydrostatic Arch; Influence Diagram

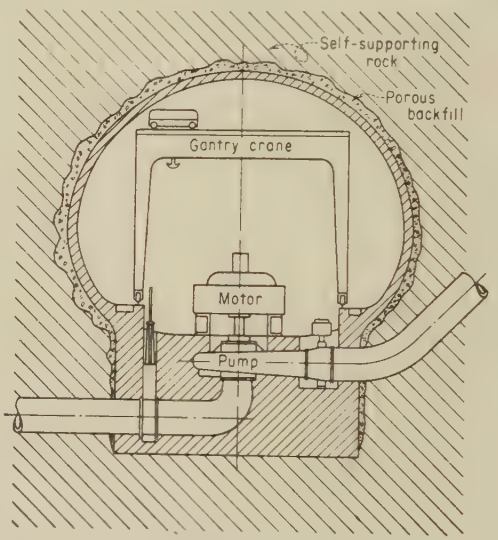

Fig. 5 A Proposed Subterranean Pumping Plant

the ends being of semidome shape of the same curvature as the arch ring.

For a given condition of exterior loading, it was found that a considerable saving in concrete and reinforcement over that required in a conventional arch could be obtained. But since the assumed conditions of exterior loading could not be controlled in practice, this design was abandoned in favor of an open concrete shaft having a rectangular central section and semicircular ends, with massive exterior buttresses and interior cross-walls for resisting the external hydrostatic and earth pressures.

Step-by-Step Motor Starting

The three Granby pumps discharge through 87-in-ID steel pipes which branch into a single 11-ft-ID concrete conduit that carries the water up to the canal flowing into Shadow Mountain Lake. The total length of the discharge line from pump to canal is approximately 3500 ft. Originally it was planned to omit the shutoff valves at the pump, and studies were made to deter-

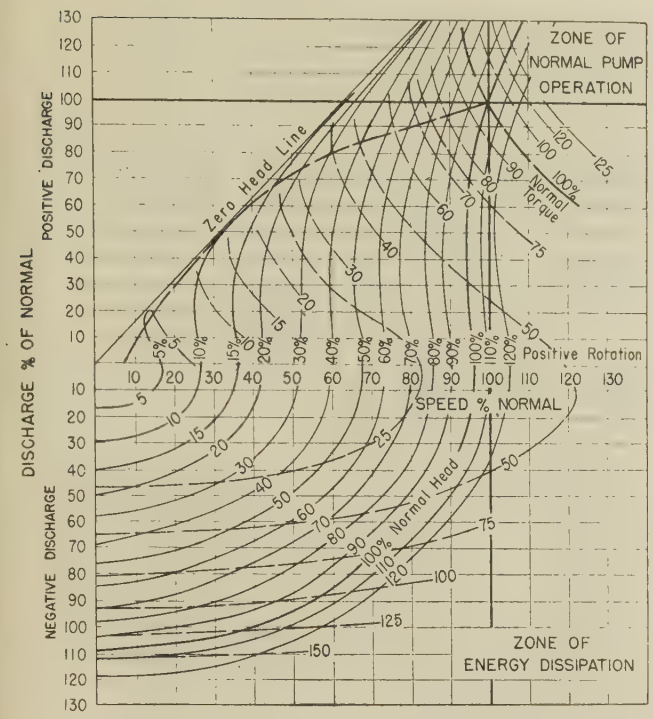

FIG. 6 DOUBLE-VOLUTE-PUMP CHARACTERISTIC DIAGRAM

mine the necessary starting characteristics for the motor and its control while the pump was accelerating and building up the head of water in the long pipe line.

An example of this type of calculation will be given, as it is believed that this method is an original approach to the problem, in which the head, discharge, power, speed, and efficiency are all variables at any instant of the starting period. To make use of this method, a pump characteristic diagram is required which will show the relationship of these several variables. Since one for the particular design used at Granby was not available, a diagram constructed from test data on model pump of quite similar type was used and is shown in Fig. 6. Since this curve has its various variables, head, discharge, torque, and speed, based on percentages of the corresponding values at the 100 per cent or rated operating point, values for the Granby pump could be readily calculated for any assumed condition during the accelerating period. In this example the motor torque is increased in uniform steps of 10 per cent up to a maximum of 110 per cent of normal, this upper value being used to provide a sufficient margin to insure prompt synchronization. It was assumed that the torque required to break away the unit from the static friction of rest would be 25 per cent of full-load torque so that the motor would not start to move until the 30 per cent torque step had been applied.

A "reservoir curve" for the discharge pipe was then plotted which gave its capacity in cubic feet, in relation to the elevation of the water surface in the pipe line. This curve was used in determining the head on the pump for each increment of time during the starting period. An example of the calculations is given in Table 1. The method in brief is as follows:

The pump is accelerated during a given time interval t_i, up to a new speed N, and from Fig. 6,[3] the corresponding percentages of head, per cent H; of discharge per cent Q; and of torque per cent T, are read. Fig. 7 gives the total friction and windage losses of the unit in kilowatts for the full range of speeds. From this curve the friction plus windage torque T_w can be found, and this added to the torque required for pumping T_p, gives the total required torque T_r, for that time interval, or

$$T_r = T_w + T_p$$

The difference between the applied motor torque T_m, as determined by the controller, and the required torque T_r, is that available for acceleration T_a, or

$$T_a = T_m - T_r$$

The acceleration so produced is

$$\frac{dn}{dt} = T_a \times \frac{308}{WR^2}$$

expressed in (rpm/sec), from which the new speed at the start

[3] "Centrifugal Pump Performance as Affected by Design Features," by R. T. Knapp, Trans. ASME, vol. 63, 1941, Fig. 15, p. 258.

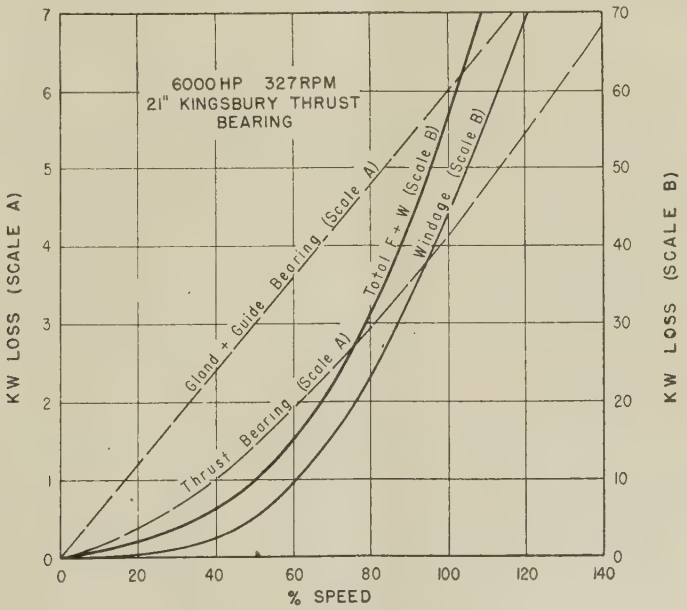

FIG. 7 FRICTION AND WINDAGE CURVES

TABLE 1 ACCELERATION DIAGRAM FOR GRANBY PUMP, LOCATION A WITH SURGE SUPPRESSOR, COMPUTATIONS FOR FIG. 8

Normal Data for Pumping Unit

H_n = 188 ft N_n = 327 R.P.M Q_n = 200 c.f.s. P_n = 6,000 H.P for motor

T_n = motor torque = 96,400 lb-ft. WR^2 = 463,000 lb-ft^2 T.W. Elev. = 8186.

ITEM	TOTAL TIME t	TIME INTERVAL t_i	HEAD IN PER-CENT OF NORMAL FOR (5) (FIG. 6)	DISCHARGE IN PERCENT OF NORMAL (FIG. 6)	SPEED IN PER-CENT OF NORMAL = (7) x N_n (FIG 6)	ACCEL. ERATION $\frac{dN}{dt}$ x $\frac{308}{WR^2}$ = (16)[ABOVE] R.P.M. per sec.	SPEED = Σ[(6)x (21)]	WINDAGE + FRICTION OF PUMPING UNIT FROM FIG 7	WINDAGE + FRICTION OF PUMPING UNIT TORQUE T_w = (70403 x(8)) ÷ (7)	WINDAGE + FRICTION OF PUMPING UNIT TORQUE IN PER-CENT OF NORMAL = (9) ÷ T_n	TOTAL APPLIED MOTOR TORQUE IN PER-CENT OF NORMAL	TOTAL APPLIED MOTOR TORQUE T_m = T_n x (11)	PUMPING TORQUE PUMP ONLY IN PER-CENT OF NORMAL (FIG. 6)	PUMPING TORQUE PUMP ONLY T_p = T_n x (13)	PUMPING TORQUE T_r TOTAL REQUIRED = T_w + T_p = (9) + (14)	TORQUE, T_a, AVAILABLE FOR ACCEL-ERATION = T_m - (T_w + T_p) = (12) - (15)	DISCHARGE Q_1 OF PUMP = (4) x Q_n	VOLUME DISCHARGED DURING INTERVAL = Q x t_i = (17) x (2)	TOTAL VOLUME DISCHARGED INTO PIPE = Σ (18)	W.S ELEV-ATION IN PIPE FOR COL. (19)	STATIC HEAD H FOR COL. (20) = (20) - T.W. ELEV. = (20) - 8186	STATIC HEAD IN PER-CENT OF NORMAL = (21) - H_n
(0)	Seconds (1)	Seconds (2)	(3)	(4)	(5)	R.P.M. per sec. (6)	R.P.M. (7)	K.W. (8)	Ft.-lbs. (9)	(10)	(11)	Ft.-lbs. (12)	(13)	Ft.-lbs. (14)	Ft.-lbs. (15)	Ft-lbs. (16)	c.f.s. (17)	Cubic feet (18)	Cubic feet (19)	feet (20)	feet (21)	(22)
1	0							0	0	0	10											
2	10	10						0	0	0	20											
3	20	10						0	0	0	30	28,920										
4	21	1	0 (0)	0	5.9	19.2	19.2	0.4	147	0.15	30	28,920	0	0	147	28,773	0	0	0			
5	22	1	1.5 (4.0)	15.5	11.7	19.1	38.3	0.9	165	0.17	30	28,920	3.5	3,374	3,539	25,381	31	31	31			
6	23	1	3.5 (6.5)	23.0	16.9	16.9	55.2	1.6	204	0.21	30	28,920	6.0	5,784	5,988	22,932	46	46	77			
7	25	2	7.0 (10.0)	38.0	26.2	15.2	85.6	2.9	239	0.25	30	28,920	7.5	7,230	7,469	21,451	76	152	229			
8	28	3	8.2 (14.0)	58.0	39.3	14.3	128.5	6.0	329	0.34	30	28,920	17.5	16,870	17,199	11,721	116	348	577			
9	31	3	11.5 (15.0)	69.0	46.5	7.8	151.9	8.5	394	0.41	30	28,920	24.0	23,140	23,534	5,386	138	414	991	8203.8	17.8	9.5
10	34	3	17.0	72.0	49.8	5.6	162.7	10.0	433	0.45	30	28,920	27.5	26,510	26,943	1,977	144	432	1423			
11	37	3	20.0	73.0	50.9	1.3	166.6	11.0	465	0.48	30	28,920	29.2	28,150	28,615	305	146	438	1861	8220.0	34.0	18.1
12	37						166.6	11.0	465		40	38,560		28,150	28,615	9,945						
13	38	1	22.0	74.0	53.0	6.6	173.2	11.5	467	0.48	40	38,560	32.5	31,330	31,797	6,763	148	148	2009			
14	40	2	25.0	75.0	55.7	4.5	182.2	13.0	502	0.52	40	38,560	35.5	33,740	34,242	4,318	150	300	2309			
15	43	3	29.0	75.5 (76.5)	58.4	2.9	190.9	14.7	542	0.56	40	38,560	38.0	36,630	37,172	1,388	151	453	2762	8238.0	52.0	27.7
16	45	2	32.0 (31.0)	76.3 (77.0)	58.9	0.92	192.7	15.4	563	0.58	40	38,560	39.4	37,980	38,543	17	152	304	3066	8246.0	60.0	31.9
17	45						192.7	15.4	563		50	48,200		37,980	38,543	9,657						
18	46	1	34.0 (32.0)	76.3 (78.0)	60.9	6.4	199.1	16.0	566	0.59	50	48,200	42.0	40,490	41,056	7,144	153	153	3219	8250.0	64.0	34.0
19	48	2	36.0 (35.5)	77.0 (80.0)	63.8	4.8	208.7	18.0	607	0.63	50	48,200	45.0	43,380	43,987	4,213	154	308	3527	8258.0	72.0	38.3
a	51	3	39.0	81.5	66.4	2.8	217.1	20.4	662	0.69	50	48,200	48.5	46,750	47,412	788	163	489	4041	8271.5	85.5	45.5
b	53	2	39.5	81.7	66.7	0.52	218.1	21.4	691	0.72	50	48,200	49.1	47,330	48,021	179	163	326	4367	8280.0	94.0	50.0
20	48						208.7	18.0	607		60	57,840		43,380	43,987	13,853						
21	49	1	39.8	78.5	66.6	9.2	217.9	20.3	656	0.68	60	57,840	49.0	47,240	47,896	9,944	157	157	3684	8262.5	76.5	40.7
22	51	2	47.0	81.5	70.7	6.6	231.1	22.8	695	0.72	60	57,840	53.0	51,090	51,785	6,055	163	326	4010	8270.7	84.7	45.1
23	54	3	52.5	83.5	74.3	4.0	243.1	26.3	762	0.79	60	57,840	57.0	54,950	55,712	2,128	167	501	4511	8283.5	97.5	51.9
24	55	1	53.5	84.0	74.8	1.4	244.5	26.7	769	0.80	60	57,840	58.0	55,910	56,679	1,161	168	168	4679	8288.0	102.0	54.3
25	55						244.5	26.7	769		70	67,480		55,910	56,679	10,801						
26	56	1	57.0	85.5	77.0	7.2	251.7	28.5	797	0.83	70	67,480	61.5	59,290	60,087	7,393	171	171	4850	8292.5	106.5	56.6
27	58	2	61.5	87.0	80.0	4.9	261.5	31.6	851	0.88	70	67,480	65.0	62,660	63,511	3,969	174	348	5198	8301.5	115.5	61.4
28	60	2	66.0	88.0	81.6	2.6	266.7	33.9	895	0.93	70	67,480	68.0	65,550	66,445	1,035	176	352	5550	8311.0	125.0	66.5
29	60						266.7	33.9	895		80	77,120		65,550	66,445	10,675						
30	61	1	69.0	90.0	83.7	7.1	273.8	35.5	913	0.95	80	77,120	73.0	70,370	71,283	5,837	180	180	5730	8315.5	129.5	68.9
31	63	2	74.0	92.0	86.1	3.9	281.6	37.7	943	0.98	80	77,120	76.0	73,260	74,203	2,917	184	368	6098	8324.5	138.5	73.7
32	64	1	76.6	92.5	86.7	1.9	283.5	39.0	969	1.01	80	77,120	77.5	74,710	75,679	1,441	185	185	6283	8330.0	144.0	76.6
33	64						283.5	39.0	969		90	86,760		74,710	75,679	11,081						
34	65	1	80.5	93.5	89.0	7.4	290.9	41.5	1,004	1.04	90	86,760	80.5	77,600	78,604	8,156	187	187	6470	8334.7	148.7	79.1
35	67	2	85.5	95.0	92.3	5.4	301.7	45.7	1,066	1.11	90	86,760	85.0	81,940	83,006	3,754	190	380	6850	8344.5	158.5	84.3
36	68	1	87.5	95.5	93.0	2.5	304.2	46.5	1,076	1.12	90	86,760	87.0	83,870	84,946	1,814	191	191	7041	8349.5	163.5	87.0
37	69	1	89.8	96.0	93.4	1.2	305.4	47.4	1,093	1.13	90	86,760	88.5	85,310	86,403	357	192	192	7233	8354.5	168.5	89.6
38	69						305.4	47.4	1,093		100	96,400		85,310	86,403	9,997						
39	70	1	92.8	97.0	95.4	6.6	312.0	50.3	1,135	1.18	100	96,400	91.5	88,210	89,345	7,055	194	194	7427	8360.5	174.5	92.8
40	72	2	97.9	98.0	98.3	4.7	321.4	54.5	1,194	1.24	100	96,400	96.0	92,540	93,734	2,666	196	392	7819	8370.0	184.0	97.9
41	74	2	100.0	99.0	99.4	1.8	325.0	56.0	1,213	1.26	100	96,400	97.5	93,990	95,203	1,197	198	396	8215	8374.0	188.0	100.0
42	74						325.0		1,213		110	106,040		93,990	95,203	10,837						
43	75	1			101.6	7.2	332.2				110	106,040										

of the next time interval t_i, is obtained. This process is continued until the required torque equals the applied motor torque, or $T_r = T_m$, at which time acceleration will cease and the controller must move up to a new step, increasing T_m by a predetermined amount, in this example by 10 per cent.

The data given in Table 1 have been plotted in Fig. 8 where per cent torque versus time in seconds is given in the upper set of curves. Here it is shown that the pump starts 20 sec after the controller closes the circuit, the torque having risen to 30 per cent in three equal increments of 10 per cent each, and has pulled into synchronism 74.5 sec after the beginning of the starting sequence, or 54.5 sec after breakaway.

In the lower set of curves the per cent of head, discharge, and speed are plotted against time. In these curves, the values of H, Q, N, and T at any instant were obtained by starting at the origin of the pump characteristic, Fig. 6, and proceeding along a smooth curve to the 100 per cent point, as indicated by the heavy dotted line, and assuming points by trial and error which satisfy the available head, torque, and speed; remembering that the head produced by the pump must always equal or exceed the static head of water in the pipe line at that instant; that the torque must not exceed the motor torque T_m, for that given step; and that the speed is in agreement with that found by the summation of the previous accelerations.

Starting by Impulse Water Wheel

One method proposed for starting the unit with a minimum of line disturbance is shown in Fig. 9. The unit would be brought up to synchronous speed by means of a small impulse water wheel mounted directly on the main shaft under the motor. Four $^7/_8$-in-diam jets, discharging under a pressure of 300 psi, impinge on the buckets of an enclosed Pelton wheel, developing up to 165 hp at the normal speed of 327 rpm, which should produce ample torque to bring the unit up to synchronism if the impeller were unwatered by compressed air. The high-pressure water for the jets would be supplied by a 400-psi 1260-gpm boiler feed pump, and the discharge from the water wheel led to the station sump, from whence it would be removed by the regular sump pump. Speed control during the period of synchronization would be by throttling the high-pressure supply, and by the use of the regular service air brakes.

The characteristic of an impulse wheel gives the maximum torque at zero speed; however, the breakaway torque of the unit would be kept down to a reasonable value by introducing pressure oil under the collar of the motor thrust bearing in sufficient amount to float the rotating parts on an oil film.

Starting Tests on Model Pump

In order to obtain data[4] for various methods of starting and stopping the pumping unit, an 8-in. motor-driven vertical pumping unit was set up in the hydraulic laboratory with the various valves and pressure-indicating devices as shown in Figs. 10 and 11. This pump, while not homologous with the Granby unit, was of a sufficiently similar type; and the "model" scale was 1:6.3 based on impeller diameters. Pressure cells, PC-1 to PC-6, operating on the principle of a Wheatstone bridge, were connected to an oscillograph to record the fluctuations of pressure in the suction and discharge lines. Photographic oscillograph records of several tests have been replotted to a common scale in Figs. 12 and 13. The input to the motor in amperes is also shown, taken from the oscillograph record, but is not a reliable indication of the power required owing to the changes in power factor for various loads on the induction motor.

The first series of tests were conducted with the setup shown in Fig. 10. To test out the impulse-starting scheme, a $^3/_{16}$-in. brass plate was attached to the top of the impeller and 30 buckets cut at a 20-deg angle by a $^1/_4$-in. $\times$ $1^1/_2$-in-diam key-seat cutter, Fig. 14. Four $^1/_4$-in-diam jets of water were arranged to impinge along the inner curve of the buckets as shown. A series of tests were run with the discharge valve closed, 9-ft positive suction head in the tank reservoir, and pressure varying from 35 to 100 psi in the line supplying the jets. It was found that a minimum of about 60 psi was required to bring the unit up to 900 rpm

[4] From the USBR, Hydraulic Laboratory Reports Nos. 113 and 150.

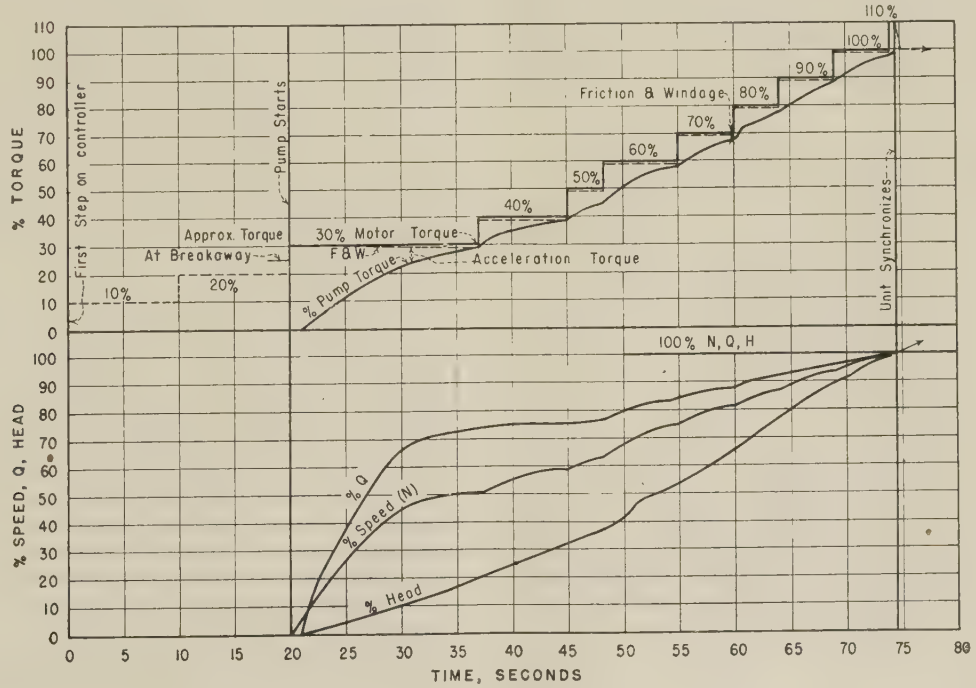

Fig. 8 Acceleration Diagram

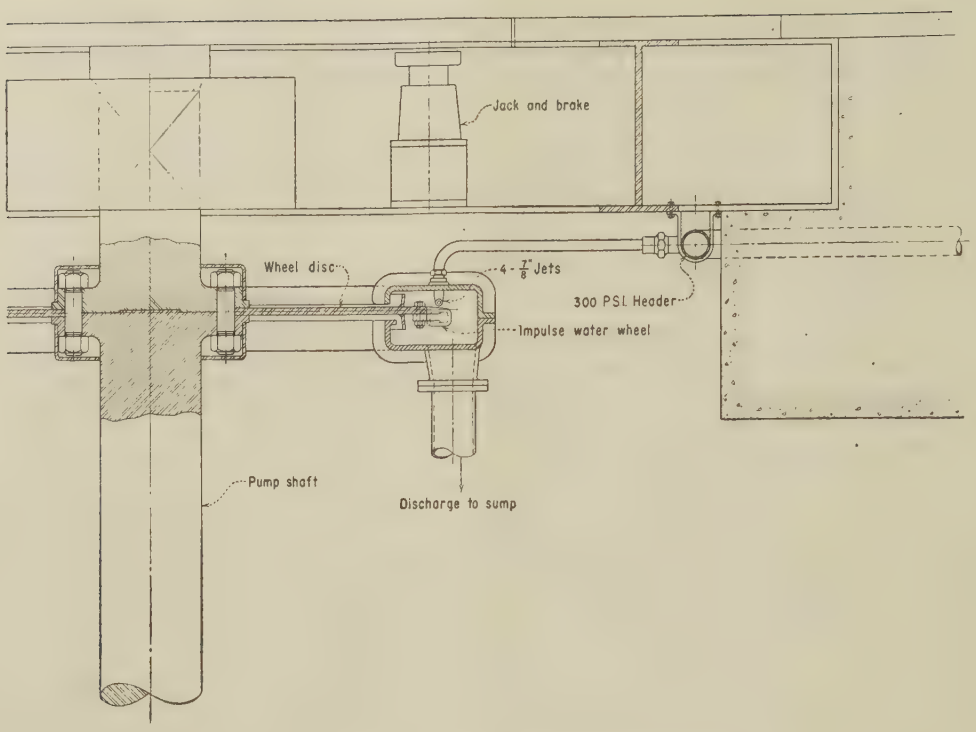

FIG. 9 HYDRAULIC STARTER, INSTALLATION DETAILS

synchronous speed. The 2-in. by-pass had to be nearly wide open to take care of the discharge from the jets.

Tests were made with the buckets in place and also with buckets filled with type metal. It was found that this design of bucket resulted in an over-all loss of efficiency of about 4 per cent, this considerable loss being largely due to the effect of water being circulated in the buckets themselves, similar to the action of the liquid in the "fluid drive" or hydraulic coupling. It it evident that any such design wherein the buckets are revolving in water during the normal operation of the pump would result in excessive losses in the prototype. However, the design indicated in Fig. 9, wherein the buckets revolve in air, would be entirely feasible, as the loss on the prototype due to air drag as computed would not exceed 1 kw or 0.02 per cent.

A second series of tests were conducted with the setup in Fig. 11. In this arrangement, a booster pump was connected to the suction pipe to give the required higher inlet head which could not be obtained with the tank reservoir, an intake valve added, and the air admitted to the suction pipe instead of to the discharge pipe.

Various tests were made and oscillograph records obtained (1) with the discharge valve open and with the throttling by intake valve, both with and without aeration or admitting air to the suction side; and (2) with the intake open and throttling by the discharge valve, air being admitted to suction side of the pump. In (1) severe surges and cavitation occurred during both the starting and stopping periods, which proved this method of operation unsuitable for the prototype. The method of pump operation adopted is based on (2) and is illustrated in Figs. 12 and 13, with the intake valve open, by-pass open, with aeration (suction vent open), and throttling by the discharge valve.

In the starting cycle, Fig. 12, the pump is started with the discharge valve closed and water depressed below the level of the impeller by compressed air. The air is then exhausted and, when the case is nearly free of air, the pump suddenly primes and shutoff head conditions are reached. As the discharge valve is opened, flow is established and the head drops to normal. In the stopping cycle, Fig. 13, the discharge valve, as it nears closure, builds up the head to shutoff conditions, then as compressed air is admitted to the suction tube, the head drops. When the level has reached the bottom of the impeller and the net pumping head is approximately zero, the motor is disengaged.

It is seen that in this final scheme of operation, Figs. 12 and 13, there are no severe surges, the heads gradually building up or dropping, and that they are always positive. For this reason this method will be adopted in the prototype installation, as it will reduce power surges as well as the likelihood of cavitation.

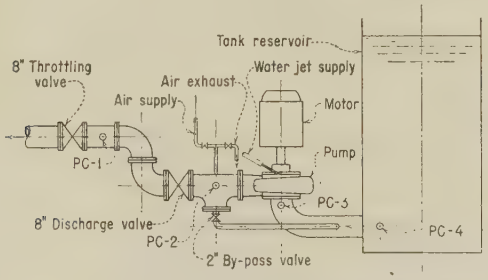

FIG. 10 MODEL PUMP SET-UP FOR IMPULSE-STARTING TESTS

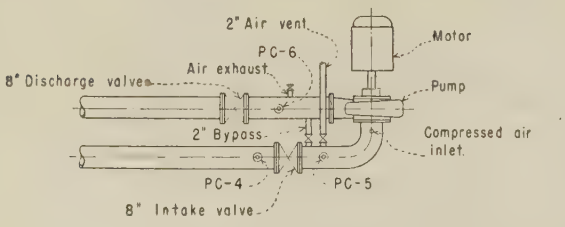

FIG. 11 MODEL PUMP SETUP FOR STARTING TESTS WITH SUCTION AND DISCHARGE VALVES

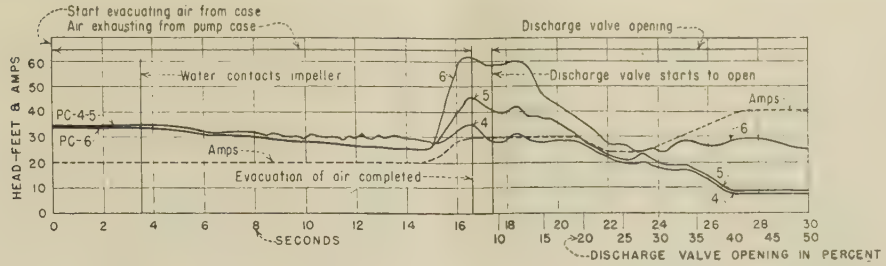

FIG. 12 STARTING CYCLE, THROTTLING BY DISCHARGE VALVE, WITH AERATION

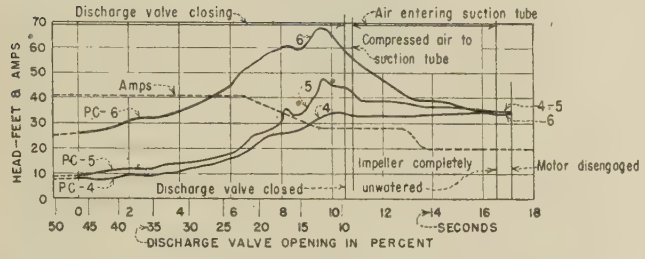

FIG. 13 STOPPING CYCLE, THROTTLING BY DISCHARGE VALVE, WITH AERATION

OPERATION OF PUMPS AT GRANBY

Since other considerations led to the adoption of a butterfly valve in both the suction and discharge passages of each pump, Fig. 1, the methods described of impulse water-wheel starting and step-by-step electric-controller starting were not used.

Ordinarily, the Granby plant will be connected to the power system on the eastern slope of the Rockies through a 115-kv transmission line. This line extends over much mountainous country, crossing the Continental Divide by way of the 11,700-ft Buchanan Pass, and, as outages due to storms, slides, etc., are likely to occur, the pumping plant has been designed so that the pumps can be started on the power from the Green Mountain plant which is located on the western slope. The two 12,000-kva units in this plant are connected through a 69-kv line, 45 miles long, to the Granby plant. When the line over the Continental Divide is out of service, the pumps would be started at reduced voltage with impellers unwatered by compressed air, the discharge butterfly valve and 8-in. by-pass both being closed. The pumps having been brought up to speed on Green Mountain power, water is then admitted to the impeller and normal operation is established. With this method, a minimum of disturbance would occur on the comparatively low-capacity Green Mountain system.

In starting from the main power system of the eastern slope full voltage will be used, the discharge butterfly valve will be closed and the pump will be full of water. The 8-in. by-pass valve will be open to allow sufficient water to circulate for cooling the pump. Under these shutoff conditions, the pump will require about 50 per cent of normal full-load power.

It may be noted here that the pump unit may be used as a synchronous condenser when the impeller is unwatered. The butterfly valve in the suction pipe is closed only when unwatering the pump for inspection and repair, since the placing of bulkhead gates at the intake structure is involved except at the lowest reservoir levels.

CONTROL OF PUMPING UNIT

The pumping unit may be controlled from two stations, one on the floor at ground level at elevation 8287.50, the other on the pump floor below at elevation 8186.25 ft. The starting procedure is divided into two parts, as follows:

1 Putting auxiliary equipment into operation. This includes guide-bearing oil pump, thrust-bearing oil pump, opening valve for supplying water to motor cooler and thrust-bearing cooler, and opening valve to pump gland seal and pump guide-bearing cooler.

2 Starting the motors through automatic-control switch gear which includes field-application equipment in cubicles adjacent to the motors.

For normal or full-voltage starting, after the motor is synchronized, a control switch is operated which opens the butterfly discharge valve while simultaneously closing the by-pass valve.

For reduced-voltage starting, the same procedure is followed, except that, in addition to the operation of the foregoing auxiliaries, cooling water is admitted to the seal rings, the air vent to the pump casing is closed, and air is admitted to the casing to depress the water surface below the impeller to a level determined by an automatic float switch.

After the motor has been synchronized at reduced voltage, open-circuit transition to full voltage will be effected. When the motor is on the line, the casing air vent is opened and the pump is allowed to fill with water when normal pumping will be established by opening the butterfly discharge valve and closing the by-pass valve.

Table 2 shows the estimated torques required by the pump, based on 6000-hp maximum motor output at 327 rpm.

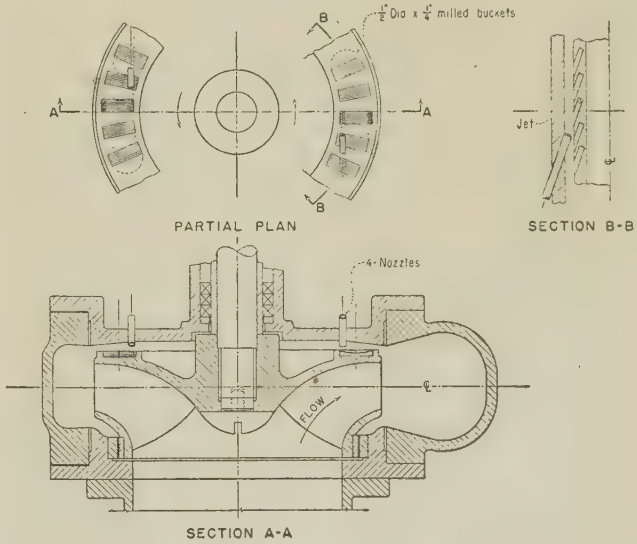

FIG. 14 IMPULSE STARTING FOR TEST PUMP

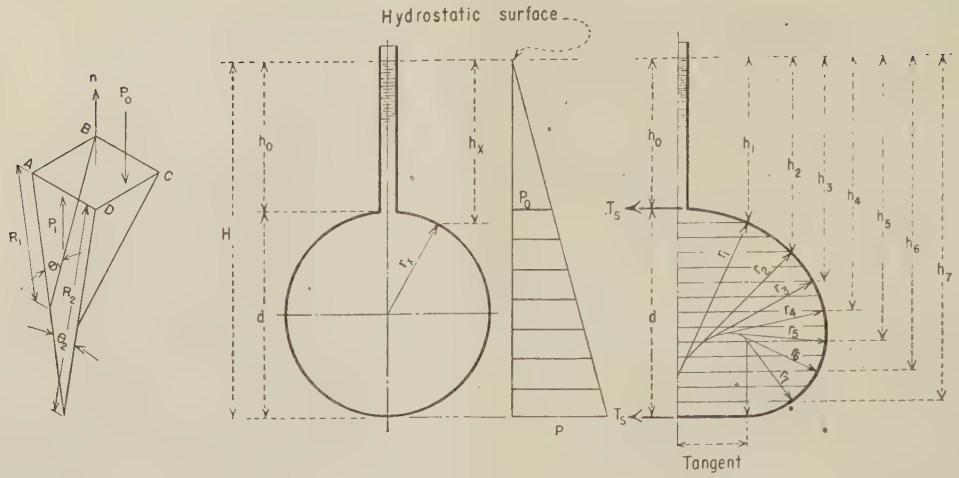

FIG. 15 DIAGRAM SHOWING BASIC FORMULAS FOR SPHEROID AND HYDROSTATIC ARCH

TABLE 2 TORQUE REQUIREMENTS OF PUMPING UNIT

	Torque ft-lb	Kva	Notes
Full load, normal pumping	96400	4920	(0.95 power factor)
Shut off, impeller submerged	49000	2410	(0.95 power factor)
Breakaway, thrust bearing oil immersed	11580	29400	(Inrush power—full voltage)
Breakaway, thrust bearing oil immersed	11580	4000	(Inrush power—38.6 per cent voltage)
Breakaway, thrust bearing supported on oil film	4800	29400	(Inrush power—full voltage)
Breakaway, thrust bearing supported on oil film	4800	4000	(Inrush power—38.6 per cent voltage)
Unit motoring at synchronous speed, impeller unwatered	1230	57	.....

SURGE TANK AND DISCHARGE VALVES

A 25-ft-diam plate-steel surge tank is connected to the 11-ft-diam discharge conduit at its lower end near the triple branch connection from the pumps. The top of the tank is at elevation 8393 or about 106 ft above the ground line, or 24 ft above the siphon invert. The bottom of the cylindrical portion of the tank is at elevation 8336, below which is a hemispherical head, 36.5 ft above the ground. A 5.25-ft-diam riser connects the hemispherical tank bottom to the discharge conduit and is designed to give a 50-ft head loss with a flow of 1000 cfs into or out of the surge tank.

With three pumps running, the maximum change in water level in the surge tank caused by the emergency closure of all three butterfly valves has been calculated and is given in Table 3.

The 76-in. butterfly discharge valves are operated by hydraulic servomotors which receive oil from a central oil-pressure system, located at one end of the building. The valves are designed for a full 90-deg opening or closing movement to be made in 24 sec under normal conditions of operation. The control mechanism consists of a governor-type four-way piston valve with solenoid-operated pilot valve. A second solenoid for emergency shutdown will operate to close the 76-in. butterfly valve at a faster rate, causing the first 67.5 deg of closing movement in 4 sec and the final 22.5 deg of closure in 6 sec, or the total closure in 10 sec. This emergency operation would be initiated by failure of power supply to the main-pump motor.

The design of the butterfly-valve control mechanisms follows closely that of the conventional gate-shaft governor for hydraulic turbines. These control mechanisms were purchased separately from the butterfly valves, and this selection permitted the use of fully developed manual and automatic controls and mechanisms for operation of the discharge valves in the same manner as for hydraulic turbines. This is particularly advantageous at Granby since some of the pumping will be done at short intervals each day to utilize off-peak secondary power. Also, the starting and stopping sequences should be as nearly automatic as good design will permit. The plant will be operated as a comprehensive unit of the power system by operators who are trained to handle hydraulic-power-plant equipment.

TABLE 3 PRESSURE SURGES DURING EMERGENCY SHUTDOWN

Reservoir elevation, ft	Butterfly valve operative	Downsurge below static, ft	Upsurge above static, ft
8280	Yes	26.6	14.3
8280	No[a]	30.3	15.7
8186	Yes	20.1	12.2
8186	No[a]	28.2	15.9

[a] In order to obtain the maximum upsurge when the butterfly valves fail to close at the prescribed time (10 sec), it was assumed that the effective closure would occur at approximately 34 sec after power failure when the water-surface elevation in the surge tank had reached a minimum value.

DISCHARGE SIPHON

The outlet from the 11-ft-diam conduit consists of a concrete siphon with crest of invert at elevation 8369 ft, the water surface in the canal to Shadow Mountain Lake being at elevation 8368.39 ft. The siphon is of circular cross section of the same diameter as the conduit and is essentially a 35-deg elbow with radius of curvature equal to 33 ft or 3 pipe diam. The upstream leg is turned into a horizontal direction with transition to a square section as it enters the canal.

To insure rapid breaking of the water column when the pump stops, an automatic type of air vent is provided at the top of the siphon. The control is arranged to insure prompt opening of the air valve under emergency conditions of power failure. A small

vacuum pump, controlled by a float in a separate float well, is used to remove the air pocket at the top of the siphon and to insure the siphon operating full at all times and at its best efficiency. The air-vent valve, vacuum pump, and float control are protected from the weather by a suitable metal cover.

The use of the automatically closing butterfly discharge valve, and siphon with automatically operated air vent, should prevent the emptying of the long discharge conduit when power to pump is cut off, and also eliminate the attendant high reverse-speed rotation of the pump as well as the necessity for refilling the long conduit after each shutdown.

Conclusions

A number of preliminary investigations have been described, from which the final designs of the Granby pumping plant and equipment were evaluated. From these investigations the following principal conclusions may be deduced:

1 A design for the subterranean plant based on the hydrostatic arch would effect a substantial saving in amount of reinforced concrete but could not be used at Granby owing to the variable external loads with resulting high bending stresses in the membrane.

2 Several satisfactory methods of starting the pump motors with a view to keeping the attendant transmission-line disturbance to a minimum are feasible. The use of supplemental model tests to investigate the power required, together with the resulting hydraulic pressure surges when starting the pump under various combinations of suction and discharge-valve openings and of air admissions, is an essential adjunct to developing fully the electrical requirements of the power-supply system.

3 From actual experiments conducted and from related investigations, it was established that normal operation could be accomplished by starting under shutoff conditions with full voltage; and for emergency operation on the limited-capacity system, starting at reduced voltage, with the pump impeller unwatered, would be required.

4 A surge tank on the discharge conduit, together with the automatically controlled butterfly discharge valve, will limit pressure fluctuations in the hydraulic system to a safe value during normal shutdown or at times of power failure. A siphon with automatic air valve gives additional protection against reverse flow with the resulting overspeed of the unit should the discharge valve fail to close promptly.

5 The use of appropriate apparatus to accomplish desired methods of operation such as gate-shaft type of servomotors for operating the disks of the butterfly valves; applying oil under pressure to the thrust shoes of the motor bearings to separate the metal surfaces prior to starting the unit, the use of compressed air in reducing starting torque, and so forth, is economically feasible.

Acknowledgment

The studies described in the paper were performed under the direction and inspiration of I. A. Winter, Head of Hydraulic Equipment Design. All engineering designs for the pumping plant are under the direction of L. N. McClellan, Assistant Chief Engineer, Electrical and Mechanical, and Walker R. Young, Chief Engineer, Design and Construction, Denver, Colo. All activities of the Bureau are under the general charge of Michael W. Straus, Commissioner, Washington, D. C.

Discussion

J. N. Bradley.[5] One of the tests on the model pump, which was made to exploit every possibility even though it appeared to be a questionable solution, brings to light another significant point which is worth attention. There is a tendency at times to stress economy of design to the point where it interferes with the basic principles of good hydraulic design. This is especially true in the case of closed-conduit structures in which a favorite remedy for an inadequate design is the makeshift addition of air vents or breather pipes at points along the conduit where subatmospheric pressures prevail. This practice often does not result in satisfactory solutions, as this discussion is intended to show. Carefully planned air vents in adequate designs serve a useful purpose, but their indiscriminate use in inadequate structures may prove quite disappointing.

Fig. 16 of this discussion shows portions of an oscillograph record from the model tests on the Granby pumps, during which throttling was accomplished by a gate valve on the suction side of the pump. Record A shows instantaneous pressures and electric current for the pump operating at 14 per cent valve opening. The pressures are quite steady at the points of measurement (pressure cells PC 4, 5, and 6) and the current to the motor is uniform, but PC 5 shows a negative pressure amounting to 24 ft of water in the model. Most certainly, this would result in cavitation in the prototype.

An air vent was installed in the suction line between the valve and the pump to relieve the low pressure in this region. The oscillogram B depicts the results for valve openings from 5 to 30 per cent. The air vent increased the pressure at P.C. 5 approximately to that of the atmosphere, as was the intention, but the pressure at PC 6, on the discharge side of the pump, has an oscillatory characteristic which varies from 5.5 to 25 ft of water. The pressure surges in the discharge line are evidenced by corresponding oscillations in the power utilized by the pump motor. The surge in current which varies from 25 to 40 is indicative of the power surges, because the power factor was near unity in this case. As the power and pressure surges are in phase in record B, this could result in a self-sustaining oscillation which could be stopped only by complete shutdown of the pump.

The practice of venting to relieve the condition, unnecessarily produced by low subatmospheric pressures, merely complicates this problem, as a mixture of air and water can be an unstable fluid, and the pressures throughout such a fluid are as unstable as the fluid itself.

In the case of the Granby pumps, where surges in pressure directly affect the power requirements of the motors, neither cavitation nor venting could be tolerated. The solution to the problem was particularly simple in that throttling could be accomplished with a valve on the discharge side of the pump, which eliminated all of these difficulties.

This rather extreme example serves to illustrate the fact that air vents are not cure-alls for closed-conduit pressure problems. When vents are used, careful consideration should be given to all possible effects that air might have on the flowing fluid.

F. M. Wilson.[6] Additional features of the electrical equipment to be used at the Granby plant will be mentioned briefly.

Reduced voltage for motor starting on the limited system, with the pump impeller unwatered, will be obtained by taps in the wye-connected low-voltage windings of the 3-phase transformers which supply the pump motors. Three taps will be provided in each low-voltage winding to give an approximate reduced range of from 30 to 50 per cent of normal voltage. The wye-connected windings will allow balanced voltages and currents for motor starting for whichever tap is determined by test in the field to be most suitable for the operating conditions.

Although the main-pump motors will operate at 6.6 kv, the

[5] Hydraulic Engineer, U. S. Bureau of Reclamation, Denver, Colo.

[6] Engineer, U. S. Bureau of Reclamation, Denver, Colo.

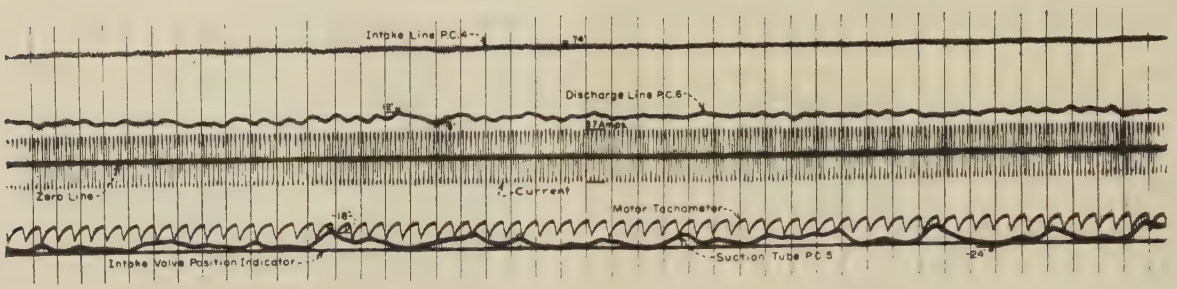

OSCILLOGRAM OBTAINED AT CRITICAL OPERATING POINT — 14 PERCENT VALVE OPENING
SUCTION TUBE NOT VENTED — BY-PASS OPEN

A

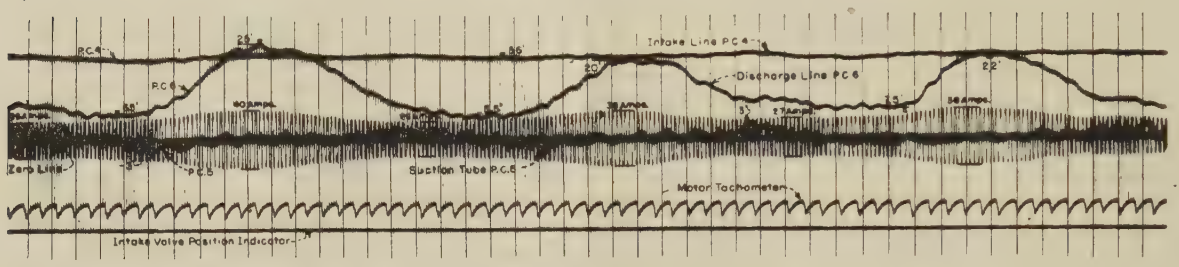

OSCILLOGRAM OBTAINED FOR CRITICAL OPERATING ZONE — 5 TO 30 PERCENT VALVE OPENING
SUCTION TUBE VENTED — BY-PASS OPEN

B

FIG. 16 GRANBY PUMP TESTS; THROTTLING ACCOMPLISHED WITH INTAKE VALVE

high altitude of this installation will require motor-control switchgear rated at 15 kv. Provision is made in this switchgear to prevent the motors from being started in case the auxiliaries do not operate properly. To keep the motor-starting-torque requirements as low as possible, an oil film will be introduced by oil pressure between the bearing surfaces of the thrust bearing before a motor is started.

Reduced-voltage starting of a unit will be initiated by a manually operated control switch at either of two stations, which will close the reduced-voltage circuit-breaker in the switchgear, applying reduced voltage to the motor, which will start and accelerate to maximum subsynchronous speed as an induction motor. The motor will then be synchronized automatically at reduced voltage by the automatic application of excitation to the motor field at the optimum conditions of speed and rotor-pole angular displacement. The reduced-voltage circuit-breaker will then be opened automatically and the full-voltage circuit-breaker will be closed automatically to apply full voltage to the motor.

The full-voltage starting sequence will be similar, except that the motor will be thrown on full voltage at the start, and no transition will be required after synchronization.

The control equipment will be so arranged that a motor will be automatically shut down by unit overspeed, excessive pump-casing water pressure, incomplete starting sequence, loss of motor-field excitation, loss of synchronism, and by operation of any of the following motor relays: Thermal overload, overcurrent, differential current, ground fault, and undervoltage. Carbon dioxide for extinguishing fire will be released automatically into the motor air housing upon operation of the motor differential-current or ground-fault relays. Automatic shutdown of a motor will close the discharge valve for that unit. For normal shutdown, the discharge valve will be closed before the motor is tripped off the line to minimize system disturbances. A speed switch on the motor will apply compressed-air-operated brakes on the motor during the shutdown operation.

I. A. WINTER.[7] The principles of the hydrostatic spheroid and arch as described by the author in studies of a subterranean pumping plant have not had as wide application in engineering practice as appears to be warranted by the interesting results obtained in the Granby studies.

The writer has found these principles to be of economic value in the design of large reinforced-concrete conduits up to 20 ft diam, and spheroids up to 200 ft diam for hydrostatic pressures not exceeding 100 ft. At higher heads, the true shape, as given by the formula, do not differ sufficiently from a circle or sphere to effect an appreciable saving in materials.

A description of the hydrostatic arch has been given by Rankine.[8] The relation of surface tension and fluid pressure for spheroids is shown in Fig. 15 of the paper. By the theory of surface tension, there is a force on AD, tangential to the free surface of magnitude $T(R_1\theta_1)$, where T is the surface tension of the liquid.[9]

The writer has derived the simplified formula

$$r_1 = \frac{H^2 - h_0^2}{4h_1} \qquad [1]$$

for the outline of the hydrostatic arch in terms of the radius at any point on the surface of the membrane. Derivation of the formula is illustrated in Fig. 15(B). This formula will be found useful for quick geometrical construction of the figure for stress analysis by the force-diagram method. In this derivation, the surface tension of the liquid is determined as a function of $(1/2\ wH^2) - (1/2\ wh_0^2)$, which is the total trapezoidal pressure normal to the vertical axis of the conduit. Since the surface tension of a liquid for a free unsupported form must be equal

[7] Engineer, U. S. Bureau of Reclamation, Denver, Colo.

[8] "Manual of Applied Mechanics," by W. J. M. Rankine, D. Van Nostrand Company, Inc., New York, N. Y., p. 190.

[9] "Encyclopedia Britannica," fourteenth edition, vol. 2, p. 987.

top and bottom, the value T_s is one half of the total internal pressure within the trapezoid or

$$T_s = \frac{w(H^2 - h_0^2)}{4} \quad [2]$$

From this consideration it follows that the radius of curvature r_x of the membrane at any point h_x may be expressed in terms of the surface tension T_s as

$$r_x = T_s/w(h_x) \quad [3]$$

Therefore $r_x h_x$ is a constant. The depth d of the conduit is $H - h_0$, which is assumed for the basis of design.

The agreement of the theoretical shape obtained by Equation [1], shown in Fig. 2 of the paper, with the force diagram for conditions without consideration of the weight of the membrane, in which there is only tensile stress, is excellent agreement in engineering procedure.

Author's Closure

Since the presentation of this paper it has been found possible to omit the surge tank on the pump-discharge line. This has resulted in a very substantial saving in cost since unsatisfactory rock conditions at the proposed site would have required a deep and very expensive foundation for the surge tank. A larger WR^2 for the motor than was assumed in the original waterhammer calculations (actually it is close to that used in the acceleration study of Table 1) together with a new profile for the discharge pipe lowered to suit existing excavation, were factors which contributed to the feasibility of eliminating the surge tank.

When these changes were considered in the subsequent waterhammer investigations, it was shown that under the most severe conditions of emergency closure, the minimum momentary drop in pressure after power failure is 14 ft below atmospheric pressure, which at this altitude is 11 ft above absolute zero; consequently a pressure rise of the instantaneous type due to water-column separation will not occur if surge tank is omitted.

The rate of closing and opening of the butterfly discharge valve has been decreased from that given in the paper. The waterhammer studies have been based on a closing cycle of the first 75 per cent of angular movement in 12 sec and the final 25 per cent of movement in 30 sec or 42 sec for the complete 90 deg of movement. The opening cycle is made the exact reverse of this to minimize complications in the control apparatus. These opening and closing cycles apply to all conditions of operation, both normal and emergency.

The author wishes to thank the discussers of this paper and appreciates the additional information and details of the tests and of the final design conveyed therein. The hydraulic problems studied in the design of a large pumping plant, such as the Granby installation, are many and varied and the p esent paper has attempted to outline briefly some of the more unusual ones. It may be mentioned in closing that the studies made in connection with the operation of the unit as affected by the long discharge line and siphon have been of great value in connection with the designs for the Grand Coulee and Tracy pumping plants, which are many times larger than the Granby plant, having pump motors rated at 65,000 hp and 22,500 hp respectively, in contrast with the 6000 hp Granby motor.

An Analysis of the Dynamic Forces in a Cam-Driven System

By JOHN A. HRONES,[1] CAMBRIDGE, MASS.

The influence of the mass, elasticity, and damping of a cam-driven system upon the magnitude and character of the forces imposed upon the cam are analyzed and discussed from a general viewpoint. Actual solutions for the force-displacement characteristics of three widely used cam contours are carried out.

THE cam is an important machine element, widely applied in machines of varied types. In Fig. 1 the basic components of the cam-follower mechanism are shown. The cam A rotates about a fixed axis at constant angular velocity. A follower B, is forced to move in conformance with the shape of the cam with which it is always in mechanical contact. The function of the cam is to cause the follower to cyclically move through the distance L and to return to its initial position. In many cases the type of motion used to produce the desired amplitude of motion of the follower is unimportant in terms of the desired output displacement, but in almost all cases the time function of x employed plays a tremendously important role in the resulting forces produced and therefore greatly influences the life, smoothness of operation, and the permissible operating speed of the machine.

In order to obtain the analytical results with which the behavior of the cam-follower mechanism may be predicted, it is necessary to develop the geometric and kinematic properties of the system for a desired follower motion.

A list of symbols used in the paper is given on page 481.

In this paper the following assumptions will be made:

1 The follower is positively driven by the cam.

2 No backlash exists in the system.

3 The driven output mass is large compared to the other moving components of the cam-driven system.

4 The cam rotates at constant angular speed.

5 The cam contour is not changed by the forces which act upon it.

6 Coulomb friction may be combined with viscous friction and the combined effects represented by an equivalent viscous damping.

Let $x_f = \phi(t)$ be the desired follower motion for one half cycle .....[1]

Then the radius vector from the center of rotation to the center of the follower roller at any time t is

$$r = [(y_0 + x_f)^2 + z_0^2]^{1/2} \text{ (See Fig 2)} \quad .....[2]$$

where r = radius vector, in.
y_0 = y co-ordinate to initial follower position, in.
z_0 = z co-ordinate to line of motion of follower, in.
R = radius of base circle, in.

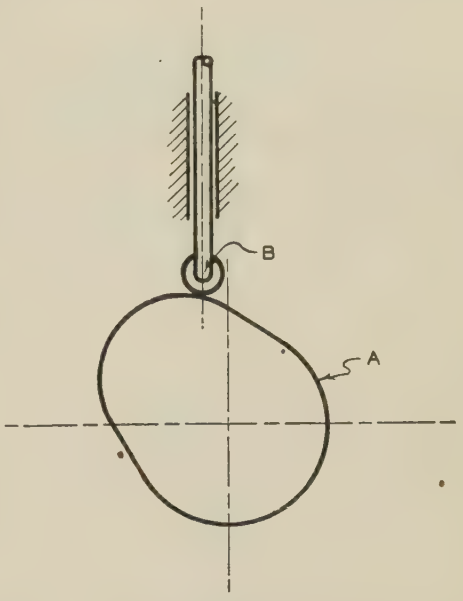

FIG. 1 BASIC CAM-FOLLOWER MECHANISM

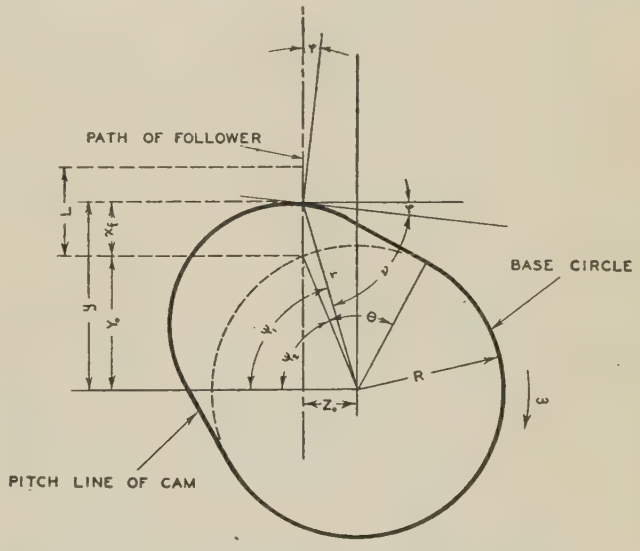

FIG. 2

Expanding Equation [2] and observing that $R^2 = y_0^2 + z_0^2$ the value of r is

$$r = [R^2 + 2y_0x_f + x_f^2]^{1/2} \quad .....[3]$$

The angular position of the cam (θ) is given by

$$\theta = \omega t \text{ radius} \quad (\omega = \text{constant}) \quad .....[4]$$

Therefore the function x_f may be rewritten as

[1] Associate Professor, Mechanical Engineering, Massachusetts Institute of Technology. Mem. ASME.

Contributed by the Machine Design Division and presented at the Annual Meeting, Atlantic City, N. J., December 1–5, 1947, of THE AMERICAN SOCIETY OF MECHANICAL ENGINEERS,

NOTE: Statements and opinions advanced in papers are to be understood as individual expressions of their authors and not those of the Society. Paper No. 47—A-46.

$$x_f = \varphi\left(\frac{\theta}{\omega}\right) \quad \ldots\ldots [5]$$

The first time derivative of Equation [3] is

$$\frac{dr}{dt} = \frac{y}{r}\frac{dy}{dt} \quad \ldots\ldots [6]$$

in terms of θ

$$\frac{dr}{d\theta} = \frac{y}{r}\frac{dy}{d\theta} \quad \ldots\ldots [7]$$

Determination of Pressure Angle

Referring to Fig. 2, the pressure angle (φ) is given by the following relationship

$$\varphi = \psi_1 - \nu \quad \ldots\ldots [8]$$

$$\tan\varphi = \frac{\tan\psi_1 - \tan\nu}{1 + \tan\psi_1 \tan\nu} \quad \ldots\ldots [9]$$

$$\tan\psi_1 = \frac{y}{z_0} \quad \ldots\ldots [10]$$

From Fig. 3

$$\tan\nu = \frac{r\,d\theta}{dr} \quad \ldots\ldots [11]$$

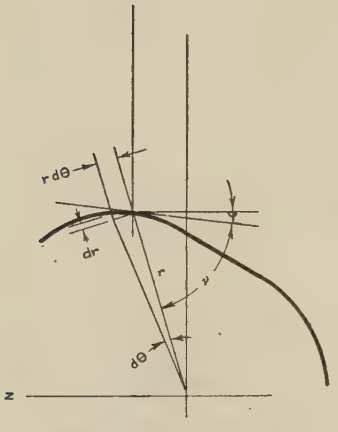

Fig. 3

By substitution of Equations [11] and [12] in Equation [10], we have

$$\tan\varphi = \frac{y^2\frac{dy}{d\theta} - z_0 r^2}{y\left[z_0\frac{dy}{d\theta} + r^2\right]} \quad \ldots\ldots [12]$$

By setting the derivative of tan φ with respect to θ equal to zero, the values of θ at which the pressure angle becomes a maximum may be determined (Equation [13a])

$$\frac{d}{d\theta}(\tan\varphi) = \frac{y^2 z_0\left(\frac{dy}{d\theta}\right)^3 - (y^4 - z_0^4)\left(\frac{dy}{d\theta}\right)^2 + z_0 r^4\left(\frac{dy}{d\theta}\right) + r^4 y\left(\frac{d^2y}{d\theta^2}\right)}{y^2\left[z_0\left(\frac{dy}{d\theta}\right) + r^2\right]^2} \quad \ldots\ldots [13]$$

Set Equation [13] equal to zero

$$y^2 z_0\left(\frac{dx_f}{d\theta}\right)^3 - (y^4 - z_0^4)\left(\frac{dx_f}{d\theta}\right)^2 + z_0 r^4\left(\frac{dx_f}{d\theta}\right) + r^4 y\left(\frac{d^2x_f}{d\theta^2}\right) = 0 \quad \ldots\ldots [13a]$$

Because of the complexity of Equation [13a] it is often more convenient to plot φ against θ using Equation [12] and to determine maximum values of the pressure angle from this plot. The maximum values of φ may, in general, be graphically obtained from the cam layout.

Properties of the Combined Follower-Output Member System

The motion of the cam follower is used to impart motion to an output of finite mass. The follower may drive the output member directly or more commonly through a system of gears and levers. The follower is coupled to the output member by a relatively low mass, low inertia, and, in general, relatively stiff system. Fig. 4 shows a possible arrangement of such a system. This system is chosen as one of many to illustrate the text. It will be observed that it in no way limits the applicability of the method to other systems. Generally the mass of the output member is very large relative to the follower and the components of the coupling system. Thus no appreciable error results by assuming the mass of all other elements of the system to be zero.

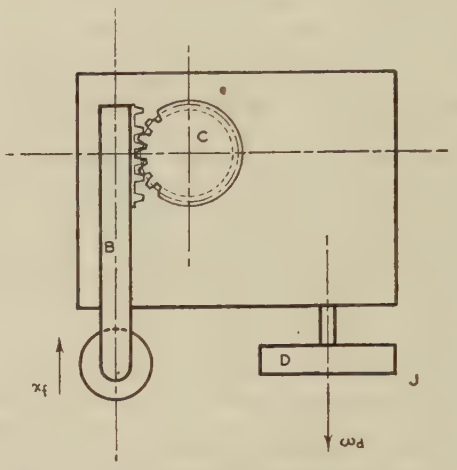

Fig. 4 Cam-Driven System

Equivalent System Stiffness

The equivalent system stiffness, K, is defined as the force required to deflect the follower one inch if the output member is rigidly held, the force being applied at the center of the roller and along the line of motion of the follower.

Equivalent Mass of Driven Member

M is the equivalent mass of the driven member referred to the displacement x. Its value in any given system is readily found by tracing the inertia force or torque back through the coupling system to the reciprocating motion x.

To illustrate the procedure, the system shown in Fig. 4 will be treated in detail. Isolate the driven member (see Fig. 5). The resultant torque acting upon it is $\frac{Jd^2\theta_d}{dt^2}$. Neglecting friction losses and mass of the coupling system, the power developed at D must be equal to that existing simultaneously at C.

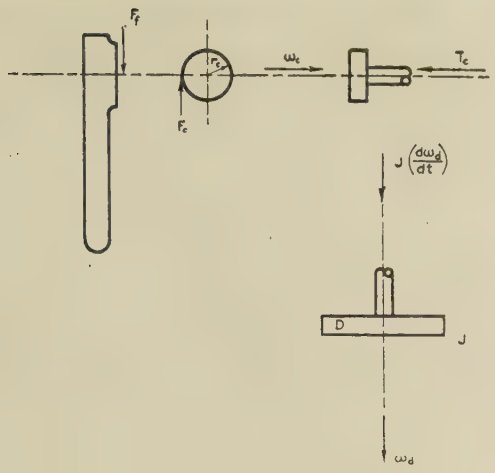

Fig. 5

$$T_c \frac{d\theta_c}{dt} = \left[J \frac{d^2\theta_d}{dt^2} \right] \frac{d\theta_d}{dt}$$

but

$$\frac{d\theta_d}{dt} = n \frac{d\theta_c}{dt}$$

$$\therefore T_c = n^2 J \left(\frac{d^2\theta_c}{dt^2} \right)$$

also

$$F_e = \left(\frac{n}{r_c} \right)^2 J \frac{d^2x}{dt^2}$$

therefore

$$M = \left(\frac{n}{r_c} \right)^2 J$$

The system shown in Fig. 6 is therefore dynamically equivalent to the actual system providing M and K bear the values indicated in the foregoing.

The force transmitted to the follower is the sum of the force developed in the equivalent spring K and the dashpot force. To determine the maximum cam load, it is therefore necessary to find this force as a function of the time for a given follower displacement $x_f = \phi(t)$.

Forces on the Cam Follower

The solid lines in Fig. 7 show the equivalent mass M and the follower at rest at the time $t = 0$. At some time t the positions are as indicated by the dotted outlines.

A summation of the forces acting on mass M yields the following result

$$M \frac{d^2x}{dt^2} + b \left(\frac{dx}{dt} - \frac{dx_f}{dt} \right) + c \frac{dx}{dt} + K(x - x_f) = 0$$

or

$$M \frac{d^2x}{dt^2} + (b + c) \frac{dx}{dt} + Kx = b \frac{dx_f}{dt} + Kx_f \ldots\ldots [14]$$

Where b is the equivalent viscous-damping factor between the follower and the output mass and c is the equivalent viscous-damping factor between the output mass and the frame. It is here assumed that the effect of static and viscous friction may be lumped together with sufficient accuracy and expressed in terms of viscous damping.

If Equation [14] is divided by M, the following result is obtained

$$\frac{d^2x}{dt^2} + 2(\zeta + \zeta_c)\,\omega_n \frac{dx}{dt} + \omega^2_n x = 2\zeta\omega_n \frac{dx_f}{dt} + \omega^2_n x_f \ldots [15]$$

where

$$\omega_n = \left(\frac{K}{M} \right)^{1/2} = \text{undamped natural frequency of output mass}$$

$$\zeta = \frac{b}{2\sqrt{KM}} = \text{damping ratio (follower)}$$

$$\zeta_c = \frac{c}{2\sqrt{KM}} = \text{damping ratio (frame)}$$

Now, if Equation [15] is divided by ω^2_n and a change of variable introduced, the following simplified relation results

$$D^2x + 2(\zeta + \zeta_c)Dx + x = 2\zeta Dx_f + x_f \ldots\ldots [16]$$

where

$$D = \frac{d}{d(\omega_n t)} = \left(\frac{1}{\omega_n} \right) \frac{d}{dt}$$

Equation [16] is a linear differential equation of second order with constant coefficients which upon solution will give the displacement of the output mass for any follower motion.

In operational form Equation [16] may be written

$$x = \left[\frac{2\zeta D + 1}{D^2 + 2(\zeta + \zeta_c)D + 1} \right] x_f \ldots\ldots [17]$$

$$\frac{dx}{dt} = \left[\frac{\omega_n D(2\zeta D + 1)}{D^2 + 2(\zeta + \zeta_c)D + 1} \right] x_f \ldots\ldots [18]$$

The component of force acting on the cam follower in the x direction is

$$F = K(x - x_f) + b \left(\frac{dx}{dt} - \frac{dx_f}{dt} \right) \ldots\ldots [19]$$

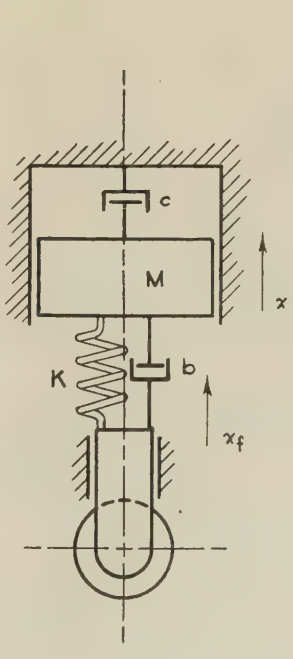

Fig. 6 Equivalent System

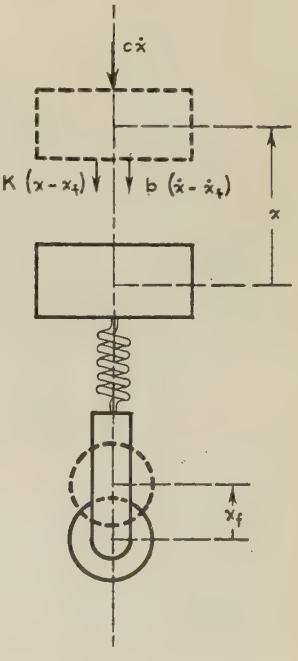

Fig. 7

Substituting Equations [17] and [18] into Equation [19], we have

$$F = \omega_n b D \left[\frac{D^2 + \left(2\zeta_e + \frac{1}{2\zeta}\right) D + \frac{\zeta_e}{\zeta}}{D^2 + 2(\zeta + \zeta_e)\, D + 1} \right] x_f \quad \ldots\ldots [20]$$

Equation [20] is a general expression in operational form of the force on the cam follower.

This may be reduced to the following form

$$F = b \left[\frac{D^2 + \left(2\zeta_e + \frac{1}{2\zeta}\right) D + \frac{\zeta_e}{\zeta}}{D^2 + 2(\zeta + \zeta_e) D + 1} \right] \frac{dx_f}{dt} \quad \ldots\ldots [21]$$

or

$$\frac{F}{M} = \omega_n \left[\frac{2\zeta D^2 + (4\zeta_e \zeta + 1) D + 2\zeta_e}{D^2 + 2(\zeta + \zeta_e) D + 1} \right] \frac{dx_f}{dt} \quad \ldots\ldots [22]$$

The choice of a suitable follower acceleration-time characteristic is of great importance. A number of different functions are used. A few of the more widely used cam contours follow:

1 *Constant Acceleration or Gravity Cam.* A cam which produces a follower motion

$$\frac{x_f}{L} = 2 \left(\frac{\theta}{\theta_0} \right)^2 \quad \ldots\ldots [23]$$

2 *Harmonic Displacement Cam.* A cam which produces a follower motion

$$\frac{x_f}{L} = \frac{1}{2} \left[1 - \cos \frac{\pi \theta}{\theta_0} \right] \quad \ldots\ldots [24]$$

3 *Cycloidal Cam.* A cam which produces a follower motion

$$\frac{x_f}{L} = \frac{1}{\pi} \left[\frac{\pi \theta}{\theta_0} - \frac{1}{2} \sin \frac{2\pi \theta}{\theta_0} \right] \quad \ldots\ldots [25]$$

The velocity and acceleration characteristics of the follower for the foregoing displacement functions are shown in Table 1.

Displacement, velocity, and acceleration curves of the follower are plotted in Figs. 8 and 9.

The follower of the constant acceleration cam has the lowest peak acceleration but starts off with a finite acceleration which remains constant until half lift position is reached where it suddenly changes to the same negative value. A sudden change back to zero acceleration occurs at full lift position.

The acceleration of the follower of the harmonic displacement cam starts off with its peak value and changes continuously passing through zero at half lift. At full lift, the acceleration undergoes a sudden change from its peak negative value to zero.

The acceleration of the cycloidal cam changes continually from zero at the start of lift to zero at full lift exhibiting no sudden changes. Its peak value is higher than each of the peaks of the previously discussed cam contours.

Determination of Cam Forces for Specific Cam Contour

If the foregoing follower motions are inserted in Equations [18] and [19], the solution of the resulting differential equations may readily be obtained. The results follow:

For constant acceleration cam

$$\frac{dx_f}{dt} = a_0 t$$

$$a_0 = 4L \left(\frac{\omega_f}{\theta_0} \right)^2$$

Substituting in Equation [22] gives the following result

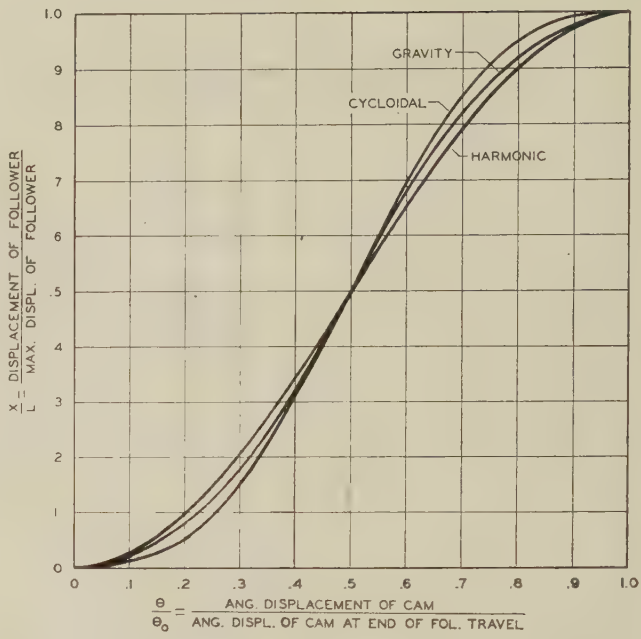

Fig. 8 Displacement Characteristics of Cam Follower

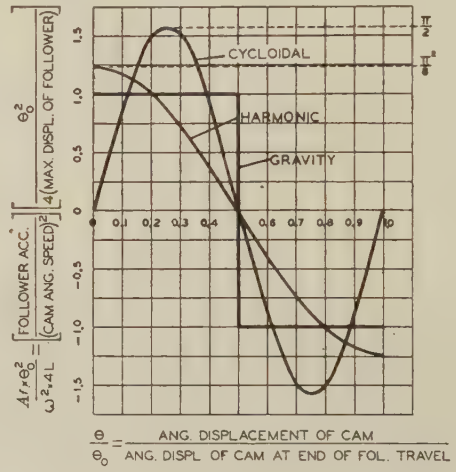

Fig. 9 Acceleration Characteristics of Cam Follower

For constant acceleration cam

$$\frac{dx_f}{dt} = a_0 t$$

$$a_0 = 4L \left(\frac{\omega_f}{\theta_0} \right)^2$$

Substituting in Equation [22] gives the following result

TABLE 1 FOLLOWER CHARACTERISTICS

Type of cam	Displacement	Velocity	Acceleration
Constant acceleration	$\frac{x_f}{L} = 2\left(\frac{\theta}{\theta_0}\right)^2$	$\frac{v_f}{L\omega_f} = \frac{4\theta}{\theta_0^2}$	$\frac{a_f}{L(\omega_f)^2} = \left(\frac{2}{\theta_0}\right)^2$
Harmonic displacement	$\frac{x_f}{L} = \frac{1}{2}\left[1 - \cos\frac{\pi\theta}{\theta_0}\right]$	$\frac{v_f}{L\omega_f} = \frac{\pi}{2\theta_0}\sin\frac{\pi\theta}{\theta_0}$	$\frac{a_f}{L(\omega_f)^2} = \frac{1}{2}\left(\frac{\pi}{\theta_0}\right)^2\cos\frac{\pi\theta}{\theta_0}$
Cycloidal	$\frac{x_f}{L} = \frac{1}{\pi}\left[\frac{\pi\theta}{\theta_0} - \frac{1}{2}\sin\frac{2\pi\theta}{\theta_0}\right]$	$\frac{v_f}{L\omega_f} = \frac{1}{\theta_0}\left[1 - \cos\frac{2\pi\theta}{\theta_0}\right]$ $\left(v_f = \frac{dx_f}{dt}\right)$	$\frac{a_f}{L(\omega_f)^2} = \frac{2\pi}{\theta_0^2}\sin\frac{2\pi\theta}{\theta_0}$ $\left(a_f = \frac{d^2x_f}{dt^2}\right)$

$$\frac{F}{Ma_g} = \left[\frac{2\zeta D^2 + (4\zeta\zeta_c + 1)D + 2\zeta_c}{D^2 + 2(\zeta + \zeta_c)D + 1}\right] \omega_n t \quad \ldots\ldots [26]$$

For harmonic displacement cam

$$\frac{dx_f}{dt} = \frac{a_h \theta_0}{\pi \omega_f}$$

where

$$a_h = \frac{L}{2}\left[\frac{\pi\omega_f}{\theta_0}\right]^2$$

By substituting in Equation [22] we have

$$\frac{F}{Ma_h} = \frac{\theta_0}{\pi\beta}\left[\frac{2\zeta D^2 + (4\zeta\zeta_c + 1)D + 2\zeta_c}{D^2 + 2(\zeta + \zeta_c)D + 1}\right] \sin\left(\frac{\pi\beta}{\theta_0}\right)\omega_n t \ldots [27]$$

where

$$\beta = \frac{\omega_f}{\omega_n}$$

For cycloidal cam

$$\frac{dx_f}{dt} = \frac{\theta_0 a_c}{2\pi\omega_f}\left[1 - \cos\frac{2\pi\theta}{\theta_0}\right]$$

where

$$a_c = 2\pi L\left(\frac{\omega_f}{\theta_0}\right)^2$$

By substituting in Equation [22] the following results

$$\frac{F}{Ma_c} = \frac{\theta_0}{2\pi\beta}\left[\frac{2\zeta D^2 + (4\zeta\zeta_c + 1)D + 2\zeta_c}{D^2 + 2(\zeta + \zeta_c)D + 1}\right]\left[1 - \cos\frac{2\pi\beta}{\theta_0}\omega_n t\right] \quad \ldots\ldots [28]$$

Solutions to Equations [26], [27], and [28] have been carried out on the differential analyzer at M.I.T. for a selected number of values of the system constants shown in Tables 2, 3, and 4. The results are plotted in Figs 10 to 15 inclusive.

The ratio of the force on the cam along the center line of the follower to the product of the equivalent output mass and the maximum acceleration of the follower is plotted against the ratio of cam displacement to the cam displacement required to produce full lift. This product, Ma, is the maximum value F would reach if the motion of the equivalent mass was the same as the cam follower. This ratio is therefore a measure of the cam force amplification resulting from the spring-dashpot coupling between the cam follower and the output. In each case the follower motion plotted occurs between two dwell periods.

Discussion of Results

With no damping present the force F oscillates at the natural frequency (ω_n). In the case of the gravity cam the peak value of the ratio $\frac{F}{Ma_g}$ during the first half of the follower motion is equal to two. Immediately after mid-position where the follower acceleration suddenly changes from a positive value to a negative one of equal magnitude a peak force ratio of three is reached. See Fig. 13.

With a harmonic follower motion an oscillation of the same frequency occurs with a peak value of two. See Fig. 14.

With the cycloidal follower motion an oscillation of the same frequency but of much smaller amplitude occurs. The peak value of the force ratio is 1.06. See Fig. 15.

As the damping ratio ζ_c (damping between output mass and the frame) is increased the transient oscillation decreases rapidly but the peak force increases rapidly with damping ratio as shown in Table 5. For damping ratios (ζ_c) greater than 0.1 with cycloidal follower motion no force reversal occurs. For the harmonic and gravity cams a very slight force reversal takes place near the end of the travel for values of ζ_c equal to or greater than 0.1. This is because of the fact that the damping forces are now large relative to the inertia forces. As the damping ratio increases the general shape of the force-time curve approaches the

TABLE 2 GRAVITY CAM

Run	β	ζ	ζ_c	θ_0
1	0.02	0.1	0.1	$\frac{\pi}{3}$
2	0.02	0.1	0.3	$\frac{\pi}{3}$
3	0.02	0.1	0.5	$\frac{\pi}{3}$
4	0.02	0.1	0.7	$\frac{\pi}{3}$
5	0.02	0.1	1.0	$\frac{\pi}{3}$

TABLE 3 HARMONIC CAM

Run	β	ζ	ζ_c	θ_0
1	0.02	0	0	$\frac{\pi}{3}$
2	0.01	0	0	$\frac{\pi}{3}$
3	0.01	0.05	0.05	$\frac{\pi}{3}$
4	0.01	0.05	0.1	$\frac{\pi}{3}$
5	0.01	0.05	0.2	$\frac{\pi}{3}$
6	0.01	0.05	0.3	$\frac{\pi}{3}$
7	0.01	0.05	0.5	$\frac{\pi}{3}$
8	0.01	0.05	0.7	$\frac{\pi}{3}$

TABLE 4 CYCLOIDAL CAM

Run	β	ζ	ζ_c	θ_0
1	0.01	0.05	0	$\frac{\pi}{3}$
2	0.01	0.05	0.05	$\frac{\pi}{3}$
3	0.01	0.05	0.1	$\frac{\pi}{3}$
4	0.01	0.05	0.2	$\frac{\pi}{3}$
5	0.01	0.05	0.3	$\frac{\pi}{3}$
6	0.01	0.05	0.5	$\frac{\pi}{3}$
7	0.01	0.05	0.7	$\frac{\pi}{3}$

TABLE 5

TYPE	ζ_c	$\frac{F}{Ma_g}$
GRAVITY	0	3
	0.1	6.5
	0.3	16.5
	0.5	26.5
	0.7	36.5
	0.9	45.5
HARMONIC	0	2.47[a]
	.05	4.32
	0.1	11.1
	0.2	16.7
	0.3	24.7
	0.5	41.4
	0.7	58.1
CYCLOIDAL	0	1.72[b]
	.05	6.28
	0.1	11.0
	0.2	21.2
	0.3	31.8
	0.5	52.5
	0.7	72.9

[a] Obtained by multiplying values in Fig. 11 by 1.236.
[b] Obtained by multiplying values in Fig. 12 by 1.57.

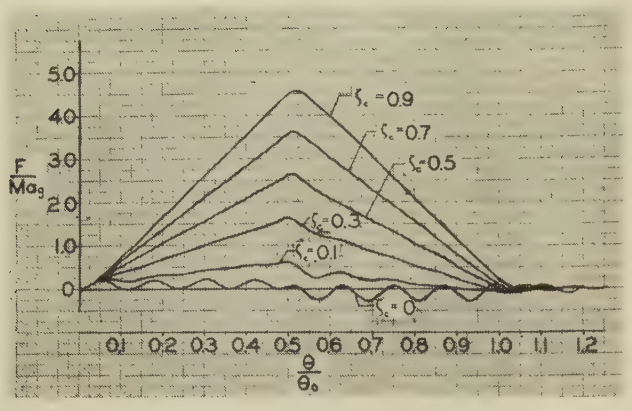

FIG. 10 RATIO OF AXIAL CAM FORCE TO THE PRODUCT OF DRIVEN MASS AND MAXIMUM FOLLOWER ACCELERATION VERSUS THE RATIO OF CAM DISPLACEMENT TO THE CAM DISPLACEMENT REQUIRED TO PRODUCE FULL LIFT
(Constant acceleration follower motion.)

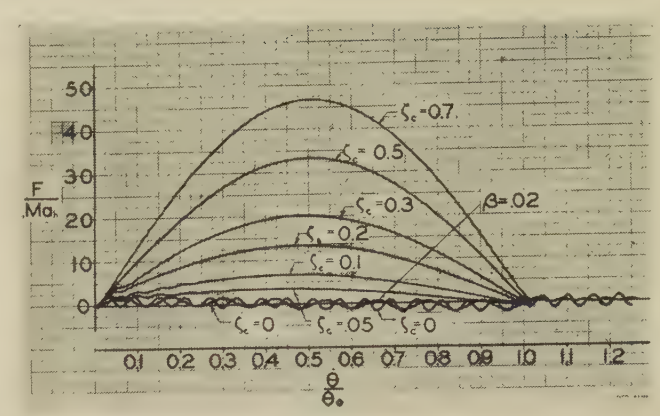

FIG. 11 RATIO OF AXIAL CAM FORCE TO THE PRODUCT OF DRIVEN MASS AND MAXIMUM FOLLOWER ACCELERATION VERSUS THE RATIO OF CAM DISPLACEMENT TO THE CAM DISPLACEMENT REQUIRED TO PRODUCE FULL LIFT
(Harmonic follower displacement.)

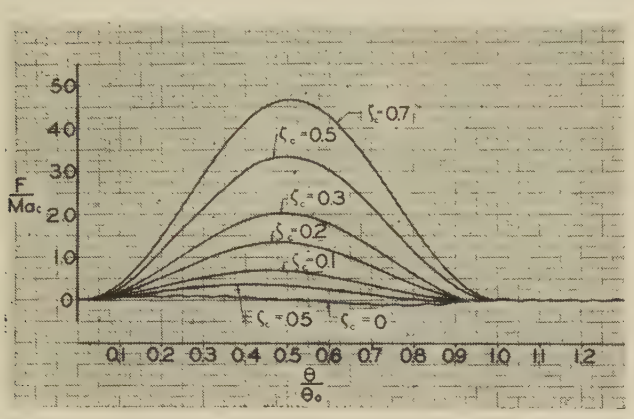

FIG. 12 RATIO OF AXIAL CAM FORCE TO THE PRODUCT OF THE DRIVEN MASS AND THE MAXIMUM FOLLOWER ACCELERATION VERSUS THE RATIO OF CAM DISPLACEMENT TO CAM DISPLACEMENT REQUIRED FOR FULL LIFT
(Cycloidal follower displacement.)

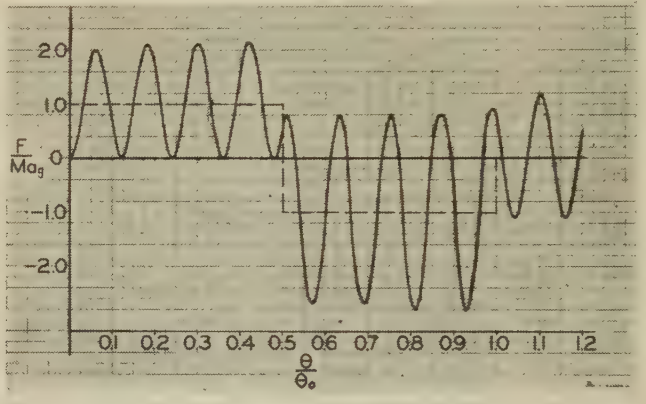

FIG. 13 RATIO OF AXIAL CAM FORCE TO THE PRODUCT OF DRIVEN MASS AND MAXIMUM FOLLOWER ACCELERATION VERSUS THE RATIO OF CAM DISPLACEMENT TO THE CAM DISPLACEMENT REQUIRED TO PRODUCE FULL LIFT.
(Constant acceleration follower motion.)

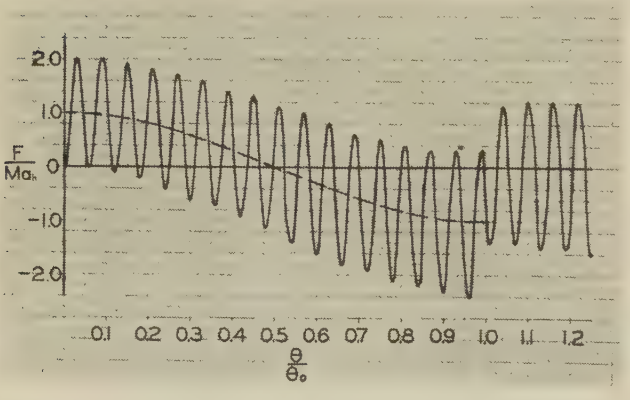

FIG. 14 RATIO OF AXIAL CAM FORCE TO THE PRODUCT OF DRIVEN MASS AND MAXIMUM FOLLOWER ACCELERATION VERSUS THE RATIO OF CAM DISPLACEMENT TO THE CAM DISPLACEMENT REQUIRED TO PRODUCE FULL LIFT
(Harmonic follower displacement.)

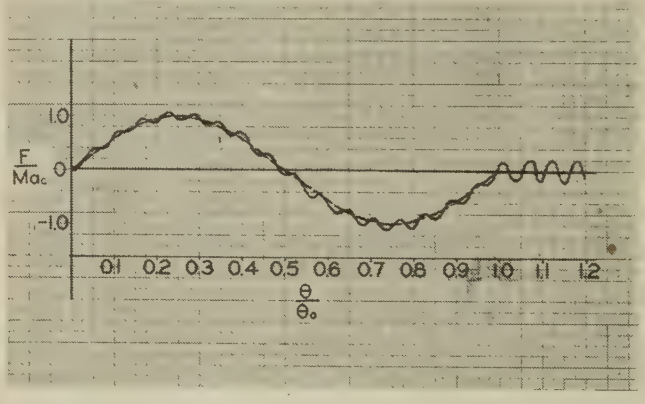

FIG. 15 RATIO OF AXIAL CAM FORCE TO THE PRODUCT OF THE DRIVEN MASS AND THE MAXIMUM FOLLOWER ACCELERATION VERSUS THE RATIO OF CAM DISPLACEMENT TO THE CAM DISPLACEMENT REQUIRED FOR FULL LIFT
(Cycloidal follower displacement.)

shape of the velocity-time curves of the cam follower. Values of $\frac{\omega}{\omega_n}$ were arbitrarily chosen and the results are shown for two values of β. Normally the natural frequency of the driven system is high relative to the frequency of rotation of the cam. Therefore ratios of $\beta = 0.01$ and 0.02 were used. The effect of changing values of β in the range of low values of β is shown in Fig. 11. In comparing the plotted results it should be remembered that $\frac{a_c}{a_g}$ is equal to 1.57 and $\frac{a_h}{a_g}$ is equal to 1.24.

The use of a cam contour of the cycloidal type produces the following desirable results at low damping ratios:

1 A lower peak force along the axis of the cam follower.

2 The amplitude of the transient force variation taking place at the natural frequency of the driven system is much smaller than that produced by the other two cam contours. This should result in longer life of the cam surface and other elements of the machine. It should yield quieter as well as smoother machine performance. Operation at increased speeds should be possible.

The maximum value of the pressure angle is greater for the cycloidal cam than for the other contours discussed if all other dimensions are held fixed and only the contour changed. However, at low values of damping ratio the maximum pressure angle occurs at nearly zero force ratio with a cycloidal cam. In the gravity cam the maximum pressure angle occurs at nearly maximum values of the force ratio.

In order to produce a cycloidal follower motion the accuracy to which the cam contour must be held is very high. An error of a few ten thousandths of an inch in the initial or final stages of the rise will seriously affect the system performance. This is also true in the case of gear action. In recent years a tremendous improvement in gear performance has resulted from the recognition of need for holding tooth contours within very close limits. A great improvement in cam operation will result when the importance of close tolerances is fully recognized and production methods used to yield the desired accuracy.

It is well to point out that the cycloidal follower displacement does not necessarily represent an optimum solution to the cam problem. However, it does offer an opportunity for tremendous improvement in dynamic performance over that obtained by either the gravity or harmonic displacement type cams. A dynamic analysis of the results produced by any other cam contour can be carried out by the methods outlined in this paper. The idealized treatment used in the foregoing has omitted the influence of a number of important factors (see list of assumptions) which it is believed may be introduced in future work.

Acknowledgment

The author wishes to express his appreciation to Mr. Frank Verzuh and Prof. Richard Taylor for their co-operation in making available the differential analyzer at M.I.T.

Discussion

W. M. Dudley.[2] The writer does not recognize the type of machine shown in Fig. 4. Is it part of some textile machinery? The writer's work has been concerned largely with valve cams for aircraft and automotive engines. In comparing with Fig. 6 of the paper, the valve system could be represented by removing the two dashpots and replacing dashpot C by the valve springs. In the work at Thompson Products, we recorded a large number of actual motions with a Western Electric Fastax camera. These were compared with the theoretical solutions for the motion of the valve, and we found slight evidence of appreciable amounts of damping. By contrast with Equations [17] and [18] of the paper, we found the motions of the valve mass by using an equation by Timoshenko.[3] This was changed from an integral to a summation with short time intervals which is the only practical procedure on the usual cams which consist of various curves fitted together. We found very good agreement between theoretical and actual valve motions.

The paper does not state specifically the relation between the natural frequency of the driven system and the cam cycle. From the data in the tables and also the plotted results, it appears that the natural frequency was about 16 times the applied frequency. This pleasant situation does not exist in valve mechanisms where the ratio at top engine speeds cannot be made more than about 8 without overstressing the springs. Also, it is possible in some cases to detect force reflections due to the mass of the spring itself. In other words, the spring behaves as a bar with distributed mass rather than a simple linear assumption. The writer advocates designing cams by specifying first the motion of the follower and then using the differential equation to find the cam profile itself. The latter is not a simple curve as it is required to meet six or seven boundary conditions. In general, no simple curve such as a cycloid or a parabola will give satisfactory performance in a valve mechanism. Likewise, the usual process of assembling pieces of different curves will never operate well at high speeds.

The writer concurs in the statement that greater accuracy is required in machining cams. We designed several experimental cams for automotive and radial aircraft engines and found difficulty in getting the cams made accurately, owing to the fact that the grinding machines use master cams or followers of a different diameter, grinding wheels of variable radius, etc. It is not too difficult to correct for such conditions, but the companies had never done it. Our cams produced very good results at high speeds in so far as valve motion was concerned. However, the cam has such a vital effect on engine performance in various ways that dynamic action is only part of the problem. Some years probably will be required to obtain valve cams which are satisfactory in all respects.

An amusing incident is recalled in which we had spent $1500 making an experimental valve cam. When it arrived we laid it on top of the conventional cam and the differences appeared very slight. The boss looked it over with great suspicion. Fortunately, however, the functional cam design operated quietly and with a limiting speed of about 600 or 700 rpm above the old cam. We did not have the advantage of differential analyzers but were able to get along very well using IBM machines to perform the calculations with punched cards.

Aside from the present paper and one by the writer[4] the only other paper to his knowledge, in which flexibility of the follower system is discussed, is one by Olmstead and Taylor.[5] They do not consider any damping in the system and confine their attention to cases of determining the motion of the follower for a given cam.

W. F. Huck.[6] Satisfactory operation of high-speed automatic machinery requires properly designed and accurately produced

[2] Associate Director, Engineering Research Department, Standard Oil Company of Indiana, Chicago, Ill. Mem. ASME.

[3] "Vibration Problems in Engineering," by S. Timoshenko, second edition, D. Van Nostrand Company, Inc., New York, N. Y., 1937, Equation [48], p. 104.

[4] "New Methods in Valve Cam Design," by W. M. Dudley, Quarterly Transactions, Society of Automotive Engineers, vol. 2, no. 1, January, 1948, pp. 19–33 and 51.

[5] "Poppet Valve Dynamics," by E. H. Olmstead and E. S. Taylor, *Journal of the Aeronautical Sciences*, vol. 6, 1938–1939, pp. 370–375.

[6] Huck Company, New York, N. Y. Mem. ASME.

cams and related mechanism. Despite their importance and interesting possibilities in transforming rotary motion into oscillatory motion of desired functional property, they have not received the attention of our technical schools which they deserve. It is therefore gratifying to see the present author's broad mathematical approach to cams.

He has treated the "gravity," "harmonic," and "cycloidal" types of acceleration/time curves. There are others which may be applied to advantage.

The shock application of force that is inherent in the gravity curve, and the resulting oscillations are illustrated in Fig. 13 of the paper. It should be noted, however, that these oscillations depend upon the relative location of the point of reversal at ordinate 0.5 and the return to zero at ordinate 1.0 with respect to the oscillation waves. It seems that these may have amplitudes approaching the value 8 or may become zero again at point 1.0. This variation depends upon the cam speed variation, since the frequency of oscillation will remain practically constant. For this reason the gravity cam is undesirable where high speeds and forces are involved.

The harmonic curve can be used to advantage for cams that have no dwell. It is undesirable if used, as indicated in Fig. 14, because abrupt application and cessation of acceleration force at the end and the beginning of dwells induce high-value oscillations also.

The more gradual application of acceleration force, in accordance with the cycloidal curve, results in greatly reduced oscillations, as shown in Fig. 15 of the paper. The writer has used cams based on these curves since 1932, with excellent results. Design standards were prepared for the following:

1 Cams with dwell at both ends of each stroke. They have an acceleration in form of a sine curve from zero to 2π, as illustrated in Fig. 9 of the paper.

2 Cams with dwell on one end of each stroke. They have an acceleration in form of a sine curve from zero to $^3/_2\ \pi$ with a constant acceleration to connect to a sine curve from $^3/_2\ \pi$ to zero acceleration for the return stroke, Fig. 16 of this discussion.

3 Cams without dwell. These have continuous accelerations in form of reversing sine curves connecting the alternatingly positive and negative constant portions.

Fig. 16 herewith indicates how velocity and displacement

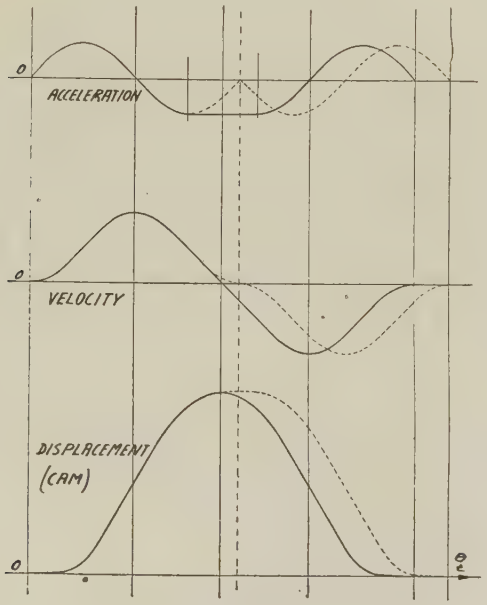

FIG. 16

curves are improved by the combination of cycloidal and constant acceleration. It results in more efficient cam dimensions for cams having reversing without dwell.

The curves, Figs. 10, 11, and 12 of the paper, seem to be obtained through the differential analyzer. For $\zeta = 0$ the curves are the same as in Figs. 13, 14, and 15, respectively, but in a different scale. For ζ values greater than zero the indicated accelerations not only become entirely positive but also reach over 45 times the basic acceleration rates. The writer cannot visualize a practical application where this would be possible. Furthermore, with the acceleration thus increased and remaining positive throughout, the maximum velocity would be attained at the ordinate 1.0. This means that the fluid friction of the illustrated hydraulic dashpot c in Fig. 6 would have to be such that it will retard the mass M during the stroke in exactly the correct value to have its acceleration, and velocity, become zero at the ordinate 1.0. The mass would have to be small in proportion to the fluid friction of c to make this possible. Because this is a rather unusual case the writer would like to see development of similar curves with damping based upon proportions of mass and damping encountered in practical applications.

The writer hopes that the subject of cams becomes an integral part of the curriculum of mechanical engineering and believes that the author has made an encouraging start.

G. J. TALBOURDET.[7] In the past, many attempts have been made to obtain a better understanding of the factors involved in designing cams to give to a follower a definite motion under various speed and load conditions. Anyone connected with this particular branch of machine design knows from experience that the problem is extremely complex. It may then be of value in the following discussion to state what may appear to be relatively simple objectives:

1 Definite motion of the driven mass.
2 Smoothness of operation with minimum noise and vibration.
3 Ability of cam and roll contacting surfaces to withstand the imposed dynamic loads.

It is a well-known fact that cam-driven mechanisms possess a flexibility which cannot be matched by any link mechanism. On the other hand, the limitations of cam-driven systems regarding speed and loads are a barrier to their general use.

The present paper is therefore of extreme interest, not only because of its excellent analytical treatment and method of attack but also for its findings, which should excite our interest and prod us to further study and to evaluate some of the factors influencing cam design to obtain optimum results.

In a treatise of this nature, some assumptions must necessarily be introduced to make it susceptible to a mathematical analysis. While the assumptions mentioned in the paper are well taken, it has been the experience of several engineers of our research division that the finish of cam and roll surfaces has also a definite influence upon the acceleration imparted to a follower. This has been further substantiated by oscillograms of the action of a fine-ground steel roll against milled and fine-ground cylindrical surfaces.

Another factor of great importance is the effect of the applied load upon the smoothness of operation of the cam-driven mechanism. We have found that the application of external forces on the driven mass during the decelerating period tends to reduce and sometimes eliminate the reversal of the forces acting on the cam surface. We feel therefore that surface finish and applied loads should also be considered in designing cams.

For many years we have been engaged in determining from

[7] Mechanical Engineer, Research Division, United Shoe Machinery Corporation, Beverley, Mass. Mem. ASME.

tests the surface-endurance limits of materials for cams to enable us to calculate the safe load-carrying capacity of cam surfaces, and it may be mentioned that the results of these tests have been invaluable in cam design. However, we are in the dark regarding the extent of the dynamic forces imposed on the surfaces of cams imparting to followers some well-known motions such as gravity, harmonic, and cycloidal, or any combination of these motions, although in some few cases we have been able, from the extent of the surface failure of a cam track and the number of repeated stresses, to obtain some indication of the critical dynamic loads imposed on the surface and to select a cam material to withstand these loads.

As early as 1930 we realized the possibilities of the cycloidal cam and also of the combination of harmonic acceleration and cycloidal deceleration, because we felt that the critical action between cam and roll occurs at or soon after the crossover, i.e., when the follower tends to continue its motion at maximum velocity, while the cam tends to constrain that motion. In that region the roll is urged by the energy stored in the follower and driven mass to leave the cam surface, with the result that when roll and cam contact again, they do so with an impact whose force may be several times that of the product of the driven mass and the deceleration of the follower. Our efforts have been directed to minimize this impact force by using a cam curve or combination of curves giving to the follower a smooth crossover, a minimum deceleration, and a zero or near-zero deceleration at the end of the motion. Whenever possible, we make the driven mechanism do work during the decelerating period.

The author's findings show, however, that the dynamic forces acting on the cam surface are greater than the product of the driven mass and the acceleration of the follower by a ratio of 3 to 1 for gravity, 2 to 1 for harmonic, and 1.06 for cycloidal cams, assuming no damping. These findings are worth noting because one of the objections raised against the use of cycloidal cams is that the maximum acceleration imparted to the follower is 1.57 times that of gravity motion, while the paper claims that the peak force, due to the cycloidal motion, is only 55.47 per cent that of gravity motion, assuming equal lift and angle of action. Furthermore, the vibratory forces at the end of the motion of the cycloidal cam follower are only a fraction of those due to the gravity and harmonic motions. These findings check with our experience with cycloidal cams which, in several speed applications, have resulted in minimum noise and vibration as well as longer life, compared to gravity and even harmonic cam curves. We hope in the future to be able to substantiate by tests the analytical results of the author.

We also realize that for similar lifts and angles of action, the differences between the co-ordinates of gravity, harmonic, and cycloidal cam curves at the initial and final stages of the lift are extremely small and very often a matter of a few ten thousandths of an inch. It requires accurate conditions of manufacture with optimum rigidity of work and cutting tool. Here again, the surface finish is an important factor which may influence appreciably the dynamic forces on the cam surface.

Since one of the objectives in cam design is to eliminate the reversal of forces on the cam surface, the effects of introducing a damping action between driven mass and frame, as shown in Figs. 10, 11, and 12 of the paper, are of great interest. However, it remains to be seen what practical value such damping would have on the life of the cam because it appears that, to avoid force reversal, the damping forces must be many times that of the product of the driven mass and the acceleration of the follower. Under such conditions, the loads imposed on the cam surface may be in excess of the load capacity of the surface and seriously affect the useful life of the cam. Some possibilities may, nevertheless, be worth investigating, such as the use of low damping ratios 0.05 or less, which may be sufficient, especially in conjunction with cycloidal follower motion to reduce to a safe value the peak load on the cam surface, while at the same time eliminating the force reversal so detrimental to the smoothness of operation and life of cam-driven mechanisms.

Author's Closure

In response to several requests a list of symbols used in the paper is given below.

List of Symbols Used

r	= distance from center of rotation of cam to center of roller follower	in.
R	= radius of base circle of cam	in.
y_0, Z_0	= y and Z co-ordinates of r when follower is in its lowest position	in.
x_f	= displacement of cam follower	in.
θ	= angular displacement of cam	rad
θ_0	= angular displacement of cam required to produce full travel of follower	rad
$\left(\omega = \frac{d\theta}{dt} = \omega_f\right)$	= angular velocity of cam	rad/sec
φ	= pressure angle	rad
ω_d	= angular velocity of driven table	rad/sec
ω_c	= angular velocity of pinion "c"	rad/sec
T_c	= torque driving pinion "c"	in-lb
$n = \frac{\omega_d}{\omega_c}$	= speed ratio	
r_c	= pitch radius of pinion "c"	in.
J	= moment of inertia of driven table	lb in. sec^2
M	= equivalent mass of driven table referred to cam follower displacement	lb sec^2/in.
x	= displacement of equivalent mass	in.
b	= viscous-damping coefficient (equivalent mass to cam follower)	lb sec/rad
c	= viscous-damping coefficient (equivalent mass to frame)	lb sec/rad
K	= equivalent system stiffness	lb per in.
ζ	= damping ratio (equivalent mass to follower)	
ζ_c	= damping ratio (equivalent mass to frame)	
$\omega_n = \frac{K}{M}$	natural undamped angular frequency of driven system	rad per sec
D	= operator $D = \left(\frac{1}{\omega_n}\right)\frac{d}{dt}$	1/rad
F	= component of force on cam surface in direction of x_f	lb
L	= cam lift	in.
$v_f = \frac{dx_f}{dt}$	velocity of follower	in per sec
$a_f = \frac{d^2x_f}{dt^2}$	acceleration of follower	in per sec^2
$a_g = 4L\left(\frac{\omega_f}{\theta_0}\right)^2$	maximum follower acceleration (gravity cam)	
a_h	maximum followed acbeleration (harmonic displacement cam)	

a_c = maximum follower acceleration (cycloidal displacement cam) in per sec^2

$$\beta = \frac{\omega}{\omega_n} = \frac{\omega_f}{\omega_n}$$

The stimulating discussion to this paper indicates wide recognition of the dynamic problems involved in high-speed cam operation. The general problem to which the schematic system shown in Fig. 4 refers is that of the cam indexing of a mass which is elastically connected to a cam follower. A large number of operations on a wide variety of automatic machines are also characterized by a similar dynamic system. Normally the speed of rotation of the cam is slow compared to that of the camshaft of an internal-combustion engine. Values of 50 to 200 rpm are common. Values over 1000 rpm are rare. The ratios of forced frequency to natural frequency discussed in this paper were therefore restricted to small quantities. As Mr. Dudley indicates the valve-cam problem involves in general higher speeds, lower driven mass, and a gas-flow problem not considered in this paper, but dealt with at some length by Mr. Dudley.[4]

As Mr. Huck indicates, the use of a harmonic displacement cam in cases where no dwell exists is justified because of the absence of transient disturbances. The suggested modification of the cycloidal displacement cam for a single dwell is permissible and should give excellent dynamic performance. Mr. Huck states that "the indicated accelerations . . . . . reach over 45 times the basic acceleration rates." This is not correct. Figs. 13, 14, 15 show that the axial cam *force* at high damping values becomes very large compared to the product of mass and follower acceleration. Reference to Equations [14] and [19] will give the following relationship for the force F

$$F = -M\frac{d^2x}{dt^2} - c\frac{dx}{dt}$$

At high values of damping the second term becomes very large while at low values of c the second term is very small. Thus at very low damping levels the force versus time plot reveals an oscillation about the follower acceleration - time plot. At high damping values the force versus time plot is of the same character as the follower velocity-time plot. In actual practice damping ratios of the order of 0.01 to 0.05 are common. Higher values were studied to explore the possibility of avoiding force reversals.

Mr. Talbourdet's comments which reflect his long experience with and able contributions to the use of cams in automatic machinery are well taken. Surface finish and accuracy of contour are vitally important. With respect to surface finish the writer feels that real steps forward in this direction rest upon a better understanding of the friction phenomenon than we now have together with a more rigorous method of measuring surface finish. The effect of introducing an applied load to the system can be analyzed by the methods of this paper. Its influence would depend upon the character of such an applied load.

The author wishes to thank those whose discussions have contributed so much to the original paper. Preliminary tests on an actual system appear to substantiate the results herein presented.

Curvature-Acceleration Relations for Plane Cams

By M. L. BAXTER, JR.,[1] ROCHESTER, N. Y.

This paper discusses cam curvature as an important limitation in cam design, and presents formulas not previously published for obtaining this curvature. Flat and circular followers are considered for both translational and rotational follower motion. Constructions for obtaining the center of curvature by graphical means are also given. The formulas are listed early in the paper in convenient tabular form for reference purposes, followed by detailed discussion and derivations.

Nomenclature

The following nomenclature is used in the paper:

Translational Motion:

ρ = radius of curvature of cam at point of contact
ρ' = for a circular follower: radius of curvature of path of follower center
b = for a circular follower: distance from cam center to center of follower, in direction of motion
= for a flat follower: distance from cam center to follower surface
r = for a circular follower: radius of follower
e = for a circular follower: offset of follower path from cam center
λ = pressure angle, as defined later
θ = cam rotation in general
$x = \frac{db}{d\theta}$ = distance proportional to instantaneous follower velocity
$y = \frac{dx}{d\theta} = \frac{d^2b}{d\theta^2}$ = distance proportional to instantaneous follower acceleration

Rotational Motion:

ρ = radius of curvature of cam at point of contact
ρ' = for a circular follower; radius of curvature of path of follower center
ρ'' = for flat follower: radius of curvature of cam where follower surface contains turning center of follower
C = center distance between turning center of cam and turning center of follower
L = for a circular follower: distance from turning center of follower to center of follower
r = for a circular follower: radius of follower
f = for a flat follower: offset of follower surface from turning center of follower
β = for a circular follower: angle between line of centers and center line of follower
= for a flat follower: angle between line of centers and follower surface
λ = pressure angle
θ = cam rotation in general
$\chi = \frac{d\beta}{d\theta}$ = quantity proportional to instantaneous follower velocity
$\psi = \frac{d\chi}{d\theta} = \frac{d^2\beta}{d\theta^2}$ = quantity proportional to instantaneous follower acceleration

Introduction

One of the more common problems facing a machine designer is that of determining the smallest cam capable of producing a prescribed motion; or conversely, determining what extremes of motion can be obtained from a cam of limited size. There are two criteria which provide the basis for the solution of this problem.

The first, and best understood, is pressure angle. This term has been variously defined with respect to cams; in this paper it will always refer to the angle between the direction of force and the direction of (instantaneous) motion. It governs the amount of side thrust on the follower guides (and on the cam milling cutter in manufacture), and depends primarily on the instantaneous follower velocity. Pressure angle is discussed in most machine-design texts, such as Berard and Waters.[2] A recent article by Sanders[3] presents a more detailed study which is recommended as background material for the analysis given in this paper.

The purpose of this paper is to consider the second criterion, cam curvature. The importance of curvature may be indicated by the following discussion, based on Fig. 1, which shows a circular follower riding on a cam. If it is desired to move the follower toward the cam center as rapidly as possible, starting at the position shown, it is apparent that the best that can be done is to cut the cam curve off sharply. The center of the follower, however, does not immediately move toward the cam center; it proceeds about a circular path representing a finite limiting deceleration for the assumed dimensions. If a greater deceleration is required, either the cam size must be increased or the roller size decreased. We may then set down as a primary rule of cam design that the required motion must not produce a radius of curvature of the pitch curve less than the radius of the follower. The amount by which this limit must be avoided in practice depends on the allowable compressive stresses in cam and follower.

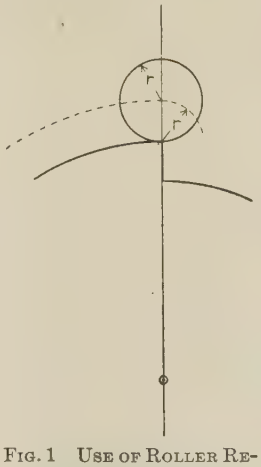

Fig. 1 Use of Roller Results in Finite Maximum Deceleration

---

[1] Mechanical Engineer, Gleason Works. Jun. ASME.

Contributed by the Machine Design Division and presented at the Annual Meeting, Atlantic City, N. J., December 1–5, 1947, of The American Society of Mechanical Engineers.

Note: Statements and opinions advanced in papers are to be understood as individual expressions of their authors, and not those of the Society. Paper No. 47—A-77.

[2] "Elements of Machine Design," by S. J. Berard and E. O. Waters, second edition, D. Van Nostrand Company, Inc., New York, N. Y., 1933.

[3] "Cam Design and Analysis for High Speeds and Torques," by Milton A. Sanders, *Product Engineering*, vol. 18, 1947, pp. 84–87.

TABLE 1 FORMULAS FOR DETERMINING CAM CURVATURE

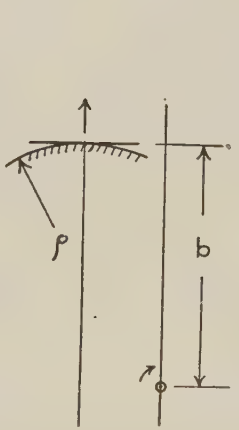

FIG. 2 FLAT FOLLOWER

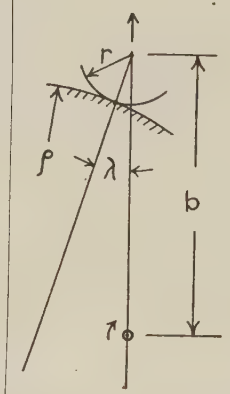

FIG. 3 CIRCULAR FOLLOWER, RADIAL MOTION

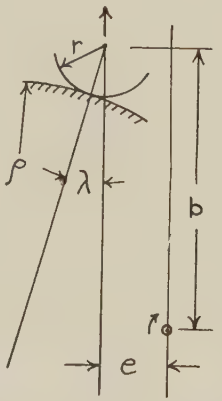

FIG. 4 CIRCULAR FOLLOWER, OFFSET MOTION

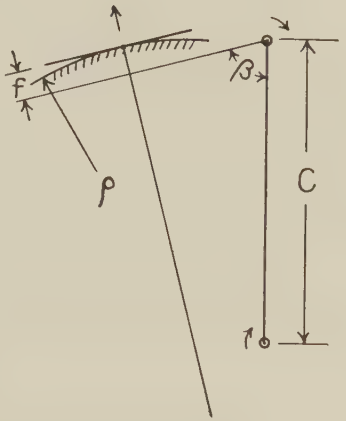

FIG. 5 FLAT FOLLOWER

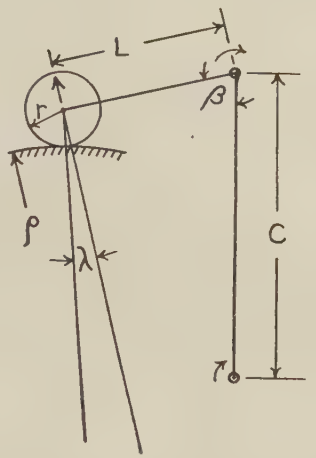

FIG. 6 CIRCULAR FOLLOWER

		Translation			Rotation	
Velocity = 0 High or low point	Pressure angle	———	$\lambda = 0$	$\tan \lambda = \frac{-e}{b}$	———	$\tan \lambda = \operatorname{ctn} \beta - \frac{L}{C \sin \beta}$
	Curvature	$\rho = b + y$	$\frac{1}{\rho'} = \frac{1}{b}\left(1 - \frac{y}{b}\right)$ $\rho = \rho' - r$	$\frac{1}{\rho'} = \frac{\cos \lambda}{b}\left(1 - \frac{y}{b}\cos^2 \lambda\right)$ $\rho = \rho' - r$	$\rho'' = C\,[\sin \beta + \psi \cos \beta]$ $\rho = \rho'' + f$	$\frac{1}{\rho'} = \frac{\cos \lambda}{C \sin \beta}\left[1 - \frac{L \cos^2 \lambda}{C \sin \beta} \cdot \psi\right]$ $\rho = \rho' - r$
Velocity ≠ 0 General case	Pressure angle	———	$\tan \lambda = \frac{x}{b}$	$\tan \lambda = \frac{x - e}{b}$	———	$\tan \lambda = \operatorname{ctn} \beta - \frac{L(1 - x)}{C \sin \beta}$
	Curvature	$\rho = b + y$	$\frac{1}{\rho'} = \frac{\cos \lambda}{b}\left[1 + \frac{\cos \lambda}{b}(x \sin \lambda - y \cos \lambda)\right]$ $\rho = \rho' - r$		$\rho'' = \frac{C}{(1 - x)^2}\left[(1 - 2x) \sin \beta + \frac{\psi}{(1 - x)} \cos \beta\right]$ $\rho = \rho'' + f$	$\frac{1}{\rho'} = \frac{\cos \lambda}{C \sin \beta}\left\{1 + \frac{L \cos \lambda}{C \sin \beta}\,[x(1 - x) \sin \lambda - \psi \cos \lambda]\right\}$ $\rho = \rho' - r$

This paper presents a method of determining the cam curvature for a given set of dimensions and for all cases of follower motion:

(*a*) Circular follower, radial translation.
(*b*) Circular follower, offset translation.
(*c*) Circular follower, rotation.
(*d*) Flat follower, translation.
(*e*) Flat follower, rotation.

The corresponding formulas are listed in Table 1. It is believed that those for a circular follower and for a rotating flat follower have never before been published. It will be seen that the formulas assume a simplified form for the special case where the follower velocity is momentarily zero. In many instances this is also the point of maximum curvature. This condition is discussed at greater length later in this paper.

Constructions are also given, based upon the theorem of three centers, for locating the center of cam curvature by geometrical means.

Characteristics of Follower Motion

To the order required for the determination of cam curvature the follower motion is sufficiently defined by the quantities x and y for translation and χ and χ for rotation. While it is unnecessary to bring in the concept of time, these quantities may be related to actual velocity and acceleration by the following equations, where

t = time

$\omega_c = \dfrac{d\theta}{dt}$ = angular cam velocity, radians per sec

$x = \dfrac{db}{d\theta}$

$y = \dfrac{dx}{d\theta} = \dfrac{d^2b}{d\theta^2}$

$\chi = \dfrac{d\beta}{d\theta}$

$\psi = \dfrac{d\chi}{d\theta} = \dfrac{d^2\beta}{d\theta^2}$

$v = \dfrac{db}{dt}$ = follower velocity, translation, in. per second

$a = \dfrac{dv}{dt} = \dfrac{d^2b}{dt^2}$ = follower acceleration, translation, in. per (second)^2

$\omega = \dfrac{d\beta}{dt}$ = follower velocity, rotation, radians per second

$\alpha = \dfrac{d\omega}{dt} = \dfrac{d^2\beta}{dt^2}$ = follower acceleration, rotation, radians per (second)^2

$$x = \frac{v}{\omega_c} \qquad y = \frac{a}{\omega_c^2} \ldots\ldots\ldots\ldots [1a, b]$$

$$\chi = \frac{\omega}{\omega_c} \qquad \psi = \frac{\alpha}{\omega_c^2} \ldots\ldots\ldots\ldots [2a, b]$$

Where the follower motion is readily defined mathematically, as for constant acceleration or harmonic motion, x and y or χ and ψ are easily obtained from this knowledge. Otherwise they may be easily obtained from a table of successive follower positions such as is often required for cam manufacture. Let

$\Delta\theta$ = tabular interval of cam rotation, deg
d_1 = average of first differences on each side of assumed tabular value, in. or deg
d_2 = second difference at assumed tabular value, in. or deg

Then

$$x = \left(\frac{180}{\pi}\right) \cdot \frac{d_1}{\Delta\theta} \qquad y = \left(\frac{180}{\pi}\right)^2 \cdot \frac{d_2}{\Delta\theta^2} \ldots\ldots [3a,b]$$

$$\chi = \frac{d_1}{\Delta\theta} \qquad \psi = \left(\frac{180}{\pi}\right) \cdot \frac{d_2}{\Delta\theta^2} \ldots\ldots [4a, b]$$

The sign of d_1 is taken as positive when the follower displacement is increasing, and d_2 is positive when d_1 is increasing algebraically.

Derivation of Formulas

The following nomenclature for points and lines is used in the derivations:

O = center of cam rotation
P = center of circular follower
Q = point of contact of cam and follower
I = instant center of relative motion
K = center of curvature of cam
N = contact normal
F = turning center of rotating follower

Primes are used to designate positions after an infinitesimal cam rotation $d\theta$.

The general method employed in the derivations is simple. The contact normal N is first determined for the original configuration; a second position N' is then obtained corresponding to an infinitesimal cam rotation $d\theta$. The intersection of these successive positions of the normal is the center of curvature.

For a flat follower, the normal is located by the position of one of its points (the instant center I) and the knowledge that it is perpendicular to the follower. For a circular follower, the normal must contain both the instant center I and the follower center P.

Circular Follower

Circular Follower—Translation. Fig. 7 shows a circular follower with center P moving along a straight path offset a distance e from the cam center O. The instantaneous position of the follower is defined by the quantity b, measured in the direction of motion. In addition we must know the values of the quantities x and y which characterize the velocity and acceleration of the follower.

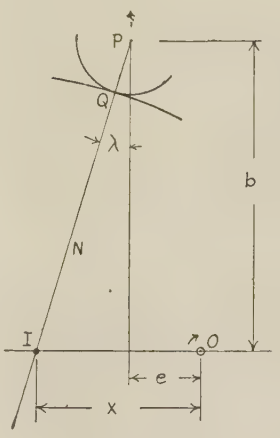

Fig. 7 Circular Follower With Translational Motion

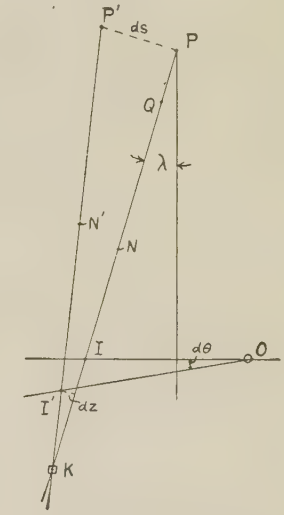

Fig. 8 Circular Follower With Translational Motion
(Position of normal after infinitesimal displacement.)

The instant center I is readily located on a line perpendicular to the follower path and containing cam center O. To satisfy the requirement that cam and follower have equal velocities at I

$$\overline{OI} = \frac{db}{d\theta} = x$$

The normal N may now be drawn through P and I, locating the point of contact Q; and the pressure angle λ is seen to be given by the equation

$$\tan \lambda = \frac{x - e}{b} \quad [5]$$

We may now consider an infinitesimal relative rotation $d\theta$; for convenience, we consider the cam to be the stationary member, see Fig. 8. Since the follower is instantaneously rotating about I, the displacement of P to P' is perpendicular to the normal and is equal to

$$\overline{PP'} = ds = \overline{PI} \cdot d\theta = b \sec \lambda \cdot d\theta$$

The displacement of the instant center I is composed of two components.

(a) Due to the follower acceleration, x increases an amount

$$dx = y \cdot d\theta$$

(b) Due to the rotation $d\theta$, I moves vertically a distance $x \cdot d\theta$. The resultant displacement of I perpendicular to the normal is

$$dz = dx \cos \lambda - x \cdot d\theta \sin \lambda$$

or

$$dz = (y \cos \lambda - x \sin \lambda) d\theta$$

The displacement in the direction of the normal may be ignored as it represents only a higher-order effect.

The new positions of P and I define the new normal N', whose intersection with N is the required center of curvature K. By similar triangles we get

$$\frac{\overline{IK}}{\overline{PK}} = \frac{dz}{ds}$$

Then, since

$$\overline{PK} = \rho'$$
$$ds = b \sec \lambda \, d\theta$$
$$dz = (y \cos \lambda - x \sin \lambda) d\theta$$
$$\overline{IK} = \rho' - b \sec \lambda$$

We get

$$\frac{\rho' - b \sec \lambda}{\rho'} = \frac{y \cos \lambda - x \sin \lambda}{b \sec \lambda}$$

Whence

$$\frac{1}{\rho'} = \frac{\cos \lambda}{b} \left[1 + \frac{\cos \lambda}{b} (x \sin \lambda - y \cos \lambda) \right] \quad [6]$$

An important special case is obtained when the follower velocity is zero, namely

$$\frac{1}{\rho'} = \frac{\cos \lambda}{b} \left[1 - \frac{\cos^2 \lambda}{b} \cdot y \right] \quad [7]$$

Also, when the follower offset, as well as velocity, is zero

$$\frac{1}{\rho'} = \frac{1}{b} \left[1 - \frac{y}{b} \right] \quad [8]$$

The radius of curvature of the cam itself is of course

$$\rho = \rho' - r \quad [9]$$

Circular Follower—Rotation. This case is somewhat more complicated. Fig. 9 shows cam center O and the center of follower rotation F separated by center distance C. The follower center P swings about F at a distance L. The instantaneous follower position is defined by the angle β, and the first and second derivatives of the follower motion are χ and ψ.

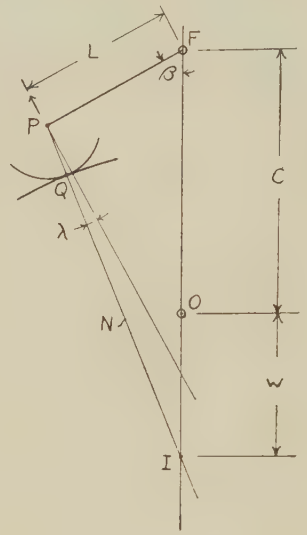

FIG. 9 SWINGING CIRCULAR FOLLOWER

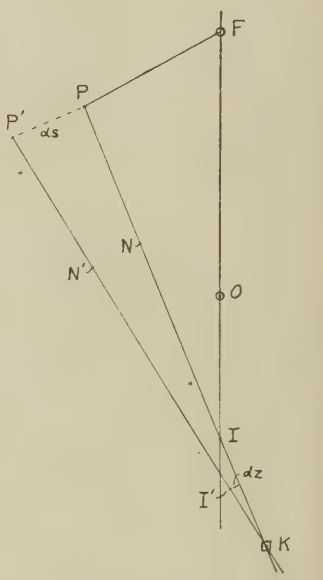

FIG. 10 SWINGING CIRCULAR FOLLOWER
(Position of normal after infinitesimal displacement.)

Here again we first locate the instant center I, which in this case lies on the line of centers at a distance from O of w where

$$\frac{w}{C + w} = \frac{d\beta}{d\theta} = \chi$$

Hence

$$w = \frac{C\chi}{(1 - \chi)} \quad [10]$$

and

$$(C + w) = \frac{C}{(1 - \chi)} \quad [11]$$

The normal N as before contains P and I, locating the point of contact Q. Solution of the triangle FPI yields the formula for the pressure angle λ

$$\tan \lambda = \operatorname{ctn} \beta - \frac{L(1 - \chi)}{C \sin \beta} \quad [12]$$

as well as the distance

$$\overline{PI} = \frac{C \sin \beta}{(1 - \chi) \cos \lambda}$$

Referring to Fig. 10, we assume again an infinitesimal rotation $d\theta$, the cam being considered stationary. The relative rotation of the follower is then $(d\theta - d\beta)$ about instant center I, from which

we obtain the displacement of point P as $\overline{PI}\cdot(d\theta - d\beta)$ perpendicular to normal N. Then, since $(d\theta - d\beta) = d\theta(1 - \chi)$

$$ds = C\frac{\sin\beta}{\cos\lambda}\cdot d\theta$$

The displacement of point I is again composed of two parts, one of which is the increase in distance w. This is most readily obtained by differentiating Equation [11], whence

$$dw = \frac{C\psi}{(1-\chi)^2}\cdot d\theta$$

where

$$\psi = \frac{d\chi}{d\theta}$$

In addition to the displacement dw along the line of centers, I rotates an angle $d\theta$ about O, giving a linear displacement perpendicular to the line of centers of $w\cdot d\theta$.

The resultant displacement perpendicular to the normal is

$$dz = dw\cos(\beta+\lambda) - wd\theta\sin(\beta+\lambda)$$

or

$$dz = \left[C\cos(\beta+\lambda)\cdot\frac{\psi}{(1-\chi)^2} - C\sin(\beta+\lambda)\cdot\frac{\chi}{(1-\chi)}\right]d\theta$$

Since $\overline{PK} = \rho'$, we again obtain from similar triangles

$$\frac{\rho' - \overline{PI}}{\rho'} = \frac{dz}{ds}$$

Substituting equations previously obtained for $\overline{PI}$, dz, and ds we get

$$\frac{1}{\rho'} = \frac{\cos\lambda}{C\sin\beta}\left\{(1-\chi) + \frac{\cos\lambda}{\sin\beta}\left[\chi\sin(\beta+\lambda) - \frac{\psi}{(1-\chi)}\cos(\beta+\lambda)\right]\right\} \quad \ldots\ldots [13]$$

While this constitutes a solution of the problem, we may simplify considerably by a transformation not given here to yield

$$\frac{1}{\rho'} = \frac{\cos\lambda}{C\sin\beta}\left\{1 + \frac{L\cos\lambda}{C\sin\beta}\left[\chi(1-\chi)\sin\lambda - \psi\cos\lambda\right]\right\}. \quad [14]$$

Furthermore, to bring out an analogy between this case and that of an offset translation we may make the following substitutions

$$C\sin\beta = b$$
$$L - C\cos\beta = e$$
$$\chi = \frac{x}{L}$$
$$\psi = \frac{y}{L}$$

to obtain the following forms, which should be compared with Equations [5] and [6]

$$\tan\lambda = \frac{x-e}{b}$$

$$\frac{1}{\rho'} = \frac{\cos\lambda}{b}\left\{1 + \frac{\cos\lambda}{b}\left[x\left(1-\frac{x}{L}\right)\sin\lambda - y\cos\lambda\right]\right\} \ldots [15]$$

Flat Follower—Translation. The curvature of a cam imparting translational motion to a flat follower has been discussed thoroughly in a recent paper by Candee;[4] Berard and Waters[2] give simple design formulas for determining the minimum cam size for a flat follower having constant acceleration or harmonic motion. No derivation is given here, but the formula is included in Table 1 for completeness.

Rotating Flat Follower. This case is similar to that of the rotating circular follower and somewhat simpler. Referring to Fig. 11, O and F are the turning centers as before, separated

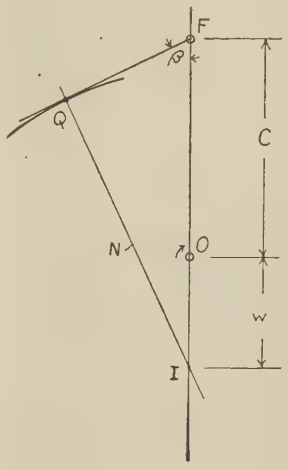

FIG. 11 SWINGING FLAT FOLLOWER

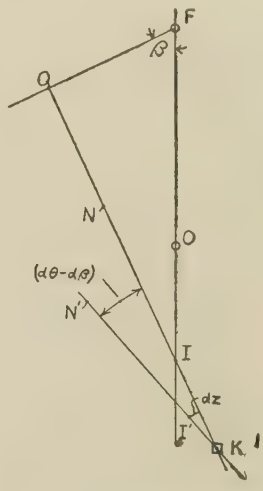

FIG. 12 SWINGING FLAT FOLLOWER
(Position of normal after infinitesimal displacement.)

by distance C. The follower consists of the line FQ, whose instantaneous position is defined by the angle β. As before

$$\chi = \frac{d\beta}{d\theta} \quad \text{and} \quad \psi = \frac{d^2\beta}{d\theta^2}$$

We locate the instant center I as before on the line of centers such that

$$\overline{OI} = w = \frac{C\chi}{(1-\chi)}$$

The normal N may then be drawn through I perpendicular to the follower, locating the contact point Q.

After a rotation $d\theta$, the two displacement components of I are, as before,

$$dw = \frac{C\psi}{(1-\chi)^2}d\theta$$

$$w\cdot d\theta = \frac{C\chi}{(1-\chi)}d\theta$$

so that the resultant perpendicular to N is

$$dz = \left[C\cos\beta\cdot\frac{\psi}{(1-\chi)^2} - C\sin\beta\cdot\frac{\chi}{(1-\chi)}\right]d\theta$$

The new normal N', remaining normal to the follower, makes an angle with the original normal N of $(d\theta - d\beta) = d\theta(1-\chi)$.

We may then use the triangle $II'K$ to obtain

$$\overline{IK} = \frac{dz}{(1-\chi)d\theta}$$

[4] "Kinematics of Disk Cam and Flat Follower," by Allan H. Candee, Trans. ASME, vol. 69, 1947, pp. 709–724.

The radius of curvature ρ'' of the cam is then $(\overline{QI} + \overline{IK})$, or

$$\rho'' = (C + w) \sin \beta + C \cos \beta \frac{\psi}{(1 - \chi)^3} - C \sin \beta \frac{\chi}{(1 - \chi)^2} \quad \ldots\ldots [16]$$

or by substitution for w and rearranging

$$\rho'' = \frac{C}{(1 - \chi)^2}\left[(1 - 2\chi) \sin \beta + \frac{\psi}{(1 - \chi)} \cos \beta\right] \ldots [17]$$

Where the follower surface is offset from its center of rotation F by an amount f, see Fig. 5, the radius of cam curvature is simply

$$\rho = \rho'' + f \ldots\ldots [18]$$

Point of Maximum Curvature

It is possible, by differentiating the appropriate curvature formula, to set up a relation between the variables for the condition of maximum curvature. In the general case such a relation is too complicated to be of practical use, and it is far shorter to calculate the curvature at several points and to plot these results to determine the worst position.

An analytical determination of the point of maximum curvature obviously requires an analytical expression for the follower motion. If we consider two of the most common follower motions, harmonic and constant acceleration, we may obtain for the simpler cases considerable information as to the location of the critical point.

Considering only translational follower motion, we may study a portion of the cam corresponding to a rotation of θ_R radians. At both ends of this interval the follower velocity is zero; the follower distance decreases during the rotation from b_X to b_N. Under these conditions, the following rules apply for the location of the point of maximum curvature:

Flat Follower. The maximum curvature always occurs where $b = b_X$ for both harmonic and constant acceleration returns. In the special case of harmonic motion where $\theta_R = 180$ deg, the curvature is constant, the cam profile is a semicircle, and represents the well-known case of the eccentric circle.

Circular Follower—Constant Acceleration. Maximum curvature occurs for $b = b_X$ when

$$\left(\frac{b_X - b_N}{b_X}\right) > 0.316\ \theta_R{}^2 \ldots\ldots [19]$$

This represents the majority of cases where danger of a cusp exists; only where a relatively large roller is used will it be necessary to investigate other points.

Circular Follower—Harmonic Motion. Here again the maximum curvature usually occurs when $b = b_X$. The necessary condition is

$$\left(\frac{b_X - b_N}{b_X}\right) > \left(\frac{\theta_R}{\pi}\right)^2\left[1 + \sqrt{\frac{7}{3} - \frac{4}{3}\left(\frac{\pi}{\theta_R}\right)^2}\right] \ldots [20]$$

Geometrical Constructions for Center of Curvature

The following constructions serve to locate the center of curvature by geometrical means. They are of great value for general points, but unfortunately fall down for certain dead-center positions.

Detailed derivations of these constructions are not given here, but it may be well to indicate in a general way the method involved. We employ an extension of the familiar theorem of three centers to a system of five bodies: the frame, the cam, the follower, the contact normal, and an auxiliary body geared to the cam and carrying the instant center of the follower relative to the cam. We locate successively the various instant centers of the system, arriving eventually at the instant center of the normal relative to the cam, which is the required center of curvature.

The constructions are shown in Figs. 13, 14, and 15. In each case it is first necessary to locate the instant center I. For the follower with straight-line motion, Fig. 13, I lies on a line OI through the cam center and perpendicular to the direction of motion at a distance x. For a rotating follower, I is located on the line of centers at a distance from the cam center of

$$w = \frac{C\chi}{(1 - \chi)}$$

The contact normal may then be drawn through I, containing point P for a circular follower, and perpendicular to the follower for a flat follower.

Just as the instant center I characterizes the velocity of the follower, point A characterizes its acceleration. OA is perpendicular to OI, and for Fig. 13, $\overline{OA} = y$. For the rotating followers in Figs. 14 and 15

$$\overline{OA} = \frac{C\psi}{(1 - \chi)^2}$$

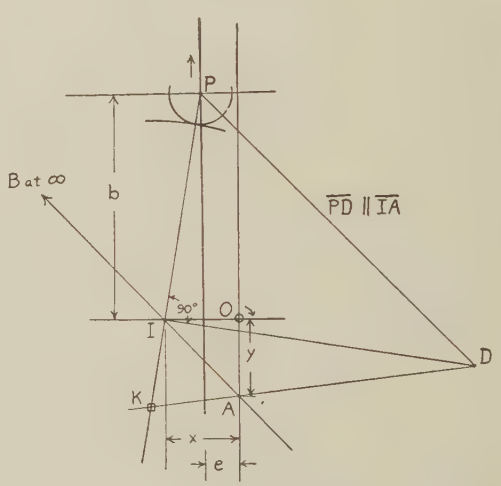

Fig. 13 Construction for Center of Curvature of Cam
(Circular follower with translational motion.)

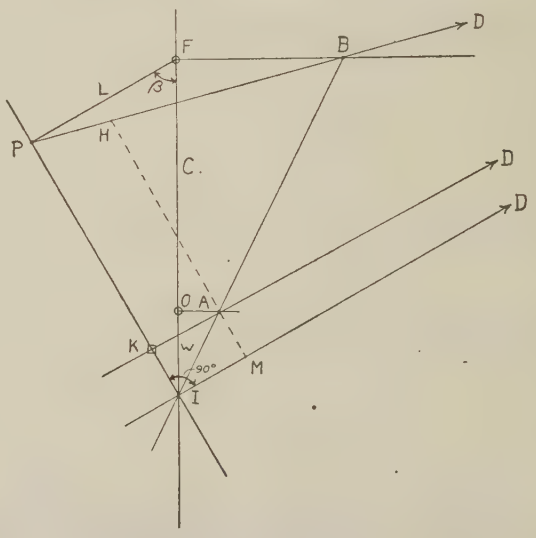

Fig. 14 Construction for Center of Curvature of Cam
(Swinging circular follower.)

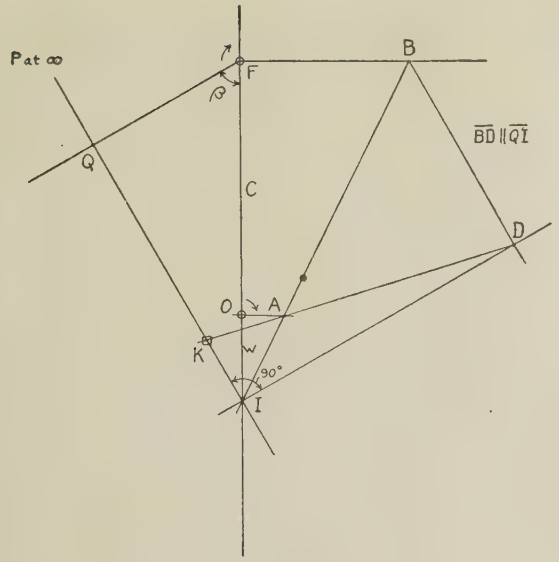

FIG. 15 CONSTRUCTION FOR CENTER OF CURVATURE OF CAM (Swinging flat follower.)

While the three figures differ somewhat in appearance, we may see that they are really identical when we consider that in Fig. 13 point B is at ∞ along line IA, while the "line of centers" is perpendicular to the direction of motion, and in Fig. 15 point P is at ∞ along line $\overline{IQ}$.

In Fig. 14 point D frequently lies at an inconvenient distance, in which case we draw the auxiliary line $\overline{HAM}$ parallel to $\overline{PI}$, so that

$$\frac{\overline{IK}}{\overline{PI}} = \frac{\overline{MA}}{\overline{HM}}$$

EXAMPLE

This example indicates how these formulas may be applied to a simple typical design problem. A series of cams is to be designed, each having the same minimum radius (perhaps governed by a hub diameter) but varying in throw from 0.4 in. to 1.0. The follower is a 1-in-diam roller constrained to move in a straight path which, extended, contains the center of rotation of the cam. The return motion is to be of the constant-acceleration type, and the problem is to find the smallest angle θ_R which can be used for this return for each throw.

The following data are given:

Minimum cam radius, R_N ..... 2.0 in.
Roller radius, r ..... 0.5 in.
Throw, T ..... 1.0, .. 0.4 in.
Minimum allowable radius of curvature of cam. 0.2 in. (assumed)

The values of b at the start and end of the return are

$$b_N = R_N + r = 2.5$$
$$b_X = b_N + T = 2.5 + T$$

Since the motion is to be constant acceleration, and $y = \frac{d^2b}{d\theta^2}$

$$(b - b_X) = \frac{1}{2} y \cdot \theta^2$$

in general, and

$$-\frac{1}{2} T = \frac{1}{2} y \left(\frac{1}{2} \theta_R\right)^2$$

for the first half of the return. Hence

$$y = \frac{-4T}{\theta_R{}^2} \qquad [21]$$

Referring to Equation [8] and considering the conditions when $b = b_X$

$$\frac{1}{\rho'} = \frac{1}{b_X}\left(1 - \frac{y}{b_X}\right)$$

We require that $\rho' = r + \Delta r = 0.7$ in. at this position. Hence

$$y = b_X\left(1 - \frac{b_X}{r + \Delta r}\right)$$

or

$$\theta_R{}^2 = \frac{4T}{b_X\left(\frac{b_X}{r + \Delta r} - 1\right)} \qquad [22]$$

Before proceeding with calculations for obtaining θ_R for each desired throw, we may check against Equation [19] to make sure that the maximum cam curvature will occur at the high point. From Equation [19] we see that this is the case when the quantity $\left[\frac{b_X - b_N}{b_X \cdot \theta_R{}^2}\right]$ is greater than 0.316.

But from Equation [22] we have

$$\left[\frac{T}{b_X \cdot \theta_R{}^2}\right] = \frac{1}{4}\left(\frac{b_X}{r + \Delta r} - 1\right)$$

Computing this quantity for values of T = 1 in. and 0.4 in., we obtain 1.0 and 0.8, respectively, and since these exceed 0.316, we know the worst position is at the high point, as assumed.

The calculations for θ_R, the minimum permissible return angle, may be tabulated as follows

T (throw)	1.0	0.8	0.6	0.4
$b_X = 2.5 + T$	3.5	3.3	3.1	2.9
$\left(\frac{b_X}{0.7} - 1\right)$	4.0	3.714	3.429	3.143
$\theta_R{}^2 = \frac{4T}{b_X\left(\frac{b_X}{0.7} - 1\right)}$	0.286	0.261	0.226	0.1755
θ_R, radians	0.535	0.511	0.475	0.419
θ_R, deg	30.7	29.3	27.2	24.0

In closing it should be remarked that Equation [22] will be found particularly useful in the preliminary stages of design as an aid in arriving at proper size relationships.

Studies in Boundary Lubrication—III The Wear of Carbon Brushes in Dry Atmospheres

By W. E. CAMPBELL,[1] AND ROSE KOZAK[2]

The dusting wear of carbon brushes is studied in dry nitrogen at atmospheric pressure. The effect of water, oxygen, and carbon dioxide on dusting wear is described, and the results compared with those of investigations carried out under partial vacuum conditions. No effect of current, up to 114 amp per sq in. is found under the conditions studied. It is shown that a highly oriented natural graphite specimen or an oriented graphite brush, operated so that the faces of the cleavage planes rub on a plane rotating copper surface, neither dusts nor produces wear on the copper surface in dry nitrogen. When operated so that the edges of the cleavage planes rub against the plate, rapid dusting wear takes place and the copper surface is deeply scored. The dusting rate of carbon brushes in dry nitrogen against several metals is given. The rate is shown to decrease as the hardness of the metal increases, the behavior of brass being exceptional. It is found to be zero on smooth chromium and rhodium surfaces. On the assumption that an adsorbed lubricant film prevents scoring of the plate by the edges of the graphite crystals, allowing them to be oriented, the results are shown to be consistent with recent theories of solid friction.

Introduction

EARLY in 1942 it was known by several of the leading manufacturers of motor generators and brushes that, under the conditions prevailing at high altitudes (20,000 to 40,000 ft), vastly accelerated wear or "dusting" of carbon brushes took place. It was also recognized that the wear was related to the low water content of the atmosphere at these altitudes. The mechanism of action of water as a wear-preventing agent was not understood, there was disagreement in the experimental findings from different sources, and no really adequate wear-preventive treatment had been developed for brushes operating at high current densities. Owing to the urgency of the situation, large-scale development studies, aimed at discovery of more effective treatments, occupied the major attention of these investigators. The present investigation was initiated in 1942, and continued to the end of 1943, because of the urgent need expressed by these manufacturers for a better understanding of the fundamental mechanism of high-altitude dusting.

The results of several other fundamental investigations have been published (1),[3] and some of the work to be presented here covers similar ground. All these studies, however, were carried out in evacuated systems at low pressures, whereas the present work was carried out at atmospheric pressure.

[1] Bell Telephone Laboratories, Murray Hill, N. J.

[2] Formerly with Bell Telephone Laboratories.

[3] Numbers in parentheses refer to the Bibliography at end of paper.

Contributed by the Research Committee on Lubrication and presented at the Annual Meeting, New York, N. Y., Nov. 26–29, 1945, of THE AMERICAN SOCIETY OF MECHANICAL ENGINEERS.

Description of Apparatus and Procedure

The apparatus consisted essentially of a device for pressing the square end of a vertically mounted brush against a rotating plate in a bell jar through which a controlled atmosphere was passed. It is shown in Fig. 1, with the gas-purification and mixing train disconnected. The brush was held in a brass block, mounted on pivots on a steel support screwed to a brass base plate. The tendency of the brush to rotate in the horizontal plane when the disk rotated was restrained by a steel spring attached to the steel support, and a horizontal pointer on the block indicated the torque. The brush was loaded by means of flat lead disks slipped over a hollow rod. A spring was placed between the end of the rod and the top of the brush. As the brush wore, the edge of the disk moved down along a vertical scale graduated in millimeters, and the reading on the scale was recorded at short time intervals. The copper test plate against which the brush was pressed was screwed on its underside to a steel disk locked to a shaft which was rotated on ball bearings at a speed of 1725 rpm. The diameter of the brush track was 2 in. The brush dimensions were $1^1/_4$ in. $\times$ $^3/_{16}$ in. $\times$ $^3/_{16}$ in.

In studying the effect of current, one lead was soldered to a silver film deposited from silver paste on the upper end of the brush and passed up through the hollow rod supporting the weights. The other lead was made through a silver-plated phosphor-bronze spring pressing against a rhodium-plated section of the rotating shaft.

A tapered hole was drilled in the brush track of some of the copper plates; a close-fitting, tapered copper insert was fitted to the holes, and polished flush with the plate. This insert could be removed at the end of a run and its surface examined by electron diffraction.

The bell jar was ground along its lower edge and was tightly clamped to a brass platform. Gas of regulated composition entered the bell jar through a ground-glass joint at the top and passed out through the upper ball bearing in the platform, thus carrying away grease vapors which might tend to contaminate the plate. The upper ball bearing was lubricated with a vacuum-stop-cock grease.

The purification train was arranged so that a measured flow of nitrogen, purified by passage over freshly reduced copper at 300 C, could be mixed with measured flows of other gases such as oxygen or carbon dioxide. The mixture was purified with activated carbon and dried with dehydrite and phosphorus pentoxide. The line could then be split and any given fraction by-passed through a water bubbler at a measured rate and remixed with the main stream. Although an efficient saturator was employed, it has been shown (2) that it is extremely difficult to saturate a gas with water by bubbling through the liquid. The partial pressures given have been based on the assumption of 80 per cent saturation of the gas. The volume of the bell jar was 10 liters, and the total flow was usually maintained at 150 liters per hr.

In boundary-lubrication studies, it has been frequently pointed out that very careful precautions should be taken to free the sur-

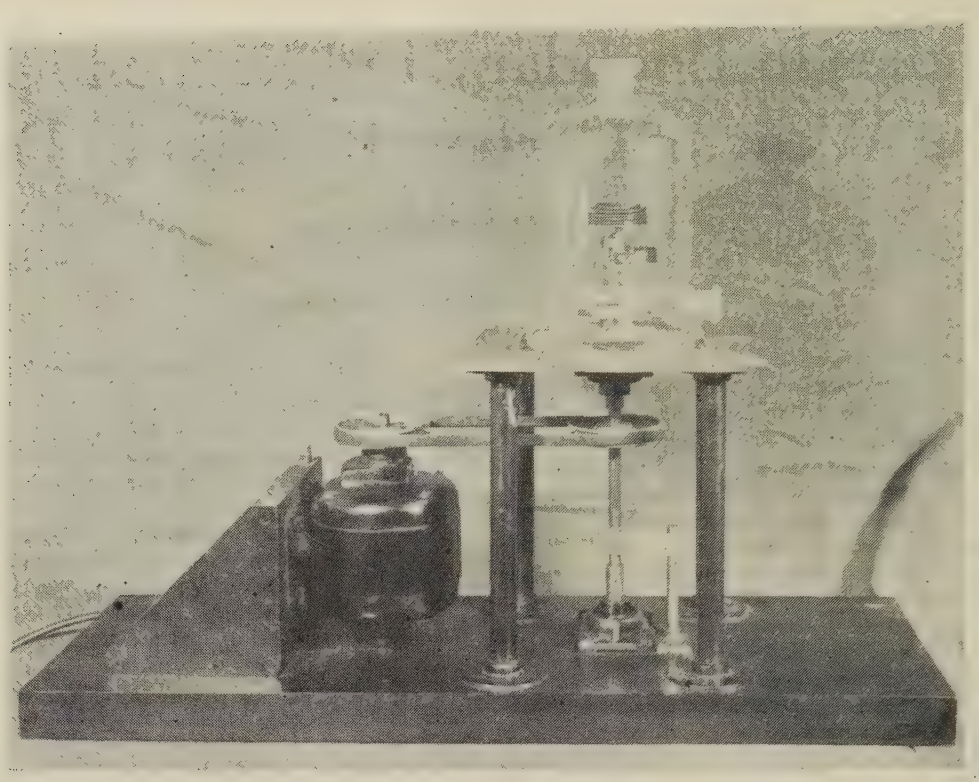

FIG. 1 APPARATUS FOR STUDYING DUSTING WEAR OF CARBON BRUSHES

faces from organic contamination (4). The same care is essential in studying carbon-brush wear, as has been convincingly demonstrated by Van Brunt and Savage (3). The plate was polished successively with 1, 0, and 0000 French emery and was cleaned by polishing with levigated alumina on wet broadcloth (4), or by cathode degreasing. The plate was held in a steel jig during cleaning, to prevent contact with the bare hands. When dry, it was removed with clean metal tongs, placed on the support, and screwed into place. The test gas was checked frequently for freedom from greasiness by allowing it to impinge directly on a freshly cleaned plate. If, after this, the plate reacted clean to the water wetting test, the gas was assumed to be sufficiently free of adsorbable grease. The brush was cleaned by heating to 500 C for 5 to 10 min. It was placed in the holder when cool, and loaded with the standard load of 2.2 kg per sq cm (31.4 psi). This load is considerably in excess of that used in practice, and was chosen in order to provide accelerated conditions.

The bell jar was clamped into place as soon as possible after cleaning the plate and brush, and the test atmosphere allowed to flow for at least 10 min before starting the motor. Unless otherwise stated, all the experiments were run with no current flowing. The brush type selected for all the studies of the variables affecting standard brush operation was an exceptionally pure grade of electrographitic carbon. It had a coke binder, and was fired originally at 2800 C. It had a scleroscope hardness of 50, a resistivity of 7×10^{-4} ohm-inches, a density of 1.75, and an ash content of 0.2 per cent. The wear versus time curves for this carbon are accurately linear. The mean of the wear rates in dry nitrogen for 20 brushes cut at random from a large block of the material was 1.3 mm per min with a maximum deviation of 0.3 mm per min. The wear-measuring device was not sufficiently sensitive to measure the wear of brushes in moist nitrogen or air over the short time periods used for an average run. Therefore the wear rates under these conditions have been designated zero throughout this paper.

Because of the variability from brush to brush, the same brush was generally used in studying a given effect. The procedure used was to run the brush in dry nitrogen for 5 min to establish the rate. The variable to be studied was then introduced, and a new rate established over a 5-min period. Successive changes in the variable were then studied in the same manner until the desired range had been covered. The rate was then redetermined in dry nitrogen to check whether the original rate could be reproduced. In all the runs recorded in this paper the original rate was always reproduced at the end of the run to within 0.1 mm per min.

The friction-measuring device did not permit very accurate measurement of friction. Under dusting conditions bad stick-slip took place, and readings were highly erratic; under no-wear conditions the friction was steady. The friction results were consistent with those reported by others (6), the coefficient running from 0.5 to 1.0 for dusting wear, and from 0.1 to 0.2 when wear was negligible.

Effect of Brush Pressure on Wear Rate With and Without Current Flow

The run was started on a clean polished plate in dry nitrogen with a pressure of 220 g per sq cm (3.13 psi), and was continued long enough to establish a steady wear rate, both with and without a current flow of 114 amp per sq in. The same procedure was adopted for each point on the curve in Fig. 2. Over the range covered, which includes the pressures commonly employed in industry, the rate of wear is an increasing function of load. This behavior is in accord with experience in field tests on commercial machines.

The current produced no measurable effect at any load studied when moisture was absent. This result is in accord with the findings of other investigators, and indicates that the dusting wear of carbon brushes in dry atmospheres is due to the absence of an adsorbed lubricating film and not primarily to erosive effects of current. The accelerating effect of current, so frequently

noted in field studies and altitude-chamber tests on standard machines, is probably due to the evaporation of organic contamination at the high brush temperatures caused by the current flow, and to the mechanical ploughing effect of irregularities in the commutator surface producing by sparking.

Effect on Brush Wear of Diluent Gases in Nitrogen

In studying the effect of diluent gases, very low concentrations were generally used first, and the amount increased until the wear reached the zero rate. Fig. 3 shows the dusting rate as a function of moisture content expressed as partial pressure of water vapor. At a partial pressure of water vapor equal to 0.6 mm of mercury the rate became zero. The effect was reversible, that is, on decreasing the water concentration to the lowest amount possible, the rate increased to the initial dry rate. The shape of the curve is quite similar to that of other investigators (5, 6), but the partial pressure at which wear ceases is somewhat lower. The difference can probably be accounted for by the difference in surface temperature resulting from operation at low pressures on the one hand and at atmospheric pressure in the present studies. In all, this experiment was repeated six times to see how closely the partial pressure of moisture necessary to stop wear could be reproduced on different brushes. The average value found from these experiments was 0.65 ± 0.1 mm of mercury.

The rate of wear versus concentration curves in Figs. 4 and 5 for oxygen and carbon dioxide were obtained in a similar manner

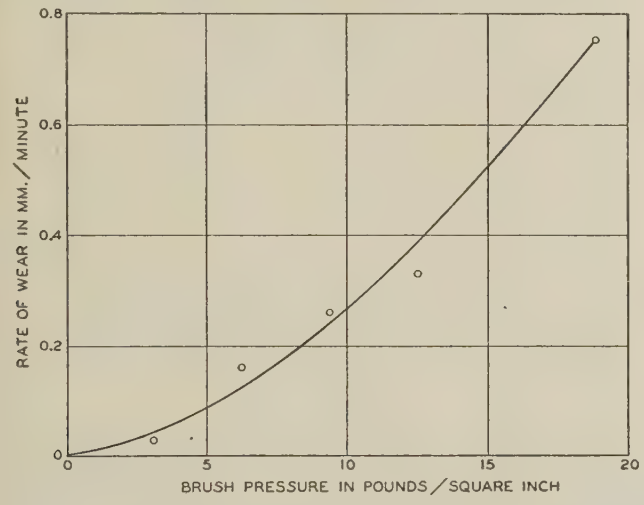

Fig. 2 Rate of Wear of Carbon Brush in Dry Nitrogen Versus Brush Pressure

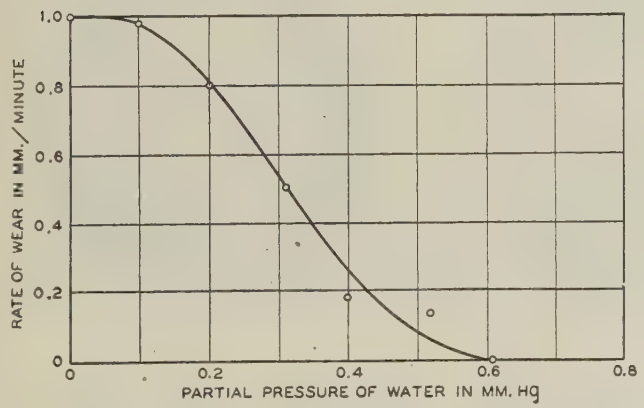

Fig. 3 Rate of Wear of Carbon Brush Versus Partial Pressure of Water in Nitrogen

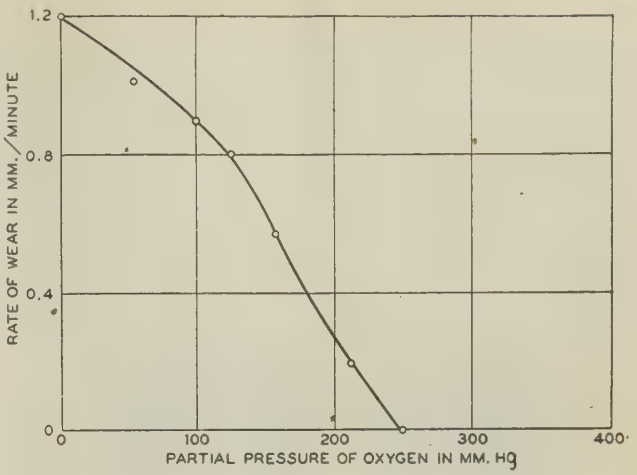

Fig. 4 Rate of Wear of Carbon Brush Versus Partial Pressure of Oxygen in Nitrogen

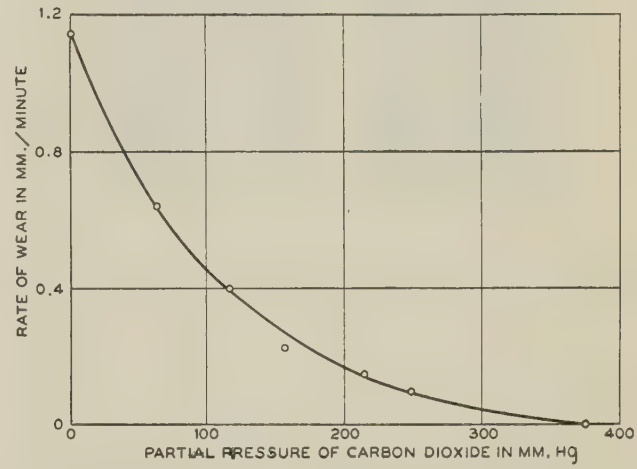

Fig. 5 Rate of Wear of Carbon Brush Versus Partial Pressure of Carbon Dioxide in Nitrogen

to that for water and are of similar type, differing only in the critical pressure required to stop wear. This is of the order of 230 mm for oxygen, and 350 mm for carbon dioxide. The result for carbon dioxide is in disagreement with the findings of Ramadanoff and Glass (6), but is in agreement with an observation made on direct current to 400-cycle aircraft inverters in these laboratories at low temperatures produced by dry ice in an enclosed space. The reason for the disagreement is not known. Similar results to those in Figs. 3, 4, and 5, were obtained on several types of carbon, including some containing copper.

Effect of Orientation of Carbon on Brush Wear

It was found early in the work that if the brush was first run in air or in moist nitrogen, it would not wear subsequently on passage of dry nitrogen. This was true when the running time in the no-wear condition was as short as 10 min. If the run was started in dry nitrogen, dusting started immediately, but stopped within a minute or two when water in sufficient quantity was introduced into the stream. On reintroducing dry nitrogen there was a lag, sometimes as long as 20 min, before dusting started again. If the copper plate was roughened, say, by abrasion with No. 1 emery cloth, and the run started in moist nitrogen, no wear took place; on drying, dusting set in after a time lag, as in the case just described.

Electron-diffraction pictures of the brush and the track after

running in the no-wear condition, showed oriented carbon on both surfaces, Fig. 6*a*. The carbon is oriented so that the faces of the cleavage planes are in the plane of the plate and of the brush face. Electron-diffraction pictures taken after running in the wear condition again showed carbon on both surfaces, Fig. 6*b*, but there was no sign of orientation. The track on the copper frequently showed copper and cuprous oxide in addition to carbon. The degree of orientation found on brushes and track in the no-wear condition was variable, but in no case was any orientation found after rapid wear, although a large number of surfaces were tested.

These results suggested strongly that an adsorbed moisture film

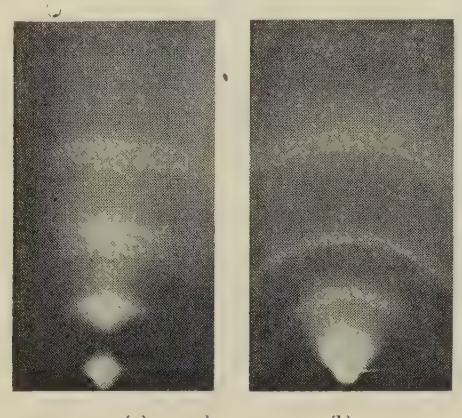

(*a*) (*b*)

FIG. 6(*a*) ORIENTED PATTERN ON CARBON BRUSH FACE AFTER RUNNING WITHOUT WEAR. (*b*) RANDOM PATTERN ON CARBON-BRUSH FACE AFTER DUSTING

acted in some way to aid orientation of the crystals, and that after orientation of the surface layers of the brush was effected, no dusting took place even in the absence of water. Reversal from a no-wear condition back to a dusting condition, when dusting had been stopped by moisture, is explicable on this theory by assuming that, during the initial wear phase, the plate was deeply grooved and torn in the brush track. While water was present in sufficient quantities, its lubricating action kept the wear and friction down, but when it was removed, the grooved track gradually destroyed the oriented layer or layers, finally exposing the disoriented, very hard edges of the crystals in the body of the brush.

This picture suggested that if the brushes were cut from a highly oriented block in such a manner that the faces of the cleavage planes rubbed against the rotating metal surface, then no dusting would be possible even in a dry atmosphere. To check on this possibility, the following experiment was carried out.

Three specimens, $^3/_{16}$ in. square and $^1/_8$ in. thick, were cut from a highly oriented natural graphite specimen and cemented to a standard brush face in such a manner that the cleavage-plane faces lay in the plane of the brush face in one case, and perpendicular to it in the other two. Strict precautions were taken throughout to prevent organic contamination of the exposed face. The brushes were then run in turn in dry nitrogen on polished copper.

The results of this experiment are shown in Fig. 7, and views of the brush tracks in Fig. 8. Identical results were obtained when the experiments were repeated with a current density of 114 amp per sq in. When the faces of the cleavage planes of the specimen were rubbing against the copper surface, after a small initial amount of wear (0.1 mm), no further measurable wear took place over a period of 9 hr; both the brushes run in the edge-on condition started dusting immediately, and were almost completely worn out in less than 40 min. After operation in the face-on condition there is no evidence of any scratching of the copper plate, Fig. 8*b*, whereas in the other two cases there is evidence of consider-

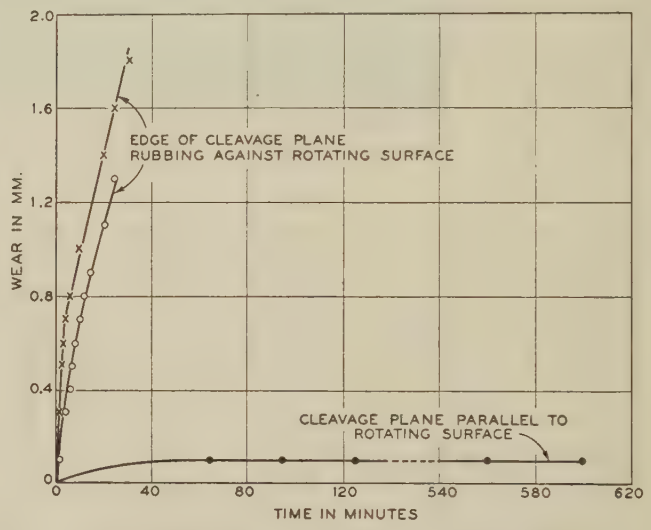

FIG. 7 WEAR VERSUS TIME OF BRUSHES CUT FROM A SPECIMEN OF HIGHLY ORIENTED NATURAL GRAPHITE IN THREE DIRECTIONS

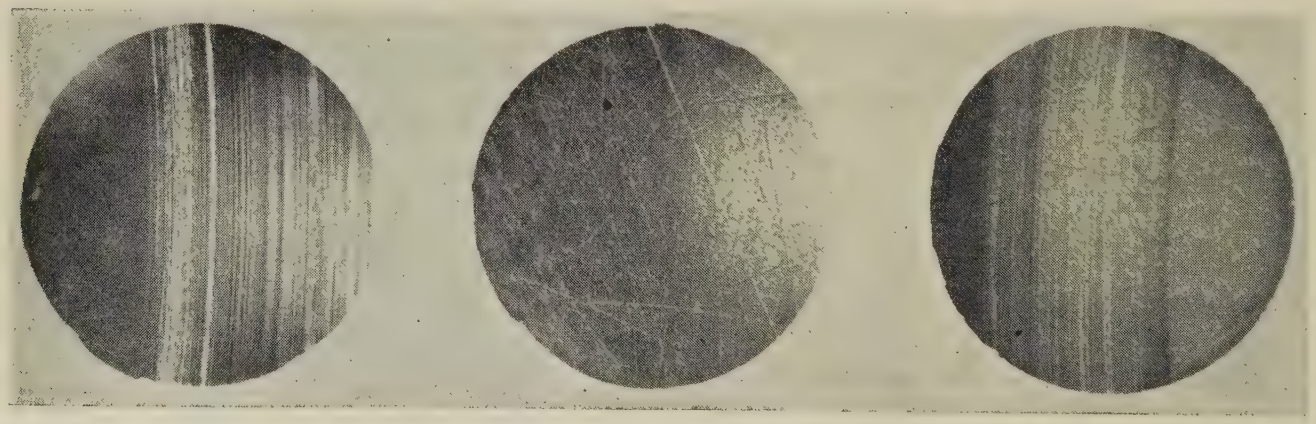

(*a*) (*b*) (*c*)

FIG. 8(*a*) TRACK ON COPPER AFTER RUBBING CONTACT WITH EDGES OF CLEAVAGE PLANES OF GRAPHITE SINGLE CRYSTAL. (*b*) TRACK ON COPPER AFTER RUBBING CONTACT WITH FACES OF CLEAVAGE PLANES OF GRAPHITE SINGLE CRYSTAL. (*c*) AS FOR (*a*) EXCEPT BRUSH WAS ROTATED THROUGH 90 DEG

able grooving, Figs. 8*a* and *c*. This is direct evidence that the edges of the graphite are hard enough to cut into the metal.

As a consequence of these findings, a large number of oriented graphite preparations were compounded to see whether operation without dusting in dry atmospheres could be achieved by operating oriented brushes in the face-on condition. A typical preparation was made by mixing pitch with finely divided graphite in benzene, evaporation of the benzene, pressing the mix in a mold at a pressure of 30 tons per sq in., and firing in graphite at 1000 C. The ratio of resistivity measured in two directions at right angles to each other ran between 3 and 10 to 1.

Wear results in dry nitrogen obtained with such a brush are shown in Fig. 9 and are in full agreement with those for the

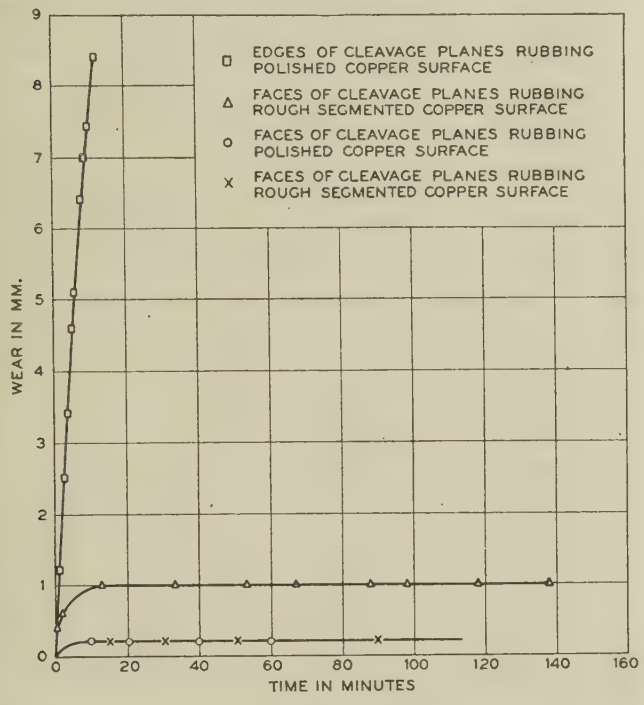

FIG. 9 WEAR VERSUS TIME OF ORIENTED CARBON PREPARATION IN DRY NITROGEN

oriented natural graphite experiment. It is of interest to note that, even on a relatively rough surface, in which radial slots were cut to simulate the segments of a commutator, the wear stopped after an initial period of relatively rapid wear. This indicates that the brush is sufficiently well oriented so that negligible wear takes place after the surface irregularities of the plate are filled and the peaks covered over with an oriented film of graphite.

EFFECT OF DIFFERENT METAL SURFACES ON CARBON-BRUSH WEAR

The wear rates in dry nitrogen of several metals are given in Table 1. The silver, gold, and nickel were electroplated onto a copper surface which had been abraded with No. 1 French emery. The chromium and the rhodium were plated on a copper surface which had been finished with No. 1 French emery, the thickness of the plates being 0.002 in. and 0.000005 in., respectively. After a wear rate had been established in dry nitrogen, the plate was replaced with one of polished copper and a rate determined. The values given in Table 1 are the ratios of these two determinations, that is, the values are referred to a rate for copper of 1 mm per min.

TABLE 1 RELATIVE RATES OF WEAR OF CARBON BRUSH IN DRY NITROGEN ON POLISHED METAL SURFACES

Metal	Rate of wear, mm per min
Silver	1.96
Gold	1.64
Copper	1.00
Nickel	0.19
Brass	0.00
Chromium	0.00
Rhodium	0.00

Although the number of metals is not very large, it is noteworthy that there is a tendency for the dusting of carbon to decrease as the hardness of the metal increases. The correlation is not perfect, the rate on brass being exceptional. Dusting of brushes never took place in dry nitrogen on a polished brass surface. If several short trials were made with a new brush for each trial, but without resurfacing the plate, dusting eventually took place at a rate of 0.5 mm per min. This is believed to be due to the progressive roughening of the metal surface which took place before the edges of the graphite slip planes were oriented into the nonwearing position. It has been shown that very high local temperatures are produced at the interface between two rubbing solids (7); although the nitrogen was carefully purified, enough oxygen was certainly present to allow a thin oxide film to form on the base metal at these temperatures. The nature of this oxide film probably determines to some extent the type of wear behavior to be expected. It is possible that the nature of the oxide film on brass is such that it aids in the prevention of dusting.

The surface of chromium, in addition to being very hard, is covered with a continuous highly protective oxide film. This combination is apparently ideal for preventing dusting of carbon under the conditions prevailing in these tests, where the surface was relatively smooth and no current was flowing. On such a surface, however, the area of metallic contact is microscopically small, because much of the load is supported by an insulating oxide film. Therefore the contact drop will be very high and poor operation electrically would be expected. Rhodium is a metal which is almost as hard as chromium, but, being a noble metal, it forms no oxide film at room temperature and therefore has good contact characteristics. To see whether carbon brushes would fail to dust on such a surface, runs were made on rhodium-plated copper. The results were the same as for chromium, a zero wear rate being obtained in dry nitrogen.

EFFECT OF ROUGHNESS OF METAL SURFACE ON BRUSH WEAR

In order to determine the effect of roughness of the metal surface, chromium and rhodium were plated on copper surfaces which had been abraded to different degrees of roughness. The results for chromium in dry and moist nitrogen are given in Table 2. For the roughest surface, the dusting rate was so high that the brush wore out in a little over 1 min in dry or moist nitrogen. For the surface sandblasted with 150-mesh emery, the dusting rate in dry nitrogen was still very high, but a small effect of moisture became evident. The effect of moisture began to become evident for the surfaces sandblasted with 180 and 200-mesh emery. The results are shown in detail in Fig. 10. The surface treated with 180-mesh emery gave a more moderate rate in dry nitrogen than the rougher surfaces but the rate was still very high in moist nitrogen. This rate decreased steadily over a period of about 4 min and eventually became zero. The surface treated

TABLE 2 EFFECT OF ROUGHNESS OF CHROMIUM SURFACE ON WEAR OF CARBON BRUSH

Surface finish	Rate of wear, mm per min — Dry N_2	Moist N_2
Sandblasted, no. 90 grit	16.3	16.3
Sandblasted, 150-mesh emery	12.2	9.2
Sandblasted, 180-mesh emery	3.8	0.0[a]
Sandblasted, 200-mesh emery	0.0[a]	0.0
Abraded, no. 1 French emery	0.0	0.0

[a] Wear rapid initially; equilibrium value given.

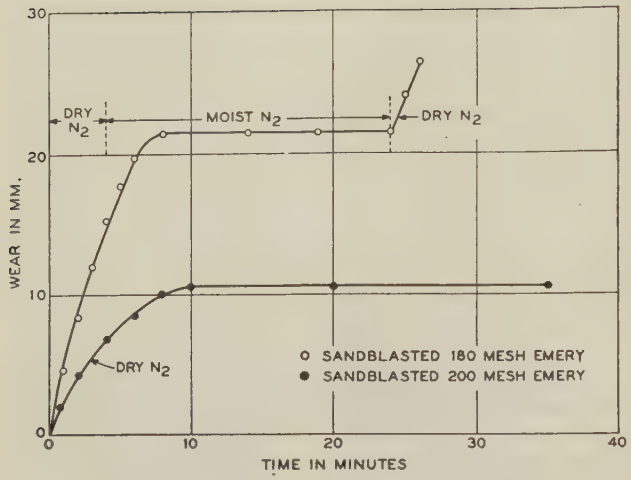

FIG. 10 WEAR VERSUS TIME OF A CARBON BRUSH ON ROUGH CHROMIUM SURFACES

with 200-mesh emery started to wear the brush at a rate of 2 mm per min in dry nitrogen but decreased during the next 10 min to zero. In a repeat run the rate was zero from the start. The brush surface was strongly oriented at the conclusion of the test and did not dust when run in dry nitrogen on polished copper. For smoother surfaces zero rates were always obtained. Similar results were obtained on rhodium-plated surfaces.

These results point to another hazard in the use of a hard material, especially if it has poor contact characteristics. Under conditions of high current loading, where sparking with consequent roughening of the surface is certain to take place, it would be expected to cause severe dusting wear even under normal atmospheric conditions.

DISCUSSION

Recent researches have indicated that when two solid metals come together, the pressure on a very small area of contact due to minute irregularities is so high that plastic flow and consequent welding take place (7, 8). The area of the welds will be determined by the hardness of the metal surfaces, and by the characteristics of the surface oxide film. The frictional force may be considered as the sum of two forces, that necessary to shear the welded junctions, and that necessary to drag the surface irregularities of the harder metal through the softer one (8).

The results obtained in the present studies are consistent with this theory, if we assume that in the absence of water, a process analogous to welding of metals takes place at points on the carbon surfaces, and if we assume further that some of these welds are brought about by carbon to carbon bonding. This would mean that dusting wear is caused at least in part by the breaking of carbon to carbon bonds (9). The water or other lubricant, by adsorbing on the surfaces, would appear to reduce the number of bonds by keeping the surfaces a greater distance apart; also by chemisorbing on those crystal edges that are exposed by bond breaking, the water lowers the friction and the crystallites are stroked into a position such that their basal planes are in the plane of the surface.

A brush surface consisting of randomly oriented graphite crystals will be relatively soft. Therefore the area of contact between such a surface and the rotating surface will be large, and the force required to shear bonds correspondingly large. The edges and corners of the crystals are clearly hard enough to scratch most metal surfaces, Fig. 8*a*, 8*c*. When motion takes place in the absence of moisture or other adsorbed lubricant, the ploughing effect of the crystal edges and of the metal projections thus created causes the ploughing component of the frictional force to be very high.

When motion takes place, a film of carbon is immediately deposited on the metal surface, with a bond strength greater than that between crystal planes. In the presence of adsorbed lubricant, both surfaces soon become cleavage faces of graphite, a condition which is ideal for minimum friction on Bowden's theory. The cleavage face of the graphite is almost as hard as diamond, so that the area of the contact between the surfaces will be low. Therefore the force necessary to break the bonds between surfaces will be very low, since it will only have to be sufficient to overcome a small number of weak bonds between cleavage planes. The ploughing force will be very low for the same reasons.

The behavior of the brushes on smooth chromium and rhodium is consistent with the foregoing condition, because these metals are hard enough to resist scratching by the crystal edges. The ploughing force will be low even in a dry atmosphere; the strongest orientation observed was, in fact, found on brushes run on a chromium surface.

The initial behavior of the oriented preparations on a rough copper surface in dry nitrogen, and of a disoriented brush on chromium plated on a rough surface, as shown in Fig. 10, are also consistent with this condition. The ploughing force accounts for the wear until the valleys are filled up, but becomes negligible when the metal surface is overlaid with an oriented layer. The friction was actually observed to fall steadily with time as wear decreased, and reached a constant low value when the wear became negligible. The difficulty in producing dusting after operation in room air, and the lag on changing from a moist to a dry atmosphere, are also consistent with this theory.

The use of oriented brush preparations in practice introduces several new problems. Such brushes will be relatively weak laterally; they will have a lower resistance tangent to the rubbing surface than normal to it, which is contrary to good practice. It is believed that these difficulties can readily be overcome by brush and holder design for most practical purposes. Brushes cut from oriented preparations have not been run on generator commutators. It is not known what effects the curved surface of the commutators will have on the ability of these brushes to resist high-altitude wear.

ACKNOWLEDGMENT

The authors wish to express their appreciation for the assistance rendered by Dr. L. H. Germer, and Dr. J. J. Lander, who carried out and interpreted the electron-diffraction measurements; to Mr. U. B. Thomas, who designed and built part of the apparatus, and to Dr. G. T. Kohman for his advice and encouragement during the course of the work.

BIBLIOGRAPHY

1 "Carbon-Brush Contact Films: Part I," by C. Van Brunt and R. H. Savage, *General Electric Review*, vol. 47, July, 1944, pp. 16–19.

"Carbon-Brush Contact Films: Part II," by C. Van Brunt, *General Electric Review*, vol. 47, August, 1944, pp. 28–35.

"High-Altitude Brush Problem," by D. Ramadanoff and S. W. Glass, Trans. A.I.E.E., vol. 63, 1944, pp. 825–829.

"Treatment of High-Altitude Brushes by Application of Metallic Halides," by H. M. Elsey, Trans. AIEE, vol. 64, 1945, pp. 576–579.

"Carbon-Brush Contact Films," by R. H. Savage, *General Electric Review*, vol. 48, October, 1945, pp. 13–20.

2 "The Quantitative Humidification of Air in Laboratory Experiments," by W. H. J. Vernon and L. Whitby, Trans. Faraday Society, vol. 27, 1931, pp. 248–255.

3 Ibid., reference (1).

4 "Studies in Boundary Lubrication," by W. E. Campbell, Trans. ASME, vol. 61, 1939, pp. 633–641.

5 See fifth item, reference (1).

6 See third item, reference (1).

7 "Electric Contacts," by R. Holm, Almquist and Wiksells, Aka-

demiska Handböcker, Hugo Gebers Vörlag, Stockholm, Sweden, 1946.

8 "The Physics of Rubbing Surfaces," by F. P. Bowden, Journal and Proceedings of the Royal Society of New South Wales, vol. 58, 1944, pp. 187–219.

9 "Graphite Lubrication," by R. H. Savage, *Journal of Applied Physics*, vol. 19, January, 1948, pp. 1–10.

Discussion

R. H. Savage.[4] The impressive experiments of the authors on the effects of the graphite-crystal orientation upon wear were continued in an additional study by the writer during the summer of 1947. For this new work several graphite specimens designated "single crystals" were obtained from Ward's Natural Science Establishment. These were supplemented by several other specimens which the writer obtained in the graphite deposits of the Adirondacks, 3 miles northwest of Ticonderoga, in the "Lead Hill" region. These were obtained by breaking open a few pegmatite rocks of Grenvillian origin[5] and separating the enclosed crystals by hand. The best of these graphite specimens were thin plates averaging 1 sq cm in area on the cleavage faces and showed slight or negligible damage from handling.

The graphite plates were mounted individually for the wear study by a mechanical device designed expressly to avoid surface contamination by foreign traces of organic or inorganic impurity either of which would tend to form adsorption films upon the carbon atoms and thus mask the intrinsic lubricating characteristics of the graphite. Each graphite plate was cut into a square or rectangular shape and was mounted firmly with one of its cleavage surfaces against the end of a carbon rod of 6.2 mm sq cross section by means of two L-shaped copper side pieces which were bolted to the carbon rod with a jeweler's screw. All of the parts used in the assembly had been cleaned and the graphite was handled with forceps.

During the mounting it was found that a few lamellae could be separated at one edge of the graphite plate with a clean razor blade, and these could then be peeled off with tweezers so as to produce fresh cleavage surfaces. In some instances there were thus formed large optical mirror surfaces. The physical properties of these graphite crystals, as revealed under the microscope, were remarkable in contrast to those of powdered graphite. It was noted, for example, that the flat cleavage face cannot stand concentrated pressure and fractures easily. The result is a fault on the surface which provides a splinter edge. If such splinter edges are developed during the process of rubbing friction, it is clear that the projecting edges may interlock with microscopic protrusions on the opposite surface so that the crystal face is ripped open.

It was further observed during the peeling of the brush faces that successive lamellae were accurately parallel and that the lines of secondary cleavage occurred consistently at the same angle (estimated to be roughly 0 deg, 120 deg, or 240 deg from a reference line perpendicular to the hexagonal axis). This indicated an almost perfect degree of orientation for this work.

The first of the crystalline graphite samples to be tried, after mounting on the carbon rod, was placed in a special brush holder so as to press against a copper rail of 2 mm width and 10 cm diam which had been formed by machining two concentric grooves in the face of the copper disk. The grooves provided clearance for the feet of the copper pieces so that only the main cleavage face of the graphite crystal bore against the brush track which was the top surface of the rail. A normal force of 100 to 200 g was used on these brushes. The copper rail was machined to as smooth a surface as could be conveniently done in the laboratory and the burrs were removed with great care. The disk was then cleaned with solvents, followed by cathodic degreasing in sodium-carbonate solution, rinsed, and dried quickly under vacuum.

When the first crystalline sample was tried as a brush with the face exactly flat on the rail, a rapid scaling occurred so that it was necessary to stop the run before a trial in a dry atmosphere could be made. It was found preferable to mount the brush at a slight angle from the normal (< 5 deg) so that the leading edge of the brush could not quite touch the rail, the load being distributed on the part of the face toward the trailing edge.

Having established stable sliding conditions a fresh oriented crystalline graphite sample was operated in a water-vapor atmosphere in our friction apparatus,[6] and the wear rate was observed to be relatively low. After a short run the water vapor was removed by condensation on a trap containing liquid nitrogen (—196 C). Within 10 sec the friction increased to 300 per cent of normal, and the wear rate became high. Within 5 min the graphite was worn through, and a deep groove had been cut in the carbon backing above it as a result of the dusting wear (see Fig. 11 of this discussion).

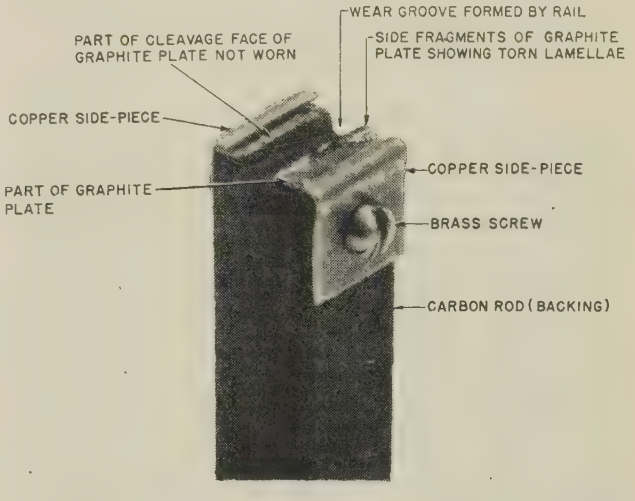

Fig. 11 Crystalline-Graphite Sample Bisected by Severe Wear When Operated in Vacuum With Cleavage Plane Approximately Parallel to Rotating Surface

In another experiment an ordinary graphite brush was operated on the rail in a rather long preliminary run intended to polish the surface and to form an oriented graphite film. After the film had been formed this brush was removed, and was replaced with a new crystalline-graphite plate mounted on a rod as described. This plate was operated first in moist air, and then in water vapor at a pressure of several millimeters (mercury), with low wear rate and low friction. Lastly, the water-vapor pressure was lowered to about 100 microns. Immediately following this, the friction became high and within 1 min the crystalline sample of nearly 1 mm thickness was worn completely through (see Fig. 12 of this discussion). The angle which the cleavage face made with the plane of motion in this run was estimated as 3 deg 2 min.

These experiments clearly indicate that graphite crystals, held with the basal plane approximately flat on a rotating copper disk, do require for their lubrication a pressure of water vapor greater than 100 microns, or some other substance in considerable concentration. In vacuum, or even in water vapor at the low pres-

[4] Research Laboratory, General Electric Company, Schenectady, N. Y.

[5] "The Adirondack Graphite Deposits," by H. L. Alling, New York State Museum Bulletin No. 199, 1918.

[6] See reference (9) of paper.

sure of 100 microns, they seize and disintegrate into small carbon fragments.

The authors' experiments show that the orientation of the

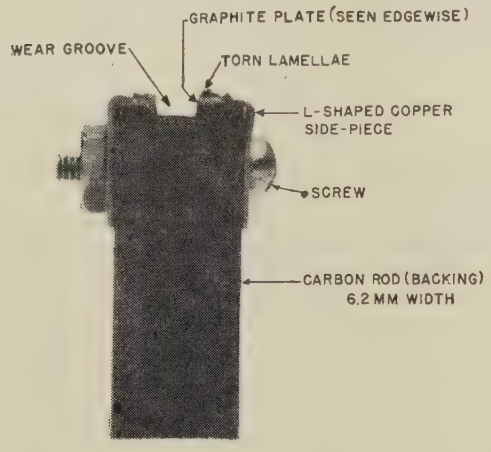

FIG. 12 CRYSTALLINE-GRAPHITE SAMPLE BISECTED BY SEVERE WEAR, AND GROOVE FORMED IN CARBON BACKING BY COPPER RAIL, WHEN OPERATED WITH CLEAVAGE PLANE APPROXIMATELY PARALLEL TO ROTATING SURFACE
(Wear rate about 1 mm per min.)

graphite is an important factor, but this supplementary work indicates that it is not the controlling factor. Its importance and function would seem to require still further clarification, possibly with special emphasis placed upon the surface finish of the metal base and upon the removal of inorganic impurities such as iron oxide which are frequently present in natural graphite and which tend to form lubricating films by adsorption upon the surface carbon atoms.[7] This viewpoint is supported not only by our recent experiments as just described, but also by the authors' observation that "the degree of orientation found on brushes and track in the no-wear condition was variable."

The writer, along with others interested in this subject, would be glad to have an additional description of the possibilities of the electron-diffraction method in estimating the degree or percentage of orientation of the crystals, and also in determining the average angle of tilt, if any, which the crystals might in some instances make with respect to the plane of the base upon which they are deposited.

The authors present a conclusion of considerable practical importance in stating that the accelerating effect of current on brush wear (noted in engineering practice) is due to evaporation of contaminants and to the mechanical effect of irregularities produced on the commutator surface by sparking. In this connection it should be noted that the authors' statements as to the effect of current "up to 114 amp per sq in." may require qualification when translated into engineering terms.

The area of real contact of a brush face may be considered to be proportional to the first power or to slightly less than to the first power of the normal force. It follows that the thermal effects of the current in the zone of interfacial contact will be roughly proportional to the number of amperes per unit of force rather than per unit of gross cross-sectional area. Thus the number of amperes per square inch has small significance when not related to the force. The writer suggests accordingly that a ratio of much greater significance than the customary expression "amperes per square inch" is the "number of amperes per unit of force."

On large machines a representative ratio is 75 amp per kg, and frequently this will represent 12 to 24 amp per sq cm (or roughly 75 to 150 per sq in.). The authors' figure of "114 amp per sq in." represents only 2 amp per kg. It would seem therefore that the authors' conclusions in regard to current effects on brush wear, as determined in their apparatus, should be applicable mainly to "low current-density equipment."

In instances where high currents are passed through brushes during periods of water-vapor lubrication, a large rise in the friction may be observed and this may be easily understood as resulting from the depletion of the adsorption film by increased evaporation rate at high surface temperature. Thus the "electrical wear" of brushes may be due not only to the evaporation of contaminants in some instances, as stated, but also in other instances, to the increased evaporation rate of the "transient" adsorption films (in distinction to contaminants), and to the erosive effects produced at high currents per unit of force (not necessarily attended by sparking).

Taken as a whole, the authors' work is an important contribution to our knowledge of graphite brush wear, and the fundamental quality of the work is unusual in the field of brush wear.

AUTHORS' CLOSURE

Mr. Savage's ingeniously conducted experiments certainly cast doubt on the fundamental lubricity of the graphite crystal cleavage faces which is assumed in our paper. He has suggested that inorganic impurities were responsible for the orientation effects described. Unfortunately, no effort was made to determine the nature and amount of impurities in the natural graphite which was used, and no sample is now available. Therefore this explanation cannot be confirmed or refuted now.

Our experimental methods were very different from his, so that some unknown variable may have caused the difference in results. Leaving this possibility aside, another explanation, which brings both sets of experiments into line, suggests itself. If it is assumed that adsorption takes place much more readily on the faces than on the edges of the crystals, then, at a given low pressure of adsorbent, a thinner layer will be present on the edges than on the faces. It would also be likely that the limiting pressure above which dusting effectively stops would be lower for the face-on than for the edge-on condition. If these assumptions are correct then we were operating over a range of partial pressure of water in which we were above the limiting pressure for the face-on, but well below it for the edge-on condition.

The dew point of the nitrogen in our experiments was —50 C to —40 C, that is, the partial pressure of water was 30 to 100 microns. Mr. Savage obtained wear on the cleavage faces of graphite in this pressure range. Since he was operating in vacuum his surface temperatures were probably very much higher than ours, which would explain a higher limiting pressure in his experiments. It is possible that 30 microns of water is sufficient to prevent wear on the cleavage faces of graphite at our lower surface temperatures.

The point regarding current and dusting is well taken. Our conclusions were not intended to apply to higher current densities than those investigated.

There is a good possibility that electron diffraction can be used successfully for estimating the degree of orientation of crystals and the angle of tilt they may make with respect to the plane of the base upon which they are deposited.

[7] It is anticipated that the efficiency of such impurities, in the role of adjuvants, may be greatly affected by the orientation of the graphite crystals at the surfaces of sliding; also that the graphite-film formation and the associated process of crystalline orientation will be affected by the surface finish.

Large Hydraulic Forging Presses

By M. D. STONE,[1] PITTSBURGH, PA.

An historical account of the art of forging is given, which traces the development of the machines used, culminating in the 14,000-ton forging presses built for the U. S. Navy during the recent war. Two forging presses of this size were built and installed at the Naval Ordnance Division Midvale Steel Company, Philadelphia, Pa., and at the Naval Ordnance Plant, South Charleston, W. Va., respectively. In one case an electric-drive pump system working in conjunction with a hydropneumatic accumulator is used as the power plant, while the other is of the steam-hydraulic type. A detailed account of the design, construction, installation, and operation of each press is given as well as comparative performance data, cost studies, and the like. Numerous other installations of heavy stamping or die-forging presses of various types and capacities up to 30,000 metric tons at the I. G. Farben Company, Germany, are described at some length.

History of Hydraulic-Press Development

THE art of forging—the working and shaping of metal—is old, dating back to almost 4000 B.C. For many centuries, however, this art was manual. It was not until about 1500 A.D. that hand hammers were replaced by tilt hammers; at first powered by water wheels, and later, around 1750, by steam engines. The tilt hammer was followed by the steam hammer, and then by the hydraulic forging press, which constitutes the subject of this paper.

By the forging press is meant that hydraulic machine whose operation cycle consists of lowering the top forging tool onto the work rapidly, applying full pressure as required at some reduced speed, and rapidly raising the top tool for further manipulation of the workpiece prior to the next forging stroke. Another requirement of the forging press is its ability to make a rapid succession of light planishing strokes, say, up to 50 per min, such as are used in rounding up a cylindrical forging. In addition, such a press should be able to be stopped and held stationary at any intermediate position within its stroke range. In this way we differentiate between the rapid-action or hammer-type press, which may operate up to several hundred strokes per minute, utilizing the inertia force of the moving head to perform work on the one hand, and the hydraulic die-forging or stamping press on the other, where relatively slow advancing and pressing speeds are involved (usually the same), as well as lifting speeds. Such latter presses have relatively smaller column spacings and the loadings are central, although extremely large pressing capacities may be involved.

In particular, we are concerned with large-size forging presses, as this paper will describe two 14,000-ton presses built for the United States Navy during the recent war, and installed at the present time in the Naval Ordnance Division, Midvale Steel Company, Philadelphia, Pa., and the Naval Ordnance Plant, South Charleston, W. Va., respectively.

The mechanical use of liquids, primarily water, as a pressure-transmitting medium, came long after its use in power machinery. Whereas water wheels and mills were in use in old Roman times and earlier, the invention of the hydraulic press was as recent as 1795, by Bramah in England, following the enunciation by Pascal in the preceding century that "water pressure exerts itself in all directions alike, in a closed container." This original press had a single cylinder in the base, with the ram acting upward.

It was not until about a half century later that Bramah's countrymen initiated the era of hydraulic machinery, when John Fox in 1847, first suggested its use as a forging machine. Its early applications were in competition with the more prevalent hammers in use at the time, particularly the then recently developed steam hammer of Naysmith, invented in 1839. The disadvantages of the Fox machine were largely eliminated in the Dubs press of 1853 and the Haswell press of 1861.

Fox's press (and similar ones built by Bessemer) was merely a Bramah press, whose bottom platen was replaced by the lower forging tool, which moved, and whose upper platen carried the fixed forging tool. Bessemer's presses introduced the idea of an adjustable upper platen by means of a large screw at the top, to allow the use of shorter-stroke hydraulic cylinders which were easier to manufacture at that time. In these presses the work was necessarily lifted each time a forging stroke was made, hence manipulation of the work could not take place until the press head was readied for the next stroke. Return of the movable forging tool of course was by gravity.

The Haswell press, and concurrently the Whitworth press, overcame the objections cited by inverting the design. It consisted essentially of an hydraulic cylinder, held in the upper platen, containing a ram which pointed downward, and had attached to its lower end a toolholder and forging tool. With these designs came the first introduction of the pull-back cylinder, to raise the tool rapidly after the forging stroke. In the Dubs press, the main cylinder was double-acting, and thus served doubly for pressing and raising. The Haswell press first introduced the idea of two separate pull-back cylinders, arranged symmetrically on either side of the main press cylinder. Whitworth later reintroduced Bessemer's earlier idea of an adjustable-stroke press, by mounting the press cylinder on a movable-top platen, whose position was varied by gear-driven nuts mounted in the movable platen engaging the threaded columns, Fig. 1.

Sir Joseph Whitworth and his managing director, Manassah Gledhill, having earlier utilized presses on a large scale for forging purposes, around 1861 fitted out several of their presses with hydraulic cranes and rotating gear for easy and rapid handling of the work, and may be said to have really put the forging press on a solid foundation as an industrial tool.

Press construction altered little until 1884, when Davy Brothers in England made a notable advance, still used in many modern presses. As will be discussed later, earlier presses were poorly designed to withstand any appreciable degree of eccentric loading, and Davy's design, shown in Fig. 2 was the first to overcome largely the previous shortcomings of column breakage, and cylinder and packing failures. The single forging cylinder was replaced by two cylinders, with pintle-type rams acting against an inverted-T-type movable crosshead. The vertical leg of the crosshead slid up and down within a central guide tube, with the bottom of the crosshead held in close sliding relationship with the four press

[1] Manager, Development Department, United Engineering and Foundry Company. Mem. ASME.

Contributed by the Metals Engineering Division and presented at the Annual Meeting, Atlantic City, N. J., December 1–5, 1947, of The American Society of Mechanical Engineers.

Note: Statements and opinions advanced in papers are to be understood as individual expressions of their authors, and not those of the Society. Paper No. 47—A-151.

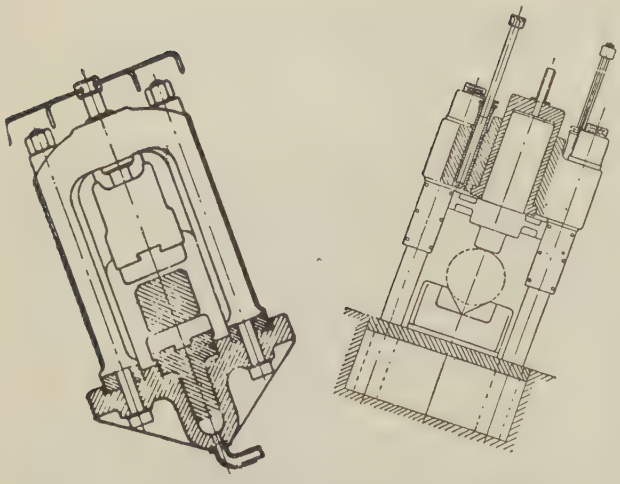

FIG. 1 EARLY BESSEMER PRESS, AROUND 1860, AND EARLY WHITWORTH PRESS, AROUND 1875

columns. Smaller presses were also constructed by Davy retaining this special form of crosshead, but utilizing a single-press cylinder, in which the vertical leg of the crosshead served the dual purpose of pressure ram and guide stalk. This latter construction was an obvious compromise.

Some few years later, Breuer and Schumacher in Cologne, who had entered the forging-press field, took another step forward in press construction adapted to off-center forging when, in 1891, they brought out a press equipped with extra oblique columns connecting the upper entablature with the press foundation as shown in Fig. 3. As will be analyzed later, this construction still further decreased press-column bending stresses, over the Davy construction, and helped still further to minimize column breakage which was of all too frequent occurrence.

The most recent press construction, which practically eliminates column bending stresses due to eccentric forging, will be described later and constitutes one of the major design advances in the new United heavy forging press, constructed for eccentric loading, such as is encountered in forging and rectifying armor plate, plate bending, and so forth.

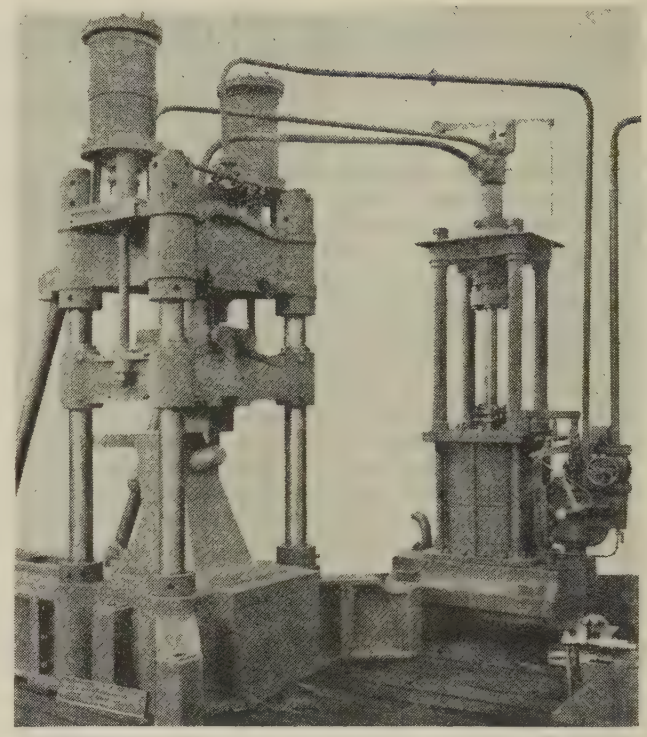

FIG. 3 EARLY STEAM-HYDRAULIC PRESS, SHOWING OBLIQUE STRUTS, BREUER AND SCHUMACHER, 1891

TYPES OF HYDRAULIC POWER PLANTS

Along with the advances made in press construction proper, were the several important steps in the types of hydraulic power plants used to actuate the press heads. The earliest presses, from Bramah on to Whitworth, all employed the direct-pumping or pure hydraulic type of power plant. In the case of Bramah, it was a hand-operated single-plunger pump. In the case of Whitworth, steam-engine-driven rapidly controllable multicylinder pumps were used. While the important invention of Bramah's associate, Maudesley, in 1796, of the U-leather, per-

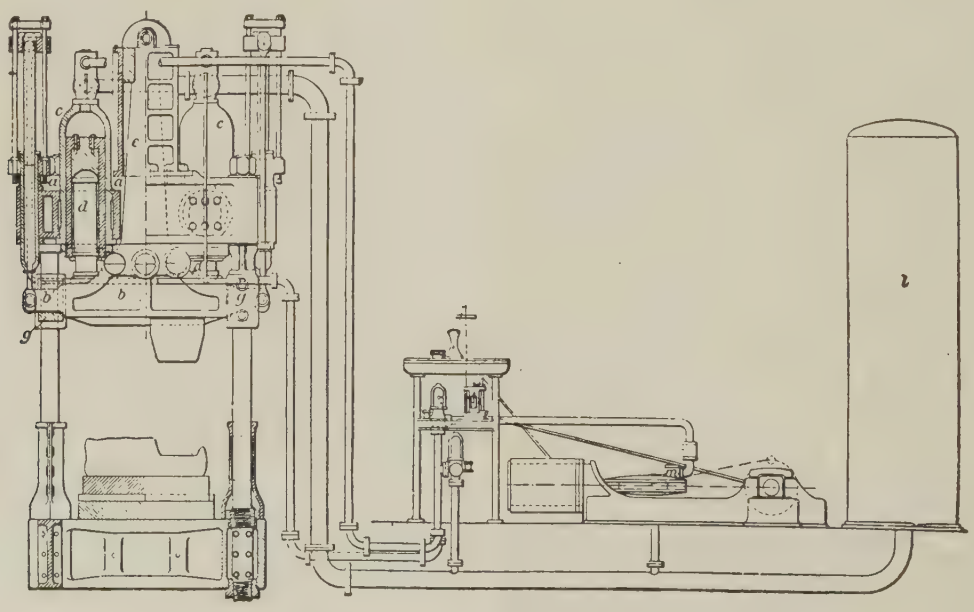

FIG. 2 FORERUNNER OF MODERN FORGING PRESS, BY DAVY BROTHERS, 1884

mitted hydraulic pressures of only a few hundred pounds per square inch to start with, Whitworth was building presses in the 1860's, utilizing hydraulic pressures of the order of 6000 psi.

It was around this time that Benjamin Walker of Leeds, introduced the idea of a dead-weight accumulator in the main pressure system. This permitted better steam economies in steam-driven pumps, which could now be fitted with flywheels, thus taking advantage of the expansive properties of the steam. Under such conditions of course the engine could not be stopped and started in accordance with variable water demands, and it was the accumulator system which permitted this necessary control. Then, too, the use of the accumulator permitted higher ram speeds without the attendant hydraulic shocks when stopping a long column of relatively incompressible water, particularly under planishing conditions.

Shortly after this time the Bochum press was built in Germany, with the first hydropneumatic accumulator used in the main hydraulic system, removing still further even those hydraulic shocks associated with the sudden stoppage of the falling weight of the accumulator itself.

The use of accumulators of course introduced the uneconomical feature of requiring that a full stroke of high-pressure water be utilized at each request of service from the press, even though much reduced pressure would suffice. For this reason, firms such as Whitworth and Davy retained the direct pumping system for a long time, and bent their efforts toward better steam-engine control to provide quick stopping, starting, and the like. The subsequent use of electric-drive pumps, and better pump-unloading devices greatly eased these problems.

Attacking the same problem along somewhat different lines, Shanks & Kohn, in 1863, patented the steam-hydraulic intensifier and applied the device to a forging press. However, the press, as then designed, was objectionably slow. In 1884, Breuer & Schumacher adopted this design and built the first commercially successful steam-hydraulic forging presses, as shown in Fig. 3. The lifting cylinders were direct steam-operated. As can be seen, the intensifier was built with the steam cylinder below, and the hydraulic cylinder above, with short hydraulic piping overhead from the intensifier to the main press cylinder.

Subsequent designs utilized an inverted type of intensifier, which claimed better accessibility of working parts, and the elimination of the relatively stiff hydraulic connection, which was said to transmit vibrations. A major disadvantage arose from the fact that the machine did not return to its initial position by gravity. The firm of Haniel & Lueg, of Dusseldorf, for instance, mounted the inverted steam-hydraulic intensifier directly on top of the forging press. While the arrangement was compact from a floor-space point of view, it involved excessive building and crane heights, but even more undesirably, it required the hot steam piston rod to dip directly into the cold pressure water. In addition, should the forging resistance be taken away suddenly, such as happens when a cutting tool comes through the work, or when a forging falls off the anvil, the combined downward action of the steam cylinder plus gravity unnecessarily punished the lower head of the intensifier cylinder.

With the early departure from the Fox type of gravity-return forging crosshead, lifting or pull-back cylinders and associated power systems became a necessary and integral part of all press installations. In the early Dubs and Haswell presses, the press heads were raised by diverting the pressure water from above the main pressure cylinder to below the pull-back cylinders, thus entailing an extra operation and its attendant delay. The early Whitworth presses of the 1860's introduced the idea of a dead-weight accumulator in the pull-back-cylinder hydraulic circuit, still utilizing the one set of pressure pumps for the dual service. The pull-back system pressure was maintained high, of the order of 4000 psi, and was provided by the steam-engine-driven pumps feeding directly into the weighted accumulators. The squeeze was obtained by allowing the water to pass directly into the press cylinder instead of into the accumulator, so that the pressure was obtained directly from the pumps to the press ram. When water was not required, a by-pass valve was opened, permitting the pumps to operate in an unloaded condition.

Introduction of Dual Hydraulic System

The Walker press, mentioned earlier, was the first to introduce the idea of two separate hydraulic systems; one for the pressing operation, and one for the lifting. Both systems utilized dead-weight accumulators, the main system working as high as 5000 psi, while the pull-back system pressure was of the order of 750 psi. This auxiliary system was also used to operate the cranes, auxiliary apparatus, and particularly a newly introduced set of horizontal cylinders located below floor level, which served to draw the anvil out so that the bottom tool could be changed easily by the overhead crane. The Bochum press operated similarly to the Walker, with the added feature that the low-pressure system was used also as a prefill system, to bring the head down more rapidly on the work prior to the application of the main squeeze.

The revolutionary Davy press of 1884 also introduced modifications in the auxiliary cylinder system. Steam was used for the first time as a source of constant pressure on the underside of the pull-back cylinders, and a low-pressure (60 psi) system, loaded by an air receiver, was utilized for prefilling the main pressure cylinder and supplying suction water for the pumps. The pumps, as mentioned earlier, were started up for each piercing operation, being driven by steam engines of the high-speed fast accelerating type, without flywheels. In later developments of the steam-hydraulic forging press, steam-powered pull-back cylinders were utilized almost universally, except for the very large presses, when the cylinders involved became too large and a special hydraulic system was again resorted to. Improvements in press operation in the later Davy machines were obtained by connecting the lower side of the pull-back cylinders to the upper side, when lowering, so that the steam was recirculated. This action served to speed up the press operation by virtue of increasing the pressure on the top side of the cylinders at the same time that it was decreased on the bottom side, and served to improve steam economy to some extent by reducing condensation losses.

Development of Press Auxiliaries

Of historical as well as contemporary interest too are the development in press auxiliaries, such as cranes, rotating gears, and the like. As mentioned earlier, the Whitworth Company first used such devices, and Walker introduced the hydraulic tool-changing rig some years later. Many years elapsed, however, until traveling forging ingot manipulators were used for handling the work rapidly in and about the press. Such machines, built along the lines of furnace chargers, were first developed in the United States about 1920, by the Alliance Machine Company. In the meantime, particularly for the larger presses handling such items as armor plate, hollow gun tubes, and the like, the old Walker tool-changing rigs were amplified into quite massive work-manipulating rigs, as well, and have become an essential adjunct to such installations.

Control Gear

Perhaps the smallest item about a forging press, and yet one of great importance, is the control gear. Great strides have been made here, too. In the original Bramah press, where practically no valve gear was involved, the press was actuated by a hand-

operated pump, and permitted to return to its starting position by opening a release valve. The utter slowness of the press was of course greatly improved in the first commercial presses. Of these, during the last quarter of the preceding century, the Whitworth and original Davy presses were controlled by two operating levers. As these were both direct-pumping presses, steam driven, one lever was required to operate the valves to both the main cylinder and the lifting cylinders, and the other to regulate the pumps by controlling the steam inlet throttle to the engines or to unload the pumps themselves, as the particular operating arrangement required.

At the beginning of this period, pressing speeds were of the order of 1 ips, with raising and lowering speeds about 2 ips, with delay times due to valve manipulation of the order of 20 to 30 sec. Thus frequencies of press operation of 2 to 3 strokes per min were the best obtainable. The Bochum press mentioned earlier, using a pneumatic accumulator in the main system and a dead-weight accumulator in the pull-back system, was the first to introduce the desirable simplification of the single operating lever which contributed greatly to the remarkable performance of the press at the time. The complete sequence of operations, four in number, was controlled from the one lever through hydraulically actuated pilot valves. The first position released the pressure from the main cylinder, permitting the press to rise automatically by virtue of the separately powered pull-back cylinders. The second position was for holding the press at any level; the third for admitting the prefill pressure; and the fourth position for admitting the high pressure. A 4000-ton press of this design was capable of operating at 30 strokes per min for planishing, and established a record performance at that time of some 30 tons of forgings per day.

With the adoption of the steam-hydraulic system by Davy Brothers in the early part of this century, a greatly improved and speeded-up control gear was developed, utilizing the single-lever mechanism, in which was introduced for the first time the "follow-up" idea in press control. This device permitted the operator to control the press as to motion and speed exactly proportional to his manual movement of the control lever, and so speeded up the operation that manipulations up to 60 strokes per min were attained in large presses, and 150 strokes per min on small presses. Several additional improvements were made subsequent to the introduction of the Davy press into this country by the author's company in 1909.

Fig. 4 shows a typical up-to-date Davy-United press system, operated from a single lever, and involving several steam-saving features, all automatically worked into the control system. As shown in the figure, the press is in the standing position, with valves *A*, *B*, and *E* closed. Valve *A*, when open, permits steam to flow from the bottom to the top of the intensifier. Valve *B* is the main steam-exhaust valve; and valve *E*, the prefiller valve, acts as a simple check to permit flow from the prefiller tank when pressure in the main cylinder is lower than that in the tank, and as a mechanically operated valve to return water to the tank at the will of the operator. Valve *C*, the main steam-inlet valve, is opened by advancing the operating lever to the "pressing" position, through the action of the floating lever. As the intensifier rises, through the action of the slanted control bar, the valve is closed again. In this way a smooth follow-up motion is obtained, as mentioned earlier. Just as valve *A* operates to connect opposite ends of the intensifier, so does valve *D* act to connect opposite ends of the pull-back cylinders, during lowering of the press head. The introduction of valves *A* and *D*, absent in the earlier control system, has led to more rapid press operation and improved steam economy.

High-Speed 14,000-Ton Press

When the problem was posed early in the recent war of constructing two 14,000-ton high-speed forging presses with the exacting requirements of heavy on-center shaft and gun-forging work, rapid planishing operations, together with heavy off-center work, such as is required in the forming and rectifying of armor plate, it was only natural that the whole art of forging-press design and operation was critically examined. Particularly was the last requirement of considerable and challenging importance—where full pressure forging, from 4 ft to 6 ft off center was specified. Many cases of cylinder-packing destruction and main-

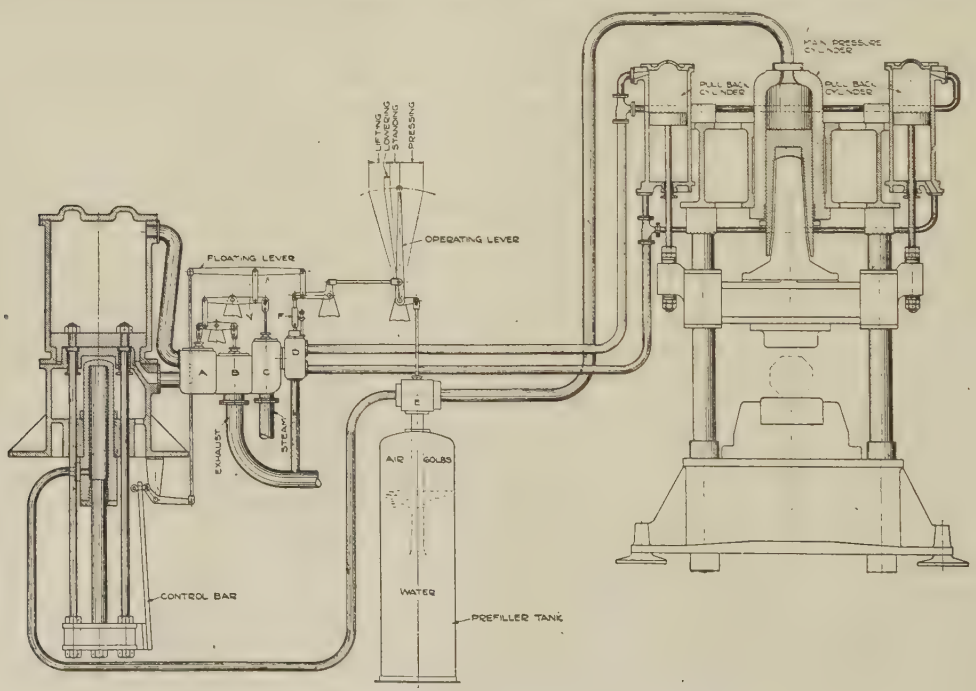

Fig. 4 Davy-United Steam-Hydraulic Press and Control Gear

column breakage, resulting in agonizing operational delays of long duration, pointed this problem up as one of prime importance.

In examining the various types of forging-press construction from this point of view, Fig. 5(*a*) shows essentially the original arrangement of press, Fig. 1(*b*), in which off-center loading is easily seen to react directly on the glands and packings. Since the distance *h*, could not be made too long without increasing the ram length abnormally, serious leakage and packing troubles readily developed. This construction was soon abandoned by the early designers.

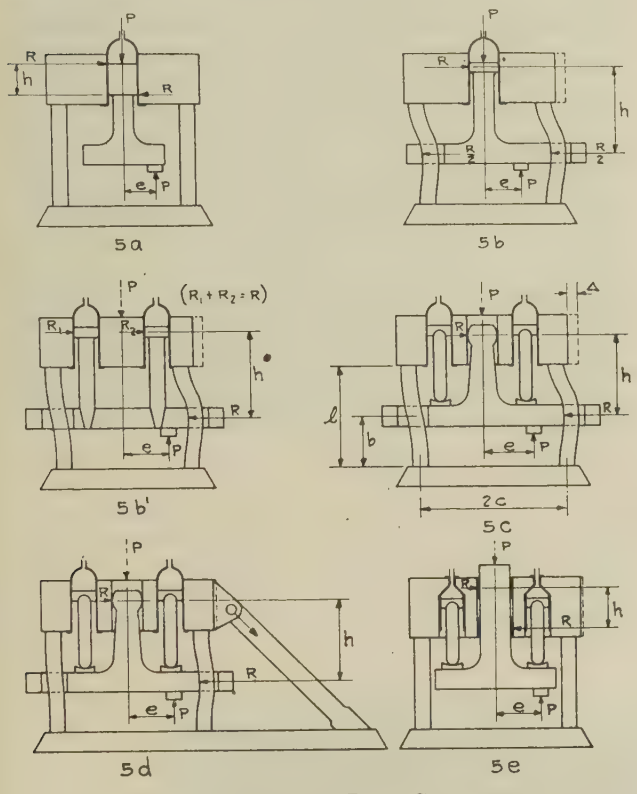

FIG. 5 VARIOUS TYPES OF PRESS CONSTRUCTION

The next innovation was the introduction of crosshead column slides, illustrated in Fig. 2, which reduced such troubles, but did not eliminate them, see Fig. 5(*b*). The distance *h*, which determines the lateral reaction due to eccentric forging, can be increased considerably in this construction, and remains constant, as well, for all press positions, as compared to the *h* in Fig. 5(*a*), which necessarily decreases as the crosshead drops to its lowest position. In this case a lessened but objectionable side pressure still exists on the top gland, and as the press column deflects under the lateral reaction (now pressing against the columns), there is the danger that a secondary lateral reaction will come into play at the lower packing and the old trouble reappear in diminished form. At the same time, secondary bending stresses are introduced in the columns, which in combination with the primary tension stresses, are potential sources of early failure.

In order to evaluate quantitatively the magnitudes of column stresses, distortions, press sway and the like, the Appendix follows through the statically indeterminate analyses of the press structures of the various types being examined. However, for all constructions shown, from statical equilibrium considerations of the crosshead structure, it follows that the total lateral reaction *R*, is related to the forging pressure *P*, and the amount of eccentricity *e*, by the relationship

$$Pe = Rh$$

where

P = total forging pressure, lb
e = eccentricity of pressure, in.
R = total reaction force lb
h = reaction couple arm, in.

Owing to the fact that it cannot always be counted on that both pairs of columns divide this lateral reaction evenly, as indicated in Fig. 5(*b*), we have seen fit to analyze all constructions on the assumption that only the right-hand pair carry the full reaction. Advanced wear, or the dropping out of a set of column-guide slippers easily results in such a condition.

In all the press constructions skeletonized in Fig. 5, when no off-center forging is being performed, the column stresses are pure tension and are given by (for 4-column presses)

$$S_t = \frac{P}{\pi d^2} \text{ psi}$$

where d = column diameter (in.). Off-center forging, however, introduces bending moments throughout the columns, with maxima occurring at different points in the columns, depending upon the construction and position of the crosshead during forging, indicated by dimension *b*. In all cases we have called 2*c* the center distance between columns the long way of the press, it being understood that any appreciable eccentric forging is always carried out along this dimension. In addition to the tension and bending stresses, we are concerned with the press sway Δ. The importance of sway is directly reflected in the stressing of connecting piping from the entablature to the auxiliary apparatus, such as intensifiers, and the like, as well as its effect upon the distortion of associated crane structures, and even the press building itself.

For the case of Fig. 5(*c*), we may evaluate the maximum bending and tension stresses, and press sway from Equations [20], [22], and [25] of the Appendix. In order to introduce reality into these evaluations, we shall consider a press whose capacity is to be 14,000 tons (28,000,000 lb), capable of forging 6 ft (e = 72 in.) off-center. The requirements further are that the column center distances shall be 23 ft × 11 ft 6 in. ($2c$ = 276 in.), daylight should be 24 ft, corresponding to column lengths between base and entablature of 40 ft (l = 480 in.), and the column diameters such that low tension stresses are obtained, say, S_t = 8000 psi, thus choose d = 34 in. ϕ. For this press, the reaction arm, h, may reasonably be made as large as 22 ft (h = 245 in.).

From an examination of the critical equations just cited, in the light of Fig. 15, it is apparent that the highest stresses occur at the top of the right-hand pair of columns, when forging at a crosshead position corresponding to about mid-span, i.e., $b = {}^1/_2 l$. We notice further that the column tension stresses increase with eccentricity, increasing some 20 per cent over on-center forging. For example, Equation [22] gives us as the maximum force per pair of columns, N_2 = 16,900,000 lb, resulting in a tension stress of 9400 psi. The maximum bending moment, from Equation [20], results in a maximum bending stress of 118,000 psi! This intolerably high value of course results only when forging at maximum load, at maximum eccentricity, at the least desirable crosshead location, and with only one pair of columns taking the eccentric thrust. Nevertheless, even under these conditions, the stresses must remain comfortably under the breaking stress. With all columns dividing the side thrust equally, the bending stresses are reduced by only 25 per cent.

In any event, the extreme and dominating importance of the secondary bending stresses is evident, and it becomes apparent why column breakage may seem inexplicable to those designers who have not undertaken to analyze their presses in detail, and who are guided by conservative tension stresses only. The sway of the press under the conditions cited would be $4^1/_4$ in.! To reduce stresses and deflections to reasonably acceptable values would mean to increase the column sizes by more than 50 per cent, requiring columns bigger than could be made and forged properly; of the order of 55 in. diam, 65 ft long, and weighing 500,000 lb each. It is evident that alternate press designs must be resorted to.

For the case of Fig. 5(*d*), the maximum bending stresses are reduced by some 40 per cent, as demonstrated in Equation [30] and Fig. 17, with the nominal tension stresses and press sway even more desirably reduced. The maximum bending stresses for $d = 34$ in. diam, are 70,000 psi, which still indicate the necessity for considering press columns of a diameter around 50 in. This construction, however, introduces an interesting innovation, and large presses of recent manufacture have employed this principle, although using the less desirable crosshead construction in Fig. 5(*b'*) (because of the uncertainty of lateral thrust load division of such a stiff-legged ram construction, due to thermal or machining inequalities). The excessive sway of earlier constructions, resulting in objectionable pipe breakage, etc., is considerably lessened in this construction, being determined primarily by the extensional deformation of the struts, to be $^3/_{16}$ in. For a press of the dimensions being discussed, a pair of such struts would necessarily be 75 ft long, have a cross-sectional area of some 400 sq in., and preferably be so constructed that they could take compression as well as tension, without buckling. This latter condition arises when eccentric forging is carried out on the side of the press opposite the struts. To make the press universal, two sets of oblique struts should be used, or to avoid the danger of buckling, forging could be limited to one side of the press only. Even for a single pair of struts, a sizable base extension of some 50 ft is required, and considerable expense involved, not counting the increased building space required.

Being dissatisfied with all these previous constructions, particularly because of the size of the press being studied, the construction shown in Fig. 5(*e*) was evolved. Here it is seen that the entire eccentric forging moment Pe, is taken within the elongated stalk guide, there being no column guides, so that essentially there is no bending moment sustained by the columns. Eccentric forging moments are thus resisted by readjusted tensions in the main column pairs, the column tensions on the side nearest the load being increased somewhat, and on the off-side, decreased, as given by Equations [52]. Thus Equation [52] indicates a maximum column tension stress of 11,700 psi, compared with the values of 118,000 psi and 70,000 psi calculated earlier.

The virtues of this construction therefore as a forging-press structure, particularly for eccentric work, are definitely established. Press sway, as well, is reduced to the relatively small amount, Equation [53], of $^1/_8$ in.; even less than for construction, Fig. 5(*d*), employing the oblique struts.

Installation Considerations

Once the choice of press structure was determined, various other considerations and advantages were studied. The minimum amount of floor space required, and the lack of necessity of struts made for easier and better servicing by cranes and rotating gear. The rigidity of the structure permitted less massive crane runways, structures, and building columns, so that clean-cut installations, as shown in Figs. 6 and 7, were possible.

A major point of design interest is indicated by the relatively high top entablatures shown in these two illustrations. Two factors led to this choice of design, i.e., desire for improved press cylinder supports, and the choice of conservative loading of pressure pads carrying lateral thrust loads due to eccentric loading. Of course a dominating consideration in designing a press of this magnitude is the limitation of transportation possibilities, both as to dimensions and weight.

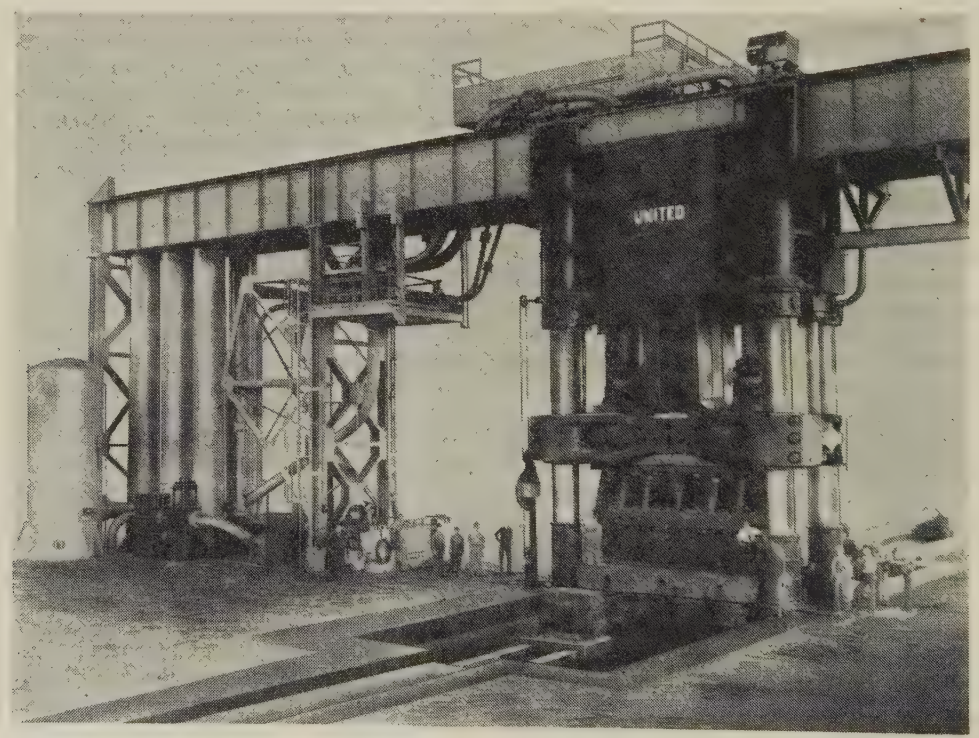

Fig. 6 The 14,000-Ton Charleston Press; Direct Pumping Plus Hydropneumatic Accumulator

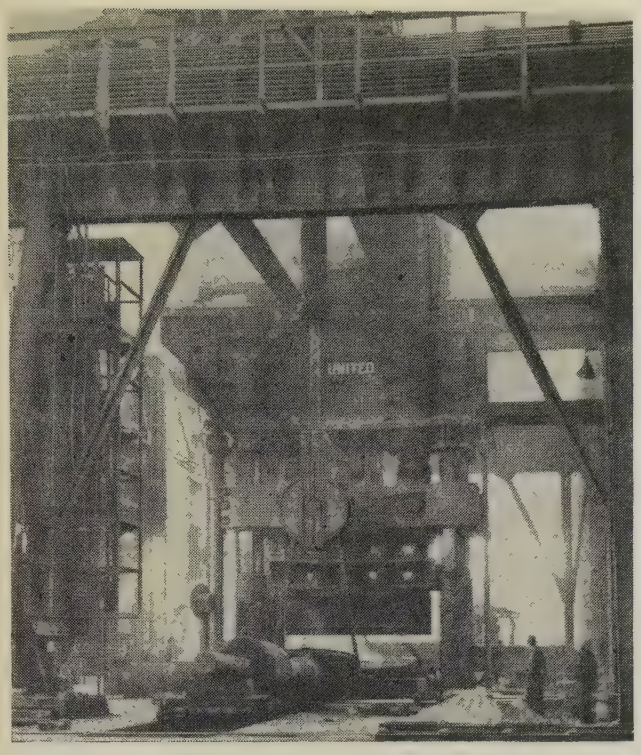

FIG. 7 THE 14,000-TON MIDVALE PRESS, STEAM-HYDRAULIC

In all previous press constructions the main pressure cylinders have been held in the upper entablatures by virtue of integral flanges around the bottom or open ends of the cylinders. Because of restricted space conditions, which always seem to exist, it has been difficult to provide generous fillet radii and flange dimensions. As a result, too many cylinder failures have occurred as a consequence of fatigue resulting from the continuous repetition of press operation. Then, too, many cylinders have failed in fatigue from compound stressing near the top of the barrel, where they are reduced in diameter to afford easy bolting of the high-pressure piping.

In the present construction, as indicated in Fig. 5(*e*), the top entablature is made deep enough so that the cylinders are supported at the top, the support being compressive in nature, and bearing against the shoulders of the cylinders. All flanges are eliminated, with their attendant design difficulties. The height of the entablature was limited to 16 ft, which easily permitted the improved-type support for cylinders designed for a 10-ft press stroke. This depth of entablature also permitted the pertinent dimension *h*, discussed previously, to be 12 ft, resulting in maximum lateral forces of 14,000,000 lb, which are properly taken against brass-clad steel pressure pads, having areas of 4500 sq in. each. The resulting bearing pressures of 3000 psi are quite comparable with current practice in mill bearings, and are continuously lubricated from an automatic high-pressure grease system. These bearing pressures usually operate at sliding velocities of less than 15 fpm.

In order to cast and transport the various massive component parts of the press properly, it was impossible to manufacture either the top entablature, the crosshead, or the press base from a single casting. As indicated in Figs. 8, 9, and 10, single castings were restricted to 340,000 lb finished weight, with maximum vertical dimensions, as transported, to 17 ft 6 in., and lateral dimensions to 10 ft. Thus the top entablature, weighing over 1,250,000 lb, was made up of four castings, two as in Fig. 9 and two as in Fig. 10, bolted and keyed together with many properly located bolts. Several of these bolts, in this and other parts of the press, are as large as 12 in. diam and 20 ft long. The crosshead which weighed in excess of 1,250,000 lb was made up as three major castings with four smaller column shoe castings bolted on. The press base, also a massive structure, was made from three major castings, bolted together. Cylinders are 63 in. diam ID, 8 in. thick and were made from single alloy forgings, weighing 100,000 lb each. The columns, as mentioned earlier, are 34 in. diam, nickel-steel forgings, bored out for internal inspection, 66 ft long, and weigh more than 200,000 lb each. Other important component parts are the pressure rams, pintles, die blocks, etc., as shown in Fig. 11 which indicates their massiveness in comparison with the erector shown leaning against one of the pintles.

Auxiliary Equipment

The auxiliaries for handling the forgings, or even the forging tools, become a major design item on presses of this magnitude. As can be seen in Fig. 6, trenches running at right angles to the major axis of the press, both front and back, house the cylinders and associated mechanisms of the so-called forging manipulators. Forgings may be straddled across the stools or chairs which will permit their rapid lateral shifting, the stools being actuated by opposed hydraulic cylinders having a 32-ft stroke. Such manipulator cylinders are powered from the same pressure system as the pull-backs, and can move large forgings requiring a shifting force of 300,000 to 400,000 lb at speeds of up to 20 fpm.

The items of control valves, shutoff valves, steam-exhaust silencers, etc., normally considered small items, take on unusual significance in presses of this magnitude. The control gear shown in Fig. 12, also visible in Fig. 6, is easily man-high, and the pre-filler valve for the Charleston press, for instance, is 8 ft × 2 ft × $2^1/_2$ ft, and weighs more than 20,000 lb.

Forging cranes, cutter-bar cranes, rotating blocks, etc., are likewise of unusual interest. Both presses are serviced by 250-ton main cranes which may be seen in Figs. 6 and 7. Just as manipulators are necessary for handling heavy plates and the like, so are rotating blocks required for forging and finishing large rounds. Fig. 7 shows a crane-suspended rotating block handling a large forging onto the manipulating gear at Midvale, whereas Fig. 13 shows a uniquely compact design of ring-spring-type block. This latter block has a spring case (shown as the cylindrical barrel in the illustration) capable of supporting a 125-ton load (one end of a 250-ton forging, for instance) and still permit a 3-in. additional extension due to misalignment on the anvil. This case, 2 ft diam × 5 ft long, can store up 450,000 ft-lb of elastic energy, and is only 10 per cent of the size of earlier coil-spring models, thus permitting closer servicing of the forging cranes. Piping between units sometimes reaches 12 in. OD, being manufactured by boring out solid forgings, and bending hot when required, or at other times being welded into forged angle blocks.

Press Transportation Problems

The matter of press transportation, in itself, was a problem, even to the transferring of castings from foundry to machine shop, as well as to final destination. Some of the heavy, but more compact pieces, could be carried on a specially designed 250-ton 16-wheel flatcar, as in Fig. 10. Other pieces, however, because of their maximum dimensions, had to be suspended between two girders of a specially constructed bridge, spanning two 125-ton cars, as in Figs. 8 and 9. In these cases the pieces cleared the rails by only 3 in., and the underpasses by 6 in. All pieces were carried on special trains, not hauling other freight, which were restricted to a 10-mph speed limit, to avoid accidental shifting or dislodgment.

FIG. 8 PART OF 14,000-TON PRESS CROSSHEAD, SHOWING MODE OF TRANSPORTATION

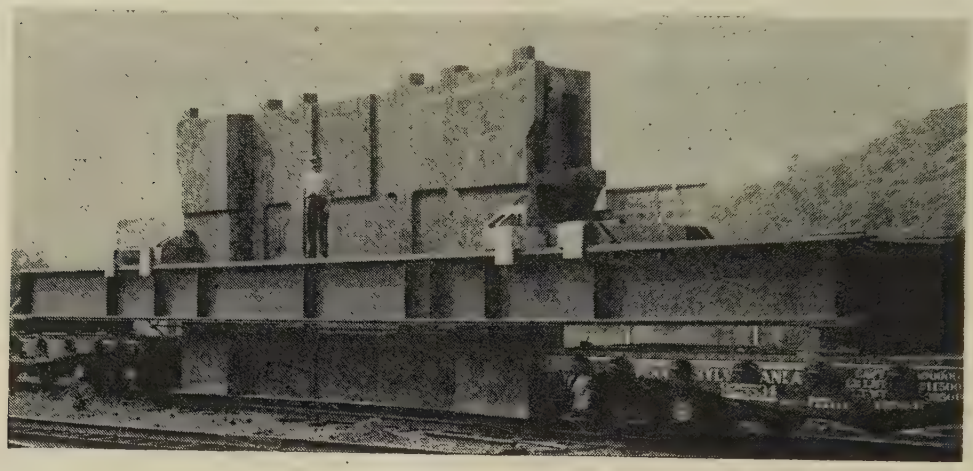

FIG. 9 PART OF 14,000-TON PRESS ENTABLATURE

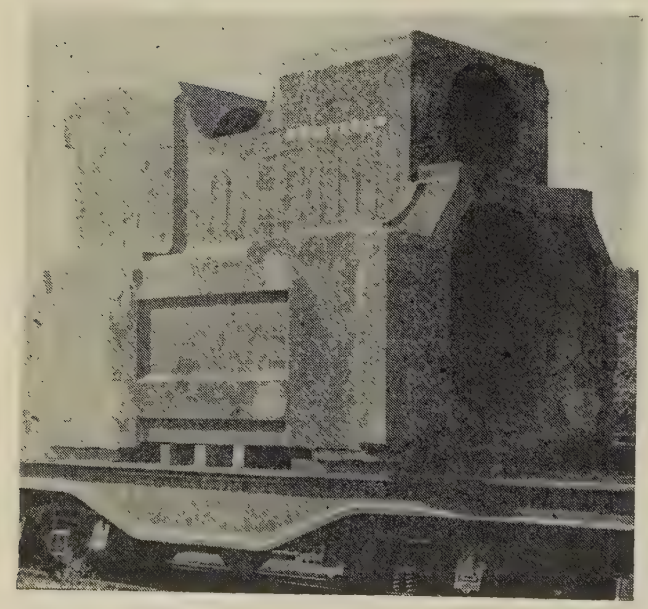

FIG. 10 ANOTHER PART OF ENTABLATURE, SHOWING RECEIVING BORES FOR MAIN AND PULL-BACK CYLINDERS

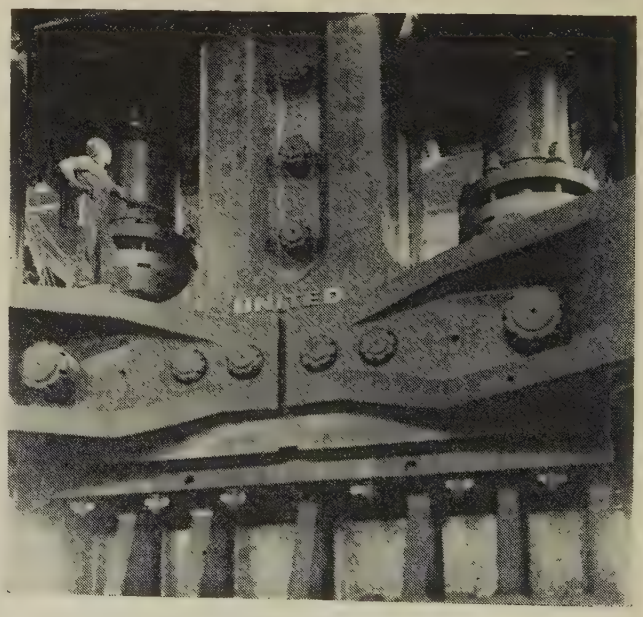

FIG. 11 CLOSE-UP OF CROSSHEAD OF 14,000-TON PRESS

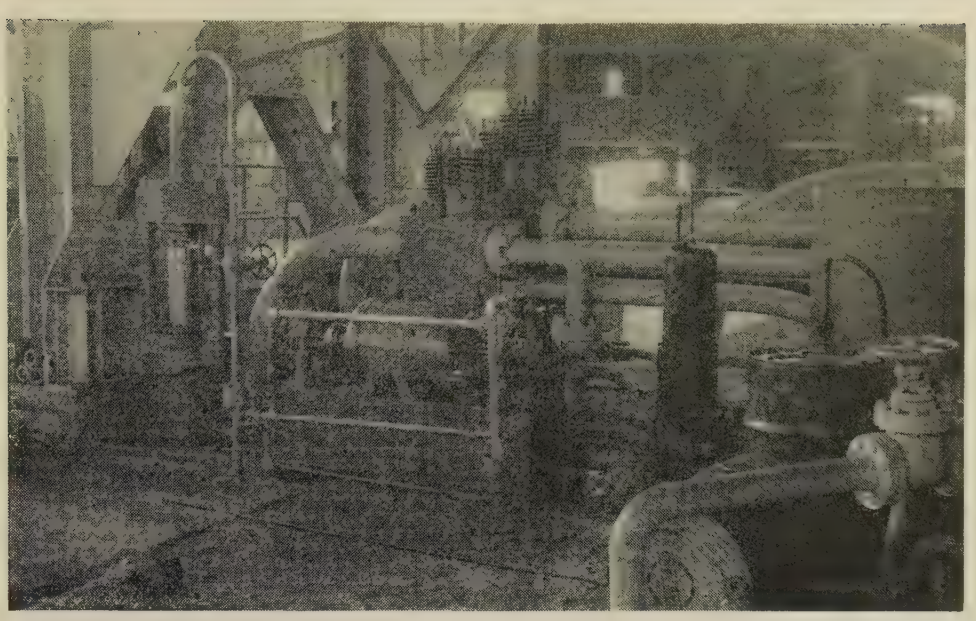

FIG. 12 OPERATING CONTROL GEAR, CHARLESTON PRESS

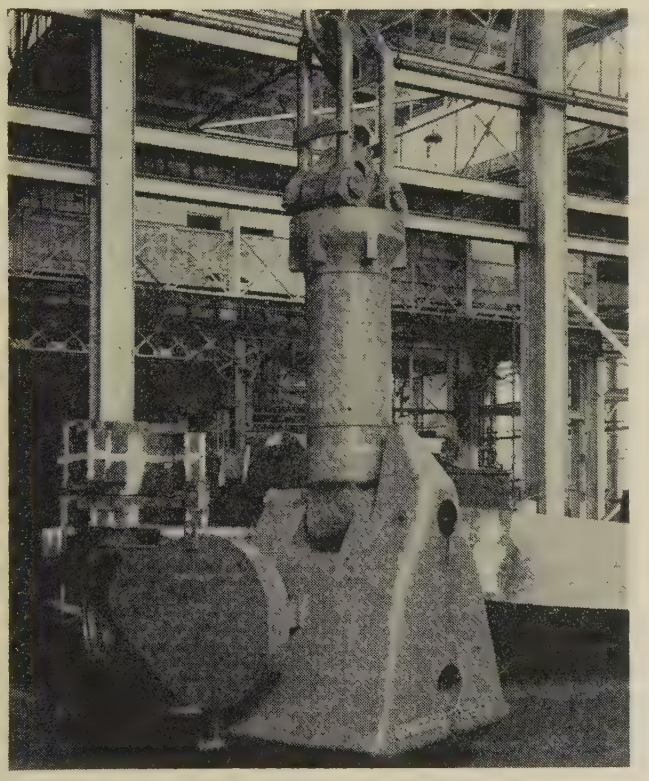

FIG. 13 125-TON ROTATING BLOCK

POWER PRESSURE PLANTS

As was mentioned earlier, two 14,000-ton presses were built; one for 6 ft off-center full-pressure forging, and one for 4 ft. As might not be unexpected, the power pressure plants in the two cases were not selected alike. In the one case, an electric-drive pump system was chosen, utilizing 4500-psi water pressure, working in conjunction with an hydropneumatic accumulator installation. In the other, a steam-hydraulic system was installed, utilizing 250-psi steam and 7700-psi water pressure. In both cases, full-capacity pressing was provided for a speed of 3 ips, with lowering and raising speeds of 12 ips, or greater. These choices pointed up the question very well, of what is the best type of pressure plant. In each case, the pull-backs were provided with adequate supplies of pressure water, and equally adequate and highly sensitive controls were provided, so that even these massive machines were easily controlled through servomechanisms to within $^1/_{16}$ in., and planishing operations could be carried out at up to 50 strokes per min.

In the case of the direct pumping press, the 4500-psi-pressure water is supplied by four 400-gpm horizontal double-acting triplex pumps, 74 rpm, each driven by a 1250-hp 720-rpm motor. The associated hydropneumatic system is composed of six 35-in-ID, 7-in-thick cylinders of multilayer construction, 49 ft high, having a total capacity of 14,500 gal. Automatic level controls were worked out so that pressure variations seldom exceed 5 per cent, even for the longest-stroke operations. Lifting and lowering of the press head is controlled by main pressure water admission to and from the two pull-back cylinders, 26 in. ID, having 13-in-diam pull rods.

In the case of the steam-hydraulic-system, the higher water pressure of 7700 psi fixed the pressure cylinders to be 48 in. ID, and because of the lesser eccentric forging requirement of 4 ft, the size and weight of this press is somewhat less than for its sister press. Steam is supplied at 250 psi, from a separate system, composed of two 100,000-lb per hr boilers. Steam from the boilers passes into a 3000-cu ft receiver, and then to two intensifiers, each having an 8-ft-diam × 10-ft 6-in. stroke steam cylinder. The intensifiers are of the latest Davy-United design, as indicated in Fig. 4, in which the hydraulic cylinders are below the steam cylinders but are operated upward through the use of two 33-ft-long, 13-in-diam tension rods, the hydraulic cylinders being $16^3/_4$ in-diam. The over-all height of each intensifier is 44 ft 2 in., of which slightly more than half is below floor level. This arrangement makes for a mechanically stable structure. By having the large steam cylinder mounted on the floor, it still retains the feature of gravity return after the power stroke, and eliminates the overhead cross-piping associated with earlier inverted constructions. Built-in dashpot construction governs the slowdown of the intensifier, as it reaches its bottom position, without undue impact or "hunting."

The reason for the receiver is immediately apparent when one considers the steam demands at maximum press-operating conditions. A press speed of 3 ips means 2 fps intensifier speed, corresponding to a required steam flow of 400,000 lb per hr, since one 10-ft stroke of the intensifiers requires 600 lb of steam, corresponding to 1000 cu ft at 250 psi. Thus steam is drawn from the receiver while the intensifiers are returning for another volume of steam. Each stroke of the intensifier system permits a press power stroke of 15 in., which more than takes care of normal forging requirements. Due to the intermittent nature of the pressure application in the steam-hydraulic press system being off during the return stroke of the intensifier for another volume of steam, the pull-back cylinders and other auxiliaries are necessarily operated from a separate source of 2500-psi constant-pressure water, the pull-back cylinders being 30 in. diam. This system is composed of two 400-gpm 2500-psi steam-driven double-acting duplex pumps, working in conjunction with two 52-in-ID 7-in-thick 45-ft-high hydropneumatic accumulators, having a capacity of 7200 gal. The use of steam-operated pull-backs would have involved too large cylinders, and complicated the press design abnormally.

Comparison of Press Performance

In connection with these presses, the opportunity was rare indeed of having two such similarly designed machines, utilizing competitive high-pressure systems, and working over an extended period on substantially the same class of work. In the interest of comparing performances data[2] were obtained as summarized in Table 1.

TABLE 1 COMPARATIVE PRESS DATA

Steam-hydraulic	Direct-pumping + accumulator
Data over 2-year period, working 2 and 3 shifts	Data over 2-year period, averaging 577 hr per month
Average power used, 33,000 lb of steam per op. hr	Average power used, 625 kwh per op. hr
Peak power demand, 220,000 lb of steam per hr	Peak power demand, 3750 kw
Steam cost, $0.53 per 1000 lb	Average power cost, $0.008 per kwhr
Forging rate, 66 tons per hr	Forging rate, 75 tons per hr
Forging rate for finished forgings, 11.2 tons per op. hr	Forging rate for finished forgings, 13.3 tons per op. hr
Steam cost.....$18.50 per op. hr	Power cost.....$ 5.63 per op. hr
Repair and maintenance supplies. 1.85 per op. hr	Repair and maintenance supplies. 8.60 per op. hr*
Repair and maintenance labor... 1.25 per op. hr	Repair and maintenance labor... 1.30 per op. hr
Total.....$21.60 per op. hr	Total.....$15.53 per op. hr

* Abnormally high.

It is interesting to observe that in each case the average power demand is only about 15 per cent of the maximum demand required and provided for. When forging is actually going on these peak demands must be satisfied, but the great amount of down time in operations of this sort is important to appreciate. In this connection we would distinguish, for instance, between a forging hour and an operating hour, the former being the actual time that the forging is in the press, and the latter, the time that the forging crew is on hand for operations. The number of forging hours per month is usually around 50 per cent of the operating hours. Of course in the case of the steam-hydraulic press, steam must be maintained continuously and thereby sustains certain stand-by losses.

As to actual forging, it is seen that the forging rate is around 6 times the production rate for finished forgings. This comes about because of the 50 per cent ratio just cited, plus the fact that large forgings are handled from 2 to 4 times before completion. In examining the actual cost figures, the much lower power rate of the electric-drive-pump system was at least partially offset by the increased repair and maintenance item, principally on the pumps themselves. The net result, however, shows about a $6 per hr lower cost for the direct pumping-accumulator system. While this figure is considerable in itself, amounting to some $40,000 per year, it must be remembered that the foregoing charges are only a fraction of the total involved in operating press plants of this magnitude. When one includes the direct labor item of a crew of some 10 men, the fixed-charges item, based upon an investment of some $3/4,000,000, administration, etc., a total figure of some $75/100/hr is obtained, based upon which $6 per hr is only some 7 per cent.

A point of considerable importance brought out by these figures is the small percentage of the total time that anything approaching full power operations are being carried out. Based upon the figures, for instance, of 300 kw as the power required for running the direct-pumping system idle, it is easily appreciated that the monthly average of 625 kw corresponds to a full pressure period of only 15 per cent of the time, and an idle time of 85 per cent. For the steam-hydraulic system the figures are about the same. These observations tend to minimize considerably the pros and cons of the various competitive systems under operating conditions, and rather emphasize the idling-power requirements. For instance, it has been variously proposed that centrifugal pumps are to be preferred over reciprocating pumps and accumulators for forging-press service, because of their lesser first cost. The fact that their operating efficiency is about 70 per cent, compared to over 90 per cent for the reciprocating-pump system, is of less importance than the fact that their idling losses are in excess of 40 per cent, as compared to 5 per cent to 10 per cent for reciprocating pumps. In this case, for example, 35 per cent as idle losses would amount to some 10,000,000 kwhr per year, or $80,000 per year, which would easily more than nullify any first-cost differences.

Operating Features

In comparing the operating features of the steam-hydraulic versus the direct-pumping plus accumulator system, we first must recognize a shortcoming of both systems, namely, that any power stroke always involves a volume of maximum-pressure water, no matter what the actual pressure required may be. Efforts to utilize the expansive properties of the steam in the steam-hydraulic system have involved too great complexity, hence the steam primarily acts as a pressure fluid. In the electric-drive pump-accumulator system, the steam in the power-generating plant is of course used more efficiently, but the pressure water thus developed is inefficiently used because of the constancy of the hydraulic pressure in the accumulator system.

In earlier days, when the Whitworth system was more generally used, i.e., 100 per cent direct pumping (no accumulator), the steam-driven pumps had to be rapidly controllable, so that then too, the best use of the steam in the pump prime movers could not be realized; for instance, flywheels were not used, and the like. If, however, a modern electric-drive pump system (with high-speed unloaders and no accumulator) were used, definitely improved operating efficiency would be realized. However, plenty of power-inrush capacity would be required to handle the sudden-demand current surges properly, and we would be confronted with even greater idle losses.

For instance, if the Charleston press were to be operated without accumulators, 4800 gpm of pumps would be required to maintain the full pressure speed of 3 ips, corresponding to 15,000 hp of drive, and accordingly an increase in idle losses to 3 times. From these considerations it seems fairly evident that the electric-drive pump-accumulator system for large hydraulic forging

[2] The information contained in Table 1 was supplied through the courtesy of Mr. C. R. Cox, president of the Carnegie-Illinois Steel Company, and Mr. Francis Bradley, president of the Midvale Steel Company.

presses is the most suitable system. For hydraulic forging presses of the more usual commercial capacities, say, from 500 to 3000 tons, where more continuous operation is to be expected, the simplicity and ease of control obtained in the direct-pumping presses without accumulators will doubtless recommend them, however, to many operators.

Other Large Presses

The magnitude of the presses discussed in this paper necessarily brings to mind other large presses built in the past. Although there have been quite a few 8000, 10,000, and 12,000-ton presses built, there are only six 14,000-ton forging presses in the world; five in the United States, and one in Germany. The first 14,000-ton press was built as long ago as 1893, by the Bethlehem Steel Company, and is still being used at its Bethlehem, Pa., plant.

When it was recognized at that early date that heavy forgings, in general, and military forgings in particular, were much superior as produced on a press than by the steam hammer, Bethlehem Steel had the courage to scrap the then recently built largest steam hammer in the world, rated at 125 tons, and undertook to build a 14,000-ton hydraulic press.[3] This press, designed and built under the direction of John Fritz, is of the Whitworth type and has operated intermittently up to the present time.

The press has 4 columns, 26 in. diam, 52 ft 7 in. long, with column spacings 17 ft 6 in. × 6 ft, and daylight of 17 ft. The press is powered from two 50 1/2-in-diam cylinders, working at a maximum pressure of 7000 psi, and having a stroke of 8 ft, internally packed. The pull-back cylinders are 13 in. diam, externally packed, and are powered from a separate 3200-psi pump-accumulator system, the pumps being originally steam-driven, but now electrically driven. The original top and bottom entablatures were of two-piece cast-iron construction, but in 1930 the top entablature was replaced by a single steel casting. The main cylinders receive high-pressure water directly from a 15,000-hp 60-rpm horizontal triplex double-acting pump, 7 3/4-in-diam cylinder × 24-in. stroke, direct-driven by a vertical triplex single-expansion steam engine, 50-in-diam cylinder × 90-in. stroke, steam at 150 psi. This huge engine-driven vertical-horizontal pump is capable of delivering 3300 gpm, corresponding to a press speed of about 3 ips which is obtained by closing the by-pass valve, or partially closing it for finer speed control. The over-all press height is 54 ft, being 37 ft above floor level, and 17 ft below.

The second 14,000-ton press built was put into operation by the Carnegie-Illinois Steel Corporation at the Charleston Naval Ordnance Plant at the close of the first world war. This press, of the oblique-strut type mentioned earlier, has four 30-in-diam columns, 51 ft 3 in. long, on column centers 19 ft × 8 ft 6 in., with 18 ft daylight. The press has 3 main cylinders, 44 in. diam, working at a maximum pressure of 7000 psi, and having a stroke of 7 ft 6 in. The objective of the three-cylinder construction is to obtain 1/3 pressure, 2/3 pressure, or full pressure by using different cylinder combinations. The pull-back cylinders are 26 in. diam, and are pressured from a separate 2500-psi pump-accumulator (dead-weight) system. The main cylinders are supplied with pressure water by 3 steam-hydraulic intensifiers, having 6-ft 4-in. diam × 7-ft-stroke steam cylinders, 12 3/4-in-diam water cylinders, thus producing 7000-psi water from 200-psi steam. A single full stroke of all the intensifiers corresponds to a 7-in. full-pressure stroke. The total weight of press and auxiliary equipment, tools and dies, is 7,250,000 lb.

The third press of this size was installed by Krupp around 1930, but no information is available as to its details other than its capacity. The last three 14,000-ton presses were built contemporaneously during the recent war, one being of the oblique-strut design described earlier, except that its pressure system is of the centrifugal pump-accumulator type, installed at the Charleston Naval Ordnance Plant; while the other two are as described in detail in this paper.

From this short recapitulation of the largest forging-press installations, we see that the United States has five of the six such presses in existence; three at the Charleston Naval Ordnance Plant, one at the Philadelphia Naval Ordnance Division of the Midvale Company, and the original at the Bethlehem Steel Company, Bethlehem, Pa. Regarding the United presses, the Midvale press is 71 ft 8 in. in total height, being 50 ft 7 in. above floor level, and 21 ft 1 in. below, and weighs 9,500,000 lb complete with auxiliary equipment, less dies and tools. The Charleston press has a total height of 74 ft 8 in., being 53 ft 7 in. above the floor, also 21 ft. 1 in. below, and weighs 11,900,000 lb complete. From these comparisons it is seen that in many respects these two most recent presses are not only the largest and heaviest forging presses ever built, but probably are the largest single machines of any type ever constructed.

Heavy Stamping or Die-Forging Presses

It is certainly in order to mention in these connections, the large-capacity presses of the heavy stamping or die-forging type alluded to in the early part of the paper. Recent machines have been built for 18,000 tons press capacity, in this country; and 15,000 tons and 30,000 tons (metric) in Germany. The function of these presses is usually to squeeze or shape between form dies, structural or mechanical parts, usually of aluminum or magnesium, in one stroke. The loads are usually central, the pressing speed and idle speed usually the same, with no particular requirements as to rapid stroking, as in planishing.

There is record of the fact that shortly before and during the early part of the recent war, the I. G. Farben Company put into operation three 15,000-metric-ton presses of the die-forging type. These presses are of 4-column construction, with columns 33 in. diam, on 15-ft × 11-ft-6-in. centers, and with daylight of 8 ft 3 in.; 19-ft 8-in. × 6-ft 6-in. press platens can be used. The presses are powered by three 55-in-diam cylinders, working at a maximum pressure of 5000 psi, the pressure being supplied from a central hydraulic system, of the motor-driven-pump hydropneumatic-accumulator type, used to operate several other machines, such as large extrusion presses, and the like. The total height of these presses is 50 ft, being 35 ft above floor level, and 15 ft below.

In this country, at the Worcester, Mass., plant of the Wyman-Gordon Company, the Reconstruction Finance Corporation had installed during the recent war, an 18,000-ton die-forging press of somewhat similar proportions. The columns are 36 in. diam, 46 ft long, and on 12-ft × 8-ft column centers, permitting the use of platens up to 7 ft, 1 in. × 12 ft 4 in., for lighter sections. The press has a maximum daylight opening of 10 ft 6 in., and a stroke of 5 ft. Pressure is obtained from a centrifugal pump-accumulator main system, working at a maximum pressure of 5400 psi. Making up this system are three 8-stage centrifugal pumps, operating in series, driven by 1000-hp 3600-rpm motors, each pump passing 800 gpm at a pressure differential of 1800 psi. Working in conjunction with these pumps are four hydropneumatic cylinders, 44 in. ID, 30 ft high, having a total volume of 9000 gal. The pull-back (more properly, push-back) cylinders, 24 in. diam, receive pressure from the main pressure system, as do the manipulator and ejector gear. The main cylinders are four in number, 48 in, diam, and arranged in line. The speed of operation of the press, being the same for idling as under pressure, is 2 1/2 ips, which full pressure speed, however, can be maintained for an 18-in. stroke, after which it must drop back to the capacity of the pumps which is about 1/2 ips. The total height of the press is 47 ft 6 in., be-

[3] Most of the data given here are from a communication from Messrs. R. B. Gerhart and W. Zollinger, chief engineers, construction and manufacturing, respectively, Bethlehem Steel Company.

ing 32 ft above floor level, and 15 ft 6 in. below, weighs 5,000,000 lb bare, and 9,000,000 lb including pumps, piping, motors, tools, dies, etc.

The 30,000-metric-ton press mentioned earlier, also installed by the I. G. Farben Company, is in reality two 15,000-ton press structures built alongside each other, to receive a common pair of long, top and bottom, die platens. Each of the two press units is of the 4-column type, having columns 32 in. diam, 69 ft 9 in. long, and on 17-ft × 6-ft column centers. By arranging these units side by side the long way of the presses, on a center distance of 18 ft, press platens having maximum dimensions 11 ft × 33 ft have been used for the die-forging of two 15-ft-long aluminum propeller blades at the same time. The press platens, because of the large span across which full pressure must necessarily be transmitted, are very deep, being of the order of 15 ft to 20 ft, and result in the abnormal height of the press, even though the maximum daylight is only 9 ft. Each press unit has four $40^1/_2$-in-diam pressure cylinders, arranged at the four corners of a rectangle, and fitted with pintle-type rams, and two 15-in-diam pull-back cylinders, all having a maximum stroke of 6 ft. Pressure is supplied to all operating cylinders from a separate pump-accumulator system, comprising three 160-gpm horizontal triplex pumps, working at a maximum pressure of 4500 psi, each driven by a 600-hp motor, and a battery of small pressure cylinders, having a probable total capacity of 6000 gal. The hydraulic system is connected to the press through two hydraulic-hydraulic intensifier units, so that pressures of 4500 psi, 6750 psi, or 3000 psi can be obtained at the press depending upon the arrangement of the valving. Each of these intensifier units is connected to each of the press units and is composed of one upper cylinder, 18 in. diam, and three lower cylinders, the outer two of which are $12^3/_4$ in. diam, and the center cylinder, $14^1/_2$ in. diam, all having an 8-ft 6-in. stroke. Each unit has a total height of 35 ft, being 25 ft above floor level, and 10 ft below. By means of the various cylinder combinations, press capacities may be adjusted to 30,000 tons, 20,000 tons, or 13,333 tons, depending upon the most suitable capacity, thus obtaining some power economy. The over-all height of the press is 81 ft, being 54 ft above floor level and 27 ft below.

Conclusion

In conclusion, we would state that we have reviewed, in general, the history and present state of the art attained in the design and construction of large hydraulic forging presses. In particular, we have attempted to explain and justify the newest type of such press which has so well lived up to all expectations, in which connection the author wishes to acknowledge the interest and courage of the United Engineering & Foundry Company in proceeding with such a departure in design, particularly under the stress of war conditions.

Appendix

Press Construction Involving Large Off-Center Loads

As mentioned in the main body of the paper, press constructions, as shown in Figs. 5(*c*, *d*, *e*), are potential designs for heavy press construction involving large off-center loads, and hence must needs be analyzed and compared critically.

In Fig. 14 are shown the various isolation and equilibrium diagrams of the Davy construction, Fig. 5(*c*). Referring to Fig. 14(*d*), it is apparent from moment considerations that

$$Rh = Pe \quad \ldots\ldots [1]$$

In Figs. 14(*b* and *c*) are shown the various statically determinate and indeterminate reactions with which we must be concerned,

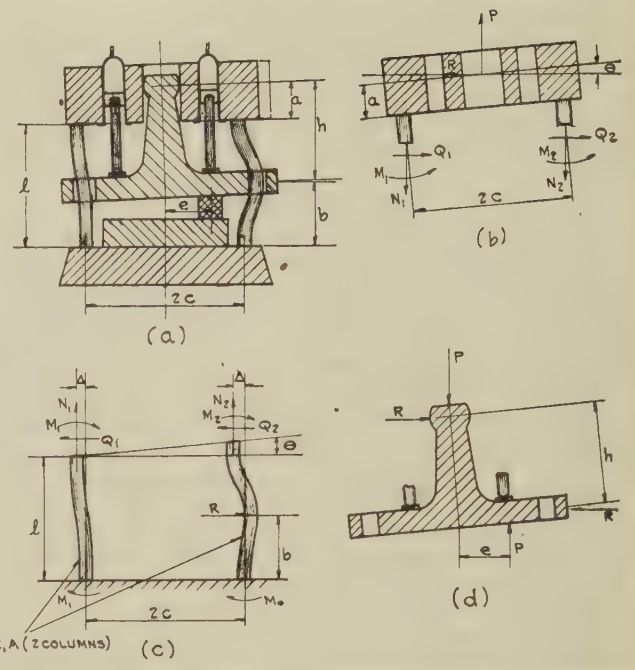

Fig. 14 Force Diagrams and Isolation Sketches; Column-Guide-Type Forging Press

particularly as to the column proper. Owing to the massiveness of the entablature and crosshead constructions, it is assumed that their body distortions are negligible with respect to the column deformations, and consequently these press components displace as rigid bodies. Referring to Fig. 14(*c*) therefore, and utilizing the basic deflection and rotation formulas as given, for instance, by Timoshenko[4]

$$\overleftarrow{\Delta} = \frac{Q_1 l^3}{3EI} - \frac{M_1 l^2}{2EI} \quad \ldots\ldots [2]$$

for the left pair of columns, and

$$\overleftarrow{\Delta} = \frac{Q_2 l^3}{3EI} - \frac{M_2 l^2}{2EI} - \frac{Rb^3}{3EI} - \frac{Rb^2(l-b)}{2EI} \quad \ldots\ldots [3]$$

for the right-hand pair of columns, where the indeterminate moments and forces are as shown in Fig. 14. The upper ends of the columns undergo rotations, which are the same for both, since the top entablature is assumed relatively rigid, thus

$$\overset{\frown}{\theta} = \frac{Q_1 l^2}{2EI} - \frac{M_1 l}{EI} = \frac{Q_2 l^2}{2EI} - \frac{M_2 l}{EI} - \frac{Rb^2}{2EI} \quad \ldots\ldots [4, 5]$$

The vertical extensions of each of the columns is given by

$$\uparrow \delta_1 = \frac{N_1 l}{AE} \quad \ldots\ldots [6]$$

and

$$\uparrow \delta_2 = \frac{N_2 l}{AE} \quad \ldots\ldots [7]$$

Now the rigid-body rotation of the entablature corresponds to the difference in the column extensions, and also must be equal to the top column end rotation, from continuity considerations, thus

[4] "Strength of Materials," by S. Timoshenko, first edition, D. Van Nostrand Company, Inc., New York, N. Y., 1930, The Macmillan Company, New York, N. Y., 1931.

$$\frac{\delta_2 - \delta_1}{2c} = \theta \quad \ldots\ldots [8]$$

From considerations of equilibrium of the entablature, isolated in Fig. 14(*b*), we have

$$P = N_1 + N_2 \quad \ldots\ldots [9]$$

$$R = Q_1 + Q_2 \quad \ldots\ldots [10]$$

and

$$\underbrace{R}_{(Q_1 + Q_2)} a + M_1 + M_2 = (N_2 - N_1)c \quad \ldots\ldots [11]$$

the last equation arising from rotational equilibrium considerations around point, *O*. The foregoing eleven equations provide sufficient relationships to solve for the eleven unknowns R, N_1, N_2, Q_1, Q_2, M_1, M_2, Δ, θ, δ_1, and δ_2.

Combining Equations [6], [7], and [8], we get

$$\frac{(N_2 - N_1)l}{2EAc} = \theta \quad \ldots\ldots [12]$$

Now, by combining Equations [2] and [3], and simplifying in the light of $Q_2 = R - Q_1$, as given in Equation [10], we get

$$[4l^3]\, Q_1 - [3l^2]\, M_1 + [3l^2]\, M_2 = [2l^3 + b^3 - 3b^2l]R \quad \ldots [13]$$

Similarly combining Equations [4] and [5], we get

$$[2l^2]\, Q_1 - [2l]\, M_1 + [2l]\, M_2 = [l^2 - b^2]R \quad \ldots\ldots [14]$$

Now, by combining Equations [11] and [12], we obtain

$$\theta = \frac{l}{2AEc} \cdot \frac{Ra + M_1 + M_2}{c}$$

which may be combined further with Equation [4], to give, after simplification

$$[l^2]\, Q_1 - \left[l\left(2 + \frac{I}{Ac^2}\right)\right] M_1 - \left[\frac{Il}{Ac^2}\right] M_2 = \left[\frac{Ial}{Ac^2}\right] R \quad \ldots [15]$$

In Equations [13], [14], and [15], we have three simultaneous equations in the three unknowns Q_1, M_1, and M_2, which may be solved in terms of R, and by virtue of Equation [1], in terms of P. However, Equation [15] may be simplified desirably by the further approximation based upon practical knowledge of the value of the quantity $I/(Ac^2)$. For two 34-in-diam columns, $I = 2 \times (\pi/64) \times (34)^4$ and $A = 2 \times (\pi/4) \times (34)^2$; and for a column spacing of $2c = 23'$, yielding $c = 138$ in., we have

$$\frac{I}{Ac^2} = \frac{(34)^2}{16(138)^2} \approx \frac{1}{250}$$

which may be neglected with respect to unity. Thus Equation [15] reduces to

$$[l^2]\, Q_1 - [2l]\, M_1 = 0$$

or

$$M_1 = Q_1 \frac{l}{2} \quad \ldots\ldots [16]$$

Solving Equations [13] and [14] simultaneously, in the light of Equation [16], we get

$$Q_1 = P \cdot \frac{e}{h}\left[\frac{1}{2} - \frac{3}{2}\left(\frac{b}{l}\right)^2 + \left(\frac{b}{l}\right)^3\right] \quad \ldots\ldots [17]$$

and consequently

$$Q_2 = P \cdot \frac{e}{h}\left[\frac{1}{2} + \frac{3}{2}\left(\frac{b}{l}\right)^2 - \left(\frac{b}{l}\right)^3\right] \quad \ldots\ldots [18]$$

Accordingly

$$M_1 = \frac{Q_1 l}{2} = \frac{Pe}{4(h/l)}\left[1 - 3\left(\frac{b}{l}\right)^2 + 2\left(\frac{b}{l}\right)^3\right] \quad \ldots\ldots [19]$$

The expression for M_2 also comes out of Equations [13] and [14], to be

$$M_2 = \frac{Pe}{4h/l}\left[1 + \left(\frac{b}{l}\right)^2 - 2\left(\frac{b}{l}\right)^3\right] \quad \ldots\ldots [20]$$

Combining Equations [9] and [11], in the light of Equation [1], we get

$$\left.\begin{aligned} N_2 &= \frac{P}{2} + \frac{Pea}{2ch} + \frac{M_1 + M_2}{2c} \\ \text{and} \qquad N_1 &= \frac{P}{2} - \frac{Pea}{2ch} - \frac{M_1 + M_2}{2c} \end{aligned}\right\} \quad \ldots\ldots [21]$$

Now, substituting Equations [19] and [20] in [21], we get finally

$$\left.\begin{aligned} N_1 &= \frac{P}{2}\left[1 - \frac{e}{c}\left(\frac{a}{h} + \frac{1 - (b/l)^2}{2h/l}\right)\right] \\ N_2 &= \frac{P}{2}\left[1 + \frac{e}{c}\left(\frac{a}{h} + \frac{1 - (b/l)^2}{2h/l}\right)\right] \end{aligned}\right\} \quad \ldots\ldots [22]$$

We are now concerned with the bending-moment diagrams of the columns. It is easy to see that for the left-hand columns, the BM is a maximum at each end, being equal, and always zero in the middle, the condition being independent of the value b, i.e., the position of the crosshead. The right-hand pair of columns has a more complex BM diagram, and we must examine the conditions at the top M_2, and as well the moments at the contact point with the crosshead, M_R, and at the base, M_0. Thus for M_R we have, referring to Fig. 14

$$M_R = Q_2 (l - b) - M_2$$

and by substituting in the values of Q_2 and M_2 as given in Equations [18] and [22], we get

$$M_R = \frac{P_e}{4h/l}\left[1 - 2\left(\frac{b}{l}\right) + 5\left(\frac{b}{l}\right)^2 - 8\left(\frac{b}{l}\right)^3 + 4\left(\frac{b}{l}\right)^4\right] \quad \ldots\ldots [23]$$

For M_0, we have

$$M_0 = Q_2 l - M_2 - Rb$$

which leads to

$$M_0 = \frac{P_e}{4h/l}\left[1 - 4\left(\frac{b}{l}\right) + 5\left(\frac{b}{l}\right)^2 - 2\left(\frac{b}{l}\right)^3\right] \quad \ldots\ldots [24]$$

Now we must further pursue the problem to evaluate all four moments, M_1, M_2, M_R, and M_0 as a function of crosshead position b. To do this most effectively, we plot the curves as shown in Fig. 15(*a*) from which it is apparent that M_2 is always the largest of the four, and is an absolute maximum for $b = 1/(3l)$, although it is nearly the same value for all values from $b = 0$ to $b = l/2$, which about covers the entire operating range. We see from Equation [22] that the tension stress, as determined by N_2, is also greater in the columns toward which the eccentric forging is carried out, and hence the most highly stressed location is at the top of the right-hand pair of columns.

To evaluate the press sway or lateral deflection of the top entablature, let us return to Equation [2], substituting the

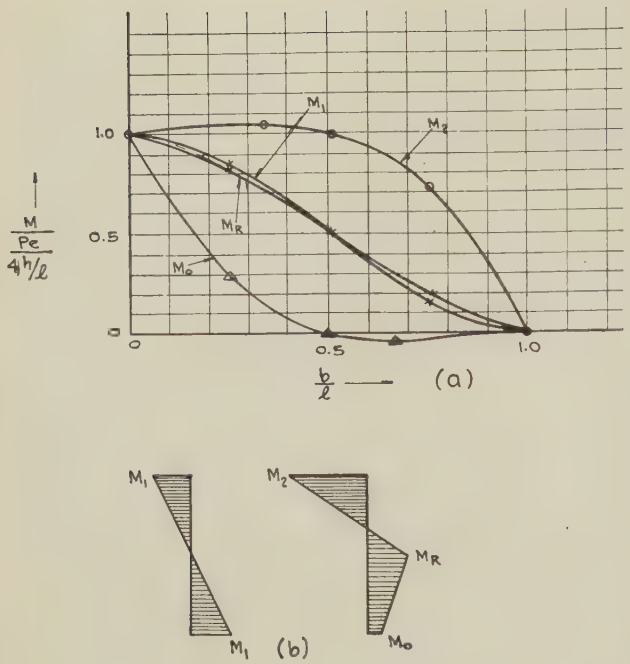

FIG. 15 BENDING-MOMENT DIAGRAM FOR COLUMN-GUIDE PRESS

values of Q_1 and M_1 from Equations [17] and [19], to obtain

$$\Delta = \frac{Pel^3}{24\,hEI}\left[1 - 3\left(\frac{b}{l}\right)^2 + 2\left(\frac{b}{l}\right)^3\right] \quad \ldots\ldots [25]$$

which shows the sway to be greatest where b is the least, all other things being equal.

PRESS CONSTRUCTION WITH STRUT

In this section, the press construction of Fig. 5(d) will be analyzed. The principal contribution and purpose of the oblique strut is to reduce the sidesway essentially to zero, and correspondingly to reduce the maximum bending stresses. In order to simplify the evaluation of this structure, which is inherently considerably more complex than the construction of the preceding section, we may proceed by superimposing on the analysis there given, the stress system introduced by applying a lateral force T, of sufficient magnitude to nullify the sidesway Δ. This neglects the elastic extension of the strut itself (which is of the order of one tenth of the sidesway before the introduction of the strut), as well as the reduced elastic extension of the right-hand pair of columns, due to the angularity of the strut.

It is apparent from Fig. 16(b) that extensional forces N_1' and N_2', are set up as a result of the lateral distortion Δ'. Our approach is to evaluate that force T, but more particularly, those values of M_1' and M_2' associated with making $\Delta' = \Delta$ (of Equation [25]). Under the system of forces in Fig. 16(c) it is known that $M' = Q'l/2$ will cause the top ends of the columns to deflect without appreciable rotation. From symmetry considerations $Q_1' = Q_2' = T/2$, from which follows that $M_1' = M_2' = (Tl/4)$. From these relations, and the expression

$$\Delta' = \frac{Q_1'l^3}{3EI} - \frac{M_1'l^2}{2EI}$$

we obtain finally

$$\Delta' = \frac{Tl^3}{24EI} \quad \ldots\ldots [26]$$

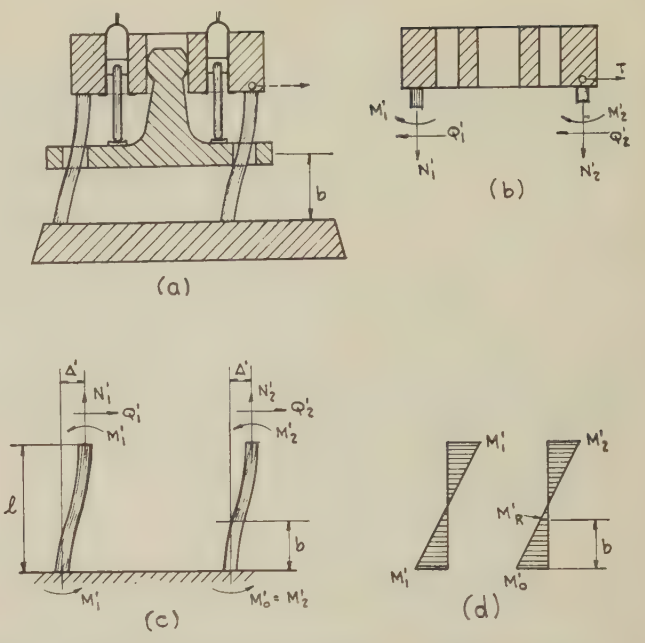

FIG. 16 ISOLATION SKETCHES AND BENDING-MOMENT DIAGRAMS, SHOWING EFFECTS OF OBLIQUE STRUTS

Equating [25] and [26], we obtain the required expression

$$T = P\frac{e}{h}\left[1 - 3\left(\frac{b}{l}\right)^2 + 2\left(\frac{b}{l}\right)^3\right] \quad \ldots\ldots [27]$$

from which we obtain

$$M_1' = M_2' = \frac{Pe}{4\,h/l}\left[1 - 3\left(\frac{b}{l}\right)^2 + 2\left(\frac{b}{l}\right)^3\right] \quad \ldots\ldots [28]$$

and also that $M_0' = M_2'$, see Fig. 16(d). From this figure also, we evaluate the bending moment M_R', corresponding to the crosshead position b, above the base, to be

$$M_R' = \frac{Pe}{4\,h/l}\left[2\left(\frac{b}{l}\right)\left\{1 - 3\left(\frac{b}{l}\right)^2 + 2\left(\frac{b}{l}\right)^3\right\}\right] \quad \ldots\ldots [29]$$

The actual bending moments, then, in the structure, Fig. 5(d) are given by superposing the values and diagrams of Figs. 15 and 16, to give

$$\left.\begin{aligned} M_1'' &= M_1 - M_1' = 0 \\ M_2'' &= M_2 - M_2' = \frac{Pe}{4\,h/l}\left[4\left(\frac{b}{l}\right)^2\left(1 - \frac{b}{l}\right)\right] \\ M_R'' &= M_R - M_R' = \frac{Pe}{4\,h/l}\left[1 - 4\left(\frac{b}{l}\right) + 5\left(\frac{b}{l}\right)^2 - 2\left(\frac{b}{l}\right)^3\right] \\ M_0'' &= -(M_0 - M_0') = \frac{Pe}{4\,h/l}\left[4\frac{b}{l}\left(1 - \frac{b}{l}\right)^2\right] \end{aligned}\right\} \quad \ldots [30]$$

The only reason for reversing the sign in the last of Equations [30] is to yield positive values, as directions mean nothing in our numerical comparison. By plotting the values of the various moments given, we obtain Fig. 17. From this plot it is apparent that for the range $b/l = 1/4$ to $1/2$ the maximum bending moments do not exceed 0.59 $Pe/[4(h/l)]$ which is about 60 per cent of the maximum values for construction Fig. 5(c) as shown

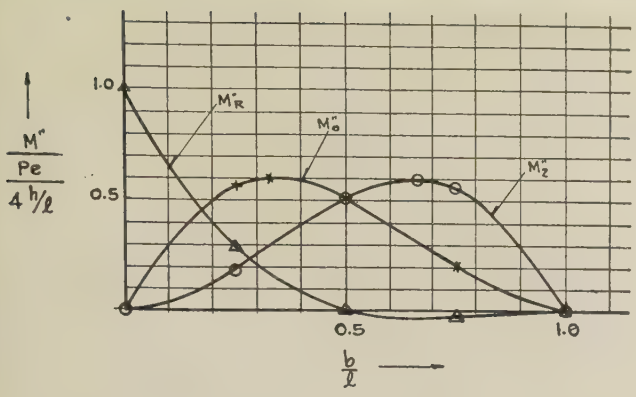

FIG. 17 BENDING-MOMENT VALUES AS FUNCTION OF CROSSHEAD POSITION, COLUMN-GUIDE PRESS PLUS OBLIQUE STRUTS

in Fig. 15, a reduction of some 40 per cent. However, if $b \approx 0$ were a practical condition, no essential reduction in maximum stress would have been accomplished.

INTERNALLY COMPENSATED GUIDE-STALK PRESS

If we now examine critically the press structure shown in Fig. 5(*e*), isolation sketches are as indicated in Fig. 18. As there is no contact between the crosshead and the columns, the

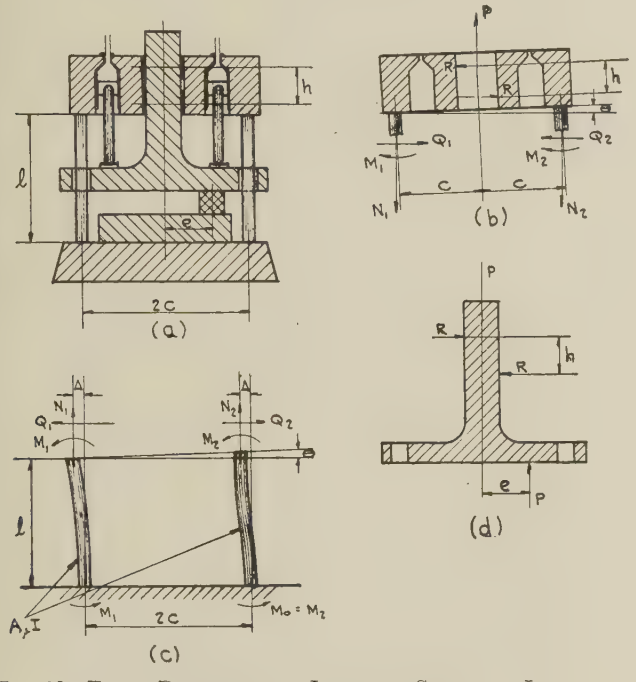

FIG. 18 FORCE DIAGRAMS AND ISOLATION SKETCHES, INTERNALLY COMPENSATED GUIDE-STALK PRESS

eccentric forging moment is balanced by pressure against the pads in the guide-stalk well, and as shown in Fig. 18(*d*), we have

$$Rh = Pe \quad [31]$$

Referring to Fig. 18(*b*), conditions of static equilibrium are

$$P = N_1 + N_2 \quad [32]$$

$$Q_1 = Q_2 \quad [33]$$

and

$$Rh - (N_2 - N_1)c = M_1 + M_2 \quad [34]$$

It is apparent that shear forces Q_1 and Q_2 can exist only if opposite in direction, as shown.

Now, as to elasticity conditions, the column extensions are given by

$$\uparrow \delta_1 = \frac{N_1 l}{AE} \quad [35]$$

and

$$\uparrow \delta_2 = \frac{N_2 l}{AE} \quad [36]$$

As to rotation of the top ends of the columns, we have

$$\overset{\curvearrowleft}{\theta} = \frac{M_1 l}{EI} + \frac{Q_1 l^2}{2\,EI} \quad [37]$$

and

$$\overset{\curvearrowleft}{\theta} = \frac{M_2 l}{EI} - \frac{Q_2 l^2}{2\,EI} \quad [38]$$

where the rotations are constrained to be the same because of the relative rigidity of the top entablature. This member can rotate only in space due to unequal column extensions, hence

$$\overset{\curvearrowleft}{\theta} = \frac{\delta_2 - \delta_1}{2c} \quad [39]$$

As to press sway or lateral column deflection, we have, again

$$\overset{\leftarrow}{\Delta} = \frac{M_1 l^2}{2\,EI} + \frac{Q_1 l^3}{3\,EI} = \frac{M_2 l^2}{2\,EI} - \frac{Q_2 l^3}{3\,EI} \quad [40,\ 41]$$

Thus here again, we have eleven equations to determine the eleven unknowns, R, N_1, N_2, Q_1, Q_2, M_1, M_2, Δ, θ, δ_1, and δ_2.

From Equations [37] and [38], we obtain by simplifying

$$M_2 - M_1 = \frac{1}{2}(Q_2 + Q_1)l \quad [42]$$

and from Equations [40] and [41], we obtain similarly

$$M_2 - M_1 = \frac{2}{3}(Q_2 + Q_1)l \quad [43]$$

By examining and comparing Equations [42] and [43], we find that these equations can be true only if $Q_1 = -Q_2$, but by Equation [33], we have $Q_1 = Q_2$, therefore

$$Q_1 = Q_2 = 0 \quad [44]$$

which condition imposes on Equations [42] and [43] the conditions that

$$M_1 = M_2 = M \quad [45]$$

Now, combining Equations [35] and [36] with [39], we get

$$\theta = \frac{(N_2 - N_1)l}{2\,AEc} \quad [46]$$

And equating Equations [46] to [37] or [38], in the light of Equations [44] and [45], we get

$$N_2 - N_1 = \frac{2\,MAc}{I} \quad [47]$$

Rewriting Equation [34] in the light of Equations [31] and [45], we also obtain

$$N_2 - N_1 = \frac{Pe - 2M}{c} \quad [48]$$

And by equating Equations [47] and [48], we get finally

$$M = \frac{Pe}{2} \cdot \frac{1}{1 + \frac{Ac^2}{I}} \quad \ldots\ldots [49]$$

Remembering now that Ac^2/I is large with respect to unity, Equation [49] may be more simply written

$$M = \left(\frac{I}{Ac^2}\right)\left(\frac{Pe}{2}\right) \quad \ldots\ldots [50]$$

Substituting Equation [50] in Equation [47] yields

$$N_2 - N_1 = P \cdot \frac{e}{c} \quad \ldots\ldots [51]$$

and Equation [32] says

$$N_2 + N_1 = P$$

From these two equations, it follows that

$$\left.\begin{aligned} N_1 &= \frac{P}{2}\left[1 - \frac{e}{c}\right] \\ \text{and} \quad N_2 &= \frac{P}{2}\left[1 + \frac{e}{c}\right] \end{aligned}\right\} \quad \ldots\ldots [52]$$

which thus completely evaluates all previous unknowns.

The virtues of this design are now apparent, since the maximum column bending moment is only a small fraction (less than 1 per cent) of the eccentric forging moment Pe. The structural resistance to this forging moment resides primarily in the modified column tension loads, which increase the maximum tension stress only by some 25 per cent. As to press sway, Equation [50] in Equation [40], in the light of Equation [45] yields

$$\Delta = \frac{Pel^2}{4EAc^2} \quad \ldots\ldots [53]$$

Streamlining Effect on Air Resistance and Smoke Lifting on Steam Locomotives

By J. F. GRIFFIN,[1] EAST CHICAGO, IND.

A test was conducted in 1946 in the wind tunnel at the Daniel Guggenheim School of Aeronautics at New York University with a $^1/_{12}$-scale model of an existing modern 4-8-4 type locomotive. To this model was added for various runs different features of streamlining or smoke-lifting deflecting plates or both. Each change constituted, in effect, a different model. This paper covers a report on the five models which proved to be of the most importance.

Introduction

Problems Prompting Investigation. All motive power has to overcome wind resistance. This resistance can be held to a minimum by suitable streamlining but on the steam locomotive the streamlining is limited to that which will not interfere with maintenance and servicing.

A steam locomotive also presents the problem of preventing smoke from curling around the cab and obstructing the vision of the engineer and fireman. This is referred to as smoke trailing and is caused by too low a velocity at the outlet of the stack for the conditions under which the locomotive is operating.

The usual correction for smoke trailing is to decrease the diameter of the exhaust tip which results in an increase in the exhaust pressure and a decrease in cylinder horsepower. The increased exhaust pressure increases the velocity at which the mixture of the gases of combustion and the exhaust steam are discharged from the stack, lifting them well above the locomotive.

A "head-on" wind velocity of 88 mph gives a mass velocity about the same as the mass velocity of the mixture of gases and steam leaving the stack on a typical locomotive operating with about 4 lb exhaust pressure. The head-on wind considered here is due to the locomotive traveling at 88 mph. Under these conditions, the tendency should be for the smoke and steam to start upward at an angle of about 45 deg in relation to the longitudinal center line of the locomotive. Since the force available, due to the velocity of the mixture from the stack, is a diminishing one and that of the wind a constant one, the wind and gravitation soon overcome the velocity of the mixture from the stack, bringing its flow down to a horizontal flow. However, the wind tends to act parallel to the axis of the locomotive and it should have a strong tendency to combat gravitation and hold the flow of gases and steam in a horizontal path unless some outside force acts to interfere with it.

It seems to be pretty well accepted, that because of the lack of suitable streamlining on the top and sides of a locomotive, eddy currents of air are formed along the upper portion. This creates a lower pressure at various points and the gases and exhaust steam flow to these low-pressure points, finally curling around the cab obstructing vision.

A test was conducted in 1946 in the wind tunnel at the Daniel Guggenheim School of Aeronautics at New York University with a $^1/_{12}$-scale model of an existing modern 4-8-4 type locomotive. To this model were added for various runs, different features of streamlining or smoke-lifting deflecting plates or both. Each change constituted, in effect, a different model.

The Huet design is described in detail in the text, but briefly it is a novel design arranged to convert air velocity into pressure so as to build up a layer of air at least to atmospheric pressure around the locomotive to reduce skin friction, and to prevent low-pressure points being formed, which would draw the smoke and exhaust steam down around the locomotive.

The main object in testing "full streamlining" was to establish what the least possible wind resistance could be with the utmost in smoothing out the lines of the locomotive, regardless of its practicability for a steam locomotive.

The general interest of The Superheater Company in all types of motive power for transportation purposes, prompted them to sponsor this test in the interest of improved motive-power performance.

Summary of Results Obtained. The results obtained on this test were such that, if they can be duplicated in road service, make it appear possible not only to reduce smoke trailing but also to decrease stack velocities; and at high speeds to effect a reduction in wind resistance. The latter would add directly to the drawbar horsepower. A decrease in stack velocities would mean a decrease in exhaust pressure which could be utilized to increase the drawbar horsepower.

Full streamlining (considered impractical from a maintenance and servicing standpoint) gave less wind resistance than any model tested. However, it was not entirely satisfactory from a smoke-lifting standpoint. When smoke-lifting deflecting plates were applied they helped the smoke lifting, but did not entirely prevent smoke trailing.

The Huet design of streamlining was almost as good as the full streamlining from a wind-resistance standpoint. Its performance from a smoke-lifting standpoint was remarkable, exceeding all other models tested by a wide margin. Even with high locomotive speeds and 1-lb exhaust pressure there was no smoke trailing, indicating stack velocities might be decreased considerably without smoke trailing.

The locomotive with the special streamlined nose and with smoke-lifting deflecting plates showed a small reduction in wind resistance. In this regard it ranked third with the five models tested. From a smoke-lifting standpoint its performance was about equal to that of the bare locomotive with smoke-lifting deflecting plates. With it there was no indication that stack velocities could be reduced.

The orthodox smoke-lifting deflecting plates applied to a bare locomotive increased the wind resistance slightly. They were quite effective from a smoke-lifting standpoint. However, their performance in this respect was not as good as the Huet design of streamlining with smoke lifters.

The bare locomotive gave considerably higher wind resistance than any streamlined models tested and showed up poorly as compared with the other models from a smoke-lifting standpoint.

---

[1] Chief Engineer, The Superheater Company, East Chicago, Ind. Mem. ASME.

Contributed by the Railroad Division and presented at the Annual Meeting, Atlantic City, N. J., December 1–5, 1947, of The American Society of Mechanical Engineers.

Note: Statements and opinions advanced in papers are to be understood as individual expressions of their authors and not those of the Society. Paper No. 47—A-82.

Tests

The test was made with several $^1/_{12}$-scale models with various features of streamlining and smoke-lifting deflecting plates. Although a number of models were tested, the five most important are covered by this paper. The same five models used for the wind-resistance test were used for the smoke-lifting test.

Types of Tests. The first series of runs were made to determine, by force measurements, the wind resistance. Drag- or wind-resistance readings were taken with each model at five wind-tunnel air velocities between 40 and 100 mph with the models set in the tunnel so that the wind was head-on. Readings were also taken at the same wind velocities with the models set at several angles in relation to the direction of the air flow in the tunnel. During the drag runs there was no exhaust from the stack.

The second series of runs were made to determine, by visual observation, the effect of the various features of streamlining and smoke-lifting deflecting plates, on smoke lifting. These observations were recorded by means of motion pictures.

The smoke-trailing runs were made with each model at wind-tunnel air velocities of 30 to 90 mph. The tunnel air velocity was brought up to 30 mph and each model was slowly rotated until the axis of the engine was at an angle of 25 deg to the axis of the wind tunnel, or in 25-deg yaw position. It was then rotated slowly back to zero yaw. The air velocity was then slowly brought up to 60 mph where this rotation was repeated. Finally the air velocity was brought up to 90 mph and the same procedure in rotation was followed. Each model was also tested with several different exhaust pressures while being subjected to the foregoing wind-tunnel speeds and the series of rotations described. When the motion pictures were made each run was labeled with the exhaust pressure simulated.

Description Of Models

An existing modern 4-8-4 type steam locomotive with its tender was selected as the base for this test. A model of it was built, and all streamlining features as well as smoke-lifting deflecting plates, were built for application to this model. A brief description of the features tested is given in Table 1.

TABLE 1

Line no.	Model features tested	Shown in figures
1	Bare modern 4-8-4 type locomotive; no streamlining, no smoke lifters	1
2	Bare modern 4-8-4 type locomotive; no streamlining but with orthodox smoke lifters as now used on a number of locomotives	2 and 3
3	Locomotive with a special streamlined nose and with smoke lifters	4 and 5
4	Locomotive with Huet streamlining and smoke lifters	6 and 7
5	Locomotive with full streamlining and smoke lifters	8

The term "bare locomotive" is used to indicate that no streamlining was used. In this paper, smoke-lifting deflecting plates are not considered streamlining.

The bare locomotive, or base model, was made of wood. It was 9.4 ft long and had a projected cross-sectional area of 0.84 sq ft. This model is covered by line 1 of Table 1 and is shown in Fig. 1.

The model representing the locomotive as actually operated on the road, is covered by line 2 of Table 1. It is shown in Figs. 2 and 3. This model was produced by adding to the bare model, smoke-lifting deflecting plates of an orthodox design now in road service on a number of locomotives.

Line 3 in Table 1 covers a locomotive with a special streamlined nose and smoke lifters. It is shown in Figs. 4 and 5. This model was produced by removing the bumper, pilot, and headlight from the base model and substituting the streamlined nose. The smoke-lifting deflecting plates used on this model are the same as used on the model described in line 2.

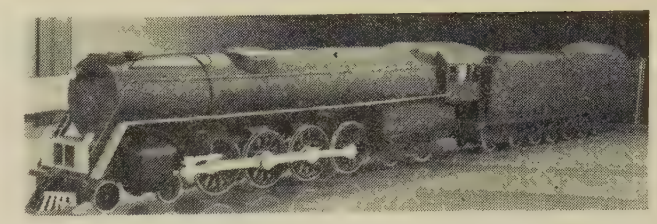

Fig. 1 Bare Locomotive—No Streamlining, No Smoke Lifters

Fig. 2 Diagram of Bare Locomotive—No Streamlining, With Orthodox Smoke Lifters

Fig. 3 Bare Locomotive—No Streamlining, With Orthodox Smoke Lifters

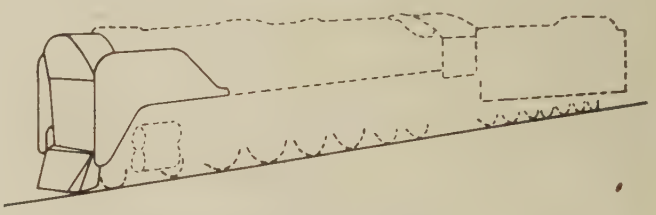

Fig. 4 Diagram of Locomotive With Special Streamlined Nose and Smoke Lifters

Fig. 5 Locomotive With Special Streamlined Nose and Smoke Lifters

Line 4 in Table 1 is the base model equipped with a novel design of streamlining, as shown in Figs. 6 and 7. This streamlining was designed by André Huet[2] and has been applied to a number of locomotives now in service in Europe. His design includes his own type of smoke-lifting deflecting plates.

Line 5 in Table 1 is the base model equipped with full streamlining. It was obtained by adding a streamlining shroud and

[2] President and General Director, Compagnie de Surchauffeurs, Paris, France. Mem. ASME.

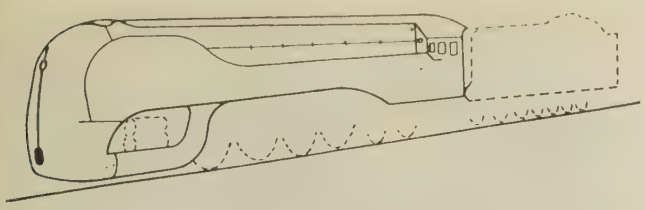

FIG. 6 DIAGRAM OF LOCOMOTIVE WITH HUET STREAMLINING AND SMOKE LIFTERS

FIG. 7 LOCOMOTIVE WITH HUET STREAMLINING AND SMOKE LIFTERS

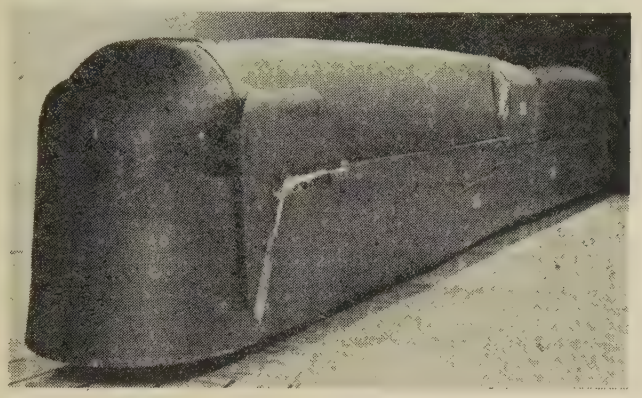

FIG. 8 LOCOMOTIVE WITH FULL STREAMLINING AND SMOKE LIFTERS

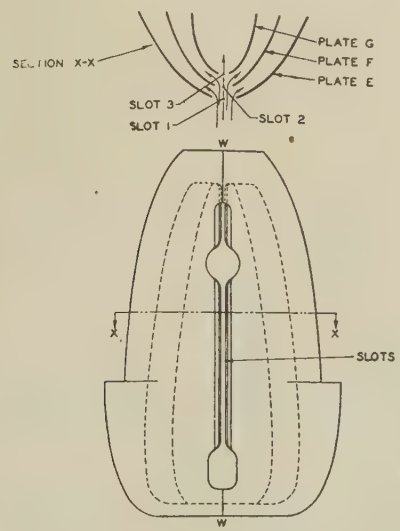

FIG. 9 FRONT VIEW OF LOCOMOTIVE WITH HUET STREAMLINING

smoke-lifting deflecting plates to the bare locomotive, as shown in Fig. 8. As previously stated, this type of streamlining is not practical, but it was included to show the optimum obtainable in the reduction of wind resistance and to determine the effect of this type of streamlining on smoke lifting. Its wind resistance was of particular interest because it is similar to the streamlining used on Diesel road engines.

Huet Type of Streamlining. The purpose of the Huet type of streamlining is to secure the greatest possible benefits from streamlining, while allowing accessibility to those parts requiring frequent servicing, and the greatest amount of maintenance.

The underlying principle of the Huet design is that fluid flowing through a properly diverging nozzle will change velocity to pressure.

Fig. 9 shows how this principle is utilized by the Huet streamlining. The lower portion of this figure shows a front view of the streamlined nose of the locomotive. The upper portion shows a plan view of a section through the streamlined nose. Referring to the upper portion, it will be noted that slots 2 and 3 in plates F and G are progressively narrower than slot 1 in plate E. Wind enters slot 1 as illustrated, and a portion of it passes between plates E and F as shown by the arrows. Some of the wind travels farther and passes between plates F and G. The divergence of these plates, in relation to each other, transforms wind velocity into pressure, enveloping the locomotive with a layer of air at a pressure higher than would otherwise exist in that proximity, thus avoiding the creation of low-pressure zones throughout the length of the locomotive.

The streamlined nose of the Huet design is made in two halves being split on line W-W. Each half is hinged to the front of the smokebox to provide easy access to the smokebox.

TEST EQUIPMENT AND METHODS

Wind Tunnel. The wind tunnel at New York University in which the test was conducted is shown diagrammatically in Fig. 10. The figure shows both a horizontal and vertical section through the tunnel which is of the type having a closed working section under atmospheric pressure and a double return. The working or testing section is 10 ft long with a 7 × 10-ft cross section. The rear portion just past the working section is built into the form of a cone and at the maximum diameter houses a 14-ft-diam 9-blade propeller, driven by a 250-hp motor. The propeller and motor will develop a wind speed of more than 125 mph in the working section. Fig. 10 also shows the location of the model in the wind tunnel.

A ground board was built into the tunnel to simulate ground

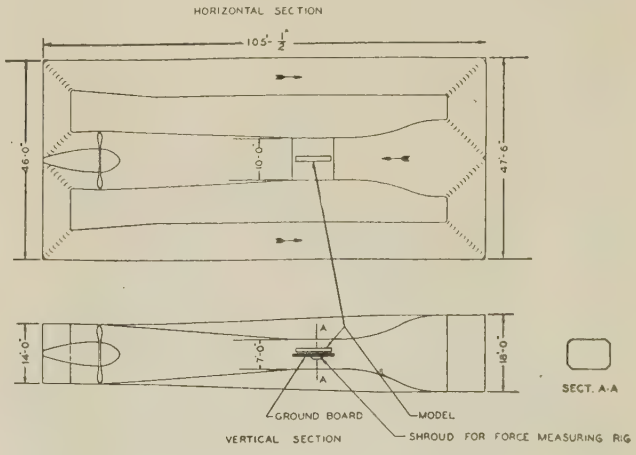

FIG. 10 WIND-TUNNEL DIAGRAM

effects. It extended from side to side of the working section, which divided the working section approximately in half, forming an upper and lower half to the tunnel at this point. The ground board was 6 in. thick and approximately 12 ft long, the front edge of which was streamlined.

Fig. 11 shows how the model was placed in the working section of the tunnel above the ground board. When the model was set in zero-yaw position its nose was 2.23 ft to the rear of the leading edge of the ground board.

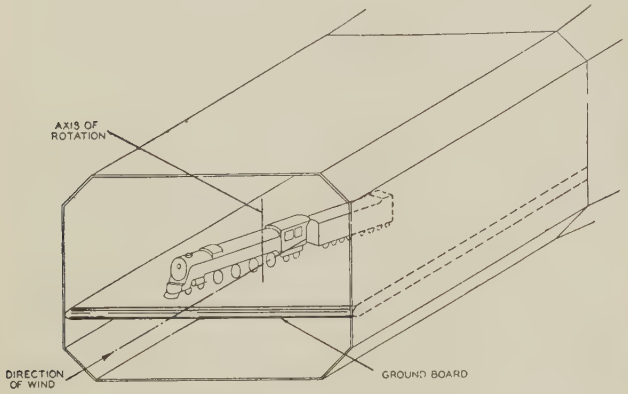

Fig. 11 Tunnel Working Section

Drag Force-Measuring Equipment. The model was rigidly mounted on a 3-in. pipe which acted as a shaft, by means of which it was attached to a T-shaped force-measuring rig. It was also used as the axis about which the model was rotated to obtain the desired angle of yaw. The shaft was located 3.56 ft to the rear of the model nose.

The T-shaped rig in which the vertical shaft rotated was provided with a clamping arrangement for holding the model rigidly in place at any desired yaw angle, while force measurements were taken.

Fig. 12 shows the T-shaped rig containing the beams to which were bonded metalectric strain gages for measuring the forces on the model. The forces measured by the strain gages were recorded by a Wheatstone-bridge control box. It will be noted that the rig was located under the ground board, a section of which was removed immediately above the rig to permit the photograph to be taken. The rig rested on three ball-bearing supporting columns, two of which acted as force-measuring beams; the third and rear column simply acted as a support. This may be seen more clearly in Fig. 13. One of the two strain-measuring and supporting beams of the rig had two sections reduced for application of strain gages. The sections were reduced to make them more sensitive to the strains imposed on them so that the recorded forces would come within the range of the control box. The reduced sections are shown in Fig. 14. The other strain-measuring and supporting beam had only one reduced section for application of a strain gage. Both strain-measuring beams were sectioned so as to record the bending in a direction parallel to the center line of the wind tunnel, while one beam only was sectioned to give the results of bending in a crosswise direction of the tunnel. However, the one with only one reduced section was secured to the base in such a manner as to permit it to act as a link with no resistance to a crossway force. In this way drag and cross-wind forces exerted by the wind on the model could be recorded.

Calibration of Drag-Measuring Equipment. Before actual testing was begun, a static calibration of the strain-gage units was made with the model mounted in place by attaching known weights to the rig. Calibration curves were prepared to indicate the equivalent forces on the model during the test. Check readings of tare

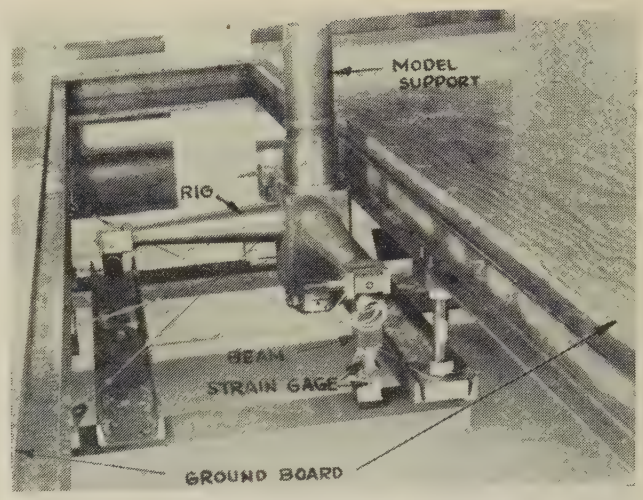

Fig. 12 T-Shaped Force-Measuring Rig (Side View)

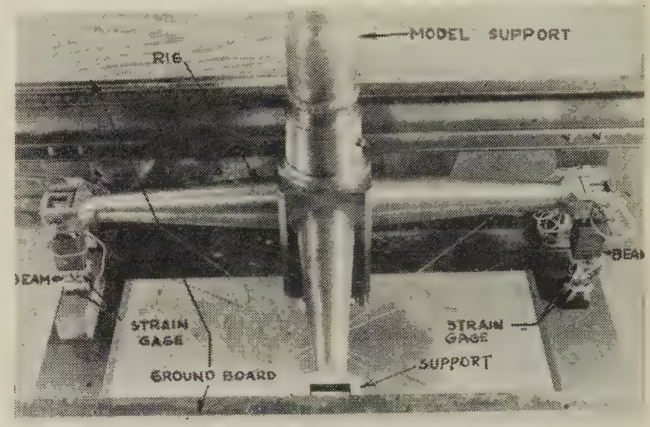

Fig. 13 T-Shaped Force-Measuring Rig (Top View)

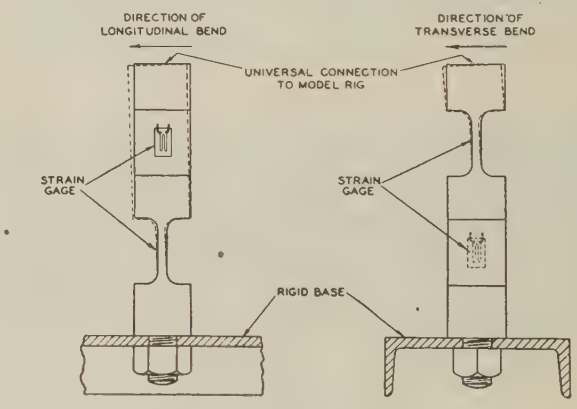

Fig. 14 Strain-Gage Beam for Drag Rig

were made before as well as after each individual run, thus accounting for any residual strains in the force-measuring system.

As previously stated, wind resistance was measured with a head-on wind as well as with the models at yaw angles of 4, 8, 12, and 25 deg.

Runs indicated that because of the lack of symmetry of the two halves of the model, or because of the vertical shaft being located slightly off center of the model, or both, corrections in the angles

when recording data had to be made. This resulted in the following corrections:

Actual angles of yaw	0°	4°	8°	12°	25°
Corrected angles of yaw	1.5°	5.5°	9.5°	13.5°	26.5°

Although the models were set at the "actual angles of yaw," all data were recorded under the angles shown as "corrected angles of yaw."

The 1.5-deg angle as compared with zero angle, has a very slight effect on the data in the direction of increasing the drag. It is of insufficient magnitude to consider in this discussion and the data so obtained are used herein as a head-on wind. Since all runs were conducted on the same basis, their results should, for all practical purposes, be comparable.

Basic Data for Smoke-Lifting Runs. Prior to making smoke-lifting observation tests, every effort was made to duplicate conditions in road service which would affect smoke lifting. These were head-on-wind velocities due to the motion of the locomotive, cross or natural winds, and the various mass velocities and densities of the mixture leaving the stack at different exhaust pressures.

To assist observations and record them by motion pictures, also to avoid the introduction of moisture into the tunnel, it was desirable to discharge "smoke only" from the stack. However, all chemicals proposed for smoke-making purposes were ruled out because they were considered injurious to health or to the wind tunnel, or presented a fire hazard. It was finally decided that "steam only" could be used without detriment to the tunnel if the runs were not of too long duration before the air in the tunnel was changed.

Basic data shown in Table 2 were assumed for this test. The outlet of the full-size locomotive stack was assumed to be 22 in. in diameter and that of the model 1.85 in. Because of the necessity for discharging from the stack steam only instead of a mixture of gases and steam, a column was added to Table 2 to show the quantities of steam exhausted from the stack of the models.

TABLE 2 BASIC DATA USED FOR SMOKE-LIFTING RUNS

Data for full size locomotive						
Total evaporation, lb per hr	Exhaust steam temperature, F	Gas temperature, F	Gas weight, lb per hr	Steam to exhaust nozzle, lb per hr	Exhaust steam pressure, psi	Model Steam, lb per hr[a]
10,000	212	448	17,000	9,000	1/4[b]	60
17,000	214	471	29,000	15,000	1	175
40,000	265	540	66,000	34,000	5	410
67,000	360	605	105,000	56,500	15	620

[a] Quantity calculated to give same mass flow at model stack using steam only as for full-size locomotive using hot gases and steam for exhaust pressures shown.
[b] Steam flow representing 1/4 lb exhaust steam pressure had insufficient volume to be of value in observations.

Smoke Pattern for Smoke-Lifting Runs. The well-known aerodynamic formula, drag per unit length $= C_d \, 1/2 \, \rho \, V^2 d$, coupled with other mathematical concepts on acceleration, scale factors, etc., was developed to a point where it indicated that if the velocity and the density of the mixture leaving the stack and the velocity and density of a head-on wind are the same for a full-size locomotive and a scale model, the smoke pattern for the model should be in proportion to the scale size.

Preliminary runs were made in a small wind tunnel to demonstrate this was a suitable application of the formula. During these runs stacks of 0.90-in. diam and of 0.45-in. diam were used. The same wind and stack mass velocities were used for each size stack. Runs were made with properly proportioned mixtures of hot gases and steam, as well as with steam only. A board marked off in numbered squares was placed in back of the jet so that the smoke pattern for each run could be determined and recorded. The results checked very closely with the formula, which proved that when operating with steam only if the same mass velocity of flow was used as existed with the proper mixture of hot gases and exhaust steam, the proper smoke pattern would be obtained and the results of the tests would be representative.

Test Data, Calculations, and Corrections

From the original test data, conversion and corrections were made as follows:

Conversion of drag data from scale-model values to prototype values.

Corrections for static pressure drop in wind tunnel.

Corrections for scale effect on skin friction.

Correction of air speed necessitated by the blocking effect of ground board and model.

Corrections to yaw angles because of lack of absolute symmetry in models or mounting of models on shaft, previously explained.

The correction for air-blocking effect was obtained by placing a Pitot static tube in the tunnel, with ground board and measuring rig shroud only, in place. Applying the law "continuity of flow per unit time is constant," the true air speed at the model was established.

Because of the relative sizes of the model and the working section of the wind tunnel, a correction in the tunnel air speed at the location of the model, due to the tunnel-wall effect, was found to be so small it could be neglected.

The drag readings for zero yaw were converted to horsepower by the formula, horsepower $= \frac{DV}{375}$, where D = drag force or wind resistance and V = velocity in miles per hour

Winds. Three types of winds will be referred to in this paper and before discussing the test results, it would be well to set up a name for each of them. Fig. 15 shows these winds and their relationship. One is due to locomotive velocity and will be called "locomotive velocity wind." It is always a head-on wind. A

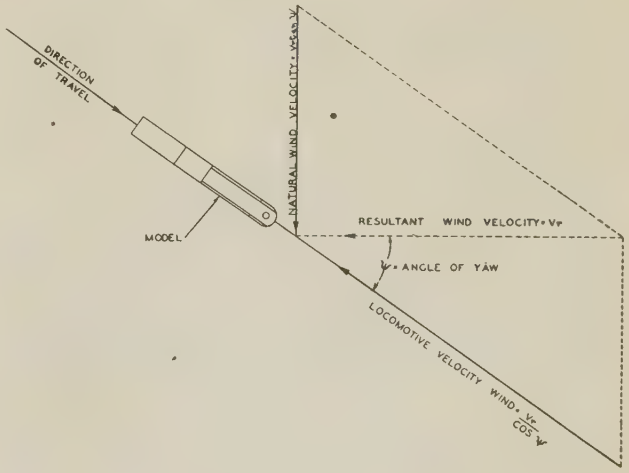

Fig. 15 Velocity Diagram

second is called "natural wind" which is due to atmospheric conditions and may be at any angle in relation to the direction of the movement of the locomotive. The third is called a "resultant wind" which is the result of combining the two.

The locomotive velocity wind and the natural wind can be resolved mathematically into a single resultant wind. However, since in a wind tunnel there is but one wind available, it will be a head-on wind when the model is set in a position with its axis parallel to the axis of the tunnel, and will be equal to the speed of the locomotive, or equal to an assumed combination of locomotive speed and natural head-on wind. When the model is rotated at an angle in the tunnel, the tunnel wind velocity acts as a resultant wind and drag readings taken during these runs are definitely in relation to the resultant wind. For each drag force and resultant wind given in the test data, the resultant wind can be resolved into two components, one being locomotive speed and the other natural-wind velocity. The natural wind can be broken down into various combinations of velocity and angularity, but each combination will result in a different locomotive speed and a different angle of yaw.

Fig. 15 shows the model rotated at an angle to the resultant or tunnel wind. In this figure the direction of the natural-wind component is shown as 90 deg to the resultant wind. It is shown at that angle to make it agree with the direction in which the cross- or natural-wind drags were recorded.

Natural Winds—at Angle to Locomotive Travel. The statement has been made in a number of papers written on wind resistance that natural winds which may be head-on or at an angle to the direction of the movement of the locomotive, are of little importance and can be omitted from consideration. Lack of supporting data indicates the desirability of studying this question sufficiently to determine its importance. It seems desirable to settle this question before going into a complete discussion of the test results.

Data obtained from the U. S. Department of Commerce Weather Bureau at Chicago, Ill., showed that the average hourly wind velocity in the Chicago district for the year 1946 was 9.4 mph. Therefore it should not be necessary to consider natural winds at any higher velocities.

The air velocity of the tunnel wind in this test was limited to a maximum of 100 mph. For this test, locomotive speeds outside the range of 60 to 100 mph were not considered. It has already been shown that natural-wind velocities greater than 10 mph should not be considered. With these limitations included, calculations were made to produce the curves in Fig. 16 and it was found that the greatest angle of yaw necessary was 9.1 deg. This is mentioned because during the drag test the model was rotated to maximum yaw angle of 25 deg actual and 26.5 deg corrected. This shows that within the limitations set for the test, angles of yaw above 9.1 deg are of no value in this discussion. It should be kept in mind that the angle of yaw is the angle relationship between the longitudinal axis of the locomotive and the direction of the resultant wind. Obviously, if the natural wind should start as a head wind and change its direction in relation to the axis of the locomotive, moving toward the rear of the locomotive, it would become an assisting force instead of a retarding force after it passes a point where it acts at an angle of 90 deg to the axis of the locomotive. The angle of yaw of 9.1 deg referred to occurs when the natural wind is at 90 deg to the axis of the locomotive, and when the wind direction moves farther to the rear the resulting wind becomes less and the angle of yaw which will produce these conditions, becomes less than 9.1 deg.

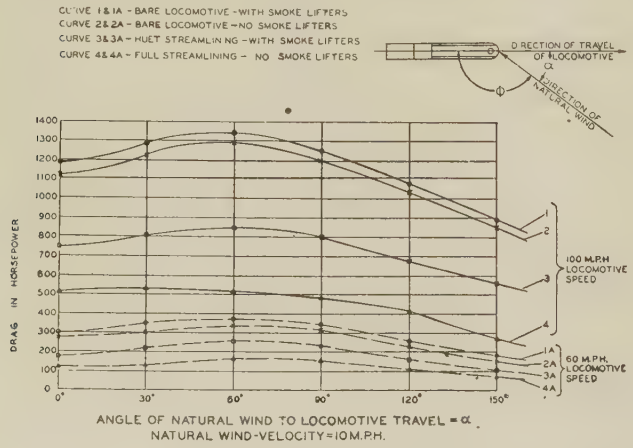

FIG. 16 DRAG EFFECT OF NATURAL WIND OF 10 MPH AT VARIOUS ANGLES

Discussion of Results of Test. Fig. 16 shows the influence on drag, or wind resistance, due to a natural wind of 10 mph, blowing at various angles in relation to the direction of the movement of the locomotive. Curves are shown for 60 and 100 mph locomotive speed.

The curves, it will be noted, cover a bare locomotive with smoke lifters, a bare locomotive without smoke lifters, a locomotive with the Huet streamlining with smoke lifters, and one with full streamlining without smoke lifters.

It will be noted that the angularity of the 10-mph natural wind has a greater influence on increasing resistance or drag on a bare locomotive than on a locomotive which has been streamlined. Apparently, streamlining, regardless of the angle of the wind, reduces the wind resistance to an appreciable degree.

Since the yearly average of natural winds is less than 10 mph, this velocity in itself indicates natural winds are relatively unimportant. Their importance is further depreciated because of the fact that although in various parts of the country they prevail in one or another general direction, there still is sufficient variation in their direction to be worth consideration in reducing their average effect. Since railroads must run trains in both directions, these winds can be a retarding force for only approximately one half of the time a given locomotive is on the road. This cuts the remaining average approximately in half.

These facts lead to the conclusion that by the time the increase in resistance, due to natural winds, shown in Fig. 16, is brought down to an average figure, their importance in negligible. In view of this, it seems reasonable that angular natural winds be omitted from further discussion and that this paper be confined to comparison of the performance of various streamlining features with head-on winds only.

It is interesting to note that most of these curves show that the greatest resistance is found when the wind is on the forward quarter at an angle of approximately 60 deg to the axis of the locomotive. The location of this point of greatest resistance coincides with that reported in an earlier paper (1).[3] This fact seems to support the statement frequently made by locomotive engineers, that a forward-quarter wind affects the locomotive speed more than a head-on or side wind.

Wind Resistance. The curves in Fig. 17 give the drag in pounds obtained with each of the models tested.

It is interesting to note that the drag coefficient obtained in this test checked closely with that in a previous paper (2). The locomotive reported on was also a $^1/_{12}$-size model of a 4-8-4 type locomotive and tender. It was a model of a Canadian National 6200 Class locomotive.

The following shows the drag coefficient and how it is obtained:

[3] Numbers in parentheses refer to the Bibliography at the end of the paper.

$$R = aAV^2$$

where R = resistance, lb
a = drag coefficient
A = locomotive sectional area, sq ft
V = speed, mph

For a bare locomotive without smoke lifters the following were obtained:

Previous test $a = 0.3308$
This test $a = 0.3541$

The difference in the drag coefficient for the previous test and this test is only about $6^1/_2$ per cent.

In addition to front-end wind resistance, there are two additional retarding forces. One is a partial vacuum at the rear of the tender and the other is skin friction; therefore the drag readings shown in Fig. 17 cannot be considered as entirely due to

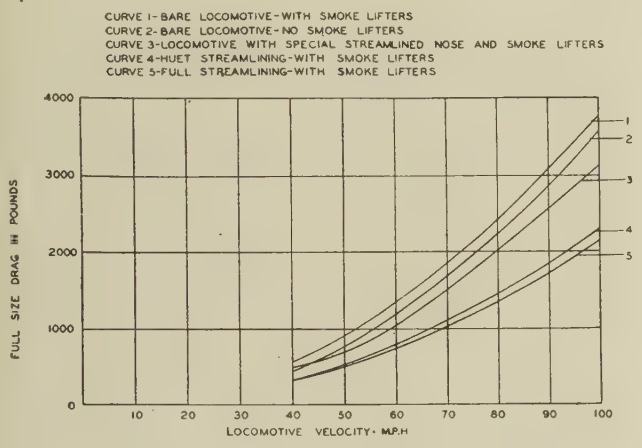

Fig. 17 Full-Size Drag Vs. Locomotive Velocity (Angle of Yaw = 0°)

front-end wind resistance. Since all five models were the same size and had the same tender, it is reasonable to assume that the drag, because of these factors, would be practically the same for all models under the same conditions of operation. In view of this, and the fact that the data are used for comparing the performance of the models, one with the other, the difference in drag of one compared with another can be used as front-end wind resistance.

Fig. 18 shows the drag readings from the curves in Fig. 17 converted to horsepower.

Fig. 19 shows how the drags in Fig. 18 change the locomotive drawbar-horsepower curve. The base of this figure is curve 1 which is a bare locomotive with smoke-lifting deflecting plates. This curve is taken from published data for an existing modern 4-8-4 type locomotive. Since this test included a model of a bare locomotive with smoke lifters and another model without smoke lifters, the difference in drag between the two was due to the smoke lifters. This difference was added to curve 1, thus producing curve 2. Curve 3 was produced by finding the difference in drag between the bare locomotive and the locomotive covered by curve 3, and adding this difference to curve 2. This same method was carried out with the remaining two curves.

A typical drawbar-horsepower curve drops off after a certain speed is reached. The base curve 1 follows this trend after reaching a speed of 60 mph. Without studying the indicator cards it might be assumed this is due to cylinder performance, but Fig. 19 indicates an important part of the drop is caused by front-end wind resistance.

Curve 5 shows the best performance with the greatest reduction

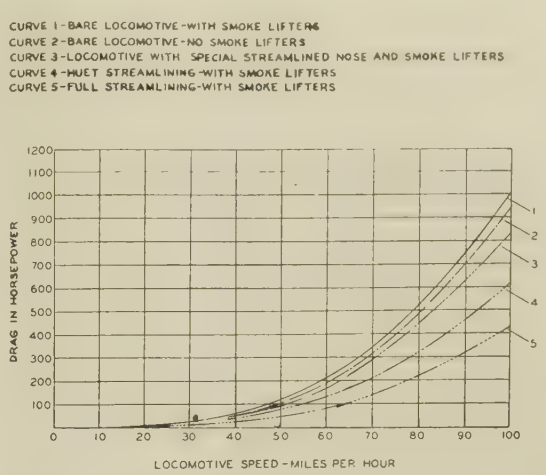

Fig. 18 Drag in Horsepower Vs. Locomotive Speed

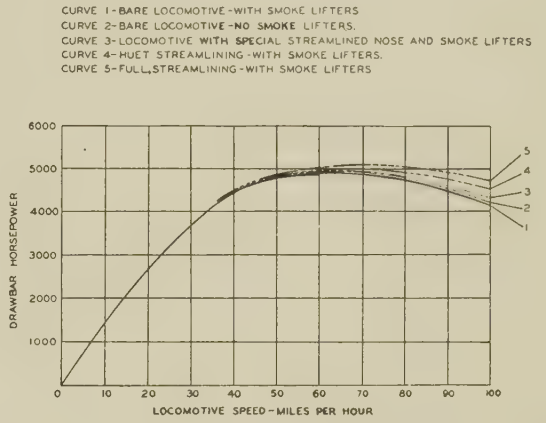

Fig. 19 Increase in Drawbar Horsepower Due to Streamlining

TABLE 3

Line no.	Locomotive features	Horsepower — 60 mph — Hp drag from test	60 mph — Total drawbar hp of locomotive	Horsepower — 100 mph — Hp drag from test	100 mph — Total drawbar hp of locomotive
1	Bare modern 4-8-4 type, no smoke lifters	196	4866	945	4220
2	Bare modern 4-8-4 type, with smoke lifters	212	4850	1005	4160
3	Locomotive with special streamline nose and smoke lifters	169	4893	834	4331
4	Locomotive with Huet streamline and smoke lifters	131	4931	628	4537
5	Locomotive with full streamline and smoke lifters	133	4929	562	4603

in wind resistance. This is the full-streamlined locomotive and as previously pointed out, has streamlining similar to that used on a Diesel road locomotive. This curve shows the advantage this type of streamlining gives the Diesel locomotive.

Front-end wind resistance is only of interest on locomotives when traveling at fairly high speeds; therefore Table 3 was prepared to show the relative locomotive drawbar horsepower at 60 and 100 mph. This tabulation is based upon the data shown in Fig. 19 and again the existing modern 4-8-4 type locomotive is used as a base. Its total drawbar horsepower is shown on line 2 as 4850 at 60 mph and 4160 at 100 mph. The remaining lines in this tabulation were prepared in the same manner as the curves in Fig. 19.

TABLE 4 ANALYSIS OF TABLE 3

Line			60 mph	100 mph
A	Cost in hp due to application of smoke lifters, line 2 vs. line 1 of Table 3	Hp	16	60
		Per cent of total locomotive drawbar hp	0.3	1.4
B	Saving in hp due to use of special streamline nose, line 3 vs. line 1 of Table 3*	Hp	27	111
		Per cent of total locomotive drawbar hp	0.6	2.6
C	Saving in hp due to use of Huet streamlining, line 4 vs. line 1 of Table 3*	Hp	65	317
		Per cent of total locomotive drawbar hp	1.3	7.5
D	Saving in hp due to use of full streamlining, line 5 vs. line 1 of Table 3*	Hp	63	383
		Per cent of total locomotive drawbar hp	1.3	9.1

* Drag used in these calculations includes that due to smoke lifters because test indicated they were essential to prevent smoke trailers.

Table 4 gives an analysis of the data in Table 3, and shows there is a small cost in drawbar horsepower due to the application of smoke lifters. As might be expected, it also shows that all types of streamlining tested gave a saving in horsepower. The saving shown by the Huet streamlining is particularly interesting since it approaches that which might be considered the optimum obtainable by using full streamlining. This Huet manages to accomplish without sacrificing accessibility to the moving parts of the locomotive for servicing and repairs.

The percentages in Table 4 are based on a locomotive developing almost 5000 drawbar horsepower. These percentages would be greater for a locomotive of less drawbar horsepower.

Smoke-Lifting Observations. During observations of smoke lifting, it was noted that smoke-lifting deflecting plates as applied to the bare locomotive were of distinct value in assisting smoke lifting; however, there was no indication that their use would permit any reduction in stack velocities; in fact, some smoke trailing was noted.

The locomotive equipped with full streamlining and smoke-lifting deflecting plates did a better job in lifting the smoke than the bare locomotive with smoke lifters, but its performance in this respect was not as good as the Huet design.

The Huet design was outstanding in its performance as regards smoke lifting. It held the smoke above the cab at high engine speeds with as low as 1 lb exhaust pressure, whereas the bare locomotive without smoke-lifting deflecting plates could not accomplish this with 15 lb exhaust pressure. The Huet design performed better with 1 lb exhaust pressure than the bare engine with smoke-lifting deflecting plates did at 15 lb exhaust pressure.

This indicates that with suitable streamlining and smoke lifters, it might be possible to decrease stack velocities to a considerable degree. If so, the stack diameter could be increased, which should permit a proportional increase in the exhaust tip.

Reduction in Exhaust Pressure. To get some idea of how this would work out, take a hypothetical case and see what a small increase, such as 10 per cent in stack and exhaust-tip diameters would mean in reducing exhaust pressures. This would result in an increase of 21 per cent in their areas which would reduce the exhaust pressures as follows:

P = exhaust pressure, psig, with original diam of exhaust nozzle

P_1 = exhaust pressure, psig, with increased diam of exhaust nozzle

$$P_1 = \frac{P}{1.46}$$

Therefore, when $P = 20$, $P_1 = 13.7$ psi
$P = 10$, $P_1 = 6.9$ psi
$P = 5$, $P_1 = 3.4$ psi

Although the foregoing figures give an indication of how much the exhaust pressure can be reduced by a slight increase in area of the exhaust tip, the following will give some idea of what the stack performance should be:

Saving in Drafting Energy. A discussion (3) of an earlier paper (4) furnishes some very interesting information on the subject of the energy consumed in the drafting of a locomotive, and how this energy is consumed. The curves in Figs. 20 and 21 were reproduced from the discussion (3) and relabeled to suit the present paper. Referring to Fig. 20, the upper curve shows the total horsepower consumed in the drafting of the locomotive. The lower curve shows the horsepower utilized in moving the gases of combustion through the boiler and smokebox and out of the stack against the differential between the pressure of the smokebox and the atmosphere. The difference between the

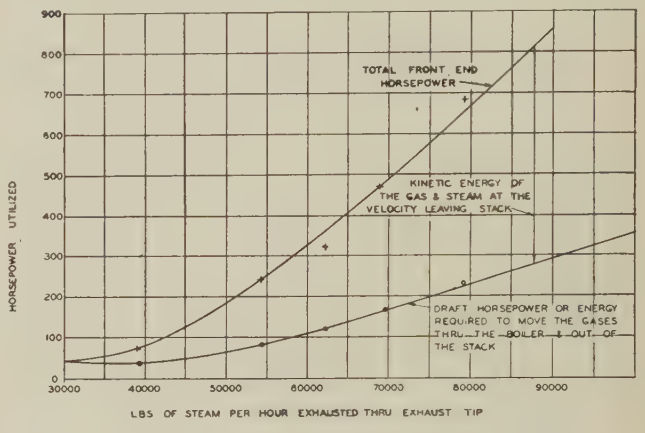

FIG. 20 HORSEPOWER UTILIZED IN DRAFTING LOCOMOTIVES

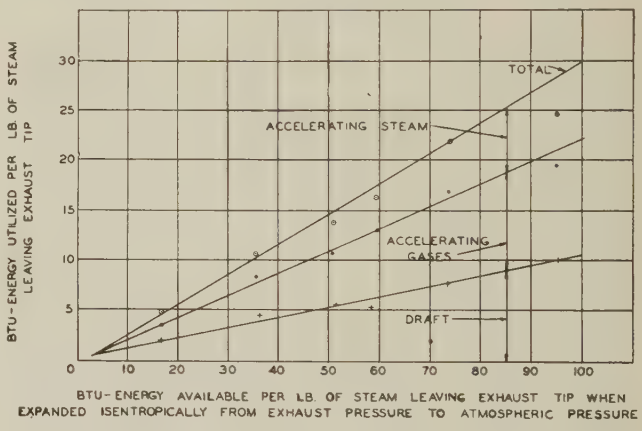

FIG. 21 BTU OF EXHAUST STEAM UTILIZED IN DRAFTING LOCOMOTIVES

upper and lower curves represents the kinetic horsepower in the mixture of gases and steam as they leave the stack. The kinetic energy in the mixture leaving the stack is that required to lift the mixture to a sufficient height above the locomotive to keep it clear of the influence of the eddy currents and low-pressure points immediately adjacent to the upper portion of the locomotive. If the velocity does not lift the mixture from the stack sufficiently, it will flow to the low-pressure points and result in smoke trailing.

At a rate of 90,000 lb of steam per hr being exhausted from the stack, a total of 850 hp was used for drafting the locomotive. Of this only 290 hp was used to move the gases of combustion out

of the boiler, and the remainder, 560 hp, or 66 per cent of the total was used in imparting velocity to the mixture.

Fig. 21 shows in terms of Btu the energy per pound of exhaust steam available for drafting purposes, plotted against the energy utilized for this purpose. In the discussion (3) it was pointed out from these curves, that at a high rate of operation 810 hp was utilized for drafting at an efficiency of 30 per cent which represents 2700 hp which had to be made available in the form of exhaust steam for drafting purposes. This of course means that a substantial exhaust pressure had to be maintained to provide this energy for drafting, and therefore its energy was not available for work in the cylinders.

Returning to the present paper regarding increasing the stack and exhaust-tip diameters, assume the stack is increased 10 per cent in diameter. This will give a decreased velocity equal to $\frac{1}{1.21}$ with a resulting decrease in kinetic energy of steam and gases equal to $\frac{1}{1.46}$. Fig. 21 shows that with 100 Btu available per pound of steam, 19.4 Btu are utilized for kinetic energy. Dividing by 1.46 gives 13.3 Btu, a saving of 6.1 Btu per pound of steam.

The cylinder efficiency varies with all conditions of operation, but a steam rate of 16 lb per ihp-hr is considered reasonably good. This corresponds to a heat drop of 159 Btu in the cylinders. Based on this figure, if 6.1 Btu diverted from the draft are utilized in the cylinder, we secure an increase of 3.8 per cent in cylinder horsepower. This, converted into additional drawbar horsepower, may be added to that saved by the reduction in front-end wind resistance.

It may be possible to increase the stack and exhaust-tip diameters considerably more than 10 per cent. If so, the benefits will increase accordingly.

A great amount of effort has been expended to improve front-end drafting and considerable progress has been made in that direction. Many who have made a study of this subject have come to the conclusion that the drafting arrangement within the smokebox requires less exhaust pressure for the flow of gases through the boiler, smokebox, and stack, than is used in actual road service, the excess being provided solely for the purpose of smoke lifting. The discussion (3) previously mentioned, and two other papers (5, 6) have all brought out this point. In the discussion (3) it was further stated that the use of a "windshield or special streamlining" would greatly improve this condition and permit a reduction in stack velocities. The observations on the present test seem to bear out this contention, and all indications are that for the present the problem is outside of the smokebox and will continue to be, until stack velocities are reduced to the point where they become too low to supply sufficient air to support combustion.

Conclusions

The wind-tunnel test results show that full streamlining on a modern locomotive gave the best performance from a wind-resistance standpoint. It shows that if applied to a locomotive having a drawbar horsepower of approximately 5000 it would increase its drawbar horsepower by 1.3 per cent at 60 mph and 9.1 per cent at 100 mph.

This streamlining being similar to that used on a Diesel locomotive indicates the advantage the Diesel enjoys because it can use this type of streamlining. With a Diesel of one or two units these percentages would be much higher because the drawbar horsepower would be lower and the wind resistance would remain the same.

From a smoke-lifting standpoint, this type of streamlining, even when equipped with smoke-lifting deflecting plates, was only second best of the models tested. Even if it were satisfactory from a smoke-lifting standpoint it would not be considered practical from a maintenance and servicing standpoint and there was no indication that stack velocities could be reduced by its use.

The Huet design with smoke-lifting deflecting plates gave the next best performance from a wind-resistance standpoint. It reduced wind resistance almost as much as did the full streamlining with smoke-lifting deflecting plates. The test indicated that with the Huet design the drawbar horsepower would be increased by 1.3 per cent at 60 mph and 7.5 per cent at 100 mph. Perhaps more important is the fact that it was the best of all models tested from a smoke-lifting standpoint. Regardless of exhaust pressure, or engine speed, it did not trail smoke around the cab within the limits of average operating conditions. By this is meant, smoke did curl over the side of the locomotive when a cross or natural wind of high velocity occurred but it was very slight when this wind was 10 mph or less, and while the locomotive was at zero to 9.1 deg angle of yaw. The Huet design accomplished this without sacrificing accessibility to those parts of the locomotive requiring servicing and the greatest amount of maintenance.

The locomotive with the streamlined nose, Figs. 4 and 5, and with smoke-lifting deflecting plates, increased the drawbar horsepower 0.6 per cent at 60 mph and 2.6 per cent at 100 mph. Although the usual benefit from a smoke-lifting standpoint was obtained by the use of the smoke-lifting deflecting plates, there was no indication that stack velocities could be reduced.

The bare locomotive with smoke-lifting deflecting plates (no streamlining) showed that the addition of the smoke-lifting deflecting plates decreased the drawbar horsepower to a negligible degree. The plates did help considerably in lifting the smoke but there was no indication that stack velocities could be reduced.

The bare locomotive had slightly less wind resistance than the bare locomotive with smoke-lifting deflecting plates. Its performance from a smoke-lifting standpoint was noticeably poor after viewing the performance of other models.

Indications from this test are that the problem of smoke lifting is located outside of the smokebox. If the application of suitable streamlining and smoke-lifting deflecting plates will, in road service, reduce or prevent smoke trailing with low exhaust pressures it may lead the way to improved locomotive performance.

With present-day improved front-end arrangements, exhaust pressures are frequently increased solely for smoke-lifting purposes and not for the purpose of handling the gases of combustion through the boiler, smokebox, and stack. It appears possible that the Huet design of streamlining may permit drastic reductions in stack velocities which means larger stacks and proportionately larger exhaust tips. This should result in an appreciable reduction in exhaust pressures and an increase in drawbar horsepower.

It is hoped that the presentation of this data may contribute in some small measure to an improvement in the performance of the steam locomotive.

Acknowledgment

The test was conducted under the general supervision of Prof. A. F. Spilhaus, member ASME, director of research, College of Engineering, New York University, and was reported by Dr. A. Ciffrin, research associate, College of Engineering, New York University. Calculations covering the quantity of steam to be used as a substitute for steam and gases, including the reduction in amount for use with a scale model, were checked and approved by Dr. J. M. Labberton, member ASME, professor of mechanical engineering, New York University. Able assistance

was also given by E. Stolper, instructor, College of Engineering, New York University, L. R. Bennett, instructor, College of Engineering, New York University, R. G. Makely, research and development division, The Superheater Company, and others, to whom the author is grateful. The models were made by E. C. Keithley, Combustion Engineering Company, Inc.

BIBLIOGRAPHY

1 "Air Resistance of Passenger Trains," by F. C. Johansen, Proceedings of The Institution of Mechanical Engineers, vol. 134, 1936, pp. 91–160.

2 "Wind Tunnel Development of Proposed External Form for Steam Locomotives," by J. J. Green, *Canadian Journal of Research*, vol. 8, no. 1, January, 1933, pp. 37–61.

3 Discussion by Lawford Fry of a paper "Relationship Between Smokebox and Boiler Proportion," by D. W. Sanford, *Journal of The Institution of Locomotive Engineers*, No. 185, May-June, 1945.

4 "Relationship Between Smokebox and Boiler Proportion," by D. W. Sanford, *Journal of The Institution of Locomotive Engineers*, No. 183, paper No. 451, January 7, 1945.

5 "Study of the Locomotive Front End, Including Tests of a Front-End Model," by Everett G. Young, Engineering Experiment Station, University of Illinois, Urbana, Ill., Bulletin No. 256, vol. 30, no. 39, May 30, 1933.

6 "Supply of Air to Coal-Fired Locomotives," by R. A. Sherman, W. H. Browne, and R. B. Engdahl, Trans. ASME, vol. 68, no. 5, 1946, pp. 467–480.

Discussion

C. E. Sperry.[4] The author, his co-workers, and his employers should be highly commended for reducing some of the theories on atmospheric frictional drag and smoke lifting to definite test results. It is gratifying to see the dramatic way in which the Huet design with smoke lifter contributes so convincingly to the safety of high-speed operations by lifting the smoke from the engineman's cab at speeds of 90 mph.

Unfortunately, these improvements do not solve the problem in high-speed passenger service, since the smoke will apparently still trail and envelop a 14-car passenger train running into a head wind or at small angles of yaw. The effect on many passengers is all too similar to flying through a cloud bank, and they generally do not know that the engineman is not encountering the same annoyance. Passenger acceptance is heavily against the reliable old steam locomotive, due to many factors such as black smoke and finely divided slate, slag, and earth which has been wastefully heated to 2800 F in the locomotive firebox and then indiscriminately showered over the countryside, but due more particularly to nation-wide advertising in consumer publications by Diesel locomotive builders.

However, it does appear altogether probable that the application of streamlining and smoke lifting to high-speed freight locomotives will contribute to the safety and economy of railroad operations. Increase in stack and exhaust passages, perhaps up to 10 per cent, is perfectly sound engineering, but railroad experience of many trials and errors raises the question of a more conservative increase in these openings. If this more conservative increase is made in conjunction with controlled admission of air to the ashpans, it may result in some over-all definite fuel saving per 1000 gross ton-miles per train-hour. The results of these wind-tunnel tests add significantly to the mass of reliable data on which mechanical engineers may base future draft improvement for successful operation at the modern high sustained locomotive operating speeds.

Lawford H. Fry.[5] The research project described by the author represents an important contribution made by the Superheater Company to steam-locomotive engineering. It not only adds to our knowledge of locomotive wind resistance, but provides definite information as to the mechanism of smoke trailing and smoke lifting.

It is to be hoped that Mr. Griffin's paper will not be treated as just another paper on streamlining, to be noted and filed.

The Huet method of streamlining offers two important advantages. In the first place it uses the forward motion of the locomotive to lift the smoke clear of the cab and thus enables the back pressure against the pistons to be reduced so as to give increased drawbar pull with no increase in steam consumption. In the second place the special streamlining reduces the locomotive resistance so that the gain in effective power is double.

Author's Closure

The points raised by Mr. Sperry are indeed interesting. Even if the addition of the Huet streamlining does not have any appreciable effect in preventing smoke from trailing around passenger cars it will have a distinct advantage of providing greater safety in locomotive operation. This will be true both on passenger and freight locomotives. The example used to show the effect of increasing the stack and exhaust tip by 10 per cent was intended merely as an illustration. Just how far this can be carried can only be determined by trial.

Mr. Fry's comments, I know, are based upon a wide knowledge of the subject, and it is hoped that this paper and Mr. Fry's discussion of Mr. Sanford's paper will serve to bring about greater efforts to utilize the benefits of streamlining to increase exhaust tips and stack diameters.

[4] Lieut. Col., Ordnance Reserve, U. S. A., Seaside Park, N. J. Mem. ASME.

[5] Director of Research, Steam Locomotive Research Institute, Inc., New York, N. Y. Fellow ASME.

Frequency-Response Measurements of a Hydraulic Power Unit

By M. R. HANNAH,[1] GREAT NECK, N. Y.

Hydraulic power units continue to find important applications in a wide variety of servomechanisms wherein high-performance power sources are required. In such applications the servo designer is concerned with the fidelity of the power unit in responding to the controlling signals, and this information is often obtained or corroborated by means of experimental data. This report outlines an investigation into the dynamic response of a typical hydraulic power unit comprising a transmission and associated stroke control. The well-known tool of frequency analysis has been employed to investigate the effects of certain system parameters on the performance of the several components of the power unit. The results have been evaluated with a view toward effecting improvement in the response of the power unit as a whole.

Introduction

ONE of the essential components of every servomechanism is a source of power whose output to a controlled member is a time-varying function of some initiating signal. The latter occurs frequently at an extremely low energy level, so that, in general, some form of amplification is required prior to the final transfer of energy from the power source to the load. Each stage of energy amplification contributes something to the total time lag with which the power source responds to a signal, and it is often necessary to determine the magnitude not only of the total time lag but also of the individual lags occurring in each of the components of the servomechanism.

One of the most convenient methods for determining these response characteristics is that of alternating-current analysis, or frequency analysis, whereby the response of the servosystem, or of any of its components, to sinusoidal inputs is determined as a function of input frequency. While the theory of alternating-current analysis as applied to servomechanisms has been much discussed (1, 2, 3),[2] the actual techniques of measurement of frequency-response characteristics have not been widely published. The purpose of this paper is to present the procedures and results of a typical investigation into the dynamic behavior of a particular hydraulic power unit. The basic measuring techniques to be described were first acquired by the author in the Automatic Control Laboratory of the Department of Electrical Engineering at the Massachusetts Institute of Technology where considerable attention has been devoted to the study of hydraulic servomechanisms.

Object of the Investigation

The primary object of the investigation was to measure the dynamic response of a Vickers model AA-16850 aircraft duplex hydraulic power unit, each half of which consists essentially of a fixed-displacement axial-piston hydraulic motor (0.378 cu in. per revolution), supplied in either direction with oil under pressure from a variable-displacement axial-piston pump (0.319 maximum cu in. per revolution). The nominal rating of the transmission is approximately 4 hp. The displacement of the pump is controlled by a small hydraulic amplifier of which the pilot or control valve is positioned by means of a differential solenoid.

It was desired to measure the response not only of the power unit as a whole but also of each of the elements making up the complete power unit. These elements were divided into the following components:

(*a*) The control solenoid, together with the pilot valve and associated linkage, as well as the power-amplifier stage which supplied the differential current to the solenoid windings. The motion (X_c) of the pilot valve in response to an input voltage (E_i) applied to the power amplifier is represented by the function

$$K_1G_1(s) = \frac{X_c(s)}{E_i(s)} \quad \ldots\ldots\ldots\ldots\ldots\ldots [1]$$

where s represents the operator $d/(dt)$.

(*b*) The hydraulic amplifier, with the power piston attached to the pump yoke. The motion (X_p) of the power piston in response to motion of the pilot valve is represented by the function

$$K_2G_2(s) = \frac{X_p(s)}{X_c(s)} \quad \ldots\ldots\ldots\ldots\ldots\ldots [2]$$

(*c*) The hydraulic transmission, comprising the pump, or A-end, the motor, or B-end, and connecting conduit, with the B-end subject only to inertia and viscous-friction loads. The B-end velocity (ω_0) in response to motion of the power piston is represented by the function

$$K_3G_3(s) = \frac{\omega_0(s)}{X_p(s)} \quad \ldots\ldots\ldots\ldots\ldots\ldots [3]$$

Fig. 1 shows a block diagram of the system elements as defined.

Measurement of Performance

The performance of each of the various elements of the power unit was assessed on the basis of its response to a constant-amplitude, variable-frequency, sinusoidal, signal voltage applied to the grids of the power-amplifier stage. No quantitative information was sought regarding the response of the elements to transient signals.

Scope of Investigation

An analysis of the performance of the transmission alone had been made previously (4). In the present investigation it was desired:

(*a*) To corroborate the transmission performance as predicted by the foregoing or similar (see Appendix) analysis.

---

[1] Armament Engineering Division, Sperry Gyroscope Company.

[2] Numbers in parentheses refer to the Bibliography at the end of the paper.

Contributed by the Industrial Instruments and Regulators Division and presented at the Annual Meeting, Atlantic City, N. J., December 1–5, 1947, of The American Society of Mechanical Engineers.

 Paper No. 47—A-70.

(*b*) To determine the variation in performance with each of several controlled parameters such as B-end load inertia, stiffness and inertia of solenoid and linkage, replenishing pressure and amplitude of input signal.

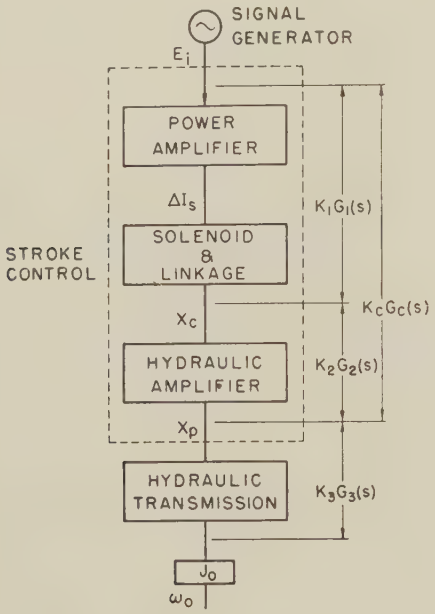

FIG. 1 DEFINITION OF ELEMENTS

(*c*) To employ the results of item (*b*) in choosing the most promising avenue of approach to the problem of improving the over-all response of the transmission and stroke control.

(*d*) To develop response equations which would approximate the observed response of the transmission and of the stroke control. These equations would be of value in any analytical representation of the hydraulic power unit as a servocomponent and would also indicate to some extent, by comparison with the observed response, the linearity of the system elements.

TECHNIQUE OF MEASUREMENT

The methods employed for the measurement of the desired quantities are summarized in Fig. 2. The most difficult measurement was that of the quantity X_c (pilot-valve motion). A simple photoelectric pick-off was developed which performed well and added very little mass or friction to the moving system of the pilot valve and solenoid linkage. A diagrammatic sketch of the pick-off is shown in Fig. 3.

The motion of the power piston was measured by means of a very small selsyn unit geared to a rack which was fixed to the lower end of the piston rod. The selsyn excitation was obtained from another similar selsyn which afforded a convenient means of adjusting the neutral position of the pick-off selsyn.

The output speed was measured by means of an alternating-current tachometer using 400-cycle excitation. The use of a direct-current generator for this measurement was avoided only because a good direct-current tachometer with high ripple frequency was not readily available. The frequency response of each of the measuring circuits, as well as that of the reference voltage circuit, was obtained in order to correct for their effects upon the measured quantities.

The phase and amplitude measurements were made by means of a cathode-ray oscillograph having a long-persistence screen. The measured voltages were taken directly to the direct-current section of the vertical amplifier, while a synchronized reference voltage was applied to the direct-current input of the horizontal amplifier.

The signal generator consisted of a specially designed com-

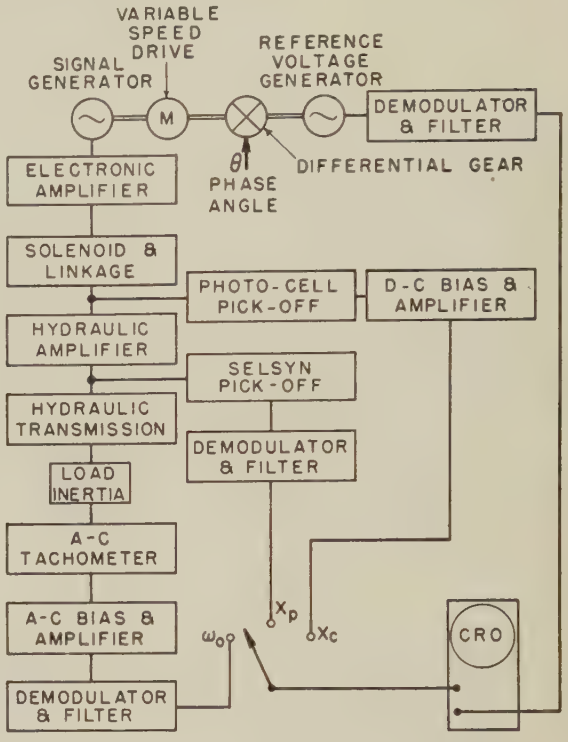

FIG. 2 BLOCK DIAGRAM OF COMPONENTS

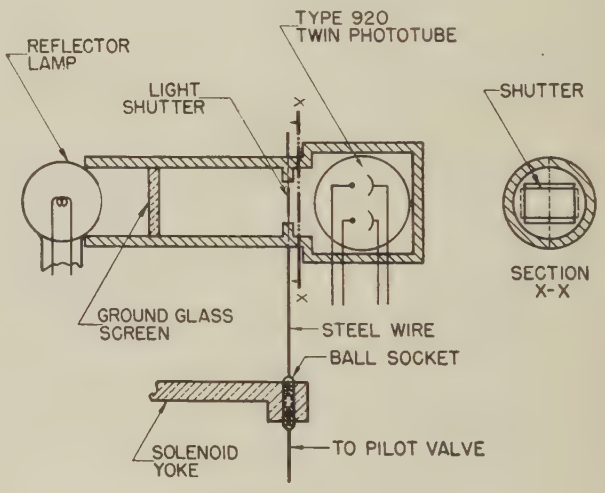

FIG. 3 PHOTOELECTRIC PICK-OFF

position potentiometer, rocked sinusoidally by means of a synchronous motor and gear train, the latter being designed to permit signal frequencies of 1 to 60 cycles per sec to be obtained in unit steps. An auxiliary direct-current motor provided frequencies as low as 0.01 cycles per sec for "zero-frequency" calibration.

RESULTS OF TESTS

Breakdown of Dynamic Response. Fig. 4 shows the response of the solenoid and linkage, i.e., from the signal voltage E_i to

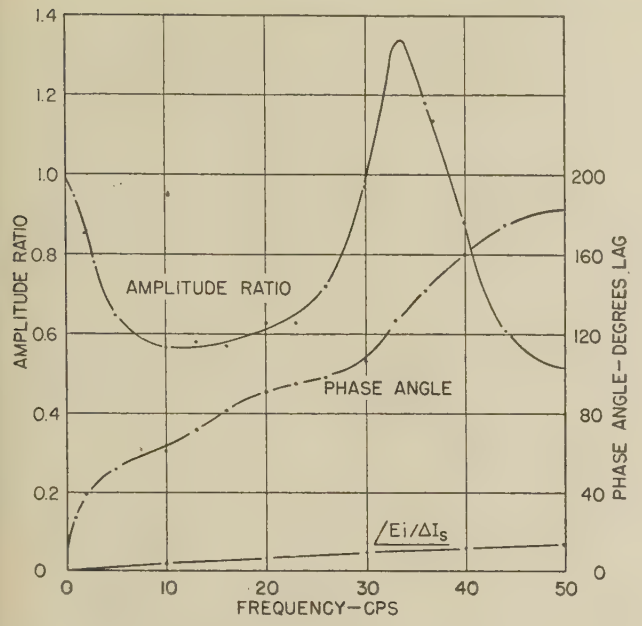

FIG. 4 RESPONSE OF SOLENOID AND LINKAGE
(Input $K/M = 3.8 \times 10^4$ sec^{-2}.)

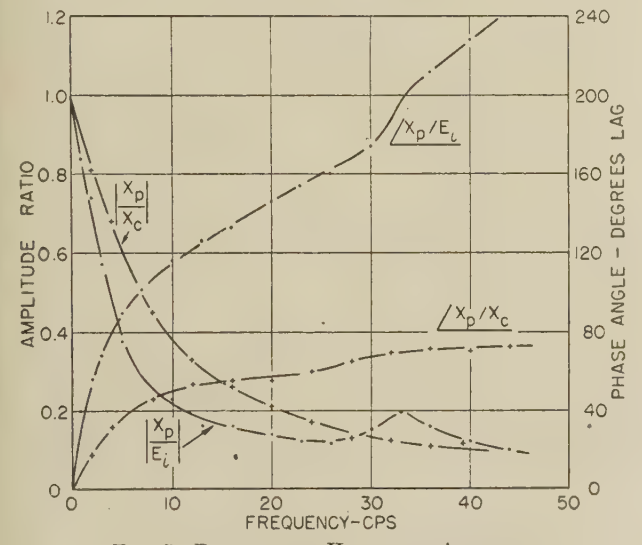

FIG. 5 RESPONSE OF HYDRAULIC AMPLIFIER
(Input $K/M = 3.8 \times 10^4$ sec^{-2}.)

the motion of the pilot valve X_c. The phase shift from input voltage to solenoid current is also shown, and is seen to account for relatively little of the total phase shift of the solenoid-linkage element. The amplitude characteristic of the solenoid current response is not shown because it was negligibly affected by frequency in the range below 60 cycles per sec.

The response of the hydraulic amplifier is shown in Fig. 5. The response functions for the hydraulic amplifier alone were obtained by dividing the response of the stroke control $K_cG_c(s)$, see Fig. 1, by the response up to the pilot valve, $K_1G_1(s)$. Similarly in Fig. 6 the response of the transmission was obtained by dividing the over-all response of the transmission and stroke control by that of the stroke control alone. The resulting amplitude and phase functions of the transmission response correspond to a particular value of output load inertia (13.3 in^2-lb).

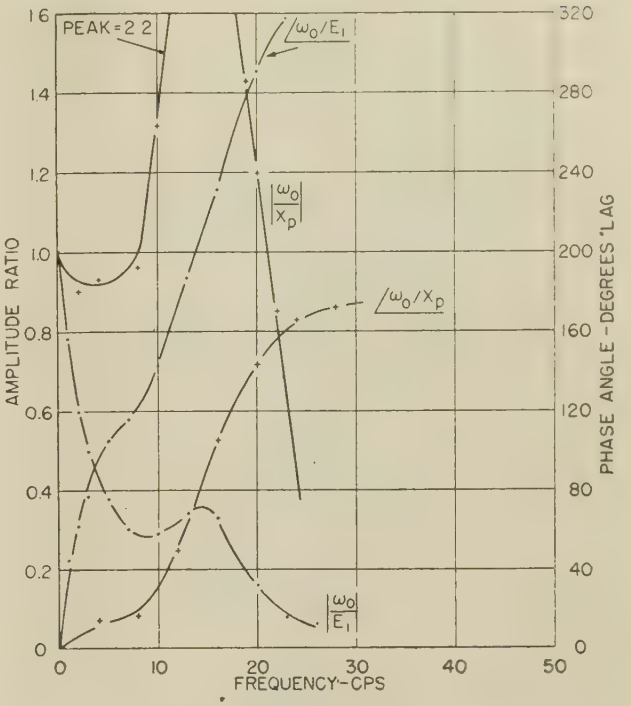

FIG. 6 RESPONSE OF HYDRAULIC TRANSMISSION
(Inertia load = 13.3 in^2-lb.)

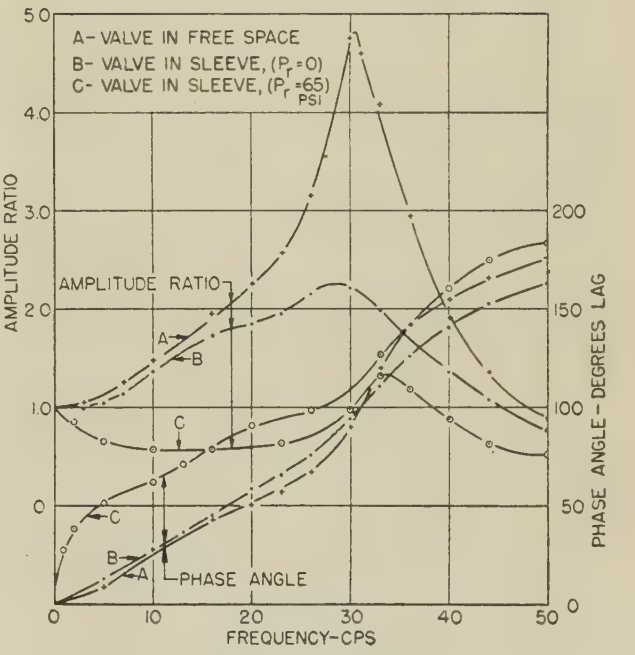

FIG. 7 RESPONSE OF SOLENOID AND LINKAGE AS A FUNCTION OF PILOT-VALVE COERCION
($K/M = 3.8 \times 10^4$ sec^{-2}.)

Coercive Reaction Upon Pilot Valve. In Fig. 7 curves A indicate the frequency response of the solenoid, linkage, and pilot valve, where the pilot valve has been removed from its sleeve and is freely suspended from the linkage. These curves are, in general, quite similar to those which represent any simple mass-spring viscously damped system with a relatively small damping ratio, and they indicate that the system could be represented by

means of a second-order linear differential equation. Curves B show the response of the same system but with the addition of the friction existing between pilot valve and sleeve. Curves C show the same system when subjected also to the hydraulic reaction forces on the pilot valve, resulting from the porting of oil to the hydraulic amplifier.

Fig. 7 shows conclusively that the hydraulic reaction upon the pilot valve results in severe damping of the valve motion. Obviously, the effect of this reaction could be lessened by increasing the stiffness of the moving system but this would in turn call for larger forces to be supplied by the solenoid.

Amplitude of Stroke. In order to gage the effect of the ratio of dead space to maximum valve travel upon the measured response of the solenoid-linkage system, the stroke amplitude was made a variable quantity. Strokes of 10, 15, and 20 per cent (zero frequency values) were employed but little variation was noted in the response up to 48 cycles per sec. The term "per cent stroke" refers to the ratio of the peak value of pilot-valve travel during any half-cycle of its motion (measured at 0.01 cycle per sec) to the travel required to raise the B-end speed from zero to maximum. Since it requires nearly 0.10 in. of travel to produce full stroke (i.e., full B-end speed), the value of per cent stroke also indicates the actual pilot-valve peak travel in thousandths of an inch.

Mass and Stiffness of Solenoid and Linkage. Fig. 8 shows the results obtained by decreasing the mass M, of the moving system and increasing the stiffness K, of the recentering springs.

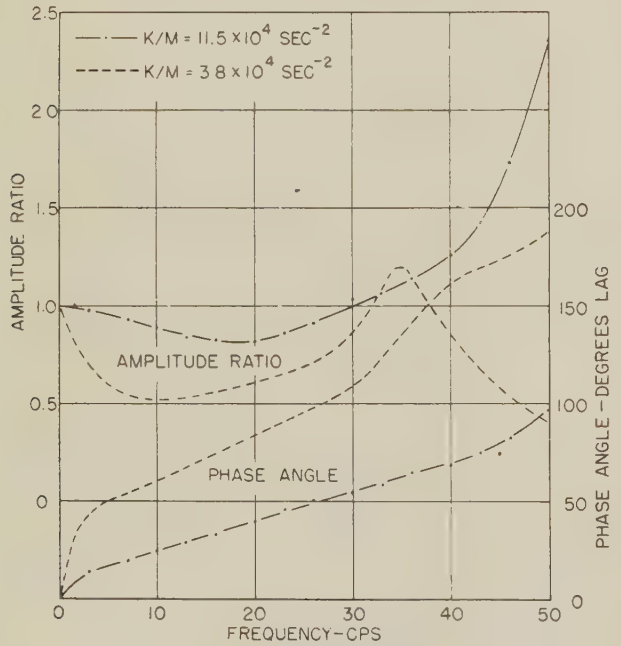

FIG. 8 RESPONSE OF SOLENOID AND LINKAGE AS A FUNCTION OF THE MASS-STIFFNESS RATIO K/M

The response of the solenoid and linkage when K/M was raised to 11.5×10^4 sec^{-2} is contrasted with the response obtained with $K/M = 3.8 \times 10^4$ sec^{-2}. The results indicate that very worthwhile improvements can be effected in the response of the stroke control by the use of a stiffer and lighter solenoid-linkage system. However, an increase in K is worth more than a decrease in M, since a stiffer system would be less affected by hydraulic reaction upon the pilot valve.

Replenishing Pressure. In view of the pronounced effect of the hydraulic coercion upon the pilot valve, as exhibited in Fig. 7, it was considered advisable to investigate the magnitude of the effect with different values of replenishing pressure, P_r. The results are shown in Fig. 9 where the response of the solenoid and linkage system is plotted for replenishing pressures of 25, 65, and 95 psi. The most pronounced effect appears in the amplitude function where, as would be expected, the lowest pressure resulted in the least coercion of the pilot valve and hence the least attenuation of motion. The phase function shows a smaller per cent variation and is less consistent throughout the frequency spectrum.

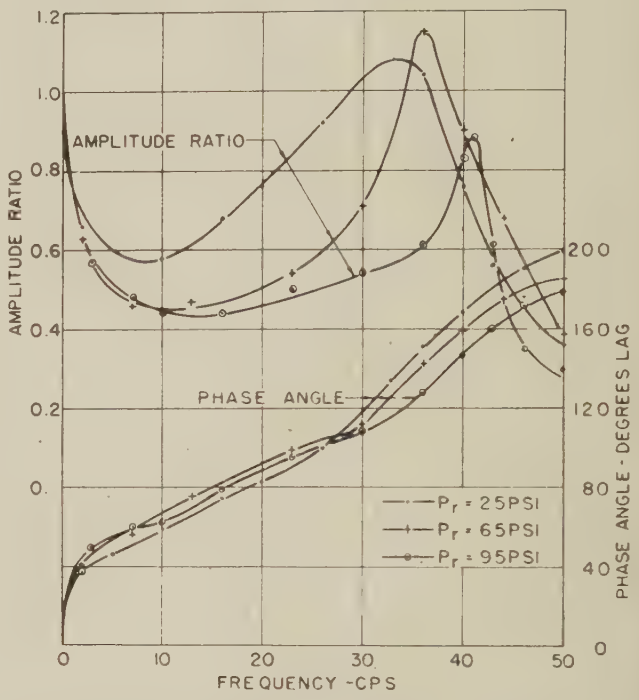

FIG. 9 RESPONSE OF SOLENOID AND LINKAGE AS A FUNCTION OF REPLENISHING PRESSURE

Magnitude of Inertia Load. The dynamic response of each of the three main elements was measured as a function of inertia load on the B-end shaft. It was apparent that the response of both the solenoid-linkage system and the hydraulic amplifier was relatively independent of output-load inertia. The effect of the inertia-load parameter upon the response of the transmission is shown in Fig. 10. Loads of 1.0, 4.9, 7.7, and 13.3 in^2-lb were employed (these values include the inertia of the hydraulic motor and tachometer).

It can be shown[3] that if the B-end viscous damping is very low, then the natural frequency of the hydraulic transmission is given by the relation

$$f_n = \frac{d_m}{2\pi\sqrt{JeV}} \quad \ldots\ldots\ldots\ldots\ldots\ldots [4]$$

where

d_m = motor displacement per radian of revolution
e = coefficient of compressibility of the oil
V = volume of oil in high-pressure side of transmission
J = B-end load inertia, including that of motor

Then, substituting rated values of $d_m = 0.06$ cu in./rad, and $e = 4 \times 10^{-6}$ in^2-lb and the measured value of $V = 2.44$ in.^{3}, with

[3] Appendix, Equation [39].

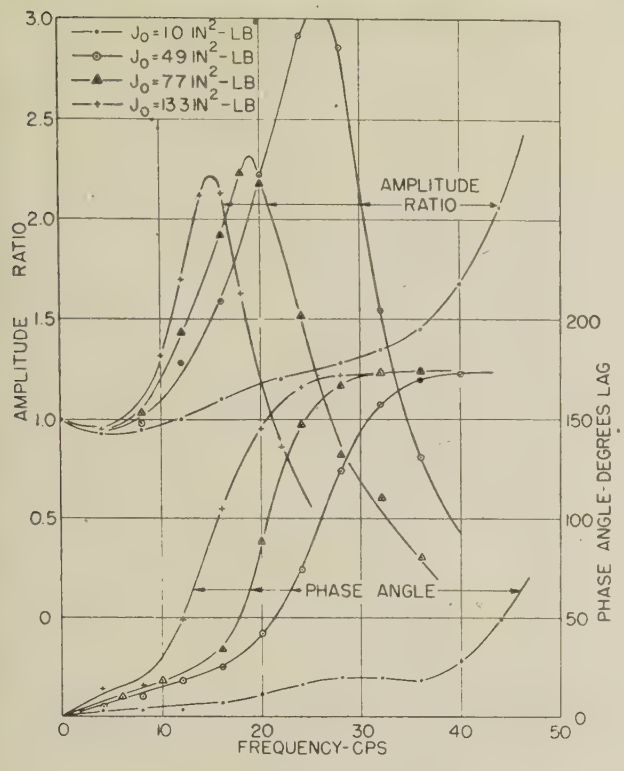

FIG. 10 RESPONSE OF HYDRAULIC TRANSMISSION AS A FUNCTION OF INERTIA LOAD

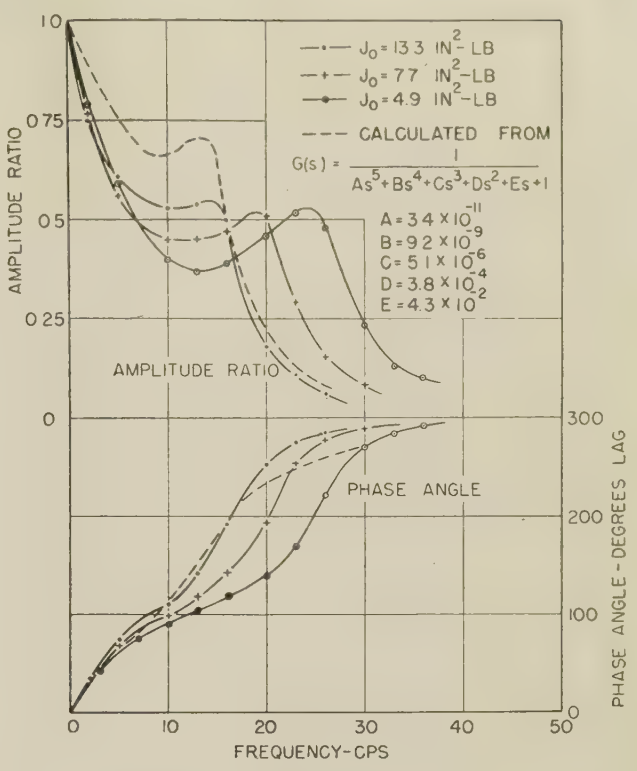

FIG. 11 OVER-ALL RESPONSE OF TRANSMISSION AND STROKE CONTROL
(Input $K/M = 11.5 \times 10^4$ sec^{-2}.)

inertia loading of 13.3, 7.7, 4.9, and 1.0 in²-lb, the following results are obtained:

Load inertia, in²-lb	Calculated natural frequency, cycles per sec	Observed natural frequency, cycles per sec	Error, per cent
13.3	17.5	16.0	8.6
7.7	21.7	21.2	2.3
4.9	27.2	26.0	4.4
1.0	60.4	49.6	18.

While the agreement of these results is well within reason, it is perhaps a fairer test of the theory to put $f_n = C/\sqrt{J}$ and to evaluate C from observed data for one load condition, say, 13.3 in²-lb. Then, using this value of C to find the natural frequency for the other load conditions, there results the following:

Load inertia, in²-lb	Calculated natural frequency, cycles per sec	Observed natural frequency, cycles per sec	Error, per cent
7.7	21.2	21.2	0
4.9	26.3	26.0	1.2
1.0	58.4	49.6	17

From either point of view the agreement of calculated with observed results is quite good (for all but the minimum-load case), particularly in view of the approximations made in reducing the expression for f_n to the simple relationship used.

Over-All Response. Fig. 11 shows the over-all response of the transmission and stroke control obtained with 10 per cent stroke and a mass-stiffness ratio $K/M = 11.5 \times 10^4$ sec^{-2} in the solenoid-linkage system. The variable parameter was inertia load, values of 13.3, 7.7, and 4.9 in²-lb being used.

ANALYTIC APPROXIMATIONS

Stroke Control. On a basis of the maximum phase shift encountered throughout the spectrum of test frequencies, it was apparent in Figs. 5 and 8 that the predominant characteristic of the response of the solenoid and linkage system was that of a second-order linear differential equation, while the response of the hydraulic amplifier was essentially that of a simple time-lag device. Consequently it was decided to approximate the response of the complete stroke control by means of a third-order characteristic equation.

Evaluating the coefficients of this equation by means of the stroke-control phase function, the calculated response was then plotted as shown in Fig. 12, for comparison with the observed response. The agreement in amplitude is quite good while the phase agreement is exceptionally good up to 50 cycles per sec. The response equation thus obtained was

$$G_c(s) = \frac{1}{2.82 \times 10^{-7}s^3 + 6.40 \times 10^{-5}s^2 + 3.72 \times 10^{-2}s + 1} \quad \ldots\ldots\ldots [5]$$

This equation factors into

$$G_c(s) = \frac{K'}{(0.033\,s + 1)\,(s + 98.5 \pm j\,341)} \quad \ldots\ldots\ldots [6]$$

Now the right-hand side of Equation [6] can be expressed in the general form

$$G_c(s) = \frac{K'}{(Ts + 1)\,(s^2 + 2\zeta\omega_n s + \omega_n^2)} \quad \ldots\ldots\ldots [7]$$

where T represents a single-order time lag, while ζ and ω_n represent, respectively, the damping ratio and the undamped natural frequency of the quadratic factor. Thus by the equality of Equations [6] and [7], the stroke control is the equivalent of a simple time lag of 0.033 sec in cascade with a two-energy-storage

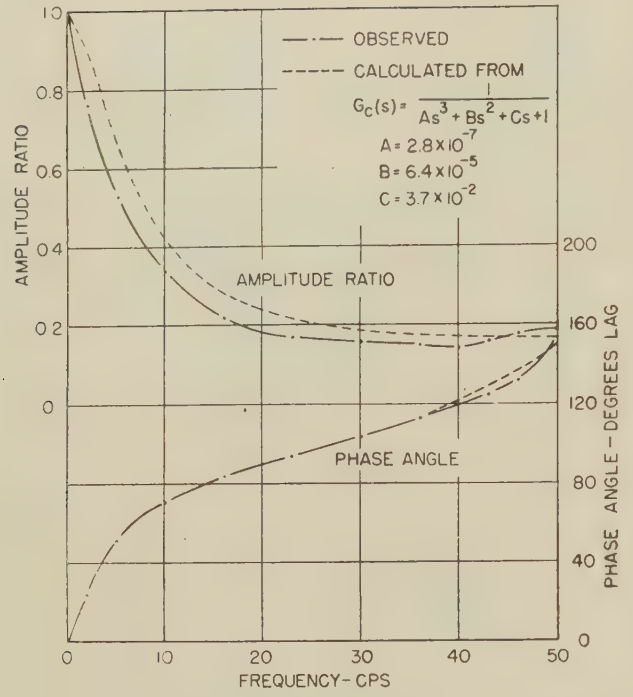

FIG. 12 CUBIC APPROXIMATION OF STROKE-CONTROL RESPONSE (Input $K/M = 11.5 \times 10^4$ sec^{-2}.)

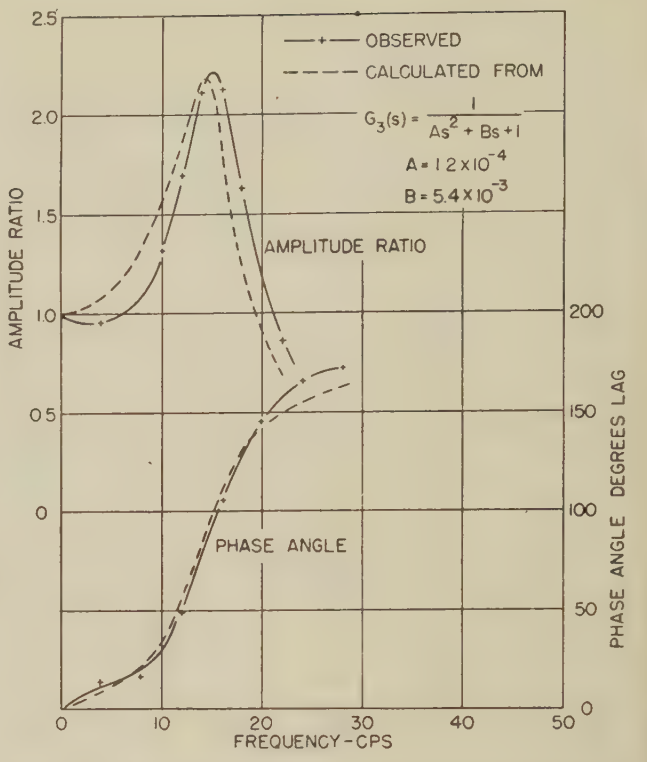

FIG. 13 QUADRATIC APPROXIMATION OF TRANSMISSION RESPONSE ($J_0 = 13.3$ in^2-lb.)

system having a damping ratio of 0.28 and an undamped natural frequency of 56.5 cycles per sec.

Transmission. The transmission response was approximated (for the $J_0 = 13.3$ in^2-lb condition) by means of a quadratic function. Fig. 13 shows the comparison of the calculated with the observed response. Here, too, the amplitude agreement is quite good, and the phase agreement very good. The response equation was

$$G_3(s) = \frac{1}{1.20 \times 10^{-4} s^2 + 5.35 \times 10^{-3} s + 1} \quad \ldots\ldots [8]$$

which yields a damping ratio of 0.25, and an undamped natural frequency of 14.5 cycles per sec.

Over-All Response. The response equations for the stroke control and transmission were multiplied together to yield

$$G(s) = \frac{1}{3.38 \times 10^{-11} s^5 + 9.18 \times 10^{-9} s^4 + 5.09 \times 10^{-6} s^3 + 3.82 \times 10^{-4} s^2 + 4.25 \times 10^{-2} s + 1} \quad \ldots\ldots [9]$$

The comparison of calculated and observed over-all response appears in Fig. 11 where it can be seen that the calculated response is somewhat optimistic in amplitude up to 16 cycles per sec but very close thereafter, while the phase-function agreement is reasonably good up to 18 cycles per sec and optimistic thereafter.

The general agreement in phase and amplitude is surprisingly good in view of the simplifications made in the representation of the physical systems by means of the low-order constant-coefficient equations used.

EVALUATION OF RESULTS

Stroke Control. Referring to Fig. 11, the useful frequency range of the combined transmission and stroke control for $J_0 = 13.3$ in^2-lb might arbitrarily be stated to be approximately 16 cycles per sec since the amplitude up to this frequency is greater than 0.5 and falls off rapidly thereafter. During the first two thirds of this range the major contributions to over-all attenuation and phase shift are made by the stroke control. At 8 cycles per sec, for example, the phase shift in the stroke control is nearly 77 per cent of the total. In view of this fact the generalization may be made that a worth-while improvement in over-all response may best be obtained through the medium of an improved stroke control. It is apparent from Fig. 8 that some improvement can be obtained by increasing still further the stiffness-to-mass ratio of the solenoid-linkage system. Such a procedure would require a solenoid (or other electromechanical conversion device) having a higher force-to-mass ratio than that of the solenoid used here. Efforts have already been expended to obtain an improved solenoid or torque motor for use in stroke-control systems (5).

However, the major improvement needs to be effected in the hydraulic amplifier itself. At 8 cycles per sec, the amplifier contributes about two thirds of the stroke-control phase shift (see Figs. 8 and 12). Now it may be shown (Appendix, Equation [25]) that the response of the amplifier can be expressed approximately by the relation

$$X_p = \frac{2AKX_c \doteq F_0 L + AP_r L}{ML s^2 + (Lf + 4A^2)s + 2KRA} \quad \ldots\ldots [10]$$

where

A = area of smaller face of power piston
K = flow rate of pilot valve per unit displacement
F_0 = reaction of pump upon yoke
L = coefficient of leakage of metered oil
P_r = replenishing pressure
M = mass of power piston, linkage, yoke, and sleeve
f = coefficient of viscous friction
R = ratio of sleeve motion to power-piston motion

This equation indicates that the hydraulic amplifier should have an undamped natural angular frequency of

$$\sqrt{\frac{2KRA}{LM}}$$

and a damping ratio equal to

$$\frac{fL + 4A^2}{\sqrt{8LMKRA}}$$

The constants f, L, R, and M offer little promise for improvement. The valve rate K might be increased a limited amount but is effective only to the $^1/_2$ power. It would appear then that the most promising approach would be to decrease the piston area which is effective to the $^3/_2$ power in the damping term. The extent to which this course might be carried would be limited by the allowable corresponding increase in the value of the replenishing pressure. It should be possible to raise P_r by a factor of 2 to 3 (65 psi is normal) without seriously increasing the coercive effects upon the pilot valve. Hence the area could be reduced by a factor of one half to one third.

If the leakage be neglected, the amplifier-response equation reduces to

$$\frac{X_p}{X_c} = \frac{1}{R} \cdot \frac{1}{(2A/RK)s + 1} \quad \ldots\ldots\ldots\ldots [11]$$

That this simplification is still a close approximation to the observed response is evident in Fig. 12 wherein the third-order characteristic equation includes the amplifier as a simple time lag. Now the time constant $2A/(RK)$ can be cut in half by the use of a four-way valve, together with a power piston having equal areas (A) on both sides. However, the gain here is offset by the fact that the hydraulic reaction upon the pilot valve is approximately double that experienced by a three-way valve of the same diameter. In other words, a given solenoid will allow a larger K to be employed with the three-way valve, so that an evaluation of the net effect upon the time constant occasioned by the use of a four-way valve requires a more extensive investigation into the matter of pilot-valve coercion than has been attempted here.

A further possibility in the matter of increasing the effective value of K lies in an improvement of the pressure regulation of the replenishing system. The gage value of P_r was observed to fall more than 50 per cent with step-function inputs to the pilot valve. Such a pressure drop results in a lower rate of flow of oil through the valve, i.e., a drop in the value of K.

Transmission. The outlook for the transmission must be evaluated on the basis of its response equation (Appendix, Equation [36])

$$\frac{N_m}{X} = \frac{\dfrac{(d_p)_{max} N_p}{d_m}}{\dfrac{JeV}{d_m^2} s^2 + \left(\dfrac{f_m eV}{d_m^2} + \dfrac{JL_t}{d_m^2}\right) s + \dfrac{f_m L_t}{d_m^2} + 1} \quad \ldots [12]$$

where

N_m = speed of B-end (motor)
N_p = speed of A-end (pump)
X = per unit stroke of A-end
d_p = displacement of pump per radian of revolution
L_t = coefficient of total leakage of pump and motor
f_m = viscous friction of motor and load

(Remaining symbols as previously defined)

The characteristic system equation yields an undamped natural angular frequency

$$\omega_n = \sqrt{\frac{f_m L_t + d_m^2}{JeV}} \quad \ldots\ldots\ldots\ldots [13]$$

and a damping ratio

$$\zeta = \frac{f_m eV + J L_t}{2\sqrt{JeV(f_m L_t + d_m^2)}} \quad \ldots\ldots\ldots\ldots [14]$$

If the viscous-friction term is relatively small (as is generally true) then these expressions reduce to

$$\text{Undamped natural frequency, } \omega_n = \frac{d_m}{\sqrt{JeV}} \quad \ldots\ldots [15]$$

$$\text{Damping ratio, } \zeta = \frac{L_t\sqrt{J}}{2d_m\sqrt{eV}} \quad \ldots\ldots\ldots [16]$$

Thus for a given transmission and load inertia the adjustable parameters can be merely V and L_t, and of these only V affects both terms by useful amounts. The leakage coefficient L_t could be used to control the damping ratio but would have an adverse effect upon the "torque stiffness" of the transmission from an open-cycle viewpoint. Consequently it appears that improvement in transmission response may be obtained readily only by reducing the high-pressure oil volume, which implies keeping the conduit distance between pump and motor as short as possible.

It should be noted that any expansion of the conduit under pressure constitutes in effect an increase in the compressibility of the oil and hence should be held to a minimum by the use of relatively strong conduit material because, since both the natural frequency and the damping ratio vary approximately as the inverse of the square root of the compressibility factor (if the viscous-friction load is small), very desirable increases in both terms can be achieved by minimizing the expansion as well as the volume of the conduit.

Notes on Procedure

Equipment Required. Although the scheme of measurement as outlined in Fig. 2 required a considerable amount of laboratory equipment, extensive use was made of standard laboratory electronic and mechanical components (6) with attendant savings in labor and time. Views of the signal generator and the hydraulic power unit appear in Figs. 14 and 15, respectively. In Fig. 15 can be seen the photoelectric pick-off with its adjustable mounting, the latter feature being necessary in order to make the zero-signal position of the pick-off shutter coincide with the neutral position of the pilot valve. The latter position was made an arbitrary value, rather than that which resulted in zero output speed at the B-end. Such a procedure is an artifice which avoids or at least minimizes the undesired effects of the dead space occurring at the neutral-stroke position. The neutral position actually employed for the pilot valve was that which yielded an output speed approximately one half of maximum, namely, 1500 rpm. The output voltage (E_i) from the signal generator then served merely to vary the output speed sinusoidally about this mean or neutral value. Consequently the output voltage from the alternating-current tachometer geared to the B-end had a steady component (i.e., a 400-cycle carrier) with a sinusoidal modulation of small amplitude. It was then necessary to remove this steady component from the tachometer signal by means of an alternating-current bias voltage of controlled phase and amplitude in order that the modulation alone might be amplified and demodulated prior to measurement on the oscillograph.

In order to minimize the effects of entrained gas upon the compressibility of the oil and of temperature upon the oil viscosity, the oil for the transmission and hydraulic amplifier was drawn continuously from a large external sump wherein the oil temperature was maintained at 60 ± 1 deg C by means of thermostati-

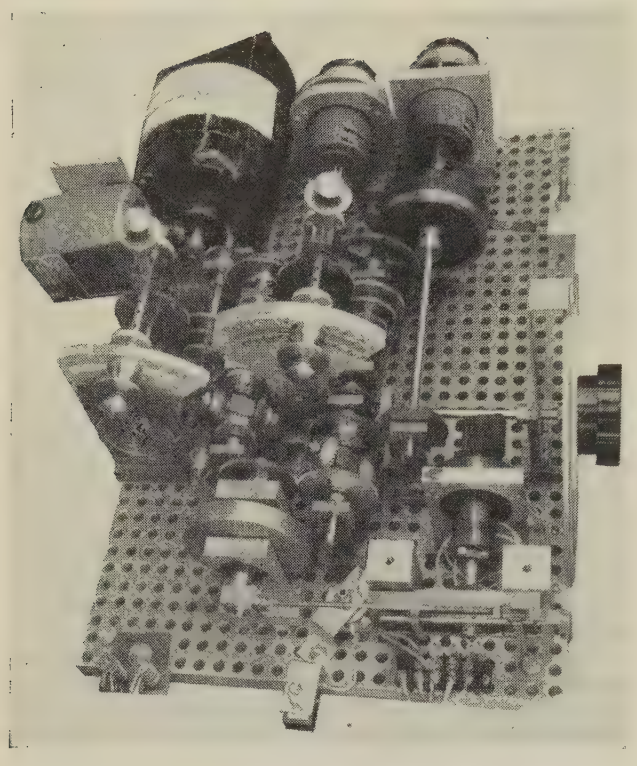

FIG. 14 VARIABLE-FREQUENCY SIGNAL GENERATOR

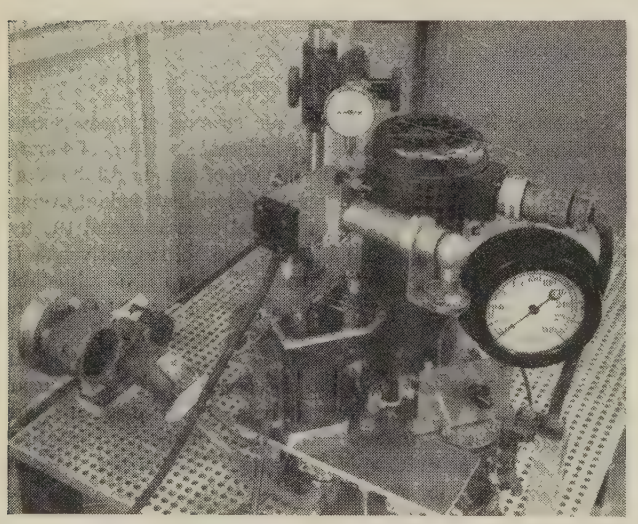

FIG. 15 HYDRAULIC POWER UNIT

cally controlled electric heaters. The oil used was AN-VVO-366 hydraulic fluid.

Method of Operation. With all measuring components and bias voltages adjusted for zero output with zero signal, the signal generator was driven at approximately 0.02 cycle per sec (referred to as "zero frequency") with sufficient output voltage to achieve the desired stroke amplitude. The gain in each measuring circuit was then adjusted to provide suitable vertical deflections of the oscillograph beam (i.e., full-scale deflection for the quantities X_p and ω_0, half-scale or less for X_c to enable the resonant peak to be read). The phase-angle dial (θ in Fig. 2), was then adjusted to cause the beam to cross the neutral axis at the same point after each half cycle, or in other words, to produce the nearest approach to a straight-line trace on the screen. In this objective the use of a long-persistence screen proved very helpful.

Then with the signal generator operating at each of several suitable speeds throughout the useful frequency spectrum, the phase and amplitude functions of the quantities X_c, X_p, and ω_0 were measured in quick succession. The amplitude in each case was the over-all vertical height of the trace on the screen (expressed as a fraction of the zero-frequency height), while the phase angle was the difference between the zero-frequency reading of the phase dial and that reading which resulted when the phase dial was rotated sufficiently to obtain a straight-line trace or the closest approximation. Coulomb friction and other effects caused the optimum trace to assume an elongated and irregular figure-eight shape, in which case the criterion for adjusment was to obtain equal loop areas. By means of this procedure the average phase-shift reading could be repeated to within 2 per cent over the range of interest.

Difficulties Encountered. The measuring technique outlined in Fig. 2 proved generally satisfactory, although certain difficulties were encountered. The major problems were those of shielding and filtering in order to minimize the 60-cycle and 400-cycle pick-up. Such noise in any of the signal voltages obscured the reading of signal amplitudes (i.e., the vertical deflections) on the oscillograph screen, while ripple in the reference voltage (horizontal deflection) increased the difficulty of applying a consistent criterion for phase adjustment.

On the other hand, the filtering-out of noise had to be held to a minimum in order to maintain a satisfactory frequency response in the measuring circuits. This was particularly important in the matter of the amplitude functions, since the attenuation of the signals in the measuring circuits narrowed the frequency range over which reliable amplitude measurements could be made.

Coulomb friction effects in the solenoid and linkage system resulted in nonsinusoidal wave form in the motion of the pilot valve which in turn obscured the phase adjustment as previously mentioned. This difficulty was considerably lessened with the use of stiffer recentering springs and stronger input signals. The photoelectric pick-off proved highly satisfactory after preliminary difficulty in making it linear. The nearly perfect frequency response of this pick-off avoided some of the labor required to correct observed data for nonperfect response in the measuring circuits.

Noise in the B-end tachometer signal was particularly troublesome, even with the use of an alternating-current tachometer. This noise appeared to be a function of A-end displacement and consequently varied in amplitude with that of the output signal. The most prominent noise frequency was in the neighborhood of 30 cycles per sec, and the fact that this lay within the range of signal frequencies made adequate filtering impossible.

Curve Fitting. The linear equations approximating the response of the stroke control and the transmission were obtained by fitting curves to the observed phase-shift functions in each case. This procedure was adopted because it was felt that the accuracy of phase measurement exceeded that of the amplitude ratio. Further, the arithmetic involved was somewhat less laborious in fitting to the phase-shift curves, particularly in the case of equations of order higher than second.

The method, briefly, consists in first choosing the order of the approximating equation, based upon the number of quadrants swept through by the phase function before approaching an asymptote. Then the equation thus chosen is converted into its phase component, and the coefficients of the latter are evaluated by substituting the necessary number of points from the observed phase-shift curve. The success of the approximation of course lies in the choice of points, care being taken to select

points which appear most in accordance with the probable trend of an equation of the order chosen. In the case of cubics or higher, the choice of points will usually be indicated by significant convolutions in the amplitude function. More precise methods of curve fitting exist but the foregoing trial-and-error approach is simple and relatively fast and is generally consistent with the accuracy of the observed data.

A simple example is the approximation of the transmission response. Since the phase-shift curve approaches 180 deg asymptotically, the equation must be second order. Then the form of the response equation is

$$G(s) = \frac{1}{as^2 + bs + 1} \quad [17]$$

or, for a sinusoidal, varying-frequency driving function where $s = j\omega$, the frequency response becomes

$$G(j\omega) = \frac{1}{(1 - a\omega^2) + jb\omega} = \frac{e^{j\theta}}{\sqrt{(1 - a\omega^2)^2 + (b\omega)^2}} \quad [18]$$

where

$$\theta = -\tan^{-1}\frac{b\omega}{1 - a\omega^2} \quad [19]$$

Since there are two unknown coefficients, two points on the observed response curve will suffice. In the case in question the points chosen (on the $J = 13.3$ in^2-lb phase curve, Figs. 10 and 13), were at frequencies of 7 and 19 cycles per sec approximately. Then substituting each of these values of ω and the tangent of its corresponding phase angle into the expression for θ, the coefficients a and b are evaluated, enabling the phase and amplitude functions to be calculated. One or more successive trials using other points may be required so that the best average fit (or the best fit over a range of particular interest) may be chosen.

Conclusion

The scope of this investigation has by no means been exhaustive. Inevitable compromise has left much useful information still to be desired. In such a category might be listed the following:

1 The effect of conduit length and diameter upon transmission response, from the standpoint of fluid friction.

2 The nature of the hydraulic reaction of the A-end upon the yoke linkage as a function of pressure and stroke amplitude.

3 The magnitude of the stroking forces as a function of frequency and of stroke amplitude.

4 The effectiveness of a suitable feedback network from the power-piston signal to the input circuit for the purpose of improving the response of the stroke control.

5 The nature of the transient pressure occurring in the conduits as a result of impulse loads.

Nevertheless, it has been shown that the over-all response of the transmission and stroke control can be represented by a linear constant-coefficient differential equation of relatively low order. Further, the response of the various elements in the power unit has been measured and compared in order to assess the merits of these elements in a servoloop and to provide a basis for the design of power amplifiers to be used to stroke larger transmissions. In addition, certain evidence has been established concerning the magnitudes of the effects of various parameters upon the dynamic behavior of the several elements in the power unit.

The evolution and refinement of measuring techniques incidental to the progress of this investigation can be expected to bear fruit in any similar work subsequently undertaken.

BIBLIOGRAPHY

1 "The Frequency Response of Automatic Control Systems," by Herbert Harris, Jr., Trans. AIEE, vol. 65, Aug.–Sept., 1946, pp. 539–546.

2 "The Analysis and Synthesis of Linear Servomechanisms" (book), by A. C. Hall, Technology Press, Massachusetts Institute of Technology, Cambridge, Mass., 1943.

3 "Servomechanism Fundamentals," by H. Lauer, R. Lesnick, and L. Matson, McGraw-Hill Book Company, Inc., New York, N. Y., 1947.

4 "Hydraulic Variable-Speed Transmissions as Servomotors," by G. C. Newton, Jr., *Journal of The Franklin Institute*, vol. 243, June, 1947, pp. 439–469.

5 "Design of a Linear Torque Motor," by R. C. Gibson, S. M. Thesis, Electrical Engineering Department, Massachusetts Institute of Technology, Cambridge, Mass., 1946.

6 "Laboratory Aids for Electro-Mechanical System Development," by G. C. Newton, Jr., and W. T. White, Trans. AIEE, vol. 166, sect. P 752, 1947, pp. 1–7.

7 "Investigation of the Frequency Response of an Hydraulic Amplifier," by M. R. Hannah, S. M. Thesis, Department of Electrical Engineering, Massachusetts Institute of Technology, 1946.

Appendix

Analysis of Hydraulic Amplifier (7)

The hydraulic amplifier may be represented diagrammatically as shown in Fig. 16. The following nomenclature will be used in the Appendix:

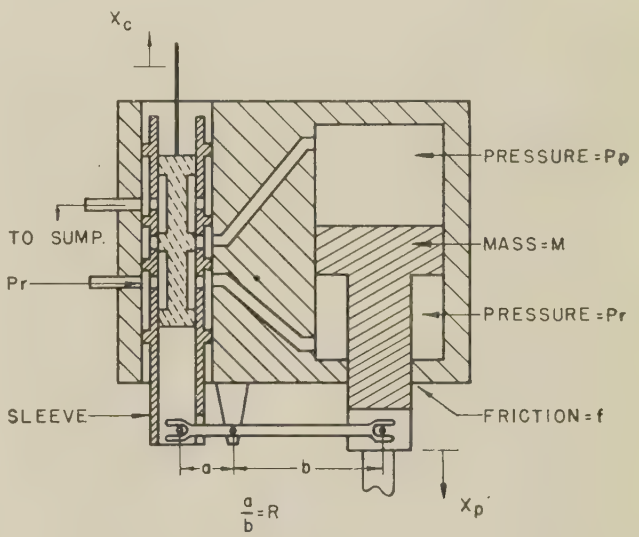

Fig. 16 Diagrammatic Representation of Hydraulic Amplifier

M = mass of power piston and yoke
f = viscous friction in moving system
X_c = position of pilot valve relative to its neutral position
X_p = position of power piston relative to its neutral position
P_p = pressure above power piston
P_r = replenishing or control pressure
A = area of smaller face of power piston
L = coefficient of leakage past power piston
R = ratio of sleeve travel to power-piston travel
F_0 = reaction of A-end upon yoke linkage

Assume that the leakage is proportional to pressure difference. Assume that the oil flow from the pilot valve is proportional to the travel of the pilot valve relative to that of the sleeve. Then valve flow rate $= K(X_c - RX_p)$, and leakage flow rate $= L(P_p - P_r)$. Therefore, neglecting the compressibility of the oil,

the total flow rate into the cylinder $= L(P_p - P_r) + 2\,AsX_p$, where s represents the operator $d/(dt)$. Then

$$K(X_c - RX_p) = L(P_p - P_r) + 2\,AsX_p \quad [20]$$

or

$$P_p = \frac{K(X_c - RX_p) - 2\,AsX_p}{L} + P_r \quad [21]$$

$$\text{Force on piston} = 2\,AP_p - AP_r \quad [22]$$

$$\text{Reaction force on piston} = (Ms^2 + fs)X_p \pm F_0 \quad [23]$$

Equating [22] and [23]

$$P_p = \frac{(Ms^2 + fs)X_p \pm F_0 + AP_r}{2A} \quad [24]$$

From Equations [21] and [24]

$$X_p = \frac{2\,AKX_c \pm F_0L + AP_rL}{MLs^2 + (Lf + 4A^2)s + 2KRA} \quad [25]$$

If the leakage be neglected

$$X_p = \frac{\frac{X_c}{R}}{\frac{2A}{RK}s + 1} \quad [26]$$

Analysis of Hydraulic Transmission

Referring to Fig. 17, let

Q_m, (Q_p) be rate of flow of oil through motor (pump)
Q_{Lm1}, (Q_{Lp1}) be direct leakage from motor (pump) to sump
Q_{Lm2}, (Q_{Lp2}) be differential leakage across motor (pump)
P_m, (P_p') be inlet pressure at motor (outlet pressure at pump)
P_r be replenishing pressure

Assume leakage is proportional to pressure difference and that

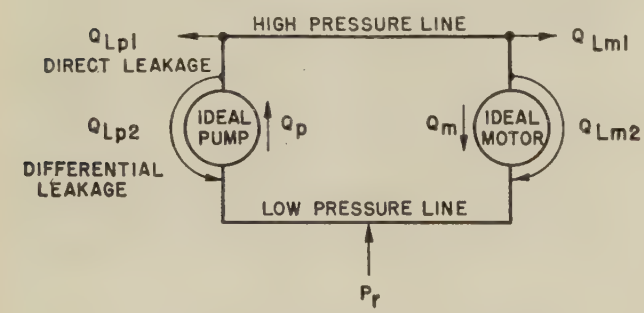

Fig. 17 Schematic Representation of Transmission

leakage may be lumped from the high-pressure side so that

$$Q_{Lp1} + Q_{Lp2} = Q_{Lp} = L_p(P_p' - P_r) \quad [27]$$

and

$$Q_{Lm1} + Q_{Lm2} = Q_{Lm} = L_m(P_m - P_r) \quad [28]$$

Hence

$$Q_p - L_p(P_p' - P_r) - L_m(P_m - P_r) = Q_m \quad [29]$$

Let

d_m, (d_p) be displacement of motor (pump) per radian of revolution
N_m, (N_p) be speed of motor (pump)

Then

$$Q_p = d_pN_p \text{ and } Q_m = d_mN_m \quad [30]$$

The theoretical motor torque is equal to the delivered torque plus the loss due to viscous friction in the motor, that is

$$d_m(P_m - P_r) = T + f_mN_m \quad [31]$$

From Equations [29] and [30]

$$d_pN_p - L_p(P_p' - P_r) - L_m(P_m - P_r) = d_mN_m \quad [32]$$

Neglect pressure drop in conduit, i.e.,

$$P_p' = P_m$$

Assume that

$$\text{Volume of oil compression} = (P_m - P_r)eV$$

where

e = coefficient of compressibility
V = volume of oil in high-pressure line $+ \pi(d_m + d_p)$

Then

$$d_pN_p = (L_p + L_m)(P_m - P_r) + d_mN_m + s(P_m - P_r)eV \quad [33]$$

Assume that the delivered torque is equal to a load torque T_0 plus an inertia reaction torque, i.e., $T = T_0 + JsN_m$, where J is the total inertia of load and motor. From Equation [31]

$$(P_m - P_r) = \frac{1}{d_m}[T_0 + N_m(Js + f_m)] \quad [34]$$

Let

$$L_p + L_m = L_t$$

From Equations [33], [34]

$$d_md_pN_p = T_0(L_t + seV) + N_m\,JeVs^2 + (L_tJ + f_meV)s + L_tf_m + d_m^2 \quad [35]$$

Let X be a per unit pump stroke so that

$$X(d_p)_{\max} = d_p$$

Then, letting T_0 be zero, the response of the transmission becomes

$$\frac{N_m}{X} = \frac{\frac{(d_p)_{\max}}{d_m}N_p}{\frac{JeV}{d_m^2}s^2 + \left(\frac{f_meV}{d_m^2} + \frac{JL_t}{d_m^2}\right)s + \frac{f_mL_t}{d_m^2} + 1} \quad [36]$$

From Equation [36] the characteristic natural angular frequency is

$$\omega_n = \sqrt{\frac{f_mL_t + d_m^2}{JeV}} \quad [37]$$

and the corresponding damping ratio is

$$\zeta = \frac{f_meV + JL_t}{2\sqrt{JeV(f_mL_t + d_m^2)}} \quad [38]$$

If the viscous-friction term f_m is relatively small then the natural frequency and damping terms reduce to

$$\omega_n = \frac{d_m}{\sqrt{JeV}} \quad [39]$$

and

$$\zeta = \frac{L_t\sqrt{J}}{2d_m\sqrt{eV}} \quad [40]$$

Discussion

H. T. Marcy.[4] The author is to be complimented on this report of a very comprehensive series of tests. In particular, the completeness with which the functions of cascade elements have been separated is a noteworthy feat. There are, however, a few omissions of data and references which constitute the subject of this discussion.

In the description of the hydraulic amplifier it is not made clear what type of oil ports are in the sliding pilot-valve sleeve. From the appearance of the data, showing rapid phase shifts at very low frequencies, it would seem that the ports are circular holes. Such a circumstance results in a nonlinear functional relationship between port area and valve opening with less port area per unit valve travel for small openings than for large. It would also be interesting to know whether the author considered the use of dither as a means of reducing pilot-valve coercion on solenoid and linkage.

The author reports much better agreement between theoretical and measured transmission characteristics than other experimenters.[5,6] He has considered, however, only the natural frequency and neglected the damping. In the following table the writer has used the measured values of the natural frequency and degree of resonance given by the author and has computed the value of the leakage coefficient L_t, which would make a proper theoretical prediction of the damping ratio:

Load inertia in²-lb, J	Observed natural frequency, cycles per sec, ω_n	Observed resonant peak	Equivalent damping ratio	Calculated leakage coef.[a] L_t, cu in./sec/psi
13.3	16.0	2.2	0.23	4.8×10^{-4}
7.7	21.2	2.3	0.22	6.0×10^{-4}
4.9	26.0	3.1	0.16	5.6×10^{-4}

[a] $L_t \backsimeq \frac{2\zeta}{\omega_n} \frac{dm^2}{J}$.

It is at once apparent that there is good consistency in the three leakage factors shown which ideally would be the same. Mr. Newton[5] previously has given a value of the total leakage of the pump and motor of this same model transmission as 0.44×10^{-3}. Thus by Equation [40] of the paper, the theoretical damping ratio is 92 per cent of the measured value for an inertia of 13.3 in²-lb. It is 72.5 per cent and 78 per cent of the measured values for inertias of 7.9 and 4.9 in²-lb, respectively.

The agreement between theory and measurement reported by the author is markedly better than that reported by other observers,[5,6] although the tendency is the same, to predict too high natural frequencies and too low damping ratios. Mr. Newton in particular reports an observed resonant frequency of 11 cycles per sec as opposed to a 19 cycle per sec theoretical value for 6.4 in²-lb of inertia with the same type transmission as used by the present author.

The observed differences between theory and practice are mutually incompatible with possible experimental errors in determining load inertia, oil compressibility, or leakage. Consequently the writer is of the opinion that there is something as yet unaccounted for in the theory. On the other hand, the existing theory does give very accurate results for a particular transmission in indicating the change which should be expected when parameters such as load inertia are varied, thus reducing the number of experiments that must be made and preserving the value of theory. Messrs. Steinhauer and Payson[6] have shown this for a radial-type unit manufactured by the Oilgear Company. They also observed the same amplitude attenuation at low frequencies with its corresponding greater than theoretical phase shift as appears in the data of the paper. From network theory, this could indicate some sort of a time lag not indicated by theory.

G. C. Newton.[7] This paper will be particularly useful to university teachers in the field of applied dynamics and automatic control. For those uninitiated in the art of frequency-response measurements for complex electromechanical systems, it is a source of information on techniques as well as an example of the detailed results of such measurements and their use. Sufficient information is provided so that extensive and practical home problems can be constructed from it. This is an acid test of the quality of a paper in the writer's opinion. To be considered "good," a technical paper of this class should include sufficient quantititative information to permit a reader to cross-check the author's conclusions and to make calculations of his own using the data presented as a basis. This paper meets this requirement to a greater degree than most.

Even with this paper, however, there are a few points which may have been omitted in the interest of conciseness but which the writer would like the author to clarify in his closure.

1 *Dither.* The writer finds no reference made to dither in the hydraulic amplifier. It is common practice to introduce a relatively high-frequency vibratory motion called dither, between the pilot valve and its sleeve in order to reduce the effects of valve overlap, valve friction, and transmission "softness" near neutral stroke. These effects generally show up as low-frequency oscillation of output displacement when the power unit is incorporated in a closed-loop system. In this particular apparatus, dither might be introduced at the fulcrum of the lever connecting the power piston and sleeve(see Fig. 16 of the paper). The writer asks the following specific questions:

(*a*) Was dither used during the frequency-response tests? If so, what were the amplitude and frequency?

(*b*) Is dither to be used in contemplated closed-loop applications of the power unit? If so, what are the amplitude and frequency?

(*c*) If no dither was used during the frequency-response tests, and if dither is to be used in closed-loop applications of the power unit, what is the justification for omitting dither in the frequency-response tests? In answering this, superposition arguments probably cannot be used because of the inherent nonlinearities of the system. (Dither, in fact, is supposed to compensate partially for certain of these nonlinearities.)

2 *Auxiliary Information Necessary for Proper Interpretation of Frequency-Response Data.* In general, frequency-response data alone are insufficient to specify the behavior of a dynamical system. If the system were linear, it is true that the frequency-response data (presumably amplitude and phase versus frequency over a finite frequency interval) would characterize the system's behavior completely. However, the systems we deal with in practice are never linear in the mathematical sense; they are, at best, only "approximately linear." The response of a nonlinear system to a sinusoidally varying excitation is not a sinusoid and a frequency response generally cannot be readily defined.

If the degree of nonlinearity over the range of variation (in frequency, amplitude, and bias) of the excitation variable is small, then the deviation of the response from a sinusoidal motion is generally small. Under these conditions a frequency re-

[4] Research Engineer, The M. W. Kellogg Company, Special Projects Department, New York, N. Y.

[5] Refer to author's Bibliography (4)

[6] "Automatic Control Characteristics of a Hydraulic Transmission," by H. Steinhauer, Jr., and E. C. Payson, B.S. Thesis in E.E., Massachusetts Institute of Technology, Cambridge, Mass., 1943.

[7] Department of Electrical Engineering, Massachusetts Institute of Technology, Cambridge, Mass.

sponse can be defined by comparing the fundamental of the response and the excitation. A change in the range of variation of the excitation variable generally changes both the deviation of the response from a sinusoidal motion and the frequency response. However, the change in frequency response is usually more readily detected than the change in the deviation of the response from a sinusoidal motion. Furthermore, certain nonlinearities are directly measurable by making a number of frequency-response measurements for different ranges of the excitation variable.

Thus it is apparent that precautions must be exercised in making frequency-response tests on practical systems, particularly in the matter of the choice of ranges of excitation variation. If complete tests are not contemplated (and seldom can they be for economic reasons), then the engineer should choose ranges of variation of the excitation variable which correspond as closely as possible to the conditions expected in the situation for which the data are to be used. For example, if the data are to be used for studies of system stability to small disturbances, then the frequency-response runs should be made at as small amplitude as possible with static bias corresponding to the operating point for which stability is to be determined. (The limit on smallness is usually set by observation difficulties.) On the other hand, if the data are to be used for calculation of performance with large excitation, then correspondingly large amplitudes should be used.

It should be recognized that the amplitude of the excitation variable should not necessarily be the one controlled during a frequency-response run. Rather, the amplitudes of variables associated with the most nonlinear elements should be controlled. In the power unit under discussion, the most nonlinear elements would seem to be the hydraulic amplifier and the transmission. The nonlinearity of the stroke control is most likely associated with some function of its output if pilot-valve overlap effects are negligible. (Such effects generally must be negligible for the satisfactory closed-loop operation of a system incorporating this power unit.) The transmission nonlinearity is probably associated with pressure and hence B-end acceleration, $\dot{\omega}_0$, for the pure inertia loading of these tests. At low frequencies the B-end acceleration is directly related to the velocity of the stroke control output ($\dot{X}_p$). Therefore it would seem more appropriate to control the amplitude of B-end acceleration rather than the input voltage to the power amplifier, E_i. By "control" the writer does not mean to make constant but to make conform to a prescribed function of such variables as are indicated by purposes of the tests. This amplitude-control function may or may not be a constant.

To summarize, frequency-response data for practical systems (i.e., systems which exhibit nonlinearity) should be accompanied by auxiliary information including the following:

(*a*) The purpose of the data in view of the nonlinearities present.

(*b*) Statements of the controlled-amplitude variable, the amplitude-control function, and reasons for these selections.

(*c*) Disclosures of actual amplitudes applying to each frequency-response run (or the equivalent) when not given elsewhere, e.g., these disclosures are necessary when amplitudes are concealed in per unit scales.

(*d*) Statements of the biases of all pertinent variables so that the operating point for which the data are supposed to apply is disclosed.

(*e*) Estimates of precision or repeatability of data.

This list does not include items such as equipment description, test method, and the like, which are normally presented with any test result.

The last item is included without prior discussion, on the basis that all scientific and engineering test results should include such information. In frequency-response tests, repeatability can be presented as a graph of phase and amplitude uncertainties versus frequency. Separate information for instrument and equipment uncertainties should be given if possible. Such estimates are recognized as being generally subject to large errors, but crude estimates are better than none. The experimentalist always interprets his data against a background of such estimates but often fails to convey them with his other results.

Finally, estimates or data describing the nonlinearities of the equipment are highly desirable. These may be in the form of static curves such as torque-speed curves and the like. Such information is not essential to the characterization of a particular frequency response but is convenient to have if the frequency-response data are to be used for estimating performance at operating points different from their own.

The author has explicitly disclosed part of the auxiliary information listed. In his paper he states, pertaining to the respective items:

(*a*) Nothing

(*b*) That the input voltage E_i, amplitude was held constant during runs and that the zero-frequency amplitudes of valve travel used were approximately 0.010, 0.015, 0.020 in. (see section "Amplitude of Stroke").

(*c*) Nothing.

(*d*) That 1500 rpm output speed (ω_0) and zero-load torque biases were used.

(*e*) Nothing.

He probably discloses implicitly much additional auxiliary information through conventions used among people "skilled in the art" which assign exact meanings to omissions in explicit disclosures. But those not skilled in the art will appreciate any clarification he may care to make in his closure.

To show the need for clarification, suppose one tries to estimate, on the basis of the explicitly disclosed facts, the working range of transmission pressure difference (one of the linearity determining variables of the transmission) corresponding to the data of Fig. 11 of the paper. To do so, it is necessary to make assumptions regarding which zero-frequency stroke amplitude was used and what the zero-frequency B-end speed for full stroke is. Assuming 10 per cent stroke and 3600 rpm, the writer's rough calculations indicate that pressure amplitudes vary from zero to roughly 1000 psi. The maximum rated pressure of the transmission is probably in the vicinity of 1000 psi. The writer can only conclude that one of the nonlinear elements has probably been worked over a very large range indeed.

Effect of Dynamic Variation in Replenishing Pressure. In the last paragraph of the section, "Evaluation of Results," the author mentions a possibility of decreasing the effective time constant of the hydraulic amplifier by better regulation of the supply pressure. Such improvement would undoubtedly occur but the overall performance of the stroke control probably would not change appreciably, in the writer's opinion, because the device acts to a considerable degree as a force balance in which the solenoid force is balanced against the coercion force. The coercion force is closely related to the flow of oil through the valve and tends to increase with increasing flow, regardless of the actual magnitude of the supply pressure. Reduction of supply pressure tends merely to allow the valve to have a wider opening for the same coercion force.

In concluding, the writer again states that he believes the author has written an excellent paper and that the comments and queries contained herein are not to be construed as criticism intended to point out flaws but rather as providing opportunities

for the author to add to his paper through the medium of his closure.

N. B. Nichols[8] and E. H. Woodhull.[9] By employing existing knowledge of linear servotheory, the performance and stability of the over-all servo can be calculated readily if the characteristics of each element in the servo are known accurately enough. Therefore if servos are to be designed by analytical methods, a fundamental knowledge of each element and its limitations is necessary before the designer can proceed to build a servo to fit a specific need. Also, improvements in servo design result either from the development of new elements or the rearrangement of elements; in either case, a fairly detailed knowledge of the dynamic characteristics of each element is necessary.

In his paper the author discusses experimental techniques for obtaining dynamic information about each element in a hydraulic power unit and follows this with a method for obtaining an approximating analytical transfer function from the experimental data, namely, constant-coefficient differential equations of low order. It is felt that the paper is timely and an important contribution to the literature of automatic control.

By using frequency-response methods, the author has done what appears to be a careful job of determining transfer functions experimentally. It is noted that he seeks to improve each element by examining the approximating analytical expression and then by recommending design changes which will increase the band pass of the element, that is, extend the cutoff frequency to a higher value. It should be pointed out that for a given servo-application, it may be that, when a compensating or equalizing network is introduced in the servoloop to obtain a desired performance characteristic, its introduction will void any advantage of a higher cutoff frequency for the hydraulic amplifier. However, it still seems desirable to make the hydraulic amplifier as fast as possible since it increases the flexibility of application and improves performance when the amplifier characteristic does become of importance.

The method used to obtain approximating equations appears convenient if an accurate and easy method of measuring phase angle is available. For those cases where phase-angle measurement is more difficult than amplitude-ratio measurement, a plot of amplitude ratio in decibels versus the logarithm of the radian frequency permits an easy method of determining the same data. The phase angle need be checked only at a few points since asymptotic intersections on the decibel-log frequency plot afford a very simple method of calculating phase angle. In fact, the phase-angle measurement can be eliminated entirely if previous experience indicates that the element is nearly linear and not of a nonminimum phase type.

K. I. Postel.[10] It is indeed a pleasure for the designer of the transmission studied to have an opportunity to comment on the paper. At the outset it seems in order to state, not so much in defense as by way of explanation, that the unit was designed at a time when static performance and weight economy were the principal considerations, and serious attention was not given to its application as a servounit until more recently.

The author states that the most promising approach to improvement of the dynamic performance would be to decrease the piston area in the hydraulic amplifier. It is interesting that we had arrived at the same conclusion independently, and that comparative tests made with a piston of one half the area show some improvement. The amount of improvement, however, is moderate because the differential pressure available to force the oil over the opening of the pilot valve is the difference between the control-pressure source and the value required to move the piston against the work. The result is that the reduced volume of oil to be ported has also less effective pressure to force it across the orifice.

The poor regulation of the control pressure under varying demand was a factor that had been overlooked by us, but one which offered a simple means of improvement.

Experimental work had been under way for some time in an endeavor to increase the pulling effort of the solenoid, but new impetus was tendered the project when the amount that could be realized was made evident by the data shown graphically in the author's Fig. 8. The higher stiffness-to-mass ratio for which results are shown in Fig. 8 was almost exactly 3 times that of the standard solenoid. An entirely different type of solenoid has been developed in which the maximum effective effort available for moving the pilot valve to signal position is more than double that of the solenoid used in the subject report, with approximately the same power input. Though we were not able to keep the mass of the armature down to the value which would also result in a stiffness-to-mass ratio double the former, we concur in the opinion of the author that an increase in stiffness is worth more than a decrease in mass because the stiffer system will be better able to overcome the hydraulic reaction of the pilot valve.

In view of the number of times mention is made of the B-end operating under viscous friction, it might be of interest to consider the nature of the actual friction losses. An equation which closely approximates the experimental results is

$$T_l = T_f + bP + cN^2$$

where

T_l = total equivalent torque loss, lb-in.
T_f = torque required to idle unit at a low speed, lb-in.
P = sum of pressures in both ports, psi
N = speed of rotation, rpm
b and c are constants

In this equation the term T_f covers the idling friction of bearings and rubbing surfaces, the term bP accounts for the increase in friction as pressure is applied, and the term cN^2 is an equivalent torque representing the pressure drop encountered within the motor as the speed is increased. For the B-end used in the transmission tested, the friction will be closely represented by

$$T_l = 0.8 + 0.002P + 0.00000023N^2$$

We regard the paper as comprehensive and competent.

H. I. Tarpley.[11] The author has used several methods to advantage in his experimental analysis of the complete Vickers Model AA-16850 power unit, namely, electrical as well as optical methods. Too little has appeared in the literature upon the measuring techniques associated with the frequency-analysis method. More details would be of interest concerning the photocell pick-off and its associated amplifier for the measurement of very small pilot-valve displacements, since optical pick-offs add little coercion to small moving parts.

The results on the hydraulic amplifier are very interesting in that this particular amplifier may be approximated by a single time-lag function, whereas frequently they may be approximated only as a quadratic function. Does this not mean that, in this particular amplifier, the second time constant is small compared to the first time constant? It would be of value to find this second time constant. It is interesting that Equation [11] of the

[8] Director of Research, Taylor Instrument Companies, Rochester, N. Y.
[9] Engineering Research Division, Taylor Instrument Companies.
[10] Development Engineer, Vickers Incorporated, Detroit, Mich.
[11] Professor of Electrical Engineering, The Pennsylvania State College, State College, Pa.

paper for this amplifier is the equation of the ideal hydraulic amplifier. This may be shown in the following way:

Ideally the valve flow equals the flow into the power cylinder, hence

$$KX_a = ASX_p$$

where

X_a = valve opening
K = valve flow constant
A = area of power piston
$S = \frac{d}{dt}$
X_p = displacement of power piston

Then

$$X_a = \frac{A}{K} S X_p$$

Hence

$$X_p = \frac{K/A}{S} X_a$$

Therefore the power piston is an ideal integrator.

The whole amplifier with its feedback sleeve linkage may be as represented in the block diagram, Fig. 18 of this discussion.

In Fig. 18

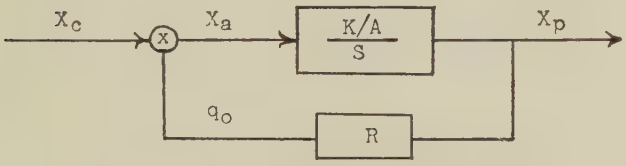

FIG. 18

R = sleeve lever multiplication ratio
X_c = displacement of pilot valve
q_o = displacement of sleeve.
$X_a = X_c - q_o = X_c - RX_p$

Hence

$$\frac{K}{AS}(X_c - RX_p) = X_p$$

and

$$\frac{K}{AS}X_c - \frac{K}{AS}RX_p = X_p$$

or

$$X_c = RX_p + X_p\left(\frac{AS}{K}\right)$$

Then

$$X_c = X_p\left(\frac{A}{K}S + R\right)$$

$$\frac{X_p}{X_c} = \frac{1}{\frac{A}{K}S + R} = \frac{1}{R}\,\frac{1}{\frac{A}{KR}S + 1}$$

This last equation is identical to the author's Equation [11], except the area of the power piston appears as $2A$; the writer has defined the power-piston area as A.

Equation [11] of the paper may be written

$$\frac{X_p}{X_c} = \frac{1}{R}\,\frac{1}{\frac{1}{K_vR}S + 1}$$

where

$K_v = K/A$ = velocity constant of the amplifier, since the amplifier time delay = $1/(K_vR)$, the problem is one of increasing the velocity constant to as large a value as possible in dealing with the ideal hydraulic amplifier.

The writer believes it would be unwise to attempt a redesign of a hydraulic amplifier by considering only its largest time constant since such a procedure might lead to an increase in the second time constant and cause no over-all improvement in the amplifier itself. As wider frequency bands are considered, we should not ignore fluid leakage, fluid compressibility, and the interaction of system elements in order to oversimplify the problem. In his conclusions the author outlines future studies which are aptly chosen, particularly the nature of the reaction of the A-end upon the yoke linkage as a function of the pressure and stroke of the A-end.

Attention should be called to the fact that a solenoid linkage and pilot-valve assembly driving a hydraulic amplifier, which in turn strokes a hydraulic transmission, is inherently a cascade of interacting elements and may have to be so considered in order to avoid oversimplification. In analyzing a cascade of elements, it is permissible to derive the over-all system function by routine multiplication of the element functions only for the case where there is no coercion between the elements. There is serious doubt that this is ever approximated in a complete hydraulic servosystem. Quantitative investigations for improvement of any element of a system may soon not ignore this fact even though nonlinear mathematics may be involved.

Author's Closure

Mr. Marcy is correct in his surmise that the amplifier valve-sleeve ports are circular holes. The inherent nonlinearity of circular ports helps to assure a stable (nonoscillatory) amplifier, although rectangular ports have been used with complete success. The matter of dither will be discussed later. Regarding the contention that the transmission response theory may be incomplete the author inclines to the view that the discrepancies between predicted and observed performance can be attributed largely to lack of constancy of the leakage coefficient L_t. Even though efforts are made to maintain the sump oil at a constant temperature the work done on the oil during compression within the transmission varies with frequency and stroke amplitude. Thus the temperature, viscosity, and the leakage coefficient of the oil in the transmission will vary even during one test with supposedly constant parameters.

In addition to the temperature variation, gradual wear or sudden scoring of mating surfaces will cause gradual or sudden changes in the leakage coefficient. Furthermore the continual shearing to which the oil is subjected results in a gradual breaking down of the molecular structure of some of the additives in the hydraulic fluid, thereby causing a gradual change in the viscosity and hence in the leakage coefficient (admittedly a second-order effect). Similarly the compressibility coefficient is a function of both the temperature and the pressure of the oil (and, in effect, of the expansion of the conduits), and therefore varies during any response measurements. These and other variables assumed in the theory to be constant lessen the likelihood of complete agreement between theory and experiment.

Mr. Newton's queries regarding the use of dither in the hydraulic amplifier may be answered as follows: (*a*) no; (*b*) yes, approximately 0.005 in. amplitude and 70 cycles per sec in terms of sleeve motion; (*c*) dither is required in order to maintain the

linearity of the amplifier in responding to very small signals (i.e., to minimize the effects of coulomb friction and dead space). The minimum amplitude employed in the tests described in the paper was 10 per cent of maximum stroke and this value was still within the linear range of the system. Table I compares the over-all response of the power unit with and without dither as a function of input amplitude (about the 50 per cent stroke bias) with a signal frequency of 10 cycles per second. Approximately similar agreement was obtained at 2 cycles per sec. Table 1 indicates the importance of dither for small input signals but suggests that for 10 per cent or larger signals the dither may be discarded without serious error. It was highly desirable to omit the dither in order that the various measured quantities might be free from dither noise which obscured the reading of phase and amplitude. The measurement of pilot valve motion was particularly difficult when dither was employed because of the transfer of dither motion from the sleeve to the pilot valve.

TABLE 1

	Amplitude ratio			Phase angle		
Per cent stroke	With dither	Without dither	Per cent difference	With dither	Without dither	Per cent difference
5	0.34	0.11	68	105	150	43
10	0.31	0.30	3	95	96	1
20	0.35	0.34	3	83	87	5
30	0.33	0.33	0	92	94	2
40	0.25	0.23	8	110	114	4

Mr. Newton's second point is well made and the author agrees that his listed "auxiliary information" is highly desirable (where space permits). Elaborating upon his summary of the paper's auxiliary information it may be said that:

(*a*) The purpose of the data was to achieve the maximum correlation between the derived response equations and the measured response. For this purpose it was, and is, felt that the use of 10 per cent stroke amplitude without dither yielded the most useful data.

(*b*) It is true that variables other than the excitation variable must not be allowed to assume large nonlinearities if a correlation of observed response with calculated response is to be attempted. However, if one employs the smallest constant excitation amplitude consistent with reasonable freedom from the effects of coulomb friction, dead space, and noise, then it would appear that an element must be hopelessly nonlinear if such a procedure could not be expected to yield usable data. The mere fact that a transmission whose relief valves are set at 1250 psi is subjected to pressures in the neighborhood of 1000 psi does not seem reason enough to go to the trouble of determining for each signal frequency just what the input amplitude should be in order to keep the transmission pressure or other variable within some arbitrary limit. It is not apparent to the author that the response data obtained with other than constant excitation amplitudes could be as readily transcribed into equation coefficients unless linear superposition is assumed. The linearity of both the stroke control and the transmission as demonstrated in Figs. 12 and 13 certainly justifies the use of a small, constant, excitation amplitude.

(*c*) All of the plotted data were obtained with 10 per cent strokes except those of Fig. 7 for which unity amplitude ratio corresponds to 15 per cent stroke.

(*d*) No comment.

(*e*) It was stated in the text that the phase angle data were employed to evaluate the coefficients of the response equations and that the phase-angle readings could be repeated to within two per cent over the range of interest. The latter condition was intended to imply that this accuracy was not maintained at the upper end of the frequency spectrum where the output amplitude in most instances would have fallen too low to permit precise phase-angle adjustments.

Messrs. Nichols and Woodhull make the timely comment that efforts to increase the bandpass of an element in a servomechanism may be nullified by the use of certain desirable compensating networks. This of course is very true, and moreover it should be remembered that a servo can be made *too* fast in some instances where the input data contains noise of disturbing magnitude and frequency. Such a condition has been discussed by R. E. Graham in his paper "Linear Servo Theory" in the *Bell System Technical Journal*, October, 1946. However, the primary application of the power unit in question was that of driving an aircraft gun turret, the successful stabilization of which required that the power unit have a relatively high natural frequency, hence the interest in widening its band-pass characteristic.

The db-log frequency techniques of response representation are unquestionably convenient for systems involving a cascade of simple time lags. Where coulomb friction, distributed and nonconstant parameters are encountered, the author would prefer to have a phase-angle plot before evaluating an approximating equation. The phase-angle measuring technique described in the paper requires more equipment than does the measurement of amplitude alone but once assembled it can be used with a wide variety of servosystems and it proved to be faster and more accurate than the corresponding amplitude measurements.

Mr. Postel's comments regarding the improvement in amplifier response which he obtained by reducing the power piston area suggest that possibly he maintained the same control pressure with the reduced as with the original piston. It is the author's view, however, that the amplifier time constant can be materially reduced if the control pressure is raised in the same ratio as the piston area is reduced so that the same energy is dissipated by a smaller volume of oil.

Professor Tarpley's comments regarding single-order versus quadratic approximations of hydraulic amplifier response suggest that one should make a distinction between low-pressure amplifiers, wherein the leakage and compressibility effects are small, and high-pressure amplifiers wherein these effects might be significant. To account for both leakage and compressibility a third-order response equation would be required. The author is completely in agreement with Professor Tarpley in his contention that one should not ignore the interaction of cascaded elements. This is particularly true in the case of the hydraulic reaction upon the pilot valve and control solenoid, which phenomenon assumes increasing importance as one attempts to decrease the amplifier time constant.

The author wishes to thank all those who have contributed to the discussion of this paper. Their constructive criticisms and additional information are indeed welcome. In particular the author would like to thank Dr. Walter T. White of the Sperry Gyroscope Co. for his valued assistance and encouragement in the preparation of this paper.

Power Turbines for Natural-Gas Expansion

By STEPHEN BENCZE,[1] JEANNETTE, PA.

Natural-gas expansion turbines are driven by gas in the same way that steam drives steam turbines. These gas-expansion turbines are supplied with energy in the form of heat energy in the gas, and they convert this into useful mechanical energy. Turbines of this type are not to be confused with the combustion type of gas turbine in which the fuel is burned and the resultant gases allowed to expand, generating power, then exhausted and thrown away. In a natural-gas turbine, the gas is allowed to expand and is exhausted into subsequent processes and may be used for combustion or chemical reduction. The gas undergoes only a change in pressure and temperature and undergoes no chemical change in passing through the turbine. Thus the conversion of power can be considered a "by-product" to the normal uses of the gas.

Applications

NATURAL-gas expansion turbines have become an exceedingly important source of power in our gas and oil fields. These units are driving generators, pumps, fans, blowers, and other equipment. They are rapidly replacing reciprocating gas engines, mainly because of the relative low initial cost and maintenance, as well as the improved over-all efficiency and physical size. It should also be noted that in an engine the gas used is burned, while in a turbine the gas is only expanded and can be further used. Thus in a turbine, the generated power is obtained at no expense for gas. Many installations have also been made for dual operation, on either steam or gas, so that if gas supply is not available or is interrupted, the turbine can be operated on steam. Units may also be geared for low-speed applications to allow for turbine operation at higher speeds, which results in better energy conversion, and also for physical size reduction of the turbine.

Turbines of this type will operate on any type of gas (natural, producer, casing head, etc.) or hot air, provided sufficient energy is available in the gas to warrant expansion. Thus design limitations of the turbines are governed by the gas used as well as the driven equipment. Many of the gases used contain hydrogen sulphide, mercaptans, sulphur compounds, and other acid-forming constituents which present many problems in design and operation and which have been overcome satisfactorily. Because gases available are generally at a relatively low pressure and temperature, gas-expansion turbines are generally of the single-stage type or are limited to few stages.

General Design

The general design of gas-expansion turbines does not differ materially from the conventional steam turbine. Standard single-stage steam turbines are generally used for these "gas" applications. Design and operating problems because of high pressures and temperatures do not generally exist, except in applications where the gas is preheated to a considerable degree before passing through the turbine. Here the use of high-temperature materials is limited. Design of casings, valves, bearings, and other basic components is the same as for steam units. Fig. 1 shows the cross section of a typical single-impulse-stage velocity-compounded mechanical-drive-type turbine, operated on natural gas.

The material problem for certain applications is of major importance, particularly where operating with "sour gases" containing hydrogen sulphide or other acid-forming constituents. Sour gas is especially corrosive in the presence of moisture, hence operation with these gases without first preheating or expanding to the dew point of the gas may become quite serious. Ordinary run of sour gases contains approximately 75 units of hydrogen sulphide. This is typical of the West Texas and New Mexico fields. Experience has shown that under favorable operating conditions and using sour gas, standard turbine materials as used for standard steam turbines, i.e., stainless or monel governor valves, stainless buckets, carbon-steel wheels and shafts, have held up satisfactorily.

One of the major problems which must be considered in designing and building a gas turbine is that of leakage. Gas leaks not only may be obnoxious, but may actually endanger life and property. All casing joints must be carefully made and tested at pressures well above the operating pressure of the unit. Special attention must also be paid to leakage past the rotating turbine shaft. There are many types of gas seals available for this application which would give entirely satisfactory results. As a general rule, carbon-type packing rings are used for sealing the turbine casing around the rotating shaft. Closer carbon-ring clearances are used on gas turbines than are used on steam turbines because of the lower temperature of the gas and also because of the low shaft temperatures which are present when the unit is running and the shaft shrinks away from the rings.

An effective seal arrangement is shown in Fig. 2. Here an ejector, with necessary valves and piping, is used to create a slight vacuum between the inner and outer carbon rings. By creating this vacuum, a slight amount of air is drawn in past the shaft under the outer ring. In effect, an air wall is set up between the two outer rings, preventing leakage. The ejector discharge is generally piped into the turbine exhaust if the inlet pressure is sufficiently high to allow the ejector to discharge against the exhaust pressure. If the exhaust pressure is too high, the ejector is piped to a low-pressure gas line.

Fig. 3 shows a simple way of sealing the shaft for relatively low gas pressures in the turbine casing. The inner seal rings are of the segmental carbon type with segments retained by a garter spring. The two outer rings are split micarta rings. Grease is packed between these two micarta rings, forming a grease seal. The leak-off from the inner rings is carried off to a suitable low-pressure line or to the outside atmosphere.

The problem of speed control and regulation of gas-expansion turbines does not differ from that encountered in steam-turbine units. Conventional governor devices of the centrifugal and hydraulic types have operated over long periods of time with assured accuracy and reliability.

Typical Performance

The mechanical performance, from the standpoint of safety and reliability is well proved by the hundreds of units which have been in continuous operation for many years. There is no reason why

[1] Assistant Division Engineer, Turbine Division, Elliott Company. Jun. ASME.

Contributed by the Oil and Gas Power Division and presented at the Spring Meeting, Tulsa, Okla., March 2–5, 1947, of The American Society of Mechanical Engineers.

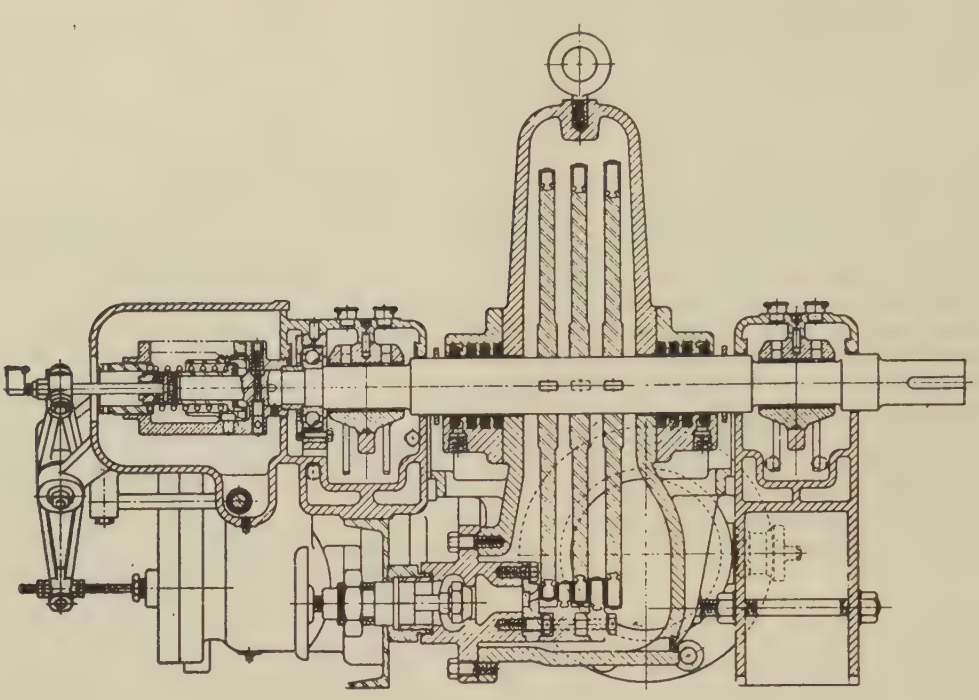

FIG. 1 SINGLE-IMPULSE-STAGE TURBINE

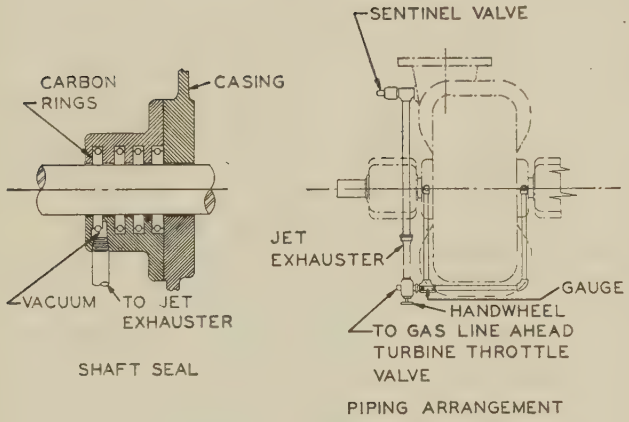

FIG. 2 SHAFT SEAL AND PIPING ARRANGEMENT

a gas-expansion turbine will not be the same dependable source of power as a steam turbine. Thermodynamic efficiencies comparable to those attained with steam turbines can readily be realized. Just as in the case of steam turbines, the thermodynamic performance of gas-expansion turbines is dependent upon the available energy in the gas for expansion, the speed and size of the unit, the design of the nozzles and buckets, as well as the inlet and exhaust flow passages. The available energy in the gas is dependent upon the turbine-inlet pressure and temperature and the exhaust pressure, as well as upon the chemical composition of the gas.

Fig. 4 shows the performance of a typical single-impulse-stage type of turbine driving a pump. The turbine is operated on 100 psig inlet pressure, 100 F inlet temperature, and 30 psig exhaust pressure with gas having a specific gravity of 0.650. Pump and turbine speed at rated horsepower is 2750 rpm.

Fig. 5 shows an interesting comparison of performance of single-impulse-stage-type turbines operated on natural gas and on steam, at the same inlet pressures and temperatures, speeds, and exhaust pressures. This curve gives approximate ratios of gas rate and steam rate per horsepower-hour at various turbine speeds and various specific gravities of the gas. Turbine-wheel

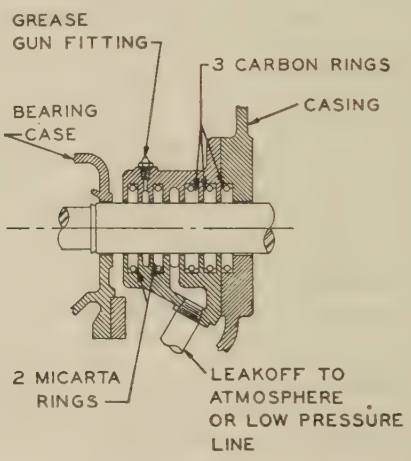

FIG. 3 LOW-PRESSURE SHAFT SEAL

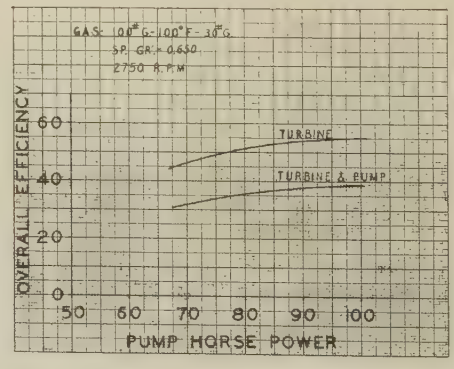

FIG. 4 SINGLE-STAGE-TURBINE PUMP-DRIVE PERFORMANCE 100 HP

dimensions, nozzle and bucket efficiencies, as well as over-all mechanical efficiencies are assumed to be the same for gas and for steam. It is seen that gas rates for comparable conditions are higher than steam rates, and this is due mainly to the difference in available energy in the gas and steam. Another factor contributing to the difference in rates for gas and steam operation is the difference in windage created by the turbine disks and buckets because of the difference in gas and steam densities and viscosities.

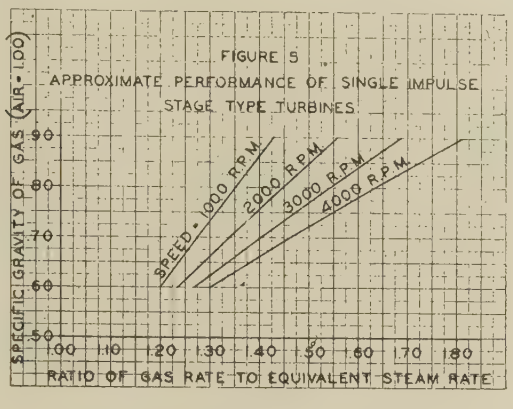

FIG. 5 APPROXIMATE PERFORMANCE OF SINGLE-IMPULSE-STAGE-TYPE TURBINES

CALCULATION OF THERMODYNAMIC PERFORMANCE

Calculating the gas consumption and changes in conditions of the gas in a turbine is somewhat more complicated than calculating the steam consumption and steam conditions in a turbine, as the equivalent of a Mollier diagram for the many compositions of gas is not available. Table 1 gives physical constants of various constituents making up the gases usually encountered in the operation of gas-expansion turbines. These physical constants apply with good accuracy in the low-temperature range encountered in these units, and are useful in calculating thermodynamic properties and changes in various gas mixtures.

Since the usual "natural gases" are mixtures of so-called permanent gases and behave according to Dalton's law, the gas mixture may be treated as a single gas with the appropriate physical constants. This concept simplifies calculations and applies accurately to all permanent gases and to all but the heaviest vapors. The necessary values for these physical constants may be found from the general gas equation

$$pV = wRT \quad \ldots\ldots [1]$$

where V denotes the total mixture volume; w_1, w_2, w_3, etc., the weights of the gas constituents; R_1, R_2, R_3, etc., corresponding gas constants and R_m the equivalent gas constant for the mixture, and T the absolute temperature deg F of the mixture. The partial pressures of the constituents of the gas when occupying the total volume V at a temperature T are expressed as

$$p_1 = \frac{w_1 R_1 T}{V}; \quad p_2 = \frac{w_2 R_2 T}{V}, \text{ etc.}$$

The total pressure p of the gas mixture is the sum of the partial pressures or

$$p = p_1 + p_2 + p_3 + \ldots\ldots$$

The total weight of the mixture is

$$w = w_1 + w_2 + w_3 + \ldots\ldots$$

From Equation [1]

$$pV = wR_mT$$

or

$$R_m = \frac{\Sigma(w_i R_i)}{w} \quad \ldots\ldots [2]$$

where subscript i denotes an individual constituent of the gas mixture.

In a similar manner, the equivalent specific heats (c_p and c_v) of the gas mixture can be determined

$$c_p = \Sigma(w_i\, c_{pi})/w \quad \ldots\ldots [3]$$

$$c_v = \Sigma(w_i\, c_{vi})/w \quad \ldots\ldots [4]$$

Then denoting the volumes that would be occupied by the constituents of the mixture at pressure p and temperature T by V_1, V_2, V_3, etc. (these are given by the volume composition of the gas)

$$V = V_1 + V_2 + V_3 + \ldots$$

and the equivalent molecular weight m_m of the mixture is

$$m_m = \Sigma\,(w_i\, V_i)/V \quad \ldots\ldots [5]$$

The foregoing equivalent constants for a mixture of gases are

TABLE 1 PHYSICAL CONSTANTS OF COMMON GASES

Name	Atomic formula	Molecular weight	Specific gravity[a] (Air = 1.00)	Specific heat of vapor[a] c_p	c_v	c_p/c_v	Gas constant R
Methane	CH_4	16.042	0.554	0.530	0.405	1.309	96.31
Ethane	C_2H_6	30.068	1.038	0.415	0.346	1.198	51.39
Propane	C_3H_8	44.094	1.522	0.376	0.324	1.161	35.03
Iso-butane	C_4H_{10}	58.120	2.006	0.357	0.312	1.144	26.59
N-butane	C_4H_{10}	58.120	2.006	0.357	0.312	1.144	26.59
Iso-pentane	C_5H_{12}	72.146	2.491	...	0.309	1.121	21.40
N-pentane	C_5H_{12}	72.146	2.491	0.347	0.309	1.121	21.40
N-hexane	C_6H_{14}	86.172	2.975	0.339	0.305	1.113	17.92
N-heptane	C_7H_{16}	100.198	3.459	0.335	0.302	1.109	15.41
N-octane	C_8H_{18}	114.220	3.944	0.330	0.311	1.060	13.51
N-nonane	C_9H_{20}	128.250	4.428	0.325	0.310	1.050	12.04
N-decane	$C_{10}H_{22}$	142.276	4.912	0.321	0.309	1.040	10.85
Ethylene	C_2H_4	28.052	0.985	0.363	0.292	1.240	55.08
Acetylene	C_2H_2	26.036	0.899	0.350	0.270	1.280	59.34
Carbon monoxide	CO	28.010	0.967	0.248	0.177	1.402	55.14
Carbon dioxide	CO_2	44.010	1.519	0.197	0.151	1.305	35.09
Hydrogen sulphide	H_2S	34.076	1.176	0.253	0.192	1.320	45.30
Sulphur dioxide	SO_2	64.064	2.264	0.154	0.123	1.250	24.10
Ammonia	NH_3	17.032	0.597	0.523	0.399	1.310	90.50
Air		28.966	1.000	0.241	0.171	1.400	53.34
Hydrogen	H_2	2.016	0.069	3.389	2.403	1.409	765.86
Oxygen	O_2	32.000	1.105	0.217	0.155	1.401	48.25
Nitrogen	N_2	28.016	0.967	0.248	0.177	1.404	54.99

[a] 760 mm 60 deg F.

in effect but weighted averages of the constants of the constituent gases.

Generally, gas mixtures are analyzed on a volumetric basis (composition by volume) instead of the weight basis (composition by weight). Weight composition can be very readily calculated from the volume composition by using the "mol" concept. (A mol is a volume measure and is equal to a quantity of gas having a weight equal to the molecular weight of the gas.)

$$w_1 = \frac{V_i m_{mi}}{V \times m_m} \quad \ldots\ldots\ldots\ldots\ldots\ldots [6]$$

This relationship will give the weight composition of a mixture in terms of the volume composition.

The equivalent ratio of specific heats of the gas mixture can be determined from Equations [3] and [4] as

$$n = c_p/c_v$$

Once the equivalent physical constants and polytropic exponent of the gas mixture is determined, calculations are simply made by the usual gas equations.

As the gas is expanded in the turbine, low temperature may be encountered in the exhaust due to the expansion and, when there are vapors in the gas mixture, as is usually the case, expansion may result in vapor condensation and also possible freezing. The theoretical temperature resulting from expansion may be determined from

$$T_2 = T_1 \left[\frac{p_2}{p_1}\right]^{\frac{n-1}{n}} \quad \ldots\ldots\ldots\ldots\ldots\ldots [7]$$

T_1 = absolute temperature at start of expansion, deg F
T_2 = absolute temperature at end of expansion, deg F
p_1 = absolute pressure at start of expansion
p_2 = absolute pressure at end of expansion
n = equivalent ratio of specific heats

Fig. 6 gives a convenient curve for determining the theoretical temperature at the end of expansion.

It should be noted that a temperature, very close to the calculated theoretical temperature at the end of the expansion, may exist at the exit of the nozzles of the turbine. However, as the gas expands in the turbine and passes through the rotating and stationary buckets and finally through the exhaust outlet of the turbine, the heat equivalent of the losses in the turbine raises the temperature of the gas to a value well above the calculated theoretical temperature. The problem of low turbine-exhaust temperatures becomes serious only with units of high-pressure-ratio design or low initial temperatures, or a combination of both.

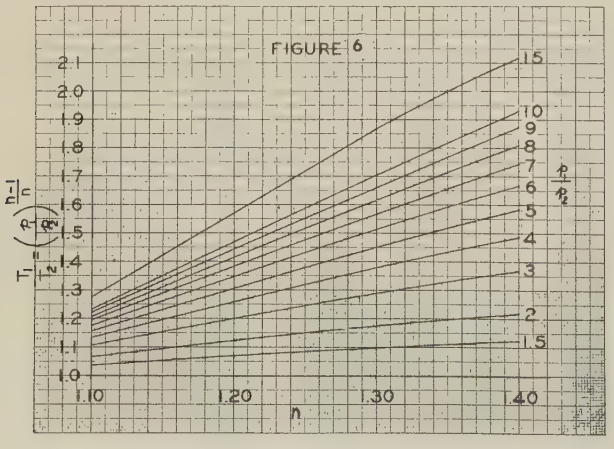

FIG. 6 CURVE FOR DETERMINING THEORETICAL TEMPERATURE AT END OF EXPANSION

When gas pressures and temperatures at the turbine inlet are such that the exhaust temperature drops below 40 F, it is advisable to preheat or raise the temperature of the gas at the turbine inlet. This preheating has been accomplished in many ways. A simple steam jacket around the gas-inlet main has been used in cases where the required degree of preheat is small. In other cases, heat exchangers or natural-gas-fired superheaters have been used.

When water vapor is present in the gas mixture, as the gas is expanded in the turbine, the temperature at the end of the expansion may reach or go below the dew-point temperature. The temperature at which condensation of the vapor content of the gas mixture starts is known as the dew-point temperature, and the gas mixture in that condition is said to be saturated with vapor. The partial pressure exerted by the vapor present in the gas mixture may be calculated readily using Dalton's law of partial pressures. The dew point then is the saturation temperature corresponding to this partial pressure of the vapor. Thus if the expansion of the gas is carried to this dew point or below it, the vapor in the gas will condense out.

The following simple calculation illustrates the method of computing the dew point of a gas mixture. Consider a gas mixture with the following weight composition to be expanded from 30 psig and 100 F to atmospheric pressure:

Weight composition		Molecular weight		Mol
CH_4	= 0.7113 divide by	16.042	=	0.04435
C_2H_6	= 0.0649	30.068	=	0.00147
C_3H_8	= 0.0384	44.094	=	0.00087
N_2	= 0.1753	28.016	=	0.00491
H_2O	= 0.0101	18.016	=	0.00056
	1.0000			0.05216

Then there is $\frac{0.00056}{0.05216} = 0.0107$ mol of water vapor per mol of gas mixture. The partial pressure exerted by the water vapor is 0.0107 (14.696) = 0.157 psia. From "Steam Tables," a pressure of 0.157 corresponds to a saturation temperature or dew point of 47 F, which is the lowest temperature to which the moist gas mixture can be expanded and cooled without condensation.

From the phenomena of supersaturation, it is known that when the gas mixture containing water vapor is expanded and the expansion crosses the saturation limit, condensation does not occur immediately but an undercooling or supersaturation up to a certain limit takes place. The vapor is cooler than the saturation temperature corresponding to the saturation pressure before condensation actually occurs. Thus before actual condensation is realized, the expansion can be carried somewhat below the dew point.

The available energy for power conversion in the turbine, resulting from the expansion of the gas, is determined from the Saint Venant relation as

$$\Delta h = \frac{R_m T_1}{778} \frac{n}{n-1}\left[1 - \left(\frac{p_2}{p_1}\right)^{\frac{n-1}{n}}\right] \quad \ldots\ldots\ldots [8]$$

where

Δh = available energy, Btu per lb
R_m = equivalent gas constant for gas mixture
n = equivalent ratio of specific heats for gas mixture
T_1 = absolute temperature at start of expansion, deg F
P_1 = pressure at start of expansion, psia
P_2 = pressure at end of expansion, psia

Fig. 6 can be used to simplify calculation of this equation, recognizing that the

$$\text{Reciprocal of } (p_1/p_2)^{\frac{n-1}{n}} = (p_2/p_1)^{\frac{n-1}{n}}$$

The energy available for conversion in the turbine is that released during expansion from the ring pressure (pressure just before the nozzles) to the exhaust pressure and not from the throttle or inlet pressure to the exhaust pressure. Thus the available energy, as given by Equation [8], should be calculated accordingly. To arrive at the nozzle-ring pressure from the throttle or inlet pressure, the throttling effect through the inlet chest, governor valves, etc., ahead of the turbine-nozzle ring must be considered. The pressure drop from the throttle or inlet to the nozzle ring is fixed by the design and is known. From this pressure drop and the inlet pressure and temperature of the gas, the pressure and temperature of the gas at the nozzle ring can be determined from the Joule-Thomson principle of throttling effect.

The efficiency of conversion in the turbine of the available energy is a function of the nozzle and bucket design, that is, the design of the flow passages. This efficiency can be determined readily by tests. Letting η = efficiency of conversion, then

$$\text{Theoretical gas rate (lb per hp-hr)} = \text{TGR} = \frac{2545}{\eta \Delta h} \quad [9]$$

The theoretical gas rate gives the necessary weight of gas flow through the turbine to realize 1 hp of converted available energy. It should be realized that the full converted power in the turbine cannot be realized at the turbine shaft because of mechanical losses, such as bearings, and also because of windage and friction losses of the turbine disks, buckets, and shrouds. The actual weight of gas flow W, to the turbine, to produce a fixed power (hp), can be determined from

$$W = \text{lb per hr} = \text{TGR} \left(\frac{\text{hp} + \text{losses}}{\text{hp}} \right) \quad [10]$$

The cubic-foot gas consumption of the turbine is readily determined from this weight flow.

The relationships given by Equations [9] and [10] can also be used to determine the approximate horsepower which can be derived from the expansion of a quantity of gas of known chemical composition, and known pressure and temperature.

The nozzle proportions for a single-stage expansion turbine can also be determined readily. From Saint Venant's equation, the velocity in feet per second that is realized from an expansion, can be expressed as

$$c = \sqrt{2g \frac{n}{n-1} R_m T_1 \left[1 - \left(\frac{p_2}{p_1} \right)^{\frac{n-1}{n}} \right]} \quad [11]$$

where g = acceleration due to gravity (= 32.16 ft per sec^2), substituting Equation [8], this may be written as

$$c = 223.7 \sqrt{\Delta h} \quad [12]$$

If Δh is taken from nozzle-ring pressure to exhaust pressure, then c is equal to the gas velocity at the nozzle-tip cross section, assuming no loss during expansion in the nozzle. The flow through the nozzle cannot be considered without losses, thus the actual velocity at the nozzle-tip cross section will be less than that calculated by Equation [12] and can be expressed as

$$c_2 = Kc \quad [13]$$

where K = nozzle velocity coefficient which is determined by test. From the work of Zeuner (1),[2] the pressure at the minimum cross section of the nozzle (throat) can be expressed in terms of the nozzle-ring pressure as

$$p_m = p_1 \left[\frac{2}{n+1} \right]^{\frac{n}{n-1}} \quad [14]$$

and the velocity at the minimum cross section can be expressed as

$$c_m = \sqrt{2g \frac{n}{n-1} R_m T_1} \quad [15]$$

Since the flow past the minimum and tip cross sections of the nozzle is constant, then

$$\frac{A_2}{A_m} = \frac{c_m}{c_2} \times \frac{v_2}{v_m} \quad [16]$$

where

A_2 = nozzle cross-section area at tip
A_m = nozzle cross-section area at throat
v_2 = specific volume of gas mixture at nozzle tip
v_m = specific volume of gas mixture at nozzle throat

From the basic gas-expansion relation

$$p_1 v_1^n = p_m v_m^n = p_2 v_2^n = \text{const}$$

we get

$$\frac{v_2}{v_m} = \left(\frac{p_m}{p_2} \right)^{1/n} \quad [17]$$

Substituting in Equation [16], we get an expression for the ratio of nozzle cross-section areas at the throat and tip as

$$\frac{A_2}{A_m} = \frac{c_m}{c_2} \left(\frac{p_m}{p_2} \right)^{1/n} \quad [18]$$

This area ratio is known as the nozzle-expansion ratio and gives the nozzle proportions that are required to handle the gas expansion from the nozzle-ring pressure to the exhaust pressure.

BIBLIOGRAPHY

1 "Theorie der Turbinen," by G. A. Zeuner, Leipzig, Germany, 1899, p. 268F.
2 "Steam and Gas Turbines," by Aurel Stodola, McGraw-Hill Book Company, Inc., New York, N. Y., 1927.
3 "International Critical Tables," 1926–1930.
4 "API Research Project 44—Tables of Physical and Thermodynamic Properties of the Hydrocarbons" American Petroleum Institute, New York, N. Y.
5 "Physical Constants of the Principal Hydrocarbons," fourth edition, Texas Company, Technical and Research Division, New York, N. Y., 1943.
6 "Handbook of Chemistry and Physics," by C. D. Hodgman, twenty-eighth edition, Chemical Rubber Publishing Company, Cleveland, Ohio, 1944.

Discussion

G. F. Gayer.[3] The author covered the subject thoroughly, both in its thermodynamic and practical aspects. No occasion for criticism could be found. However, some interest may attach to the following description of gas leakage disposing apparatus which differs from the ones described by the author.

On our single-valve mechanical-drive turbines, where the leak-

[2] Numbers in parentheses refer to the Bibliography at the end of the paper.

[3] Chief Engineer, Westinghouse Electric Corporation, Sunnyvale, Calif. Mem. ASME.

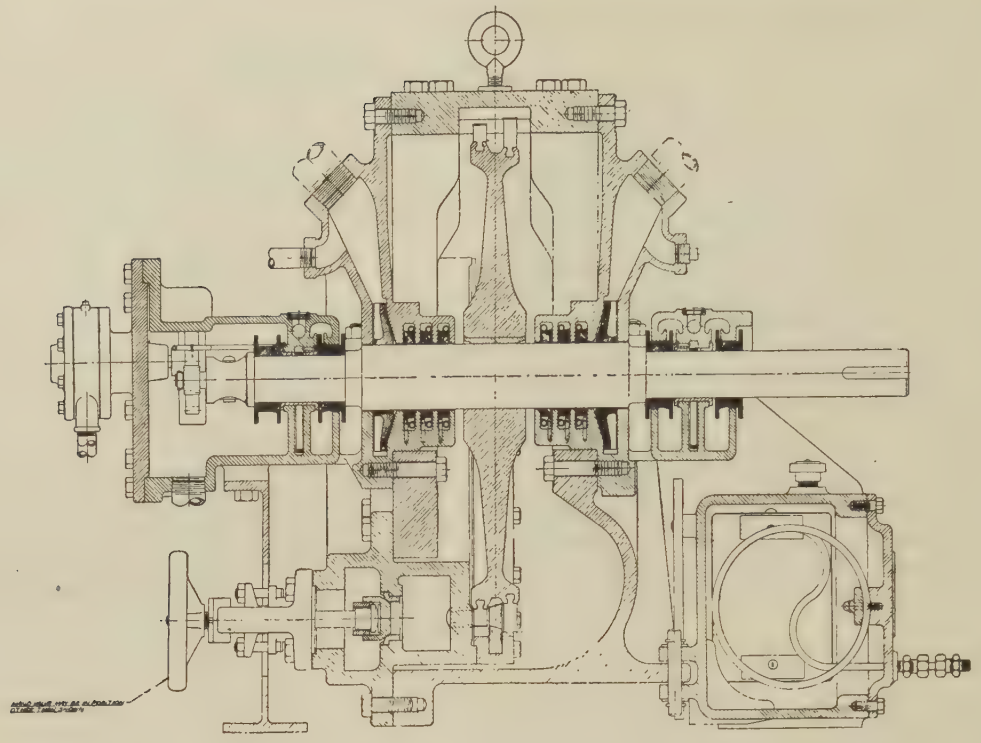

FIG. 7 CENTRIFUGE IMPELLER

age along the shaft is the principal one with which we have to contend, our practice is to use centrifugal impellers of the type shown in Fig. 7 of this discussion. These impellers installed on the outer end of the carbon glands create vacuum at their suction, which causes air to enter the outer end of the gland case and prevents gas from leaving it, both air and leaking gas being piped to the atmosphere outside the building. The slight gas leakage from two valve stems is also discharged through this system.

On multistage generator-drive turbines, where leakages along the governor-valve stem, throttle-valve stem, auxiliary oil-pump drive-turbine shaft, pressure-regulator stem have to be disposed of in addition to the leakage along the main turbine shaft, ejectors were used in a way described by the author, except that two ejectors were installed, one being used, with the other serving as a stand-by. Either ejector can be isolated from the system by closing proper valves. A vacuum of 5 in. of mercury was obtained with one ejector in the leak-off line. In case the vacuum fell to about 2 in. of mercury, a specially provided vacuum switch would operate an alarm bell, giving the operators an opportunity to switch to the other of the two ejectors and make necessary repairs of the first one. If in spite of this the vacuum drops to 1 in. of mercury, a hydraulic low-vacuum trip will trip the main throttle valve, thus shutting down the unit. The system is arranged so that the normal vacuum must be established before the throttle valve can be opened. Thus the operating personnel is protected from gas leakage resulting either from mishap to the gas-disposal apparatus or from improper operating procedure.

AUTHOR'S CLOSURE

The sealing arrangement described by Mr. Gayer is noteworthy and apparently has been used quite extensively by his company. This is another method of sealing that has been used for gas-expansion turbines and that has proved a very satisfactory arrangement. The sealing arrangements described in this paper are by no means the only satisfactory methods that have been used. Many other arrangements have been tried and have proved quite satisfactory.

It should be noted, however, that in Mr. Gayer's arrangement, the gas leakage is mixed with air and discharged and lost to the atmosphere. In the seal arrangement described in the paper and shown in Fig. 2, the gas leakage is piped into the turbine exhaust or into a low-pressure gas line. Thus there is a minimum gas loss in the system.

The leakage arrangement for multistage generator-drive turbines described by Mr. Gayer illustrates a system designed for maximum reliability and maximum protection. Such an arrangement has been used with great success in specific installations where the utmost of protection is necessary. The dual ejector system, the low-vacuum trip control of the main throttle valve and the low-vacuum-throttle interlock are protective arrangements accepted as quite standard for gas-expansion applications.

Performance Characteristics of Tight White-Oak Laminated-Stave and Solid-Stave Barrels

By R. S. KURTENACKER[1] and D. L. PATRICK[2]

The glued laminated wooden arch, which in the last 10 years has found popular acceptance in the building industry, has recently found application in the construction of barrels. This is, perhaps, one of the most drastic changes made in barrel design in many decades. Although great progress has been made in developing and improving mechanical devices for fabricating barrels, the general features of construction have remained unchanged. The use of laminated staves, together with plywood heads, results in an entirely new style of construction for which certain advantages are claimed. Such barrels, as well as barrels made of solid-wood staves and heads, were the subject of a study at the Forest Products Laboratory. The investigation was made in co-operation with the General Plywood Corporation. The purpose of the investigation was to study the performance characteristics of tight barrels of two constructions. One consisted of laminated staves and plywood heads, while the other was of solid staves and multiple-piece heads. All the barrels used in this study were supplied by the co-operator.

Fabrication of Laminated-Stave Barrels

In conventional cooperage a period of about 6 months elapses between the cutting of the tree and the completion of the barrel. This time is reduced considerably in the laminated process because of the short time needed for drying the veneer. The manufacture of this patented laminated barrel may be separated into five steps as follows:

1 Manufacture of the veneer.
2 Fabrication of head and staves.
3 Fabrication of hoops.
4 Final machining of head and staves.
5 Assembly of the barrel.

Manufacture of Veneer. The manufacture of the veneer from which the heads and staves are made follows closely the standard practice of rotary-cut veneer manufacture. From the lathe, the veneer goes to the clipper, where the defects are cut out and the veneer is cut to the required width. After it is clipped, the veneer is kiln-dried to a moisture content between 8 and 11 per cent.

Fabrication of Heads and Staves. Fabrication of the heads and staves is begun by the application of resin adhesive through the use of a glue spreader. The glue is then dried until it loses its tackiness. The veneers are graded so that the best material may be put on the inside of the barrel. The stave material is then made up into books, consisting of four layers of veneer, and pressed under a pressure of 200 psi. Application of proper heat causes polymerization of the resin bonding agent and the staves are ready for final machining.

In making the heads, polymerization of the bonding agent is accomplished by the use of a steam-heated hydraulic press operating at a temperature of 300 F and a pressure of 250 psi.

Fabrication of Hoops. The steel hoops, which are received cut to length, are punched to receive the rivets, rolled into a circular shape, riveted, and flared to the proper shape.

Final Machining of Staves and Heads. The final machining of the staves and heads is accomplished by mass-production methods. This is possible because of uniform-size staves, which are held in the shape they will have in the barrel when they are jointed. The heads are cut into circular shape and are beveled properly in a machine called a head rounder.

Assembly of Barrel. The assembly of the laminated-stave barrel is similar to standard cooperage with one important exception. These barrels use molded laminated staves and are assembled dry without steaming. Since no moisture has been added at this point, none must be removed later as is necessary in the usual manufacture of barrels. This tends to eliminate loosening of the hoops, which sometimes results from later shrinkage of the staves.[3]

General Description of Barrels Tested

All barrels used in this study were white oak unlined and uncharred and had a rated capacity of 50 gal. The barrels were assembled with six steel hoops, each of which was assembled with two rivets. All bungholes were approximately 2 in. diam and were tapered with the small diameter on the inside of the barrel. All bungs were manufactured of yellow poplar.

Solid-Stave Barrels. The solid-stave barrels, which were obtained by the co-operator through purchase on the open market, were made of white oak. The staves varied in number from 30 to 36 per barrel and averaged $34\frac{3}{16}$ in. in length. The thickness of the staves was $\frac{3}{4}$ to $\frac{25}{32}$ in., while the width of the staves measured at the bilge varied between a minimum of $\frac{15}{16}$ in. and a maximum of $5\frac{3}{16}$ in. The bilge circumference was approximately 79 in. All bung staves (the stave containing the bunghole) were more than $3\frac{1}{4}$ in. wide.

The heads, which were of multiple-piece solid white-oak construction, were so located in the croze that the chime extended approximately $\frac{11}{16}$ to $\frac{13}{16}$ in. beyond the outside head surface. All solid-stave barrels had heads that were $\frac{13}{16}$ in. thick and were fabricated of at least six pieces but not more than eight pieces. The headpieces were assembled with two hickory dowels, $\frac{5}{16}$ in. diam, to each head joint and located at about one third of the length of the joint from its ends.

Laminated-Stave Barrels. The laminated-stave barrels, which were fabricated at the Container Division of General Plywood Corporation, New Albany, Ind., were made of white-oak veneer. The laminated staves were made of four layers of $\frac{3}{16}$-in-thick

[1] Engineer, Forest Products Laboratory, Madison, Wis.
[2] Chemical Engineer, General Plywood Corporation, Louisville, Ky.

Contributed by the Wood Industries Division and presented at the Annual Meeting, Atlantic City, N. J., December 1–5, 1947, of The American Society of Mechanical Engineers.

 Paper No. 47—A-127.

[3] For more complete details of the production procedure, see "Roll Out the Barrels," by C. W. Hill, *Cosgroves Magazine*, July, 1947.

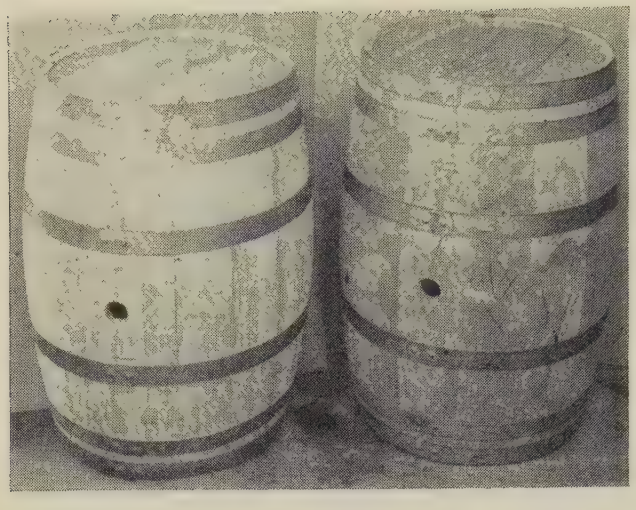

FIG. 1 LAMINATED-STAVE PLYWOOD-HEAD BARREL AT RIGHT AND SOLID-STAVE, MULTIPLE-PIECE, SOLID-WOOD-HEAD BARREL, LEFT, SHOWING WIDE VARIATION OF STAVE WIDTHS IN SOLID-STAVE BARREL AND UNIFORM WIDTH OF STAVES IN LAMINATED-STAVE BARREL
(The chime designs in the two barrels which are apparent here are also shown in cross section in Fig. 2.)

rotary-cut white-oak veneer laminated together with a phenol-resin glue. The finished staves were approximately $^3/_4$ in. thick. The length of the staves averaged $34^7/_8$ in. All except six of the laminated-stave barrels had 14 staves of identical size. These six barrels had 12 "full-size staves" and three "two-thirds-size staves." All full-size laminated staves were approximately $5\ ^9/_{16}$ in. wide at the bilge, while the two-thirds-size laminated staves were approximately $3^3/_4$ in. wide at the bilge. The bilge circumference was approximately 78 in.

The heads of these barrels were plywood construction fabricated of five plies of $^3/_{16}$-in-thick rotary-cut white-oak veneer bonded together with a phenol-resin glue. These heads were $^{15}/_{16}$ in. thick and were so located in the croze that the chime extended approximately $1^1/_{16}$ in. beyond the outside surface of the barrel. Some of the construction details of the two kinds of barrels are pictured in Figs. 1 and 2.

METHOD OF TESTING

All tests in this study were conducted with the barrels filled with water. A separate group of five barrels with laminated staves and five barrels of solid staves was subjected to each of the following five tests:

(*a*) Compression test on bilge.
(*b*) Compression test on edge.
(*c*) Internal hydrostatic-pressure test.
(*d*) Drop test on bilge.
(*e*) Diagonal drop test on chime.

Compression Test on Bilge. For the compression test on bilge a 25,000-lb-capacity universal testing machine was used. The barrels were placed between the upper and lower machine platens so that the vertical axis of the barrel (head to head) was parallel to the testing-machine platens. The barrel was then filled with water and bunged. In order to apply a concentrated load at the bilge, steel blocks (15 in. long × 7 in. wide × $4^5/_8$ in. thick) were placed between the top and bottom machine platens and the barrel. These were placed with the length of the block crosswise of the barrel, and the point of initial contact centered on the blocks, Fig. 3. By the use of metal drainage pans and a platform scale, the amount of water which leaked from the barrel under test could be recorded. The compression load was applied by the top platen moving downward at a constant rate of speed of 0.2 ipm.

Compression Test on Edge. For the compression test on edge, the same testing machine and arrangement of equipment, except for the load-concentration blocks which were omitted, were employed as in the compression test on the bilge. The sequence of operations differed in that the barrels were loaded and bunged before placing them in the testing machine. The barrels were supported upon one contact point of the bottom chime and the load was applied by the top machine platen moving downward on the top chime at a contact point. A diagonal line through the barrel from contact point to contact point was perpendicular to the machine platens.

Internal Hydrostatic-Pressure Test. Each barrel was supported in a horizontal position for the internal hydrostatic-pressure test. Again the platform scale and drainage pans were used to record water leakage. The barrel to be tested was fitted with a threaded metal bung plug securely screwed into the bung hole until a tight seal was made. Through the center of the bung plug was a threaded hole. By means of pipe and pipe fittings, there was attached to this plug a water inlet valve, a bleeder valve, and a 60-lb pressure gage reading in $^1/_4$-lb increments. The water inlet valve was attached to the city water supply, and by means of the bleeder valve the barrel and connecting pipes were filled with water so as to exclude as much air as possible.

By the use of the inlet valve, the test was started by raising the pressure to 2 psi and holding it there for 2 min. The amount of water leakage, if any, was recorded after the 2-min interval. The pressure was then raised to 4 psi and held for 2 min. This process was continued, increasing the pressure 2 psi each time and holding it for a period of 2 min, until failure, or until leakage from the barrel was in excess of 1 lb per min.

It is recognized that this internal hydrostatic-pressure test does not represent a condition that would actually be met in use. Under normal conditions the barrels are not filled to the extent that all air is expelled. Instead, adequate space is left to compensate for the expansion of the contents. To study the performance of the barrels without prolonged observations, however, the hydrostatic-pressure test as described was used.

Drop Test on Bilge. The barrels for the drop test on the bilge were filled, bunged, and weighed before dropping. They were then supported at the top and bottom chime with a set of metal grab hooks so that the lengthwise axis of the barrel was parallel to a metal plate resting on a concrete floor. The barrels were lifted by means of a hoist and were dropped by actuating a tripping device located between hoist load hook and grab hooks.

For the first drop the barrel was raised to a height of 3 in. and dropped. The height of the next drop was 6 in., and the succeeding drops were increased by height increments of 3 in. per drop. All drops for any one barrel were upon the same point on the bilge. After each drop there was a 3-min waiting period after which the barrel was weighed to determine the outage, if any. This was continued until the barrel had lost at least one half of its contents.

Diagonal Drop Test on Chime. The test procedure for the diagonal drop test on the chime was identical to that of the drop test on the bilge, except that the barrel was supported by the grab hooks in such a way that the barrel was tilted so that the force of the drop impact was received by a point on the bottom chime. Each drop was upon the same point of the bottom chime.

OBSERVATIONS, TEST RESULTS, AND DISCUSSIONS

Observations Made Prior to Scheduled Tests. During the filling of the barrels with water it was noticed that the solid-stave barrels had small leaks caused by wormholes that had to be plugged. There were also other wormholes that had been plugged previously. The laminated-stave barrels were tighter in this respect and did not contain any wormholes that had to be plugged.

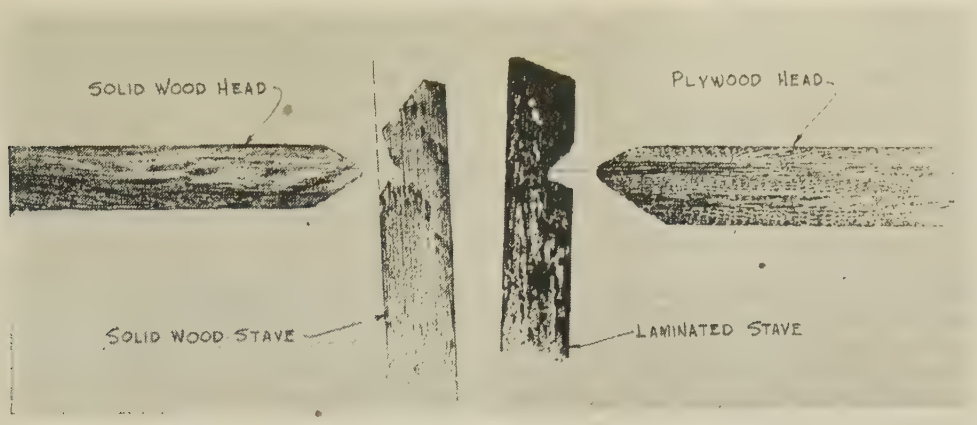

FIG. 2 ACTUAL CROSS-SECTION WOOD PRINTS OF CHIME, CROZE, AND HEAD OF SOLID-STAVE BARREL, LEFT, AND LAMINATED BARREL, RIGHT

There was some seepage around the croze of the solid-stave barrels. After the barrels had had a chance to swell, this seepage was usually eliminated. The laminated-stave barrels showed no seepage around the croze nor between staves while being filled.

Subsequent to testing and during the testing program, the difference in the design of the chime and croze of the solid-stave barrel and laminated-stave barrel became evident. The difference in the two designs of chime and croze is shown by the cross-sectional illustration, Fig. 2.

Under a pressure or force applied to a small portion of the chime arc, it was observed that the wood structure of the solid-stave chime became indented and compressed the wood fibers while, under the same conditions, the wood structure of the laminated-stave chime became fractured by splitting or breaking across the grain at the croze.

The better performance of the solid-stave chime under these conditions and during subsequent testing could be partially explained by considering obvious differences in chime and croze design. The cross-sectional print shows that the chime for the laminated stave is approximately $^1/_4$ in. higher (or longer) than the chime for the solid stave when measured from the same relative point in the croze. Also the solid stave is thicker at the croze than is the laminated stave. It can be shown that a greater unit stress will occur at the croze of the laminated stave than at the croze of the solid stave if an equal force is applied to the end of each type of chime.

The tendency of the chime and croze to break across the grain of the stave did not seem to affect seriously the ability of the laminated-stave barrel to resist leakage at that point. The performance of the laminated-stave chime can be improved by a slight change in design.

Compression Test on Bilge. The results of the compression test on the bilge showed that the laminated-stave barrels, by sustaining an average maximum load of 10,292 lb at an average compression of 3.05 in., withstood greater compressive loads with less deformation than the solid-stave barrels, which withstood an average maximum load of 9275 lb at average compression of 4.06 in.

The test results also indicated that the laminated-stave barrels with an approximate average outage of only 6.5 lb of water just prior to maximum load appeared to be tighter than the solid-stave barrels tested, which had an average outage of 62 lb just prior to maximum load.

A typical failure of the solid-stave barrels was usually a splitting of the staves parallel to the grain or a breaking across the grain of the stave.

The laminated staves had some slight splitting parallel to the grain and near the edge of the stave. This was apparently caused by the loading block being pushed into the barrel with the result that the staves were splintered at the edges near adjacent staves. There was also some splitting and fracturing of outer laminations.

FIG. 3 LAMINATED-STAVE PLYWOOD-HEAD BARREL ARRANGED IN 25,000-LB TESTING MACHINE FOR COMPRESSION TEST ON BILGE

Compression Test on Edge. In the compression tests on edge, the laminated-stave barrels reached an average maximum load of 21,446 lb at an average compression of 3.64 in., as compared to an average maximum load for the solid-stave barrels of 19,141 lb at an average compression of 5.04 in. This test also provided information on the relative tightness of the barrels tested. When the maximum load was reached, the average outage of the five laminated-stave barrels was 1.6 lb of water, as compared to the average outage for the five solid-stave barrels of 122 lb of water. It may be of interest to note that two of the solid-stave barrels had lost more than one half of their water contents at maximum load, while at the same point in the tests, two of the laminated-stave barrels had not lost a sufficient amount of their water contents to register on the scale.

The typical failure of the laminated-stave barrels when tested in diagonal compression usually developed in the following sequence: (*a*) Top and bottom chime crushed at points of contact; (*b*) top and bottom chime split near glue line of laminations from the croze and broke off at the croze without serious leakage; (*c*) individual staves slipped past each other longitudinally, causing

the top head to buckle; (*d*) the staves continued to slide past each other until the stress created at the top croze caused the top head to slip out of the croze.

The final failure of the solid-stave barrel usually developed in the following manner: (*a*) Crushing of top and bottom chimes at points of contact; (*b*) staves slipping past each other longitudinally; (*c*) top and bottom headpieces slipping past each other parallel to the grain; (*d*) top or bottom head or both starting to buckle; (*e*) top or bottom head failing at point of inflection of buckling.

In the compression test on edge, as well as in the previously discussed compression test on the bilge, the solid-stave barrels showed more slippage of their staves and headpieces than the laminated-stave barrels. This increased slippage in the solid-stave barrels undoubtedly accounted in part at least for their lower resistance to distortion. Any longitudinal movement of the staves of the barrels would create bending stresses in the barrel heads because the croze was forced out of line. The multiple-piece solid-wood heads, which apparently were not assembled with adhesive, only had the two hickory dowels in each joint as the principal means of resisting any tendency for movement of one headpiece past the adjacent headpiece. On the other hand, the plywood head, owing to the inherent characteristics of its one-piece construction, presented a better means of resisting the stresses created in the barrel head by the longitudinal movement of the staves tending to force the croze out of line. This characteristic of the plywood heads to resist the tendency for the croze to be forced out of line might very well have been an important factor contributing to the over-all stiffness qualities of the laminated-stave barrel.

Internal Hydrostatic-Pressure Test. In the internal hydrostatic-pressure tests, the principal failures for both the laminated-stave barrel and the solid-stave barrel occurred in the heads.

The laminated-stave barrels withstood greater internal pressures and also exhibited greater tightness than the solid-stave barrels. The laminated-stave barrels with plywood heads failed at an average of 29 psi, while the solid-stave barrel with multiple-piece head failed at an average pressure of 15 psi. In the laminated-stave barrels a leakage of 1 lb of water did not occur until an average pressure of 27.6 psi was attained, while the solid-stave barrels had a leakage of 1 lb at an average pressure of only 5.6 psi.

In the multiple-piece head, the reed flagging was forced from between the joints in the head, and the barrel leaked so that pressure could not be maintained. In two instances, an individual piece in a head broke across the grain. In the plywood-headed barrel, the failures were first apparent by a breaking across the grain or split parallel to the grain of the outer plies, but there was no leakage through the heads until the break was completely through the entire head. Sometimes part of the head that failed pulled from the croze, but other times it remained tight in the croze.

In considering the results of the tests where the final failure was breaking of the heads, it is difficult to analyze all the factors influencing the resistance of the heads of these barrels to the forces set up by the internal pressure of the hydrostatic-pressure test or to the surge of water resulting from the drop tests (to be discussed later). Although the plywood heads were $^1/_8$ in. thicker than the solid-wood heads, it is felt that perhaps this did not affect the performance of the plywood heads so much as the fact that the plywood heads were of one-piece construction, as compared to the multiple-piece solid-wood heads.

Drop Test on Bilge. In the drop test on bilge, the laminated-stave barrels gave better performance than the solid-stave barrels that were tested. The approximate cumulative amount of work absorbed at an outage of 1 lb of water was 5932 ft-lb for the laminated-stave barrels against 1793 ft-lb for the solid-stave barrels. At final failure, the approximate cumulative amount of work absorbed was 17,293 ft-lb for the laminated-stave barrels. The comparable figure for the solid-stave barrels was 5246 ft-lb, or only about one third of the value obtained for the laminated-stave barrels.

Cumulative work absorbed was determined by taking the summation of the products obtained by multiplying the individual height of drops, in feet, by the gross weight of the barrel before the drop.

The laminated-stave barrels withstood average maximum drop heights of approximately 48 to 51 in., while the solid-stave barrels withstood average maximum drop heights of 24 to 27 in.

When the solid-stave barrels were dropped, the staves receiving the impact tended to flatten out, thus moving past the other staves and setting up a stress in the heads near the croze. This, coupled with the surge of the water contents, finally resulted in the heads slipping out of the croze, and the breaking across grain of individual headpieces. These breaks generally occurred at the point where the dowels were located.

When the laminated-stave barrels were dropped, the staves receiving the contact also tended to flatten out and in so doing caused the head hoops to loosen and to start slipping off the end of the barrel. When this happened, leaks developed at the croze.

The laminated-stave barrels bounced after the initial impact on the bilge and on the return impact the chime received an additional partial blow and eventually became broken off at the croze. As a result, the heads were forced out of the croze because they had to absorb the inertia or liquid surge of the water contents when the barrel was dropped.

Diagonal Drop Test on Chime. In the diagonal drop test on the chime, which is a severe test of the ability of a barrel to absorb shock and resist distortion, the laminated-stave barrels again withstood more drops than the solid-stave barrels even though the chime of the laminated-stave barrel was usually damaged on the first drop (3 in. height). During the following drops, the chime of the laminated-stave barrel at the point of contact continued to crush, break, and split at the croze. There was no serious leakage from this point of contact until the head slipped out of the croze or fractured from arresting the inertia of the water contents. The head also fractured at the point of drop contact. Failure always occurred in the bottom head and developed when it broke across the grain or slipped out of the croze.

The approximate cumulative amount of work absorbed at an outage of 1 lb of water was 4349 ft-lb for the laminated-stave barrels, against 1976 ft-lb for the solid-stave barrels. At final failure, the comparable figures were 5940 ft-lb for the laminated-stave barrel against 2532 ft-lb for the solid-stave barrel or less than one half of the value obtained for the laminated-stave barrel. The laminated-stave barrels withstood average maximum drop heights of approximately 27 to 30 in., while the solid-stave barrels withstood average maximum drop heights of 24 to 27 in.

In the solid-stave barrels, the chime receiving the impact withstood the impacts better than the chimes of the laminated-stave barrels. While the edges of the solid-stave chimes were crushed at the point of contact, they did not fracture nor shear off as did the chimes of the laminated staves. The bottom head of the solid-stave barrels broke across the grain at the location of the dowels or else slipped out of the croze.

Conclusions

Although it is apparent from this study that the barrels manufactured with laminated staves and plywood heads gave better performance in the laboratory tests than the barrels manufactured with solid staves and multiple-piece solid-wood heads, it should be remembered that this conclusion, as well as those which follow, refers specifically to the two groups of barrels provided for

the investigation. In the solid-stave barrels, the width of the staves varied greatly, and the number of staves was about double the number used in the laminated-stave barrels. Similar laboratory tests of solid-wood barrels having staves comparable in size and number to those of the laminated-stave barrels might easily yield entirely different results.

The laminated-stave barrels tested sustained greater average maximum loads and with less distortion than the solid-stave barrels in both the compression test on bilge and the diagonal compression test on edge.

The solid-stave barrels were more susceptible to loss of liquid contents during filling and during testing than were the laminated-stave barrels. The solid-stave barrels leaked and failed structurally at lower internal hydrostatic pressures, and they suffered greater outage during the other tests than the laminated-stave barrels.

The laminated-stave barrels withstood more drops and from greater heights than the solid-stave barrels before serious structural failures occurred.

The solid-stave barrels were lighter in weight and suffered less damage to the chime than the laminated-stave barrels. The tendency for the laminated-stave chime to break or split readily at the croze during the edgewise drop and compression tests did not seriously affect its resistance to leakage. It appears possible to improve the performance of the laminated-stave chime by a slight change in its design.

This study did not provide information regarding the ability of the barrels to resist leakage under storage conditions conducive to alternate shrinking and swelling of the wood, nor did it indicate their adaptability for aging of alcoholic beverages.

Discussion

E. G. Stern.[4] This report on the performance characteristics of tight white-oak barrels brings to light outstanding test data in favor of the laminated-stave plywood-head barrel.

Both the solid and the laminated staves of the tested barrels were $^3/_4$ in. thick. The laminated stave had a chime of $1^1/_{16}$ in., and the solid stave had a chime of $^{11}/_{16}$ to $^{13}/_{16}$ in. This difference in the length of chimes may be an explanation for failure of the laminated-stave chime in the edge-compression test, since the larger chime of the laminated stave provided a larger lever of the eccentrically loaded barrel edge. Thus splitting or breaking across the grain failures occurred, while the shorter lever in the shorter chime of the solid stave did not result in excessive internal stresses. The reported deficiency of the laminated stave may be attributed to the particular design of the chime and not be inherent to the laminated construction.

The staves under observation were solid or parallel-laminated with four layers of $^3/_{16}$-in-thick veneers. It is believed that a cross-laminated stave with three parallel-laminated veneers and with one cross-laminated veneer, that is, the second veneer from the inside having grain perpendicular to the other three veneers, would have certain merits worthy of investigation. Contrary to the need for balancing veneers of flat panels, an unbalanced compound-shaped stave is entirely feasible. Such cross-laminated construction would result in a greater dimensional stability: (1) allowing final machining of croze, howel, and chime in a single operation before assembly of the staves; (2) with complete interchangeability of machined staves during replacement of staves in finished barrels; (3) with more permanently tight barrels; (4) with continuously tight hoops; (5) preventing lengthwise splitting of staves, reported to be a serious limitation in the performance tests. It is evident that replacement of a parallel-laminated veneer with a cross-laminated layer also would result in certain property decreases. Should this weakening be too critical, it may be justified to increase the four layers of veneers by one, although it is possible that increased production cost and time may outweigh the advantages attained.

An explanation would be desirable why the laminated staves are not of uniform width, that is, why twelve "full-size" and three "two-third-size" staves are used.

It would also be of interest to learn what patent claims were granted for the discussed type of construction.

Is it advantageous to mold rotary-cut veneers in their natural curvature in order to prevent splitting of veneers during molding, or is it feasible to mold veneers in disregard of such a possible advantage?

The statement is made that the laminated-stave plywood-head barrel is lighter than the solid barrel. Data on the test weights of both types of barrels would be welcome.

Authors' Closure

It appears that Mr. Stern has thoroughly studied and considered the paper and has realized some of the problems it presents. His analysis of the failure of the laminated-stave chime parallels quite closely our own explanation of this problem.

The suggestion made about a possible cross-laminated stave appears to be feasible. Mr. Stern has given considerable thought to this idea and he has not lost sight of the fact that even though a cross-ply might create certain advantages, it might at the same time result in certain property reductions.

The use of the "two-thirds-size" stave is purely for the purpose of economy. By the use of staves of this size, veneer material may be utilized which has had some slight defect removed to make the veneer of proper quality but not of sufficient width to make a "full-size" stave.

As to the patent claims, it is understood that T. D. Perry, an engineer with Resinous Products and Chemical Company, Philadelphia, Pa., has the history of the patent rights of the laminated-stave barrel.

If the statement is made in this paper that the laminated-stave barrels tested were lighter in weight than the solid-stave barrels tested, it is an error and the authors are sorry that such was the impression. The following table gives some average descriptive data for the barrels tested.

	Laminated-stave barrel	Solid-stave barrel
Bilge, circumference, in.	78	79
Barrel height, average, in.	$34^7/_8$	$34^1/_8$
Capacity, gal.	50 to 55	50 to 55
Weight, average, lb.	75.1	70.6

[4] Research Professor and Head, Department of Wood Construction, Director, Wood Research Laboratory, Virginia Polytechnic Institute, Blacksburg, Virginia. Mem. ASME.

An Investigation of the Variation in Heat Absorption in a Pulverized-Coal-Fired Water-Cooled Steam-Boiler Furnace

I—Variations in Heat Absorption as Shown by Measurement of Surface Temperature of Exposed Side of Furnace Tubes

By L. B. SCHUELER,[1] NEW YORK, N. Y.

This report is one of several current formal reports (1)[2] covering the activities of the ASME Special Research Committee on Furnace Performance Factors. These investigations were undertaken early in 1945, as one of the direct contributions of the Committee to the fundamental knowledge of heat-transfer processes in water-cooled boiler furnaces. The present investigation is still under way and this report is an introduction to and description of the project along with a presentation of significant data procured and analyzed up to December, 1946. The investigation is being carried out on boiler No. 11 at the Tidd Plant of The Ohio Power Company, Brilliant, Ohio. Directly co-operating with the Committee in the installation of apparatus, testing, and analysis of data are the American Gas and Electric Service Corporation, Combustion Engineering Company, and U. S. Bureau of Mines, Pittsburgh Experiment Station. It was at the initial suggestion and invitation of Mr. Philip Sporn, a member of the main Committee, that a comprehensive investigation of furnace-heat absorption on a full-scale unit was held desirable, and one of the Tidd Plant boilers was made available to the Committee for such an undertaking.

Introduction

THIS report covers the results of tests conducted under the auspices of the ASME Special Research Committee on Furnace Performance Factors to investigate the variation and distribution of heat absorption in a specific water-cooled boiler furnace under various conditions of operation. The use of a multiplicity of thermocouples installed in furnace-wall tubes of a large central-station boiler provides the first comprehensive picture of the heat-absorption pattern in such a furnace. The heat-absorption rate is involved indirectly in that the furnace-wall-tube skin temperatures are measured with thermocouples, and the absorption rate is known to be related directly thereto as a function of the tube-temperature elevation above boiler-water saturation temperature. A similar method of measuring heat absorption has been used for some time, as reported by E. G. Bailey (2), and involves the use of thermocouples embedded in wall blocks at various depths to determine the temperature gradient.

The provision of a vertical tilting mechanism for the burners permitted producing wide variations in tube temperatures, and corresponding heat-absorption rates, as desired.

Three series of tests comprising 14 complete individual tests have been run and analyzed and are reported herein. The tests cover measurements of temperatures of 135 furnace-wall tube-face thermocouples and 4 cold-side tube thermocouples to measure base saturation temperature, along with all supporting operating data and notes. All thermocouples are wired to a single 7-bank 21-point potentiometer recorder which records thermocouple temperatures consecutively and continuously throughout the testing period. The tests are designed to develop the influence of some of the more basic operating variables such as rating, excess air, burner position, and furnace-wall cleanliness. The wall cleanliness was under some degree of control as produced by use of wall soot-blowing elements in the upper portion of the furnace. Other influences, such as variation of wall-tube cleanliness (or conversely, permanent dirtiness or "aging") and flame distribution were also sought.

The ΔT (furnace-tube temperature minus saturation temperature) values have been averaged for each thermocouple and subjected to analytical treatment to determine the relation between them and the better-known design and operating variables. These ΔT values have also been plotted as isotherms to provide a convenient "picture" of the relative heat-absorption pattern in the furnace for each test. Several analyses of variation in ΔT values during a given test have been made, and these illustrate the cyclic fluctuation in tube temperature as caused by variable ash coverage. Photographs of furnace walls, taken during one of the testing periods, are shown and can be related reasonably to the wall-tube ΔT patterns in a number of cases.

Other analyses indicate the substantial vertical gradient in furnace heat absorption, and the pronounced effect of tilting the burner nozzles both on local and over-all heat-absorption levels. An empirical constant is presented to permit direct conversion of the over-all average furnace ΔT into equivalent total heat absorption. This constant is subject to critical checking and is not firmly substantiated but is offered to stimulate possible further analysis of the data by others.

Object of Investigation

The object of that portion of an extensive boiler-furnace-performance investigation reported herein is to measure the relative heat-absorption rate at the various selected points of a water-cooled steam-boiler furnace under various operating conditions. The means of measurement of heat-absorption rate are indirect,

---

[1] Assistant Mechanical Engineer, American Gas and Electric Service Corporation. Mem. ASME.

[2] Numbers in parentheses refer to the Bibliography at the end of the paper.

Contributed by the Special Research Committee on Furnace Performance Factors in co-operation with the Fuels, Power, and Heat Transfer Divisions and presented at the Semi-Annual Meeting, Chicago, Ill., June 16–19, 1947, of The American Society of Mechanical Engineers.

that is, tube furnace-face surface temperatures are measured by means of thermocouples, and the relative absorption rate is assumed to be directly proportional to the elevation of tube-surface temperature above boiler-water saturation temperature. This temperature difference ΔT, is assumed to be closely proportional to the heat-absorption rate at the point of measurement, but is not intended to be an accurate index of the absolute heat-absorption rate at that point, although some estimates of this latter item will be given as a matter of general interest. By successive testing periods it is believed that some general trends in the characteristics of furnace absorption and their variation with time, cleanliness, rating, and other factors can be established. In this way a more detailed understanding of the process of heat absorption in a furnace will be made available to supplement the present limited knowledge which is restricted more or less to overall effects.

Apparatus Used

The boiler on which the tests are being carried out is a conventional three-drum bent-tube unit with a dry-ash-removal hopper-bottom furnace and with pulverized-coal firing through corner burners into the completely water-cooled furnace. The general arrangement of the unit is shown in Fig. 1. The furnace-wall tubes on all four sides are bare 3-in-OD tubing on $3^1/_8$-in. centers and are backed by vertical steel sealing strips between tubes. The furnace-roof tubes are 3-in-OD tubing with 1-in-wide fins on the center line and arranged on 6-in. centers. The boiler screen consists of 4 rows of 3-in-OD tubes, on $12^1/_2$-in. centers, laterally. The unit is designed for 1525 psi pressure, and design operating conditions are 1375 psi and 925 F steam at the superheater outlet at 475,000 lb per hr maximum continuous output. The burners fire tangentially from each corner to a 2-ft 6-in-diam center-firing circle and are provided with vertically adjustable coal and air nozzles which have an adjustment range of 30 deg tilt up or down from the normal horizontal position. This feature permits considerable variation in distribution of furnace heat release, and corresponding absorption, to be produced as desired, and has been extensively explored during the test program here reported.

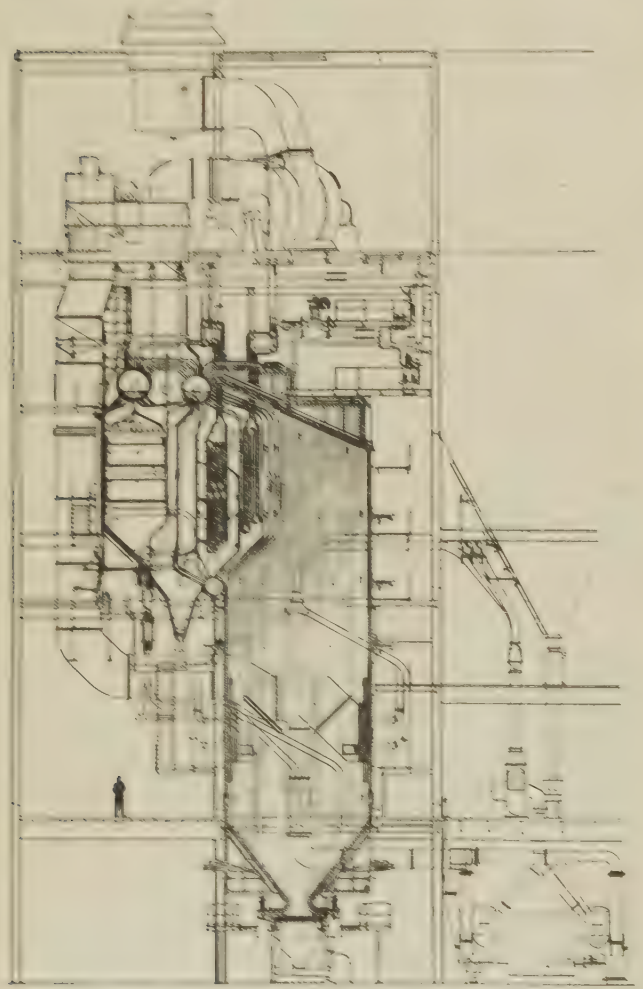

Fig. 1 General Arrangement of Boiler No. 11

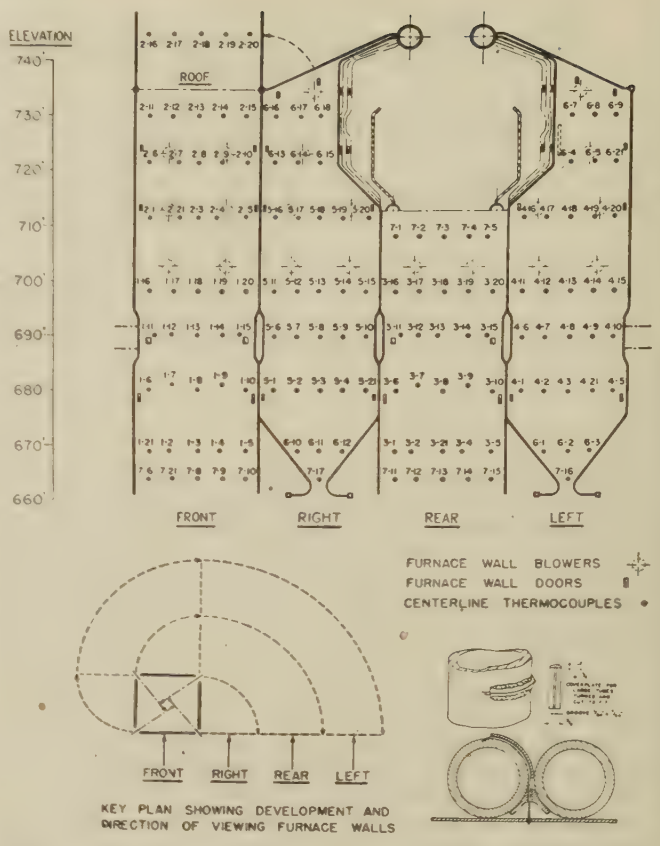

Fig. 2 Key Plan and Thermocouple Location Identification Diagram

The thermocouples which measure temperatures of the outer tube surface are installed substantially as described by Humphreys (3), and consist of chromel-alumel No. 22 gage glass insulated duplex wire which passes through a $^1/_8$-in-diam hole in the sealing strip between the wall tubes and then through the groove in the guard ring which is welded to the tube. The hot junction is made at the furnace face center line, or tangent, of the tube in all cases. The location arrangement and installation details of thermocouples are shown in Fig. 2, which is a development of the furnace walls and roof. Also shown are furnace inspection doors, furnace-wall soot blowers and burner-nozzle center lines for the four corners. No thermocouples are installed in the extension of the rear wall tubes which form the boiler front screen due to difficulty in carrying leads out of the hot gas zone. The thermocouple designation numbers are given in Fig. 2 and will be referred to as such in all subsequent data and curves. It should be noted that this diagram represents thermocouple location as viewed from "outside" the furnace.

There are a total of 135 furnace-tube center-line thermocouples and 4 furnace cold-face saturation base thermocouples installed, and each of these is carried outside the wall into a 3-in. pipe nipple which is welded to the outer furnace casing. A cap is fitted on the end of each to minimize air leakage into the furnace. The wires come out of the pipe nipple through a $^1/_4$-in. hole and pass into a "Wiremold" conduit system which picks up all wires and carries them to the recording instrument. This provides substantial protection for the extended testing program involved. The thermocouple wires are brazed to chromel-alumel lead wires directly at the entrance to the Wiremold channel. This channel has a readily removable cover over its entire length so that access for inspection or repair is facilitated. All thermocouple lead wires are carried to a single 140-point Leeds & Northrup potentiometer-recorder which consecutively records the temperature of all thermocouples, or any preselected group, or individual ones.

The instrument is a conventional 21-point high-speed Micromax unit supplemented by a switching unit which has 7 groups of 21 contacts which are switched on and off automatically and in sequence in any preselected manner. Thermocouples are identified by numbering from 1 to 21 for all of the 7 groups and are further identified by a group-bank identification number which is one of the 21 points and prints at the upper extremity of the chart range to identify the group being recorded.

Normal operating time is approximately 12 sec for each point so that a complete cycle of 139 temperatures and 7 identification numbers are recorded in about 30 min. This represents a reasonable compromise between extremely high-speed recording, which gives a more detailed record of rapid fluctuations in temperatures but involves an impracticality in the volume of data to be analyzed, and a conventional slow-speed instrument which does not reveal many of the significant variations in temperature over shorter time intervals. The instrument is mounted near the boiler, and is shown in Fig. 3 which is a photograph of the actual installation. During testing periods the instrument is operated continuously and requires only infrequent attention in the way of checking galvanometer balance for evidence that it is functioning properly. The saving in man power during tests by use of this instrument is very considerable, and it has proved itself a very worth-while investment.

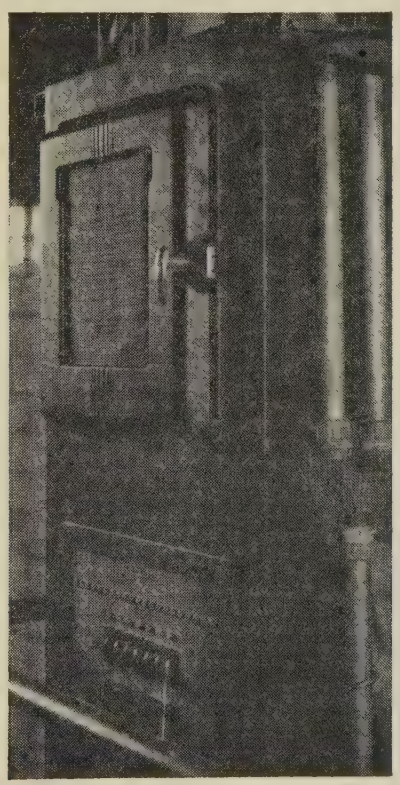

Fig. 3 L & N 140-Point Potentiometer-Recorder

General operating data are provided by the existing boiler-unit instrumentation and include all necessary flowmeters, temperature and pressure recorders, and a flue-gas oxygen analyzer. Coal scales weigh all coal fed to the boiler under test, and samples can be taken readily for analysis. A generous and well-located quota of furnace inspection doors is provided for visual observation of furnace-wall and flame conditions during testing periods. The furnace-wall soot blowers permit means for establishing a basic "clean" condition at the start of tests whenever desired. The wall soot-blower installation, as shown in Fig. 2, does not permit cleaning all portions of the walls but only that above the burners. The surface below approximately elevation 690 ft is not affected appreciably by the operation of blowers.

Report on Tests

There have been three[3] series of complete tests run and analyzed and these are reported herein. The essential operating data, along with several supporting items derived from the data, are given in Table 1. The first series of tests (Nos. 1, 2, 3, and 4) were carried out about 3 months after initial operation of the boiler. During this period operation was quite steady at about 400,000 lb of steam per hr output. The soot-blower installation had not been completed so that the furnace walls had considerable ash covering which was not disturbed during this first series of tests. This series was considered more as a "shake-down" run for the apparatus as well as the test crew, but the data are none the less complete and as accurate and well taken as for any of the later tests, and are interesting in that they represent "uncontrolled" conditions as to furnace-wall cleanliness. The full range of burner-nozzle tilting was explored during this first series. These tests and all others reported in Table 1 were carried out in conjunction with and simultaneous with other tests reported elsewhere (1). The duration of the tests was established by the requirements of these other investigations.

The second series of tests (Nos. 10, 11, 13, 14, and 15 in Table 1) somewhat paralleled those of the first series although a higher rating was planned but could not be reached due to limitation of pulverizer capacity by the high-moisture coal at that time. The soot blowers were in operation and were used to clean the furnace walls prior to each test, except No. 10 which was run with "dirty walls" to provide a basis for comparison with data of the first series of tests. The remainder of this series substantially duplicated runs of the first series except for wall cleaning and for the intermediate tilt position of test No. 14, where only lower burners were tilted downward. A small number of thermocouples which had failed or showed inconsistent readings during or after the first series of tests were renewed prior to this second series so that an almost complete quota of points was used.

The third series of tests (Nos. 17, 18, 19, 20, and 21) were conducted with the view of exploring the effect of two other variables not previously covered, namely (*a*) variable load, and (*b*) variable excess air. All these tests were preceded by the usual wall-cleaning process so as to establish what was considered a normal uniform basis of wall cleanliness in so far as was possible

[3] A fourth series of tests were subsequently run, and the operating data and some of the analytical data are reported in the accompanying Appendix.

TABLE 1 SUMMARY OF OPERATING AND TEST DATA FOR ALL COMPLETE TESTS

Test Number		1	2	3	4	10	11	13	14	15	17	18	19	20	21
Date		12/18/45	12/19/45	12/20/45	12/21/45	2/26/46	2/27/46	2/28/46	3/1/46	3/2/46	6/4/46	6/5/46	6/6/46	6/7/46	6/8/46
Duration,	Hours	6-1/2	7	6-2/3	5	9-2/3	7	4	7-1/2	5-2/3	8	8	8	8	8
Furnace Condition		Dirty	Dirty	Dirty	Dirty	Dirty	Cleaned	Cleaned	Cleaned	Cleaned	Cleaned	Cleaned	Cleaned	Cleaned	Cleaned
No. Pulverizers in Operation		2	2	2	2	2	2	2	2	2	2	2	2	2	2
No. Burners in Operation		8	8	8	8	8	8	8	8	8	8	8	8	8	8
Upper Burners Inclination,	Deg	0	Up 30	Down 30	0	0	0	Up 30	0	Down 30	0	0	0	0	0
Lower Burners Inclination,	Deg	0	Up 30	Down 30	0	0	0	Up 30	Down 30	Down 30	0	0	0	0	0
Integrators:															
Steam Flow,	M lb/hr	448	411	407	419	416	390	410	416	421	422	522	419	429	323
Feedwater Flow,	M lb/hr	429	395	388	401	394	372	394	399	403	402.5	503	402	410	318
Desup. Water Flow,	M lb/hr	0	0	0	0	0	0	0	0	0	0	0	0	0	0
North Coal Scales,	M lb/hr	22.2	21.66	21.1	21.3	22.25	20.4	20.6	20.1	19.5	18.33	24.3	17.87	18.94	13.9
South Coal Scales,	M lb/hr	22.5	21.43	20.9	21.25	22.4	21.1	20.9	21.1	21.3	21.5	25.0	20.54	19.54	14.33
Temperature Recorders:															
Primary Steam,	F	752	774	748	769	776	730	732	714	710	756	753	736	726	703
Secondary Steam,	F	863	894	844	869	900	839	847	808	797	870	865	847	834	803
Superheat leaving Desup.	F	140	159	135	151	169	123	130	110	103	168	160	147	136	118
Gas entering Preheater,	F	634	622	590	600	614	581	590	583	587	613	635	595	587	562
Gas leaving N. ID Fan,	F	320	319	305	303	314	294	298	298	293	316	331	313	313	304
Gas leaving S. ID Fan,	F	297	299	286	283	291	273	276	278	272	293	306	293	294	288
Air leaving FD Fan,	F	84	94	93	87	100	91	91	97	85	106	105	109	114	116
Air entering Preheater,	F	86	106	105	104	99	90	90	97	84	105	104	107	114	115
Air leaving Preheater,	F	542	537	506	509	524	497	506	501	501	524	539	519	513	500
Water entering Econ.	F	420	422	413	424	387	380	387	384	386	419	427	420	410	414
Water leaving Econ.	F	520	520	495	507	497	478	483	477	478	510	515	502	490	486
N. Pulverizer Coal-Air,	F	156	152	152	153	150	150	157	148	139	151	151	155	164	170
S. Pulverizer Coal-Air,	F	142	150	157	157	149	149	160	150	142	142	153	144	154	166
Excess Air:															
Economizer Outlet,	%	30	30	30	30	29	30	28	27	26	35.8	28.2	28.1	19.1	28.1
Furnace Outlet,	%	27.5	25	25	27	25	28	24	26	26	35.1	26.7	24.2	15.7	27.4
Indicators:															
Steam Drum Pressure,	psig	1400	1357	1347	1369	1353	1339	1345	1347	1348	1352	1393	1344	1346	1309
Steam Main Pressure,	psig	1285	1267	1260	1276	1261	1259	1261	1259	1260	1262	1262	1260	1260	1259
SH. By-pass Damp. Opening	%	10	8	0	0	0	0	0	0	0	0	0	0	0	0
Raw Coal Analysis: *															
Heat Content (as recd.),	Btu/lb	11400	11020	10970	11150	10910	10680	11510	11280	11230	11590	11620	11600	11940	11820
Heat Content (M&A Free),	Btu/lb	14340	14240	14240	14270	14150	14070	14310	14320	14300	14360	14370	14390	14500	14480
Moisture (as recd.),	%	8.0	9.5	9.5	9.0	9.6	10.8	8.9	9.0	8.8	7.7	7.3	7.7	5.6	5.3
Ash (as recd.),	%	12.5	13.1	13.5	12.9	13.3	13.3	10.7	12.3	12.7	11.6	11.8	11.7	12.1	13.1
Volatile (as recd.),	%	34.3	33.1	33.0	33.6	33.4	33.0	34.2	34.3	34.4	35.5	36.1	35.5	37.2	37.2
H (M&A Free),	%	5.5	5.5	5.4	5.4	5.4	5.4	5.5	5.5	5.5	5.5	5.5	5.6	5.7	5.7
C (M&A Free),	%	80.6	80.5	80.2	80.3	80.0	79.9	80.8	80.4	80.4	80.6	80.2	80.5	80.8	80.7
N (M&A Free),	%	1.5	1.5	1.5	1.5	1.3	1.3	1.5	1.3	1.4	1.4	1.5	1.5	1.4	1.3
O (M&A Free),	%	10.3	10.5	10.9	10.7	10.9	10.9	10.4	10.1	9.8	9.7	9.7	9.4	8.9	9.1
S (M&A Free),	%	2.1	2.0	2.0	2.1	2.4	2.5	1.8	2.7	2.9	2.8	3.1	3.0	3.2	3.2
Ash Temperatures:															
Initial Deformation,	F	2470	2520	2520	2490	2370	2140	2520	2170	2150	2330	2120	2120	2160	2240
Softening,	F	2540	2560	2600	2550	2470	2360	2570	2430	2400	2490	2170	2190	2470	2470
Fluid,	F	2720	2680	2680	2650	2570	2540	2700	2570	2570	2600	2420	2520	2610	2590
Pulverized Coal Fineness:															
Through No. 50 USS Sieve,	%	-	-	-	-	-	-	-	-	-	99.6	99.1	99.8	99.7	99.9
Through No.100 USS Sieve,	%	-	-	-	-	-	-	-	-	-	96.6	93.8	97.4	97.6	98.8
Through No.200 USS Sieve,	%	-	-	-	-	-	-	-	-	-	80.8	75.3	85.0	85.5	89.4
Heat Input in Fuel,	MKB/hr	509	475	461	473	488	443	478	464	458	462	574	446	460	334
Heat Available to Furnace,	MKB/hr	532	494	476	489	506	458	495	480	474	483	597	459	472	343
Avg. Furnace Exit Gas HVT,	F	-	-	-	-	1929	1819	1859	1747	1674	1827	1890	1824	1859	1691
Avg. Furnace Wall TC ΔT,	F	42	36	41	41	38.1	37.8	37.7	45.6	46.5	40.2	48.2	39.8	41.8	35.7

* Coal for all tests: Meigs Creek (No. 9), Duncanwood Mine, Harrison County, Ohio.

with such equipment. Burners were maintained horizontal in all tests so as not to obscure the effect of the other variables. A high rating of 503,000 lb per hr (feedwater flow) was carried on test No. 18, although the fuel input for this test corresponds closely to that of normal maximum design output of 475,000 lb and 925 F steam temperature, the test steam temperature being considerably lower due to the combined effect of clean walls and horizontal burner position.

The behavior of thermocouples was checked on several occasions when the boiler was being taken out of service. The record of temperatures at such times indicated proper calibration of all satisfactory couples as following the saturation temperature characteristic. The few cases of abnormal readings for some couples indicated immediate replacement for these.

Discussion of Data

The test data given in Table 1 are averages of the data taken periodically during each test run. Operating conditions were maintained reasonably uniform for the entire period of each test so that arithmetic averaging, as it is being done, is probably quite acceptable and representative.

Referring further to Table 1, the following additional comments are made to amplify and clarify the data reported:

(*a*) The item of "Furnace condition" represents a statement as to whether the walls are "dirty" from previous operation and without cleaning prior to testing, or whether they have been "cleaned" by blowing the wall soot blowers just prior to starting the test.

(*b*) It is well known that the boiler-output level indicated by "Feedwater flow" is reasonably accurate, particularly at higher ratings.

(*c*) The fuel and ash data are from composited samples taken frequently during the test period, and all proximate analyses and ash-softening temperature data are by the U. S. Bureau of Mines. A more detailed account of these items is given in another paper (1).

(*d*) The item "Excess air at economizer outlet" is by a Bailey oxygen recorder which is carefully checked prior to and during each test. It represents analysis of gas from a single sampling point at the center of the gas flue leaving the economizer. A traverse of the entire flue at this level shows slightly higher average excess air, as would be expected.

(*e*) The item "Excess air at furnace outlet" is by water-cooled sampling-tube traverse and Bailey oxygen recorder and is described more fully elsewhere (1). It is given here merely to indicate fairly reasonable agreement and consistency in data from the two locations.

(*f*) The item "Average furnace-exit-gas temperature" is by water-cooled single-shield exposed-junction high-velocity thermocouple traverse and is described more fully elsewhere (1). It is given here and referred to later to indicate comparison of over-all furnace absorption by exit-gas temperature and by wall-tube temperature.

(*g*) The derived quantities "Heat input in fuel" and "Heat available to furnace" are given to provide a more fundamental basis of establishing furnace heat release. In both cases, quantities are heat-released above 80 F. "Input in fuel" is the product of fuel fired and calorific value, while "Heat available" is the net sensible heat to the furnace.

(*h*) The item "Average furnace wall $TC - \Delta T''$ is obtained by arithmetic averaging of all furnace-wall temperatures recorded during a specific test period, and subtracting the boiler saturation temperature for that period, as determined from the average of all saturation thermocouple readings. No correction is made for slight variation in saturation temperature due to variable hydrostatic head at the particular elevation or average elevation considered.

In addition to the physical and analytical data reported in Table 1, there were certain "visual" data which were acquired and some of which are reported here. This involves the actual inspection of furnace conditions by observers throughout the tests and the recording of these observations. The complete record of these cannot be given here, due to their length, but short excerpts will be quoted to indicate their nature, as follows:

Test No. 19 (refer to Fig. 17 for photographic record).

Front Wall—Elev. 679′–0″ [Fig. 17 (*e*) and (*f*)]:

A.M.—The front wall was approximately 75 per cent covered with $^1/_2$-in-thick sponge ash beginning at the center half about 1 foot above the operating floor and increasing in width up to the burner level. Most of the tubes appear to have a thin clean strip on the side opposite the direction of burner rotation.

P.M.—The same general type of deposit was on this wall as previously noted, except that it appeared to have grown slightly thicker and several large strips had peeled off the center.

Right Wall—Elev. 689′–0″ [Fig. 17 (*d*)]:

A.M.—From the front, it appears that two thirds of the right wall was from 80 per cent to 90 per cent covered with a sheet of semi-fused slag approximately $^1/_2$ in. thick. From the rear it could be seen that practically all of these deposits were heavy strips located on the center and side of each tube toward which the firing was directed.

P.M.—The condition of this wall was similar to that previously noted except that the covering extended back slightly farther and many of the strips had increased in thickness up to 1 inch and extended over to the adjacent strip forming almost continuous coverage.

Left Wall—Elev. 689′–0″ [Fig. 17 (*c*)]:

A.M.—The front two thirds of the wall was covered with a deposit similar to that noted for the right wall.

P.M.—Deposits on the front two thirds of the wall had increased similarly to that noted for the right wall.

A complete summary of test average ΔT values for all thermocouples is given in Table 2. It will be noted that there are occasional blank spots which indicate data to be lacking owing to faulty or failed thermocouple conditions. The points 6–19, 6–20, 7–18, and 7–19 are the saturation-base couples, which are averaged to establish the basic zero ΔT. The data given in this table are used in all subsequent analyses in this report where averages for the total test period are used.

Analysis and Interpretation of Data

An examination of the wall-tube ΔT values, as determined from successive recorder readings of specific couples, is of interest, particularly where these couples are in zones of high heat release

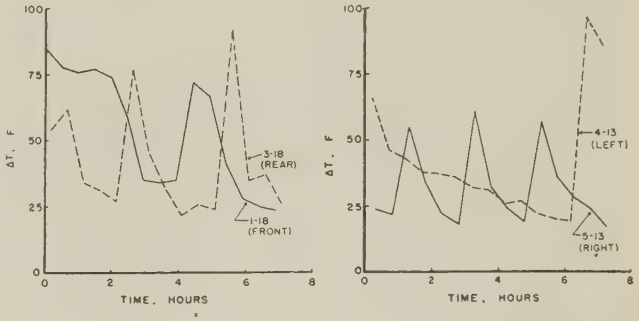

Fig. 4 Behavior of Thermocouples at Mid-Point in Each Wall, Elevation 698 Ft, Where Sponge Ash Was Being Deposited at a Relatively Rapid Rate; Test No. 11

TABLE 2 CENTER-LINE THERMOCOUPLE AVERAGE TEMPERATURE DIFFERENTIALS FOR ALL COMPLETE TESTS

Test #	1	2	3	4	10	11	13	14	15	17	18	19	20	21
TC #														
1-21	37	17	71	32	23	20	12	39	51	25	33	22	22	22
1-2	57	15	96	35	20	20	6	45	61	27	36	24	24	24
1-3	40	15	80	31	21	20	7	47	70	27	37	28	30	23
1-4	31	15	76	29	19	17	8	57	66	19	34	31	32	19
1-5	23	15	45	28	18	17	7	45	45	17	30	28	30	16
1-6	51	20	60	52	33	32	22	48	50	35	50	39	42	36
1-7	54	21	30	37	40	41	24	53	64	37	60	23	32	30
1-8	17	20	11	19	14	14	9	8	10	7	9	6	9	9
1-9	23	21	35	55	37	39	20	54	46	41	56	19	38	33
1-10	33	20	39	53	34	33	21	52	51	35	44	45	47	31
1-11	85	54	50	61	44	42	37	67	80	43	62	58	64	62
1-12	87	51	58	62	53	49	40	77	82	69	82	51	44	74
1-13	90	55	59	95	61	61	53	74	71	70	104	79	97	40
1-14	75	53	56	69	42	58	62	75	75	17	32	25	44	47
1-15	68	44	41	66	59	51	57	69	55	55	75	60	58	49
1-16	91	62	28	40	37	41	66	44	67	84	65	90	82	70
1-17	89	61	29	32	69	59	78	76	77	82	40	62	56	47
1-18	88	92	37	47	67	54	30	92	90	68	49	46	58	29
1-19	59	72	24	29	41	59	77	76	75	65	48	44	52	42
1-20	56	53	32	58	57	55	63	62	52	59	73	56	57	50
2-1	45	73	37	43	42	56	58	42	46	49	69	56	61	42
2-21	43	32	8	24										
2-3	60	48	31	35	44	57	65	46	52	37	44	42	41	35
2-4	49	57	31	27	19	46	67	47	53	42	56	49	53	38
2-5	48	58	28	41	38	43	50	37	41	42	57	50	53	38
2-6	43	44	26	33		32				30	36	30	33	23
2-7	40	50	30	38		46								
2-8	37	37	27	28	36	36	37	28	33	33	42	38	40	30
2-9	36	37	25	27	17	34	38	31	36	29	36	33	36	27
2-10	36	38	23	31	32	31	33	24	26	29	38	33	36	26
2-11	36	38	21	29	32	26	30	19	21	25	31	27	27	21
2-12	36	40	22	30	35	31	34	22	25	30	36	38	32	25
2-13	36	41	24	31	36	32	34	24	29	30	38	32	35	26
2-14	32	33	22	27	29	22	24	20	24	21	27	25	25	19
2-15	30	31	21	26	28	23	23	19	22	22	30	25	25	19
2-16	29	32	20	26	29	25	27	20	23	27	31	28	29	22
2-17	29	35	23	27	32	29	33	26	31	29	34	32	34	25
2-18	36	45	32	34	39	34	39	31	34	35	41	37	39	29
2-19	36	43	32	32	37	32	37	31	34	33	37	35	36	28
2-20	29	29	22	28	30	25	26	23	27	24	32	27	26	21
3-1	28	52	8	23	14	14	5	45	43	13	31	25	27	15
3-2	22	16	59	27	18	18	7	43	56	18	35	29	30	19
3-21	35	24	84	31	23	19	16	37	60	19	33	25	26	12
3-4					23	20	16	36	53	23	29	20	21	19
3-5	92	29	110	45	23	19	11	33	44	26	35	22	23	25
3-6	44	21	32	40	29	29	16	47	50	32	49	44	46	33
3-7	20	17	22	32	28	27	16	15	15	30	41	22	13	10
3-8	4	17	22	54	39	39	18	47	58	42	62	51	53	46
3-9		14	8	49	39	40	20	44	53	42	49	44	46	43
3-10	37	20	61	48	38	37	21	41	45	40	47	41	40	40
3-11	39	30	42	48	48	44	41	49	50	37	49	51	48	55
3-12	58	37	45	70	73	65	45	64	62	61	75	79	76	90
3-13	58	29	56	59	62	61	48	76	74	49	69	55	49	50
3-14	68	72	61	60	68	53	68	72	63	71	82	71	77	73
3-15	62	56	48	59	65	52	55	65	51	57	73	58	63	51
3-16	45	23	37	32	58	53	72	55	43	58	43	55	51	48
3-17	40	32	33	30	37	56	86	71	54	83	27	29	52	81
3-18	43	45	38	28	38	42	84	80	58	47	26	46	54	56
3-19	39	41	27	28	56	52	65	61	52	69	31	40	40	33
3-20	51	58	45	54	64	59	66	63	49	65	78	67	69	63
4-1	31	20	50	35	29	27	16	28	34	34	41	34	35	37
4-2	9	17	27	49	38	36	21	40	51	45	53	41	44	45
4-3	43	23	31	67	45	43	25	42	51					
4-21	38	25	50	63	43	40	27	63	63	46	63	43	43	41
4-5	96	28	84	58	31	30	24	50	55	33	43	31	28	22
4-6	70	30	35	53	66	53	31	55	53	63	70	64	68	67
4-7	94	49	52	78	79	69	48	75	81	88	106	80	84	81
4-8	79	48	57	73	68	39	47	51	49	76	78	71	71	56
4-9	63	58	67	57	66	55	54	68	67	55	58	27	37	32
4-10	74	61	55	61	55	49	47	54	36	62	83	72	72	50

Test #	1	2	3	4	10	11	13	14	15	17	18	19	20	21
TC #														
4-11	67	49	50	60	62	70	78	62	46	63	83	69	75	59
4-12	48	31	54	55	46	64	88	72	69	80	60	62	69	55
4-13	48	36	80	49	61	42	41	52	82	90	65	25	33	48
4-14	47	61	63	56	57	49	71	70	74	87	85	76	73	66
4-15	66	82	57	67	67	67	67	70	67	70	99	73	74	57
4-16	55	64	37	51	77	70	87	49	43	66	76	68	69	48
4-17					66	76	91	48	43	70	83	76	84	58
4-18	22	39	26	30	38	51	62	42	41	51	55	45	45	42
4-19	28	61	36	31	42	47	63	47	46	41	53	46	49	36
4-20	60	66	35	45	44	48	51	46	46	38	54	44	47	36
5-1					40	40	24	52	53	39	58	53	55	35
5-2					41	42	23	72	62	39	64	33	31	29
5-3					40	42	22	79	70	38	62	30	33	27
5-4	28	22	52	60	42	44	24	86	50	41	70	58	67	44
5-21	24	19	34	36	27	25	19	50	51	24	34	34	32	25
5-6					49	37	26	68	54	53	61	74	79	60
5-7	25	39	49	70	57	54	39	70	61	77	85	53	91	65
5-8	68	35	58	78	68	52	44	60	54	45	70	60	34	61
5-9	80	43	59	86	80	76	44	77	70	62	31	36	36	62
5-10	59	37	36	67	61	55	45	50	50	55	73	50	52	59
5-11	46	39	26	92			69		55					
5-12	74	60	46	67	30	23	48	70	63	35	34	20	29	56
5-13	61	19	35	41	32	32	29	63	59	37	24	25	30	50
5-14	61	47	41	52	58	71	105	80	59	77	89	43	51	53
5-15	59	48	42	63	64	58	70	59	42	65	79	67	62	43
5-16	49	47	25	37	22	38	41	33	37	42	57	46	47	34
5-17	38	25	25	40	19	56	68	44	45	58	77	68	71	51
5-18	36	42	30	37	15	48	74	45	41	44	56	48	48	41
5-19	29	35	22	34	27	42	64	37	29	37	49	42	44	33
5-20	32	36	22	35	44	41	59	34	24	35	45	41	42	34
6-1					18	16	10	29	35	20		17	18	19
6-2		4	77	16	18	16	8	34	42	20	25	19	18	20
6-3	14	7	69	19	17	15	8	33	41	19	23	18	17	18
6-4	34	40	34	33	26	33	37	25	36	42	38	40	28	
6-5	37	50	33	35	41	38	45	31	32	40	49	44	45	34
6-21	36	47	25	33	35	31	35	27	29	31	40	34	36	27
6-7	73	42	34	37	41	35	37	26	26	33	38	32	33	23
6-8	44	37	31	29	36	31	34	24	25	29	35	30	31	22
6-9	36	36	27	28	33	26	29	20	23	27	32	27	27	21
6-10	29	21	39	27	22	21	12	40	42	22	31	27	28	19
6-11	34	16	40	27	18	17	10	42	41	12	21	18	17	11
6-12	33	14	41	26	17	16	10	44	42	15	24	24	23	16
6-13	35	44	30	37	34	31	30	28	30	33	45	37	37	27
6-14	37	36	26	36	36	33	35	28	30	32	47	37	39	28
6-15	34	39	14	33	25	29	35	28	28	29	35	25	26	25
6-16	32	33	19	31	28	28	27	23	25	27	34	29	29	21
6-17	36	36	22	33	34	31	29	23	26	28	38	31	32	24
6-18	28	29	19	27	28	27	26	22	23	26	33	23	25	19
6-19	*													
6-20	*													
7-1	42	47	29	51	50	49	66	37	28	45	64	52	51	43
7-2	44	39	36	48	36	64	88	51	35	55	77	68	71	48
7-3	29	57	22	10	52	52	34	50	35	53	59	49	44	41
7-4	17	63	23	38	64	59	75	45	34	53	61	48	35	40
7-5	25	46	24	34	51	48	60	37	30	44	50	39	35	34
7-6	19	13	52	21	14	13	8	19	27	14	20	13	12	12
7-21	10	11	61	16	14	13	8	25	42	15	19	11	10	15
7-8	53	19	89	24	16	14	12	36	59	16	23	13	14	12
7-9	25	12	51	18	13	10	8	30	40	9	20	16	16	10
7-10	17	11	35	16	13	12	7	32	36	11	23	18	19	11
7-11	13	10	28	17	12	11	5	29	32	10	22	17	16	10
7-12	12	9	46	17	12	12	7	31	41	10	22	18	17	10
7-13	10	9	59	16	12	11	7	30	46	10	21	18	16	10
7-14	13	10	64	17	12	11	6	22	43	13	20	11		
7-15	14	11	62	19	12	12	6	19	31	14	21	13	13	15
7-16	11	9	49	17	12	11	6	16	24	13	16	11	10	13
7-17	11	9	28	17	12	12	6	24	30	13	23	18	20	13
7-18	*													
7-19	*													

* External saturation base thermocouple.

and ash concentration. This is shown for several such couples in Fig. 4 which shows the behavior of thermocouples at the midpoint of each wall at elevation 698 ft where sponge ash was being deposited at a relatively rapid rate during test No. 11. It should be noted that the furnace is almost square, and the burners are similarly arranged at each corner so that firing similarity is substantially uniform with respect to all walls. The concentration of ash and the combustion activity are at or near maximum intensity at this level due to extreme turbulence and probable greatest recirculation rate, so that extremely high or low absorption rates would be expected depending upon ash coverage.

The variation in tube ΔT is shown to be quite irregular for the selected points shown in Fig. 4. Thermocouple 5–13, which is at the center of the right wall, shows a clearly discernible cycle of ash accumulation and falling off, the period being about 2 hr. Thermocouple 4–13 at the center of the left wall appears to have a cycle of about 8 hr but with greater variation in ΔT. The midpoint thermocouples in the front and rear walls, 1–18 and 3–18, show still different characteristics both as to cycle period and ΔT range.

It is obvious from examination of these records that the heat absorption of closely spaced bare-tube walls adjacent to the burners in a dry-ash furnace can be quite irregular and generally unpredictable. This same process of ash accumulation and shedding occurs over surfaces farther removed from the burners but to a lesser extent. While the "local" effect appears of great magnitude, the "over-all" effect is probably greatly reduced by the great diversity in period and magnitude of the condition, as clearly shown in Fig. 4. The variations shown also tend to confirm the opinion of some that furnace performance should not be judged from individual tests but rather from a very great number of tests under all potential conditions so that the "range" of performance is fully explored and considered.

The furnace-wall-tube average test ΔT values have been indicated on a furnace-wall outline development for those tests of significance, as indicated in Figs. 5 to 16, inclusive. These have been augmented by tube ΔT "isothermal lines" to better visualize the heat-absorption pattern for all the walls. Also shown are the burner position and the average ΔT for the various levels at which thermocouples are installed. A brief interpretation of the data shown in Figs. 5 to 16 is given herewith to illustrate certain over-all deductions.

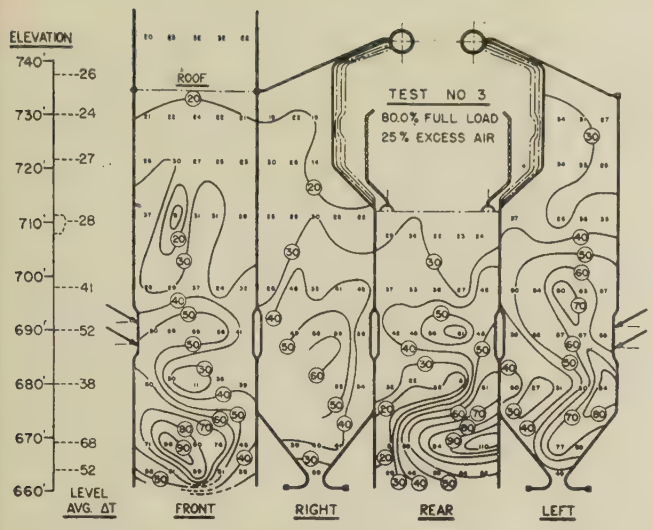

FIG. 5 ISOTHERMAL ΔT DIAGRAM, TEST NO. 3

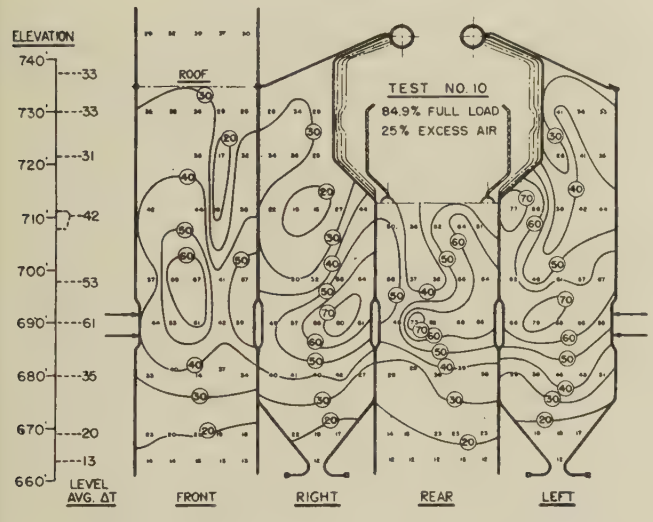

FIG. 6 ISOTHERMAL ΔT DIAGRAM, TEST NO. 10

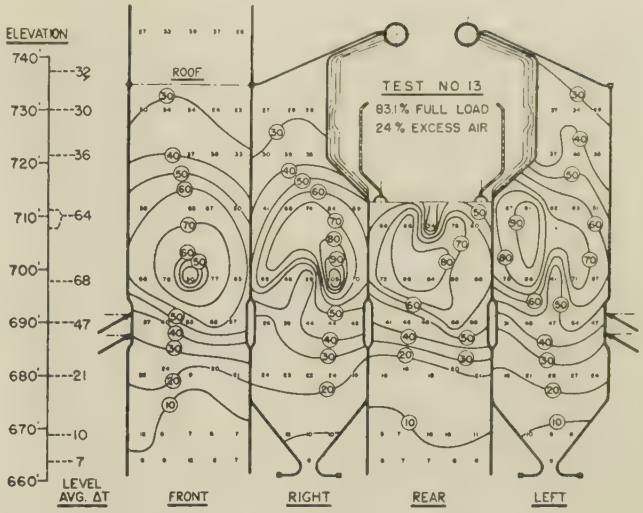

FIG. 7 ISOTHERMAL ΔT DIAGRAM, TEST NO. 11

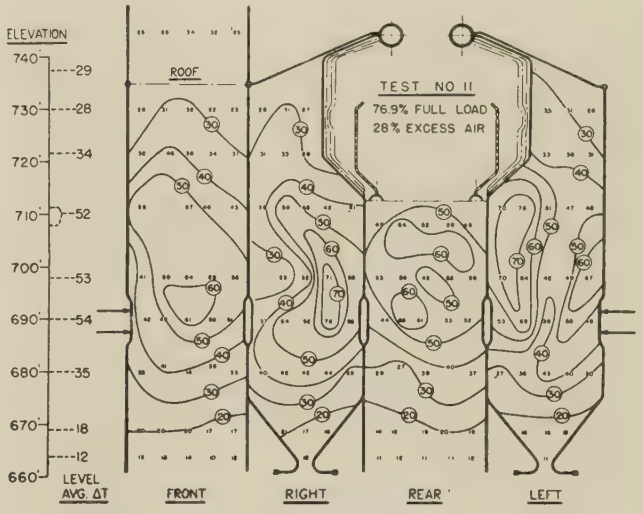

FIG. 8 ISOTHERMAL ΔT DIAGRAM, TEST NO. 13

Fig. 5 (test No. 3). The dirty furnace walls are evidenced by low absorption (ΔT) areas in the burner zone which are covered with ash for all or a great part of the time. This produces extremely high-level average ΔT's at elevation 668 ft although prolonged operation with burners tilted downward, as for this test, would probably result in eventual ash covering at this lower level.

Fig. 6 (test No. 10). The walls were dirty for this test although the data indicate, and visual observation of wall conditions during the test confirm, that they were not as dirty as for the first series of tests, and there are fewer apparent areas of heavy ash coverage, and correspondingly very low ΔT, than for test No. 3. The lower portion of the furnace is absorbing at considerably lower rates with horizontal burners than with downward tilted burners. The upper portion of the furnace is absorbing at higher rates, both because of burner position and greater residual heat in gases leaving the partly dirty central portions of the furnace. This indicates quite clearly the substantial compensating influence of a clean furnace zone which recovers a very great proportion of heat following a dirty zone. Several "islands" of dirty surface are evident in the upper part of the front and right walls and operation of wall blowers would have removed this ash quite effectively.

Fig. 7 (test No. 11). The beneficial effect of cleaning walls with soot blowers is evident in comparing this clean-wall test with the two previous dirty-wall tests. The absence of islands of heavy ash accumulation is noticeable, although it must be remembered that the ΔT values shown are averaged from readings over a period of 7 hr, and the walls, although cleaned just prior to the start of the clean-wall tests, do acquire a coating of ash in the burner zone during the course of the test period. This will be demonstrated more clearly later.

Fig. 8 (test No. 13). This is a clean-wall test with all burners tilted upward and the movement of high-absorption zones upward is quite evident. The very low absorption rate below the burner level is particularly marked, and its effect is significant on over-all furnace performance. An island of heavy ash and low absorption is evident on the front wall directly in the flame path. Also of interest is the rapid ΔT gradient at this zone as evidenced by close-spaced isothermal lines. A similar small zone of extremely high absorption is seen on the right wall and the sharp gradient downward is evident.

Figs. 9 and 10 (test No. 14). This is another clean wall test but with the upper burners horizontal and the lower burners tilted down 30 deg. Two diagrams have been included from this test, the first, Fig. 9, showing average ΔT values for a $1^1/_2$-

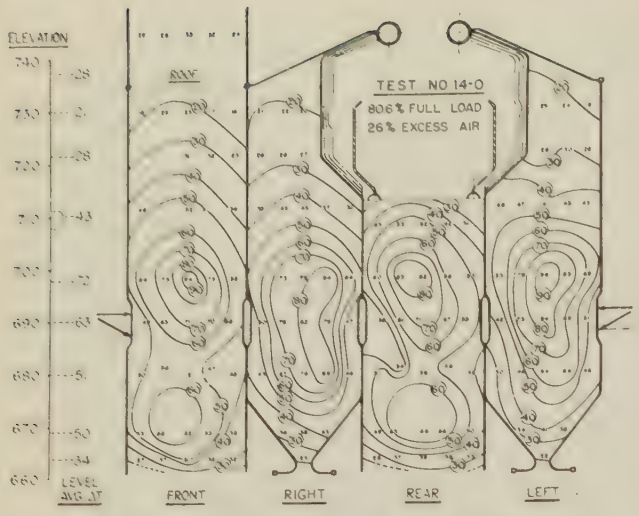

FIG. 9 ISOTHERMAL ΔT DIAGRAM, JUST BEFORE TEST NO. 14

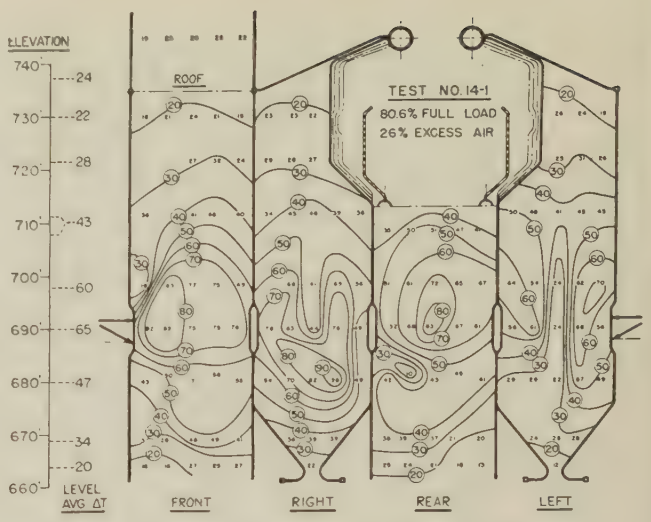

FIG. 10 ISOTHERMAL ΔT DIAGRAM, AT END OF TEST NO. 14

hr portion of the $2^1/_2$-hr period elapsing between operation of wall soot blowers and the beginning of the formal test. The second, Fig. 10, shows average ΔT values for the last $1^1/_2$ hr of the test period. Fig. 9 shows the effect of the "spread" burner position clearly in that two high-absorption zones are discernible in both front and rear walls, and which are clearly produced by flame direction from the two burner levels. The uniformity of absorption over a considerable height of the furnace and the high rate for this area indicate the beneficial effects of this particular burner arrangement and the extreme wall cleanliness.

Fig. 10 indicates the effect of ash coverage accumulated during the test period, and the corresponding reduction in absorption rate over considerable wall area. The disappearance of the high-absorption islands in the hopper zone at about elevation 670 ft shows the appreciable effect of ash coverage in this area. A further study of this test and the details of ash behavior and effects will be given later.

Fig. 11 (test No. 15). This shows a clean test with both burner levels tilted 30 deg downward. High ΔT values in the lower furnace and hopper areas are evident as a result of downward flame direction. The high over-all ΔT average and low furnace-exit-gas temperature given in Table 1 for this test indicate the very beneficial over-all effect of this burner arrangement, while Fig. 11 indicates in more detail the uniformly high absorption level over a greater portion of furnace height than for any other burner arrangement.

Fig. 12 (test No. 17). This is a clean test at normal rating and with all burners horizontal but with high excess air, 35 per cent leaving the furnace as compared to normal 25 per cent. The only new item of significance to note in this test is the relatively wide spacing of the isothermals, except for several areas in the burner zone, which indicate absence of ash deposits with correspondingly greater uniformity in absorption. This greater stability of furnace cleanliness with higher excess air may be a desirable method of operation for certain abnormal conditions.

Fig. 13 (test No. 19). This is similar to the previous run except that normal excess air of 25 per cent leaving the furnace was used. Other than a noticeable increase in ash coverage on the walls, this run needs no further comment. It was run to establish a means for proper judgment of excess-air influence.

Fig. 14 (test No. 20). This is also similar to tests Nos. 17 and 19, except that low excess air, 16 per cent leaving the furnace, was used. The further influence of more ash coverage is noted, although the effect of higher flame temperature is predominant in its influence on over-all average ΔT for the test periods involved. A further analysis of the excess-air runs will be covered later.

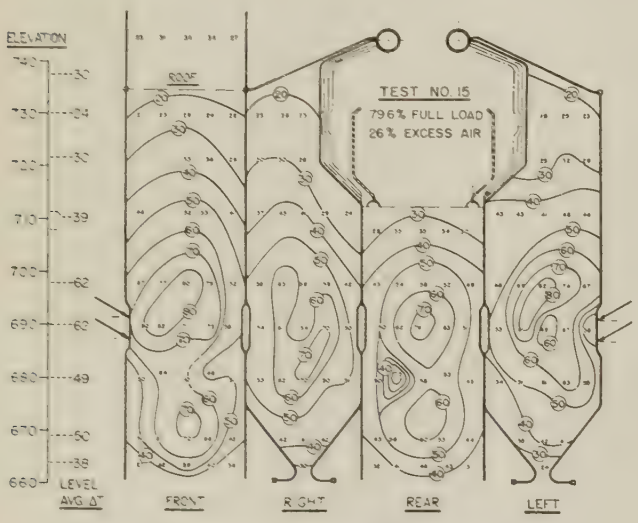

FIG. 11 ISOTHERMAL ΔT DIAGRAM, TEST NO. 15

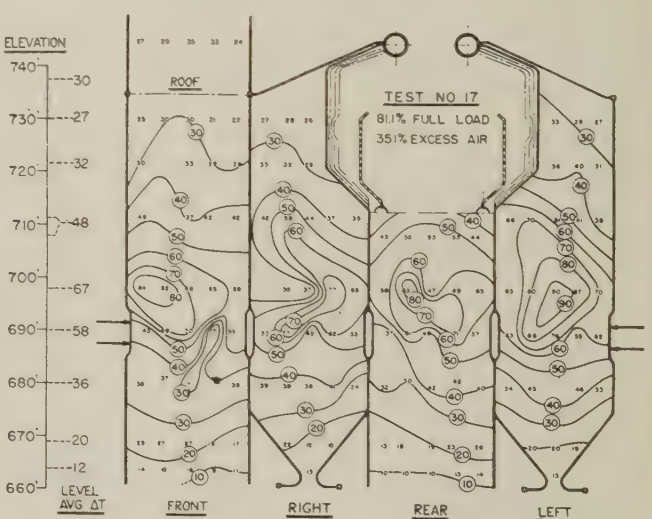

FIG. 12 ISOTHERMAL ΔT DIAGRAM, TEST NO. 17

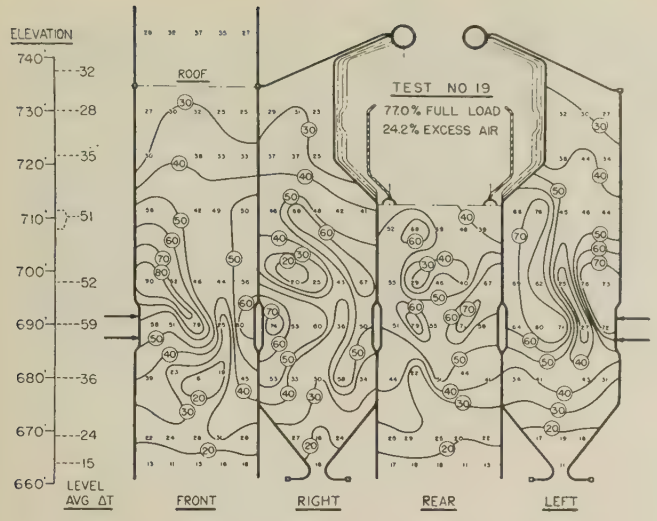

FIG. 13 ISOTHERMAL ΔT DIAGRAM, TEST NO. 19

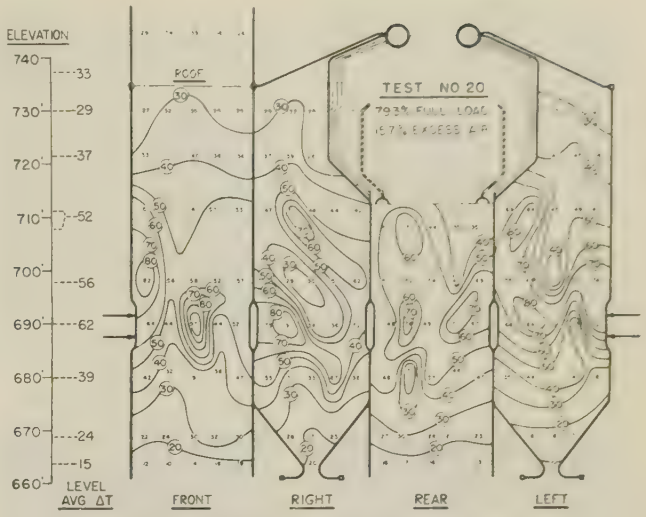

FIG. 14 ISOTHERMAL ΔT DIAGRAM, TEST NO. 20

Fig. 15 (test No. 18). This is a maximum-rating run with clean furnace conditions, normal excess air, and with all burners horizontal. The higher level of all ΔT values at this higher rating is quite evident. There is also a concentration of high absorption at the immediate burner level, and some evidences of heavy ash accumulation in this zone are noted, although these are tempered by the sweeping action of the burners which appears to inhibit heavy ash formation on walls in the direct flame flow path. A considerably longer test run under these same conditions appears desirable to study the possible variations in absorption pattern over a considerable period of time.

Fig. 16 (test No. 21). This is a lower rating run with clean furnace conditions, normal excess air, and with all burners horizontal. The generally lower ΔT values, except at the burner level, indicate clearly the effect of rating alone on over-all furnace absorption. The somewhat higher ΔT values directly in line with the burners are evidently the effect of direct flame impingement which would not be expected to vary so greatly with rating. The wide spread between isothermal lines indicates the general absence of heavy ash coverage, as would be expected at reduced rating.

In an attempt to correlate the test data with visual data in the form of a photographic record, numerous pictures were taken during each of the last series of tests. While location of observation doors and unfavorable furnace-wall visibility interfered with obtaining clearly detailed and informative photographs, several were obtained some of which are presented here.

Figs. 17(a) to 17(f), inclusive, show various views of the furnace walls taken during test No. 19. The viewed and viewing locations and gas-flow direction past the walls are given for each photograph and a check of the ΔT isothermals in Fig. 13 shows the following: 1 Fig. 17(a) and isothermals indicate slight ash coverage on the near side of the wall tubes at elevation 724 ft. 2 Fig. 17(b) and isothermals show clean tubes on the near side at elevation 724 ft, as contrasted to the other half as just described. This unequal condition is probably due to horizontal rotation of gas body resulting from tangential firing. The firing rotation is counterclockwise looking down so that the ash coverage is on the side of approaching flow, while the clean side is that from which flow is receding. 3 Fig. 17(c) and isothermals indicate relatively clean wall tubes and high absorption with the flame from the upper burner visible. 4 Fig. 17(d) and isothermals show considerable ash coverage and correspondingly low absorption in the upper foreground with lesser amount of ash coverage beyond. The agreement here is particularly good. 5 Fig. 17(e) and

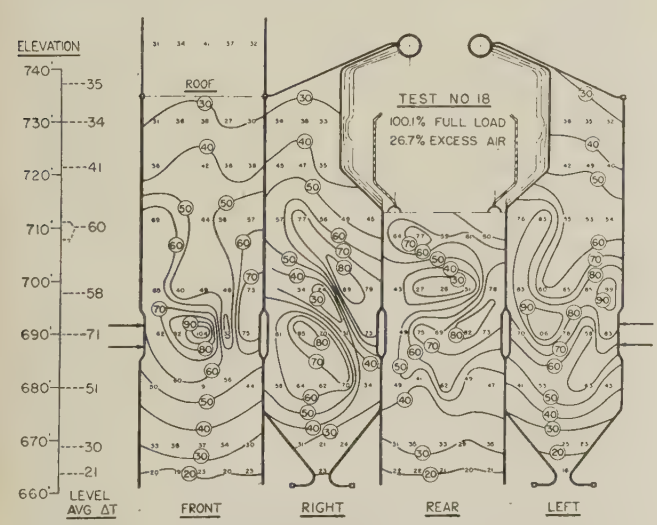

FIG. 15 ISOTHERMAL ΔT DIAGRAM, TEST NO. 18

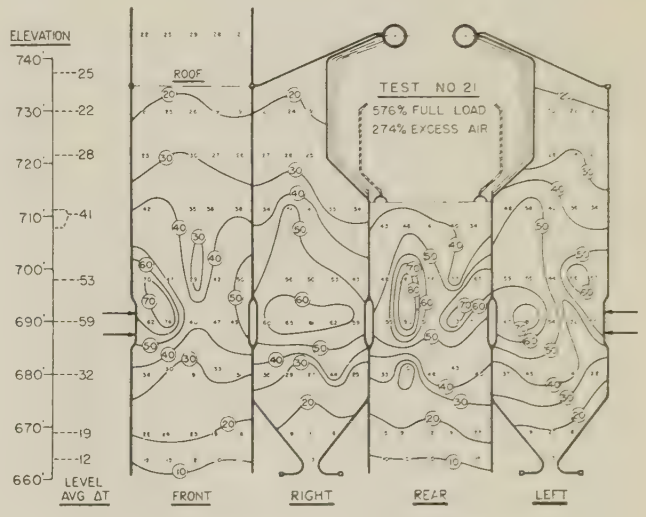

FIG. 16 ISOTHERMAL ΔT DIAGRAM, TEST NO. 21

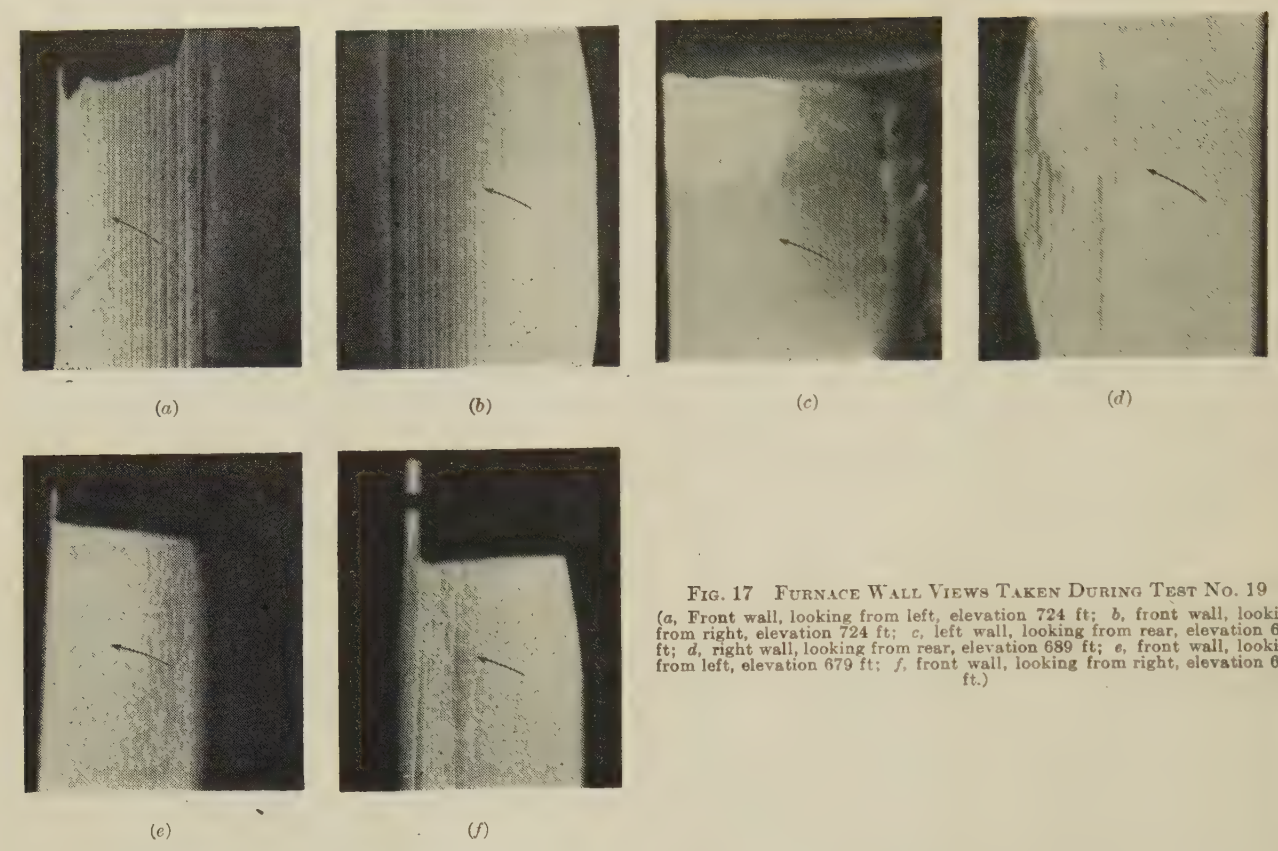

(*a*) (*b*) (*c*) (*d*)

(*e*) (*f*)

FIG. 17 FURNACE WALL VIEWS TAKEN DURING TEST NO. 19
(*a*, Front wall, looking from left, elevation 724 ft; *b*, front wall, looking from right, elevation 724 ft; *c*, left wall, looking from rear, elevation 689 ft; *d*, right wall, looking from rear, elevation 689 ft; *e*, front wall, looking from left, elevation 679 ft; *f*, front wall, looking from right, elevation 679 ft.)

isothermals both indicate considerable ash coverage, and zone of dark patches of ash correspond well with the low ΔT island where the 6 F value is shown. 6 Fig. 17(*f*) and isothermals again show ash at the same elevation as viewed previously from the other side. The agreement is again good with cleaner surface and higher absorption indicated in the immediate foreground, and more ash with lower absorption farther away until the view is obscured by haze in the region of heavy ash noted in viewing from the other side.

Another interesting and revealing analysis of the tube-temperature data is shown in Figs. 18 to 22, inclusive. In these the average ΔT for each level of thermocouple groups is plotted against furnace elevation to provide a heat-absorption "contour" for the four walls at various elevations.

Fig. 18 shows the level average ΔT values for various heat inputs, all other factors such as cleanliness, burner position, and excess air being unchanged. It is noted that a band of reduced absorption at about 35 ft is indicated for the high-rating test (No. 18), indicating a slagged condition. This is also apparent in the isothermal study of Fig. 15 for this test. A lesser amount of ash covering at this same level is noted for the intermediate rating test (No. 19). The low-rating test (No. 21) shows no pronounced level of ash covering to influence effective heat absorption. It is noted that the intermediate and low-rating tests show about the same ΔT values at the burner level and slightly above. This may indicate that the area actively swept by flame from the burners is not subject to appreciable reduction in absorption rate below a certain rating level. It is hoped that this condition can be explored further to confirm this possibility.

The effect of variation in burner-nozzle position on level average ΔT is clearly shown in Fig. 19 which covers four tests (Nos. 2, 3, 4, and 10), which are at similar rating, and in which wall blowers were not operated before each test. The extremely high ΔT values for test No. 3 in the hopper area at the 5-ft level with all burners tilted 30 deg downward is of considerable surprise. The effect of ash coverage at the 17-ft level, and a secondary high-absorption level at the 27-ft level and rapidly diminishing rate in the upper portion of the furnace show the compensating influences which tend to influence the over-all absorption value. The two tests (Nos. 4 and 10) with horizontal burners show similar characteristics, as would be expected, but with some noticeable differences due to extent and location of ash coverage. The other extreme, test No. 2, with all burners tilted 30 deg upward, shows a marked difference in level average ΔT pattern but also is free of the more heavily slagged areas in the lower portion of the furnace. It should be noted that for dirty-wall tests, as shown, the effect of burner position on level average ΔT values is most pronounced, but the over-all result is of a much more uniform nature.

The effect of burner-nozzle position variation on level ΔT for clean furnace walls is shown in Fig. 20. In general, the effect is similar to that for the dirty-wall operation except that heavily slagged levels are less in evidence. The improvement in over-all and local absorption characteristics with all burners down 30 deg (test No. 15), and with the lower-level burners down 30 deg (test No. 14), is clearly evident. Further improvement in "equalizing" the pattern of heat absorption in furnaces is to be desired and the tilting burner can be a material aid in studying this problem and in producing a degree of uniformity.

The significance of excess-air variation on furnace performance was explored and results are shown in Fig. 21. It will be noted that the low and intermediate excess-air tests (Nos. 20 and 19) show a slagged-zone effect at the 35-ft level, while the high excess-air test (No. 17) shows no such condition. As a result, the total absorption for the high air test was about equal to that for the intermediate air test. This fact is not always recognized by designers in their effort to obtain "apparent" improvement in furnace performance by reducing excess air for dry-ash units. It is likely that extended operation for the extreme low excess-air

TEST NO.	HEAT AVAILABLE MKB/HR	% FULL LOAD
• 18	597	100.1
△ 19	459	77.0
○ 21	343	57.6

ALL BURNERS HORIZONTAL
FURNACE WALLS BLOWN BEFORE EACH TEST

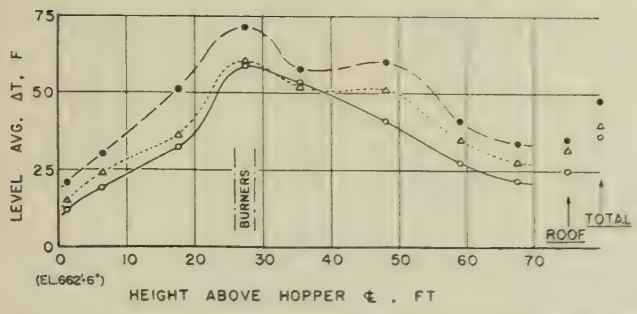

FIG. 18 FURNACE TUBE LEVEL AVERAGE ΔT VARIATION WITH LOAD

TEST NO.	HEAT AVAILABLE MKB/HR	% FULL LOAD	AVG EXCESS AIR LEAVING FURNACE, %
• 17	483	81.1	35.1
○ 19	459	77.0	24.2
△ 20	472	79.3	15.7

ALL BURNERS HORIZONTAL
FURNACE WALLS BLOWN BEFORE EACH TEST

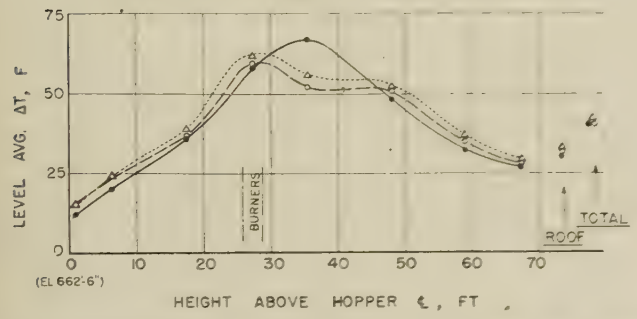

FIG. 19 FURNACE TUBE LEVEL AVERAGE ΔT VARIATION WITH BURNER INCLINATION, FURNACE NOT CLEANED

condition would result in more slag accumulation and consequent reduction in absorption level below that indicated here.

Another study of level average ΔT values is shown in Fig. 22 in which case a single test (No. 14) is analyzed to determine the variation in cleanliness with time, as indicated. In this test, the upper burners were horizontal and the lower ones tilted 30 deg downward which accounts for the relatively high ΔT values in the hopper zone. It is noted that the hopper zone, just below the active flame path of the lower burners, and the upper zone at the 35-ft level, above the flame path of the upper burners, are both subject to appreciable variation in cleanliness and corresponding ΔT values. The intermediate zone, from the 18 to the 30-ft level, in the flame paths is not influenced materially and this may be due to the sweeping action of the flame preventing ash deposition and accumulation beyond a stable limit. This "sweeping" action of the flame over the wall tubes and the apparent beneficial effect in stabilizing absorption in the affected area at a reasonably high level may well warrant much careful study and investigation. An extension of this principle to a substantial portion of the furnace surface would likely be most effective if the practical details of its accomplishment could be worked out properly.

A yet more detailed analysis of test No. 14 is shown in Fig. 23 in which the level average ΔT values are plotted directly from

TEST NO.	HEAT AVAILABLE MKB/HR	% FULL LOAD	BURNER INCLINATION UPPER	LOWER
▼ 2	494	83.0	UP 30°	UP 30°
△ 3	476	80.0	DOWN 30°	DOWN 30°
○ 4	489	82.1	0	0
• 10	506	84.9	0	0

FURNACE WALLS NOT BLOWN BEFORE THESE TESTS

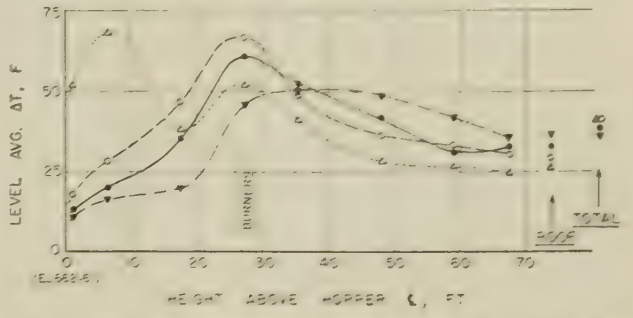

FIG. 20 FURNACE TUBE LEVEL AVERAGE ΔT VARIATION WITH BURNER INCLINATION, FURNACE CLEANED

TEST NO.	HEAT AVAILABLE MKB/HR	% FULL LOAD	BURNER INCLINATION UPPER	LOWER
○ 11	458	76.9	0	0
▼ 13	495	83.1	UP 30°	UP 30°
• 14	480	80.6	0	DOWN 30
△ 5	474	79.6	DOWN 30°	DOWN 30

FURNACE WALLS BLOWN BEFORE EACH TEST

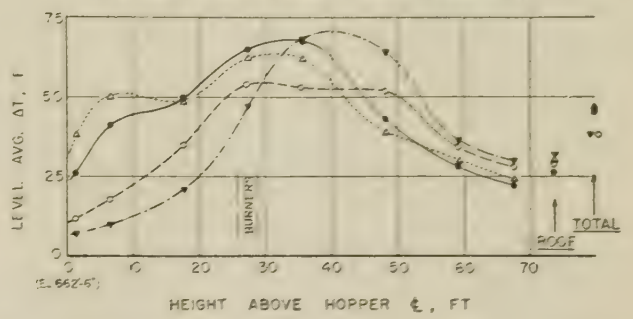

FIG. 21 FURNACE TUBE LEVEL AVERAGE ΔT VARIATION WITH EXCESS AIR

TEST NO.	HEAT AVAILABLE MKB/HR	% FULL LOAD	BURNER INCLINATION UPPER	LOWER
14	480	80.6	0	DOWN 30°

FURNACE WALLS BLOWN 7:00 AM TO 7:45 AM

LEGEND:
- ○ BEFORE TEST PERIOD (7:50 AM TO 9:10 AM)
- • AT END OF TEST PERIOD (4:00 PM TO 5:30 PM)
- △ AVG. FOR TEST PERIOD (9:45 AM TO 5:30 PM)

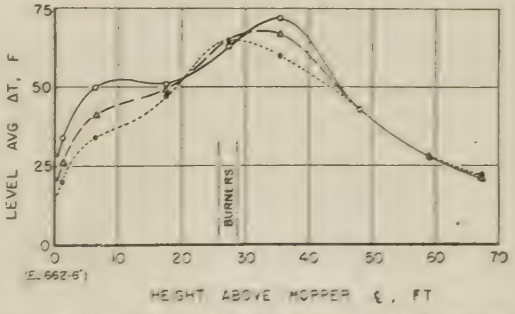

FIG. 22 FURNACE TUBE LEVEL AVERAGE ΔT VARIATION WITH TIME FOR TEST NO. 14

the recorder-chart data. Actually, the plot represents "faired" averages of the chart data so as better to visualize the trends. Again, it is seen that ash accumulations are reducing the absorption efficiency at the 664-ft and 669-ft levels which are well down in the hopper and somewhat below the direct flame path from the lower burners, and at the 698-ft level, which is slightly above the flame path of the upper burners. The 680-ft and 690-ft levels, more in the direct flame path, retain their high absorption level fairly well. This is more clearly indicative of the tendency for slag to deposit and accumulate just outside the turbulent-flame path, while a beneficial sweeping action appears to maintain cleanliness in the direct flame path. The data cover about 10 hr of operation, and it may be that further operation without additional wall cleaning may modify these indicated conditions. The upper part of the furnace is seen to be reasonably stable, as would be expected, while the over-all furnace average ΔT is decreasing to reflect the marked drop in efficiency of the areas affected by slag.

An interesting portrayal of the over-all average ΔT values is shown in Fig. 24 in which they are plotted against total heat available, above 80 F. The furnace-wall cleanliness conditions and burner-nozzle positions are indicated to add to the descriptive value of the plot. The letter designations for the various points refer to the various test series, as described. The data indicate primarily the substantial effect of burner-nozzle tilting and the benefits of downward tilting for this particular unit. The expected long-range effect of furnace-tube "aging," and consequent loss of absorption efficiency, is not the least bit in evidence from a study of these data, although such effect might well be obscured by internal tube fouling which would produce

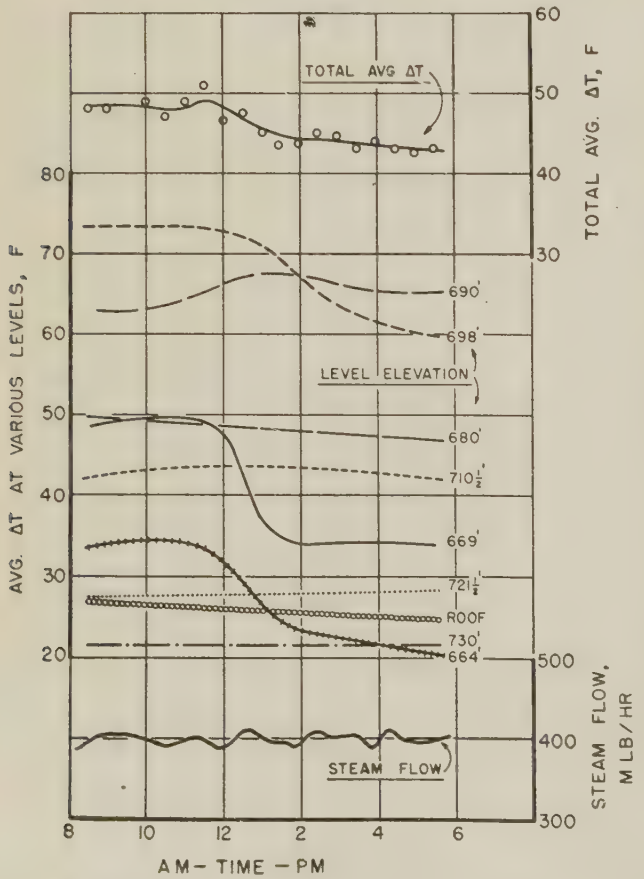

Fig. 23 Furnace Tube Level Average ΔT Variation With Time for Test No. 14

LETTER	TEST NUMBERS	AGE OF BOILER
A	1, 2, 3, 4	3 MONTHS
B	10, 11, 13, 14, 15	6 MONTHS
C	17, 18, 19, 20, 21	9 MONTHS

FURNACE CONDITION: CLEANED ○ DIRTY ●

ARROW INDICATES BURNER INCLINATION

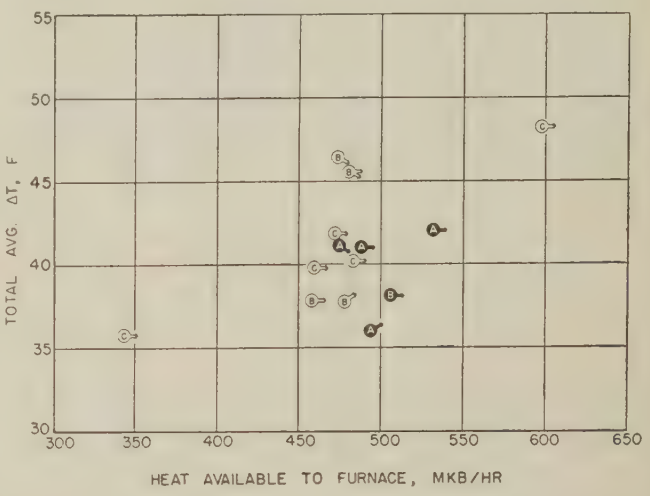

Fig. 24 Furnace Tube Total Average ΔT Variation With Heat Available Above 80 F for All Complete Tests

abnormally high tube-metal temperatures. The effect of rating, or heat input, is clearly evident although more confirming points at the high and low extremes are needed to establish a more firm basis for this characteristic. The furnace cleanliness conditions produce a marked effect on over-all absorption but probably not as great as might be expected primarily due to the powerful "equalizing" effect of radiant heat throughout the entire furnace.

Any attempt to calculate a furnace efficiency from the data obtained is of course subject to many possible errors of both constant and variable nature. The ΔT values are subject to possible variation with age of thermocouple leads, with variation in inside tube cleanliness condition and with variation in inside-film conductance. Along with these are the factors of proper selection of equivalent furnace surface, weighting of thermocouple data with respect to surface and the partial circumferential distortion of heat flow through cylindrical tubes on close centers and with nonuniform radial heat flow. However, in order that a set of comparative figures be made available for study, we have assumed a number of factors and calculated others to arrive at an efficiency value on the following basis:

U metal[a] = 1040 Btu/ft², hr, F (calc.) (referred to tube OD)
U film = 5000 Btu/ft², hr, F (assumed) (referred to tube OD)
U over-all = 860 Btu/ft², hr, F (calc.) (referred to tube OD)

[a] Tube OD = 3 in.; ID = 2.40 in.; K = 348 Btu/ft²-hr/in.

S = 6430 sq ft (measured projected furnace surface)

ΔT = average furnace center-line thermocouple temperature difference

Total furnace heat absorption = $U\,S\,\Delta T = 5{,}500{,}000 \cdot \Delta T$ Btu per hr

The furnace efficiency then becomes

$$\text{Efficiency} = \frac{5{,}500{,}000\ \Delta T}{\text{heat available}} \times 100$$

Table 3 gives the calculated efficiency on this basis for all the tests reported herein. These efficiency figures can be compared with those obtained from other means of testing, particularly

the furnace-exit-gas-temperature survey. Such comparisons should be carefully judged to take into account the possible sources of error in both determinations Serious consideration

TABLE 3 CALCULATED EFFICIENCY FOR TESTS

Test no.	Heat available, MKB/hr	Avg ΔT, F	Heat absorbed, MKB/hr	Efficiency, per cent
1	532	42	231	43.4
2	494	36	198	40.0
3	476	41	225	47.3
4	489	41	225	46.0
11	506	38.1	210	41.5
12	458	37.8	208	45.4
13	495	37.7	208	42.0
14	480	45.6	251	52.3
15	474	46.5	256	54.0
17	483	40.2	221	45.8
18	597	48.2	265	44.4
19	459	39.8	219	47.8
20	472	41.8	230	48.7
21	343	35.7	197	57.4

should be given to acid cleaning the boiler prior to each testing period so as to reduce substantially the possible great variation in tube temperatures resulting from variable internal tube fouling.

Conclusions

The following statements are made as tentative conclusions and should be recognized as being based on a limited amount of data covering performance of a single specific boiler furnace. The performance of other furnaces, or this furnace under other conditions not explored as yet, may serve to modify or to refute such conclusions. However, these are drawn with the purpose of presenting a positive viewpoint based on the limited facts at hand so that further investigation and possible controversy will be stimulated by differences in opinion or judgment.

The variation in furnace-wall-tube absorption, as determined by tube-temperature measurement, shows over-all heat absorption to be influenced materially by (*a*) rating, (*b*) ash accumulation, (*c*) flame position, and (*d*) excess air for combustion. All four were investigated and the rating, flame position, and excess air are directly controllable while the ash accumulation on wall tubes can be controlled indirectly to some extent by the use of furnace-wall soot blowers.

A study of the furnace-wall heat-absorption data and isotherms, which are plots of the wall-tube temperatures above saturation base, indicates some interesting conditions which are described briefly, as follows:

(*a*) High absorption rates are attained in the path of burner flame, as would be expected. This could be demonstrated unmistakably and adjusted, as desired, by varying the vertical tilt of the burner nozzles.

(*b*) The heat-absorption rate in the burner zone is quite irregular as influenced by periodic accumulation and shedding of ash on the tubes in this area. The effect of this condition on over-all furnace performance is rather small due to the great diversity in period and magnitude of the action.

(*c*) The tests with various excess-air levels indicate greater furnace-wall absorption stability at high excess air, although highest furnace efficiency would probably be obtained with low excess air and periodic wall cleaning to remove the ash and slag deposits which form more readily.

The illustrations and descriptions of furnace-wall isotherms and the other analyses of the test data are probably only of passing interest to many who may feel that the conditions shown are "normal." To some it may appear that they are more favorable than was suspected. However, the extreme variation in ΔT values, both high and low, and their variable position as influenced by flame position should be of significance and concern to the furnace designer. Variation in ΔT values of 10:1 or 15:1 magnitude for a given thermocouple (see points 3–8, 3–9, and 4–2 in Table 2), as influenced by flame position and ash coverage, are not conducive of highest furnace efficiency and indicate the desirability of further study and better understanding of these effects.

The data indicate and illustrate the considerable extent of local instability of furnace-wall conditions. While these local effects are of great magnitude, they also are sufficiently diversified both as to period and location that their combined effect is considerably neutralized.

In general, it is concluded that the tube-metal temperatures, as measured, do give a reasonably good representation of relative heat-absorption rates throughout the furnace, and such information can be of considerable value in analyzing details of furnace geometry, burner design and location, slagging characteristics, and numerous other detailed considerations.

Acknowledgments

The author wishes to state that this report is a compilation of data recorded and analyzed greatly by the efforts and co-operation of others. The Subcommittee on Furnace Testing, consisting of John Blizard, B. J. Cross, F. G. Ely, J. H. Harlow, A. R. Mumford, W. T. Reid, and H. Weisberg, did much to set up a workable test program and follow it through with their able direction. The Combustion Engineering Company furnished materials and men whose help was of high caliber. The Babcock & Wilcox Company, and Foster Wheeler Corporation cooperated graciously in the loan of special testing equipment. The Ohio Power Company, Tidd Plant, supervisory and operating personnel were most helpful in the arrangements for and conduct of all tests. The work of the author's associate, Mr. G. W. Bice, both in conducting and analyzing the tests, has been outstanding and is a substantial contribution to the project. The co-operative work of the U. S. Bureau of Mines on the entire test project was of considerable magnitude and inestimable importance in all phases of the work and the Directors and Staff are to be highly complimented.

BIBLIOGRAPHY

1 II—"Furnace Heat Absorption Efficiency as Shown by the Temperature, Composition, and Flow of Gases Leaving the Furnace," by W. T. Reid, Paul Cohen, and R. C. Corey, in this issue of Transactions, pp. 569–586.

III—"Variations in Heat Absorption as Shown by Density and Velocity Measurements of the Fluid Within a Tube," by A. R. Mumford and C. G. R. Humphreys, in this issue of Transactions, pp. 587–600.

IV—"Comparison and Correlation of the Results of Furnace-Heat-Absorption Investigations," by A. R. Mumford and G. W. Bice, in this issue of Transactions, pp. 601–614.

2 "Some Factors in Furnace Design for High Capacity," by E. G. Bailey, Trans. ASME, vol. 50, 1928, pp. 253–283.

3 "Thermocouples for Furnace-Tube Surface Temperature Measurements," by C. G. R. Humphreys, *Combustion*, vol. 16, December, 1944, pp. 53–55.

Appendix

The fourth series of tests (Nos. 24, 25, and 26) were run to establish further the effect of time on furnace-wall cleanliness both as to long-range effects and over short periods, say several days. Test No. 24 was a maximum-load run without wall cleaning to establish this condition in relation to earlier tests. Test No. 25 was a 60-hr continuous test run at maximum load with furnace walls cleaned just prior to the tests. The data have been broken down into five short periods during the main test and corresponding to those periods during which furnace-exit-gas temperature and composition data were taken. These tests are identified as follows:

TABLE 4 SUMMARY OF OPERATING AND TEST DATA FOR FOURTH SERIES TESTS

Test Number		24	25A	25B	25C	25D	25E	26
Date		12/10/46	12/11/46	12/12/46	12/12/46	12/13/46	12/13/46	12/14/46
Duration	Hours	3	3-1/2	2-1/3	2-1/2	3	3	5
Furnace Condition		Dirty	Cleaned	-	-	-	-	Cleaned
No. Pulverizers in Operation		2	2	2	2	2	2	2
No. Burners in Operation		8	8	8	8	8	8	8
Upper Burners Inclination	Deg	0	0	0	0	0	0	0
Lower Burners Inclination	Deg	0	0	0	0	0	0	0
Integrators:								
Steam Flow,	M lb/hr	525	468	505	503	511	511	412
Feedwater Flow,	M lb/hr	470	425	459	459	466	466	373
Desup. Water Flow,	M lb/hr	0	0	0	0	0	0	0
North Coal Scales,	M lb/hr	26800	24750	23600	26300	25600	25100	17700
South Coal Scales,	M lb hr	26600	24350	26000	25000	24700	24100	21700
Temperature Recorders:								
Primary Steam,	F	750	741	752	739	766	744	742
Secondary Steam	F	866	849	869	855	887	860	858
Superheat leaving Desup.,	F	160	153	161	151	178	157	165
Gas entering Preheater,	F	602	593	603	591	607	600	571
Gas leaving N. ID Fan,	F	322	309	322	313	298	297	296
Gas leaving S. ID Fan,	F	296	286	296	289	271	270	273
Air leaving FD Fan,	F	92	82	94	98	56	62	77
Air entering Preheater,	F	103	93	99	109	67	73	86
Air leaving Preheater	F	524	510	524	511	515	509	495
Water entering Econ.,	F	373	365	370	369	374	374	356
Water leaving Econ.,	F	476	470	476	472	482	477	461
N. Pulverizer Coal-Air,	F	138	140	145	147	148	148	149
S. Pulverizer Coal-Air,	F	146	149	151	153	154	149	143
Excess Air:								
Economizer Outlet,	%	15	25	19	17	22	18	31
Furnace Outlet,	%	11.3	24.7	16.8	15.6	17.9	16.8	28.3
Indicators:								
Steam Drum Pressure,	psig	1392	1349	1377	1367	1372	1380	1340
Steam Main Pressure,	psig	1320	1265	1290	1283	1298	1300	1280
SH. By-pass Dump. Opening	%	0	0	0	0	0	0	0
Raw Coal Analysis: *								
Heat Content (as rec'd),	Btu/lb	11130	11050	11650	11310	11540	11880	11910
Heat Content (M&A Free),	Btu/lb	14190	14180	14480	14330	14440	14540	14540
Moisture (as rec'd),	%	10.0	10.7	8.7	9.9	8.4	7.1	6.4
Ash (as rec'd),	%	11.5	11.4	10.9	11.2	11.7	11.1	11.7
Volatile (as rec'd)	%	33.2	32.1	33.4	33.1	33.6	34.5	35.6
H (M&A Free),	%	5.3	5.3	5.5	5.4	5.5	5.5	5.6
C (M&A Free),	%	80.3	80.3	81.1	80.6	80.9	81.0	81.2
N (M&A Free),	%	1.5	1.6	1.6	1.4	1.6	1.5	1.6
O (M&A Free),	%	10.4	10.3	9.1	9.9	9.4	9.1	8.8
S (M&A Free),	%	2.5	2.5	2.7	2.7	2.6	2.9	2.8
Ash Temperatures:								
Initial Deformation,	F	2090	2050	2150	2120	2210	2140	2220
Softening,	F	2210	2150	2220	2200	2310	2260	2420
Fluid,	F	2470	2520	2470	2420	2520	2520	2540
Pulverized Coal Fineness:								
Through No. 50 USS Sieve,	%	99.2	98.4	99.2	98.3	97.9	99.3	99.9
Through No. 100 USS Sieve,	%	93.7	91.4	92.5	90.6	88.2	95.5	98.3
Through No. 200 USS Sieve	%	75.0	70.4	72.5	68.7	61.3	81.1	88.0
Heat Input in Fuel,	MKB/hr	594	543	578	580	580	584	470
Heat Available to Furnace,	MKB/hr	611	561	597	596	598	602	483
Avg. Furnace Exit Gas HVT,	F	2015	1855	1925	1945	2025	2000	1865
Avg. Furnace Wall TC ΔT,	F	52.1	48.7	51.6	51.3	50.5	52.2	41.4

* Coal for all tests: Meigs Creek (No. 9), Duncanwood Mine, Harrison County, Ohio

Test no.	Hours during 60-hr run which apply
25A	0 to $3\frac{1}{2}$
25B	21 to $23\frac{1}{3}$
25C	$25\frac{1}{4}$ to $27\frac{3}{4}$
25D	45 to 48
25E	50 to 53

Test No. 26 was a recheck test on earlier runs at the normal load condition with furnace walls cleaned.

The operating data for the fourth series of tests are given in Table 4 which follows the same pattern as Table 1.

The average ΔT values for all thermocouple readings at each location are given in Table 5 (on opposite page) which follows the same arrangements as Table 2.

The calculated furnace absorption and efficiency data, corresponding to Table 3, are given in Table 6.

TABLE 6 CALCULATED FURNACE-ABSORPTION AND EFFICIENCY DATA

Test no.	Heat available, MKB/hr	Avg ΔT, deg F	Heat absorbed, MKB/hr	Efficiency, per cent
24	611	52.1	287	47.0
25A	561	48.7	268	47.8
25B	597	51.6	284	47.6
25C	596	51.3	282	47.3
25D	598	50.5	278	46.5
25E	602	52.2	287	47.7
26	483	41.4	228	47.2

An analysis of data taken during test No. 25 indicates no appreciable reduction in furnace efficiency over the 60-hr test period, and the apparent increase near the end of the test period is somewhat disconcerting. The only evident reason for this may be the great improvement in pulverized-coal fineness which was registered for this part of the run and which can be attributed in whole, or part, to lower moisture content of the fuel.

TABLE 5 CENTER-LINE THERMOCOUPLE AVERAGE TEMPERATURE DIFFERENTIALS FOR FOURTH SERIES TESTS

Test #	24	25A	25B	25C	25D	25E	26
TC #							
1-21	34	41	34	40	33	33	35
1-2	38	47	38	41	36	36	38
1-3	34	45	35	39	38	34	36
1-4	33	36	34	35	36	33	31
1-5	26	24	24	25	30	27	22
1-6	53	67	50	57	57	54	54
1-7	41	58	38	51	50	39	15
1-8	32	37	33	38	34	29	23
1-9	53	48	48	51	64	57	37
1-10	38	36	40	42	49	49	39
1-11	93	92	91	97	97	79	95
1-12	89	73	85	89	69	68	68
1-13	121	75	88	103	116	96	29
1-14	76	55	60	60	64	70	30
1-15	73	63	77	74	86	100	66
1-16	148	69	174	121	101	114	73
1-17	199	116	192	193	152	52	78
1-18	52	82	76	82	84	69	47
1-19	84	68	36	38	33	31	59
1-20	75	64	69	71	24	64	62
2-1	96	85	88	90	92	79	68
2-21	63	94	81	83	66	68	66
2-3	30	77	53	56	30	61	53
2-4	18	75	59	67	20	52	60
2-5	74	61	69	67	69	67	50
2-6	45	43	46	48	46	42	36
2-7	36	58	65	64	57	56	48
2-8	53	61	61	64	55	57	46
2-9	36	43	42	50	40	49	36
2-10	51	43	47	48	50	48	37
2-11	36	31	35	35	34	33	26
2-12	54	46	52	50	53	50	41
2-13	46	42	45	45	45	43	35
2-14	37	34	37	37	36	33	27
2-15	39	31	35	35	40	36	27
2-16	37	33	35	36	36	33	28
2-17	42	37	39	40	39	40	30
2-18	48	42	45	44	45	45	35
2-19	44	39	44	45	45	42	35
2-20	37	31	36	34	40	35	28
3-1	25	24	24	24	32	26	22
3-2	22	20	23	22	28	25	20
3-21	29	32	22	28	30	25	20
3-4	33	35	32	37	32	30	34
3-5	24	24	22	25	21	18	21
3-6	26	28	31	30	36	41	35
3-7	27	29	30	30	33	36	33
3-8	37	38	41	40	41	48	43
3-9							
3-10	27	31	30	36	30	36	37

Test #	24	25A	25B	25C	25D	25E	26
TC #							
3-11	43	41	64	48	62	73	68
3-12	68	65	84	73	82	105	90
3-13	70	66	70	64	61	57	26
3-14	76	77	72	77	89	112	45
3-15	70	70	79	79	80	90	79
3-16	75	67	80	71	79	75	65
3-17	48	86	83	85	69	106	30
3-18	107	45	97	82	89	95	45
3-19	96	56	28	71	69	74	57
3-20	96	77	94	87	97	95	75
4-1	18	17	16	19	20	21	23
4-2	29	32	24	33	28	27	35
4-3	46	61	41	46	45	49	42
4-21	64	83	59	62	59	61	60
4-5	57	75	62	64	62	63	55
4-6	60	62	68	69	63	72	72
4-7	76	84	80	81	93	100	92
4-8	79	95	75	44	87	82	15
4-9	93	20	23	42	18	82	17
4-10	78	60	72	48	90	86	62
4-11	94	84	90	83	80	74	27
4-12	41	66	50	27	27	23	34
4-13	57	49	43	34	38	61	63
4-14	117	150	115	127	120	79	109
4-15	76	96	86	92	80	108	42
4-16	89	75	87	89	81	74	62
4-17	91	87	96	95	86	82	77
4-18	57	67	67	69	54	68	56
4-19	41	71	73	71	49	67	53
4-20	86	73	78	77	74	75	61
5-1	50	46	49	51	62	57	43
5-2	45	41	44	46	59	60	40
5-3			37	21	55	60	40
5-4	48	42	44	45	56	64	50
5-21	28	25	28	27	32	34	29
5-6	54	41	47	51	71	75	70
5-7	68	53	64	65	69	75	40
5-8	74	63	68	69	49	59	15
5-9	89	72	65	69	94	94	50
5-10	59	51	62	58	69	81	65
5-11	54	50	37	41	27	32	22
5-12	52	21	28	52	41	20	
5-13		23	40	30	29	33	15
5-14	76	84	68	46	38	33	28
5-15	78	64	82	71	71	82	43
5-16	80	61	66	63	58	63	52
5-17	72	76	72	71	52	67	64
5-18	44	57	53	55	32	52	48
5-19	55	50	57	57	57	64	45
5-20	55	43	48	51	57	57	41

Test #	24	25A	25B	25C	25D	25E	26
TC #							
6-1	21	20	18	21	20	20	24
6-2	19	23	19	20	19	20	23
6-3	21	29	21	23	22	22	25
6-4	37	33	51	46	51	51	40
6-5	18	49	60	51	59	57	44
6-21	47	41	43	46	43	43	36
6-7	51	40	46	42	44	43	32
6-8	35	29	34	30	31	33	25
6-9	38	33	41	34	38	35	28
6-10	26	24	25	24	24	27	24
6-11	20	20	19	18	21	20	17
6-12	17	19	18	19	20	22	20
6-13	60	50	54	58	60	55	41
6-14	55	52	61	63	62	58	44
6-15	35	34	34	37	29	39	29
6-16	37	32	35	37	39	38	28
6-17	39	37	39	41	44	41	35
6-18			32	37	37	39	28
6-19	*						
6-20	*						
7-1	73	56	69	72	74	74	55
7-2	81	73	85	87	72	80	68
7-3	29	47	78	78	69	75	60
7-4	58	66	74	71	55	70	59
7-5	62	57	64	63	58	62	53
7-6	18	25	19	21	18	17	17
7-21	19	24	17	20	18	16	17
7-8	26	29	23	25	25	22	23
7-9	14	16	13	14	16	13	13
7-10	13	14	14	14	20	17	13
7-11	12	13	14	14	18	15	12
7-12	15	17	14	16	18	15	17
7-13	18	21	16	18	19	15	17
7-14	18	24	18	18	18	13	20
7-15	18	27	19	19	16	15	21
7-16	13	17	14	14	10	10	14
7-17	14	14	15	14	19	15	15
7-18	*						
7-19	*						

* External saturation base thermocouple

An Investigation of the Variation in Heat Absorption in a Pulverized-Coal-Fired Water-Cooled Steam-Boiler Furnace

II—Furnace Heat Absorption Efficiency as Shown by the Temperature, Composition, and Flow of Gases Leaving the Furnace[1]

By W. T. REID,[2] PAUL COHEN,[3] and R. C. COREY[4]

As part of an investigation of the factors affecting the performance of furnaces, the heat-absorption efficiency of the furnace of a pulverized-coal-fired dry-bottom steam boiler was determined from the sensible heat in the gases at the furnace outlet. The sensible heat was determined from the temperature of the gases, which was measured by traversing the furnace outlet with a high-velocity thermocouple, and from the quantity of gas leaving the furnace, which was computed from the composition of the gas and the rate of fuel firing. Data are given for the distribution at the furnace outlet of excess air, gas temperature, and mass flow. The effect on furnace heat-absorption efficiency is shown for variations in (*a*) the heat available in the furnace, (*b*) the excess air, (*c*) the angle of inclination of the burners, and (*d*) the condition of the furnace with respect to deposits of ash and slag on the heat-absorbing surfaces. The data of this investigation were correlated by a modified form of the Hudson-Orrok equation, which relates empirically the furnace heat-absorption efficiency to the weight of wet gases at the furnace outlet, per unit heat available in the furnace, and the heat available in the furnace per square foot of projected radiant heating surface.

Introduction

THIS paper summarizes four series of determinations of the furnace heat-absorption efficiency of a central-station pulverized-coal-fired steam-boiler furnace and presents the effects on furnace heat-absorption efficiency of variations of load, excess air, inclination of the burners, and cleanliness of the furnace. The unit studied is boiler No. 11 of the Tidd Station, Ohio Power Company, Brilliant, Ohio, a three-drum bent-tube boiler with a dry-bottom tangentially fired furnace with vertically adjustable burners. It is rated at 475,000 lb of steam per hr at 1375 psig and 925 F at the superheater outlet. The determinations of furnace heat-absorption efficiency were part of a comprehensive investigation of this unit by the Special Research Committee on Furnace Performance Factors of the ASME and were made by the Combustion Research Section of the Bureau of Mines concurrently with the other studies reported in this symposium, as part of the Bureau of Mines co-operative research program with the Committee to study the effect of ash and slag on furnace performance.

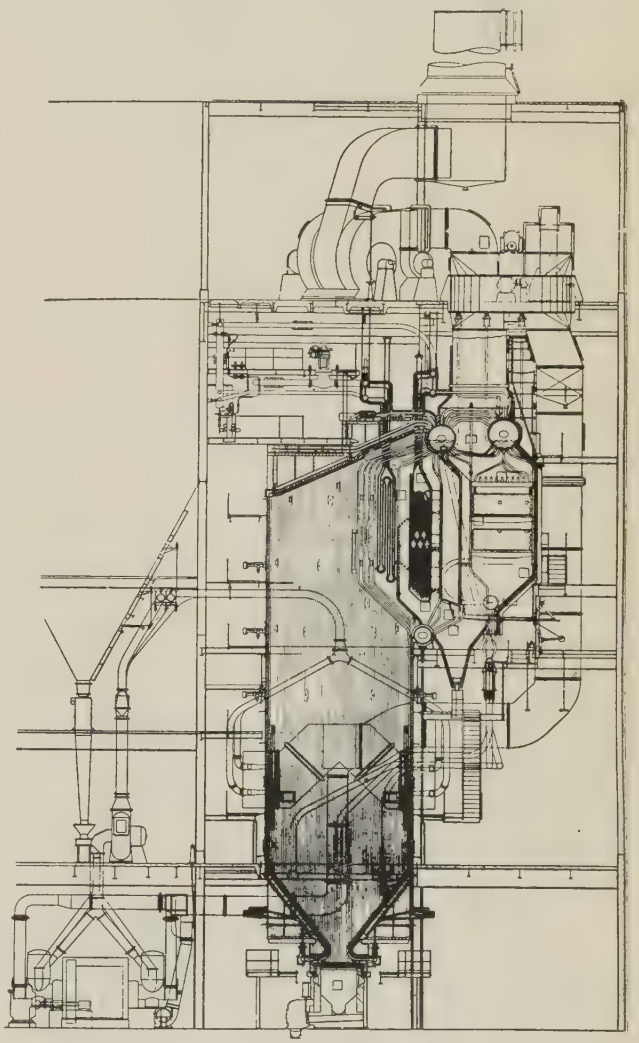

Fig. 1 Sectional Elevation of Steam-Generating Unit

[1] Published by permission of the Director, Bureau of Mines, U. S. Department of the Interior.

[2] Consulting Fuel Engineer, Bureau of Mines; Assistant Supervisor, Battelle Memorial Institute, Columbus, Ohio. Mem. ASME.

[3] Fuel Engineer, Combustion Research Section, Bureau of Mines, Pittsburgh, Pa. Mem. ASME.

[4] Supervising Engineer, Combustion Research Section, Bureau of Mines, Pittsburgh, Pa. Mem. ASME.

Contributed by the Special Research Committee on Furnace Performance Factors in co-operation with the Fuels, Power, and Heat Transfer Divisions and presented at the Semi-Annual Meeting, Chicago, Ill., June 16–19, 1947, of The American Society of Mechanical Engineers.

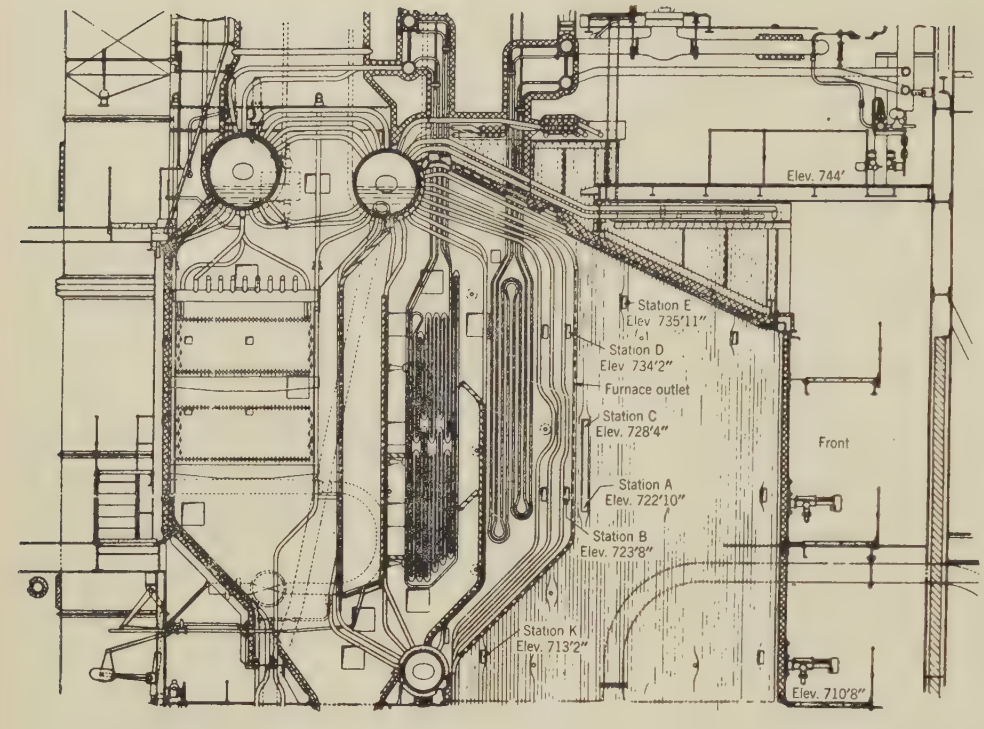

FIG. 3 LOCATION OF PROBE STATIONS ON LEFT SIDE OF BOILER
(Stations B-R, D-R, E-R, and K-R at corresponding levels and positions on right side of boiler.)

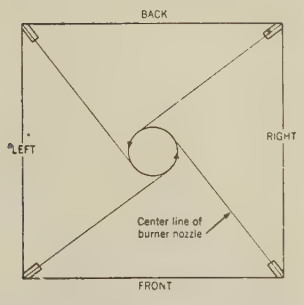

FIG. 2 FIRING CIRCLE AND DIRECTION OF ROTATION OF GASES FOR HORIZONTAL SETTING OF BURNERS; LOOKING DOWN

Twenty-six tests were made to determine the furnace heat-absorption efficiency from the sensible-heat content in the gases leaving the furnace. The sensible heat was calculated from measurements of the temperature of the gases with a single-shield high-velocity thermocouple (HVT), and of the excess air of the gases with a Bailey oxygen recorder. The measurements were made at positions approximating the furnace outlet, within the available means of access to the furnace. In some of the tests, the velocity of the gases leaving the furnace was determined with a water-cooled double-impact Pitot tube. Complete records of the original data and calculations are in the Committee files, and therefore are not repeated here. However, complete details of the test procedures, equipment, and methods of calculation are presented with sufficient data to permit evaluation of the results.

METHODS OF TEST AND CALCULATION

Description of Furnace. Fig. 1 is a sectional elevation of the steam-generating unit, showing the general arrangement of the various components.

The furnace is tangentially fired, with two burners in each corner, firing to a circle $2^1/_2$ ft in diam, each burner being individually adjustable from an inclination of 30 deg downward to 30 deg upward from the horizontal. Two ball-mill pulverizers supply the fuel, each mill supplying one burner in each of the four corners. The direction of rotation of the flame is shown schematically in Fig. 2. Each furnace wall consists of 3-in-OD bare tubes on $3^1/_8$-in. centers and the roof of 3-in-OD finned tubes on 6-in. centers. The slag screen and the convection surface at the furnace outlet are 3-in-OD bare tubes on $9^1/_2$-in. centers and are so arranged with respect to the inspection doors available for inserting the test probes that some traverses had to be made behind the first row of tubes. The area of projected radiant heating surface in the furnace is 6430 sq ft, including the plane of the furnace outlet, which has a developed area of 672 sq ft.

Location of Test Points. The elevation of the six test stations on the left or north side of the boiler is shown in Fig. 3 which is a sectional side arrangement from the lower drum to the top of the boiler. The right or south side of the boiler has test stations directly opposite and corresponding to those on the left side, with the exception of *A* and *C*, thus making a total of ten test stations. The right-side stations bear the same letter designations as the corresponding left-side stations but are distinguished from the latter by the addition of the letter *R*. Fig. 4 is a plan view of the furnace, between the front wall and the last row of boiler tubes, showing the location of the test stations with respect to the front of the furnace, and the positions at which readings were taken. Positions on the right side of the furnace are distinguished from those on the left by primes. Because of its proximity to the wall, no readings were taken at position 1.

Fig. 5 is a map of the developed furnace outlet area, as observed from the front wall, corresponding to two intersecting planes passing through the screen tubes, bounded on the sides by the side-wall tubes, on the top by the roof tubes, and on the bottom by the rear-wall tubes. The furnace outlet is also shown by the heavy dashed line in Fig. 3. The developed furnace outlet is 31 ft high, 21 ft 8 in. wide, and has an area of 672 sq ft.

Equipment Used. The temperature of the gas at the indicated sampling positions was determined by means of one of three

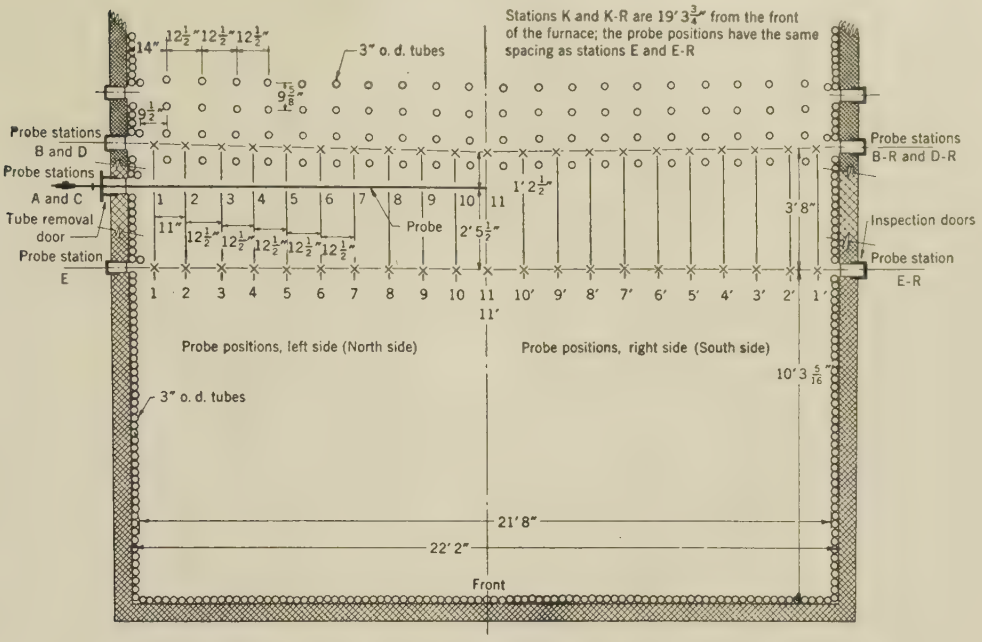

FIG. 4 PLAN VIEW OF FURNACE, SHOWING PROBE STATIONS AND POSITIONS

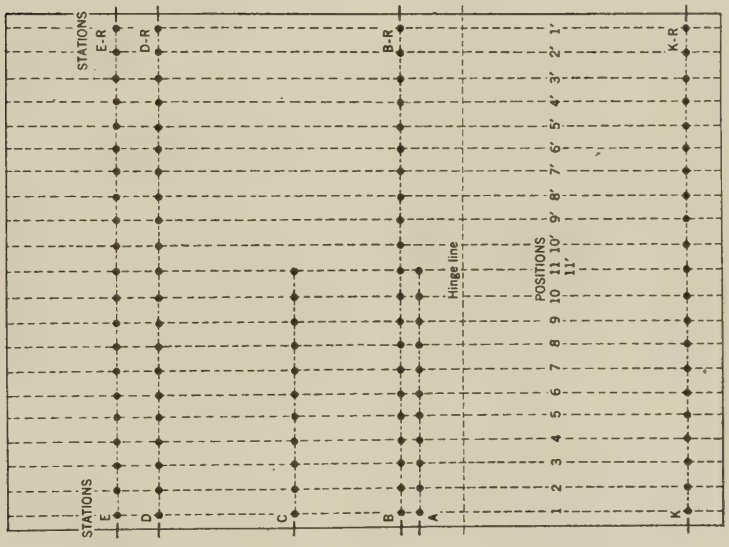

FIG. 5 FURNACE-OUTLET AREA, SHOWING SAMPLING STATIONS AND POSITIONS

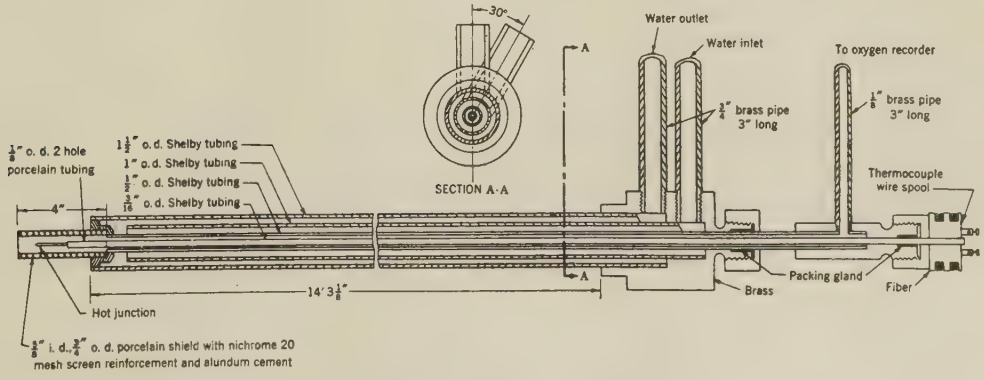

FIG. 6 HIGH-VELOCITY THERMOCOUPLE

single-shield high-velocity thermocouples mounted in a water-cooled support, the details of which are shown in Fig. 6. One of these units was equipped with a 22-gage platinum-rhodium thermocouple for temperature measurements at stations *K* and *K-R*, and the other two with 22-gage chromel-alumel thermocouples for measurements at the other stations where the temperatures were lower and within the permissible range of this material. Simultaneous readings of excess air and gas temperature were obtained by connecting the offtake of the high-velocity thermocouple to the Bailey oxygen recorder with which the boiler was equipped. The pump of this instrument produced higher rates of gas flow past the thermocouple junction than could be obtained with an air aspirator operating at the pressure available in the station service line. In addition to furnishing a simple means for maintaining the flow of gases required for the HVT, this expedient shortened the time required to make a test and assured that the gas temperature and composition were determined under identical conditions. Frequent Orsat analyses of the gas entering the recorder indicated it to be entirely dependable in all except one series of tests, and in that case the check analyses permitted correction of the observed data to a satisfactory degree of accuracy.

The temperatures of the gases at the furnace exit, as determined by the single-shield high-velocity thermocouple, HVT, require correction for two reasons, i.e., the mass velocity of the gas through the couple in these tests was about 5000 psf per hr, instead of the optimum mass velocity of 13,000 to 15,000 psf per hr; and even at the optimum mass velocity of the gases, the couple may indicate a temperature different from the true gas temperature, depending on the radiant heat-transfer characteristics of the environment. Mullikin[5] has shown that true gas temperatures are closely attained by the multiple-shield high-velocity thermocouple, MHVT, and has given a curve from which the necessary corrections may be obtained.

Since the present corrections to the HVT data involved the additional factor of mass velocity, it was decided, after completion of the regular series of tests, to make direct comparisons of the HVT and the MHVT in the Tidd furnace. These supplementary tests were made during the week of June 2, 1947, and the results were available too late to include in the presentation of the paper. However, the details of the test procedure and the results are given in the discussion of this paper by F. G. Ely, who participated in the tests. It was found that the average temperatures of the gases at the furnace outlet, indicated by the HVT, were approximately 85 deg F too low. Calculations of the heat absorption in the furnace are reported for both the observed exit-gas temperatures with the HVT and for the observed exit-gas temperatures corrected by adding 85 deg F, and designated MHVT. However, all correlations made in the paper have been based on the corrected MHVT data.

In the second series of tests, the velocity of the gas was determined in the planes parallel to the side walls of the furnace for all odd-numbered sampling positions except No. 1. The water-cooled double-impact Pitot tube, shown in Fig. 7, was used for this purpose. The directions of the gas flow in planes parallel to the side walls of the furnace were found by rotating the axis of the Pitot tube until a maximum pressure difference was indicated, the angle being obtained from a dial mounted on the instrument. Gas-velocity measurements also were made in the first series of tests, but only with the axis of the Pitot tube in the horizontal direction. Subsequent analysis of the data showed this technique to be inadequate; therefore it was modified as described previously.

Methods of Calculation. (*a*) *Temperature and Excess-Air Data.* Because the sampling stations are limited to the access doors and therefore are not distributed uniformly over the furnace outlet area, a direct numerical average of the observations would give undue weight to some and insufficient weight to others. Therefore averages of the data were calculated according to the weighting key shown in Fig. 8, in which the furnace outlet area is divided into five vertical bands, numbered 1 to 5 from left to right, and six horizontal strips designated K_1, K_2, *A*, *C*, *D*, and *E* from bottom to top, thus making 30 equal sections. Fig. 8 also indicates the scheme followed in computing the average values of the variables for each section of the furnace outlet area. The values for temperature and excess air used in calculating the averages for the sections are those of the data from the corresponding stations, with the exceptions noted in Fig. 8. For example, the average for section No. 2 would be computed by giving unit weight to the data of positions Nos. 5, 6, 7,

[5] "Gas Temperature Measurement and the High-Velocity Thermocouple: Temperature, Its Measurement and Control," by H. F. Mullikin, Rheinhold Publishing Corporation, New York, N. Y., 1941, pp. 775–804.

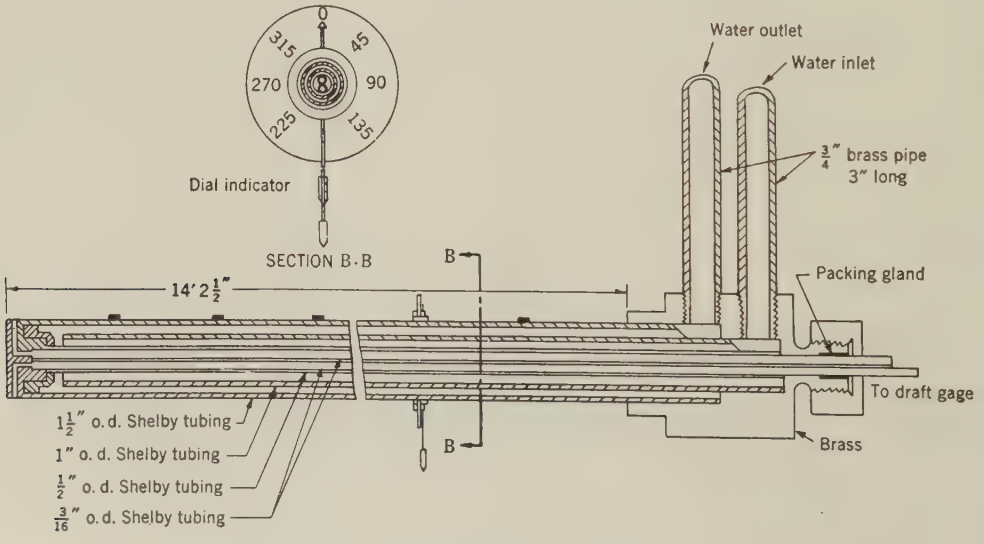

Fig. 7 Double-Impact Pitot Tube

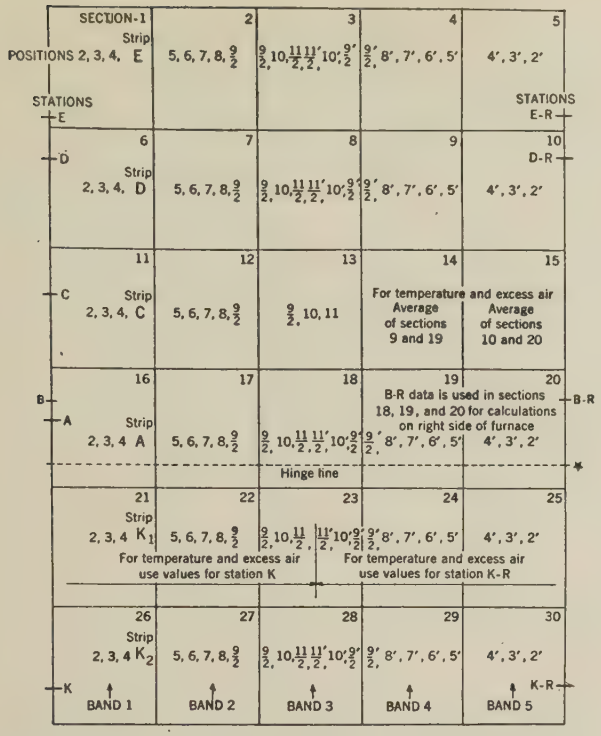

FIG. 8 WEIGHTING KEY FOR COMPUTING AVERAGE VALUES OF TEMPERATURE AND EXCESS AIR FOR ALL SECTIONS OF FURNACE-OUTLET AREA

and 8 of station *E* and one-half weight to position No. 9 of station *E*. This method serves not only to weight the data systematically according to area, but also gives some idea of the spatial distribution of the values of gas temperature and excess air.

(*b*) *Velocity Data.* The velocity data obtained in the second series of tests were treated in a similar manner to that just described, but the methods were more complicated and will not be described here. The report to the Committee on the second series of tests contains a complete review of this phase, including data and detailed summaries. The final results of the velocity calculations were values of the effective mass velocity, *M*, of the gases leaving the furnace, in pounds per square foot and second for each of the sections of the furnace-outlet area, which could be further treated in the same manner as the values of temperature and excess air for each of the sections.

(*c*) *Calculation of Heat Content of Gases Leaving the Furnace.* Calculations of the sensible-heat content of the gases leaving the furnace were made from the average values of the temperature and excess-air data for the thirty sections of the furnace outlet. The total sensible-heat content of the gases leaving the furnace is obtained by multiplying the rate of coal feed *F*, lb of MAF coal per hr, by $\overline{Hu}$, the sensible-heat content of the gases formed from the combustion of 1 lb of MAF coal for the "average" conditions of temperature and excess air at the furnace outlet. The derivations of the formulas used, and curves for ready calculation of the necessary quantities, are given in Appendix 1 of this paper.

(*d*) *Calculation of Heat Available, Heat Absorbed, and Heat-Absorption Efficiency in the Furnace.* The heat available in the furnace was computed as the sum of the "net" heat available in fuel fired, corrected for an average carbon loss of 0.8 per cent of the gross heating value of the fuel, plus the sensible-heat content of the preheated air entering the furnace. The latter was calculated in each test from the excess air at the furnace outlet and the temperature and moisture content of the preheated air. Allowance was made for 10 per cent air infiltration to the furnace and for calculated values of air leakage to the pulverizers, as well as tempering air. A further correction was made for radiation losses from the furnace, equal to one half the radiation loss for the whole unit; this was taken for all tests as 0.2 per cent of the gross heating value of the fuel fired.

The heat absorbed is the difference between the net heat available in the furnace and that carried out as sensible heat in the gases at the furnace outlet, and the furnace heat-absorption efficiency is expressed as the percentage of the net heat available in the furnace that is absorbed in the furnace. The net heat available in the furnace and the heat absorption in the furnace are calculated in terms of unit furnace area by dividing by 6430 sq ft, the projected radiant heating surface of the furnace. The details of these calculations are given in Appendix 2.

Summary of Test Conditions and Results

The operating data and the results obtained in the four series of tests are summarized in Tables 1, 2, 3, and 4. For each test there are given the operating conditions; the proximate analysis of the fuel, including heating value and ash-softening temperature; the average HVT and MHVT gas temperature, and the excess air at the furnace outlet; the calculated values of heat available in the furnace; weight of wet gases and sensible heat at the furnace outlet; heat absorbed in the furnace; and furnace heat-absorption efficiency. Wherever pertinent, the data are expressed on the basis of HVT and MHVT temperatures.

First Series, Tests Nos. 1, 2, 3, and 4. The boiler was placed in operation on September 25, 1945, and thereafter was operated without cleaning of the furnace until after the completion of the first series of tests, made during the week of December 17, 1945. It may be assumed that after operating for a period of 3 months without cleaning, the furnace walls were quite dirty. The four tests of this series, Nos. 1, 2, 3, and 4, were planned to determine the effect of the inclination of the burners on furnace heat-absorption efficiency for this condition of the furnace walls, and for a steam flow of about 420,000 lb per hr, and excess air of 30 per cent at the economizer outlet. The data are summarized in Table 1.

The test technique in this first series was incomplete and not comparable with later tests. No data were obtained at stations *K* and *K-R*, but the velocities of the gases were determined at the test positions across the furnace by the method previously described. The heat content of the gases leaving the furnace, calculated from the velocity data, averaged only 29 per cent of the heat content calculated from the rate of fuel firing. This was attributed in part to the methods used for the velocity measurements, but mostly to the failure to make observations at stations *K* and *K-R*, and to the use of too small a value for the area of the furnace outlet. Although not ideally located in the furnace, stations *K* and *K-R* therefore were established and included in the tests of the subsequent series.

Item 29 of Table 1 reveals that the furnace heat-absorption efficiency, based upon MHVT temperatures, varied in the expected manner from the indicated value of 50.9 per cent for test No. 3, in which all burners were inclined at —30 deg, to 44.3 per cent for test No. 2, in which all burners were inclined at +30 deg. Of the two tests made with the burners horizontal, the result of test No. 4, with an indicated furnace heat-absorption efficiency of 50.4 per cent, seems to be high, and that of test No. 1, 46.1 per cent, seems to be low, compared to the values for the other burner settings. It is apparent that these data cannot yield even true relative values of furnace heat-absorption efficiency; the ratios between the furnace heat-absorption efficiencies given in Table 1 and the true values for each particular test must be expected to vary with the angle of inclination of the burners. In a later part of this paper a method is given whereby an approximation to the

TABLE 1 SUMMARY OF TEST CONDITIONS AND RESULTS.[a] FIRST SERIES, TESTS NOS. 1, 2, 3, AND 4

		1	2	3	4
1	Test number				
2	Date	12–18–45	12–19–45	12–20–45	12–21–45
3	Steam flow, lb per hr	446,000	411,000	405,000	419,000
4	Rate of fuel firing, as fired, weight lb per hr	44,700	43,090	42,000	42,500
5	Inclination of burners, Upper	0	+30	—30	0
6	from horizontal, degrees, Lower	0	+30	—30	0
7	Condition of furnace walls	Dirty[b]	Dirty[b]	Dirty[b]	Dirty[b]
8	Excess air at economizer outlet, per cent	30	30	30	30
	Coal, proximate analysis, per cent as fired				
9	Moisture	8.0	9.5	9.5	9.0
10	Volatile matter	34.3	33.1	33.0	33.6
11	Fixed carbon	45.2	44.3	44.0	44.5
12	Ash	12.5	13.1	13.5	12.9
13	Btu per lb, as fired	11,400	11,020	10,970	11,150
14	Ash-cone softening temperature, F	2,540	2,560	2,600	2,550
15	Temperature of preheated air, F	542	537	506	509
16	Heat available in furnace[c], kB per hr	532,000	494,000	475,000	490,000
17	kB per hr and ft²	82.7	76.8	73.9	76.2
18	Excess air at furnace outlet, per cent	28	27	25	26
19	Average temperature of gases, HVT	1,920	1,970	1,780	1,785
20	at furnace outlet, F, MHVT	2,005	2,055	1,865	1,870
21	Weight wet gases at furnace outlet, lb per hr	532,000	494,000	468,000	486,000
22	Total sensible heat in wet gases, HVT	273,000	262,000	221,000	230,000
23	at furnace outlet, kB per hr, MHVT	287,000	275,000	233,000	243,000
24	Heat absorbed in furnace, HVT	259,000	232,000	254,000	260,000
25	kB per hr, MHVT	245,000	219,000	242,000	247,000
26	Heat absorbed in furnace, HVT	40.3	36.1	39.5	40.4
27	kB per hr and ft², MHVT	38.1	34.1	37.6	38.4
28	Furnace heat-absorption HVT	48.7	47.0	53.5	53.1
29	efficiency, per cent MHVT	46.1	44.3	50.9	50.4

[a] No data taken at stations K and K-R; not comparable with other tests.
[b] Furnace had not been cleaned for several months prior to test, and was not cleaned during course of tests.
[c] Corrected for radiation and carbon loss, infiltration of air to furnace, and leakage of air to pulverizer.

true furnace heat-absorption efficiencies for these tests is obtained.

Second Series, Tests Nos. 10, 11, 13, 14, and 15. The second series of five tests were made during the week of February 25, 1946, and are summarized in Table 2. Again, the primary purpose of the tests of this series was to determine the effect of the inclination of the burners on furnace heat-absorption efficiency for much the same conditions of heat release, and excess air at the economizer outlet, as occurred in the first series of tests, but in this case for a clean furnace. Except in the case of test No. 10, the first in the series, which was intended to serve as a link between the first and second series of tests, each test was preceded by a complete cycle of furnace-cleaning operations. The burner arrangements studied included all those of the first series with the addition of a test wherein the upper burners were horizontal and the lower burners were inclined at —30 deg. As noted in Table 2, it was not possible to obtain complete data for test No. 13, with all burners inclined at +30 deg; therefore the results for that test were calculated on the same basis used for tests Nos. 1 to 4 of the first series.

Comparison of the calculated furnace heat-absorption efficiencies, item 29 of Table 2, which are based upon MHVT temperatures, reveals that with the exception of test No. 13, the results obtained are in the proper qualitative relationship. Tests Nos. 10 and 11 are not comparable because of a considerable difference in heat-release rates.

The relationship of the furnace heat-absorption efficiencies to the inclination of the burners for the 9 tests of the first and second series is shown graphically in Fig. 9. In this figure the observed furnace heat-absorption efficiency (MHVT) for each test is plotted against the angle of inclination of the burners; test No. 14, upper burners horizontal, lower burners inclined at —30 deg, has been plotted arbitrarily at —15 deg. In each case are indi-

TABLE 2 SUMMARY OF TEST CONDITIONS AND RESULTS. SECOND SERIES, TESTS NOS. 10, 11, 13, 14, AND 15

		10	11	13[a]	14	15
1	Test number					
2	Date	2–26–46	2–27–46	2–28–46	3–1–46	3–2–46
3	Steam flow, lb per hr	421,000	396,000	414,000	424,000	426,000
4	Rate of fuel firing, as fired weight, lb per hr	44,650	41,500	41,500	41,200	40,800
5	Inclination of burners, Upper	0	0	+30	0	—30
6	from horizontal, degrees, Lower	0	0	+30	—30	—30
7	Condition of furnace walls	Dirty[b]	Clean[c]	Clean[c]	Clean[c]	Clean[c]
8	Excess air at economizer outlet, per cent	29	30	28	27	26
	Coal, proximate analysis, per cent as fired					
9	Moisture	9.6	10.8	8.9	9.0	8.8
10	Volatile matter	33.4	33.0	34.2	34.3	34.4
11	Fixed carbon	43.7	42.9	46.2	44.4	44.1
12	Ash	13.3	13.3	10.7	12.3	12.7
13	Btu per lb, as fired	10,910	10,680	11,510	11,280	11,230
14	Ash-cone softening temperature, F	2,470	2,360	2,570	2,430	2,400
15	Temperature of preheated air, F	524	497	506	501	501
16	Heat available in furnace[d], kB per hr	505,000	458,000	495,000	480,000	473,000
17	kB per hr and ft²	78.5	71.2	77.0	74.6	73.6
18	Excess air at furnace outlet, per cent	24	28	26	26	26
19	Average temperature of gases, HVT	1,930	1,820	1,730	1,745	1,665
20	at furnace outlet, F, MHVT	2,015	1,905	1,815	1,830	1,750
21	Weight wet gases at furnace outlet, lb per hr	498,000	468,000	494,000	478,000	472,000
22	Total sensible heat in wet gases, HVT	259,000	227,000	226,000	221,000	207,000
23	at furnace outlet, kB per hr, MHVT	272,000	239,000	238,000	233,000	219,000
24	Heat absorbed in furnace, HVT	246,000	231,000	269,000	259,000	266,000
25	kB per hr, MHVT	233,000	219,000	257,000	247,000	254,000
26	Heat absorbed in furnace, HVT	38.3	35.9	41.8	40.3	41.4
27	kB per hr and ft², MHVT	36.2	34.1	40.0	38.4	39.5
28	Furnace heat-absorption HVT	48.7	50.4	54.3	54.0	56.2
29	efficiency, per cent MHVT	46.1	47.8	51.9	51.5	53.7

[a] No data taken at stations K and K-R; this test calculated on same basis as tests Nos. 1–4.
[b] Furnace had not been cleaned for several days prior to test.
[c] Furnace blowers operated for one hour, just prior to test.
[d] Corrected for radiation and carbon loss, infiltration of air to furnace, and leakage of air to pulverizer.

cated the test number, condition of the furnace, and extent of the survey on which the calculation was based. It is apparent that these data are of little value in the form in which they have been plotted in Fig. 9. In a subsequent part of this paper it will be shown, however, that when these data are corrected to a uniform basis, they give a fair representation of the effect of the angle of inclination of the burners on furnace heat-absorption efficiency.

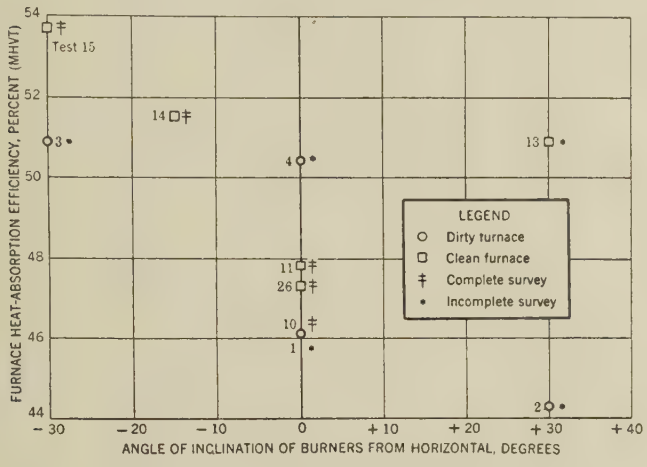

FIG. 9 OBSERVED FURNACE HEAT-ABSORPTION EFFICIENCY FOR VARYING INCLINATION OF BURNERS

(Average steam flow, all tests, 418,000 lb per hr. Average excess air at economizer outlet, all tests, 29 per cent.)

Third Series, Tests Nos. 17A, 17B, 18A, 18B, 19A, 19B, 20A, 20B, 21A, and 21B. The third series of tests was made during the week of June 5, 1946, to determine the effect of boiler rating and excess air on the heat-absorption efficiency of the clean furnace. By making two complete surveys each day, one in the morning directly after the furnace-cleaning operations, and the other in the afternoon, without further cleaning, the effect of this short time interval on furnace heat absorption could be noted. To isolate the variables, one group of tests, Nos. 17, 19, and 20, were made at an approximately constant steam flow of 420,000 lb per hr, but with excess air at the economizer outlet varying from 36 to 20 per cent. The other group was made at approximately constant excess air at the economizer outlet of 28 per cent, and steam flow varying from 315,000 to 523,000 lb per hr. The burners were horizontal in all the tests of this series.

The test conditions and results are summarized in Table 3; the morning surveys are designated by the letter *A*, the afternoon surveys by the letter *B*. The furnace heat-absorption efficiencies for the tests with varying excess air and constant steam flow are plotted in Fig. 10; those of the tests at constant excess air and varying steam flow are plotted in Fig. 11. The lines connecting the points on these plots are dashed rather than full, to indicate that the relationships they imply probably do not correspond to uniform conditions of the furnace walls.

Fig. 10 indicates a decrease in furnace heat-absorption efficiency for both the morning and afternoon tests of about 1.9 per cent for an increase in excess air from 20 to 28 per cent at an average steam flow of 420,000 lb per hr. Fig. 11 shows that at 28 per cent excess air, there is a decrease of 2.8 per cent in the furnace heat-absorption efficiency for the morning tests for each 100,000 lb per hr increase in steam flow; the average change for the afternoon tests is about 2.1 per cent for each 100,000 lb per hr increase in steam flow, but the curve has a different form.

The most striking feature of the results of these tests is the considerable variation in furnace heat-absorption efficiency between the morning and afternoon surveys of some of these tests.

TABLE 3 SUMMARY OF TEST CONDITIONS AND RESULTS. THIRD SERIES, TESTS NOS. 17A, 17B, 18A, 18B, 19A, 19B, 20A, 20B, 21A, AND 21B

		17A[a]	17B[b]	18A[a]	18B[b]	19A[a]	19B[b]	20A[a]	20B[b]	21A[a]	21B[b]
1	Test number										
2	Date	6-4-46	6-4-46	6-5-46	6-5-46	6-6-46	6-6-46	6-7-46	6-7-46	6-8-46	6-8-46
3	Steam flow, lb per hr	420,000	422,000	523,000	518,000	417,000	414,000	426,000	419,000	315,000	316,000
4	Rate of fuel firing, as fired, weight lb per hr	40,190	39,040	49,490	49,330	38,320	38,050	38,500	38,710	27,830	28,550
5	Inclination of burners {Upper	0	0	0	0	0	0	0	0	0	0
6	from horizontal, degrees {Lower	0	0	0	0	0	0	0	0	0	0
7	Condition of furnace walls	Clean[c]	Clean[d]	Clean[c]	Clean[d]	Clean[c]	Clean[d]	Clean[c]	Clean[d]	Clean[c]	Clean[d]
8	Excess air at economizer outlet, per cent	36	36	28	29	28	28	20	18	28	28
9	Coal, proximate analysis, per cent as fired										
10	Moisture		7.7		7.3		7.7		5.6		5.3
11	Volatile matter		35.5		36.1		35.5		37.2		37.2
12	Fixed carbon		45.2		44.8		45.1		45.1		44.4
13	Ash		11.6		11.8		11.7		12.1		13.1
14	Btu per lb, as fired		11,590		11,620		11,600		11,940		11,820
15	Ash-cone softening temperature, F		2,490		2,170		2,190		2,470		2,470
16	Temperature of preheated air, F		521		536		514		511		495
17	Heat available {kB per hr		475,000		542		520		512		502
	in furnace[e] {kB per hr and ft²	488,000		598,000	597,000	458,000	456,000	472,000	474,000	338,000	347,000
18	Excess air at furnace outlet, per cent	75.9	73.9	93.0	92.8	71.2	70.9	73.4	73.7	52.6	54.0
19	Average temperature of gases at {HVT	35	35	26	28	23	26	17	15	27	28
	furnace outlet, F {MHVT	1,835	1,820	1,890	1,890	1,795	1,850	1,815	1,905	1,665	1,720
20	Weight wet gases at furnace outlet, lb per hr	1,920	1,905	1,975	1,975	1,880	1,935	1,900	1,990	1,750	1,805
21	Total sensible heat in wet gases {HVT	517,000	503,000	593,000	601,000	452,000	459,000	445,000	439,000	344,000	357,000
22	at furnace outlet, kB per hr {MHVT	253,000	244,000	302,000	305,000	217,000	228,000	217,000	226,000	151,000	162,000
23	Heat absorbed in furnace, {HVT	267,000	258,000	318,000	321,000	229,000	240,000	227,000	238,000	160,000	172,000
24	kB per hr {MHVT	235,000	231,000	296,000	292,000	241,000	228,000	255,000	248,000	187,000	185,000
25	Heat absorbed in furnace, {HVT	221,000	217,000	280,000	276,000	229,000	216,000	245,000	236,000	178,000	175,000
26	kB per hr and ft² {MHVT	36.5	35.9	46.0	45.4	37.5	35.5	39.7	38.6	29.1	28.8
27	Furnace heat-absorption {HVT	34.4	33.7	43.5	42.9	35.6	33.6	38.1	36.7	27.7	27.2
28	efficiency, per cent {MHVT	48.1	48.6	49.5	48.9	52.6	50.0	54.0	52.3	55.3	53.3
29		45.3	45.7	46.8	46.2	50.0	47.4	51.9	49.8	52.7	50.4

[a] Morning test; approximately 8:30 a.m. to 11:00 a.m.
[b] Afternoon test; approximately 1:00 p.m. to 3:30 p.m.
[c] Furnace blowers operated for 1 hr. prior to each morning test.
[d] No further cleaning since preceding survey.
[e] Corrected for radiation and carbon loss, infiltration of air to furnace, and leakage of air to pulverizer.

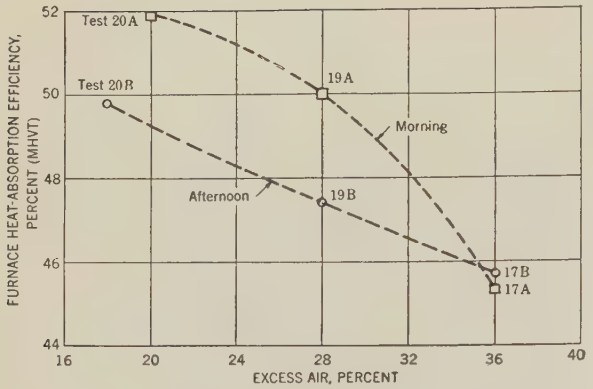

Test No.	Steam flow,[1] pounds per hour	Excess air,[1] percent	Furnace heat-absorption efficiency, percent
17A	420,000	36	45.3
17B	422,000	36	45.7
19A	417,000	28	50.0
19B	414,000	28	47.4
20A	426,000	20	51.9
20B	419,000	18	49.8

[1] Average of panel-board data for test period

FIG. 10 RELATION BETWEEN FURNACE HEAT-ABSORPTION EFFICIENCY AND EXCESS AIR AT CONSTANT STEAM FLOW; MHVT

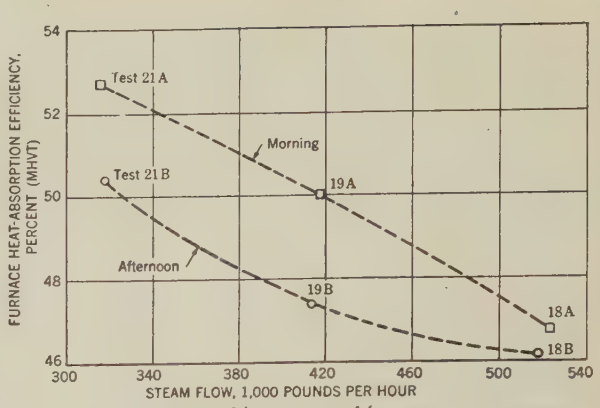

Test No.	Steam flow,[1] pounds per hour	Excess air,[1] percent	Furnace heat-absorption efficiency, percent
18A	523,000	28	46.8
18B	518,000	29	46.2
19A	417,000	28	50.0
19B	414,000	28	47.4
21A	315,000	28	52.7
21B	316,000	28	50.4

[1] Average of panel board data for test period

FIG. 11 RELATION BETWEEN FURNACE HEAT-ABSORPTION EFFICIENCY AND STEAM FLOW AT CONSTANT EXCESS AIR; MHVT

Excepting test No. 17, for which the opposite effect was obtained, the furnace heat-absorption efficiencies in the afternoon were lower than those of the morning tests, by 0.6 to 2.6 per cent. These variations are considerable, especially in view of the short time elapsing between the two tests made each day. They prompted further study of the effect of the accumulation of ash and slag on the efficiency of furnace heat absorption.

Fourth Series, Tests Nos. 24, 25A, 25B, 25C, 25D, 25E, and 26. The test conditions and results of the fourth series of tests are summarized in Table 4. These tests were made during the week of December 9, 1946, and were planned to determine the effect on furnace heat-absorption efficiency of the gradual accumulation of ash on the walls of the originally clean furnace, other factors remaining constant. To accelerate the deposition of ash on the furnace walls, the boiler was operated at a high rating of about 510,000 lb of steam per hr; the excess air at the economizer outlet varied considerably in these tests from the desired value of 20 per cent. All burners were horizontal. For reference purposes, test No. 24 was made with a dirty furnace but otherwise with operating conditions the same as those that followed. Test No. 25, the significant test of this series, was started at noon on December 11, and continued for 60 hrs until midnight on December 13. Test surveys were made between 1:00 and 4:00 p.m. on December 11, (25A); between 9:00 and 11:00 a.m., and 1:30 and 3:30 p.m. on December 12, (25B and 25C, respectively); and between 9:00 and 12:00 a.m. and 2:00 and 5:00

TABLE 4 SUMMARY OF TEST CONDITIONS AND RESULTS. FOURTH SERIES, TESTS NOS. 24, 25A, 25B, 25C, 25D, 25E, AND 26

		24	25A[a]	25B[b]	25C[c]	25D[d]	25E[e]	26
1	Test number							
2	Date	12-10-46	12-11-46	12-12-46	12-12-46	12-13-46	12-13-46	12-14-46
3	Steam flow, lb per hr	527,000	468,000	505,000	503,000	511,000	511,000	411,000
4	Rate of fuel firing, as fired weight, lb per hr	53,400	49,100	49,600	51,200	50,300	49,200	39,400
5	Inclination of burners, Upper	0	0	0	0	0	0	0
6	from horizontal, degrees, Lower	0	0	0	0	0	0	0
7	Condition of furnace walls	Dirty[f]	Clean[g]	Not Clean[h]	Not Clean[h]	Not Clean[h]	Not Clean[h]	Clean[i]
8	Excess air at economizer outlet, per cent	15	25	19	17	22	18	31
	Coal, proximate analysis, per cent as fired							
9	Moisture	10.0	10.7	8.7	9.9	8.4	7.1	6.4
10	Volatile matter	33.2	32.1	33.4	33.1	33.6	34.5	35.6
11	Fixed carbon	45.3	45.8	47.0	45.8	46.3	47.3	46.3
12	Ash	11.5	11.4	10.9	11.2	11.7	11.1	11.7
13	Btu per lb, as fired	11,130	11,050	11,650	11,310	11,540	11,880	11,910
14	Ash-cone softening temperature, F	2,210	2,150	2,220	2,200	2,310	2,260	2,420
15	Temperature of preheated air, F	529	510	527	511	515	509	500
16	Heat available in furnace,[j] kB per hr	612,000	561,000	597,000	595,000	598,000	603,000	486,000
17	kB per hr and ft²	95.2	87.2	92.8	92.5	93.0	93.8	75.6
18	Excess air at furnace outlet, per cent	11	25	17	16	18	17	28
19	Average temperature of gases at furnace outlet, F, HVT	2,015	1,855	1,925	1,945	2,025	2,000	1,865
20	MHVT	2,100	1,940	2,010	2,030	2,110	2,085	1,950
21	Weight wet gases at furnace outlet, lb per hr	550,000	558,000	557,000	551,000	560,000	558,000	490,000
22	Total sensible heat in wet gases at furnace outlet, kB per hr, HVT	302,000	277,000	290,000	291,000	307,000	301,000	243,000
23	MHVT	315,000	292,000	305,000	305,000	322,000	316,000	256,000
24	Heat absorbed in furnace, kB per hr, HVT	310,000	284,000	307,000	304,000	291,000	302,000	243,000
25	MHVT	297,000	269,000	292,000	290,000	276,000	287,000	239,000
26	Heat absorbed in furnace, kB per hr and ft², HVT	48.2	44.2	47.7	47.3	45.3	47.0	37.8
27	MHVT	46.2	41.8	45.4	45.1	42.9	44.6	35.8
28	Furnace heat-absorption efficiency, per cent, HVT	50.7	50.6	51.4	51.1	48.7	50.1	50.0
29	MHVT	48.5	47.9	48.9	48.7	46.1	47.6	47.3

[a] Start of 60-hr test; test period 1 to 4 p.m.
[b] Test period, 9 to 11 a.m.
[c] Test period, 1:30 to 3:30 p.m.
[d] Test period, 9:00 to 12:00 a.m.
[e] Test period, 2:00 to 5:00 p.m.; end of 60-hr test.
[f] Furnace not cleaned; walls very dirty.
[g] Cleaned by furnace blowers and hand lancing, prior to test.
[h] Not cleaned since start of 60-hr test.
[i] Cleaned by furnace blowers and hand lancing, prior to test
[j] Corrected for carbon and radiation loss, infiltration of air to furnace, and leakage of air to pulverizer.

p.m. on December 13, (25D and 25E, respectively). Test No. 26 was made on December 14, to furnish additional information for other test conditions.

At first glance these data are confusing. Item 29 of Table 4 shows, for example, that despite a decrease in the amount of heat available, the furnace heat-absorption efficiency (MHVT) of test 25A (clean furnace), is slightly lower than that for test 24 (dirty furnace). This may be due to the higher excess air in test 25A. Furthermore, test 25B shows a higher furnace heat-absorption efficiency than 25A, and no significant decrease in furnace heat-absorption efficiency occurs until test 25D, when it was 46.1 per cent. Thereafter, however, the furnace heat-absorption efficiency again rises, this time to 47.6 per cent. Consideration of these data demonstrates the necessity for eliminating the effect of all variables except the one being studied, which in this case was the condition of the furnace walls with respect to ash and slag deposits. This point will now be discussed further.

Correlation of Test Results: Effect of Heat Release, Excess Air, Burner Position, and Condition of Furnace Walls on Furnace Heat-Absorption Efficiency

In the tests reported in this paper four major independent variables affect the furnace heat-absorption efficiency. These variables are as follows: (1) the condition of the furnace walls; (2) the method of firing (inclination of the burners, and kind and fineness of the coal); (3) the rate of heat release in the furnace (heat available); and (4) the excess air at the furnace outlet. Although several procedures have been described in the literature for evaluating the condition of the walls of furnaces, they provide only gross estimates suitable for comparing different methods of firing, that is, by stoker, pulverized coal, oil, or gas. Consequently, in so far as these tests are concerned, the condition of the furnace walls, or rather the effect of this factor, is a quantity to be derived from the test results. The conditions generally described in these tests as "dirty" or "clean" can have wide ranges of significance for furnace heat absorption.

The ideal procedure in a correlation of this kind would be to determine the relationships between furnace heat-absorption efficiency and furnace operating conditions for a standard condition of the furnace walls. The latter could be defined most readily as an absolutely clean furnace. It might be argued, however, that absolutely clean furnace walls are impossible to achieve under actual operating conditions, since ash deposits begin to accumulate as soon as the unit is lit off. For practical purposes, however, a near approach to a standard condition might be to make the tests as soon as possible after the unit is placed into operation. Thereafter, tests made on the unit could be adjusted to a standard basis for variations of furnace heat release and excess air, to permit evaluation of the effects of ash and slag deposits on the walls.

Since this practice was not followed in these tests, a delay of several months being necessary between starting the unit and the first series of tests, it is impossible to separate entirely the effects of the conditions of the furnace walls in making correlations of furnace heat-absorption efficiency with furnace heat-release rates and excess air, or factors proportional to them. An alternative procedure has been used, which, although it cannot avoid the dilemma, nevertheless is of some aid in evaluating the data of these tests.

It is assumed that to a first approximation the relationship between furnace heat-absorption efficiency and the furnace heat-release rate and excess air is given by the Hudson-Orrok[6] equation, which was modified to use the quantitative data available in these tests. In view of the empirical[7,8] basis for this equation, this assumption undoubtedly is sufficiently good for the present purpose. As modified, the Hudson-Orrok equation is

$$\mu = \frac{100}{1 + CAQ^{1/2}} \quad [1]$$

where

μ = furnace heat-absorption efficiency, per cent
C = constant, characteristic of furnace geometry and design, nature of fuel fired, and condition of furnace walls. Also, it may be a function of A and Q
A = pounds of wet flue gas at furnace outlet per kB heat available in furnace
Q = heat available in furnace, kB per hour and square foot projected radiant heating surface

This equation is used primarily to adjust data to a uniform basis when a series of tests is made under closely similar operating conditions. In these circumstances, the applicability of the equation for large variations of A and Q is not of concern. Although C may change with these variables, it will be sufficiently constant for the small range of the variables in the tests being compared. In comparing tests for widely different operating conditions, two reasons for the variation of C are of interest: (1) changes in the condition of the furnace walls; (2) the inapplicability of the Hudson-Orrok equation. If changes in the condition of the furnace walls could be shown to be absent, or the effect of such changes could be evaluated, it would then be possible to establish the true relationship between furnace heat-absorption efficiency and the heat available in the furnace per square foot of projected radiant heating surface, and the weight of wet gases at the furnace outlet per kB heat available in the furnace.

The application of this method of analysis to the correlation of the data obtained in these tests follows.

Effect on Furnace Heat-Absorption Efficiency of Heat Available per Square Foot of Projected Radiant Heating Surface, and Weight of Wet Gases at Furnace Outlet per kB of Heat Available. As previously noted, the third series of tests, Nos. 17–21, was made to determine the effect on the furnace heat-absorption efficiency of load and the excess air. Two surveys were made in each test, separated by an interval of only a few hours. Table 5 shows the calculation of the characteristic constant C of the modified Hudson-Orrok equation for these tests. In line with the discussion just given, the point of first interest is the variation between the morning and afternoon surveys of a given test. This variation is shown by item 10 of Table 5, which gives R, the ratio of C for the afternoon and morning tests. It will be noted for two of the five tests, Nos. 17 and 18, that C varied by a maximum of 1 per cent, whereas for the other three tests the variation amounted to from 7 to 11 per cent. The extreme variation of C for all tests, between a low value of 0.1147 for test 20A and a high value of 0.1309 for test 19B, amounted to 14 per cent.

Two factors contribute to the variations of R obtained in these five tests. The first is the error in the determination of μ. The probable error of a single determination is unknown but undoubtedly large enough to be significant. The second is the variation in the conditions of the furnace walls encountered in these tests. Thus if a variation in the characteristic constant C, amounting to 11 per cent is possible between two surveys of the

[6] "Radiation in Boiler Furnaces," by R. N. Broido, Trans. ASME, vol. 47, 1925, pp. 1148–1155; discussion by G. A. Orrok.

[7] "Review of Methods of Computing Heat Absorption in Boiler Furnaces," by W. J. Wohlenberg and H. F. Mullikin, Trans. ASME, vol. 57, 1935, pp. 531–540.

[8] "Evaluation of Effective Radiant Heating Surface and Application of the Stefan-Boltzmann Law to Heat Absorption in Boiler Furnaces," by H. F. Mullikin, Trans. ASME, vol. 57, 1935, pp. 517–529.

TABLE 5 CALCULATION OF CHARACTERISTIC CONSTANT C OF MODIFIED HUDSON-ORROK EQUATION THIRD SERIES, TESTS NOS. 17A, 17B, 18A, 18B, 19A, 19B, 20A, 20B, 21A, AND 21B; MHVT DATA

		17A	17B	18A	18B	19A	19B	20A	20B	21A	21B
1	Test number										
2	Furnace heat-absorption efficiency, μ, per cent	45.3	45.7	46.8	46.2	50.0	47.4	51.9	49.8	52.7	50.4
3	$100 - \mu$	54.7	54.3	53.2	53.8	50.0	52.6	48.1	50.2	47.3	49.6
4	$(100 - \mu)/\mu$	1.207	1.188	1.137	1.165	1.000	1.110	0.927	1.008	0.897	0.984
5	A, pounds wet gas at furnace outlet, per kB heat available in furnace	1.059	1.059	0 992	1.007	0.987	1.007	0.943	0.926	1.018	1.029
6	$(100 - \mu)\ \mu A$	1.140	1 122	1.146	1.157	1.013	1.102	0.983	1.089	0.881	0.956
7	Q, heat available in furnace, kB per hr and ft²	75.9	73.9	93.0	92.8	71.2	70.9	73.4	73.7	52.6	54.0
8	$Q^{1/2}$	8.72	8.60	9 64	9.63	8.44	8.42	8.57	8.59	7.25	7.35
9	C = characteristic constant	0.1307	0.1305	0.1189	0.1201	0.1200	0.1309	0.1147	0.1268	0.1215	0.1301
10	$R = \frac{C_B}{C_A}$	0.998		1.010		1.091		1.105		1.071	

same test, then the extreme variation of 14 per cent for all the surveys is not unreasonable. The consequences of this argument would then be that the modified form of the Hudson-Orrok equation is a fair representation of the variation of furnace heat-absorption efficiency with the chosen variables, within the limits of reproducibility of the conditions of these tests. If it is assumed, however, that all the morning surveys corresponded to identical conditions of the furnace, the exponent of A in Equation [1] will be approximately 2 instead of 1, and the range of R values will be of the same magnitude as just noted. This result is due almost entirely to the effect of test No. 17A. Such a relationship between furnace heat-absorption efficiency, and the weight of wet gases at the furnace outlet per kB heat available in the furnace is at wide variance with theoretical predictions and other experimental evidence.

In view of these considerations it is concluded that, within the demonstrated limits of the variation of the conditions of the furnace walls, the relationship between the furnace heat-absorption efficiency and the furnace heat release and excess air is that given by the modified form of the Hudson-Orrok equation.

The fusibility of the ash of the coals fired should be related to the rate of accumulation of ash on the furnace walls, which is indicated by R, item 10 of Table 5. However, reference to item 14 of Table 3 shows that any such agreement is only partly true, since the softening temperature of the ash was high in tests Nos. 17, 20, and 21, and low in tests Nos. 18 and 19, whereas rapid slagging of the furnace apparently occurred in tests Nos. 19, 20, and 21. This lack of correspondence is emphasized by the fact that test No. 18 was made at the highest heat-release rate of any of these tests, and with the low softening temperature of the ash, should have shown the most slagging.

Rate of Accumulation of Ash and Slag on the Furnace Walls. The fourth series of tests, Nos. 24 and 25A-E, was made to determine the effect of accumulation of ash and slag on furnace performance for an extended period of operation at high rating and fairly low excess air. The unadjusted data, described previously, do not present a clear picture of the behavior of the furnace because of distortions introduced by the unavoidable variation of operating conditions from test to test. These variations are sufficiently small, however, to justify the procedure outlined for adjusting data to a uniform basis by means of the modified form of the Hudson-Orrok equation. The calculations of the characteristic constant C of this equation for these tests are given in Table 6. Item 10 of this table shows for each survey the mean time elapsed since the start of this 60-hr test. Item 11 is the value of μ calculated for each test for uniform values of Q and A, which are, respectively, 92.8 and 0.933. These values correspond to about 600,000 kB per hr heat available in the furnace and 20 per cent excess air at the economizer outlet, for the coal used in test No. 25B.

The variation of the calculated furnace heat-absorption efficiencies (MHVT) with the time elapsed after the start of the 60-hr test is shown graphically in Fig. 12. The value of μ for test No. 24 made the day previous to the start of the 60-hr test is plotted at the proper time interval preceding the test. A horizontal dotted line has been drawn through this point to the zero time axis to indicate the condition of the furnace prior to cleaning, assuming that no further changes had occurred.

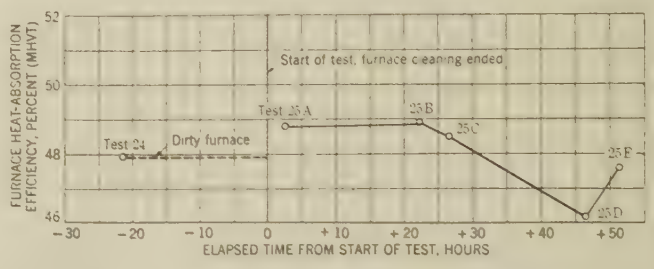

FIG. 12 VARIATION OF CALCULATED FURNACE HEAT-ABSORPTION EFFICIENCY, MHVT, WITH TIME AFTER START OF 60-HR TEST (Calculated values for conditions of test No. 25B.)

Fig. 12 indicates primarily that the furnace-cleaning operations produced a significant effect on furnace heat-absorption efficiency, increasing the calculated value (MHVT) from 47.9 to 48.8 per cent. This relatively clean state persisted for almost 24 hr, when there began a rapid decrease in furnace heat-absorption ef-

TABLE 6 CALCULATION OF CHARACTERISTIC CONSTANT C OF MODIFIED HUDSON-ORROK EQUATION, FOURTH SERIES, TESTS NOS. 24, 25A, 25B, 25C, 25D, 25E, AND 26; MHVT DATA

		24	25A	25B	25C	25D	25E	26
1	Test number							
2	Furnace heat-absorption efficiency, μ, per cent	48.5	47.9	48.9	48.7	46.1	47.6	47.3
3	$100 - \mu$	51.5	52.1	51.1	51.3	53.9	52.4	52.7
4	$(100 - \mu)/\mu$	1.062	1.088	1.045	1.053	1.169	1.101	1.114
5	A, pounds of wet gas at furnace outlet, per kB heat available in furnace	0.899	0.995	0.933	0.926	0.936	0.925	1.008
6	$(100 - \mu)/\mu\ A$	1.181	1.093	1.120	1.137	1.249	1.190	1.105
7	Q, heat available in furnace, kB per hr and ft²	95.2	87.2	92.8	92.5	93.0	93.8	75.6
8	$Q^{1/2}$	9.76	9.34	9.63	9.62	9.64	9.69	8.69
9	C, characteristic constant	0.1210	0.1170	0.1163	0.1182	0.1296	0.1228	0.1271
10	Mean time from start of 60-hr test, hr	−21.5	2.5	22.0	26.5	46.5	51.5	
11	Calculated value of μ for $Q = 92.8$, $A = 0.933$, corresponding to 600,000 kB per hr and 20 per cent excess air at economizer outlet, for the coal used in test 25B	47.9	48.8	48.9	48.5	46.2	47.6	

ficiency which persisted for another 24 hr, at which time a minimum value of 46.2 per cent was obtained. Thereafter the furnace heat-absorption efficiency increased to 47.6 per cent in 5 hr. It is worthy of note that the final value is almost identical with that obtained in the reference test for the dirty furnace.

Reference to table 4 shows that the softening temperature of the ash was quite uniform throughout the 60-hr test, although considerably lower than some of the values for the tests of the third series.

The results of the fourth series are basically similar to those of the third series, in so far as the rate of accumulations of slag is concerned. Thus the difference in furnace heat-absorption efficiency between two surveys on the same day ranged from 0.2 to 1.5 per cent for the fourth series and from 0.6 to 2.6 per cent in the third series, reference being made to the unadjusted MHVT data of both series.

Effect of Inclination of Burners on Furnace Heat-Absorption Efficiency. It will be recalled that in the first series of tests made for the purpose of determining the effect of burner inclination on furnace heat-absorption efficiency, the temperature and excess-air survey at the furnace outlet was not as complete as those made in the later tests of this investigation. Consequently the results of the first series of tests are not comparable, in their present form, with those of the second series of tests. The following procedure has been used in an attempt to adjust the results of the first series to the same basis as the rest of the tests, and thus permit the correlation of all the tests made to study the effect of inclination of the burners.

Because the surveys made in the second series of tests were complete, it was possible to calculate the total sensible-heat content of the gases leaving the furnace both by the complete method, using all the data, and by the incomplete method, using only the data from the positions at which samples were taken in the first series. The ratio of the values of the total sensible-heat content of the gases leaving the furnace, thus obtained from a test of the second series, may be taken as a factor for adjustment of the test of the first series made at the same setting of the burners. This procedure could not be applied to the tests with all burners inclined at +30 deg, because the data of the second series for this burner setting (test No. 13) also were incomplete. In this case it was necessary to resort to a linear extrapolation of the factors for the other burner settings. The results of these calculations are given in Table 7A and are plotted in Fig. 13(*a*) which shows the extrapolation used to obtain the factor for the tests made with all burners inclined at +30 deg. The line of Fig. 13(*a*) is drawn through the point for test No. 10, because this test was made with a dirty furnace and thus corresponds more closely to the conditions of the first series of tests. These factors are used to compute corrected values for the furnace heat-absorption efficiency for tests Nos. 1, 2, 3, 4, and 13, as shown in Table 7B.

The results of all tests made to determine the effect of inclination of the burners on furnace heat-absorption efficiency are summarized in Table 8. Included therein are the corrected values for tests Nos. 1, 2, 3, 4, and 13, the results of tests Nos. 10 11, 14, and 15, and that for test No. 26, which was made under operating conditions closely approximating those of test No. 11. Table 8 also shows the calculation of the characteristic constant C for all of these tests. The values of the weight of wet gases at the furnace outlet required for the calculation of C for tests Nos. 1, 2, 3, 4, and 13, were obtained by a procedure similar to that used to obtain the corrected values for these tests of the total sensible-heat content of the gases at the furnace outlet. The calculation of the correction factors for the weight of wet gases at the furnace outlet are included in Table 7A and are plotted in Fig. 13(*b*) to obtain the correction factor for tests with all burners inclined at +30 deg. The calculation of the corrected values of the weight of wet gases at the furnace outlet for tests Nos. 1, 2, 3,

TABLE 7A RATIOS OF TOTAL SENSIBLE-HEAT CONTENT AND WEIGHT OF WET GASES AT FURNACE OUTLET FOR COMPLETE AND INCOMPLETE SURVEYS OF TESTS WITH VARYING INCLINATION OF BURNERS; MHVT DATA

		10		11		13		15	
1	Test number								
2	Nature of survey	Complete	Incomplete	Complete	Incomplete	Complete	Incomplete	Complete	Incomplete
3	Inclination of burners, Upper	0		0		+30		−30	
4	Inclination of burners, from horizontal degrees, Lower	0		0		+30		−30	
5	Condition of furnace walls	Dirty		Clean		Clean		Clean	
6	Average excess air at furnace outlet, per cent	24	22	28	25	...	26	26	20
7	Average temperature of gases at furnace outlet, deg F, MHVT	2015	1935	1905	1845	...[a]	1815	1750	1805
8	Total sensible-heat content of gases at furnace outlet, MkB per hr	272	255	239	226	...	238	219	217
9	ρ, ratio of total sensible-heat content of gases at furnace outlet, complete survey: incomplete survey	1.067		1.058		1.124[a]		1.009	
10	Weight of wet gases at furnace outlet, M lb per hr	498	489	468	458	...	494	472	451
11	P, ratio of weight of wet gases at furnace outlet, complete survey: incomplete survey	1.018		1.022		0.989[b]		1.047	

[a] Extrapolated value, Fig. 13(*a*).
[b] Extrapolated value, Fig. 13(*b*).

TABLE 7B CALCULATION OF CORRECTED VALUES OF FURNACE HEAT-ABSORPTION EFFICIENCY, AND WEIGHT OF WET GASES AT FURNACE OUTLET FOR TESTS NOS. 1, 2, 3, 4, AND 13; MHVT DATA

		1	2	3	4	13
1	Test number					
2	Inclination of burners, Upper	0	+30	−30	0	+30
3	Inclination of burners, from horizontal degrees, Lower	0	+30	−30	0	+30
4	Condition of furnace walls	Dirty	Dirty	Dirty	Dirty	Clean
5	Heat available in furnace, kB per hr	532000	494000	475000	490000	495000
6	Total sensible-heat content of gases at furnace outlet, incomplete survey, kB per hr	287000	275000	233000	243000	238000
7	ρ, correction factor for total sensible-heat content of gases at furnace outlet	1.067	1.124	1.009	1.067	1.124
8	Corrected total sensible-heat content of gases at furnace outlet, kB per hr	306000	309000	235000	259000	268000
9	Corrected value for heat absorbed in furnace, kB per hr	226000	185000	240000	231000	227000
10	Corrected furnace heat-absorption efficiency, per cent	42.5	37.4	50.5	47.1	45.9
11	Weight of wet gases at furnace outlet, incomplete survey, lb per hr	532000	494000	468000	486000	494000
12	P, correction factor for weight of wet gases at furnace outlet	1.018	0.989	1.047	1.018	0.989
13	Corrected value for weight of wet gases at furnace outlet, lb per hr	542000	489000	490000	495000	489000

4, and 13 are included in Table 7B. In Table 8 are given the calculated values of the furnace heat-absorption efficiency for uniform values of Q and A, of 73.9 and 1.022, respectively, equivalent to heat available in the furnace of 475,000 kB per hr and excess air at the economizer outlet of 30 per cent, for the coal used in test No. 11.

Fig. 14 is a plot of the calculated values of furnace heat-absorption efficiency for the stated operating conditions, as a function of inclination of the burners, for the dirty-furnace conditions of tests Nos. 1, 2, 3, 4, and 10, and the clean-furnace conditions of tests Nos. 11, 13, 14, 15, and 26. Test No. 14, upper burners horizontal, lower burners inclined at —30 deg, has not been plotted, since it cannot be assumed that it necessarily represents any specific intermediate point. The curve for the dirty-furnace conditions has been drawn through the mean of the values of tests Nos. 1, 4, and 10, all burners at 0 deg, although it is quite probable that the condition of the furnace walls varied considerably in these three tests. The curves are drawn full between —30 and 0 deg, but dotted between 0 and +30 deg, because the +30-deg points are based upon extrapolated values for the correction factors applied to tests Nos. 2 and 13.

Although the two curves differ markedly, primarily because of the difference in the results for tests Nos. 2 and 13, there is a considerable improvement of Fig. 14 over Fig. 9. The large difference in furnace heat-absorption efficiency between tests Nos. 2 and 13 has not been greatly affected by the adjustments to which

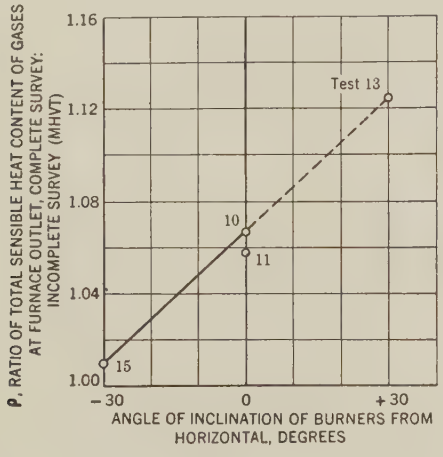

Fig. 13(*a*) P Ratio of Total Sensible-Heat Content of Gases at Furnace Outlet for Complete and Incomplete Surveys, as a Function of Inclination of Burners

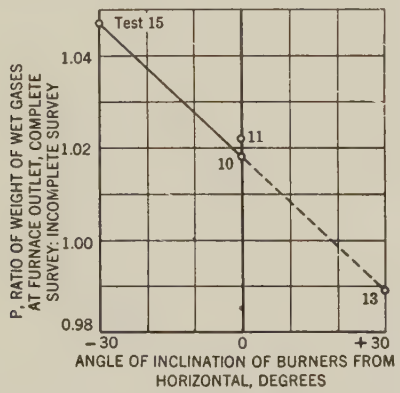

Fig. 13(*b*) P, Ratio of Weight of Wet Gases at Furnace Outlet for Complete and Incomplete Surveys, as a Function of Inclination of Burners

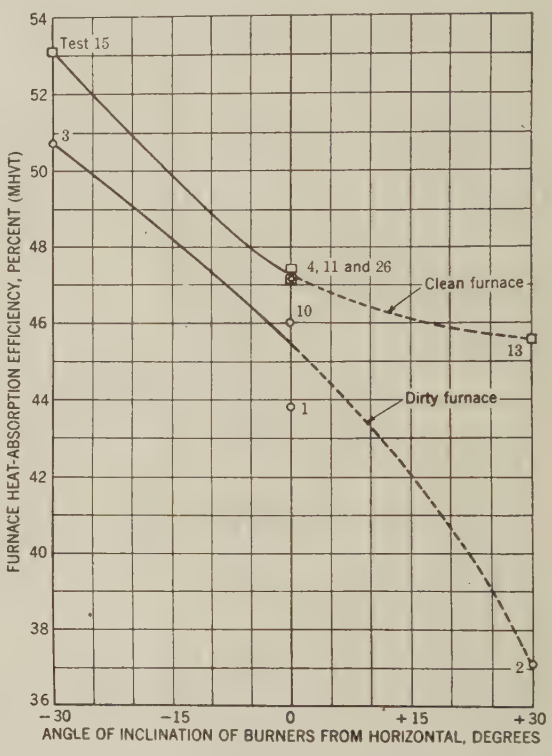

Fig. 14 Effect of Inclination of Burners on Furnace Heat-Absorption Efficiency, MHVT, for a Clean or Dirty Furnace (Calculated for operating conditions of test No. 11.)

TABLE 8 CALCULATION OF CORRECTED CHARACTERISTIC CONSTANT C, OF MODIFIED HUDSON-ORROK EQUATION FOR TESTS MADE TO DETERMINE EFFECT OF INCLINATION OF BURNERS; MHVT DATA

1	Test number	1	2	3	4	10	11	13	14	15	26
2	Inclination of burners, Upper	0	+30	—30	0	0	0	+30	0	—30	0
3	from horizontal, degrees, Lower	0	+30	—30	0	0	0	+30	—30	—30	0
4	Condition of furnace walls	Dirty	Dirty	Dirty	Dirty	Dirty	Clean	Clean	Clean	Clean	Clean
5	Furnace heat-absorption efficiency, μ, per cent	42.5[a]	37.4[a]	50.5[a]	47.1[a]	46.1	47.8	45.9[a]	51.5	53.7	47.3
6	$100 - \mu$	57.5	62.6	49.5	52.9	53.9	52.2	54.1	48.5	46.3	52.7
7	$(100 - \mu)/\mu$	1.353	1.674	0.980	1.123	1.169	1.092	1.179	0.942	0.862	1.114
8	A, pounds of wet gas at furnace outlet per kB heat available in furnace	1.019[b]	0.990[b]	1.032[b]	1.010[b]	0.986	1.022	0.988[b]	0.996	0.998	1.008
9	$(100 - \mu)/\mu A$	1.328	1.691	0.950	1.112	1.185	1.068	1.193	0.946	0.864	1.105
10	Q, heat available in furnace, kB per hr and ft^2	82.7	76.8	73.9	76.2	78.5	71.2	77.0	74.6	73.6	75.6
11	$Q^{1/2}$	9.09	8.76	8.60	8.73	8.86	8.44	8.77	8.64	8.58	8.69
12	C, characteristic constant	0.1461	0.1930	0.1105	0.1274	0.1337	0.1265	0.1360	0.1095	0.1007	0.1272
13	Calculated value of μ for $Q = 73.9$, $A = 1.022$, corresponding to 475000 kB per hr and 30 per cent excess air at economizer outlet, for coal used in test 11	43.8	37.1	50.7	47.2	46.0	47.3	45.6	50.9	53.1	47.2

[a] Corrected values, Table 7B.
[b] Derived from corrected values of weight of wet gases at furnace outlet, Table 7B.

the data have been subjected; the unadjusted values differ by 7.6 per cent, the adjusted values by 8.5 per cent. Because the same factors were used to correct the data of both tests, regardless of the condition of the walls, some error may have been introduced, but not such as substantially to change the relationship between these two tests. It must be concluded therefore that Fig. 14 is fairly representative of the conditions for which the first two series of tests were made. This figure indicates a decrease in the heat-absorption efficiency for the dirty furnace of 13.6 per cent between the conditions of all burners inclined at —30 deg and all burners inclined at +30 deg, and a decrease for the clean furnace of 7.5 per cent for the same variation of inclination of the burners.

Distribution of Gases at Furnace Outlet

The distribution of the gases at the furnace outlet and the variation of the properties of the gases with position may be expected to vary with many of the factors studied in this investigation, but greatest of all with the inclination of the burners. As previously noted, measurements of the gas velocity were made in the tests of the second series at all odd-numbered sampling positions except No. 1. Five tests were made in this series: (1) No. 10, all burners horizontal, dirty furnace; (2) No. 11, all burners horizontal, clean furnace; (3) No. 13, all burners inclined at +30 deg, clean furnace; (4) No. 14, upper burners horizontal, lower burners inclined at —30 deg, clean furnace; and (5) No. 15, all burners inclined at —30 deg, clean furnace. No data were taken at stations *K* and *K-R* in test No. 13, and this test is not included in this discussion.

The distribution of the velocity, composition, and temperature of the gas at the furnace outlet could be presented by plotting the respective values on a map of the furnace outlet area similar to Fig. 5, and then drawing lines of constant velocity, composition, and temperature. This procedure is complicated and presents difficulties familiar to all who have attempted to apply it to the fluctuating conditions which obtain at the furnace outlet. The method of presentation used here is simpler and more graphical and presents the results in a form that will be shown to correspond to significant operating conditions of the boiler.

It will be noted in Fig. 8 that the developed furnace outlet has been divided into five vertical bands and six horizontal strips. The data for velocity, temperature, and composition of the gases for each test have been used to calculate average values of temperature and excess air, and of the percentage of the total mass flow for each of the five vertical and the six horizontal strips of the developed furnace outlet area. The temperature and excess-air averages were calculated by weighting with respect to the mass-velocity data.

Distribution of Excess Air. In the course of the tests of the second series, traverses were made at the economizer outlet of this boiler, and the gas samples were analyzed in an Orsat apparatus. These traverses showed in every case that the excess air at the left or north side of the economizer was significantly lower than that at the right or south side. It is evident from the distribution of excess air across the furnace outlet that this condition originated in the furnace. These data are given in Table 9 and plotted in Fig. 15. Examination of the figure reveals that, with the exception of test No. 14, the excess air at the left side is lower than at the right side of the furnace outlet. The gases entering the superheater vary in composition systematically from the left to the right side of the furnace and flow through the superheaters and economizer is essentially parallel.

Included in Table 9 and plotted in Fig. 16 are the weighted mean values of excess air for the six horizontal strips, *E*, *D*, *C*, *A*, K_2, and K_1. For tests Nos. 10, 11, and 14, the excess-air values for all strips lie between 22 and 31 per cent, and the data show no marked systematic variations with position. For test No. 15 the distribution is quite different from the others; the excess air varies widely, with a minimum of about 11 per cent at strip *A* and a maximum value of about 35 per cent for strips K_2 and K_1.

Distribution of Mass Flow. The percentage of the total mass flow of the gases leaving the furnace in each part of the furnace-outlet area is given in Table 10, and is plotted in Figs. 17 and 18,

TABLE 9 DISTRIBUTION OF AVERAGE EXCESS AIR AT FURNACE OUTLET; TESTS NOS. 10, 11, 14, 15

	Excess air, per cent			
Test no.	10	11	14	15
Vertical band				
1	16.2	21.6	30.7	21.5
2	20.7	26.9	26.3	17.7
3	24.5	25.0	23.4	22.8
4	28.2	28.8	28.5	28.2
5	31.4	35.9	18.8	29.0
Horizontal strip				
E	28.0	25.7	22.6	15.7
D	27.9	28.5	26.6	24.2
C	25.8	29.2	30.1	20.2
A	26.9	25.8	28.5	10.8
K_2	23.7	30.8	27.2	34.7
K_1	22.9	30.1	25.8	35.1

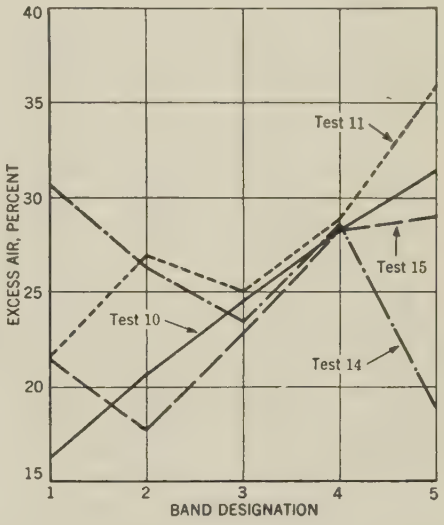

Fig. 15 Distribution of Average Excess Air at Furnace Outlet, Vertical Bands

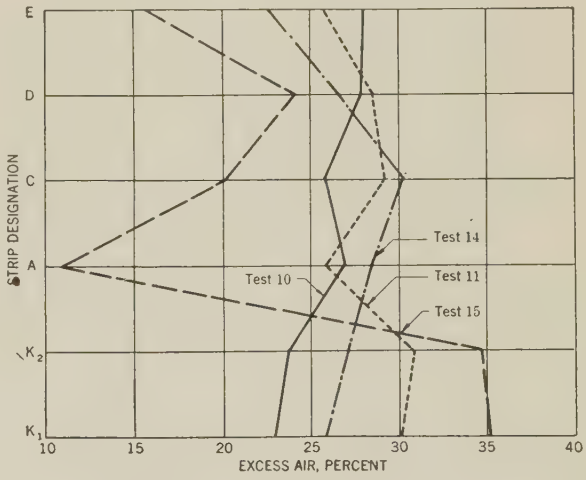

Fig. 16 Distribution of Average Excess Air at Furnace Outlet, Horizontal Strips

for the distribution in vertical bands and horizontal strips, respectively.

Referring to Fig. 8, the gases leaving the furnace in a given band at the lower portion of the furnace outlet mix primarily with gases leaving the furnace higher up in the same vertical band. That this parallel flow persists beyond the superheater has been indicated previously from the comparison of the distribution of the excess air at the furnace outlet and at the economizer outlet.

TABLE 10 DISTRIBUTION OF AVERAGE MASS FLOW AT FURNACE OUTLET; PER CENT OF TOTAL MASS FLOW FOR ALL SECTIONS OF FURNACE OUTLET; TESTS NOS. 10, 11, 14, 15

	Mass flow, per cent of total			
Test no.	10	11	14	15
Vertical band				
1	16.1	16.8	27.4	28.5
2	18.2	17.8	23.3	24.5
3	18.1	18.0	17.6	18.6
4	20.8	19.7	13.7	12.8
5	26.8	27.7	18.0	15.6
Horizontal strip				
E	20.7	26.6	25.0	32.1
D	18.9	19.9	16.6	24.2
C	10.9	9.5	7.4	12.6
A	11.1	6.0	7.9	6.2
K_2	20.2	17.6	20.7	14.6
K_1	18.2	20.4	22.4	10.3

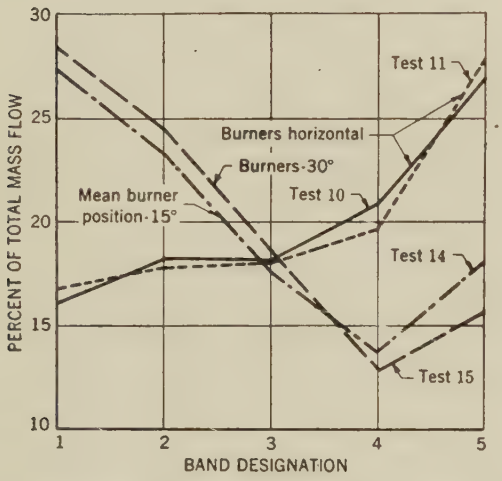

FIG. 17 DISTRIBUTION OF AVERAGE MASS FLOW AT FURNACE OUTLET, VERTICAL BANDS

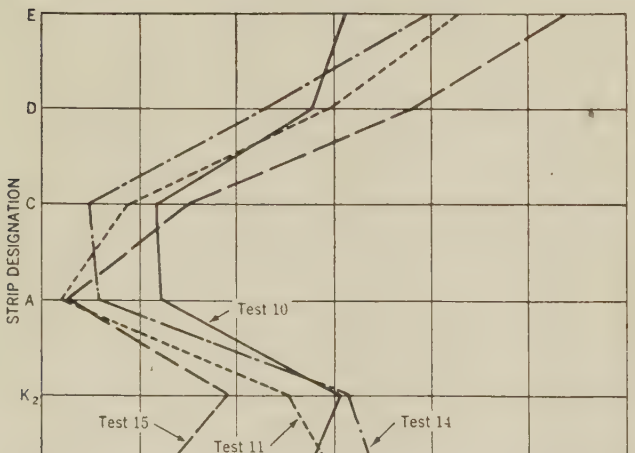

FIG. 18 DISTRIBUTION OF AVERAGE MASS FLOW AT FURNACE OUTLET, HORIZONTAL STRIPS

The most interesting features of Fig. 17 are the considerable asymmetry of the mass flow and the similarity between curves for tests having essentially the same arrangement of the burners. For example, the curves for tests Nos. 10 and 11, both with all burners horizontal, are almost identical, with low mass flow at the left side increasing slowly toward the center, then more rapidly at the right where the mass flow at band 5 is about two thirds greater than that of band 1. The curves for test No. 14, with upper burners horizontal and bottom burners inclined at —30 deg, and for test No. 15, with all burners inclined at —30 deg, also are quite similar to each other, but in this case the flow pattern is reversed from that of tests Nos. 10 and 11. The mass flow is highest at the left, in band 1, decreasing almost linearly to a minimum at band 4, where the mass flow is less than one half that of band 1. Finally, the mass flow increases again at band 5.

The distributions of mass flow for the horizontal strips K_1, K_2, A, C, D, and E, plotted in Fig. 18, are quite similar for the four tests and reflect the geometry of the furnace outlet. The mass flow is high at the top of furnace, strips D and E, is low at the center, strips C and A, and is high again at the lower inclined portion of the furnace outlet, strips K_1 and K_2.

Distribution of Temperature. The weighted mean values of the temperature of the gases for the five vertical bands and the six horizontal strips of the furnace outlet have been computed from the values of temperature, and mass velocity, for all the sections of the furnace outlet. The results of these calculations are given in Table 11; the temperature distributions for the vertical bands are plotted in Fig. 19, and the temperature distributions for the horizontal strips are plotted in Fig. 20.

TABLE 11 DISTRIBUTION OF AVERAGE TEMPERATURE AT FURNACE OUTLET; TESTS NOS. 10, 11, 14, 15

	Temperature, deg F, MHVT			
Test no.	10	11	14	15
Vertical band				
1	2085	1900	1685	1665
2	2135	1960	1880	1825
3	2065	1920	1955	1850
4	1970	1880	1930	1830
5	1870	1820	1745	1710
Horizontal strip				
E	1845	1785	1765	1825
D	1870	1785	1740	1740
C	1915	1850	1760	1730
A	1985	1895	1865	1785
K_2	2200	2020	1880	1730
K_1	2205	2030	1905	1715

Fig. 19 shows that the temperature distribution for vertical bands is asymmetrical for tests Nos. 10 and 11, with high values at band 1, rising to a peak at band 2, and then decreasing rapidly to band 5. The temperature distributions for tests Nos. 14 and 15 are symmetrical, with peak values at band 3. The differences between the bands of maximum and minimum temperature are 265 F, 140 F, 270 F, and 185 F for tests Nos. 10, 11, 14, and 15, respectively. The temperature levels for the various tests are of course in line with the average temperatures previously cited for the total outlet gas of each test.

Temperature distributions for the horizontal strips, Fig. 20, follow a much more uniform pattern. With the exception of test No. 15, the temperatures are highest at the bottom of the furnace outlet, strips K_1 and K_2, and decrease toward the top of the furnace. In test No. 15, the temperature is lowest at K_1 and K_2, with a maximum at E. The temperature differences between the strips of maximum and minimum temperature are 360 F, 245 F, 165 F, and 110 F, for tests Nos. 10, 11, 14, and 15, respectively.

General Discussion of Errors

In view of the large number of tests required to cover all the significant variables affecting furnace heat-absorption efficiency, no provision could be made in the test program for repetitive

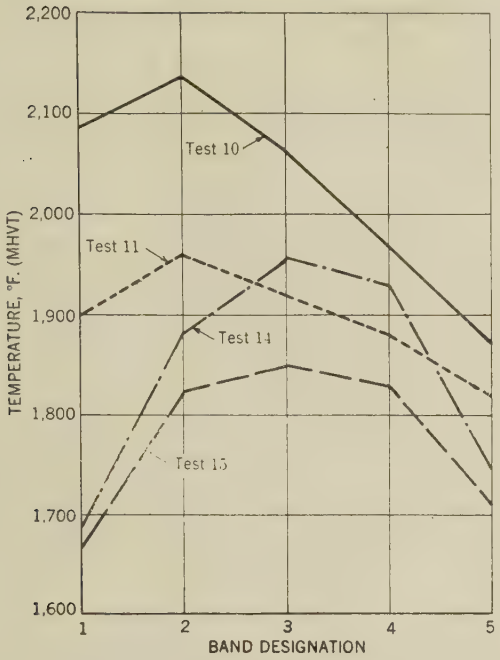

FIG. 19 DISTRIBUTION OF AVERAGE TEMPERATURE AT FURNACE OUTLET, VERTICAL BANDS

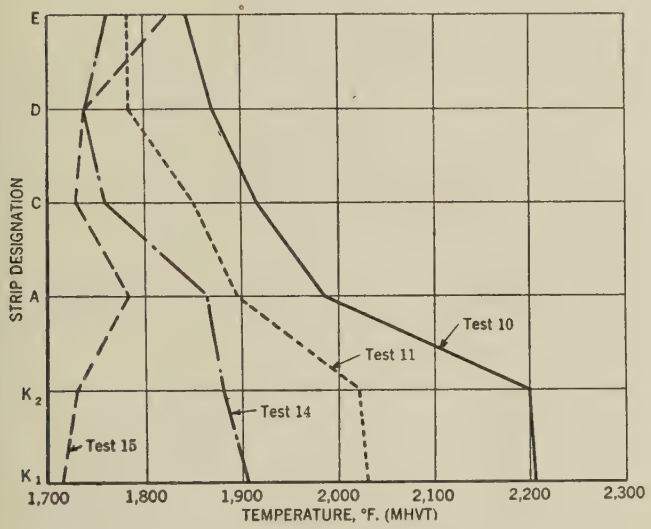

FIG. 20 DISTRIBUTION OF AVERAGE TEMPERATURE AT FURNACE OUTLET, HORIZONTAL STRIPS

testing under comparable conditions to establish the precision of the measurements. An estimate can be made, however, of the effect on the furnace heat-absorption efficiency of reasonable assumed values of the probable errors of the various observations which enter into the calculation of the furnace heat-absorption efficiency. This analysis, too detailed to be presented here, results in a value of 0.5 per cent for the probable error of single determinations of the furnace heat-absorption efficiency. Systematic errors of observations, as distinguished from the random errors on which the foregoing analysis is based, have a considerably greater effect because they are propagated without reduction in the average value. Thus the corrections applied in this paper to the temperature observations, to place them on the MHVT basis, may be in error by as much as ±30 deg F. Errors of this magnitude would change the absolute values of furnace heat-absorption efficiency reported in this paper by about 1 per cent but would not greatly affect the relative values.

This discussion has assumed tacitly that the furnace was operating so that the averages being calculated remained constant during the course of the test, even though fluctuations were known to be occurring at the various positions at the furnace outlet. In some of the tests of this investigation, significant variations in operating conditions occurred over periods of time comparable to that required for a traverse. Since each traverse can represent only the conditions under which it is made, any variation of operating procedure from the conditions for which test data are desired will be reflected in the final results.

Repeated tests for nominally identical conditions would provide an estimate of the reproducibility of all the factors influencing furnace heat-absorption efficiency, and its determination, including the reproducibility of furnace-wall conditions, which was previously discussed. Since the effect of the variations of furnace-wall conditions may well exceed that of all the other factors, it is apparent that investigations of this type require a large number of tests for the proper evaluation of the effect of the operating variables on furnace heat-absorption efficiency.

CONCLUSIONS

In order to provide basic data on furnace performance and to determine the relationship between the temperature gradient through furnace-wall tubes and the rate of heat transfer, the over-all heat-absorption efficiency of the Tidd furnace was measured by conventional methods. These consisted of determining the sensible heat in the products of combustion leaving the furnace outlet by measuring their temperature with a high-velocity thermocouple, and calculating their mass flow from the rate of burning of the fuel and the composition of the gas. Measurements of the velocity of the gases at the furnace outlet with a double-impact Pitot tube were only partly satisfactory because of the complicated flow patterns of the gases.

To reduce the data from all of the tests to a common level, use was made of a modified form of the Hudson-Orrok equation, which relates the furnace heat-absorption efficiency to the mass flow of flue gas, the heat available in the furnace, and a constant depending upon the furnace design and condition. Thus unavoidable variations in load and in excess air could be corrected for with reasonable assurance.

The test results show that an increase in the rate of heat release in the furnace decreases the heat-absorption efficiency, the amount of change being somewhat greater when the walls of the furnace are clean than when they are dirty. As a first approximation, an increase in steam output from 300,000 lb per hr to 500,000 lb per hr was found to lower the furnace heat-absorption efficiency of the clean furnace from 53.0 to 47.5 per cent; whereas for a dirty furnace, the same change of load lowered the efficiency from 51.0 to 46.3 per cent. Increase in excess air, for a given rating, also lowered the efficiency. For example, with a dirty furnace, doubling the excess air in the normal operating region lowered the heat-absorption efficiency approximately 4 per cent.

Accumulations of ash and slag on the walls of the furnace have a noticeable effect on furnace heat absorption. In some tests the furnace heat-absorption efficiency decreased 2.6 per cent, 4 to 6 hr after the furnace was cleaned by wall blowers. In other tests it was found that cleaning caused an increase in furnace heat-absorption efficiency, which amounted to only 0.9 per cent. The efficiency remained constant for 24 hr after cleaning the furnace, and then decreased 2.7 per cent during the subsequent 23 hr. Thereafter, the efficiency increased slightly so that the final value, after a total period of 52 hr since cleaning, was only 1.2 per cent less than that of the clean furnace. These changes

in furnace heat-absorption efficiency, if interpreted as being due solely to the behavior of the ash deposits on the furnace walls, suggest that a cyclic process occurs, in which ash accumulates and detaches from the walls in a rather regular manner.

Increasing the length of the path of the products of combustion by inclining the burners downward had the expected effect of increasing the furnace heat-absorption efficiency. When corrected to the same test conditions, the furnace heat-absorption efficiency of the dirty furnace was 13.6 per cent greater with the burners inclined 30 deg downward than when they were inclined upward 30 deg; the corresponding variation for the clean furnace was 7.5 per cent.

The composition and flow of gases was not uniform across the furnace outlet. In the series of tests in which the inclination of the burners was varied, the excess air at the left side of the furnace outlet was, with but one exception, lower than at the right side, the ratio being 1:2 in some tests. However, the vertical distribution of excess air was nearly constant. The distribution across the furnace outlet of the flow of gases was characteristic of the inclination of the burners. When the burners were inclined downward, the mass flow was more than twice as great at the left side of the furnace outlet as at the right side, but with the burners horizontal, the opposite effect was observed. The geometry of the furnace outlet was reflected in the vertical distribution of the flow of gases, which was greatest at the top of the furnace.

The distribution across the furnace outlet of the temperature of the gases also varied with the inclination of the burners. When the burners were horizontal, the temperature was highest at the left side of the furnace outlet; but when the burners were inclined downward, the temperature distribution was quite symmetrical, with a maximum at the center of the furnace outlet. The vertical distribution of the temperature of the gases was normal, with highest temperatures at the bottom of the furnace outlet.

Consideration of the probable error of the measurements indicates that it will be 0.5 per cent as a maximum. The considerable variations between tests made during intervals as small as 4 to 6 hr, which was probably due to changes in the condition of the furnace walls, indicate the necessity for large numbers of tests in such investigations, if the effect of the other operating variables is to be correctly deduced. It is apparent that the mechanism of the deposition of ash on the walls of dry-bottom furnaces, and the effect of such deposits as a thermal insulator, require further clarification.

Acknowledgments

The authors gratefully acknowledge, with appreciation and thanks, the contributions to this investigation made by the following:

The Special Research Committee on Furnace Performance Factors of The American Society of Mechanical Engineers, who afforded the Combustion Research Section the opportunity to participate in this important project, and the individual Committee members, who gave their unstinted advice and help whenever required.

Dr. A. C. Fieldner, Chief, Fuels and Explosives Branch, and Dr. Louis C. McCabe, Chief, Coal Division, Bureau of Mines, who gave the authority to do the work, and who made many helpful suggestions.

The engineers and assistants of the Combustion Research Section: Messrs. W. S. Landers, J. W. Myers, J. Jonakin, C. H. Schwartz, J. J. Pfeiffer, G. Kollar, and J. P. Stein, who capably made the difficult tests that form the basis for this paper.

Mr. Howard Andrews, Superintendent of Operation of the Tidd plant, and his staff, who lent willing and able assistance in the arrangements for all the tests.

The engineering, research, and test staffs of the Combustion Engineering Company, and the American Gas and Electric Service Corporation, who gave the benefits of their broad experience in field investigations of this kind.

Appendix 1

Calculation of Total Sensible Heat Content of Gases Leaving Furnace

The sensible heat content H_u of the gases resulting from the combustion of 1 lb of MAF coal

$$H_u = W_D h_D + (W_A W_v + W_c) h_W$$

where W_D = weight of gases formed from the combustion of 1 lb of MAF coal with dry air. It is calculated from the composition of the coals used in these tests, Meig's Creek (No. 9), Duncanwood Mine, Harrison County, Ohio, and is plotted as a function of excess air in curves similar to the one shown in Fig. 21, for tests Nos. 10 and 11.

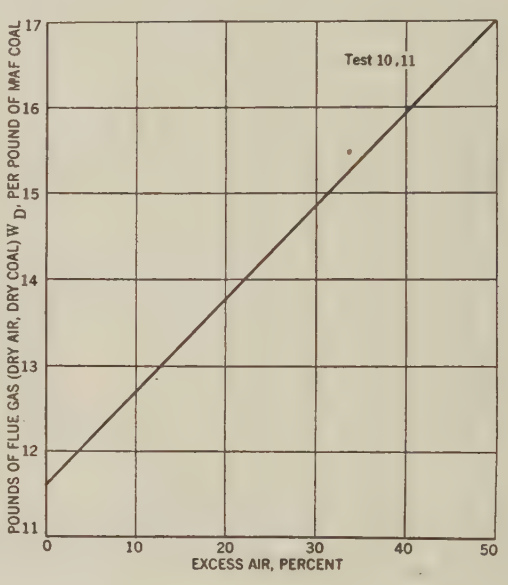

Fig. 21 Typical Plot Giving Pounds of Flue Gas—Dry Air, Dry Coal—per Lb MAF Coal as a Function of Excess Air

h_D = sensible heat content per pound of flue gas resulting from the combustion of MAF coal with dry air. It is given as a function of temperature and excess air in Fig. 22.

W_A = pounds of dry air required to burn 1 lb of MAF coal; equal to $W_D - 1$.

W_v = pounds of moisture in air per pound of dry air; obtained from wet- and dry-bulb readings at forced-draft-fan floor.

W_c = pounds of moisture in coal, as fired, per pound of MAF coal.

h_W = sensible heat of water vapor at atmospheric pressure. It is given as a function of temperature in Fig. 22.

$\overline{H}_u$ is the value of H_u computed for the average values of excess air and temperature for the thirty sections of the furnace outlet, and is used in the calculations of this paper.

The sensible-heat-content charts were calculated from the recent tables of Heck.[9]

[9] "The New Specific Heats," by R. C. H. Heck, *Mechanical Engineering*, vol. 62, 1940, pp. 9–12.

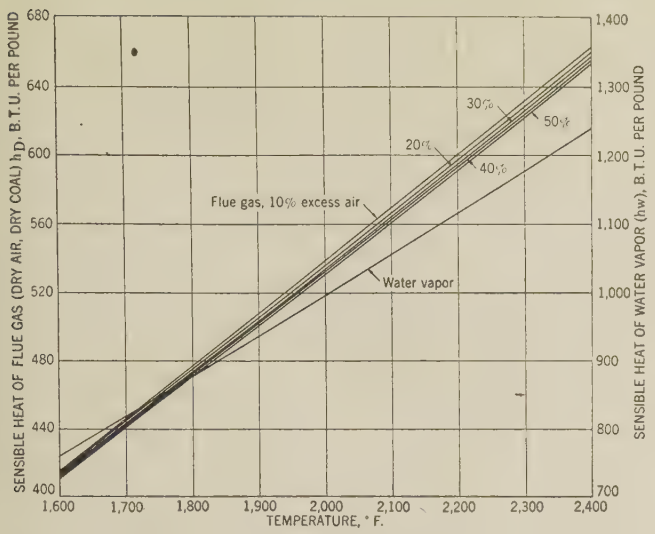

FIG. 22 CHART FOR CALCULATING SENSIBLE HEAT OF WET FLUE GAS, 80 DEG F BASE

K = total sensible-heat content of gases leaving the furnace, kB per hr

$$K = \frac{F}{1000} \times \overline{H}_u$$

where F is the rate of coal feed, pounds MAF coal per hour.

Appendix 2

HEAT AVAILABLE IN FURNACE, HEAT ABSORPTION IN FURNACE, FURNACE HEAT-ABSORPTION EFFICIENCY

(1) H_A, the sensible heat content per pound of preheated air

$$H_A = W_A h_A + W_A W_v h_W'$$

where

h_A = heat content of dry air, Btu per lb
h_W' = heat content of moisture in air, Btu per lb
h_A and h_W' are given as functions of temperature in Fig. 23.

(2) S, the total heat available in furnace, kB per hr

$$S = \frac{F}{1000}(B_N - 0.01\, B_G + \varphi\, H_A)$$

where B_N is the net heating value of the coal, Btu per lb MAF coal.

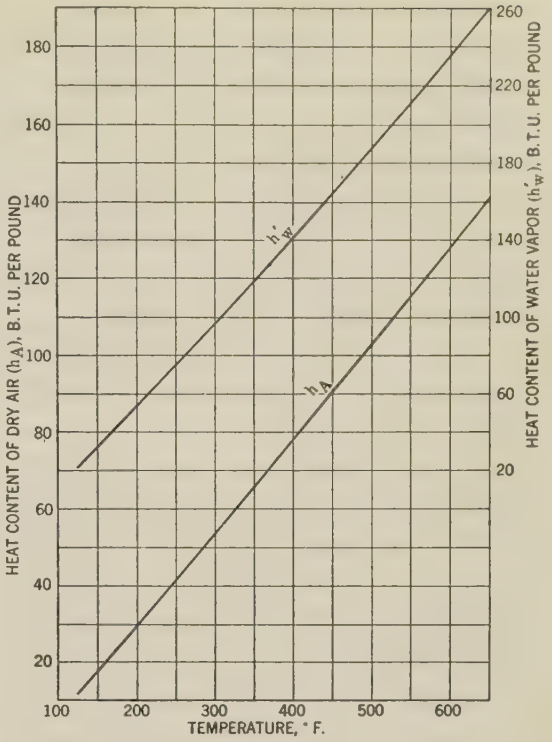

FIG. 23 HEAT-CONTENT CHART FOR PREHEATED AIR, 80 DEG F BASE

B_G is the gross heating value of the coal, Btu per lb MAF coal, and 0.01 B_G is the correction for radiation and unburned-carbon losses, equal to 1 per cent of the gross heating value of the coal.

φ is the fraction of air entering the furnace which is preheated; this allows for 10 per cent air infiltration to furnace and for air leakage to pulverizer.

(3) T, total heat absorbed in furnace, kB per hr

$$T = S - K$$

(4) μ, furnace heat-absorption efficiency, per cent

$$\mu = 100\,\frac{T}{S}$$

(5) Q, heat available in furnace, and U, heat absorbed in furnace, kB per sq ft-hr

$$Q = \frac{S}{6430}$$

$$U = \frac{T}{6430}$$

An Investigation of the Variation in Heat Absorption in a Pulverized-Coal-Fired Water-Cooled Steam-Boiler Furnace

III—Variations in Heat Absorption as Shown by Density and Velocity Measurements of Fluid Within a Tube

By A. R. MUMFORD[1] and C. G. R. HUMPHREYS,[2] NEW YORK, N. Y.

The determination of heat-transfer rates by differential measurements of static pressure and by inlet velocity resulted in lower values and less consistent values than the rates determined by measurement of the surface temperature of the tube. The difference between the two methods can be attributed to a difference in the velocity of steam and water within the tube generally resulting in indications of higher density, as measured at the cold side of the tube, then as computed from the hot-surface temperature measurement and the water velocity entering the tube. Because the effect of rate of heat transfer, total heat absorption, relative rates of absorption along the length of the tube, and velocity of water entering the tube could not be easily segregated the relative velocities of steam and water could not be correlated with the other factors, and further field work on density, as determined differentially from static pressures, is not recommended. Laboratory work in which separate control of the variables is more practical may provide valuable data on bubble slip and circulation factors.

Objectives

In order to establish the relation between the surface temperature of the hot side of a furnace tube and the heat absorbed by that tube, one experimental tube in about the middle of the right wall was selected and equipped with velocity, quality, and density-measuring devices. The quality determination was made near the point where the tube discharged into a common upper header. Velocity measurements were made in the vertical section of the tube about 3 ft above the point of first exposure to any heat but well below the point of active heat absorption. Density of the fluid within the tube was measured differentially by static pressures along the active length of the tube. The surface temperature of the exposed side of the tube was measured by center-line couples which constituted part of the temperature study of the entire furnace, and by couples disposed circumferentially at the principal center-line couple points. The establishment of the relationship between surface temperature and heat absorption, as determined by density variations and velocity, or by quality and velocity, would provide an independently determined factor for the combined heat-transfer coefficient of the tube wall and inside film.

Experimental Tube Arrangement; Density Measurements. Five simple pressure taps were installed in tube No. 40, right wall, at points indicated in Fig. 1, to measure pressure differentials between the hot leg in the boiler tube and the cold leg in the external connections between any pair of pressure taps. From these data we hoped to determine the average density of the fluid in the hot leg. The formula for determination of Q, average volumetric quality of the mixture of steam and water between any two pressure taps, from measurements of the differential between the hot and cold legs is developed in Appendix 1.

Fig. 2 shows the assembly of manometers using mercury as the manometer fluid. For taps, or density connections, 1 to 2, 1 to 3, or 1 to 2, and 2 to 3, 20-in. Meriam high-pressure manometers were used; for 1 to 4, 1 to 5, or 3 to 4, and 4 to 5, 40-in. Meriam high-pressure manometers were used. The readings were fairly steady during the test period probably because of inertia in the long connections. Leakage was rarely experienced and easily rectified despite the large number of valves necessary. Manometers functioned perfectly and the insufficiency of the method is not apparently chargeable to instrumentation.

Circumferential Thermocouples. Fig. 1 shows exactly where thermocouples are located in all walls for measurements of surface temperatures. These, described in Part I of this symposium,[3] were for records of tube center-line temperatures. The manner of placing couples is a modification of the method first described in (1)[4] and possesses definite advantages over that earlier method. It is described in detail in (2) and shown in Fig. 3.

Also, at boiler No. 11, we employed what are called circumferential couples, Fig. 1. Such couples were placed on a selected tube at or near the center of each wall and at some of the same elevations used for center-line thermocouples. The same means of couple installation was used, but couples were located at 30 deg and 60 deg on either side of the center-line couple at each location chosen. Thus five couples measured circumferential temperatures at these locations, and reference to Tables 1 and 2 is illustrated by a simple example as follows:

The five couples 5–8A, 5–8B, 5–8, 5–8C, and 5–8D are identified thus: 5–8 is the center-line couple in the right wall; B and C are set 30 deg from the center-line couple; A and D are set 60 deg from the center-line couple. All center-line-couple temperatures were recorded and all circumferential temperatures were meas-

[1] Development Engineer, Research Department, Combustion Engineering Company, Inc. Fellow ASME.

[2] Engineer, Research Department, Combustion Engineering Company, Inc. Mem. ASME.

Contributed by the Special Research Committee on Furnace Performance Factors in co-operation with the Fuels, Power, and Heat Transfer Divisions and presented at the Semi-Annual Meeting, Chicago, Ill., June 16–19, 1947, of The American Society of Mechanical Engineers.

[3] Part I appears on page 553 of this issue of the Transactions.

[4] Numbers in parentheses refer to the Bibliography at the end of the paper.

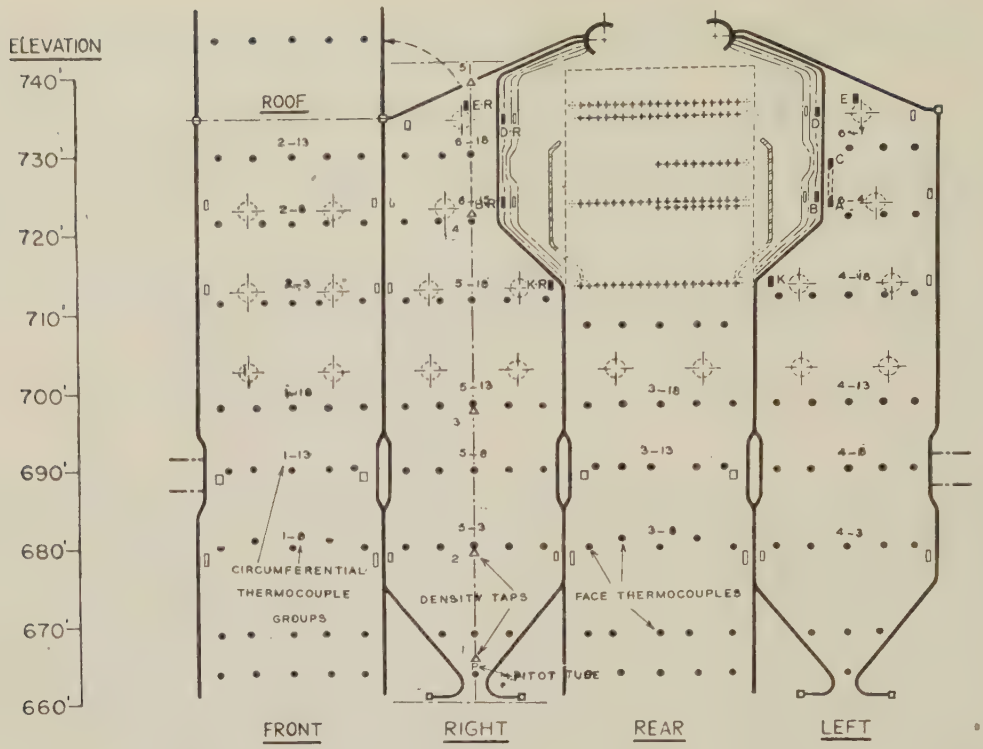

FIG. 1 LOCATIONS OF TEST POINTS AND THERMOCOUPLES

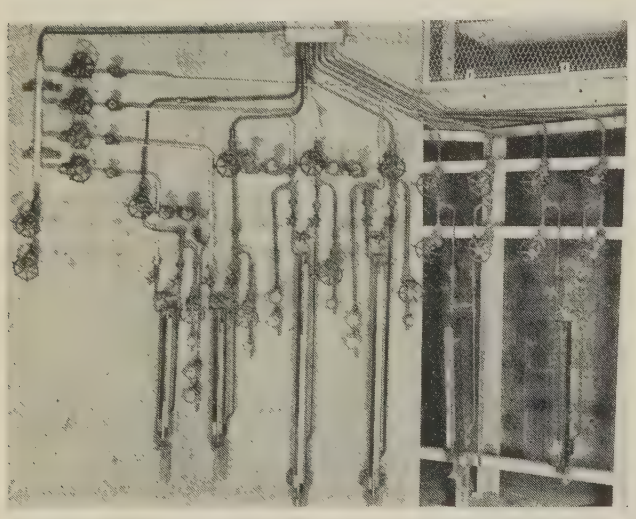

FIG. 2 MANOMETERS FOR DENSITY AND VELOCITY MEASUREMENTS

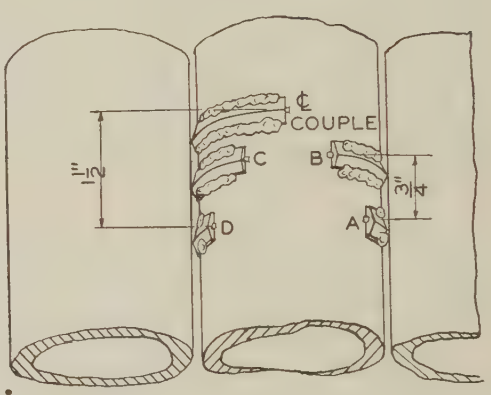

FIG. 3 CIRCUMFERENTIAL THERMOCOUPLES ON HOT SIDE OF FURNACE-WALL TUBE

ured using an indicating millivolt potentiometer. Fig. 1 shows points where circumferential couples are installed; a total of 105 couples.

Fluid-Velocity Measurements. Measurement of water flowing into tube No. 40 on the right side wall utilized the modified Pitot tube described by Ravese (3). The actual tube is shown in Fig. 4. At the point of insertion a small pad was welded to the tube on the cold side, and a $^1/_4$-in. tapped hole was made exactly at right angles to the tube. Any burrs were removed, and the internal diameter was measured before insertion of the Pitot tube. The Pitot tube was then seal-welded in place. The point of velocity measurement is at one third of the internal tube diameter where a fair average flow exists (4, 5). The differential pressure was indicated in a 20-in. Meriam high-pressure manometer using dyed carbon tetrachloride as the manometer fluid. A leg correction was made to take into account the small difference in elevation of the Pitot-tube connections. This correction is very small where high velocities are encountered, but where pressure differences exist as low as a few inches of water it must be taken into account.

Table 3 summarizes the average velocities measured. In these measurements, as in the density measurements, the length of the connections introduced sufficient inertia so that the readings of the manometers were very steady and, in fact, the readings did not change significantly during the periods of testing. The constancy of the readings was a condition of the circuit and not due to leaks which were few and speedily corrected. The manometers were not sluggish and were cleaned and overhauled before each test.

Quality Determinations. The quality of the mixture at the

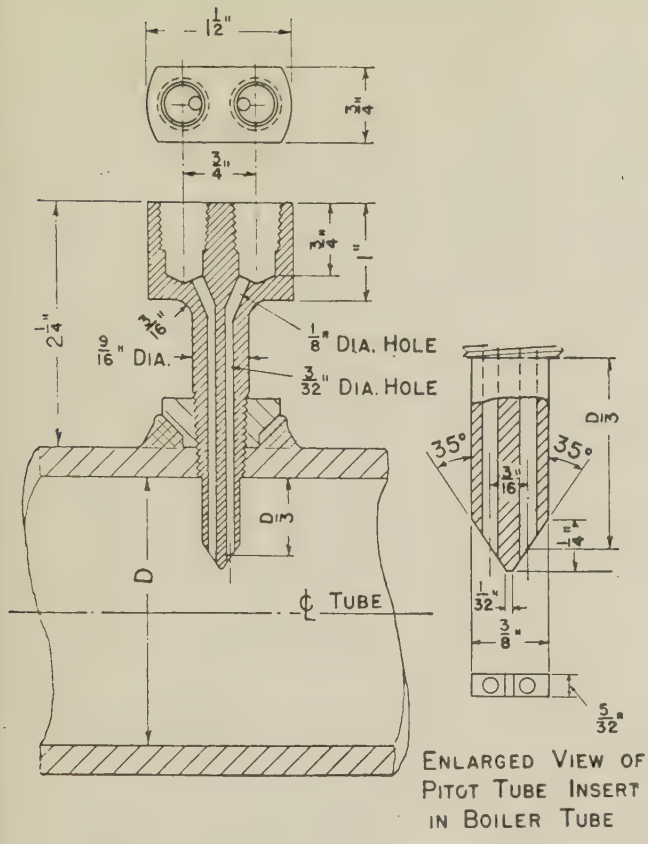

FIG. 4 PITOT TUBE IN FURNACE-WALL TUBE

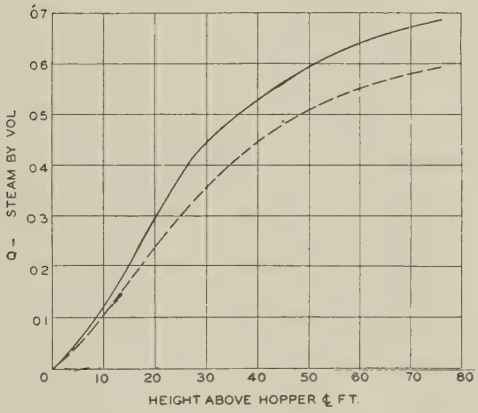

FIG. 5 QUALITY OF FLUID IN EXPERIMENTAL TUBE FROM ΔT AND FROM DENSITY: AVERAGE

top of the tube was to be measured by a heat-exchanger type of calorimeter handling a sample withdrawn from the tube through a standard ASME sampling nozzle. This procedure has been described in (6). Although the calorimeter had been acid-cleaned before the start of the tests, difficulty was experienced in balancing the flows and temperatures. The few available test men could not devote sufficient time to determine the difficulty and make the other scheduled observations, so this determination of quality was abandoned.

Density Studies. The observations of pressure differentials are given in Table 3. The computed values of the average quality of the mixture between the several points is also noted in this table.

The results of the determination of quality from measurement of differential static pressure are shown by curves connecting the average values for each test from Nos. 10 to 26.

Before discussing briefly the results of each test, an examination of the average results may aid in indicating the difficulties of this method of relating heat absorption to surface temperatures. Although of no significance in the study of the performance of the furnace, the averages do aid in an examination of the method.

In Fig. 5 are plotted the variation in Q with height above the hopper center line, as determined both by the density method and by the surface-temperature and tube-inlet-velocity relation for the experimental tube. The values of Q from the density measurements are lower at all points along the tube than are those values of Q from the surface-temperature measurements. The divergence of the curves increases steadily along the lower half of the length of the tube but remains essentially the same during the upper half of the length.

If it is assumed that the values determined from the surface temperatures are true values of the steam made, then the velocities of steam determined from this curve must be accepted as true values. Because all heat was absorbed on one side of the tube only it is easy to imagine a lack of uniformity in the mixture over any horizontal section of the tube. The mixture can be thought of as richer in steam on the portion of the section nearer the furnace and richer in water on the portion of the section nearer the casing. Such differences in uniformity of the mixture in a furnace tube have been pictured as resulting in a rolling motion of the fluid rising through the tube with the side of the section richer in water rising at a slower speed than the side of the section richer in steam. Others have termed this type of phenomena "bubble slip."

The conclusions are that a difference in velocity of the steam and water exists, with the steam rising faster near the heated surface than the water near the casing side. Such a difference in velocity would explain the lower qualities indicated by density than by temperature differentials, particularly when it is recalled that the density taps were taken from the casing side of the tube. If the water velocities are computed from the density measurements, and the steam velocities from the ΔT measurements a comparison of the average velocities of each is possible. This comparison is shown in Fig. 6. The steam velocity rises above the water velocity, and the divergence increases as the value of Q increases. If the difference between the steam and water velocities is plotted against Q, two straight lines can be drawn through the points intersecting at a Q of 0.575, and a differential velocity of 0.6 fps. If the intersection represents a break in the differential-velocity line, the upper part of which is heading for the steam

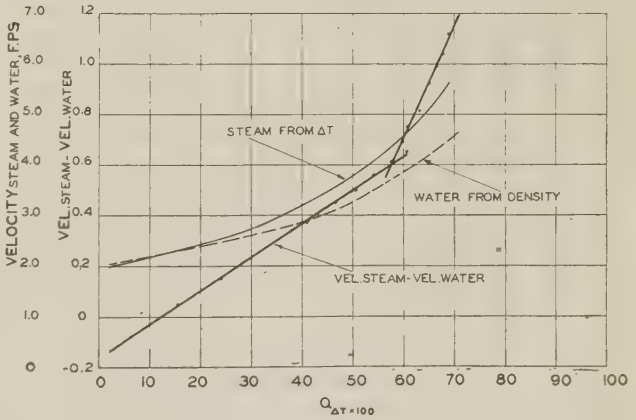

FIG. 6 AVERAGE STEAM AND WATER VELOCITIES IN EXPERIMENTAL TUBE

TABLE 1 AVERAGE TEMPERATURE DIFFERENTIALS SHOWN BY CIRCUMFERENTIAL THERMOCOUPLES

Test No.	1	2	3	4	10	11	13	14	15	17	18	19	20	21	24	25A	25B	25C	25D	25E	26
TC No.																					
1-8A	28	16	28	52	25	46	28	64	56	41	56	14	41	32	69	50	60	61	64	40	24
1-8B	22	-	12	29	26	39	24	27	23	39	56	9	32	23	51	54	47	49	25	14	25
1-8	-	-	-	-	46	14	10	-	14	4	8	5	15	9	36	37	29	32	34	26	22
1-8C	-	-	-	-	19	-	-	-	-	-	-	-	-	-	72	-	-	62	133	117	-
1-8D	-	-	-	-	26	-	20	-	-	56	18	33	117	83	54	48	55	53	66	56	36
1-13A	22	15	25	45	26	20	42	61	44	8	35	29	29	17	58	23	33	29	52	42	8
1-13B	66	46	60	72	65	51	50	68	47	43	81	65	76	48	84	66	48	70	100	75	18
1-13	106	55	67	101	71	61	57	74	69	69	105	73	93	43	136	78	84	88	110	93	27
1-13C	73	48	74	72	54	53	56	86	69	63	91	78	97	51	91	74	91	88	109	94	30
1-13D	22	20	59	35	42	15	50	72	54	21	38	30	33	36	23	15	23	27	36	32	27
1-18A	32	29	14	22	44	34	17	31	30	46	28	31	35	15	24	30	16	15	19	16	34
1-18B	52	28	12	28	27	31	19	47	41	63	31	28	36	23	61	45	59	55	49	58	39
1-18	74	90	43	48	28	77	23	49	89	68	47	45	50	29	59	72	76	79	82	65	44
1-18C	62	49	-	24	44	31	-	39	8	40	18	9	31	20	54	76	59	55	73	53	51
1-18D	77	83	47	52	39	66	52	44	67	66	57	31	41	25	30	52	38	32	31	22	39
2-3A	81	72	37	49	12	40	54	42	50	32	41	31	33	24	-	15	33	23	19	32	20
2-3B	44	33	29	38	14	53	62	51	60	43	56	48	55	38	16	75	40	44	30	67	48
2-3	53	42	33	38	19	62	74	56	23	36	46	43	50	36	20	75	58	54	36	59	57
2-3C	28	43	28	15	18	37	64	52	58	25	29	28	32	32	13	46	47	48	40	39	31
2-3D	18	56	30	26	11	42	56	42	48	28	35	34	40	32	12	25	38	42	52	49	26
2-8A	12	4	28	16	8	39	46	35	38	32	45	41	45	25	37	38	38	37	32	37	33
2-8B	47	41	35	39	34	48	52	39	47	40	54	48	57	36	26	60	62	59	58	59	53
2-8	29	26	24	27	24	38	42	32	39	33	71	39	46	29	44	60	58	58	56	55	49
2-8C	13	15	24	18	12	35	40	38	49	26	32	32	39	25	44	37	31	39	26	38	32
2-8D	12	20	38	17	6	30	66	45	48	49	63	57	66	34	71	61	65	69	76	61	-
2-13A	22	23	22	24	18	28	32	20	26	25	33	31	38	23	45	28	42	41	47	37	35
2-13B	8	4	9	9	28	25	29	20	25	20	28	24	30	18	42	27	38	36	41	35	31
2-13	40	38	32	33	27	34	38	26	33	31	39	35	41	28	45	42	42	41	46	44	36
2-13C	19	14	16	19	12	21	32	25	31	24	33	26	34	22	45	37	36	38	41	37	32
2-13D	6	3	6	8	8	26	29	21	26	19	29	25	29	18	40	36	36	35	38	35	29
3-8A	4	-	-	-	-	-	-	8	15	-	-	-	-	-	-	-	-	-	-	-	-
3-8B	-	-	9	6	39	41	24	21	14	21	14	12	19	12	26	29	32	28	32	35	30
3-8	-	-	28	50	46	50	29	53	58	47	65	55	63	43	36	38	47	43	43	47	46
3-8C	29	-	-	-	9	-	22	-	-	-	-	-	-	-	35	36	44	37	38	41	42
3-8D	21	-	49	39	24	35	21	20	8	26	18	5	20	12	24	29	30	26	27	29	31
3-13A	20	-	43	41	34	27	28	17	76	16	30	25	35	12	51	58	38	54	30	36	28
3-13B	69	13	59	71	69	76	43	67	78	24	81	42	34	16	66	75	81	78	59	50	27
3-13	56	16	62	52	62	52	57	78	82	46	82	56	56	43	67	65	70	66	66	57	26
3-13C	32	7	42	38	49	41	43	67	75	29	43	33	36	34	56	59	53	53	40	43	24
3-13D	14	16	43	32	36	38	47	82	94	28	28	45	46	34	58	66	29	34	49	39	9
3-18A	24	9	20	23	35	28	52	41	84	36	25	29	43	28	27	38	32	31	18	19	10
3-18B	24	21	25	19	28	25	73	68	50	27	22	29	47	49	34	31	44	47	36	40	18
3-18	26	34	36	18	37	39	93	86	63	36	29	45	62	63	116	76	101	93	90	92	46
3-18C	49	36	45	28	37	43	81	84	56	63	36	56	64	66	69	55	62	53	52	48	23
3-18D	68	-	46	41	42	44	52	75	54	78	54	56	46	55	69	50	51	39	36	30	16

velocity at a Q value of 1.0, then, on the average, a change in the character of flow must take place at a Q value of about 0.6. The averaging of the Q values from each source is inadmissible from a standpoint of the study of furnace performance but it may aid in clarifying the reasons for the lack of co-ordination between density measurements and temperature-differential measurements.

The individual curves of Q values from density and temperature differentials show variation which indicate that the application of co-ordinating factors derived from the averages are unwarranted because of the individual variations in burner position, rating, and cleanliness.

In Fig. 7, for test No. 10, is shown the only instance in which the Q values derived from density exceeded those derived from the temperature differentials. The temperature-differential Q curve shows a higher rate of heat absorption in the area from about 5 ft above the hopper center line to a distance of about 45 ft above the hopper.

In Fig. 8, for test No. 11, the temperature-differential Q curve is consistently above that determined from densities. The $\Delta T - Q$ curve reflects the presence of an insulating deposit of ash about 30 ft above the hopper.

In Fig. 9, for test No. 13, the final value of the two curves is satisfyingly close. The presence of ash is indicated again by the ΔT—Q curve about 35 ft above the hopper. The fact that the burners were tilted up for this test is reflected in the low rate of increase in Q near the hopper.

In Fig. 10, for test No. 14, the Q curve, obtained from density, breaks to a nearly constant value between points 3 and 5 but this is not reflected in the $\Delta T - Q$ curve. The rapid rise in Q values near the hopper indicates and confirms the effect of tilting the lower of two burners in each corner downward 30 deg while the upper was directed horizontally.

In Fig. 11, for test No. 15, the final value of Q is only slightly higher than at point 4. The two curves agree for the first 10 or 12 ft above the hopper, but then diverge, probably indicating the increase in relative steam velocities as the Q value increases.

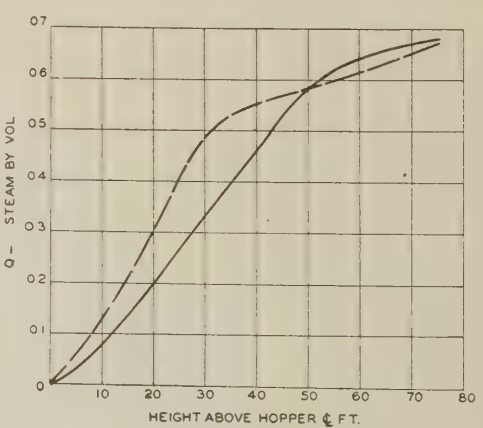

FIG. 7 TEST NO. 10; QUALITY OF FLUID IN EXPERIMENTAL TUBE FROM ΔT AND FROM DENSITY

TABLE 2 AVERAGE TEMPERATURE DIFFERENTIALS SHOWN BY CIRCUMFERENTIAL THERMOCOUPLES

Test No. TC No.	1	2	3	4	10	11	13	14	15	17	18	19	20	21	24	25A	25B	25C	25D	25E	26
4-3A	–	–	–	–	–	–	–	–	–	20	8	13	18	15	40	26	30	22	35	35	28
4-3B	17	–	12	44	45	44	24	28	15	49	55	38	46	39	47	54	20	44	42	41	45
4-3	46	18	34	66	54	49	29	48	56	–	–	–	–	–	53	67	19	46	51	49	40
4-3C	52	19	–	–	39	23	–	31	22	54	62	39	51	44	53	67	50	54	47	45	53
4-3D	51	17	33	48	44	37	24	58	28	45	46	32	40	30	50	59	46	42	42	41	46
4-8A	39	13	59	16	27	15	15	29	29	25	23	21	26	20	42	31	26	26	48	39	9
4-8B	70	31	52	71	70	33	44	43	51	91	71	71	67	63	72	64	57	47	77	70	14
4-8	69	37	54	67	71	41	48	54	51	80	80	72	78	60	102	92	41	56	94	85	16
4-8C	27	16	47	22	23	10	14	31	26	16	17	15	31	25	47	43	40	41	38	37	8
4-8D	49	36	45	65	78	62	58	48	67	88	62	75	73	62	80	66	80	48	94	91	17
4-13A	19	36	17	30	87	63	64	59	62	77	80	39	54	44	26	27	26	22	26	46	38
4-13B	19	21	25	–	38	22	31	24	54	32	80	20	32	21	24	25	28	21	29	35	39
4-13	43	35	75	48	64	46	35	59	87	97	66	28	34	41	52	38	44	35	40	55	59
4-13C	38	36	61	51	76	58	50	53	71	59	86	41	46	43	38	52	42	36	62	60	63
4-13D	23	36	33	28	72	50	58	67	72	74	87	42	44	63	47	38	46	40	54	44	82
4-18A	10	37	27	25	37	36	48	30	33	24	22	23	24	14	22	19	22	23	24	26	25
4-18B	26	43	34	34	29	52	61	40	40	43	44	37	35	31	50	46	56	57	52	57	51
4-18	32	34	30	34	38	53	60	43	44	56	55	43	47	42	50	62	64	64	56	64	59
4-18C	33	54	35	26	38	42	57	42	44	41	64	43	47	34	50	47	54	56	56	64	45
4-18D	4	47	30	8	17	23	48	33	34	25	27	27	31	22	42	16	22	26	38	30	16
6-4A	46	38	27	36	41	37	38	26	25	30	37	28	34	19	44	38	48	45	54	46	40
6-4B	30	27	26	32	41	40	40	25	26	38	41	36	42	23	35	30	26	35	38	46	43
6-4	33	37	27	34	33	37	39	25	27	40	44	40	45	28	37	33	53	46	53	47	43
6-4C	21	28	30	24	42	35	37	29	32	32	38	31	35	23	41	36	47	42	49	43	35
6-4D	3	11	26	16	26	34	36	29	32	32	37	31	35	25	31	25	31	31	36	31	25
6-7A	17	14	13	16	31	25	23	16	18	25	27	24	28	17	25	23	27	24	40	24	21
6-7B	24	22	17	24	40	32	30	19	21	32	34	30	35	21	34	32	36	34	38	33	30
6-7	25	26	22	27	43	34	33	23	26	35	38	33	38	24	40	36	39	35	40	35	29
6-7C	15	27	25	23	41	33	31	26	28	31	34	30	36	20	17	16	19	15	24	17	18
6-7D	12	13	18	18	33	27	25	20	24	25	29	27	31	19	25	26	25	24	33	24	23
5-3A	3	9	6	4	25	19	18	42	51	19	18	11	13	12	16	16	22	16	–	–	–
5-3B	–	–	6	5	26	31	15	–	–	–	–	–	–	–	25	16	17	16	21	16	18
5-3	–	–	–	–	46	49	23	83	79	52	63	33	39	30	–	11	38	37	32	16	46
5-3C	24	7	51	31	13	20	4	64	60	–	–	–	–	–	33	28	30	28	44	38	33
5-3D	–	–	–	8	26	28	13	20	32	17	13	7	12	11	19	20	14	9	32	30	22
5-8A	6	5	34	12	26	15	16	31	34	18	24	16	15	23	26	21	36	26	24	37	18
5-8B	57	13	58	44	65	29	43	43	48	24	66	33	29	42	58	52	58	62	33	45	19
5-8	74	19	63	75	71	56	46	63	51	52	71	62	38	58	73	62	75	69	40	50	20
5-8C	47	17	79	59	54	66	50	85	86	81	78	38	35	50	54	20	51	34	48	82	25
5-8D	13	–	25	18	42	23	19	39	59	29	23	21	20	37	28	10	28	29	29	37	11
5-13A	–	–	4	33	44	34	20	26	34	24	15	20	21	31	22	40	50	57	60	12	14
5-13B	41	18	25	47	27	13	22	44	54	36	24	23	26	42	46	31	32	33	51	20	16
5-13	45	17	27	36	28	13	23	64	62	49	28	40	34	52	55	60	44	35	48	30	17
5-13C	29	21	14	45	44	52	45	68	53	49	36	29	32	46	68	60	71	54	70	43	15
5-13D	31	23	16	47	49	52	40	63	55	34	23	19	27	33	72	70	78	62	82	43	18
5-18A	8	–	17	7	12	43	53	43	34	40	49	32	29	22	9	21	32	27	29	26	26
5-18B	22	18	25	19	10	47	56	32	39	51	58	45	45	33	18	44	44	52	36	37	44
5-18	27	34	32	32	19	53	77	44	44	52	56	49	51	39	34	50	53	55	40	50	50
5-18C	12	22	28	17	18	43	67	40	38	42	37	36	40	29	16	36	44	48	33	46	37
5-18D	7	10	15	10	11	32	50	32	18	36	38	33	37	29	17	27	30	44	34	41	33
6-15A	–	–	3	2	8	33	31	25	18	36	42	33	36	21	30	27	28	28	30	29	25
6-15B	40	9	16	29	34	42	37	30	34	43	50	41	47	33	46	43	49	47	49	42	40
6-15	23	12	19	23	24	31	33	29	28	37	35	22	26	27	52	31	40	35	35	35	31
6-15C	4	–	14	9	12	25	27	22	23	31	30	26	28	21	30	19	20	27	22	26	22
6-15D	–	–	5	2	6	20	21	16	29	27	25	21	23	14	21	21	12	17	18	14	14
6-18A	5	23	24	21	18	35	38	29	28	36	38	31	31	17	47	47	48	48	55	53	44
6-18B	22	16	18	22	28	31	26	19	24	36	40	32	34	19	48	42	44	45	53	41	37
6-18	21	18	20	21	27	28	21	21	19	32	33	24	27	22	–	19	33	36	26	36	28
6-18C	3	–	7	6	12	19	16	13	18	26	23	18	22	17	26	25	30	28	26	27	20
6-18D	–	–	3	4	8	19	16	13	18	25	23	18	26	12	30	27	28	30	34	29	23

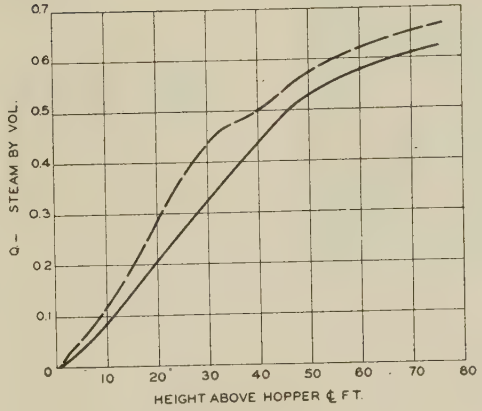

FIG. 8 TEST NO. 11; QUALITY OF FLUID IN EXPERIMENTAL TUBE FROM ΔT AND FROM DENSITY

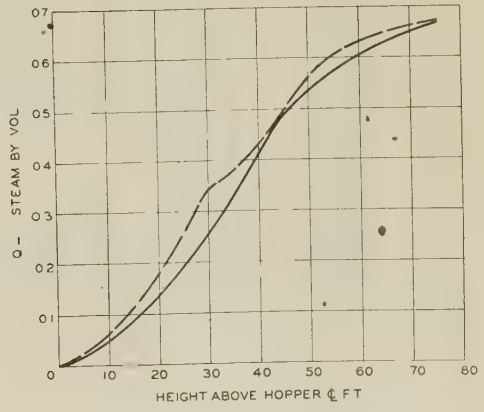

FIG. 9 TEST NO. 13; QUALITY OF FLUID IN EXPERIMENTAL TUBE FROM ΔT AND FROM DENSITY

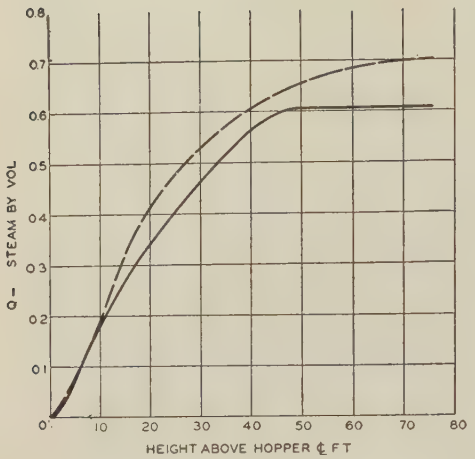

FIG. 10 TEST NO. 14; QUALITY OF FLUID IN EXPERIMENTAL TUBE FROM ΔT AND FROM DENSITY

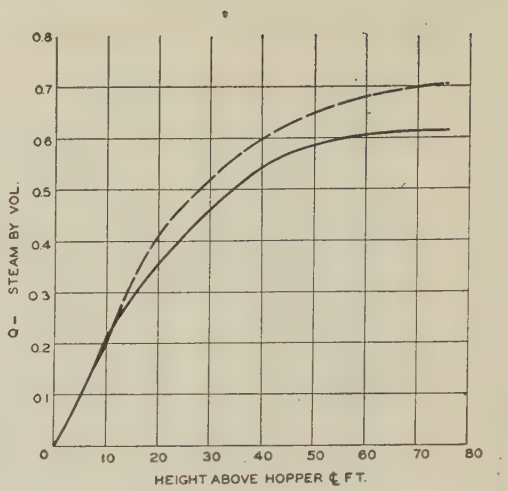

FIG. 11 TEST NO. 15; QUALITY OF FLUID IN EXPERIMENTAL TUBE FROM ΔT AND FROM DENSITY

TABLE 3 QUALITY AND VELOCITY DATA

Average Entering Velocity fps	Density Tap Nos. Test No.	Average Differential Pressures, between Density Taps, inches of mercury 1 - 2	1 - 3	1 - 4	1 - 5	2 - 3	3 - 4	4 - 5
1.90	10	4.21	12.29	27.49	38.06			
2.02	11	4.29	12.31	26.81	37.39			
1.90	13	4.01	11.23	25.80	36.74			
2.43	14	5.01	14.52	30.39	40.90			
2.35	15	5.17	14.75	30.20	40.78			
1.80	17	4.35	13.20	26.90	36.10	8.50	14.10	10.40
1.74	18	4.70	14.15	29.65	40.55			
1.88	19	4.53	13.05	27.45	37.60	8.20	13.50	10.10
1.78	20	4.65	13.30	27.40	37.80	8.60	14.40	10.50
2.13	21	4.10				7.60	13.10	9.60
2.11	24	4.45				8.51	13.99	10.14
1.87	25A	4.30				8.01	13.5	9.93
2.08	25B	4.40				8.25	13.96	10.17
2.12	25C	4.54				8.25	14.06	10.24
2.09	25D	4.61	13.46	27.25	37.45			
2.08	25E	4.49	13.22	27.68	38.20	8.72	14.13	10.36
1.89	26	4.13				7.93	12.80	9.73

Test No.	Average Quality of Mixture in tube between Density Taps as derived from above data 1 - 2	1 - 3	1 - 4	1 - 5	2 - 3	3 - 4	4 - 5
10	0.0652	0.1838	0.3445	0.4165	0.2693	0.5490	0.6624
11	0.0797	0.1880	0.3277	0.3894	0.2666	0.5046	0.6010
13	0.0429	0.1302	0.2958	0.3740	0.1934	0.5057	0.6420
14	0.1215	0.3070	0.4377	0.4757	0.4052	0.6034	0.6059
15	0.1909	0.3178	0.4311	0.4713	0.4098	0.5747	0.6092
17	0.0794	0.2299	0.3262	0.3567	0.3389	0.4486	0.4609
18	0.1183	0.2739	0.4019	0.4533	0.3860	0.5649	0.6282
19	0.1061	0.2242	0.3437	0.3918	0.3039	0.4958	0.5556
20	0.1200	0.2363	0.3412	0.3953	0.3199	0.4748	0.5791
21	0.0643	0.1655	0.2852	0.3446	0.2403	0.4374	0.5472
24	0.0905				0.3058	0.4659	0.5560
25A	0.0905				0.2627	0.4371	0.5311
25B	0.0885				0.2845	0.4658	0.5599
25C	0.1063				0.2848	0.4768	0.5683
25D	0.1162	0.2432	0.3376	0.3892	0.3352	0.4576	0.5655
25E	0.0986	0.2305	0.3500	0.4023	0.3261	0.5019	0.5810
26	0.0574				0.2572	0.3915	0.5165

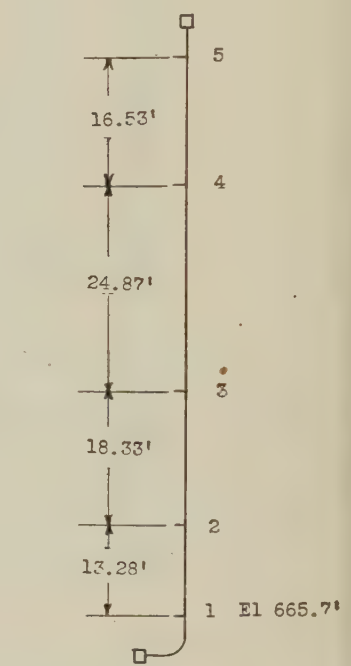

EXPERIMENTAL TUBE
LOCATION OF DENSITY TAPS

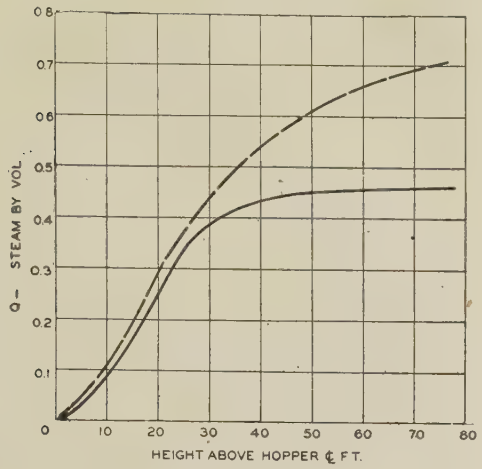

FIG. 12 TEST NO. 17; QUALITY OF FLUID IN EXPERIMENTAL TUBE FROM ΔT AND FROM DENSITY

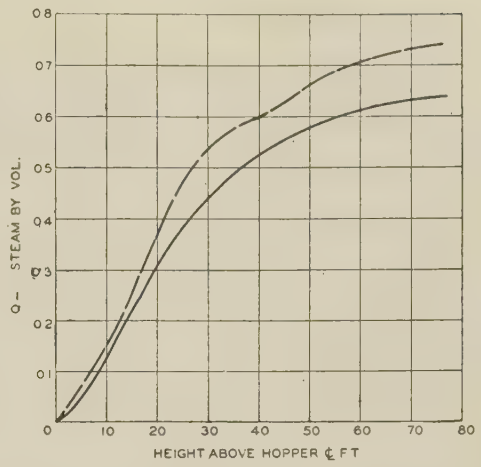

FIG. 13 TEST NO. 18; QUALITY OF FLUID IN EXPERIMENTAL TUBE FROM ΔT AND FROM DENSITY

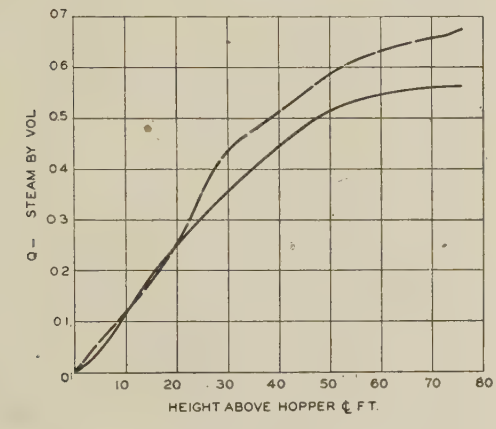

FIG. 14 TEST NO. 19; QUALITY OF FLUID IN EXPERIMENTAL TUBE FROM ΔT AND FROM DENSITY

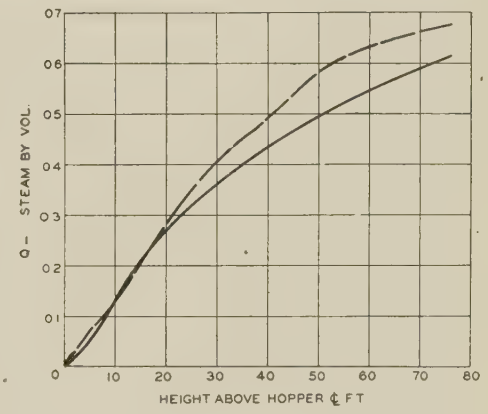

FIG. 15 TEST NO. 20; QUALITY OF FLUID IN EXPERIMENTAL TUBE FROM ΔT AND FROM DENSITY

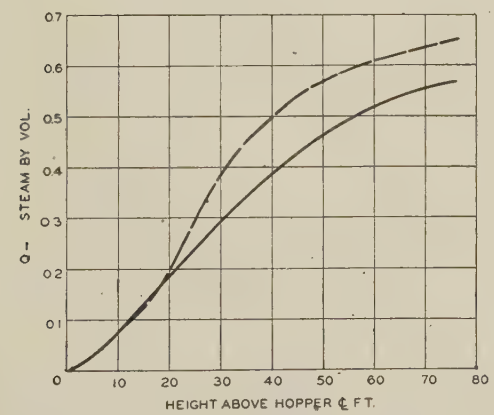

FIG. 16 TEST NO. 21; QUALITY OF FLUID IN EXPERIMENTAL TUBE FROM ΔT AND FROM DENSITY

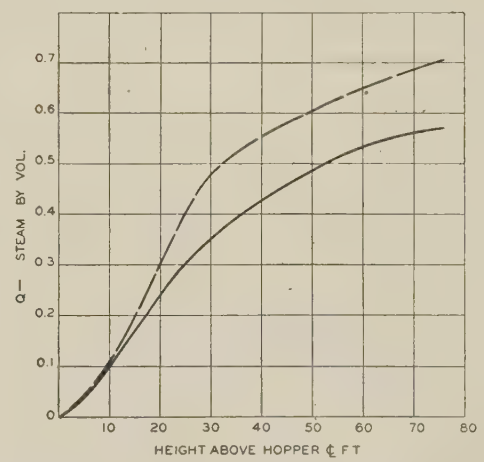

FIG. 17 TEST NO. 24; QUALITY OF FLUID IN EXPERIMENTAL TUBE FROM ΔT AND FROM DENSITY

The downward tilt of the burners caused the rapid increase in Q values near the hopper.

In Fig. 12, for test No. 17, the density Q curve levels off at a low value in the upper half of the tube, and no explanation is apparent. No such effect is seen in the ΔT — Q curve. For this and all succeeding tests the burners remained horizontal, but the rating, excess air, and dirtiness were varied. Test no. 17 was made with 35 per cent excess air at the furnace outlet and the same heat input as tests Nos. 14 and 15.

In Fig. 13, for test No. 18, the effect of decreasing the excess air from 35 to 27 per cent and an increase in input from 462 to 574 MM Btu is reflected. The curves are generally higher than those for test No. 17 and the ΔT — Q curve reflects the presence of ash 35 or 40 ft above the hopper.

In Fig. 14, for test No. 19, the excess air was held at 25 per cent, and the input dropped to 446 MM Btu. The curves are generally lower with the ΔT — Q curve again reflecting the presence of ash.

In Fig. 15, for test No. 20, the input was held about constant but the excess air was dropped to 16 per cent. No significant difference between tests Nos. 19 and 20 is apparent on the Q curves.

In Fig. 16, for test No. 21, the input was dropped to 334 MM Btu, the lowest value of the series, at normal excess air. The low value of input is not reflected in the ΔT — Q curve but may be the reason for the somewhat lower values of the Q curve from density. However, the lack of consistent variations in the Q values from density indicates that the relative velocities of steam and water are influenced by several other possible factors.

In Fig. 17, for test No. 24, the input was 594 MM Btu, the highest value, and the excess air low at 11 per cent, the lowest value. The Q curve from density is low and does not reflect the high input, but the ΔT — Q curve does reflect the high input. No effect of ash deposits on the experimental tube is evident.

In Fig. 18, for test No. 25A, the first of a series in which the wall blowers were not operated, the excess air was normal at 25 per cent, and the input high at 543 MM Btu. The Q curve from density is quite low but the ΔT — Q curve is normal reflecting only a slight ash deposit.

In Fig. 19, for test No. 25B, the input was raised slightly to 578 MM Btu and the excess air dropped to 17 per cent to accelerate ash deposition. The two curves diverge rapidly but except for a slightly more noticeable flattening of the ΔT — Q curve about 30 ft above the hopper do not indicate any pronounced accumulation of ash.

In Fig. 20, for test No. 25C, no significant changes in input or excess air were made. However, the effect of the deposit of ash is more pronounced.

In Fig. 21, for test No. 25D, operating conditions were held as in the preceding tests but the ash deposit apparently fell off because the ΔT — Q curve does not show the characteristic flattening.

In Fig. 22, for test No. 25E, operating conditions were the same as before. Ash deposits were present, however, as evidenced by the characteristic flattening of the ΔT — Q curve.

In Fig. 23, for test No. 26, the input was dropped back from 584 to 470 MM Btu and the excess air restored to about normal at 28 per cent. It is interesting to note that the Q curve from density is linear for the upper two thirds of the length of the tube. The flattening of the ΔT — Q curve is quite pronounced at slightly above the burner elevation.

Circumferential Temperature Studies. One tube in about the center of each wall was equipped with circumferentially disposed thermocouples at several of the elevations used for center-line couples. In a previous study (1), it was found that the surface temperature of tangent tubes was almost saturation tempera-

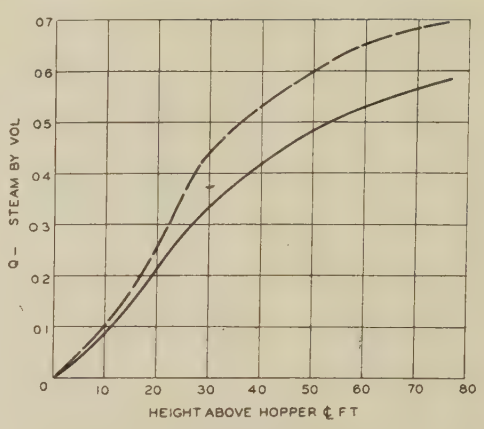

FIG. 18 TEST NO. 25A; QUALITY OF FLUID IN EXPERIMENTAL TUBE FROM ΔT AND FROM DENSITY

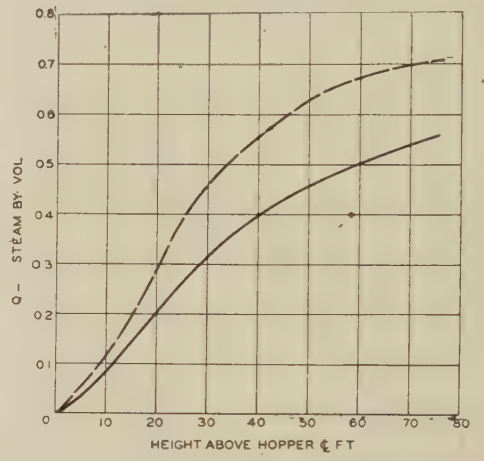

FIG. 19 TEST NO. 25B; QUALITY OF FLUID IN EXPERIMENTAL TUBE FROM ΔT AND FROM DENSITY

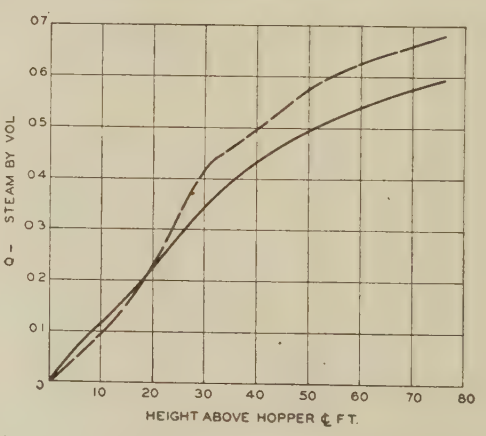

FIG. 20 TEST NO. 25C; QUALITY OF FLUID IN EXPERIMENTAL TUBE FROM ΔT AND FROM DENSITY

ture at the point of tangency. Using the assumption, in this case, that the surface temperature at the two points of tangency was 3 deg F above saturation, an average surface temperature for the exposed semicircumference was computed for each elevation of each tube equipped with circumferential couples. This average was expressed as a distribution factor by dividing it by the center-line couple. The average of all center-line couples in each wall at each elevation was modified by the distribution factor and applied to the developed area of the wall in the region

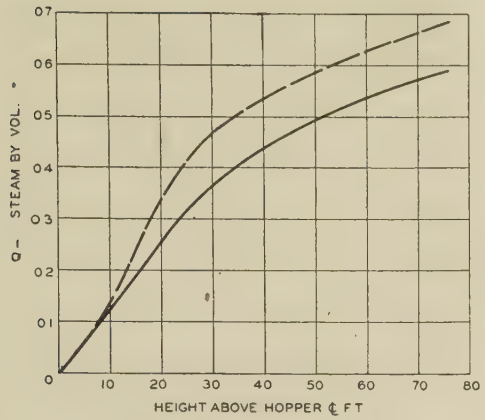

FIG. 21 TEST NO. 25D; QUALITY OF FLUID IN EXPERIMENTAL TUBE FROM ΔT AND FROM DENSITY

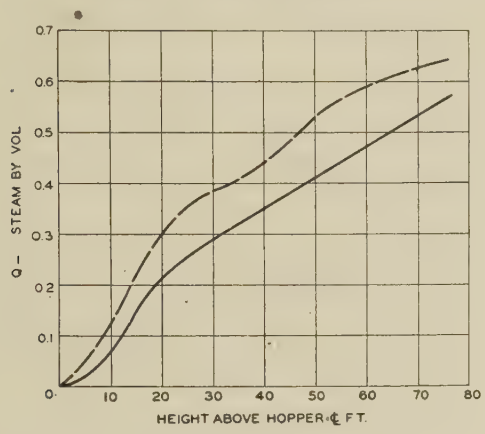

FIG. 22 TEST NO. 25E; QUALITY OF FLUID IN EXPERIMENTAL TUBE FROM ΔT AND FROM DENSITY

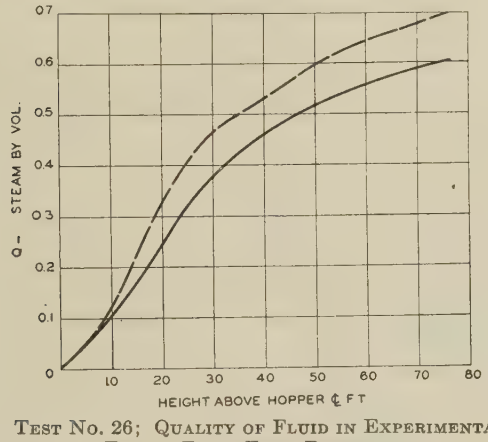

FIG. 23 TEST NO. 26; QUALITY OF FLUID IN EXPERIMENTAL TUBE FROM ΔT AND FROM DENSITY

estimated to be represented by that elevation of center-line couples. The total heat absorption of the furnace computed from such modified data was, in general, somewhat higher than other methods and probably could have been brought into line if it had been consistently high. However, the results were not consistently high and did not reflect variations in firing direction or other controlled variables to the same extent as did the other methods. It seems obvious that the use of a single tube in about the center of each wall provides an insufficient sample for the establishment of dependable distribution factors for an entire wall. Furthermore, the close proximity of several welded guard rings provides a place of lodgment for ash particles which would not find similar lodgment a few inches away. The use of circumferential couples to establish distribution factors to reflect cleanliness factors is, however, indicated as an available method to confirm visual observation and calculated or observed factors, provided a sample of perhaps three tubes distributed along a wall is used.

The heat absorption in the experimental tube was computed separately using its own surface-temperature-distribution factors and is plotted for each test from No. 10 to No. 26. The average center-line ΔT for the entire furnace is plotted on the same chart for each test with the experimental tube heat absorption for general comparison. It is obvious that the variations shown by the modified ΔT method are not reflected to the same extent by the average ΔT for the entire furnace, indicating insufficient sampling.

In Fig. 24, for test No. 10, the heat absorbed, as indicated by the arch under the curve, looks to be about the same as that of the average ΔT for the entire furnace if a factor of about 1000 Btu per deg ΔT were used. The greater peak at 30 ft and the lower values at 47 ft probably indicate differences in the cleanliness condition of the experimental tube, as compared to the average cleanliness condition indicated by the center-line couples.

In Fig. 25, for test No. 11, the variations were less sharp, and the experimental tube indicated a somewhat cleaner condition than the average for the furnace. The peak absorption shifted to a slightly higher elevation (50 ft), although there was no change in the direction of firing.

In Fig. 26, for test No. 13, although the peaks for the experimental tube and for the furnace average are at about the same elevation with the burners pointed up 30 deg, the shape of the curve for the experimental tube shows the pronounced effect of local ash deposits.

In Fig. 27, for test No. 14, the curves are in fair agreement. With the downward direction of the lower four burners, the effect of utilizing the lower furnace cooling surface more effectively is clearly evident.

In Fig. 28, for test No. 15, with all burners directed downward, the peak absorption for the experimental tube is at 24 ft. The average of the center-line couples for the entire furnace is some-

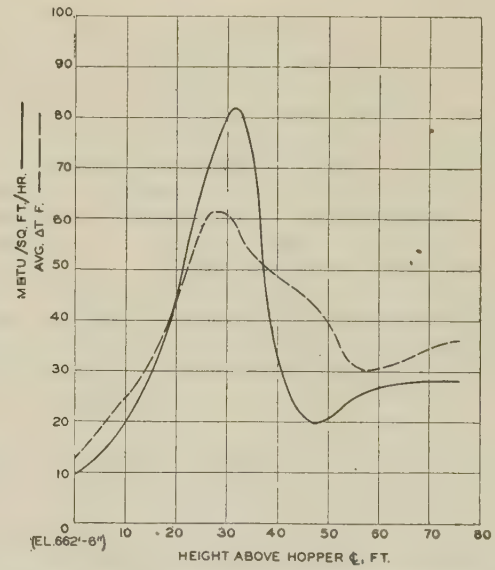

FIG. 24 TEST NO. 10; HEAT ABSORPTION IN EXPERIMENTAL TUBE AND AVERAGE ΔTS FOR ENTIRE FURNACE

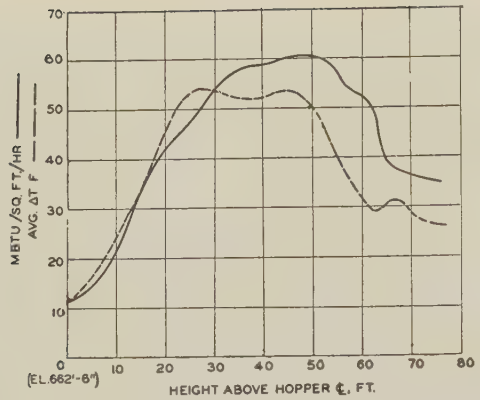

FIG. 25 TEST NO. 11; HEAT ABSORPTION IN EXPERIMENTAL TUBE AND AVERAGE ΔTS FOR ENTIRE FURNACE

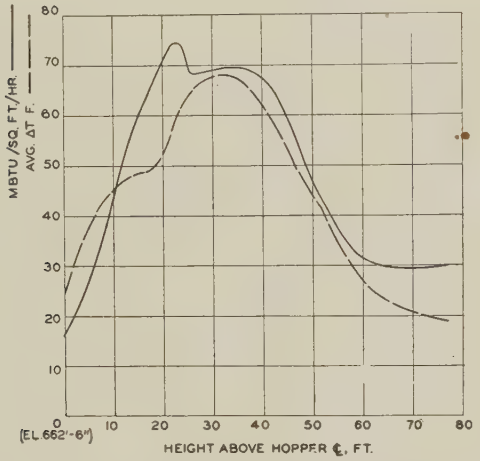

FIG. 27 TEST NO. 14; HEAT ABOSRPTION IN EXPERIMENTAL TUBE AND AVERAGE ΔTS FOR ENTIRE FURNACE

what lower. In Figs. 27 and 28 the shoulder in the average curve at about 15 ft is attributed to the sloping hopper walls on the front and rear which, probably, are scrubbed effectively by the gases as they rotate in the furnace when the burners are pointed down.

In Fig. 29, for test No. 17, the burners were directed horizontally as they were for all the remaining tests. The excess air was high at 35 per cent, but this did not prevent ash accumulating at the 35-ft point. The same ash accumulation is not shown by the average curve for center-line couples.

In Fig. 30, for test No. 18, at high input and normal excess air the two curves show the effect of ash accumulation at the same elevation. Obviously, however, the amount of the accumulation differs as between the experimental tube and the average and confirms the necessity for a broad sample.

In Fig. 31, for test No. 19, the two curves are entirely different at moderate input and normal excess air. The only plausible explanation of the differences is local ash accumulation, perhaps accentuated by the guard rings. At any rate, we can certainly conclude that one tube cannot be taken as representing the entire furnace.

In Fig. 32, for test No. 26, with moderate input and low excess air (16 per cent), the experimental tube indicates a generally higher ash accumulation in the first 40 ft.

In Fig. 33, for test No. 21, with normal excess air and the lowest input of the tests (334 MM Btu), the upper parts of the curves are in fair agreement, but the lower parts show that the experimental tube was lower than the average.

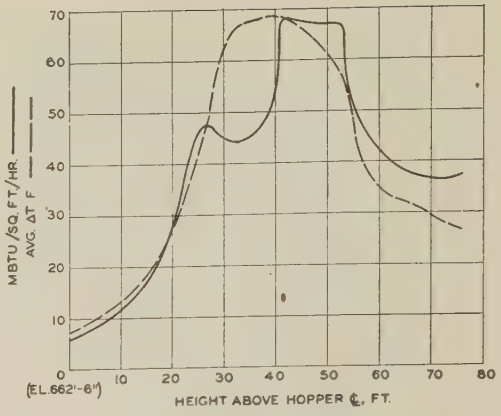

FIG. 26 TEST NO. 13; HEAT ABSORPTION IN EXPERIMENTAL TUBE AND AVERAGE ΔTS FOR ENTIRE FURNACE

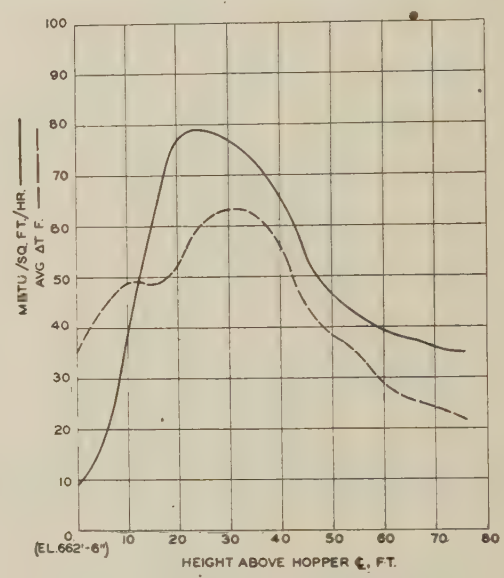

FIG. 28 TEST NO. 15; HEAT ABSORPTION IN EXPERIMENTAL TUBE AND AVERAGE ΔTS FOR ENTIRE FURNACE

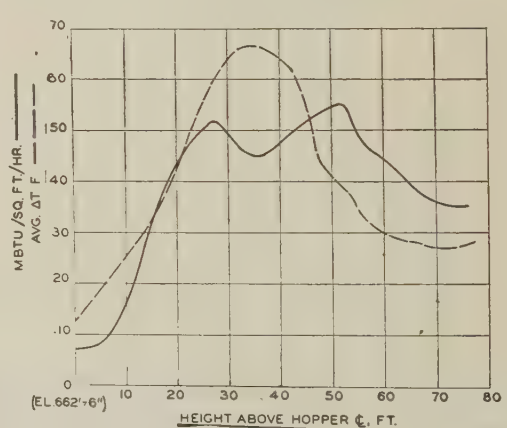

FIG. 29 TEST NO. 17; HEAT ABSORPTION IN EXPERIMENTAL TUBE AND AVERAGE ΔTS FOR ENTIRE FURNACE

In Fig. 34, for test No. 24, at high input and low excess air, the experimental tube indicated, in addition to differences in ash accumulation from the average, an increasing rate of absorption at the top 20 ft. This may be due to too high an indicated distribu-

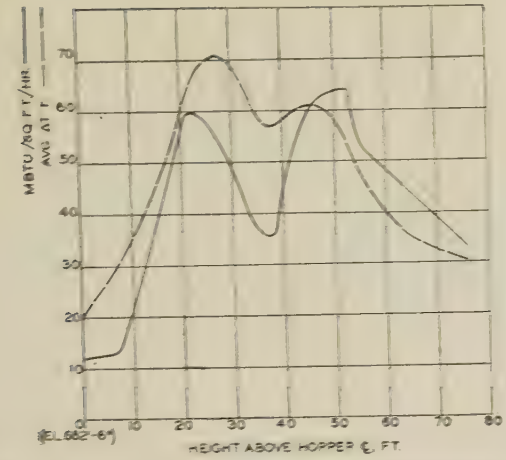

FIG. 30 TEST NO. 18; HEAT ABSORPTION IN EXPERIMENTAL TUBE AND AVERAGE ΔTS FOR ENTIRE FURNACE

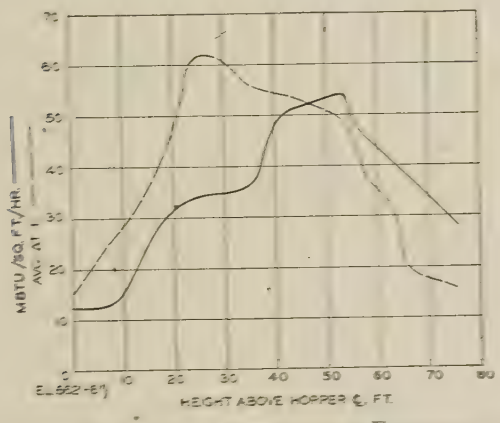

FIG. 32 TEST NO. 20; HEAT ABSORPTION IN EXPERIMENTAL TUBE AND AVERAGE ΔTS FOR ENTIRE FURNACE

tion factor or to reflected heat from ash accumulations at lower elevations.

In Fig. 35, for test No. 25A, operation was at normal excess air and fairly high input. A very high distribution factor at 17 ft resulted in the indicated peak. Such a factor results when the center-line temperature is low, perhaps because of a highly localized ash deposit, and the circumferential couples read normal temperatures. In other respects this figure shows the difference in ash deposits.

In Fig. 36, for test No. 25B, the input was high and the excess air 17 per cent. Emphasis is drawn to the nonrepresentative character of the performance of a single tube. The average ΔT curve shows none of the variations shown by the experimental tube.

In Fig. 37, for test No. 25C, the input and excess air were unchanged from the previous period but ash had been allowed to accumulate. The average curve shows little change from the previous period but the curve for the experimental tube does differ quite materially. Again we have the indication of rising heat absorption at the upper 20 ft.

In Fig. 38, for test No. 25D, we find an indication of a very high rate of absorption at the top of the experimental tube. Although this might be due to reflected heat if the value was moderate, it is more likely that a highly localized ash deposit on the center-line couple is the reason, and to assume that such a distribution factor applies for a longer length of tube than that actually covered by the couples leads to an error.

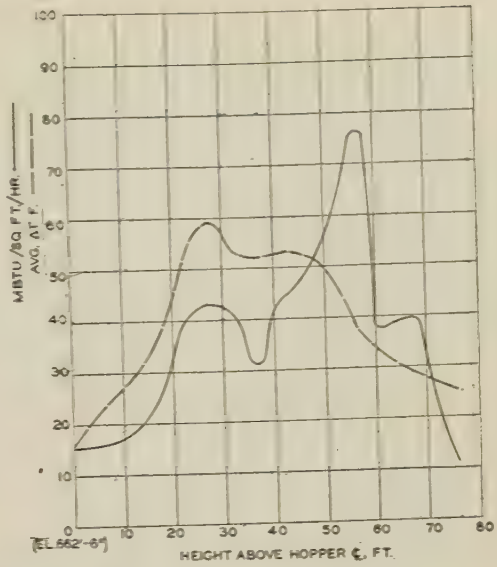

FIG. 31 TEST NO. 19; HEAT ABSORPTION IN EXPERIMENTAL TUBE AND AVERAGE ΔTS FOR ENTIRE FURNACE

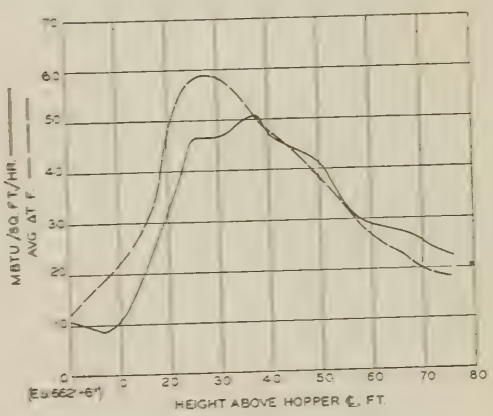

FIG. 33 TEST NO. 21; HEAT ABSORPTION IN EXPERIMENTAL TUBE AND AVERAGE ΔTS FOR ENTIRE FURNACE

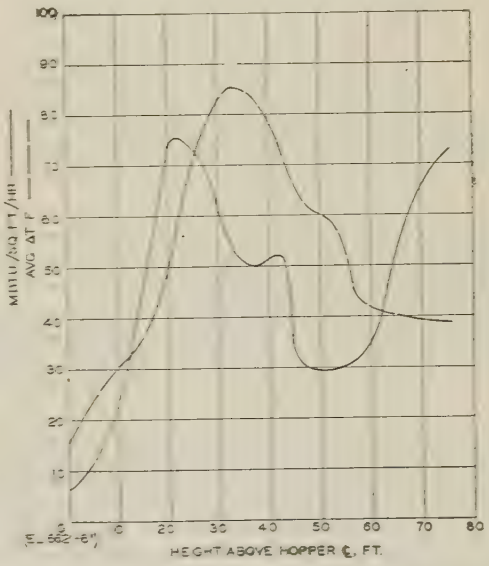

FIG. 34 TEST NO. 24; HEAT ABSORPTION IN EXPERIMENTAL TUBE AND AVERAGE ΔTS FOR ENTIRE FURNACE

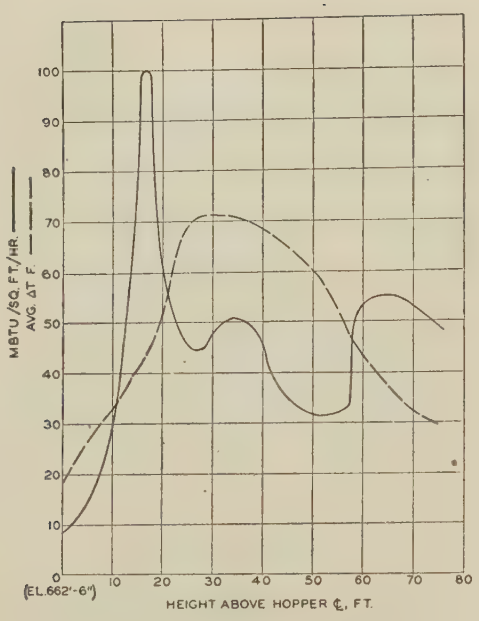

FIG. 35 TEST NO. 25A; HEAT ABSORPTION IN EXPERIMENTAL TUBE AND AVERAGE ΔTS FOR ENTIRE FURNACE

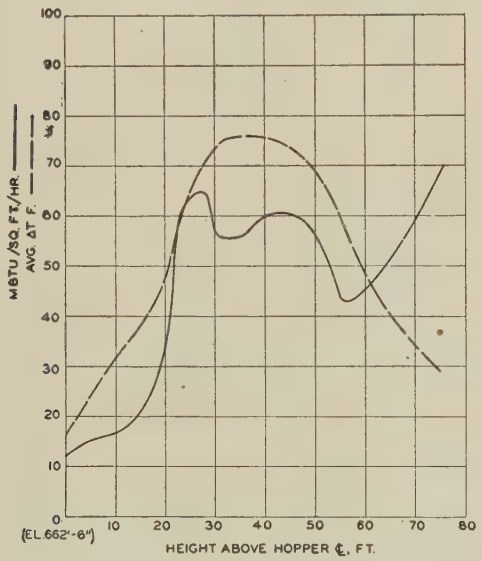

FIG. 37 TEST NO. 25C; HEAT ABSORPTION IN EXPERIMENTAL TUBE AND AVERAGE ΔTS FOR ENTIRE FURNACE

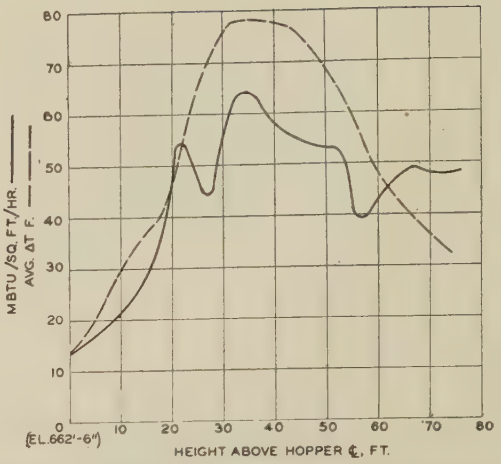

FIG. 36 TEST NO. 25B; HEAT ABSORPTION IN EXPERIMENTAL TUBE AND AVERAGE ΔTS FOR ENTIRE FURNACE

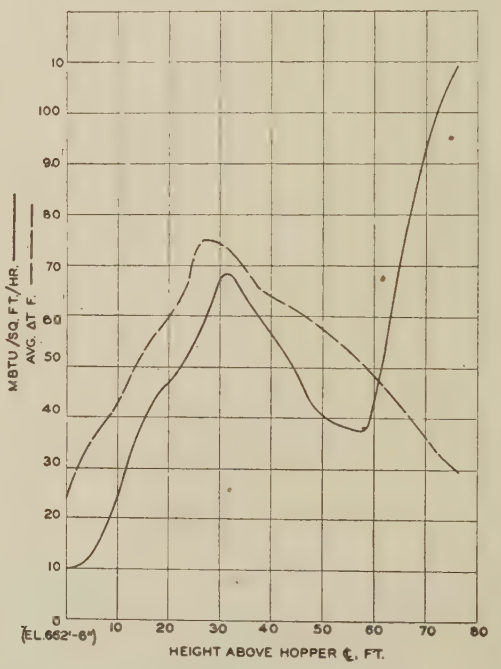

FIG. 38 TEST NO. 25D; HEAT ABSORPTION IN EXPERIMENTAL TUBE AND AVERAGE ΔTS FOR ENTIRE FURNACE

In Fig. 39, for test No. 25E, only minor variations in the curves are evident, and these again emphasize the fact that a single tube is only accidentally representative of the furnace.

In Fig. 40, for test No. 26, at moderate input and normal excess air, ash accumulation is reflected both in the furnace average curve, and to a greater extent in the experimental-tube curve.

CONCLUSIONS

A comparison of the average quality of the fluid flowing in an experimental tube, as determined by computation from the surface temperature of the tube at the center line at several elevations and the water velocity entering the tube, and as determined by differential static pressures measured along the tube, shows the latter to be lower at all points. The indicated reason for the lower values obtained from static pressures is that the steam occupies more of the section near the heat-receiving side and the water more of the section near the casing side where the pressure taps were located. This apparently resulted in an indication of higher density than the average by the pressure-tap method. Extension of the connection to the hydraulic radius instead of ending it at the inner surface might have increased the derived quality. However, the variations in the difference between the two methods made the co-ordinating factors derived from the averages of doubtful value. Because the surface-temperature method did co-ordinate well with the difference between the heat input and heat leaving the furnace, it was used as the standard of comparison.

Certain computations of steam and water velocities, based upon average quality indications, indicate that the steam flows faster than the water at an increasing rate up to a quality of more than 0.5 and less than 0.6, and thereafter the rate of increase in velocity changes slope and the increase is faster. However, the records of individual tests show wide variations from

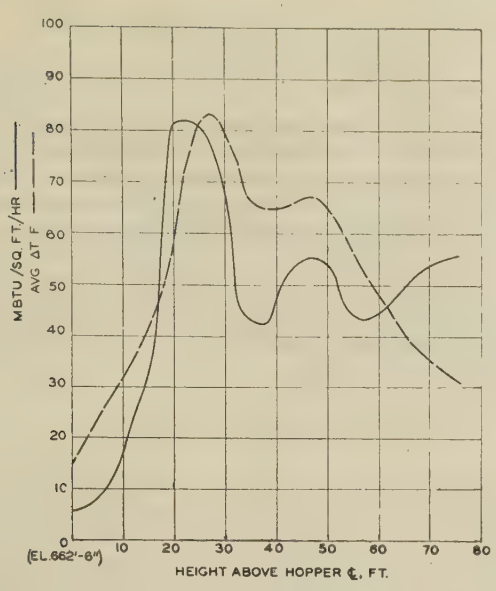

FIG. 39 TEST NO. 25E; HEAT ABSORPTION IN EXPERIMENTAL TUBE AND AVERAGE ΔTS FOR ENTIRE FURNACE

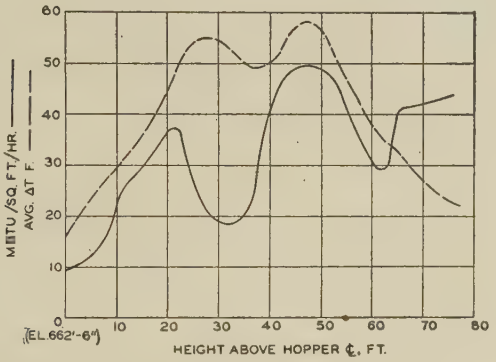

FIG. 40 TEST NO. 26; HEAT ABSORPTION IN EXPERIMENTAL TUBE AND AVERAGE ΔTS FOR ENTIRE FURNACE

the average and indicate that the individual test differences in steam and water velocities are influenced by many factors which could not be controlled individually in the field. Therefore the hope of determining a Btu rate per degree ΔT was not realized by the method of densities and little hope was held out that changes in experimental technique would improve the results.

The extensive investigation of the possibility of deriving a cleanliness or effectiveness factor from the indications of circumferential couples indicated that the use of a single tube in each wall, for this purpose, did not provide a sufficiently extensive sample. Although total heat absorptions in the furnace were of the right order of magnitude, generally being somewhat higher than the absorptions indicated by the center-line couples, the variations in heat absorption caused by changes in firing direction, excess air, and rating were not consistently reflected. The use of more elevations on perhaps three distributed tubes in each wall might prove to be sufficient sample and thus provide an effectiveness factor independent of visual observation.

Although the results of the investigation at Tidd in the two phases covered by this part of the report were negative in one phase and partly negative in the other, our understanding of the factors affecting furnace performance has been increased and should improve the effectiveness of investigations still to be carried out at other plants.

BIBLIOGRAPHY

1 "Studies of Heat Transmission Through Boiler Tubing at Pressures From 500 to 3300 Pounds," by W. F. Davidson, T. H. Hardie, C. G. R. Humphreys, A. A. Markson, A. R. Mumford, and T. Ravese, Trans. ASME, vol. 65, 1943, pp. 553–591.

2 "Thermocouples for Furnace-Tube Surface Temperature Measurements," by C. G. R. Humphreys, *Combustion*, vol. 16, December, 1944, pp. 53–55.

3 "Measurement of Boiler Circulation by Means of Pitot Tubes," by T. Ravese, *Combustion*, vol. 16, October, 1944, pp. 43–45.

5 "Heat Transmission," by W. H. McAdams, McGraw-Hill Book Company, Inc., New York, N. Y., 1942, pp. 99–102.

5 "Elementary Mechanics of Fluids," by H. Rouse, John Wiley & Sons, Inc., New York, N. Y., 1946, p. 197.

6 "Qualitative Determination of Steam-Water Mixtures," by T. Ravese and C. G. R. Humphreys, *Combustion*, vol. 16, January, 1945, pp. 37–39.

Appendix 1

DEVELOPMENT OF FORMULA USED FOR COMPUTING VOLUMETRIC QUALITY OF MIXTURE IN EXPERIMENTAL TUBE

In the experiment the difference in weight of the column of fluid within the tube and the column of water in the instrument connections outside the tube was balanced by the mercury column in the manometer so that

"Weight of mixture within tube" plus "weight of mercury column" equals "weight of outside water leg"

The effect of friction was to retard flow and act as an increased weight on the left-hand side of the equation. The force required to accelerate the mixture reacted against the fluid and therefore would also have the effect of increasing the weight of the fluid within the tube. Both friction and acceleration force were found to be small and affected the quality determined by only a small percentage. However, friction was included but accelerating force was omitted. The basic equation then became

"Weight of mixture within the tube" plus "weight of mercury column" plus "friction" equals "weight of outside water leg"

If

Q = steam by volume in mixture, per cent
X = steam by weight in mixture, per cent
l = length of tube between measuring points, ft
∂s = density of steam, lb per cu ft
∂w = density of water, lb per cu ft
v_g = specific volume of steam, cu ft per lb
v_f = specific volume of water, cu ft per lb

then the weight of the mixture within the tube can be written

$$[x\partial s + (1 - x)\partial w]l, \text{ lb per sq ft}$$

or

$$\left[\frac{Q}{v_g} + \frac{(1 - Q)}{v_f}\right]l, \text{ lb per sq ft}$$

The latter, involving the steam by volume, is the expression used.

If

M = height of mercury column, in.
∂_M = density of mercury, lb per cu ft (849 at 100 F)

then the weight of the mercury column can be written

$$\frac{M}{12}\partial_M = \text{lb per sq ft} \quad \text{or} \quad \frac{M}{12} \times 849 = 70.75M$$

If

V = velocity of mixture, fps
v = specific volume of mixture, cu ft per lb
D = internal diameter of tube, ft

then the friction can be represented by the expression

$$\frac{2fV^2l}{v_g D} \text{ lb per sq ft}$$

in which f is taken as 0.006 and g is taken as 32.2.

Because V and v are unknown, it is desirable to convert them into the desired unknown and measured or tabular values so that the friction can be represented

$$\frac{2fV_0^2 l}{gDv_f^2}\left[v_f + \frac{Qv_f v_{fg}}{Qv_f + v_g - Qv_g}\right]$$

in which V_0 is the velocity of water as measured near the entrance to the tube. By reducing constants we have

$$\frac{0.0019\, w_0^2}{v_f^2}\left[v_f + \frac{Qv_f v_{fg}}{v_g - Qv_{fg}}\right]$$

The weight of the water column can be represented as

$$\left[l + \frac{M}{12}\right]\partial w_{100} \text{ lb per sq ft}$$

This formula although cumbersome reduces to a simple quadratic and is readily solved for Q.

Appendix 2

Conversion of Heat Rates Into Quality by Volume

The ΔT for the face couples on the experimental tube, obtained from the recorder and from less frequent readings by a portable potentiometer, were averaged. A factor of 1000 Btu per deg F was used to evaluate the rate of heat transfer. This factor was developed from $k = 29$ for the tube wall, and a film conductance of 12,000 Btu per deg F. Using the entering velocity, decreased slightly to compensate for the small amount of steam made below the elevation of the Pitot tube, the heat absorbed was converted to quality on the weight basis, and then to quality on the volume basis.

Appendix 3

Development and Application of Distribution Factors

The distribution factor has been defined as the ratio of the average tube ΔT around the exposed semicircumference to the ΔT at the center line of the tube. Because it was physically impossible to install thermocouples at the tangent points of the tubes after the tubes were in place, a ΔT of 3 deg F was assumed for each of the points and included in making up the average. The distribution factor reflects surface-ash accumulations and, if the sample is sufficient, would eliminate or confirm personal observations. The factor can be used to modify the center-line ΔT and provide a modified average ΔT which can be applied to the developed exposed furnace-tube area rather than the projected furnace-tube area.

An Investigation of the Variation in Heat Absorption in a Pulverized-Coal-Fired Water-Cooled Steam-Boiler Furnace

IV—Comparison and Correlation of the Results of Furnace Heat-Absorption Investigations

By A. R. MUMFORD[1] and G. W. BICE,[2] NEW YORK, N. Y.

In this part of the symposium the three preceding sections of the report are compared, and satisfactory co-ordination is accomplished for the first two sections. The tube-surface temperature measurements show furnace heat absorptions which can be co-ordinated with the absorptions indicated by the surveys of the gas conditions at the furnace outlet by applying a correction to the gas-temperature measurement, or by varying the tube-to-water film conductance. A method of evaluating furnace cleanliness is developed and applied. A suggested basis of comparing furnaces is discussed.

DURING the past year and a half, four series of furnace-performance tests have been conducted on boiler No. 11 at the Tidd Plant of The Ohio Power Company, under the sponsorship of the ASME Special Research Committee on Furnace Performance Factors. Three individual phases of this test work are reported in detail elsewhere in this issue (1, 2, 3),[3] which are component parts of the investigation, and will be referred to as Part I, Part II, and Part III, respectively, hereafter. The purpose of this paper is to compare and correlate data from these three papers and to draw such general conclusions as may be warranted.

The location of test points for each of these phases of the investigation has been given separately in the individual reports. All of these test points, together with furnace-door and wall soot blower locations, are included on a single diagram in Fig. 1, which is a development of the furnace envelope, all walls being viewed from outside the setting as indicated in the "key plan" at the lower left of the diagram.

Factors Affecting Furnace Performance

A complete list of all the variable factors which might conceivably affect the performance of a fuel-fired furnace would be lengthy, and it is doubtful that any two engineers would compile identical lists. Therefore no attempt to list all such factors will be made herein.

The number of more important variables to be investigated is reduced materially in this report because only a single wall construction and one specific fuel are considered.

In the test work at Tidd Plant the effects of four major variables were investigated as follows:

1 Heat available (approximately proportional to rating).
2 Excess air.
3 Direction of fuel firing.
4 Relative cleanliness of water-cooled heat-absorbing surfaces.

The range of heat available values investigated was from 52,600 to 95,000 Btu per hr-sq ft of flat projected water-cooled surface. These correspond to from 56.6 to 102.2 per cent of normal full-load rating on the boiler unit.

The range of excess air values investigated was from 11 per cent to 35 per cent at the furnace outlet. Normal operating excess air is about 25 per cent at the furnace outlet.

Variation in the direction of fuel firing was obtained by tilting the burners. The investigation included tests with all burners tilted up 30 deg, all burners horizontal, all burners tilted down 30 deg, and a special case with the upper-row burners horizontal and the lower row tilted down 30 deg.

Relative cleanliness of the furnace walls constituted the most difficult variable to evaluate. Previous tests have been described as being on the basis of furnace walls either "dirty" or "clean." Because the degree of wall cleanliness varied from test to test, the foregoing classification has been found entirely inadequate. A detailed treatment of a method of evaluating furnace cleanliness will constitute a later section of this paper.

Methods for Determining Furnace Performance

Several different methods for determining heat absorption in a water-cooled furnace are available. These methods may be classified under two general categories: (*a*), calculations from formulas using empirical factors; and (*b*), actual measurements using a sampling technique.

An excellent example of the theoretical approach to furnace-performance calculation has been given by Wohlenberg (4), in which such basic radiation heat-transfer concepts as the Stefan-Boltzmann law, Kirchhoff's law, and Lambert's cosine law are combined with analytical geometry and physics to produce a number of formulas and curves. Due to the lack of data regarding the behavior of many fundamental physical constants at elevated temperatures, the uncertainty involved in making several necessary assumptions and the volume of computations involved, such theoretical methods of predicting furnace performance have not yet come into general use. Instead, empirical calculations based largely on previous test work on fur-

[1] Development Engineer, Research and Development Department, Combustion Engineering Company, Inc. Fellow ASME.
[2] Engineer, Mechanical Engineering Department, American Gas & Electric Service Corporation. Mem. ASME.
[3] Numbers in parentheses refer to the Bibliography at the end of the paper.

Contributed by the Special Research Committee on Furnace Performance Factors in co-operation with the Fuels, Power, and Heat Transfer Divisions and presented at the Semi-Annual Meeting, Chicago, Ill., June 16–19, 1947, of The American Society of Mechanical Engineers.

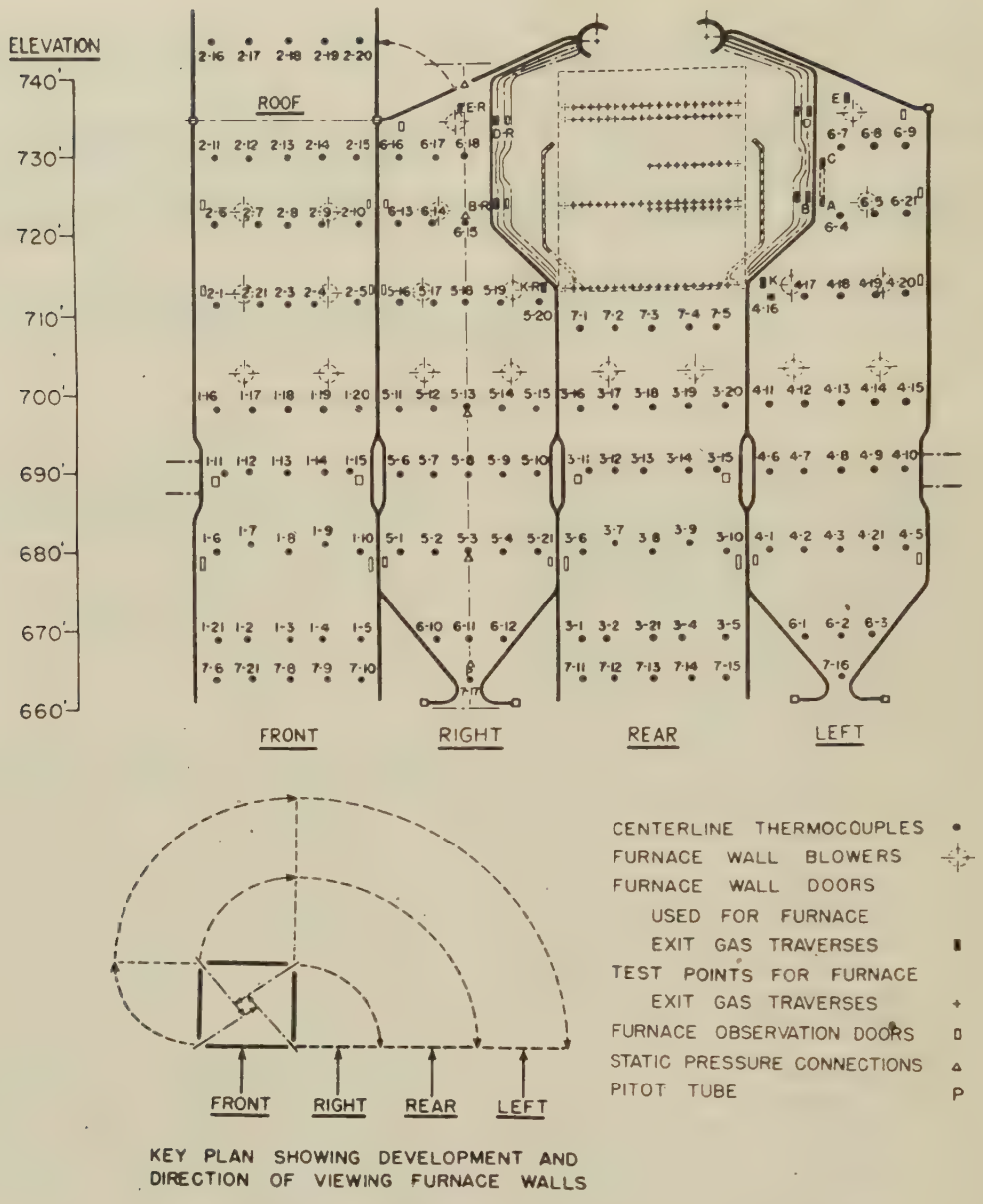

FIG. 1 KEY PLAN AND DEVELOPMENT SHOWING LOCATION OF ALL TEST POINTS

naces of similar size, design, fuel and firing method have been found to be more practical, and are currently used almost exclusively by boiler manufacturers in predicting furnace performance for new and proposed boiler units.

Several different methods employing experimental procedure have been used to measure heat absorption in water-cooled furnaces (5, 6, 7). Possibly the most dependable of these methods involves measurement of gas temperatures leaving the furnace by water-cooled high-velocity thermocouples. Several other methods of measuring gas temperature leaving the furnace have been tried, a few being the use of optical pyrometers, the determination of sound velocity through the gas, and the use of radiation pyrometers and calorimeters. Spot heat-absorption rates in various representative individual tubes in furnace walls have been determined by measuring the temperature differential between the outer tube-metal surface and the fluid within the tube by means of fixed tube-face thermocouples. Heat-absorption rates in various furnace zones have been measured by "thermal probes" (controlled-flow water-heating elements). The heat absorbed by individual tubes has also been determined by measuring the velocity and quality of the fluid at the inlet, and the quality at various incremental locations along the tube. While these are the most common experimental methods in use, several others have been tried, such as thermopiles, radiation windows, segregated tubes, etc.

TESTS

The actual furnace test work undertaken at Tidd Plant has been described quite thoroughly in Parts I, II, and III and will not be dealt with herein, except to outline what data have been excluded from this comparison and correlation, and to explain briefly the reasons for such exclusions.

In the course of this investigation four series of tests have been conducted. The first series, consisting of tests Nos. 1, 2, 3, and 4, was run at boiler age 3 months. Furnace outlet gas temperature and composition traverses for these first four tests were

complete as no data were obtained to evaluate K and K-R (refer to Par. 1). During test No. 1 the instrument recording furnace wall-tube temperatures was not in dependable operating condition. Furthermore, during all four tests load variations were excessive due to early preliminary tempering from wet coal being supplied. In view of these difficulties, results from all parts of the first series have been omitted entirely in making this comparison and correlation.

The second series consisting of tests Nos. 10, 11, 13, 14, and 15 was run at boiler age 6 months. Reliable data were obtained during all of these except test No. 13, during which no exit gas temperature or composition-traverse data were obtained, so that K and K-R; therefore all data from these tests with the exception of No. 13 as mentioned, have been used in the comparison and correlation.

The third series consisting of tests Nos. 17, 18, 19, 20, and 21 were run at boiler age 9 months. During these tests furnace exit gas temperature and composition traverses were repeated separately for each half of each 8-hr test as in Part II. These data during tests Nos. 17 and 19 showed only slight variation during the two halves of each test and have been averaged and considered as single 8-hr tests in the comparison and correlation. The furnace exit gas temperature and composition traverse data for the two halves of tests Nos. 19, 20, and 21 have been kept separate and numbered 19A, 19B, 20A, etc., as in Part II.

The fourth series consisting of tests Nos. 24, 25, and 26 were run at boiler age 15 months. Test No. 25, which was a 16-hr test, has been divided into five parts to correspond with the five exit gas temperature and composition traverses as in Part II.

A careful examination of the tabulated data from the previous papers (1, 2, 3) will reveal a number of slight discrepancies. These have resulted from differences in calculation procedure used by the various investigators. For convenience in comparing the various data, these differences have been reduced by recalculating where necessary, and a new tabulation including heat quantities available, heat quantity absorbed, and excess air at the furnace outlet are shown in Table 1.

Comparison of Basic Data

In Part II mention was made of the possibility that Mumford's (multiple-shield) high-velocity thermocouple radiation correction is similar to those reported by Mumford. It might be applicable to the observed temperatures from the single-shield high-velocity thermocouple used. Since, however, no experimentally determined corrections were available for the specific design of thermocouple actually used, it was decided to forego using any such correction in Part II. However, an acceptable correlation between these data and the wall tube ΔT data from Part I was obtained by applying Mumford's radiation correction to the observed gas temperatures. This is shown graphically in Fig. 2 in which total heat absorptions, as computed from furnace wall ΔT averages, have been plotted against total heat absorptions as computed from the exit-gas temperature and composition traverses on both an HVT and an MHVT basis. It is obvious from this plot that the heat absorptions, based upon MHVT temperatures, are in much better agreement with the wall ΔT heat absorptions than those based upon HVT temperatures. Therefore MHVT corrected heat absorptions will be used in the remainder of this paper.

[1] ΔT heat absorptions for each wall were calculated using a heat-transfer rate corresponding to a mean temperature of the hot gases and a mean temperature of the metal midway between the inside and outside surfaces of the metal tube. The mean temperature of the metal was used here for the sake of convenience only, as the difference between the mean metal temperature and the inside metal temperature would be relatively small.

TABLE 1 SUMMARY OF FURNACE-PERFORMANCE DATA

TEST NUMBER		10	11	13	14	15	17	18	19A	19B	20A	20B	21A	21B	24	25A	25B	25C	25D	25E	26
EXCESS AIR AT FURNACE OUTLET	%	29	28	26	26	26	35	27	23	26	25	17	15	16	27	28	17	16	16	17	28
BURNER INCLINATION:	DEG.	0	0	UP 30	0	DN 30	0	0	0	0	0	0	0	0	0	0	0	0	0	0	0
UPPER:	DEG.	0	0	UP 30	DN 30	DN 30	0	0	0	0	0	0	0	0	0	0	0	0	0	0	0
LOWER:																					
AVERAGE GAS TEMP. AT FURNACE OUTLET:	F	1930	1825	-	1795	1870	1830	1830	1795	1850	-	-	-	-	-	1930	1865	1825	1805	1825	1865
HVT BASIS	F	2000	1890	-	1795	1730	1830	1935	1840	1910	-	-	-	-	-	1990	1915	2015	2000	2015	1925
MHVT BASIS																					
TOTAL HEAT QUANTITIES:																					
INPUT IN FUEL	MKB/HR	488	493	478	469	458	462	574	459	457	446	-	-	-	480	538	347	534	578	580	470
AVAILABLE ABOVE BOF	MKB/HR	505	468	495	480	473	482	500	468	480	458	472	474	473	473	493	307	511	537	508	485
AVAILABLE ABOVE SAT. TEMP.	MKB/HR	441	398	432	418	412	415	500	418	429	418	418	413	416	416	437	297	540	525	508	422
ABSORBED, HVT BASIS	MKB/HR	298	231	-	289	266	243	294	242	228	265	242	298	-	-	298	197	489	526	508	442
ABSORBED, MHVT BASIS	MKB/HR	227	215	-	248	256	221	272	228	-	219	232	298	-	-	298	-	394	394	391	392
ABSORBED, WALL TUBE ΔT BASIS	MKB/HR	210	208	208	241	246	205	272	-	-	-	-	178	174	197	288	-	366	307	367	279
																287	-	368	384	378	278
UNIT HEAT QUANTITIES:																					
INPUT IN FUEL	BTU/SQ.FT-HR.	78600	71300	77000	74600	73600	74000	92900	73900	71100	71800	73500	73700	73600	74600	86800	56000	86000	93200	93600	75800
AVAILABLE ABOVE BOF	BTU/SQ.FT-HR.	68600	61900	67200	64100	64100	64400	80900	62200	61900	62000	64400	64800	64700	64800	74000	47200	78000	81600	81800	62600
AVAILABLE ABOVE SAT. TEMP.	BTU/SQ.FT-HR.	58300	53900	-	60800	57400	55200	77700	57600	59800	57600	57700	58100	58000	58000	68000	46200	78000	81600	82000	57700
ABSORBED, HVT BASIS	BTU/SQ.FT-HR.	39300	33400	-	38400	35600	33000	42800	37600	35800	37000	38000	41000	40000	40000	48100	-	64200	70300	69400	56100
ABSORBED, MHVT BASIS	BTU/SQ.FT-HR.	32700	32400	32400	30000	30600	34400	41200	-	-	39000	-	41000	40000	40000	48100	-	64200	70300	69400	56100
ABSORBED, WALL TUBE ΔT BASIS	BTU/SQ.FT-HR.																				
UNIT HEAT QUANTITIES *																					
FURNACE THERMAL EFFICIENCY, BASED	%	48.7	50.9	-	54.0	56.2	48.3	49.2	52.7	50.0	-	52.3	-	55.3	53.3	-	50.6	50.6	51.4	48.7	50.1
UPON HEAT AVAILABLE ABOVE BOF	%	45.0	46.9	-	51.3	53.3	44.2	45.5	49.7	46.8	-	51.3	49.0	-	50.2	-	47.2	47.4	47.7	47.6	48.6
FROM HVT ABSORPTION	%	41.6	45.4	42.0	52.3	54.1	45.9	44.4	-	-	47.8	-	-	48.7	-	47.4	46.9	47.8	47.6	46.5	47.0
FROM MHVT ABSORPTION																					
FROM WALL TUBE ΔT ABSORPTION																					

*HEAT QUANTITIES PER UNIT AREA OF FLAT PROJECTED WATER-COOLED FURNACE HEATING SURFACE.

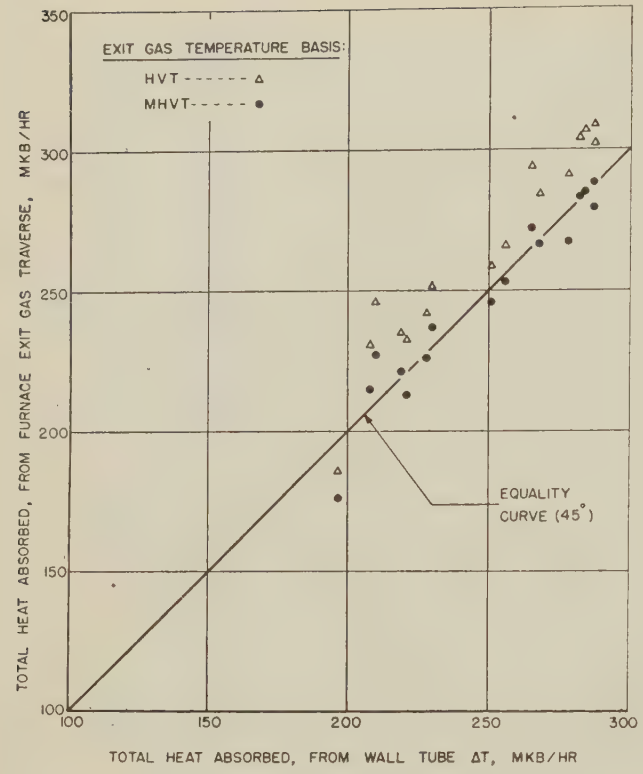

FIG. 2 COMPARISON OF HEAT ABSORPTION COMPUTED FROM WALL TUBE ΔT DATA WITH HEAT ABSORPTION COMPUTED FROM FURNACE EXIT GAS TRAVERSE DATA ON BOTH AN HVT AND AN MHVT TEMPERATURE BASIS

Heat-absorption rates per square foot of flat projected water-cooled surface have been plotted against heat available above 80 F per sq ft of flat projected water-cooled surface in Fig. 3. Although average curves have been drawn, a close inspection will reveal that the agreement of individual points with the curves is erratic. This apparent lack of agreement is due principally to variations in the relative cleanliness condition of the furnace from test to test. Notwithstanding the cleanliness condition, the general effects of changes in excess air and burner position are quite evident.

The behavior of burner position is especially interesting, as it illustrates clearly the effect of varying the effective volume of the furnace cavity by changing the location of the active combustion zone by varying the firing direction of the burners. To reduce this to basic concepts, the mass of hot furnace gases should be considered separately as they exist at any instant of time. Under any given set of conditions, a definite amount of heat will be radiated out from this mass of gases. Should it be surrounded by clean heat-absorbing surfaces having true black-body heat-absorbing characteristics, maximum heat transfer will occur.

Returning to the specific case of the Tidd furnace, let it be assumed that all burners are tilted up 30 deg and that all heat-absorbing surfaces are completely clean and have true black-body heat-absorbing characteristics. From numerous furnace inspections it is known that the lower surface of the mass of hot gases would not extend below a horizontal plane passed through the center line of the lower row of burners. Should the existing furnace hopper bottom be replaced with a water-cooled floor, composed of tangent tubes and coincident with this horizontal plane, the same total heat transfer would occur on the new floor as on the existing hopper bottom, even though the flat projected water-cooled surface would be reduced, and even though the intensity of heat transfer would be increased.

To go a step farther, assume that instead of this flat floor a water-cooled hopper bottom extending down an additional 100 ft were installed. Although the flat projected water-cooled furnace surface would be greatly increased, total heat transfer to the surface below the bottom plane of the flame would remain unchanged. This should indicate one of several possible errors involved in judging furnace performance solely on the basis of heat available per square foot of flat projected water-cooled furnace surface, as has become so common recently.

In the Tidd furnace, as the burners were tilted upward from the down position at a constant firing rate, the level at which combustion was completed moved upward toward the furnace exit. With the burners in the down position, a maximum amount of furnace cooling surface was available to cool the gases before they reached the furnace exit, while with the burners in the up position a minimum amount of furnace cooling surface was available to cool the gases after completion of combustion. In each case the amount of furnace cooling surface and the amount of available heat was the same, and the ratio would not indicate the change in temperature of the gases leaving the furnace as a result of burner tilting.

A sounder basis of comparison would be the heat available per square foot of flat projected water-cooled surface corrected by the ratio of enve ope surface of the volume of radiating gases to the envelope surface of the total furnace cavity. Application of such a basis to the curves of Fig. 3 representing the horizontal and upward burner positions, would bring them into approximate agreement with the highest curve representing the downward position of the burners, and therefore would indicate the changes in effective furnace absorption brought about by changing the direction of firing.

Furnace thermal efficiencies have been plotted against heat available above 80 F per sq ft of flat projected water-cooled surface in Fig. 4. Agreement of the individual points with the curves is poor; however, it is again apparent that burner position (or flame envelope area) has a pronounced effect upon furnace performance.

EFFECT OF SLAG AND ASH ON FURNACE WALLS

The relationships shown in Figs. 3 and 4 illustrate the effect on furnace performance of the first three of the four factors enumerated under "Factors Affecting Furnace Performance." The fourth factor, relative cleanliness of water-cooled heat-absorbing surfaces, is undoubtedly the factor which is largely responsible for the failure of individual points on these graphs to agree more closely with the average curves. Relative cleanliness of water-cooled heat-absorbing surfaces is practically indeterminate and cannot readily be evaluated accurately. In a great many cases, it has been the explanation offered for nonagreement of data from various tests on the same or similar furnaces.

Rather than merely recognizing the disturbing influence of this cleanliness factor in pulverized coal-fired water-cooled furnaces, an effort should be made to observe and analyze the extent of slag and ash deposits, and if possible to evaluate the magnitude of their influence on furnace performance.

During each of the tests considered in this comparison and correlation, one or more[5] thorough visual examinations of all furnace surfaces were made, and observed conditions were recorded in detail in the form of "Furnace Observation Reports." These reports were rather lengthy and are not reproduced in full. However, an example is given in the Appendix.

[5] See Appendix for tabulation listing number of complete "Furnace Observation Reports" available.

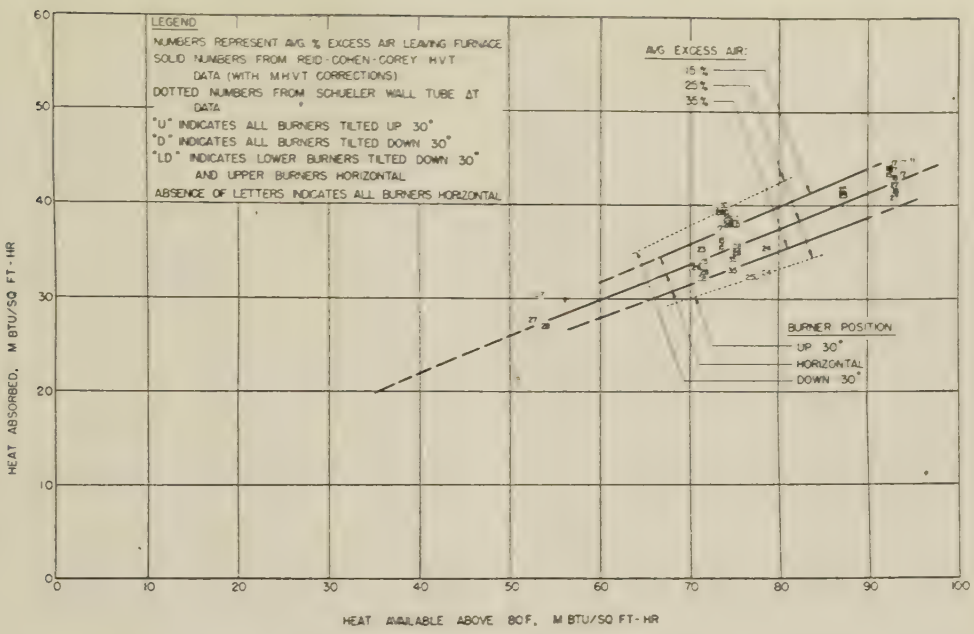

FIG. 3 HEAT-ABSORPTION RATES COMPUTED FROM WALL TUBE ΔT DATA AND FURNACE EXIT GAS TRAVERSE DATA WITH MHVT TEMPERATURE CORRECTIONS

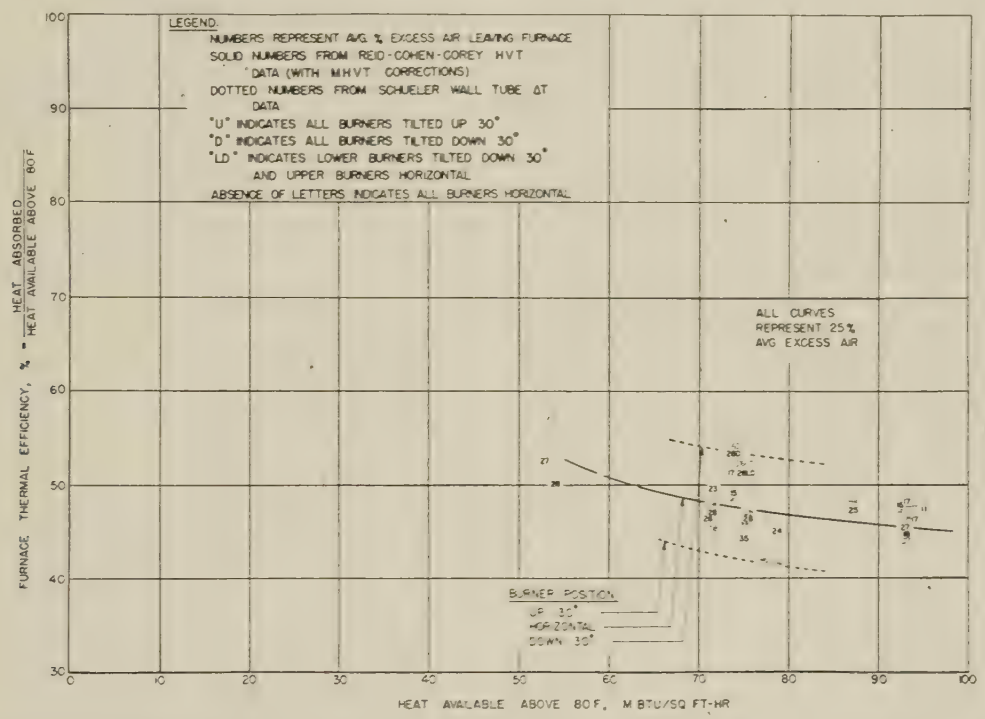

FIG. 4 FURNACE THERMAL EFFICIENCIES BASED UPON HEAT AVAILABLE ABOVE 80 F FROM WALL TUBE ΔT DATA AND FURNACE EXIT GAS TRAVERSE DATA WITH MHVT TEMPERATURE CORRECTIONS

"S-A" AND EFFECTIVENESS FACTORS

In order to evaluate the effect on furnace performance of slag and ash deposits adhering to the water-cooled surfaces, some means must be established for translating the descriptions of prevailing conditions, contained in the furnace observation reports, into numerical factors. This has been done by the use of S-A (slag and ash) factors and effectiveness factors. As used herein, these factors may be defined as follows:

(*a*) The S-A factor of a given increment of water-cooled surface, all portions of which are in approximately the same cleanliness condition, is defined as the ratio of the actual heat-absorbing capacity of the surface to the heat-absorbing capacity of the same surface when completely clean.

(*b*) The effectiveness factor of any zone in a water-cooled furnace is defined as the average, weighted according to area, of the S-A factors of all of the separately considered increments

within that zone. Following the same line of reasoning, the effectiveness factor for the total furnace would be the average, weighted according to area, of the effectiveness factors for the various zones comprising the total furnace.

The general procedure used in determining zone effectiveness factors was similar for all zones where prevailing cleanliness conditions were described in sufficient detail in the furnace observation reports. This procedure consisted of estimating the percentage of each wall (or roof or section of outlet screen) covered with slag or ash of each thickness range. Each percentage was then multiplied by the S-A factor assigned to its thickness range, and these were totalized. Actual values of S-A factors and slag or ash thickness ranges used, together with the S-A number identification, are given in Table 2. The relationship represented by the S-A factors of Table 2 is shown graphically in Fig. 5.

TABLE 2 S-A (SLAG-ASH) FACTORS

S-A number identification	Average thickness of slag or ash deposit, in.	S-A multiplying factor
S-A 0	0 to 1/8	1.0
S-A 1	1/8 to 1/4	0.7
S-A 2	1/4 to 1	0.5
S-A 3	1 and over	0.3

Selection of these particular slag-ash ranges was to a large extent arbitrary, whereas selection of the multiplying factors was guided by the test data.

The thickness ranges used were chosen as representing commercially clean surface (S-A 0), thinly covered surface (S-A 1), moderately covered surface (S-A 2), and heavily covered surface (S-A 3). Use of a greater number of thickness ranges would complicate the observer's task unduly, and probably would not increase the accuracy of the resultant effectiveness factors appreciably.

Values for the S-A multiplying factors were selected as a result of studies of the behavior both of individual wall-tube thermocouples and of averages of wall-tube thermocouples for entire walls or sections of walls. Referring to Fig. 5, the lowest expected theoretical S-A multiplying factor would approach 0.2 with very heavy ash coverage. Such coverage would probably reduce heat absorption of the covered surface even more than this; however, some compensating increase in over-all furnace absorption would be expected due to reradiation from the hot face of the slag or ash covering.

Referring to Fig. 6, "Behavior of tube wall ΔT at mid-point

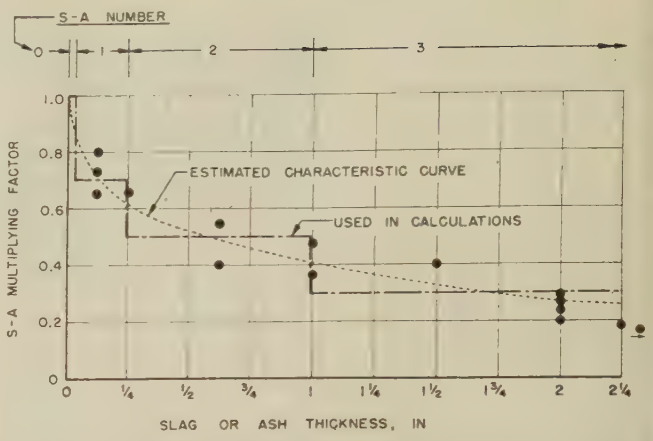

FIG. 5 S-A OR SLAG-ASH FACTORS AND IDENTIFICATION NUMBERS FOR VARIOUS SLAG OR ASH THICKNESSES

in each wall, elevation 698 ft, where ash was alternately building up and falling off, test No. 11," it can be seen that the ratios of minimum ΔT to maximum ΔT during the 7-hr period under consideration were 0.27, 0.24, 0.28, and 0.20 for the front, rear, right, and left walls, respectively. The "Estimated Characteristic Curve" in Fig. 5 was based upon these and other similar ratios from the available test data.

It is hoped that additional experimental work in the future will include data suitable for use in either verifying or modifying these S-A multiplying factor values.

In order to evaluate furnace effectiveness factors, the furnace has been divided into five "zones." The areas, in square feet of flat projected water-cooled heat-absorbing surface and in per cent of total area, are given in Table 3. These are shown diagrammatically in Fig. 7 which is a development of the furnace envelope, viewed as shown in the key plan, Fig. 1.

TABLE 3 DIVISION OF FURNACE INTO ZONES FOR S-A FACTOR EVALUATION

Zone identification	Projected area sq ft	Per cent area
Hopper zone	945	14.7
Lower burner zone	905	14.1
Upper burner zone	1300	20.2
Mud drum zone	1730	26.9
Outlet zone	1550	24.1
Total furnace	6430	100.0

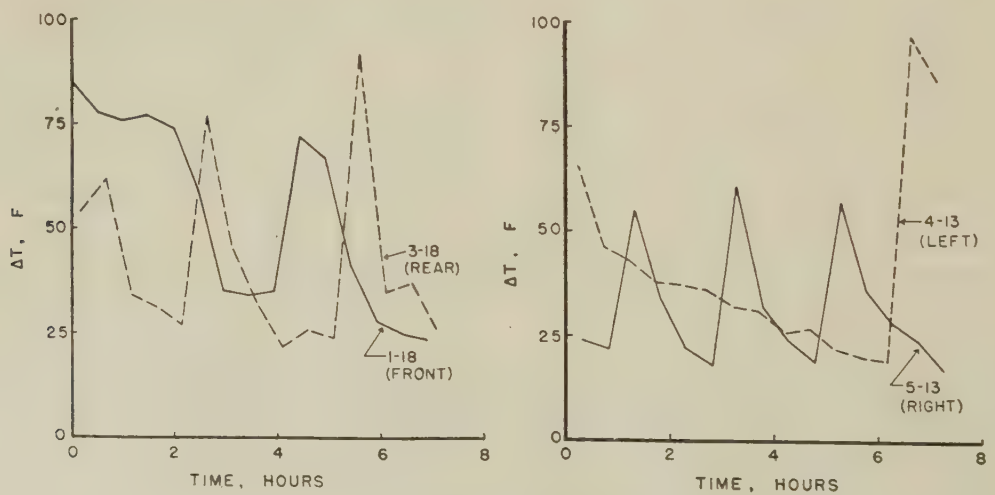

FIG. 6 BEHAVIOR OF TUBE WALL ΔT AT MID-POINT IN EACH WALL, ELEVATION 698 FT, WHERE ASH WAS ALTERNATELY BUILDING UP AND FALLING OFF, TEST NO. 11

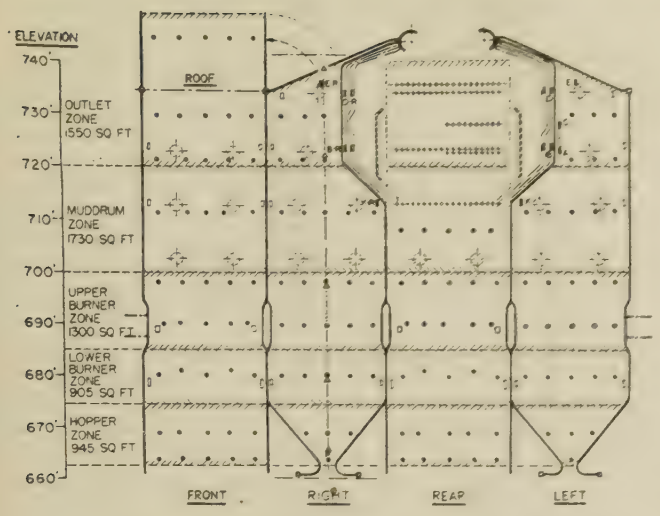

FIG. 7 DIVISION OF FURNACE INTO ZONES FOR EVALUATION OF EFFECTIVENESS FACTORS

CONDITION OF HEATING SURFACES

Facilities for observing the condition of heating surfaces and the specific procedure used in determining S-A factors are discussed in some detail as follows:

Hopper Zone. All surfaces in this zone were plainly visible from doors at elevation 679 ft. In general, the hopper slopes and adjacent side walls remained relatively clean. Only during tests Nos. 14 and 15, when burners were tilted downward, were sufficient ash deposits present to warrant mention in the furnace observation reports. Thus for all other tests, an effectiveness factor of 0.98 was assigned to all surfaces in this zone.

Lower Burner Zone. Practically all surfaces in this zone were also plainly visible from the doors at elevation 679 ft. Conditions for all four walls in this zone were described at length in all furnace observation reports for all tests; therefore the general procedure was followed in determining effectiveness factors.

Upper Burner Zone. This was the only zone in the furnace where it was impossible to see all walls clearly. Approximately 60 per cent to 80 per cent of the right and left walls were visible from the front and rear wall corner doors at elevation 689 ft during all tests except test No. 15, when the coal-air stream from the upper burners seriously obstructed vision. The front and rear walls could not be seen from this level at any time as the secondary-air ducts blocked both walls completely. The uppermost portions of all four walls could, however, be seen from a very steep angle and to a limited extent from the doors at elevation 713½ ft during many of the tests.

The assignment of reasonably accurate effectiveness factors for this zone was quite difficult for obvious reasons; however, it was decided to estimate the total effectiveness factor from the 60 to 80 per cent of the side walls visible from elevation 689 ft, and to modify this figure slightly for such observations as were available from elevation 713½ ft. The effectiveness factor for this zone for test No. 15, when visibility was almost zero, was assumed to be the same as the average for the two observations made during test No. 14.

Mud-Drum Zone. Practically all surfaces in this zone were visible from the doors at elevation 713½ ft. Conditions for the walls and lower portion of the furnace outlet screen were described in detail in the furnace observation reports for all tests except tests Nos. 14 and 15, when surfaces were simply reported to be clean. Where conditions were described completely, the general procedure was followed in determining effectiveness factors. For test No. 14, the effectiveness factor was taken as 0.98 during the first observation, and 0.96 during the second observation. During test No. 15 the effectiveness factor was assumed to be equal to the average for the two parts of test No. 14, or 0.97.

Outlet Zone. All surfaces in this zone (walls, outlet screen, and roof) were clearly visible from doors at elevations 724 ft and 734 ft. Out of the 27 observations made, complete statements concerning surface conditions in this zone were reported for 18 observations, and the general procedure was followed in determining effectiveness factors. For the remaining nine observations, when the zone was simply reported to be clean, an effectiveness factor of 0.98 was used.

The percentage of area at each S-A number for each zone is given in Table 4 for all tests. It is to be noted that several of the tests have been subdivided into two parts, and test No. 25 into five parts, in this table. This has been done so that effectiveness factors could be obtained for each separate furnace observation report, where two or more reports showed significant changes in the cleanliness condition during a given test. Effectiveness factors computed from these percentages for all five zones and for the total furnace are also given in Table 4.

Computed effectiveness factors for the individual zones varied from a maximum of 0.98 for the hopper and outlet zones during many of the tests[6] to a minimum of 0.68 for the lower burner zone during test No. 20B (second half of a low excess air run), when the walls were described as being about one quarter covered with "a sheet of semifused slag," and somewhat over one-quarter covered with "strips of sponge ash," averaging ¾ in. thick. Total furnace effectiveness factors varied from a maximum of 0.95 for tests Nos. 13, 14A, and 21A to a minimum of 0.86 for tests Nos. 18B and 25E. Thus while the range of effectiveness-factor variation for individual zones was fairly wide, the range for the total furnace was surprisingly small, covering only about 10 per cent.

CIRCUMFERENTIAL TUBE SURFACE TEMPERATURES

An extensive investigation of the possibility of confirming the empirically evaluated effectiveness factors was undertaken by applying the surface temperature distribution factors obtained from the single tube in the center of each wall equipped with circumferential thermocouples to the center-line temperatures measured for the remainder of the wall. On the hypothesis that ash deposits would build up between tubes and gradually accumulate to cover the entire circumference, the circumferential temperatures were critically examined and distribution factors developed for each elevation on each wall. These factors were simply ratios of the average ΔT around the circumference to the center line ΔT.

In general, these factors were found to be considerably lower than the effectiveness factors based on visual observations and resulted in furnace efficiencies which were inconsistent in most cases. The assumption that a single tube in the center of a wall could be taken as representative of the entire wall was evidently erroneous due to insufficient sampling. Additional tubes equipped with circumferentially disposed thermocouples might have eliminated some of the inconsistencies. However, the welded guard ring used on this type of measuring device is a potential point of lodgment for ash and might result in an indication of a lower temperature than would exist an inch or more from the measured point.

[6] The highest zone effectiveness factor value used in any case was 0.98, as a certain amount of ash in the form of a dust coating was always present except possibly in the areas affected by wall soot blowers immediately following their operation.

TABLE 4 ESTIMATED PER CENT AREA PER ZONE COVERED BY FOUR S-A CLASSIFICATIONS AND RESULTANT CALCULATED EFFECTIVENESS FACTORS

TEST NUMBER		10	11	13	14A	14B	14	15	17A	17B	17	18A	18B	18	19A	19B	19	20A	20B	20	21A	21B	21	24	25A	25B	25C	25D	25E	26
HOPPER ZONE	% AT S-A 0				85	75		87																						
	% AT S-A 1				15	15		13																						
	% AT S-A 2				0	10		0																						
	% AT S-A 3				0	0		0																						
LOWER BURNER ZONE	% AT S-A 0	52	62	87	66	53		60	84	84		82	82		63	63		77	70		71	71		81	84	83	83	80	80	80
	% AT S-A 1	26	21	11	12	16		13	6	6		4	4		16	16		12	14		14	14		5	6	7	7	7	7	8
	% AT S-A 2	12	12	0	10	10		13	4	4		5	5		16	16		9	12		14	14		4	5	4	4	3	3	2
	% AT S-A 3	10	5	2	12	21		14	6	6		9	9		5	5		2	4		1	1		10	5	6	6	10	10	10
UPPER BURNER ZONE	% AT S-A 0	86	66	80	85	60		73	86	70		70	45		70	65		63	38		73	70		62	75	68	63	50	51	46
	% AT S-A 1	7	8	9	8	20		14	7	10		10	10		15	10		7	15		12	10		8	10	7	10	15	12	10
	% AT S-A 2	0	8	0	0	10		5	7	15		15	25		15	15		15	25		10	10		12	5	10	12	15	15	22
	% AT S-A 3	7	18	11	7	10		8	0	5		5	20		0	10		15	22		5	10		18	10	15	15	20	22	22
MUDDRUM ZONE	% AT S-A 0	50	95	88					87	87		88	60		88	80		88	72		93	86		70	83	74	68	61	53	80
	% AT S-A 1	20	4	3					9	9		12	16		10	15		10	12		6	9		7	1	9	10	12	15	9
	% AT S-A 2	12	1	2					1	1		0	12		1	3		2	11		1	5		8	1	6	7	11	12	5
	% AT S-A 3	18	0	7					3	3		0	12		1	2		0	5		0	0		15	15	11	15	16	20	6
OUTLET ZONE	% AT S-A 0	89							95	88		93	93		93	93		93	93		95	95		88	96	95	95	92	90	92
	% AT S-A 1	5							5	7		4	4		5	5		6	6		4	4		6	2	3	3	5	5	4
	% AT S-A 2	3							0	5		2	2		2	2		1	1		1	1		4	0	0	0	0	2	2
	% AT S-A 3	3							0	0		1	1		0	0		0	0		0	0		2	2	2	2	3	3	2
EFFECTIVENESS FACTORS: HOPPER ZONE		.98	.98	.98	.96	.91	.93	.96	.98	.98	.98	.98	.98	.98	.98	.98	.98	.98	.98	.98	.98	.98	.98	.98	.98	.98	.98	.98	.98	.98
LOWER BURNER ZONE		.79	.84	.96	.83	.75	.79	.80	.92	.92	.92	.90	.90	.90	.84	.84	.84	.91	.87	.89	.88	.88	.88	.90	.92	.92	.92	.90	.90	.90
UPPER BURNER ZONE		.93	.81	.90	.93	.82	.88	.88	.94	.86	.90	.86	.70	.78	.88	.82	.95	.80	.68	.74	.88	.85	.87	.79	.88	.82	.81	.74	.74	.71
MUDDRUM ZONE		.75	.98	.93	.98	.96	.97	.97	.95	.95	.95	.96	.81	.88	.96	.93	.94	.96	.87	.92	.98	.95	.96	.83	.89	.87	.83	.80	.76	.91
OUTLET ZONE		.95	.98	.98	.98	.98	.98	.98	.98	.95	.96	.97	.97	.97	.97	.97	.97	.98	.98	.98	.98	.98	.98	.95	.98	.98	.98	.96	.96	.96
TOTAL (WEIGHTED AVG.)		.87	.93	.95	.95	.90	.92	.93	.95	.93	.94	.94	.86	.90	.93	.91	.92	.93	.87	.90	.95	.93	.94	.88	.93	.91	.90	.87	.86	.89
ORIGINAL DESIGNATION *		D	C	C	C	-	C	C	C	-	C	C	-	C	C	-	C	C	-	C	C	-	C	D	C	-	-	-	-	C

*C - INDICATES CLEAN D - INDICATES DIRTY

TABLE 5 FURNACE-PERFORMANCE DATA CORRECTED TO A THEORETICAL CLEAN BASIS BY USE OF EFFECTIVENESS FACTORS

TEST NUMBER		10	11	13	14	15	17	18	19A	19B	19	20A	20B	20	21A	21B	21	24	25A	25B	25C	25D	25E	26
EXCESS AIR AT FURNACE OUTLET	%	24	28	25	24	26	35	27	23	26	25	17	15	16	27	28	27	11	25	17	15	18	17	28
FURNACE EFFECTIVENESS FACTOR		0.87	0.93	0.95	0.92	0.93	0.94	0.90	0.93	0.91	0.92	0.93	0.87	0.90	0.95	0.93	0.94	0.88	0.93	0.91	0.90	0.87	0.86	0.89
CORRECTED TOTAL HEAT QUANTITIES: ABSORBED, MHVT BASIS	MKB/HR	261	231	-	267	272	227	302	245	235	-	260	267	-	187	187	-	327	286	313	314	307	324	254
ABSORBED, WALL TUBE ΔT BASIS	MKB/HR	241	224	219	273	275	235	294	-	-	238	-	-	256	-	-	209	326	288	312	313	319	334	256
CORRECTED UNIT HEAT QUANTITIES: ABSORBED, MHVT BASIS	BTU/SQ.FT-HR	40600	35900	-	41500	42300	35300	47000	38100	36600	-	40400	41500	-	29100	29100	-	50300	44500	48700	48800	47700	50400	39500
ABSORBED, WALL TUBE ΔT BASIS	BTU/SQ.FT-HR	37500	34800	34000	42400	42800	36500	45700	-	-	37000	-	-	39800	-	-	32500	50700	44800	48500	48700	49500	52000	39800
CORRECTED FURNACE THERMAL EFFICIENCY BASED UPON HEAT AVAILABLE ABOVE 80 °F: FROM CORRECTED MHVT ABSORPTION	%	51.7	50.4	-	55.6	57.5	47.1	50.6	53.4	51.4	-	55.0	55.3	-	55.3	53.9	-	53.5	51.0	52.4	52.8	51.4	53.7	52.4
FROM CORRECTED WALL TUBE ΔT ABSORPTION	%	47.7	48.9	44.2	56.9	58.1	48.7	49.2	-	-	52.0	-	-	54.1	-	-	61.0	53.3	51.3	52.2	52.6	53.3	55.4	52.8
CORRECTED FURNACE UNIT EFFICIENCY BASED UPON HEAT AVAILABLE ABOVE SAT. TEMP.: FROM CORRECTED MHVT ABSORPTION	%	59.1	58.0	-	63.9	66.0	54.7	58.0	61.2	59.1	-	62.8	64.0	-	63.9	62.1	-	60.6	58.5	59.6	59.9	58.3	61.0	60.2
FROM CORRECTED WALL TUBE ΔT ABSORPTION	%	54.7	56.3	50.6	55.2	66.7	56.6	56.5	-	-	59.7	-	-	61.5	-	-	70.4	60.4	58.9	59.4	59.7	60.6	62.9	60.6

Furnace Performance Corrected to Clean Basis

The individual test points in Figs. 3 and 4 were not in sufficiently close agreement with their average curves to represent the degree of correlation which might have been expected from various tests of the same furnace fired with coals of similar analyses. In order to obtain a better correlation, and also to establish a sounder basis for comparison with other similar furnaces fired with the same or different coals, the heat-absorption rates have been corrected to a theoretical clean furnace condition through the use of effectiveness factors as evaluated from the furnace observation reports. Furnace performance data, corrected to this theoretical clean basis, are given in Table 5. The corrections have been made by dividing the various absorption values by their corresponding total furnace effectiveness factors.

Fig. 8 shows corrected heat-absorption rates plotted against heat available above 80 F. A comparison of this plot with the corresponding uncorrected plot in Fig. 3 will reveal that the average curves have been raised about 10 per cent and that the individual points are in much better agreement with their average curves.

Upon several occasions it has been suggested that furnace efficiencies should be based on the heat available above saturation temperature rather than above 80 F. In a complete steam-generating unit, certain component parts, such as an economizer and an air preheater, are capable of absorbing heat at a thermal level below boiler saturation temperature; therefore a thermal level corresponding to an established standard entering-air temperature of 80 F has been accepted as a basis for calculating overall efficiency. When consideration is limited to a furnace composed of steam-generating tubes only, the capability for absorbing heat at a thermal level below saturation temperature does not exist. Thus it would seem that a logical argument could be advanced to support the use of the saturation temperature.

Since it is beyond the scope of this paper to attempt to judge which basis is actually the more valuable for comparing furnace performance, corrected efficiencies have been calculated on both bases and are included in Table 5.

Fig. 9 shows corrected furnace thermal efficiencies based upon heat available above 80 F. A comparison of this plot with the corresponding uncorrected plot in Fig. 4 will reveal that here again, as in the case of heat-absorption rates, the corrected values are correspondingly higher than the uncorrected values, and the individual points are in good agreement with their average curves.

Fig. 10 shows corrected furnace unit efficiencies based upon the heat available above saturation temperature (585 F). Efficiencies on this basis are of course higher than upon the more common heat available above 80 F basis. Individual points are in excellent agreement with the average curves in the graph; furthermore, the curves appear to be increasing toward 100 per cent efficiency at zero heat available, which is probably the logical trend for them to take, considering the thermal level upon which they are based.

Conclusions

The following conclusions drawn from this comparison and correlation apply only to Tidd boiler No. 11, and to the type of coal used during the investigation.

Either of two general types of test technique have been found suitable for measuring furnace performance, i.e., determination of local rates of heat absorption of the walls by a relatively large number of uniformly distributed tube-face thermocouples; and determination of the sensible heat in the gases leaving the furnace by high-velocity thermocouple and orsat traverses.

An acceptable correlation of heat-absorption values can be obtained from these two methods by using a heat-transfer rate corresponding to a metal conductivity of 29 Btu/sq ft-hr-F/ft, and a steam-water film conductance of 5000 Btu/sq ft-hr-F for the former, and specific heats according to Heck (9), and thermocouple radiation corrections according to Mullikin (8) for the latter.

Only one tube was used for studies of variation in density and comparison with heat absorption as computed from tube-surface temperature measurements. Obviously the evaporation in this one tube could not be applied to the furnace because it could not be classed as a representative sample. However the final quality of the mixture leaving the tube, as computed from the surface temperature measurements, and the velocity of the water near the entrance to the tube did not agree too closely with the final qual-

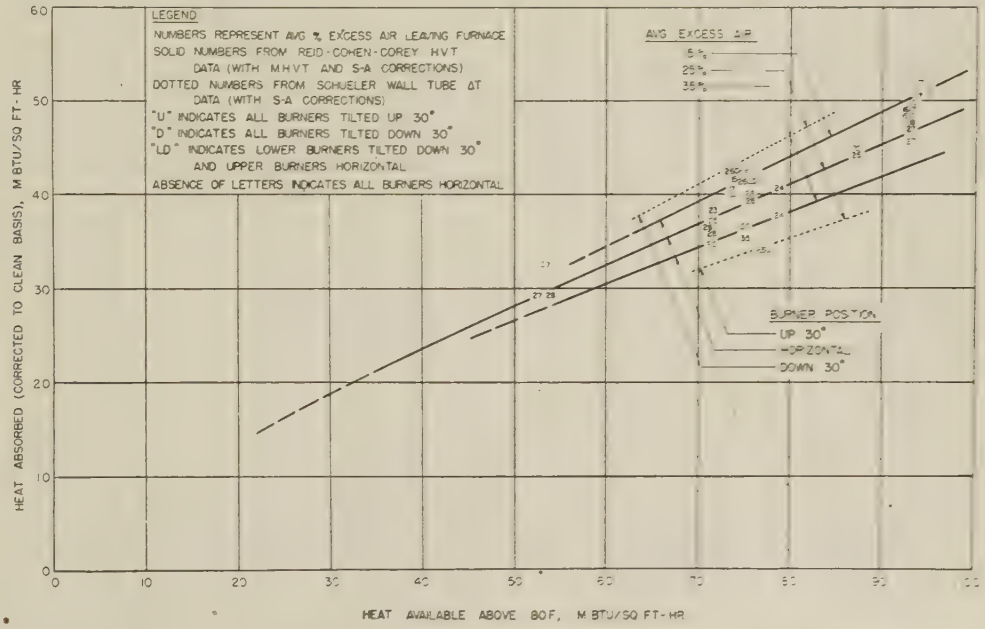

Fig. 8 Heat-Absorption Rates Corrected to Clean Furnace Condition Through Use of Effectiveness Factors

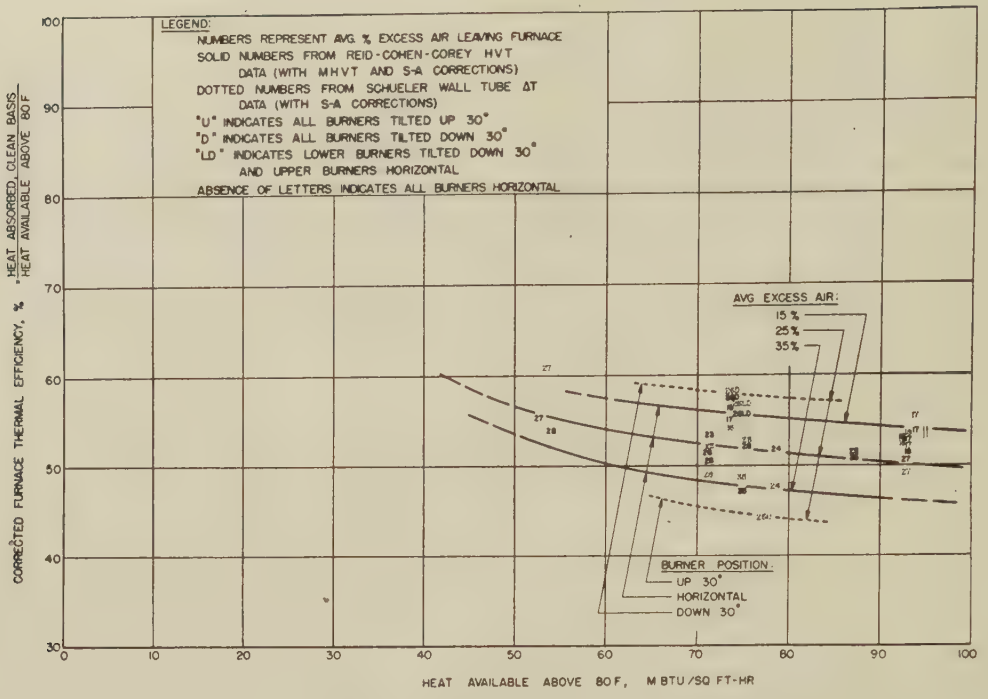

FIG. 9 FURNACE THERMAL EFFICIENCIES BASED UPON HEAT AVAILABLE ABOVE 80 F AND CORRECTED TO CLEAN FURNACE CONDITION THROUGH USE OF EFFECTIVENESS FACTORS

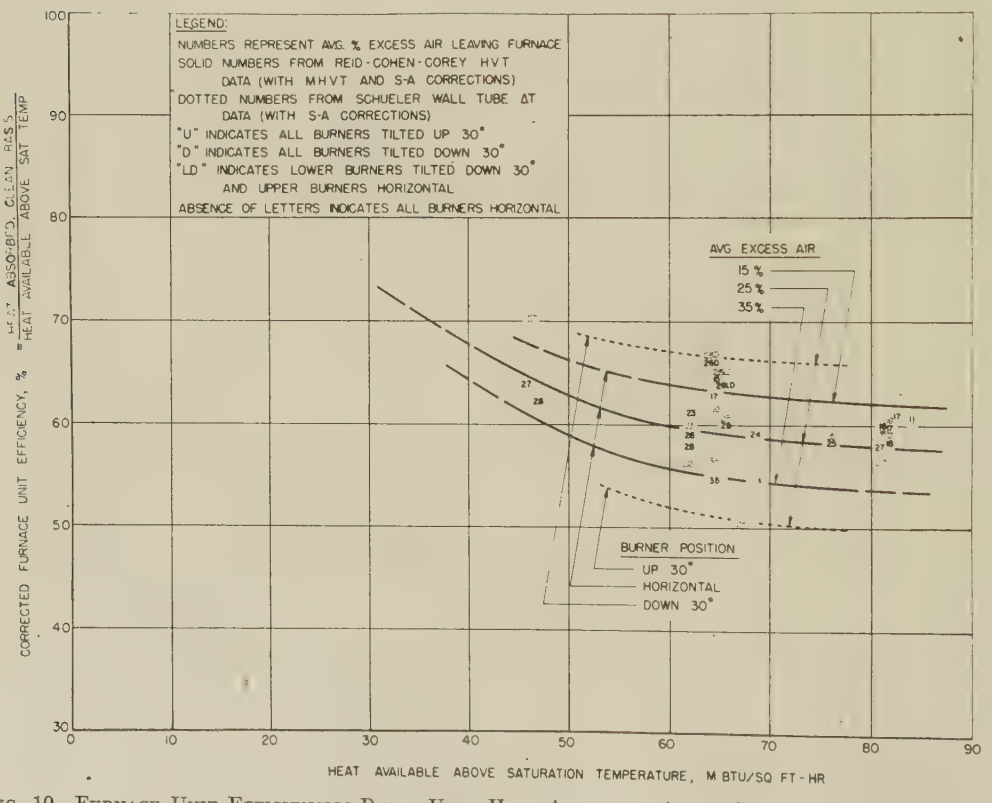

FIG. 10 FURNACE UNIT EFFICIENCIES BASED UPON HEAT AVAILABLE ABOVE SATURATION TEMPERATURE AND CORRECTED TO CLEAN FURNACE CONDITION THROUGH USE OF EFFECTIVENESS FACTORS

ity as determined by density measurements. These values are given in tabular form in Part III of the symposium. Intermediate values of quality determined by each method did not agree very well and the conclusion was reached that the density method is too strongly influenced by other factors, such as possibility of excessive slip on the hot side of the tube, to be an accurate measurement.

The average furnace heat-absorption rate increases, but the furnace efficiency decreases, as the heat available increases, as shown in Figs. 3 and 4. The efficiency curves appear to be approaching a constant gradually at the higher heat available values.

The average furnace heat-absorption rate increases approximately 0.7 per cent for each 1 per cent decrease in excess air leaving the furnace over the range of 15 to 35 per cent.

The average furnace heat-absorption rate decreases 11 per cent when all burners are tilted up 30 deg and increases approximately 13 per cent when all burners are tilted down 30 deg on the as-measured basis, Fig. 3. When corrected to a clean furnace basis, the decrease due to tilting all burners up 30 deg becomes approximately 16 per cent, while the increase due to tilting all burners down 30 deg remains about 13 per cent, Fig. 8. The relatively large effect of furnace cleanliness upon heat absorption with the burners up can be attributed to the decrease in ash deposition on the walls in the lower portion of the furnace which are not subjected to impingement of the hot ash particles carried by the flame.

The effect of relative cleanliness upon furnace performance represents the most difficult of the variables to evaluate; however, by making thorough observations of all visible furnace heat-absorbing surfaces and interpreting such observations carefully by means of the S-A factor procedure outlined herein, furnace "effectiveness factors" may be computed. By using these effectiveness factors to correct measured heat-absorption rates, performance of the furnace under a theoretical "clean" condition can be approximated. This should permit future comparison of the performance of differently shaped furnaces fired with various fuels, regardless of the relative cleanliness of the furnace heat-absorbing surfaces due to age, cleaning facilities and schedules, load-variation cycles, fuel analyses, etc. In this investigation, use of total furnace effectiveness factors varying from 0.86 to 0.95 have made possible a much better correlation of data from the various tests than was possible without their use.

A Suggestion for Future Similar Investigations

An improvement over the method used during the Tidd investigation for reporting relative furnace cleanliness conditions is available, and is recommended for any future similar work in which the evaluation of effectiveness factors is deemed advisable. This would involve use of a pad of small diagrams of a development of the furnace envelope, to scale (similar to those used for Fig. 1 and 2), on which estimated percentages of deposit corresponding to each S-A number could be written for various incremental areas. The areas to be used could be sketched in during each inspection to suit prevailing conditions. These could be interpreted quite easily, even after long periods of time, and would constitute a much more precisely defined basis for computation of effectiveness factors than would written descriptions of the type used in the Tidd investigation.

BIBLIOGRAPHY

1 Symposium Part I, this issue of Transactions, pp. 553–568.
2 Symposium Part II, this issue of Transactions, pp. 569–586.
3 Symposium Part III, this issue of Transactions, pp. 587–600.
4 "Heat Transfer by Radiation," by W. J. Wohlenberg, Purdue University Engineering, Experiment Station, Bulletin No. 75, vol. 24, August, 1940.
5 "Studies of Heat Transmission Through Boiler Tubing at Pressures from 500 to 3300 Pounds," by W. F. Davidson, P. H. Hardie, C. G. R. Humphreys, A. A. Markson, A. R. Mumford, and T. Ravese, Trans. ASME, vol. 65, 1943, pp. 553–579.
6 "An Experimental Investigation of Heat Absorption in Boiler Furnaces," by W. J. Wohlenberg, H. F. Mullikin, W. H. Armacost, and C. W. Gordon, Trans. ASME, vol. 57, 1935, pp. 541–554.
7 "Distribution of Heat Absorption and Factors Affecting Performance of Twin Branch 2500-Psi Boiler," by F. G. Ely and L. B. Schueler, Trans. ASME, vol. 66, 1944, "Furnace Performance Factors" section, pp. 23–30.
8 "Gas-Temperature Measurement and the High-Velocity Thermocouple," by H. F. Mullikin, Reinhold Publishing Corporation, New York, N. Y., 1941, "Temperature—Its Measurement and Control in Science and Industry" section, pp. 775–804.
9 "The New Specific Heats," by R. C. H. Heck, *Mechanical Engineering*, vol. 62, 1940, pp. 9–12.

Appendix

The number and times of all complete furnace observations made, together with start and finish times for the test and wall soot blower operation (if any) are given in Table 6.

Furnace observations were made, in all cases, by one of the authors, usually accompanied by one or two of several other participating engineers who corroborated the opinions formulated before they were written down in their original rough form.

In Part I a few phrases were quoted from the furnace-observation reports for test No. 19, and the descriptions contained therein were compared with furnace wall photographs and the corresponding over-all average isothermal diagram. In order to exhibit more clearly how S-A factors were selected and averaged to obtain zone effectiveness factors, the two furnace observation reports for test No. 18 will be quoted in their entirety herein, and original calculations reproduced, as follows.

TABLE 6 LOG OF COMPLETE FURNACE-OBSERVATION REPORTS

Test No.	Soot-blower oper. time, finish	Time of tests—Start	Time of tests—Finish	Number of furnace observations	Time of observations—Start	Time of observations—Finish
10	....	12:20 pm	10:00 pm	2	1:00 pm	1:45 pm
					9:00 pm	9:30 pm
11	8:00 am	9:20 am	4:20 pm	2	9:00 am	9:30 am
					4:15 pm	4:45 pm
13	8:00 am	12:40 pm	4:40 pm	2	10:15 am	10:45 am
					4:15 pm	4:45 pm
14	8:00 am	10:00 am	5:30 pm	2	10:30 am	11:00 am
					4:30 pm	5:00 pm
15	8:00 am	9:40 am	3:20 pm	2	10:20 am	11:00 am
					3:15 pm	3:45 pm
17	8:05 am	8:30 am	4:30 pm	2	9:30 am	10:30 am
					3:00 pm	4:00 pm
18	7:45 am	8:00 am	4:00 pm	2	8:30 am	9:45 am
					2:30 pm	3:45 pm
19	7:30 am	8:00 am	4:00 pm	2	8:45 am	9:45 am
					2:40 pm	3:30 pm
20	7:30 am	8:00 am	4:00 pm	2	8:15 am	9:30 am
					2:30 pm	3:20 pm
21	7:05 am	7:30 am	3:30 pm	2	8:45 am	9:45 am
					2:15 pm	3:00 pm
24	....	1:10 pm	4:10 pm	1	2:20 pm	3:00 pm
25A	11:00 am	11:50 am	3:20 pm	1	12:45 pm	2:00 pm
25B	(*a*)	9:05 am	11:25 pm	1	9:00 am	10:00 am
25C	(*a*)	1:15 pm	3:45 pm	1	3:30 pm	5:00 pm
25D	(*b*)	9:00 am	12:00 n	1	9:00 am	10:00 am
25E	(*b*)	2:00 pm	5:00 pm	1	4:15 pm	5:15 pm
26	7:30 am	8:00 am	1:00 pm	1	8:20 am	9:00 am

(*a*) Tests Nos. 25B and 25C were conducted the day following test No. 25A.
(*b*) Tests Nos. 25D and 25E were conducted the second day following test No. 25A.

FURNACE OBSERVATION REPORT—TEST NO. 18

8:00 am to 4:00 pm (EST) June 5, 1946

Furnace-wall soot blowers were operated from 6:45 a.m. to 7:45 a.m.

Location	First observation 8:30–9:45 a.m.	Second observation 2:30–3:45 p.m.
Elevation 679 ft:		
Front wall	The center half of the front wall was approximately 50 per cent covered with sponge ash from about 2 ft above the operating floor up to the lower burner level. The ash was a maximum of 1 in. thick near the bottom to 3 or 4 in. thick just below the lower burner level.	The condition of this wall was unchanged, except for a possible increase in the thickness of sponge ash near the burners.
Right wall	The front half of the right side wall was approximately 50 per cent covered with sponge ash and semifused slag starting 4 ft above the operating floor and increasing up to burner level. This deposit was approximately 1/4 in. minimum thickness to 2 in. maximum thickness near the burners. Small vertical strips of this deposit were noted to be peeling off occasionally.	This wall appeared to be slightly dirtier than during the previous inspection.
Rear wall	The right half of the rear wall was approximately 25 per cent covered with 1/4-in-thick sponge ash from 3 ft above the operating floor.	There was no apparent change in the condition of this wall.
Left wall	The rear half of the left side wall was approximately 25 per cent covered with dry ash up to 1/2 in. thick starting about 3 ft above the operating floor.	There was no apparent change in the condition of this wall.
Burners	Flame from the right rear burners was impinging or sweeping along the right half of the rear wall.	Similar flame impingement, but of a less steady nature, was noted. There was no indication of unusual heavy ash or slag deposits resulting from this impingement.
Elevation 689 ft. (*Burner Level*):		
Right wall	The rear two thirds of the right side wall was approximately 50 per cent covered with a thin semifused slag and sponge ash; thickness appearing to be 1/2 to 3/4 in. This deposit was almost a continuous sheet just to the rear of center.	The rear two thirds of the right side wall was approximately 80 per cent covered with a thick hard semifused slag; thickness being approximately 1/2 to 2 in. This deposit was the heaviest and most continuous at the elevation between the two burners. At the center a 1-ft-wide strip was bare, apparently having fallen off just prior to this inspection.
Left wall	The front half of the left side wall was approximately 50 per cent covered with sponge ash of 1/2 in. average thickness.	The front three fifths of the left side wall was approximately 90 per cent covered with sponge ash. One spot, from one third to one half of the distance back contained slag extending out 6 to 10 in. thick. At the upper burner level deposit was heavier extending back approximately three fourths of the way and ranging in thickness from 1/2 to 3 in.
Front and rear walls were not visible at this elevation.		
Elevation 713 1/2 ft. (*Mud-Drum Level*):		
Front wall	Light spotty ash deposits were scattered over the sides of the tubes into which the firing circle was directed.	There was no apparent change in the condition of this wall at mud-drum level; however, down about 8 ft there appeared to be considerably more ash, and as near as could be seen there was semifused slag just above the burners.

Right wall	The condition of the right wall was the same as that of the front wall, except that possibly light spotty deposits were slightly larger individually.	The right side wall was considerably dirtier than at the first inspection, being approximately 75 per cent covered with nodules of sponge ash at this level and increasing almost to a solid cover from 1 to 3 in. thick down 8 or 10 ft below the mud drum.
Rear wall	Small spotty deposits of sponge ash were scattered over most of the rear wall and were relatively numerous.	There was no apparent change in the condition of this wall just below mud-drum level; however, 8 to 10 ft down the deposit appeared to be considerably heavier.
Left wall	The left wall appeared to be clean. It is quite probable that the same type of deposit, as noted on the front walls, was on the sides of the tubes not visible from the door (front) from which this wall was viewed.	The rear half of this wall was covered with plainly visible thin dry nodules of sponge ash. Approximately 8 ft below this level the wall appeared to be covered with 1 to 4 in. of semifused slag.
Boiler screen	Semifused slag was just beginning to form on the bottom half of the slag screen tubes.	The bottom of the slag-screen tubes was covered with semifused and running slag; thickness being approximately 1 in. on the left-hand side and 3 in. on the right-hand side.
Elevation 724 ft:		
Front wall	There were light spotty ash deposits visible from the left wall door; however, these deposits were not visible from the right wall door.	There was no apparent change in the condition of this wall.
Right wall	There were light spotty ash deposits on part of the right wall at this elevation.	There was no apparent change in the condition of this wall.
Left wall	The left wall appeared to be clean.	The left wall appeared to be clean.
Boiler screen	On the left-hand side the front one third of the tubes had 1/8 to 1/4 in. of dust. On the right-hand side the front half of the tubes had up to 1 in. of semifused slag which was spotty and uneven.	The only change in the condition of the slag screen was an increase in thickness of the semifused slag on the right side from 1 to 2 in. and more nearly uniform than before.

Elevation 734 ft:

All walls and the roof were clean at this elevation, except for what appeared to be a normal thin coating of dust.

There appeared to be more flame (or incandescent gas) at the top of the furnace than noted previously, except when burners were tilted upward 30 deg.

Evaluation of Surface Increments in Terms of S-A Numbers and Calculation of Effectiveness Factors

Hopper Zone (14.7 per cent of total area): A zone-effectiveness factor of 0.98 was assigned, as no deposits were noted during either of the two furnace observations; this in accordance with adopted procedure described in the preceding text.

Lower Burner Zone (14.1 per cent of total area): First and second observations were combined for evaluation in this zone as follows:

Front..... 5 per cent at S-A 2
20 per cent at S-A 3
Right..... 5 per cent at S-A 1
5 per cent at S-A 2
15 per cent at S-A 3
Rear.....10 per cent at S-A 1
Left.....10 per cent at S-A 2

Σ at S-A 1 = 15 ÷ 4 = 3.75 per cent → 4 per cent
Σ at S-A 2 = 20 ÷ 4 = 5.0 per cent → 5 per cent
Σ at S-A 3 = 35 ÷ 4 = 8.75 per cent → 9 per cent
by difference, S-A 0 = 82 per cent
100 per cent

Zone effectiveness factor = (82 + 4 × 0.7 + 5 × 0.5 + 9 × 0.3) ÷ 100 = 0.90

Upper Burner Zone (20.2 per cent of total area): As explained in the text, the front and rear walls were not visible in the upper burner zone; therefore it has been necessary to assume that their over-all condition was equivalent to the average of the right and left walls.

First observation (18A):

Right.....10 per cent at S-A 1
15 per cent at S-A 2
10 per cent at S-A 3
Left.....10 per cent at S-A 1
15 per cent at S-A 2

Σ at S-A 1 = 20 ÷ 2 = 10 per cent
Σ at S-A 2 = 30 ÷ 2 = 15 per cent
Σ at S-A 3 = 10 ÷ 2 = 5 per cent
by difference, S-A 0 = 70 per cent
100 per cent

Zone effectiveness factor = (70 + 10 × 0.7 + 15 × 0.5 + 5 × 0.3) ÷ 100 = 0.86

Second observation (18B):

Right.....10 per cent at S-A 1
25 per cent at S-A 2
20 per cent at S-A 3
Left.....10 per cent at S-A 1
25 per cent at S-A 2
20 per cent at S-A 3

Σ at S-A 1 = 20 ÷ 2 = 10 per cent
Σ at S-A 2 = 50 ÷ 2 = 25 per cent
Σ at S-A 3 = 40 ÷ 2 = 20 per cent
by difference, S-A 0 = 45 per cent
100 per cent

Zone effectiveness factor = (45 + 10 × 0.7 + 25 × 0.5 + 20 × 0.3) ÷ 100 = 0.705

Mud-Drum Zone (26.9 per cent of total area):

First observation (18A):

Front.....10 per cent at S-A 1
Right.....15 per cent at S-A 1
Rear and Screen.....15 per cent at S-A 1
Left.....10 per cent at S-A 1

Σ at S-A 1 = 50 ÷ 4 = 12.5 per cent → 12 per cent
by difference, S-A 0 = 87.5 per cent → 88 per cent
100 per cent

Zone effectiveness factor = (88 + 12 × 0.7) ÷ 100 = 0.964

Second observation (18B):

Front.....15 per cent at S-A 1
10 per cent at S-A 2
Right.....20 per cent at S-A 1
15 per cent at S-A 2
15 per cent at S-A 3
Rear and screen.....15 per cent at S-A 1
15 per cent at S-A 2
15 per cent at S-A 3
Left.....15 per cent at S-A 1
10 per cent at S-A 2
10 per cent at S-A 3

Σ at S-A 1 = 65 ÷ 4 = 16.25 per cent → 16 per cent
Σ at S-A 2 = 50 ÷ 4 = 12.5 per cent → 12 per cent
Σ at S-A 3 = 50 ÷ 4 = 12.5 per cent → 12 per cent
by difference, S-A 0 = 60 per cent
100 per cent

Zone effectiveness factor = (60 + 16 × 0.7 + 12 × 0.5 + 12 × 0.3) ÷ 100 = 0.808

Outlet Zone (24.1 per cent of total area): First and second observations were combined for evaluation in this zone as follows:

Front..... 5 per cent at S-A 1
Right..... 5 per cent at S-A 1
Left..... 0 per cent
Screen.....10 per cent at S-A 1
10 per cent at S-A 2
5 per cent at S-A 3
Roof..... 0

Σ at S-A 1 = 20 ÷ 5 = 4 per cent
Σ at S-A 2 = 10 ÷ 5 = 2 per cent
Σ at S-A 3 = 5 ÷ 5 = 1 per cent
by difference, S-A 0 = 93 per cent
100 per cent

Zone effectiveness factor = (93 + 4 × 0.7 + 2 × 0.5 + 1 × 0.3) ÷ 100 = 0.971

TABLE 7 COMPUTATION OF TOTAL FURNACE EFFECTIVENESS FACTORS

Zone	Area, per cent	Effectiveness factor — Test No. 18A	Effectiveness factor — Test No. 18B	Effectiveness factor — Test No. 18 (avg)	Effectiveness factor × per cent area — Test No. 18A	Effectiveness factor × per cent area — Test No. 18B	Effectiveness factor × per cent area — Test No. 18 (avg)
Hopper	14.7	0.98	0.98	0.98	14.4	14.4	14.4
Lower burner	14.1	0.90	0.90	0.90	12.7	12.7	12.7
Upper burner	20.2	0.86	0.70	0.78	17.4	14.1	15.8
Mud drum	26.9	0.96	0.81	0.88	25.8	21.8	23.7
Outlet	24.1	0.97	0.97	0.97	23.4	23.4	23.4
	100.0				93.7	86.4	90.0
Total furnace		0.94	0.86	0.90			

An Investigation of the Variation in Heat Absorption in a Pulverized-Coal-Fired Water-Cooled Steam-Boiler Furnace

Discussion[1]

W. F. Davidson.[2] In Part I, Figs. 5 to 16 show, on a developed diagram of the furnace walls, the averages of the measured values of ΔT. "Isotherms" are then drawn, and these form the basis for some of the discussion. It is disturbing to observe, on studying these figures, that the pattern of the isothermals is so often discontinuous across the "hinge lines" between the walls. For instance, in Fig. 5, at the lower part of the furnace the "40" isotherm for the left wall seems to have no continuation on the rear wall, but rather to join, approximately, with both a 60 and a 70 isotherm. A 100 isotherm, shown as an open line on the rear wall, seems to come next to a 40 isotherm on the left wall.

This is not to argue that conditions on the adjacent wall surfaces may be quite different, but only to say that the changes will not be discontinuities.

On the basis of the data, to explore the possibilities of developing a set of isotherms which would not show these discontinuities, Figs. 5, 10, and 15 of the paper have been selected and redrawn. The results are shown as Figs. 1, 2, and 3 of this discussion. A comparison with the original figures will show that in most areas the changes have not been great, but that in other areas, especially near the corners of the furnace, they have been significant.

[1] The discussion of papers in this Symposium has been combined into a composite of all four papers. Where reference is to individual papers, the "Part" number in question will be designated, rather than the title and authors. Footnotes and illustrations will be numbered consecutively throughout the discussion.

[2] Research Engineer, Consolidated Edison Company of New York, New York, N. Y. Fellow ASME.

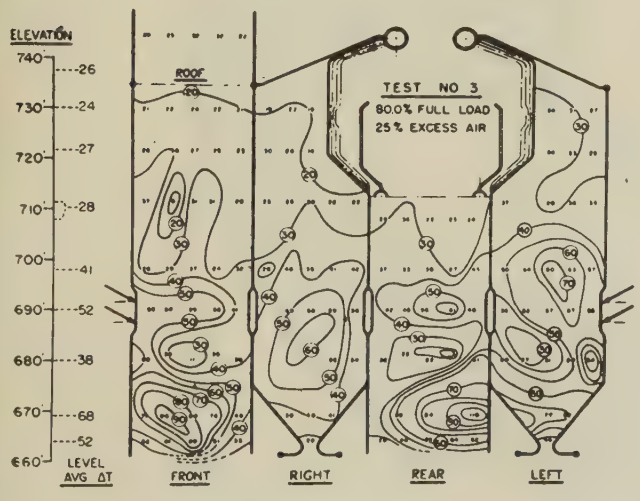

Fig. 1 Revised Isothermal ΔT Diagram Test No. 3
(Revision of Fig. 5, Part I.)

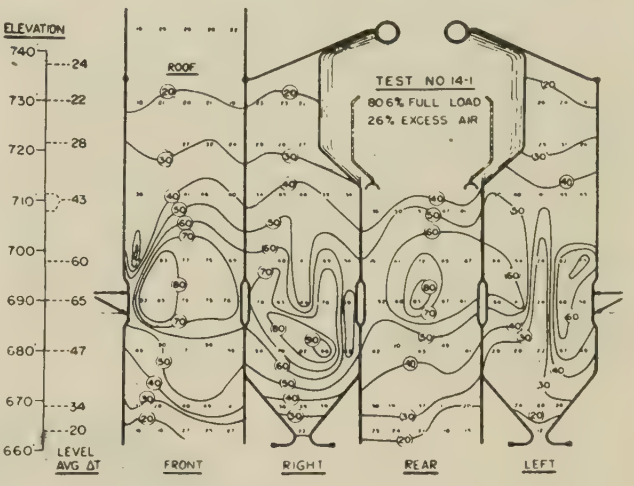

Fig. 2 Revised Isothermal ΔT Diagram at End of Test No. 14
(Revision of Fig. 10, Part I.)

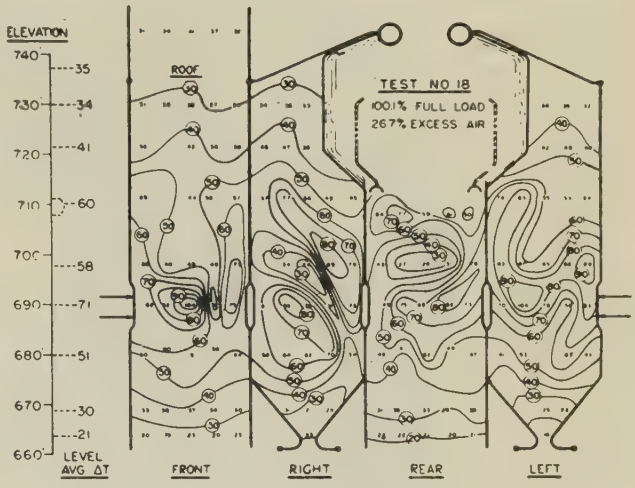

Fig. 3 Revised Isothermal ΔT Diagram, Test No. 18
(Revision of Fig. 15, Part I.)

As an incidental result, it is evident that one set of data may yield quite different "pictures" depending on the "artistic temperament" of the draftsman.

F. G. Ely.[3] In considering furnace heat absorption it is well to bear in mind that this is not measured directly, but is

[3] Research Engineer, Research and Development Division, The Babcock & Wilcox Company, Alliance, Ohio. Mem. ASME.

calculated as a difference between two quantities which are measured by very different basic means. Therefore it is important that all factors involved in the calculation be used as nearly as possible in terms of absolute values, and of these the measurement of furnace gas temperature is probably the most difficult.

This discussion is essentially a report of supplementary work carried out recently at Tidd Station, under the auspices of the Committee, for the purpose of checking the accuracy of gas-temperature measurement when using a single-shield high-velocity thermocouple, and for a preliminary verification of the need for applying correction to the reported gas temperatures, as discussed in Part IV of the symposium.

It is commonly accepted that the temperature indicated by a thermocouple in a furnace would be influenced by the rate of gas flow over the hot junction, which tends to heat the thermocouple up to true gas temperature, and by radiant transfer to or from the couple depending on its exposure and the nature of surrounding surfaces. In water-cooled furnaces, remote from zones of active combustion, a bare exposed thermocouple invariably will read below true gas temperature. By placing a refractory shield around the thermocouple junction much of the radiant effect is overcome. The use of multiple shielding, with all portions heated by the gas stream, further reduces the influence of surrounding surfaces. Rate of gas-mass flow over the thermocouple junction is a direct and important factor in developing equilibrium at or near the true temperature of the gas.

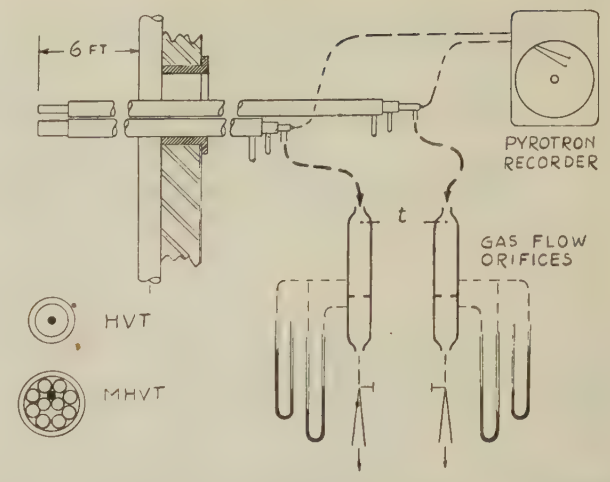

Fig. 4 Schematic Arrangement of Equipment and Method Used for Comparing HVT and MHVT Measurement of Furnace Gas Temperature at Tidd Plant

Equipment used for checking these conditions at Tidd Station is indicated in Fig. 4 of this discussion, which shows the high-velocity thermocouple (HVT) used on the original tests, assembled with a multiple-shield thermocouple (MHVT) in close proximity, and the two inserted to a distance of 6 ft into the

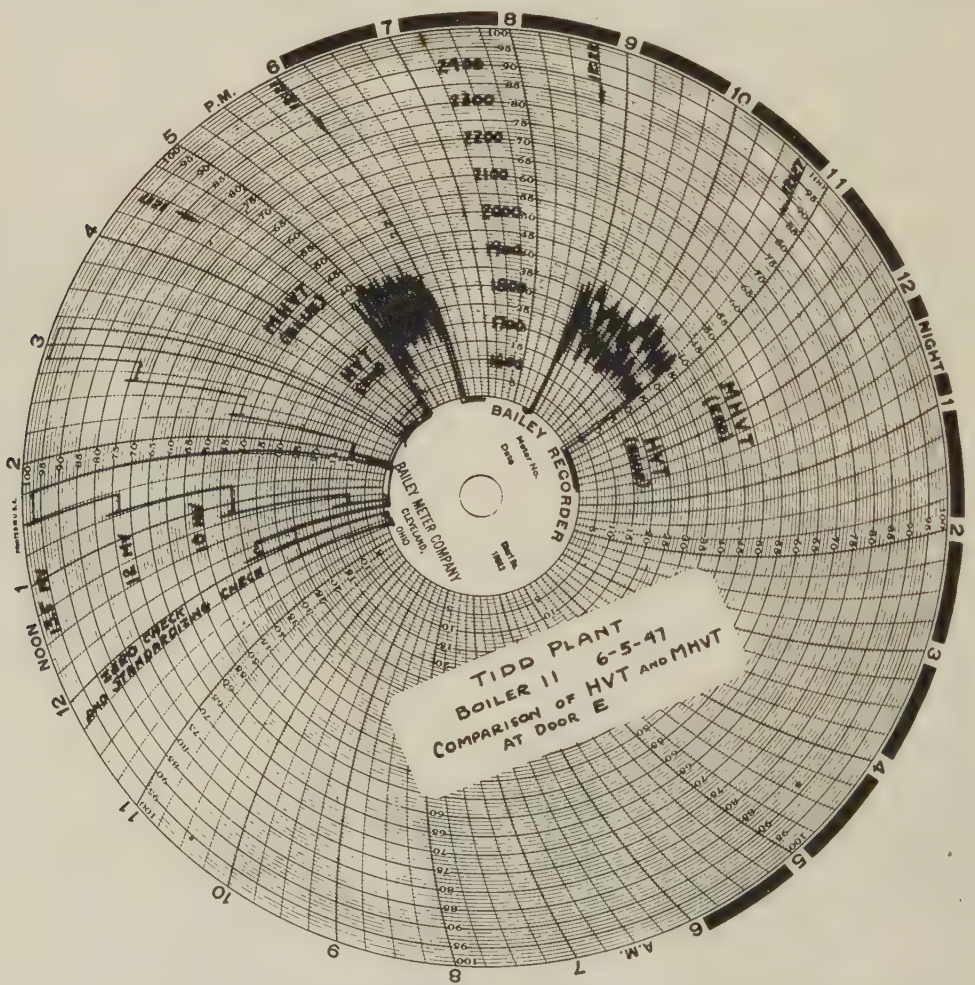

Fig. 5 Typical Chart Showing Simultaneous Records of Furnace Gas Temperature as Measured by HVT and MHVT Equipment Shown in Fig. 1

furnace cavity at door location E. Provision was made for measuring the rate of gas flow aspirated over each thermocouple, and the lead wires were connected to a two-pen Bailey electronic temperature recorder, with high-speed clock, for simultaneous measurement of comparative temperature records. Multiple shielding of the MHVT junction was composed of ten small porcelain tubes packed into the enclosing shield tube in such a manner that gas could be drawn through all spaces of the assembly, and the thermocouple junction itself was shielded by at least two porcelain surfaces from surrounding walls of the furnace. (In the dust-laden gases it was found that the small spaces rapidly became choked by fly ash, but reasonable records were obtained for periods of several minutes immediately after the gas flow was started.)

A characteristic chart record is illustrated in Fig. 5 of this discussion. To the best of the writer's knowledge, this is the first time that a continuous record has been obtained from an HVT measuring furnace gas temperatures. The timing of the clock is such that 2 hr on the printed chart corresponds to 5 min of operating time. Both pens were given a preliminary check against four set values of millivoltage impressed by a portable potentiometer, and were then connected to the two thermocouples to produce the record shown between 12:17 and 12:21 p.m. Lead wires were then interchanged and the records were continued from 12:22 to 12:27 pm. It is of general interest to note the rather rapid fluctuation in gas temperature, with amplitude of 50 to 100 deg F shown by both thermocouples, but of immediate interest to note that the record of the single-shielded HVT was approximately 100 deg F below the record of the multiple-shielded MHVT. During this run the mass flow of gases over the HVT was maintained at a value corresponding to that used in the original furnace tests, while the mass flow over the MHVT junction was held at a high value in order to be well above any critical point of its characteristics.

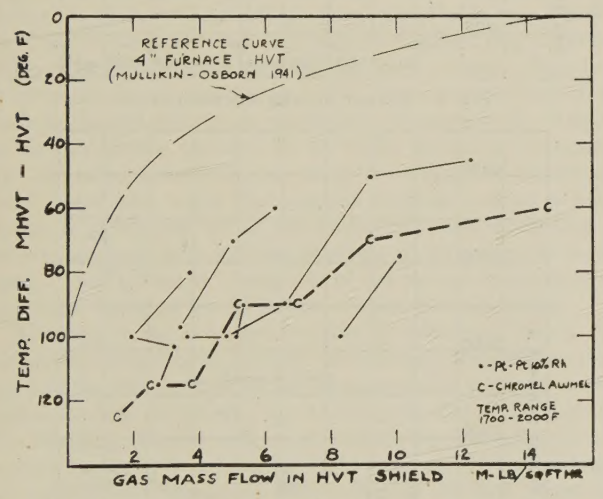

Fig. 6 Effect of Gas Mass Flow on Measurement of Temperature by Single-Shield HVT

Fig. 6 herewith shows a correlation of data from a number of comparative tests run in this manner, but in which the mass flow over the HVT junction was varied and that of MHVT held at the same high value. The solid curves are for a platinum thermocouple and the dash curve for a chromel-alumel thermocouple, both being compared to a platinum thermocouple in the MHVT. It will be noted that a distinct trend to higher readings was indicated as mass flow was increased from lower values, which fairly approximates the slope of the reference curve reported by Mullikin, in reference (5) of the author's Bibliography. (Part IV).

Dealing now with the gas-temperature values reported for the Tidd furnace tests, in which mass flow over the HVT was restricted to about 4000 psf per hr by limited capacity of the aspirator used, it appears that an error of approximately 40 deg F can be ascribed to low aspiration rate, and that an additional 60 deg F is accounted for by difference in shielding effect between the HVT and MHVT equipment. Corrections to the reported data of about this magnitude were found necessary for reasonable correlation with the furnace-tube temperature survey as reported in Part IV.

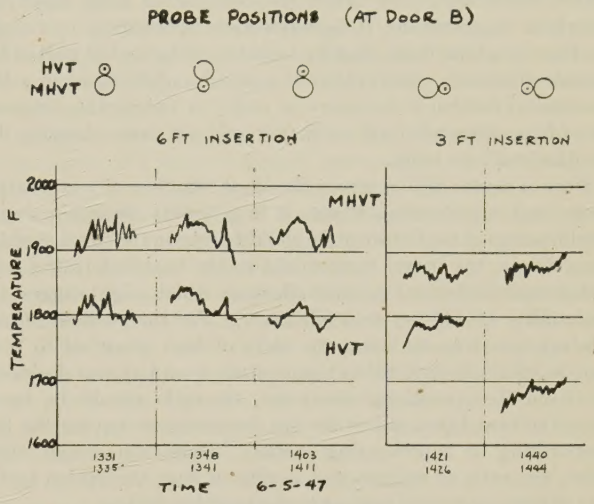

Fig. 7 Comparison of HVT and MHVT Records Under Various Conditions of Exposure and Location in Furnace

An interesting disclosure of the effect of thermocouple exposure is indicated in Fig. 7 of this discussion, where comparisons of HVT and MHVT are shown for different probe positions at door location B. Here the major portion of boiler screen and superheater was located to the left of the thermocouples, and the upper furnace cavity was located to the right. The records show general similarity in following major changes of gas temperature but indicate that the single-shield couple was most severely influenced by its surroundings.

Further explorations of this nature are needed, at different locations in the furnace and at different zones of temperature, to establish a complete basis of correction for the reported tests. It is strongly recommended that in future work of the Committee the problem and techniques of measuring true gas temperature be thoroughly investigated and developed for practical use.

A. A. Orning.[4] The heat-transfer data of Part I, estimated from measured furnace-tube-wall temperatures, indicate that a major portion of the heat release occurs in a small portion of the furnace volume. The "isothermal ΔT diagrams" are often irregular, due, at least in part, to irregular ash or slag deposits which were properly of primary interest to the Special Research Committee. These irregularities make it doubly difficult to estimate the location and size of the zone of intense heat release. However, it appears quite certain that the ability to change the portion of the total heat release absorbed in the furnace by tilting the burners results from a change in the location of the region of intense heat release.

Shifts in the portion of the heat absorbed with rating are also

[4] Coal Research Laboratory, Carnegie Institute of Technology, Pittsburgh, Pa. Mem. ASME.

probably due to changes in position or size of this region. These changes might well be the subject of more direct investigations. As a minimum, it might be interesting to have data on flame intensity as indicated by a total radiation pyrometer sighted at various angles through the furnace wall doors.

In Part IV some consideration is given to the question of the most appropriate basis for calculating the "furnace heat-absorption efficiency." The suggestion "that furnace efficiencies should be based upon the heat available above saturation temperature rather than above 80 F," because "the capability for absorbing heat above saturation temperature does not exist" is somewhat misleading. Heat is required for producing superheated steam and, even before the combustion gases reach the superheat temperature, it becomes more economical to extract the heat in a tube bank than by transfer to the cooled wall of the furnace chamber. Absorption of a portion of the heat in a less economical fashion is necessary in order to reduce the temperature of the suspended ash so that it will not cause slagging difficulties in a tube bank.

Since a steam boiler serves the dual function of evaporating water and superheating steam, it is generally desirable that a fixed fraction of heat absorption should occur in the furnace walls. Accordingly, the better term would be the heat-absorption ratio rather than the heat-absorption efficiency which might suggest the desirability of 100 per cent efficiency. For the purpose of correlating heat-transfer data, the ratio of heat absorbed to total heat input above saturation temperature would appear desirable, but from the operational viewpoint, the ratio should be based upon the heat input above the gas temperature leaving the last evaporating or superheating section. From the design viewpoint, the ratio of real interest is that of heat absorption to the cost per square foot of radiant heat-absorbing surface.

E. M. Powell.[5] Several interesting observations can be made from the data presented which might be more readily appreciated if given in terms of gas temperature rather than the designer's term, absorption efficiency. For instance, the operator has at his command three primary methods for regulating the temperature of the gases entering the convection boiler surface and superheater. These are the variation of excess air, the control of ash accumulation on the furnace walls by the operation of furnace-wall blowers, and the variation of the angle of burner inclination. The tests have been planned so that these factors can be isolated and evaluated individually.

In Fig. 10 of Part II are plotted six tests showing the variation of furnace heat-absorption efficiency with excess air for both clean and dirty furnace walls at essentially a constant rating. Using the modified Hudson-Orrok equation in a similar manner to that described by the authors, correcting the data to a constant rate of heat release of 74,000 Btu/hr/sq ft and calculating the corrected average gas temperature leaving the furnace, the following can be observed (see Fig. 8 of this discussion):

The morning tests with a clean furnace show gas temperatures of 1800, 1785, and 1792 F, corresponding to 35, 23, and 17 per cent excess air leaving the furnace, respectively. In other words, there is essentially no variation of gas temperature with excess air. The afternoon tests with a dirtier furnace show gas temperatures of 1797, 1838, and 1870 F, with 35, 26, and 15 per cent excess air leaving the furnace, respectively, or a total variation of 73 deg F. Because of the sequence in which the tests were run, allowing ash to accumulate at a constant excess air and rating, the following can be concluded: With 35 per cent excess air, no ash will accumulate on the furnace walls since there was no change in gas temperature, and the rate of accumulation will increase as the excess air is reduced. This is particularly interesting since the starting point of gas temperature is the same for all tests.

Similar calculations from Fig. 8 of Part IV, also indicate practically no change in gas temperature with excess air.

The long-term effect of ash accumulation and thorough cleaning is illustrated in Fig. 12 of Part II. Converting these corrected points to gas temperature shows a decrease due to cleaning at the start of the test of 45 deg F. The maximum increase in gas temperature after cleaning was 90 deg F (test No. 25D),

[5] Combustion Engineering Company, Inc., New York, N. Y. Jun. ASME.

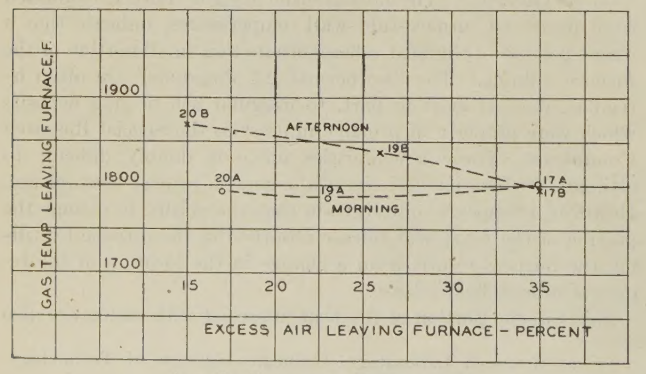

Fig. 8 Effect of Excess Air

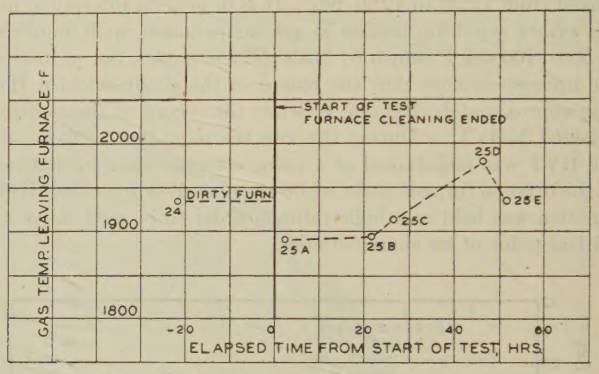

Fig. 9 Effect of Ash Accumulation

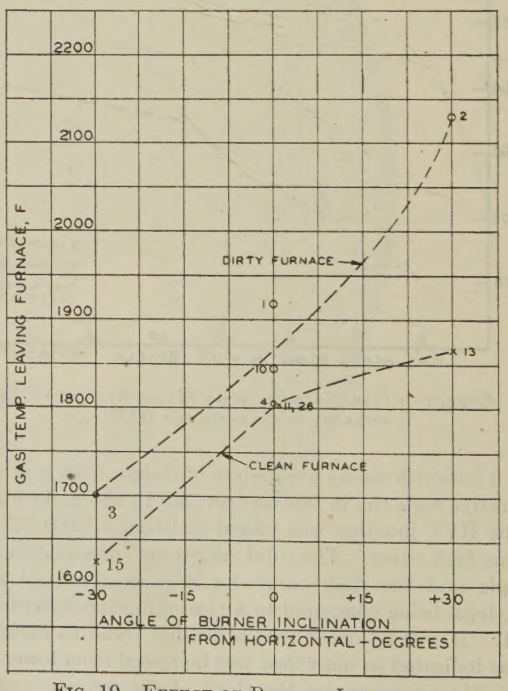

Fig. 10 Effect of Burner Inclination

after which the temperature returned to that existing before cleaning or 45 deg F above that for a clean furnace (see Fig. 9 of this discussion).

The third important variable, burner inclination, is illustrated in Fig. 14, Part II. Converted to temperature these data indicate a total change of 430 deg F, as the burner inclination is varied from —30 deg to +30 deg with a dirty furnace (see Fig. 10 of this discussion). The change with a clean furnace is essentially the same as with a dirty furnace between —30 deg to horizontal. Test No. 13 was incomplete, as stated in the paper, and probably does not represent the true temperature as plotted. Confirming this opinion, other tests on units of this type have indicated that greater changes in gas temperature can be realized by tilting the burners upward above horizontal than tilting below horizontal, substantially as shown by the dirty-furnace tests. The correlation, given in Fig. 8 of Part IV, shows a total variation of 385 deg F between burner inclination of —30 deg to +30 deg of which 140 deg F is below horizontal, and 245 deg F above horizontal. These temperatures were calculated at a release rate of 79,000 Btu/hr/sq ft.

In conclusion these tests demonstrate that the maximum gas-temperature change that can be effected by a reasonable change in excess air may be as much as 75 deg F, and the effect of wall blowers may be 50 to 100 deg F. By comparison, the added flexibility in operation resulting from the application of tilting burners and the corresponding variation of 400 deg F can be readily appreciated.

Author's Closure—Part I

Mr. Davidson's critical appraisal of the isothermal patterns included in Part I, while of interest, is hardly in accordance with the known facts involved in the tests. The contention that "conditions" on the adjacent wall surfaces . . . will not be discontinuities" is simply not in agreement with these facts.

In many instances, visual examination of the furnace walls during the tests revealed definite discontinuities in slag deposits, i.e., "dirty" areas, covered with slag or semifused slag of various thicknesses, immediately adjacent to "clean" areas. Such lines of discontinuity occurred both within the confines of individual walls, and at the right-angle junctions of adjoining walls. Regular or smooth-flowing patterns for all walls, especially in furnace-wall zones near the burners, would be subject to questioning much more than would the irregular patterns evident to some degree in practically all of the isothermal plots reproduced in Part I, and especially in those applying to dirty furnace conditions. The "off-center" firing line of the burners is probably an important factor in the formation of these discontinuities.

Referring to the proposed revision of isothermal lines in the vicinity of furnace wall corners, the constant temperature lines approaching the corners of the furnace should logically be expected to drop off sharply, due to the geometry of the furnace. The shielding afforded each corner zone by the wall adjacent and at right angles to it reduces the solid angle and correspondingly the radiant heat transfer to that portion of the wall. Also, the beneficial sweeping of walls by the hot gases is probably very much diminished in these corner areas so that convection transfer is also at a minimum.

It appears pertinent to describe briefly procedure used in selecting isothermal line paths for Figs. 5 to 16 inclusive of Part I. In all cases, the patterns used for these isothermal plots were carefully worked out by the author and his associates in the project, and were in no case turned over to others not directly associated with the test work. No attempt whatsoever was made to impart an artistic touch to the data. The plots were coordinated, as far as possible, with the "furnace observation reports" referred to in both Parts I and IV and with other related data obtained during the tests.

Authors' Closure Part II

The authors wish to thank Mr. Ely and Mr. Powell for their contributions to this paper. Mr. Ely has estimated, on the basis of data from direct comparisons of single and multiple-shield, high-velocity thermocouples, that a positive correction of 100 deg F to the SHVT is required to place the temperatures on the basis of the MHVT. This value agrees very well with the weighted average value of 85 deg F, derived by the authors from the same data used by Mr. Ely and applied to all of the temperature data given in the present paper. Mr. Powell has modified Figs. 10, 12, and 14, to show the effect of excess air, time, and burner angle on the temperature of the gases leaving the furnace. The conclusions he reaches are of definite interest to boiler designers and operators.

It should be mentioned at this point that the present paper is a revised form of a paper originally presented at the Semi-Annual Meeting in June, 1947, the revisions consisting of corrections of gas temperatures to the MHVT basis, based upon direct comparisons of the SHVT and MHVT under actual operating conditions of the Tidd furnace. Since comparison tests could not be made during the course of the furnace-efficiency tests, Mr. Ely and the Combustion Research staff of the Bureau of Mines made them only a few weeks prior to the presentation of the paper and therefore too late to include with the other data. The revised paper given here, however, has incorporated a correction of 85 deg F, and gas temperatures and enthalpies are reported on the SHVT and MHVT bases for comparison.

The conventional MHVT becomes plugged very rapidly with ash in pulverized-coal furnaces and generally the SHVT has been used for measuring gas temperatures. However, since the SHVT is known to give lower temperatures than the MHVT, corrections are applied to SHVT data to place them on the MHVT basis. It has been agreed by the Furnace Performance Factors Committee that such corrections are unique to each furnace and depend largely upon the ratio of radiant to convective surface to which the shield is exposed. Therefore, part of the pending work by the Committee will be to devise and test various types of shields that are suitable for service in pulverized-coal furnaces, and yet as effective as the conventional MHVT with regard to indicating the true gas temperature.

Authors' Closure—Part IV

Mr. Orning's analysis of the significance of the relative proportion of furnace heat-absorbing (radiant) surface to tube bank (convection) surface is quite sound. From the designer's point of view, this ratio is of paramount importance when considering over-all boiler unit performance, especially as regards required superheated steam temperature. However, as should be evident from all four parts of the investigation, no attempt has been made to either test or analyze the performance of the entire boiler unit.

In reply to the more specific question concerning the advisability of using "heat available above saturation temperature" as a basis for presenting furnace performance data, it should be stated that this was done only after a very careful analysis of the possible implications involved therein. It was finally agreed that this would provide a more nearly equitable basis for comparing the relative heat-absorbing capacity of the particular furnace under test, with its characteristic shape and firing arrangement, with the heat-absorbing capacity of other furnaces with different shapes and firing arrangements. Furthermore, it is the only basis of evaluating the absolute absorption.